

ABSTRACT

CONNER, DAVID MICHAEL.

Synthesis and Reactivity of Ruthenium Amine and Amido Complexes.

(Under the Direction of Dr. T. Brent Gunnoe)

Late transition metal complexes with non-dative and π -donating ligands are important substrates in a variety of synthetic transformations including C-N or C-O bond forming processes and C-H bond activation reactions. Examples of such complexes are few relative to early and middle transition elements in high oxidation states, and the understanding of the chemistry of such systems with amido, oxide, imido, or oxo ligands has lagged compared to related M-C or M-H linkages.

A series of Ru(II) amido complexes of the type TpRu(L)(L')NHR ($\text{L} = \text{L}' = \text{PMe}_3$ or P(OMe)_3 or $\text{L} = \text{CO}$ and $\text{L}' = \text{PPh}_3$; $\text{R} = \text{H}$, Ph , or ^tBu) were prepared and characterized. These complexes exhibit basic reactivity and will deprotonate C-H bonds as evidenced by the reactivity with weak acids such as 1,4-cyclohexadiene or phenylacetylene. The nucleophilicity of the complexes was also examined by reaction with ethylbromide. In addition, oxidation of the phenyl amido complexes with AgOTf , Cp_2FePF_6 , or I_2 resulted in 4,4' carbon-carbon coupling of the aryl group of the anilido ligands to produce the bimetallic complexes $[\text{TpRu(L)(L')NHC}_6\text{H}_4\text{-}]_2[\text{X}]_2$ ($\text{X} = \text{OTf}^-$, PF_6^- , or I^-).

The five-coordinate amido complexes $(\text{PCP})\text{Ru(CO)NHR}$ ($\text{PCP} = \text{C}_6\text{H}_3(\text{CH}_2\text{P}^t\text{Bu}_2)_2$; $\text{R} = \text{H}$ or Ph) were synthesized and characterized. The parent amido complex was prepared by deprotonation of $(\text{PCP})\text{Ru(CO)(NH}_3\text{)Cl}$ and the phenyl amido

complex was prepared by reacting (PCP)Ru(CO)OTf with LiNHPH. The reactivity of the parent amido complex with phenylacetylene, dihydrogen, and hydrocarbons was studied. Density functional theory was applied to the activation of H₂ and CH₄ by (PCP')Ru(CO)NH₂ (PCP' = C₆H₃(CH₂PH₂)₂) to yield (PCP')Ru(CO)(NH₃)X (X = H or Me). Additionally, the complex (PCP)Ru(CO)Me was prepared. The complexes (PCP)Ru(CO)X (X = Me, NH₂, and NHPH) undergo intramolecular C-H bond activation reactions with a ^tBu arm of the PCP ligand to produce the cyclometalated complex (PCP*)Ru(CO) (PCP* = C₆H₃(CH₂P^tBu₂){P(^tBu)(C(CH₃)₂CH₂)} and methane, ammonia, or aniline, respectively.

**Synthesis and Reactivity of Ruthenium Amine and
Amido Complexes.**

by

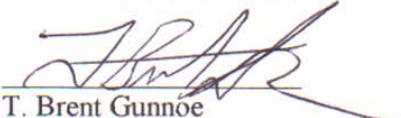
David Conner

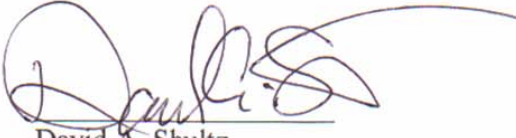
A dissertation submitted to the graduate faculty of
North Carolina State University
in partial fulfillment of the requirements for the
Doctor of Philosophy Chemistry

CHEMISTRY

Raleigh, North Carolina
2004

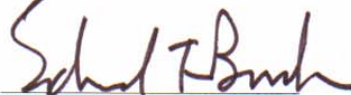
APPROVED BY:


T. Brent Gunnoe


David A. Shultz

Chair of Advisory Committee


James M. Martin


Edmond F. Bowden

DEDICATION

This work is dedicated to Rufus. The man without whom none of what follows would be possible. May the rumors of your demise be greatly overstated.

BIOGRAPHY

David Michael Conner was born in Audubon, Pennsylvania on August 21, 1975 to James and Laura Conner. The early years were entirely unremarkable except for the trivial facts that his diet consisted of blended leftovers and his older brother spent a great deal of time pinning him down to poke his eyes mercilessly. David has worn glasses for sometime and has been known to eat the same dish at Golden Dragon for over month straight.

At the age of five, David experienced the trauma of kindergarten wherein he cried unceasingly for the first three days. At the time, his teacher, Miss Yannic, assumed that the wailing was a result of separation anxiety; however, the true cause lay in that fact that upon arrival to school David realized a full thirteen years of schooling lay ahead. He surmised this period was over twice his life span and many times more than the life he could recall (and that time didn't even include college). Thus, even as a child David never really seemed to think like normal people. The irony of course is David spent not only the next thirteen years, but nearly the next twenty-six in the academic world.

His current plans involve adjusting to and enjoying life outside academia, and – well to be entirely truthful – never-ever-ever-ever-ever going to school again. Toodles!

ACKNOWLEDGMENTS

A great debt is owed to many people for their aid in completion of this work. Three of those deserve honorable mention, for without their aid and mentoring my goals and current level of success would never have been realized. First, Dr. Edward Rajaseelan of Millersville University. His faith in me has served as a beacon always summoning me to strive onward. Second, Dr. Gerfried Pruckmayr of The DuPont Corporation. Gerfried's advice such as, "Know everything, that way if I have a question, you'll have the answer" has always served me well. As a mentor, I can think of none better. Lastly, to my advisor Brent Gunnoe, enough thanks can not be expressed because I can not imagine going through graduate school under the direction of anyone else. Brent is a hell of a great guy and so I apologize to him if all the headaches I caused over the years have caused him to develop an addiction to painkillers.

Before I get disowned, let me express deepest gratitude to my parents for all they have done to help complete my education. Seemingly I have been a considerable investment to be able to use the phrase "this one isn't a loser." Congratulations on the bragging rights and thanks!

My wonderful fiancé Jen Carrozzino needs to be thanked heartily for all the help and support she has provided throughout the past few years. Graduate school is difficult and graduate research can be unqualified melancholy, yet even the darkest hours always seemed bright because she was near. I am truly blessed to have suckered in someone so grand. I love her and she is in fact better than ice-cream.

Thanks to all the Gunnoe Group members (past and present), especially the other members who were there in the beginning – Jayaprakash, Ben Arrowood (who taught me the value of always looking over my shoulder), and Melissa Travis. Also to Liz, Marty, Jubo, Yuee, John, Colleen, Laurel, and Karl, keep striving and keep the faith. I am sure you will all be horrendously successful because you all F-ing rock. I am honored to have worked with such an incredible troupe.

On a personal level let me thank the following... Shadow (my dog) for hours of fun. Mia the Bee for being a great friend and confidant for so many years. The Order of the Barley for never needing an excuse to drink. Matt Eagleson for teaching me the value of apathy. Matt's mother for - well she knows. Sam Raimi for creating such classics as the Evil Dead Trilogy, and Xena – Warrior Princess. Dennis J. Fleming for unapologetically being Dennis J. Fleming. Joe Ryan and Ryan Fuierer for making graduate school much more fun. Dr. Sankar for keeping the NMR's up and running. Shemp - the funniest Stooge. Dr. Paul Boyle for existing and doing his job so I don't have to. The one eyed man and G Heilman. The Angry Samoans and punk rock in general. And lastly to my true friend Dee Dee Allen, thanks so much for trying to save my soul – good luck with that! Best regards to all who read this and GO PACK!

TABLE OF CONTENTS

List of Figures	x
List of Tables	xvi
List of Schemes	xix
List of Symbols, Abbreviations, and Terms	xxviii
Chapter 1: Introduction	1
1.1 Introduction and Importance of Late Transition Metal Complexes with Non-Dative and π -Donating Ligands.	1
1.2 A Brief Survey of Relevant Late Transition Metal Amido Complexes.	4
1.3 Bonding in Late Transition Metal Complexes that Possess Non-Dative and π -Donating Ligands.	5
1.3.1 An Approach to Bonding in Late Transition Metal Complexes With π -Donating Ligands Using the Theory of π -conflict.	7
1.3.2 An <i>E-C</i> Approach to Bonding in Late Transition Metal Complexes with Non-Dative Ligands.	10
1.4 General Reactivity of Late Transition Metal Complexes with Non-Dative π -Donating Ligands.	14
1.5 Carbon-Hydrogen Bond Activation and Relevance to Late Transition Metal Amido Complexes.	22
1.5.1 C-H Activation by Early Transition Metal Imido Complexes.	27
1.5.2 Activation of Non-Polar Bonds by Late Transition Metal Complexes that Possess Heteroatomic π -Donating Ligands.	28
1.6 Rationale for the Choice of Ligand	32
References	37

Chapter 2: Synthesis of Octahedral Ruthenium Amido Complexes and Initial Studies.	41
2.1 Introduction.	41
2.2 General Comments on Synthesis of TpRu(L)(L')NHR Complexes.	46
2.2.1 Synthesis of Tp Amido Precursor Complexes.	47
2.2.2 Synthesis of TpRu(PMe ₃) ₂ OTf, TpRu{P(OMe) ₃ } ₂ OTf, and TpRu(CO)(PPh ₃)OTf, and Their Reactivity with Alkali Amides.	51
2.2.3 Synthesis of Cationic Amine Complexes.	57
2.3 Synthesis of Octahedral Ruthenium (II) Amido Complexes.	67
2.4 Electrochemical Studies of the Amido Complexes.	70
2.5 ¹ H NMR Chemical Shifts of the Amido Proton.	71
2.6 Variable Temperature ¹ H NMR Spectra of the Amido Complexes.	72
2.6.1 Dynamic ¹ H NMR of the TpRu(L)(L')NHR Amido Complexes.	77
2.7 General Experimental Methods.	86
References	102
Chapter 3: Detailed Studies of the Amido Complexes.	105
3.1 Introduction.	105
3.2 Linear Free Energy Relationship Studies of Ruthenium (II) Aryl Amido Complexes.	107
3.3 Determination of the pK _a of the Phenyl Amine Complexes and Ligand Effect on the pK _a .	113
3.4 UV-vis Studies of the Ru(II) Anilido-Malononitrile Equilibrium Reactions.	119
3.5 Reaction of the Amido complexes with Weak Acids and Studies of the Reaction with Phenylacetylene.	122
3.6 Reaction of the Phenyl Amido Complexes with Phenylacetylene.	129

3.7 Reaction of the Amido Complexes with 1,4-Cyclohexadiene.	136
3.8 Reaction of $\text{TpRu}(\text{PMe}_3)\text{NHPH}$ with Ethylbromide.	140
3.9 Experimental Details.	142
References.	156
Chapter 4: Aryl Coupling with Ruthenium Anilido Complexes.	158
4.1 Introduction and Importance of Biaryl Species.	158
4.1.1 Aryl-Aryl Bond Formation by Late Transition Metal Arylamido and Aryloxo Complexes.	159
4.1.2 Common Synthetic Methods to Form Aryl-Aryl Bonds.	163
4.1.3 Potential Synthetic Utility of Aryl-Aryl Coupling by Oxidation of Late Transition Metal Amido Complexes.	166
4.2 Oxidation of $\text{TpRuL}_2\text{NHPH}$ $\text{L} = \text{CO}, \text{PMe}_3, \text{ or } \text{P}(\text{OMe})_3$	168
4.3 Dynamic NMR Spectroscopy of the Complexes $[\text{TpRuL}_2(\text{NHC}_6\text{H}_4^-)][\text{OTf}]_2$	175
4.4 Solid-State Structure of $[\text{TpRu}\{\text{P}(\text{OMe})_3\}_2\text{NH}(\text{C}_6\text{H}_4^-)]_2[\text{OTf}]_2$	178
4.5 Mechanism of Formation of the Binuclear Complexes $[\text{TpRuL}_2\text{NHC}_6\text{H}_4^-]_2[\text{OTf}]_2$	180
4.6 Effect of Base and Variation of Oxidant on the Oxidative Coupling of $\text{TpRuL}_2\text{NHPH}$	187
4.7 Attempts at Catalytic Imine Formation.	191
4.8 Experimental Section.	193
References.	199
Chapter 5: Synthesis and Reactivity of Coordinatively Unsaturated Ruthenium(II) Amido Complexes.	201
5.1 Introduction and Importance of Unsaturation.	201

5.2 Synthesis of Unsaturated Amido Complexes.	204
5.2.1 Preparation of (PCP)Ru(CO)(NH ₃)Cl, [(PCP)Ru(CO)(NH ₃) ₂][OTf], and (PCP)Ru(CO)NH ₂	209
5.3 Reactivity of (PCP)Ru(CO)NH ₂ with Phenylacetylene or Dihydrogen.	215
5.4 C-H Bond Activation of Methane by (PCP)Ru(CO)NH ₂	226
5.5 Attempted C-H Bond Activation of Benzene.	235
5.6 Theoretical Studies of C-H versus H-H Bond Activation by (PCP)Ru(CO)NH ₂ . .	236
5.7 Reactivity of the Cyclometalated Complex.	243
5.8 Experimental Section.	247
References.	258
Appendix A: Crystallographic data and Structural Refinements	260
Appendix B: Variable Temperature ¹ H NMR Spectra of the Binuclear Complexes ...	375

List of Figures

Figure 1.1 A	^1H NMR spectrum on a Tp metal complex with C_3 symmetry.	35
Figure 1.1 B	^1H NMR spectrum on a Tp metal complex with σ -symmetry.	35
Figure 1.1 C	^1H NMR spectrum on an asymmetric Tp metal complex.	35
Figure 1.2	The PCP ligand. PCP ligands allow for tuning of steric and electronic effects through alteration of the phosphine substituent R, and variation of the X allows for further tuning of electronic effects.	36
Figure 2.1	^1H NMR spectrum of $\text{TpRu}(\text{PMe}_3)_2\text{Cl}$ in CDCl_3	49
Figure 2.2	^1H NMR spectrum of $\text{TpRu}\{\text{P}(\text{OMe})_3\}_2\text{Cl}$ in CDCl_3	50
Figure 2.3	X-ray diagram of $\text{TpRu}\{\text{P}(\text{OMe})_3\}_2\text{Cl}$ (H omitted).	51
Figure 2.4	$\text{TpRu}(\text{L})(\text{L}')\text{X}$ systems used as precursors to octahedral Ru(II) amido complexes.	48
Figure 2.5 A	^1H NMR spectrum of $\text{TpRu}\{\text{P}(\text{OMe})_3\}_2\text{Cl}$ in CDCl_3	53
Figure 2.5 B	^1H NMR spectrum of the proposed adduct of formed by addition of AgOTf to $\text{TpRu}\{\text{P}(\text{OMe})_3\}_2\text{Cl}$	54
Figure 2.5 C	^1H NMR spectrum of $\text{TpRu}\{\text{P}(\text{OMe})_3\}_2\text{OTf}$ in CDCl_3	55
Figure 2.6	^1H NMR spectrum of $\text{TpRu}(\text{PMe}_3)_2\text{OTf}$ in C_6D_6	56
Figure 2.7	^1H NMR spectrum of $\text{TpRu}\{\text{P}(\text{OMe})_3\}_2\text{OTf}$ in CDCl_3	57
Figure 2.8	^1H NMR spectrum of $[\text{TpRu}\{\text{P}(\text{OMe})_3\}_2\text{NH}_2\text{Ph}][\text{OTf}]$ in CDCl_3	61
Figure 2.9	^1H NMR spectrum of $[\text{TpRu}(\text{PMe}_3)_2\text{NH}_2\text{Ph}][\text{OTf}]$ in CDCl_3	62
Figure 2.10	X-ray diagram of $[\text{TpRu}(\text{PMe}_3)_2\text{NH}_2\text{Ph}][\text{OTf}]$	63
Figure 2.11	X-ray diagram of $[\text{TpRu}\{\text{P}(\text{OMe})_3\}_2\text{NH}_2\text{Ph}][\text{OTf}]$	63
Figure 2.12	X-ray diagram of $[\text{TpRu}(\text{PMe}_3)_2\text{NH}_3][\text{OTf}]$	65
Figure 2.13	X-ray diagram of $\text{TpRu}\{\text{P}(\text{OMe})_3\}_2\text{NHPh}$	68

Figure 2.14	Transition state theory states the molecules collide to form an activated complex AB^\ddagger . The activation energy ΔG^\ddagger is the energy from reactants to AB^\ddagger	75
Figure 2.15	Example of a dynamic NMR experiment. At low temperature the slow exchange results in an exchange that is “frozen out.” Warming results in an increase in rate of exchange and results in coalescence.	79
Figure 2.16	Variable temperature ^1H NMR spectroscopy of $\text{TpRu}(\text{PMe}_3)_2\text{NHPPh}$. ..	81
Figure 2.17	Variable temperature ^1H NMR spectra of $\text{TpRu}\{\text{P}(\text{OMe})_3\}_2\text{NHPPh}$	82
Figure 3.1	LFER studies use substituted arenes because of the ability of the aryl ring to electronically communicate to a remote reaction site.	108
Figure 3.2	Hammett plot of $\log K_{\text{eq}}$ for aryl amido exchange reaction. $\rho = 4.1$; $r^2 = 0.97$	112
Figure 3.3	^1H NMR spectrum of the reaction of $\text{TpRu}(\text{PMe}_3)_2\text{NHPPh}$ with one equivalent of malononitrile (room temperature).	117
Figure 3.4	^1H NMR spectrum of the reaction of $\text{TpRu}(\text{PMe}_3)_2\text{NHPPh}$ with two equivalent of malononitrile (room temperature).	118
Figure 3.5	^1H NMR spectrum of the reaction of $\text{TpRu}(\text{PMe}_3)_2\text{NHPPh}$ with one equivalent of malononitrile ($-90\text{ }^\circ\text{C}$).	118
Figure 3.6	Isosbestic point of $\text{TpRu}(\text{PMe}_3)_2\text{NHPPh}$ seen with addition of malononitrile.	121
Figure 3.7	Isosbestic point of $\text{TpRu}\{\text{P}(\text{OMe})_3\}_2\text{NHPPh}$ seen with addition of malononitrile.	121
Figure 3.8	Kinetics of the reaction of $[\text{TpRu}(\text{PMe}_3)_2\text{NH}_2\text{R}][\text{OTf}]$ with CD_3CN . ($\blacktriangle = \text{R} = \text{}^t\text{Bu}$; $\blacksquare = \text{R} = \text{Ph}$).	127
Figure 3.9	Plot of k_{obs} versus concentration of $\text{TpRu}(\text{PMe}_3)_2(\text{OTf})$	132
Figure 3.10	^1H NMR spectrum of $[\text{TpRu}(\text{PMe}_3)_3][\text{OTf}]$ in CDCl_3	134
Figure 3.11	^1H NMR spectrum of $\text{TpRu}(\text{PMe}_3)_2\text{H}$ in C_6D_6	138
Figure 3.12	First order kinetic plot for the reaction of $\text{TpRu}(\text{PMe}_3)_2\text{NHPPh}$ with ethyl bromide. ($k_{\text{obs}} = 8.6 \times 10^{-6} \text{ M}^{-1} \text{ s}^{-1}$)	141

Figure 4.1	Examples of important biaryl species. A. Ascididemin is a marine alkaloid shown to have biological activity. B. Neoamphimedine is a marine alkaloid shown to have biological activity. C. Vancomycin is a very powerful antibiotic. D. Sartans are a class of drugs used to treat high blood pressure.	159
Figure 4.2	^1H NMR spectrum of $[\text{TpRu}\{\text{P}(\text{OMe})_3\}_2(\text{NHC}_6\text{H}_4^-)]_2[\text{OTf}]_2$ in CDCl_3	171
Figure 4.2 A	^{31}P NMR spectrum of $[\text{TpRu}\{\text{P}(\text{OMe})_3\}_2(\text{NHC}_6\text{H}_4^-)]_2[\text{OTf}]_2$ in CDCl_3	171
Figure 4.3	^1H NMR spectrum of $[\text{TpRu}\{\text{P}(\text{OMe})_3\}_2(\text{NHC}_6\text{H}_4^-)]_2[\text{OTf}]_2$ in CD_3CN	172
Figure 4.3A	^1H NMR spectrum of $[\text{TpRu}\{\text{P}(\text{OMe})_3\}_2(\text{NHC}_6\text{H}_4^-)]_2[\text{OTf}]_2$ in $\text{DMSO}-d_6$	172
Figure 4.4	^1H NMR spectrum of $[\text{TpRu}(\text{CO})_2(\text{NHC}_6\text{H}_4^-)]_2[\text{OTf}]_2$ in $\text{DMSO}-d_6$	173
Figure 4.5	^1H NMR spectrum of $\text{TpRu}(\text{PMe}_3)_2(\text{NHC}_6\text{H}_4^-)]_2[\text{OTf}]_2$ in $\text{DMSO}-d_6$	174
Figure 4.6	X-ray structural diagram of $[\text{TpRu}\{\text{P}(\text{OMe})_3\}_2\text{NHC}_6\text{H}_4^-]_2[\text{OTf}]_2$	178
Figure 5.1	Pincer ligands allow tuning of steric and electronic effects through the phosphine substituent R, and, the variation of the X allows additional tuning of electronic effects.	204
Figure 5.2	Spectroscopic handles for $(\text{PCP})\text{Ru}(\text{CO})\text{X}$ complexes. A CO absorptions (IR) B ^1H resonances in the ^1H NMR spectrum.	205
Figure 5.3	^1H NMR spectrum of $(\text{PCP})\text{Ru}(\text{CO})(\text{Cl})(\text{NH}_3)$ in CDCl_3	210
Figure 5.4	^1H NMR spectrum of $(\text{PCP})\text{Ru}(\text{CO})\text{NH}_2$ in C_6D_6	212
Figure 5.5	^1H NMR spectrum of $(\text{PCP})\text{Ru}(\text{CO})\text{OTf}$ in C_6D_6	213
Figure 5.6	^1H NMR spectrum of $[(\text{PCP})\text{Ru}(\text{CO})(\text{NH}_3)_2][\text{OTf}]$ in CDCl_3	215
Figure 5.7	^1H NMR spectrum of $(\text{PCP})\text{Ru}(\text{CO})(\text{NH}_3)(\text{H})$ C_6D_6 with NH_3 in solution.	222

Figure 5.8	^1H NMR spectrum of $\text{Ru}(\text{CO})\{\text{C}_6\text{H}_3\text{-2-(CH}_2\text{P}^t\text{Bu}_2\text{)-6-(CH}_2\text{P}^t\text{Bu)-}(\text{CMe}_2\text{CH}_2)\}$ in C_6D_6	228
Figure 5.9	^{31}P NMR spectrum of $\text{Ru}(\text{CO})\{\text{C}_6\text{H}_3\text{-2-(CH}_2\text{P}^t\text{Bu}_2\text{)-6-(CH}_2\text{P}^t\text{Bu)-}(\text{CMe}_2\text{CH}_2)\}$ in C_6D_6	228
Figure 5.10	^1H NMR spectrum of $(\text{PCP})\text{Ru}(\text{CO})\text{Me}$ in C_6D_6	230
Figure 5.11	First order kinetic plot time for cyclometalation of $(\text{PCP})\text{Ru}(\text{CO})\text{Me}$ and $(\text{PCP})\text{Ru}(\text{CO})\text{NH}_2$ at $40\text{ }^\circ\text{C}$ (■ = $(\text{PCP})\text{Ru}(\text{CO})\text{NH}_2$ and ▲ = $(\text{PCP})\text{Ru}(\text{CO})\text{Me}$	231
Figure 5.12	Eyring plots for the cyclometalation reactions of $(\text{PCP})\text{Ru}(\text{CO})(\text{X})$ ($\text{X} = \text{Me}$ or NH_2). The ΔH^\ddagger for both reactions is $18(1)$ kcal/mol, and the ΔS^\ddagger is $-23(4)$ and $-18(4)$ for NH_2 and Me respectively.	233
Figure 5.13	Mass spectrometry spectrum of the reaction of the cyclometalated complex and CH_4 and ND_3 . Isotopic scrambling prevented the determination of whether the amido complex $(\text{PCP})\text{Ru}(\text{CO})\text{NH}_2$ activates methane.	234
Figure 5.14	B3LYP/SBK(d) optimized geometry of $(\text{PCP}')\text{Ru}(\text{CO})(\text{NH}_2)$ model reactant showing pertinent bond lengths and bond angles as calculated by Prof. Tom Cundari of the University of North Texas.	238
Figure 5.15	Based on theoretical calculations of methane activation, this reaction is anticipated to be thermodynamically favorable; however, a significant enthalpic loss for the Ru-N bond occurs in the transition from a non-dative amido ligand to a dative amine ligand.	240
Figure 5.16	The addition of NH_3 increases the rate of disappearance of $(\text{PCP})\text{Ru}(\text{CO})\text{Me}$, possibly due to formation of $(\text{PCP})\text{Ru}(\text{CO})\text{NH}_2$ from methane elimination from $(\text{PCP})\text{Ru}(\text{CO})(\text{Me})(\text{NH}_3)$	242
Figure 5.17	^1H NMR spectrum of the decomposition product of the cyclometalated complex under N_2 atmosphere.	244
Figure 5.18	Mass spectrum of isobutylene.	245
Figure A1	ORTEP diagram of $\text{TpRu}\{\text{P}(\text{OMe})_3\}_2\text{Cl}$	260
Figure A2	ORTEP diagram of $[\text{TpRuP}(\text{Me}_3)_2\text{NH}_2\text{Ph}][\text{OTf}]$	272

Figure A3	ORTEP diagram of [TpRu{P(OMe) ₃ } ₂ NH ₂ Ph][OTf]	283
Figure A4	ORTEP diagram of [TpRu(PMe) ₃] ₂ (NH ₃)[OTf]	297
Figure A5	ORTEP diagram of TpRu{P(OMe) ₃ } ₂ NHPh	310
Figure A6	ORTEP diagram of [TpRu{P(OMe) ₃ } ₂ NHC ₆ H ₄ -] ₂ [OTf] ₂	322
Figure A7	ORTEP diagram of [TpRu{P(OMe) ₃ } ₂ NHC ₆ H ₄ -] ₂ [OTf] ₂	339
Figure B1	¹ H NMR spectrum of [TpRu{P(OMe) ₃ } ₂ NC ₆ H ₄ -] ₂ [OTf] ₂ in CD ₃ CN at -45 °C.	375
Figure B2	¹ H NMR spectrum of [TpRu{P(OMe) ₃ } ₂ NC ₆ H ₄ -] ₂ [OTf] ₂ in CD ₃ CN at -40 °C.	376
Figure B3	¹ H NMR spectrum of [TpRu{P(OMe) ₃ } ₂ NC ₆ H ₄ -] ₂ [OTf] ₂ in CD ₃ CN at -30 °C.	377
Figure B4	¹ H NMR spectrum of [TpRu{P(OMe) ₃ } ₂ NC ₆ H ₄ -] ₂ [OTf] ₂ in CD ₃ CN at -20 °C.	378
Figure B5	¹ H NMR spectrum of [TpRu{P(OMe) ₃ } ₂ NC ₆ H ₄ -] ₂ [OTf] ₂ in CD ₃ CN at -5 °C.	379
Figure B6	¹ H NMR spectrum of [TpRu{P(OMe) ₃ } ₂ NC ₆ H ₄ -] ₂ [OTf] ₂ in CD ₃ CN at 15 °C.	380
Figure B7	¹ H NMR spectrum of [TpRu{P(OMe) ₃ } ₂ NC ₆ H ₄ -] ₂ [OTf] ₂ in CD ₃ CN at 40 °C.	381
Figure B8	¹ H NMR spectrum of [TpRu{P(OMe) ₃ } ₂ NC ₆ H ₄ -] ₂ [OTf] ₂ in CD ₃ CN at 50 °C.	382
Figure B9	¹ H NMR spectrum of [TpRu{P(OMe) ₃ } ₂ NC ₆ H ₄ -] ₂ [OTf] ₂ in CD ₃ CN at 60 °C.	383
Figure B10	¹ H NMR spectrum of [TpRu{P(OMe) ₃ } ₂ NC ₆ H ₄ -] ₂ [OTf] ₂ in CD ₃ CN at 70 °C.	384
Figure B11	¹ H NMR spectrum of [TpRu{P(OMe) ₃ } ₂ NC ₆ H ₄ -] ₂ [OTf] ₂ in CD ₃ CN at 95 °C.	385

Figure B12	^1H NMR spectrum of $[\text{TpRu}(\text{PMe}_3)_2\text{NC}_6\text{H}_4\text{-}]_2[\text{OTf}]_2$ in 80% CD_3CN 20 % $\text{DMSO-}d_6$ at 60 °C.	386
Figure B13	^1H NMR spectrum of $[\text{TpRu}(\text{PMe}_3)_2\text{NC}_6\text{H}_4\text{-}]_2[\text{OTf}]_2$ in 80% CD_3CN 20 % $\text{DMSO-}d_6$ at 40 °C.	387
Figure B14	^1H NMR spectrum of $[\text{TpRu}(\text{PMe}_3)_2\text{NC}_6\text{H}_4\text{-}]_2[\text{OTf}]_2$ in 80% CD_3CN 20 % $\text{DMSO-}d_6$ at 30 °C.	388
Figure B15	^1H NMR spectrum of $[\text{TpRu}(\text{PMe}_3)_2\text{NC}_6\text{H}_4\text{-}]_2[\text{OTf}]_2$ in 80% CD_3CN 20 % $\text{DMSO-}d_6$ at 30 °C.	389
Figure B16	^1H NMR spectrum of $[\text{TpRu}(\text{PMe}_3)_2\text{NC}_6\text{H}_4\text{-}]_2[\text{OTf}]_2$ in 80% CD_3CN 20 % $\text{DMSO-}d_6$ at 10 °C.	390
Figure B17	^1H NMR spectrum of $[\text{TpRu}(\text{PMe}_3)_2\text{NC}_6\text{H}_4\text{-}]_2[\text{OTf}]_2$ in 80% CD_3CN 20 % $\text{DMSO-}d_6$ -20 °C.	391
Figure B18	^1H NMR spectrum of $[\text{TpRu}(\text{PMe}_3)_2\text{NC}_6\text{H}_4\text{-}]_2[\text{OTf}]_2$ in 80% CD_3CN 20 % $\text{DMSO-}d_6$ -30 °C.	392
Figure B19	^1H NMR spectrum of $[\text{TpRu}(\text{PMe}_3)_2\text{NC}_6\text{H}_4\text{-}]_2[\text{OTf}]_2$ in 80% CD_3CN 20 % $\text{DMSO-}d_6$ -40 °C.	393

List of Tables

Table 2.1	Selected Bond Distances for [TpRu(L) ₂ NH ₂ Ph][OTf]	64
Table 2.2	Selected Bond Angles for [TpRu(L) ₂ NH ₂ Ph][OTf]	64
Table 2.3	III/II reduction potentials of the TpRu(L)(L') complexes	71
Table 2.4	¹ H NMR Chemical Shifts of the amido NH resonance	72
Table 2.5	Rotational barriers about Ru-N and N-C bonds	82
Table 3.1	UV-Vis data for the Ru(II) amine and amido complexes in THF	120
Table 4.1	Barriers to isomer interconversion for the binuclear complexes.	178
Table 4.2	Selected bond distances for [TpRu{P(OMe) ₃ } ₂ NHC ₆ H ₄ -] ₂ [OTf] ₂	179
Table A.1	Crystal Data and Structure Refinement for TpRu{P(OMe) ₃ } ₂ Cl	260
Table A.2	Atomic Coordinates and Thermal Parameters (x, y, z and u) for TpRu{P(OMe) ₃ } ₂ Cl	262
Table A.3	Anisotropic Displacement Parameters for TpRu{P(OMe) ₃ } ₂ Cl	265
Table A.4	Bond Distances for TpRu{P(OMe) ₃ } ₂ Cl	267
Table A.5	Bond Angles for TpRu{P(OMe) ₃ } ₂ Cl	268
Table A.6	Crystal Data and Structure Refinement for [TpRu(PMe ₃) ₂ NH ₂ Ph][OTf]	272
Table A.7	Atomic Coordinates and Thermal Parameters (x, y, z and u) for [TpRu(PMe ₃) ₂ NH ₂ Ph][OTf]	273
Table A.8	Anisotropic Displacement Parameters for [TpRu(PMe ₃) ₂ NH ₂ Ph][OTf]	276
Table A.9	Bond Distances for [TpRu(PMe ₃) ₂ NH ₂ Ph][OTf]	278
Table A.10	Bond Angles for [TpRu(PMe ₃) ₂ NH ₂ Ph][OTf]	281

Table A.11	Crystal Data and Structure Refinement for [TpRu{P(OMe) ₃ } ₂ NH ₂ Ph][OTf]	284
Table A.12	Atomic Coordinates and Thermal Parameters (x, y, z and u) for [TpRu{P(OMe) ₃ } ₂ NH ₂ Ph][OTf]	286
Table A.13	Anisotropic Displacement Parameters for [TpRu{P(OMe) ₃ } ₂ NH ₂ Ph][OTf]	289
Table A.14	Bond Distances for [TpRu{P(OMe) ₃ } ₂ NH ₂ Ph][OTf]	292
Table A.15	Bond Angles for [TpRu{P(OMe) ₃ } ₂ NH ₂ Ph][OTf]	296
Table A.16	Crystal Data and Structure Refinement for [TpRu(PMe) ₃] ₂ (NH ₃)[OTf]	297
Table A.17	Atomic Coordinates and Thermal Parameters (x, y, z and u) for [TpRu(PMe) ₃] ₂ (NH ₃)[OTf]	299
Table A.18	Anisotropic Displacement Parameters for [TpRu(PMe) ₃] ₂ (NH ₃)[OTf]	302
Table A.19	Bond Distances for [TpRu(PMe) ₃] ₂ (NH ₃)[OTf]	304
Table A.20	Bond Angles for [TpRu(PMe) ₃] ₂ (NH ₃)[OTf]	306
Table A.21	Crystal Data and Structure Refinement for TpRu{P(OMe) ₃ } ₂ NHPh ..	310
Table A.22	Atomic Coordinates and Thermal Parameters (x, y, z and u) TpRu{P(OMe) ₃ } ₂ NHPh	312
Table A.23	Anisotropic Displacement Parameters for TpRu{P(OMe) ₃ } ₂ NHPh ...	315
Table A.24	Bond Distances for TpRu{P(OMe) ₃ } ₂ NHPh	318
Table A.25	Bond Angles for TpRu{P(OMe) ₃ } ₂ NHPh	320
Table A.26	Crystal Data and Structure Refinement [TpRu{P(OMe) ₃ } ₂ NHC ₆ H ₄ -] ₂ [OTf] ₂	323
Table A.27	Atomic Coordinates and Thermal Parameters (x, y, z and u) for [TpRu{P(OMe) ₃ } ₂ NHC ₆ H ₄ -] ₂ [OTf] ₂	325

Table A.28	Anisotropic Displacement Parameters for [TpRu{P(OMe) ₃ } ₂ NHC ₆ H ₄ -] ₂ [OTf] ₂	329
Table A.29	Bond Distances for [TpRu{P(OMe) ₃ } ₂ NHC ₆ H ₄ -] ₂ [OTf] ₂	335
Table A.30	Bond Angles for [TpRu{P(OMe) ₃ } ₂ NHC ₆ H ₄ -] ₂ [OTf] ₂	337
Table A.31	Crystal Data and Structure Refinement [TpRu{P(OMe) ₃ } ₂ NHC ₆ H ₄ -] ₂ [OTf] ₂	340
Table A.32	Atomic Coordinates and Thermal Parameters (x, y, z and u) for [TpRu{P(OMe) ₃ } ₂ NHC ₆ H ₄ -] ₂ [OTf] ₂	342
Table A.33	Anisotropic Displacement Parameters for [TpRu{P(OMe) ₃ } ₂ NHC ₆ H ₄ -] ₂ [OTf] ₂	351
Table A.34	Bond Distances for [TpRu{P(OMe) ₃ } ₂ NHC ₆ H ₄ -] ₂ [OTf] ₂	357
Table A.35	Bond Angles for [TpRu{P(OMe) ₃ } ₂ NHC ₆ H ₄ -] ₂ [OTf] ₂	359

List of Schemes

Scheme 1.1	Potential for bond activation of polar and non-polar substrates by late transition metal complexes with non-dative and π -donating and heteroatomic ligand.	2
Scheme 1.2	Lipoxygenase converts 1,4-dienes to hydroperoxides by H-atom abstraction. This enzyme has been modeled using Fe(III) oxide complexes.	3
Scheme 1.3	Model of π -conflict. Heightened reactivity results from occupation of an antibonding orbital.	8
Scheme 1.4	Amido/oxide ligand exchange reactions. π -conflict rationalizes the thermodynamic preference for oxide ligand is due decreased π -donation.	9
Scheme 1.5	Resonance structures of bonding between late transition metals and non-dative and π -donating ligands. As bond polarization increases, the electrostatic component of bond increases and results in a stronger, yet reactive, M-X moiety.	11
Scheme 1.6	Exchange reactions of $(\text{PMe}_3)_4\text{Ru}(\text{H})(\text{CH}_2\text{Ph})$ with aniline and p-methylphenol favor π -donating oxide or amido ligands. This results suggests the importance of the ionic nature in M-X bonding.	12
Scheme 1.7	Meta versus para donating substituent does not significantly impact K_{eq} of exchange reactions for the complex $\text{Cp}^*\text{Ni}(\text{PEt}_3)\text{NHTol}$. This result suggests π -conflict has a minimal effect on the bonding in such M-N linkages.	13
Scheme 1.8	Common mechanism of β -hydrogen elimination.	14
Scheme 1.9	β -hydride elimination reactions for late transition metal amido and oxide complexes. These reaction have also been inferred by unobserved intermediates.	15
Scheme 1.10	Reductive elimination from a late transition metal amido complex to form an aryl amine.	17
Scheme 1.11	Aryl-aryl coupling in late transition metal complexes with nondative and π - donating ligands that possess an aryl substituent.	17

Scheme 1.12	σ -bond metathesis reaction scheme.	18
Scheme 1.13	Insertion reactions of late transition metal amido and oxide complexes. A - CO insertion. B – Cumene and heterocumene insertion. C – Olefin insertion.	19
Scheme 1.14	Studies of palladium catalyzes aryl amination indicate the rate of reaction is increased by more donating amido substituents (X) and more electronwithdrawing aryl substituents (Y).	21
Scheme 1.15	Proposed scheme for amination of olefins. The nucleophilicity of the amido ligand is key to the reactivity.	22
Scheme 1.16	C-H bond activation of ethylene oxide by Cp*Ir(PMe ₃)H ₂ . Ordinarily the epoxide functionality is considerably more reactive.	24
Scheme 1.17	General methods for metal-mediated C-H bond activation.	24
Scheme 1.18	Mechanism of electrophilic activation of methane using late transition metals in strong acidic media.	26
Scheme 1.19	C-H activation by 1,2-addition across the M=N bonds using early transition metals.	27
Scheme 1.20	C-H activation by 1,2-addition across the M=N bonds using late transition metals.	29
Scheme 1.21	Potential catalytic cycle for C-H functionalization using 1,2-addition with late transition metal imido or oxo complexes.	29
Scheme 1.22	Studies focused on the features that impact on amido reactivity, including metal identity, metal oxidation state, substituents on the non-dative ligand, as well as ancillary ligand identity.	30
Scheme 1.23	Bifunctional activation occurs between basic nucleophilic ligand and electrophilic metal center. We sought to investigate the chemistry of such complexes.	30
Scheme 1.24	The proposed mechanism of CO ₂ into the Ru-Zr bond via a bifunctional activation resulting from the combination of an electron-rich and an electron-deficient metal center.	31
Scheme 1.25	Bifunctional activation of carbon monoxide by an iridium imido complex. The activation results from the metal center acting as a Lewis acid and the nitrogen of the imido ligand acting as a Lewis base.	32

Scheme 1.26	The Scorpionate ligand. Scorpionates are a versatile class of ligand often used for their ability to sterically protect the metal center, while serving as an unreactive spectator ligand. The name is derived from the way their coordination mode resembles the attack of a scorpion.	32
Scheme 2.1	Reduction of an Os(VI) nitrido using PhMgBr to form an Os(IV) amido complex.	42
Scheme 2.2	Salt metathesis strategy generate transition metal amido or oxide complexes X = Halide, M' = Alkali, Y = NR ₂ or OR.	42
Scheme 2.3	Synthesis of a late transition metal amido complex from an alkyl complexes. Salt metathesis is carried out with the triflate.	43
Scheme 2.4	Example of an alkyl exchange reaction to form late transition metal oxide or amido complex.	43
Scheme 2.5	Synthesis of a late transition metal amido or oxide by heteroatomic exchange of free amine or alcohol with an amido or oxide ligand (X/Y = NR ₂ or OR).	44
Scheme 2.6	Oxidative addition of alcohols to form a platinum (IV) oxide complex. (R = Me, or Et).	45
Scheme 2.7	Oxidative addition of an amine to an unsaturated PCP Ir metal center to form an amido complex (R = H or Ph).	46
Scheme 2.8	Preparation of TpRu(PMe ₃) ₂ Cl and TpRu{P(OMe) ₃ } ₂ Cl by refluxing by phosphine displacement of TpRu(PPh ₃) ₂ Cl.	47
Scheme 2.9	Proposed intermediate in the synthesis of TpRu(L)(L')OTf.	52
Scheme 2.10	Preparation of cationic amine complexes by displacement of amine (NH ₂ R, R= H, Ph, or ^t Bu).	59
Scheme 2.11	Proposed route of decomposition of TpRu(CO) ₂ NHR (R = Ph or ^t Bu), CO insertion into the amido bond of TpRu(CO) ₂ NHR at elevated temperatures.	69
Scheme 2.12	Delocalization of the amido lone pair into an aryl substituent.	77
Scheme 2.13	Amido bonding models. A. Donation to metal. B. Single bond with one lone pair. C. Ligand delocalization.	77

Scheme 2.14	Hindered rotation about the N-C _{ipso} bond and multiple bonding character results in broad aryl resonances in the ¹ H NMR at room temperature. .	80
Scheme 2.15	Hindered rotation about the Ru-N _{amido} bond.	80
Scheme 2.16	Three-center, four-electron interaction of the anilido complex.	84
Scheme 2.17	Hindered rotation in Tp [*] W(CO) ₂ NHPh. The barrier to rotation is anticipated to be larger for the d ⁴ metal center compared to d ⁶ complexes because the amido ligand can more effectively π-donate.	85
Scheme 2.18	Summary of bond rotational barriers for the TpRu(L)(L')NHPh amido complexes.	86
Scheme 3.1	Nucleophilic addition to free carbon monoxide by <i>trans</i> -(DMPE) ₂ Fe(NH ₂)(H).	105
Scheme 3.2	Investigation of the reactivity of octahedral ruthenium amido complexes. We sought to determine the effect on reactivity of the amido substituent R, the oxidation state x and the ancillary ligand L and L'.	107
Scheme 3.3	The σ parameter is determined from the pK _a of meta and para substituted benzoic acids.	108
Scheme 3.4	The σ ⁺ and σ ⁻ parameters. These parameters are used for LFER studies where the arene is in resonance with the reaction site.	109
Scheme 3.5	Hammett study of the TpRu(PMe ₃) ₂ NHPh amido complex. Exchange reactions with <i>p</i> -NH ₂ C ₆ H ₄ -X (X = OMe, Me, F, CF ₃ , or NMe ₂) were studied.	114
Scheme 3.6	The Ru(II) d ⁶ anilido complexes are more basic than related W(II) d ⁴ systems. The amine complexes are not deprotonated in the presence of excess aniline.	115
Scheme 3.7	Equilibrium between the amido complexes and malononitrile.	115
Scheme 3.8	Reactions of <i>trans</i> -(dmpe) ₂ Ru(H)(NH ₂) with weak acids. The acetylide ion was found to displace ammonia while the bulky fluorenyl anion did not.	123
Scheme 3.9	Reactivity studies of the parent amido complexes TpRu(L)(L')NH ₂ with phenylacetylene or fluorine.	124

Scheme 3.10	Reactivity of amine-acetylide ion pair complexes.	127
Scheme 3.11	Examination of the amine ligand lability by reaction of the complexes [TpRu(PMe ₃) ₂ (NH ₂ R)][OTf] (R = Ph or ^t Bu) with CD ₃ CN.	127
Scheme 3.12	Reaction of the amido complexes TpRuL ₂ NHPh (L = PMe ₃ or P(OMe) ₃) with phenylacetylene at 80 °C yields the Ru respective acetylide complexes.	130
Scheme 3.13	Reaction of Cp [*] Ir(PMe ₃)(Ph)(OH) with ethylene. The triflate complex Cp [*] Ir(PMe ₃)(OTf) was found to catalyze this reaction.	131
Scheme 3.14	Proposed mechanism of the reaction of TpRu(PMe ₃) ₂ NHPh with phenylacetylene.	133
Scheme 3.15	Reaction of the triflate complex TpRu(PMe ₃) ₂ OTf with phenylacetylene yields the vinylidene complex [TpRu(PMe ₃) ₂ (C=CHPh)][OTf].	135
Scheme 3.16	Reaction of the vinylidene complex [TpRu(PMe ₃) ₂ (C=CHPh)][OTf] with aniline yields the Fischer carbene TpRu(PMe ₃) ₂ {CC(H ₂ Ph)(NHPh)}.	136
Scheme 3.17	Reaction of TpRu(PMe ₃) ₂ NH ^t Bu with 5 equiv of 1,4-CHD. This reaction forms the ruthenium-hydride complex TpRu(PMe ₃) ₂ H and benzene.	137
Scheme 3.18	Proposed pathway for the isomerization of 1,4-CHD to 1,3-CHD via deprotonation of 1,4-CHD to yield a cyclohexadienyl.	139
Scheme 3.19	Reaction of the amido complex TpRu(PMe ₃) ₂ NHPh with ethylbromide.	141
Scheme 4.1	Oxidation of Pt(PEt ₃)Cl(NHPh) results in aryl-aryl bond formation and C- H bond cleavage. This reaction yields two platinum metal centers bridged by a diimine ligand.	160
Scheme 4.2	Oxidation of the Rh μ-imido complex results in radical coupling at the 4 position of the imido ligand.	161
Scheme 4.3	Oxidation of 2,6-dimethylphenyl catalyzed by Cu(II). Radical coupling at the 4 position yields the biphenylquinones, and nucleophilic attack at the para position forms polymer.	162
Scheme 4.4	Oxidative coupling of naphthols to form chiral binaphthols.	162
Scheme 4.5	The Ullmann reaction couples aryl iodides in the presences of copper to form a biaryls and copper(II) iodide.	163

Scheme 4.6	Symmetric vs. unsymmetric coupling for a mixture of two aryl-halides. Homocoupling yields two symmetric products and hetrocoupling yields an unsymmetric product.	164
Scheme 4.7	The Stille reaction is used to form aryl-aryl bonds by reacting aryl-tin reagents with aryl-halides in the presence of a palladium catalyst.	165
Scheme 4.8	Mechanism of the Stille reaction. Initiation occurs by oxidative addition of aryl-halide or aryl-triflate to Pd(0), followed by transmetalation generate Pd(Ar)(Ar'), subsequently reductive elimination forms the biaryl bond and regenerates the catalyst.	165
Scheme 4.9	Oxidation of aniline. This reaction results in N-C bond formation through radical coupling.	167
Scheme 4.10	Oxidation of sterically hindered arylamines results in carbon-carbon bond formation through radical coupling.	168
Scheme 4.11	Oxidation of the phenyl amido complexes results in 4,4'-coupling of the phenyl group (L = CO, PMe ₃ , or P(OMe) ₃).	169
Scheme 4.12	“Syn” and “Anti” geometrical isomers due to relative orientations of {TpRuL ₂ } fragments about rigid π-system.	176
Scheme 4.13	Proposed mechanism for the formation of C-C bond in the oxidation of TpRuL ₂ NHPh (L = CO, PMe ₃ , or P(OMe) ₃ ; [Ru] = TpRuL ₂).	180
Scheme 4.14	Proposed aryl-aryl bond formation based on a nucleophilic mechanism ([Ru] = TpRuL ₂).	181
Scheme 4.15	Formation of bridging binuclear amido complexes based on nucleophilic aromatic substitution.	182
Scheme 4.16	The second step in the mechanism of formation of Ru(II) imine product based on deprotonation of the para protons followed by oxidation with residual oxidant ([Ru] = TpRuL ₂).	184
Scheme 4.17	Mechanism of imine formation based on H-atom abstraction by Ru(III) amido on an unobserved bridged intermediate.	185
Scheme 4.18	Oxidation of TpRu(PMe ₃) ₂ (OH) results in formation to TpRu(PMe ₃) ₂ (OTf) and water by hydrogen atom abstraction.	186

Scheme 4.19	Potential cycle to catalytically convert aniline(s) to benzidine(s) by metal-mediated oxidation in the presence of base ([Ru] = TpRuL ₂).	187
Scheme 4.20	Oxidation of DMA. DMB can not be directly formed because over-oxidation occurs due to the oxidation potential of DMB versus DMA. The oxidation potential DMB is about 0.4 V less than DMA.	188
Scheme 4.21	Reaction of [TpRuL ₂ (NH ₂ Ph)][OTf] with base and oxidation results in the formation of the binuclear complex (L = PMe ₃ or P(OMe) ₃ ; [Ru] = TpRuL ₂).	191
Scheme 4.22	A possible resonance structure for the Ru(II) binuclear imine complex is bridged Ru(III) amido complex. Metathesis reactions are well known for oxo and amido ligands bound to late transition metals ([Ru] = TpRuL ₂).	191
Scheme 4.23	Cleavage of a M-N imine bond by treatment with 5 equivalents of hydrochloric acid ([Pt] = Pt(PEt ₂)Cl).	192
Scheme 5.1	C-H activation pathways. 1,2-Addition reactions are driven by electrophilic metal centers and polar M-N bonds. H-atom abstraction is driven by a favorable reduction of the metal center.	201
Scheme 5.2	C-H bond activation reactions for high d-electron count amido and oxide complexes.	202
Scheme 5.3	Activation of non-polar bonds using coordinatively unsaturated late transition metals with amido ligands. We anticipated polar and basic/nucleophilic amido moiety would promote functionalization. ...	203
Scheme 5.4	Metathesis reactions of (PCP)Ru(CO)Cl with LiNH ₂ or NaNH ₂ were unsuccessful for preparation of the complex (PCP)Ru(CO)NH ₂	206
Scheme 5.5	Proposed pathways for reaction of (PCP)Ru(CO)Cl and LiNH ₂ in the presence of ammonia.	208
Scheme 5.6	The addition of ammonia to (PCP)Ru(CO)Cl results in immediate coordination of NH ₃	209
Scheme 5.7	Preparation of (PCP)Ru(CO)NH ₂ . (PCP)Ru(CO)Cl(NH ₃) was prepared insitu and deprotonated using NaN(SiMe ₃) ₂	211
Scheme 5.8	Preparation of (PCP)Ru(CO)OTf by halide abstraction from (PCP)Ru(CO)Cl using Me ₃ SiOTf.	213

Scheme 5.9	Reaction of (PCP)Ru(CO)(NH ₂) with phenylacetylene results in immediate deprotonation to form (PCP)Ru(CO)(C≡CPh).	216
Scheme 5.10	Intra vs. inter molecular deprotonation of phenylacetylene. Intermolecular forms an ion pair, while intramolecular activates phenylacetylene towards deprotonation upon coordination to Ru.	216
Scheme 5.11	Preparation of the acetylide complex (PCP)Ru(CO)(C≡CPh) was achieved by reaction of (PCP)Ru(CO)OTf and LiC≡CPh.	217
Scheme 5.12	We attempted to prepare the intramolecular deprotonation intermediate (PCP)Ru(CO)(NH ₃)(C≡CPh), by addition of NH ₃ to (PCP)Ru(CO)(C≡CPh); however, only partial conversion was observed even under harsh condition.	218
Scheme 5.13	Modes of η^2 -H ₂ bonding. H ₂ σ -donates from the H-H bonding electrons and π -accepts through the σ^* orbital.	219
Scheme 5.14	Pathways for η^2 -H ₂ bond scission. A – proceeds via oxidative addition and B – proceeds via base promoted heterolytic bond cleavage.	220
Scheme 5.15	Proposed scheme for the activation of dihydrogen by (PCP)Ru(CO)NH ₂ . Heterolytic bond cleavage occurs in the presence of the basic amido ligand.	221
Scheme 5.16	Formation of (PCP)Ru(CO)(NH ₃)(H) by initial oxidative addition of H ₂	223
Scheme 5.17	Morris et al. suggest that η^2 -H ₂ and η^1 -N ₂ bond similarly to a metal center based on a comparable orbital diagrams.	224
Scheme 5.18	The combination of TpRu(PMe ₃) ₂ NH ₂ with dihydrogen results in no reaction after several hours.	226
Scheme 5.19	(PCP)Ru(CO)NH ₂ undergoes an intramolecular C-H activation with the ^t Bu substituent to yield a cyclometalated complex and ammonia.	227
Scheme 5.20	Methane C-H bond activation by (PCP)Ru(CO)NH ₂ would form (PCP)Ru(CO)Me. This complex was synthesized by reacting (PCP)Ru(CO)Cl with methyl lithium. The complex (PCP)Ru(CO)Me undergoes cyclometalation.	230

- Scheme 5.21** (PCP)Ru(CO)Ph is the anticipated product of benzene activation by (PCP)Ru(CO)NH₂. This complex was independently prepared by reaction of (PCP)Ru(CO)OTf and phenylmagnesiumbromide. 236
- Scheme 5.22** Addition of NH₃ to solutions of (PCP)Ru(CO)Me result in formation of the amine complex (PCP)Ru(CO)(Me)(NH₃). Subsequently, this amine complex converts to the cyclometalated complex. 241
- Scheme 5.23** The Ru(II) pincer complex (PCP)RuH has been reported to form nitrogen complexes by formation of a dimer that can subsequently add two equivalents of N₂. 243
- Scheme 5.24** Conversion of the cyclometalated complex to a Ru(II) phosphido by elimination of isobutylene. 245
- Scheme 5.25** Pathways for the decomposition of the cyclometalated complex. **A** - elimination of an isobutylene fragment. **B** - Initiation of dehydrogenation chemistry. 246

List of Symbols, Abbreviations, and Terms

Cp	Cyclopentadienyl anion
Cp*	Pentamethyl Cyclopentadienyl anion
Cy	Cyclohexyl
depe	Bis(diethylphosphino)ethane
Bipy	2,2' - Dipyridyl
DMA	N,N-dimethylaniline
DMB	Dimethylbenzidine
dmpe	Bis(dimethylphosphino)ethane
DMSO	Dimethylsulfoxide
dppe	Di-phenyl-phosphinoethane
dppm	Bis-diphenylphosphino-methane
dtpe	Di-tertbutly-phosphinoethane
HSAB	Hard Soft Acid Base Theory
FFER	Linear free energy relationship
Me	Methyl
OTf	Trifluoromethansulfonate
PCP	2,6-(CH ₂ P ^t Bu ₂) ₂ C ₆ H ₃
Ph	Phenyl
PY5	2,6-bis(2-pyridyl-methoxymethane)pyridine
OTf	Trifluoromethanesulfonate
^t Bu	Tertbutly

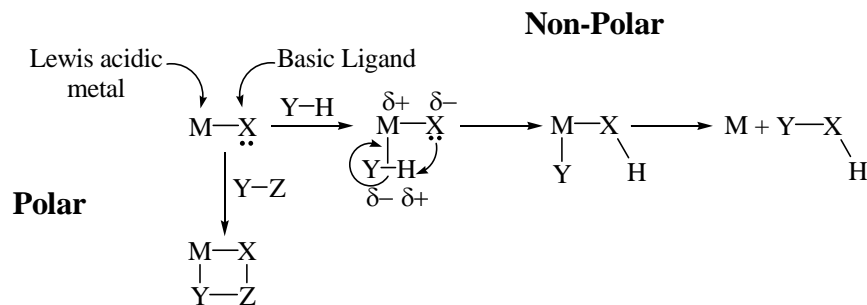
THF	Tetrahydrofuran
Tp	Hydridotrispyrazolylborate
Tp [*]	Hydridotris(3,5-dimethylpyrazolyl)borate

Chapter 1: Introduction

1.1 Introduction and Importance of Late Transition Metal Complexes with Non-Dative and π -Donating Ligands.

The past few decades have been a time of prolific growth for the field of homogeneous catalysis.¹ The advantages of milder reaction conditions and improved selectivities are the driving forces that have fueled this development. Along these lines, transition metal complexes that possess non-dative and π -donating ligands have received significant attention because of their important role in catalytic processes.^{2,3,4} Complexes with anionic heteroatomic ligands are known to be important intermediates in carbon-heteroatom bond forming reactions, and they are increasingly being identified in biological systems.^{5,6,7,8} Until recently, the number of isolable examples of such complexes with late transition metals has been few relative to those complexes containing early and middle transition elements in high oxidation states.^{9,10,11,12,13,14} Thus, understanding of the chemistry of M-X (M = late transition metal; X = amido, oxide, sulfide, imido, or oxo) linkages has lagged compared to other ligands such as alkyl, hydride, or carbonyl.^{10,11} The Gunnoe Group has been studying the synthesis and reactivity of amido and oxide complexes of Ru, Cu, and Pt. The focus and contributions of our research have been to develop synthetic routes in which various features of the complex can be systematically varied in order to explore the impact on ligand-based reactivity. The ultimate goal includes a better understanding of the nature and scope of the chemistry of amido, oxide, imido, and oxo ligands coordinated to high d-electron count metal centers. In addition, we ultimately envision exploitation of metal-based Lewis acidity in tandem with ligand-based basicity for the development of

synthetic transformations of polar as well as non-polar substrates (Scheme 1.1). Herein,



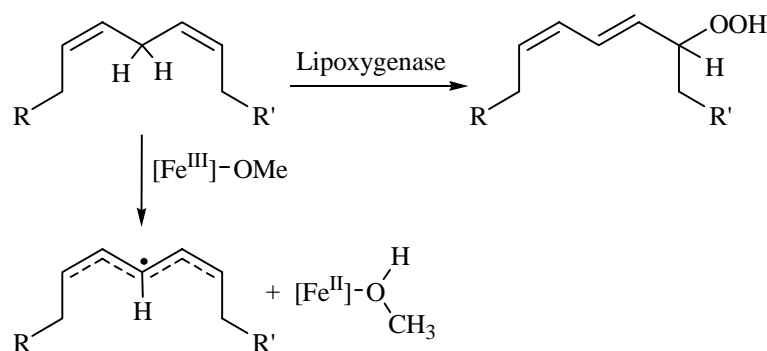
Scheme 1.1 Potential for bond activation of polar or non-polar substrates by late transition metal complexes with non-dative and π -donating heteroatomic ligands.

reactions with non-polar bonds are the focus. Specifically, this research has focused on synthesis and reactivity of amido ($M-NR_2$) complexes of ruthenium.

Late transition metal complexes with amido or nitrene ligands have been implicated in several catalytic reactions. Of particular importance is their role in C-N bond forming reactions such as aziridination, hydroamination of olefins, and arylamination.^{2,5,6,7,15} The significance of these reactions is derived from the occurrence of C-N bonds in many natural products, pharmaceuticals, as well as conducting polymers or other electronic materials.^{15,16,17} Significant advancements have been made in the past decade in late transition metal mediated amination chemistry, and palladium catalyzed arylamination is now a widely used synthetic organic tool. A search for “palladium amination” at www.pubs.acs.org yields nearly 2500 hits, and a review by Prof. Stephen Buchwald, one of the foremost authors in this field, has been cited nearly 400 times. This synthetic organic tool has, as stated by Nicolaou, “begun to leave an impact of the landscape of chemical synthesis” yielding previously inaccessible targets such as quadrigemine C, a tryptophan related alkaloid.^{18,19}

The most industrially significant catalytic process involving late transition metal complexes with non-dative heteroatomic ligands is the Wacker process, which is used to synthesize acetaldehyde from ethylene and dioxygen.^{2,11} While the definitive mechanism of this reaction has not been established, some evidence supports a mechanism whereby migratory insertion of a coordinated olefin into a metal hydroxide bond occurs; although, intermolecular nucleophilic attack by hydroxide ion on a coordinated olefin is also mechanistic possibility.^{2,11}

Late transition metal complexes with non-dative ligands have been demonstrated to abstract hydrogen atoms from weak C-H bonds.^{8,20,21} An important biological example of C-H bond activation based on a non-dative ligand is lipoxygenase, a non-heme based iron enzyme that converts 1,4-dienes to hydroperoxides. The key step in the mechanism of this enzyme is proposed to involve H-atom abstraction to generate a radical which is trapped with oxygen (Scheme 1.2).^{8,22} Stack et al. have modeled lipoxygenase and studied H-atom



Scheme 1.2 Lipoxygenase converts 1,4-dienes to hydroperoxides by H-atom abstraction. This enzyme has been modeled using Fe(III) oxide complexes.

abstraction using octahedral Fe(III) oxide complexes such as [Fe^{III}(PY5)(OMe)][OTf]₂ (PY5

= 2,6-bis(2-pyridyl-methoxymethane)pyridine).^{8,22} This complex abstracts hydrogen atoms from weak C-H bonds (e.g., 1,4-cyclohexadiene) to form $[\text{Fe}^{\text{II}}(\text{PY5})(\text{HOME})][\text{OTf}]_2$ (Scheme 1.2). The rate of H-atom abstraction was directly related to C-H bond dissociation energy, thus providing support for the proposed mechanism of lipoxygenase. Other late transition metal complexes exhibit similar chemistry and are discussed in greater detail later in this chapter.

1.2 A Brief Survey of Relevant Late Transition Metal Amido Complexes.

A number of groups have made significant contributions to the study of late transition metal complexes with non-dative π -donating ligands. Perhaps the most significant work has been developed by the group of Prof. Robert Bergman who reported the synthesis and detailed study of a host of such late transition metals complexes with these linkages. Most germane to our research are Bergman et al.'s studies of the complexes $\text{trans}-(\text{dmpe})_2(\text{H})\text{M}(\text{NH}_2)$ (M = Fe or Ru; dmpe = bis(dimethylphosphino)ethane), $(\text{PMe}_3)_4\text{Ru}(\text{H})(\text{X})$ (X= H, OAr, NHPH, NH_2 and CH_2Ph), and $\text{Cp}^*\text{Ni}(\text{PMe}_3)(\text{X})$ (Cp^* = pentamethylcyclopentadienyl; X = NAr_2 , OAr, OR, and SAr).^{23,24,25} The importance of these studies is discussed in greater detail below. In addition, this group has also reported the synthesis and chemistry of related complexes with the metals Re, Fe, Ru, Ir, and Rh.¹¹ Note, iron and rhenium are generally not considered late transition metals, but Fe(II) and Re(I) amido complexes have been demonstrated to react similarly to their Ru(II) and Ir(III) amido counterparts.^{11,23} The Bergman group has also reported chemistry with the related imido linkages including the complexes Cp^*OsNR (R = ^tBu or aryl substituent) and $\text{Cp}^*\text{IrN}^t\text{Bu}$.

Such complexes are rare examples of isolable terminal imido ligands with late transition metals, and unlike their common middle transition middle counterparts are highly reactive.^{26,27,28} These complexes have been shown to undergo novel reactivity including NR transfer reactions.²⁶

Mayer et al. have reported the synthesis and reactivity of the Os (IV) amido complex $\text{TpOs}(\text{Cl})_2\text{NHPPh}$,²⁹ and Roundhill et al. have reported the complexes $\text{CpRu}(\text{PPh}_3)_2\text{NMe}_2$, $\text{CpRu}(\text{Cy}_2\text{PCH}_2\text{CH}_2\text{PCy}_2)\text{NHR}$ ($\text{R} = \text{H, Me, and 1-octane}$).³⁰ In addition to these reports, the Hillhouse group has reported amido, imido, and phosido complexes with Ni.³¹ Other germane reports involve the reactivity of Pt and Ru amido complexes reported by Bercaw et al. including the studies of $(\text{dppe})\text{Pt}(\text{Me})\text{X}$ ($\text{dppe} = \text{Di-phenyl-phosphinoethane}$; $\text{X} = \text{NHAr}$ or OAr).³²

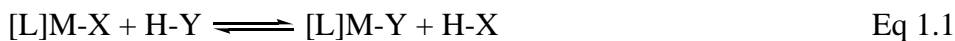
1.3 Bonding in Late Transition Metal Complexes that Possess Non-Dative and π -Donating Ligands.

The scarcity and apparent reactive nature of late transition metal complexes that possess non-dative and π -donating ligands have prompted consideration of the M-X ($\text{X} = \text{amido, oxide, imido, or oxo}$) bonding.^{9,10} Hard-soft acid-base (HSAB) theory has been applied to rationalize the chemistry of late transition metal complexes with heteroatomic non-dative π -donating ligands.^{33,34} According to this theory, a bonding mismatch between soft, late transition metals and hard donor ligands should result in weak bonds and highly reactive M-X moieties. For example, HSAB theory predicts weak bonding would raise the ground

state energies providing transformations such as β -eliminations, often observed for such complexes, with kinetically facile and thermodynamically favorable routes.^{9,10}

HSAB theory is qualitative/empirical and many exceptions exist.^{35,36} In contrast to the predictions of HSAB theory, thermodynamic studies by Bercaw et al., Bergman et al., as well as our own studies indicate that late transition metal non-dative bonds can be relatively strong.^{12,25,32,37} For example, the relative M-X bond dissociation energies of $\text{Cp}^*\text{Ru}(\text{PMe}_3)_2\text{X}$ (X = H, OH, OR, NR_2 , CCR, and SH) and $(\text{dppe})\text{PtMeX}$ (dppe = $\text{PPh}_2\text{CH}_2\text{CH}_2\text{PPh}_2$; X = OH, OR, NR_2 , and SH) have been reported to be between 30 and 70 kcal/mol for X = NAr_2 and OH respectively.

Amido and oxide ligands of late transition metals commonly undergo σ -bond metathesis reactions with amines or alcohols to form equilibria that can be used to delineate the relative M-X bond strengths from equilibrium concentrations (Equation 1.1).



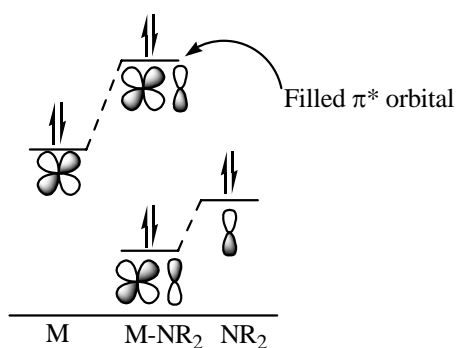
If no gases are evolved and the number of molecules remains constant, the entropy of exchange in equation 1.1 can be assumed to be negligible if entropy changes due to solvent reorganization are ignored. With these assumptions, $\Delta G \cong \Delta H = -RT \ln(K_{\text{eq}})$. Since the approximate H-X bond energies often are known, the relative M-X bond energies can be calculated.^{38,39} Bercaw et al. have reported the Ru-O bond in $\text{Cp}^*\text{Ru}(\text{PMe}_3)_2\text{OH}$ is about 9 kcal/mol stronger than a Ru-H and about 30 kcal/mol stronger than the Ru-N bond of $\text{Cp}^*\text{Ru}(\text{PMe}_3)_2\text{NPh}_2$; the Ru-N bond was approximated to be 30 kcal/mol as determined by thermolysis and relative bond dissociation determined by K_{eq} . HSAB theory would predict the softer N-based ligand should have a stronger bond with a moderately soft late transition

metal than the harder O-based ligand, and that the soft base H^- should form stronger bonds with Ru^{+2} than OH^- .^{35,36}

Similar exchange reactions conducted by the Bergman group using the complexes $(\text{PMe}_3)_4\text{Ru}(\text{H})\text{X}$ ($\text{X} = \text{H}, \text{OAr}, \text{NHPh}, \text{and CH}_2\text{Ph}$) provide thermodynamic data whereby the relative order of bond strengths was determined to be $\text{Ru-H} > \text{Ru-OPh} > \text{Ru-NHPh} > \text{Ru-CH}_2\text{Ph}$.¹⁰ Bergman et al. have also used para-substituted anilines to examine electronic effects on the M-N amido bond. Hammett studies of exchange reactions between $\text{Cp}^*\text{Ni}(\text{PEt}_3)(\text{NHPh})$ and NH_2Ar using σ_p^- parameters revealed a preference for electron-withdrawing para-substituents with $\rho = 3.4$. This group has also observed the same preference for the iridium complex $\text{Cp}^*\text{Ir}(\text{OPh})(\text{Ph})(\text{PMe}_3)$, although detailed studies were not performed.⁴⁰ Mayer et al. have reported systems exhibiting similar preferences for para-substituted rhenium phenoxide complexes $\text{Re}(\text{O})(\text{OPh})(\text{MeC}\equiv\text{CMe})_2$, electron-withdrawing groups at the para-position stabilized the Re-O bond.⁴¹ A Hammett plot using σ values revealed a ρ of +0.71.

1.3.1 An Approach to Bonding in Late Transition Metal Complexes with π -Donating Ligands Using the Theory of π -Conflict.

The studies of the bond dissociation energies and their relative trends indicate HSAB theory provides an inadequate description of late transition metal bonding with non-dative ligands. A better model would account for the relatively high bond dissociating energy of the M-X bond yet provide an explanation for the highly reactive ligands as well.



Scheme 1.3 Model of π -conflict. Heightened reactivity results from occupation of an antibonding orbital.

The π -conflict theory suggests that heightened reactivity can arise from filled-filled π -interactions while maintaining relatively strong M-X bonds (Scheme 1.3).^{9,42} While early transition metal and middle transition metal complexes in high oxidation states typically possess empty d-orbitals of correct symmetry to engage in π -bonding, late transition metal systems often have occupied d-orbitals. In this scenario, both the π bonding and π^* antibonding molecular orbitals are occupied. With the net π -bonding interaction being thermodynamically unfavorable, the bond strength is derived from M-X σ -bonding. The result is a highly reactive and nucleophilic "X" ligand. The π -conflict model is similar to the filled-filled interactions which cause weakening of the N-N bond in hydrazine or F-F.^{9,10} For example, based on the H-X bond strengths and normal periodic trends, the expected F-F bond strength should be 80-100 kcal/mol; however, the bond dissociation energy of F₂ is approximately 37 kcal/mol.^{9,43}

π -Conflict has also been employed to account for thermodynamic trends in bonding. For example, the observed thermodynamic preferences for oxide ligands over amido ligands is rationalized by the stronger π -donating ability of nitrogen-based ligands (Scheme 1.4).^{9,42}



Scheme 1.4 Amido/oxide ligand exchange reactions. π -Conflict rationalizes the thermodynamic preference for oxide ligands over amido ligands is attributable to decreased π -donation of the oxide.

Hence, less donating oxide ligands reduce the extent of π -conflict and are thermodynamically favored. In addition, ligands with aryl substituents are favored over non-aryl analogs. This trend has been attributed to the aryl ring's ability to delocalize the amido lone pair thus mitigating the $d\pi$ - $p\pi$ repulsions. Similarly, exchange reactions of para-substituted aryl amido ligands favor electron-withdrawing substituents because they allow for increased delocalization of the nitrogen lone pair into the aryl ring.

The importance of π -bonding for ligand-based reactivity is highlighted by comparing the reactivity of complexes with the stabilizing interactions between a ligand lone pair and an empty metal orbital to systems that cannot accept electrons through π -donation. For example, Ru(II) complexes of the type $\text{TpRu}(\text{L})(\text{L}')\text{NHPh}$ ($\text{L} = \text{L}' = \text{PMe}_3$ or $\text{P}(\text{OMe})_3$; and $\text{L} = \text{CO}$, $\text{L}' = \text{PPh}_3$) deprotonate weak organic acids such as malononitrile ($\text{p}K_{\text{a}} \sim 12$ in CH_2Cl_2).^{44,45} In contrast, the related Os(IV) complex $\text{TpOs}(\text{Cl})_2\text{NHPh}$ is not protonated by HCl; however, treatment with triflic acid (HOTf) results in partial conversion to the amine complex $[\text{TpOs}(\text{Cl})_2\text{NH}_2\text{Ph}][\text{OTf}]$ with the amido complex being fully protonated by treatment with two equivalents of triflic acid.²⁹ The observation that the amido complex is in equilibrium suggests the $\text{p}K_{\text{a}}$ of the amine complex is close to that of HOTf ($\text{p}K_{\text{a}} \sim -3$). Thus, there is a significant reduction, approximately 15 orders of magnitude, in $\text{p}K_{\text{a}}$ between the d^6 ruthenium aniline complex and the d^4 osmium aniline complex.

1.3.2 An *E-C* Approach to Bonding in Late Transition Metal Complexes with Non-Dative Ligands.

Bergman et al. have rationalized the reactivity of late transition metal complexes with oxide or amido ligands based on Drago's *E-C*-theory of bonding.^{10,11} This theory separates bond enthalpy into covalent and electrostatic components. The enthalpy for a bond dissociation ($AB \rightarrow A + B$) can be determined by equation 1.2 where *E*, the electrostatic component, is the measure of the capacity for electrostatic interactions, and *C*, the covalent component, is the tendency to form covalent bonds.

$$-\Delta H = E_A E_B + C_A C_B \quad \text{Eq. 1.2}$$

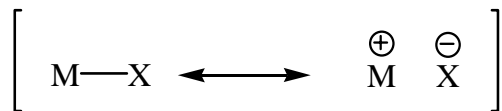
$E_A E_B$ and $C_A C_B$ represent properties of the molecule being formed, and so additional terms are needed to describe the homolytic bond strength. $T_A R_B$ where T_A is the transference of the positive component of the bond and R_B is the receptance of the negative component. The bond dissociation energy can be described by equation 1.3.^{11,35}

$$\text{BDE} = E_A E_B + C_A C_B + T_A R_B \quad \text{Eq. 1.3}$$

The product $T_A R_B$ describes the energy of the shifting charge in neutral radicals to polar bonding in the molecule. Ionic bonds have large $E_A E_B$ and $T_A R_B$ terms while covalent bonds have large $C_A C_B$ terms.

The reactivity of late transition metal complexes with non-dative π -donating ligands "M-X" is rationalized by fact that the ligand "X" is considerably more electronegative than the metal. The M-X bond is polar, and it is the highly polar bond which accounts for the

reactive nature of the ligand because significant electron density is localized on the heteroatom (Scheme 1.5).¹¹



Scheme 1.5 Resonance structures of bonding between late transition metals and non-dative and π -donating ligands. As bond polarization increases, the electrostatic component of bond increases and results in a stronger, yet reactive, M-X moiety.

This ionic model accounts for both the reactivity and the thermodynamic trends. The highly nucleophilic nature of the non-dative ligand results from significant negative charge localization on the electronegative heteroatom. The thermodynamic preference for oxide over amido ligands can be attributed to the increased polarity of oxide ligands resulting in stabilization of the complex due to the substantial $E_A E_B$ component of the bond enthalpy. Similarly, aryl substituents with electron-withdrawing groups are favored, again due to the stabilization of charge density on “x.”

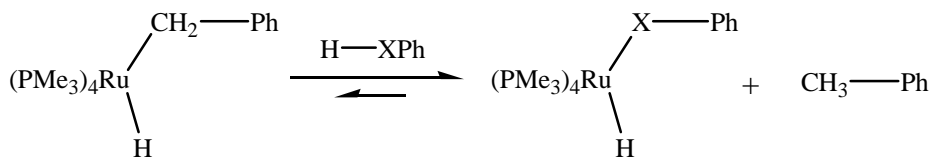
Based on the π -conflict model (Scheme 1.3), reactions resulting in no lone pair at the ligand’s α -atom should be favored. For example, exchanges which result in the formation of an alkyl or aryl ligand should be favored over oxide or amide ligands. However examples of the opposite preference are known whereby metal alkyl complexes are protonated by phenol (Equation 1.4). For example, the complex $(\text{PMe}_3)_3\text{RhMe}$ reacts with *p*-tolyl phenol to form



the respective phenoxide.⁴⁶ And $\text{Ni}(\text{Me})_2(\text{bpy})$ has been reported to undergo similar reactions with aromatic thiols and HOCH_2CF_3 .⁴⁷ The thermodynamic preferences of these reactions

have been suggested to indicate π -conflict does not account for such reactivity; however, definitive conclusions could be complicated by irreversible loss of methane resulting in conversion the phenoxide products.

Hartwig et al. recently reported that (PCP)Ir(H)Ph undergoes reversible exchange with aniline to form (PCP)Ir(H)(NHPH) and benzene.⁴⁸ Thermodynamic studies of this reaction revealed the K_{eq} of exchange to be 105 (approximately a ten fold preference for the π -donating amido ligand over a phenyl ligand). The authors attributed the thermodynamic preference for the amido ligand to a strong ionic Ir-N bond. In fact, this preference results not only from differences in the Ir-Ph versus Ir-NHPH bond dissociation energy, but from the difference in bond dissociation energy of aniline N-H versus benzene C-H (88 vs 110 kcal/mol respectively). Assuming no entropy effects, the energy difference (based on K_{eq}) is approximately -11 kcal/mol; thus indicating the Ir-N_{amido} is about ten kcal/mol weaker than the Ir-C_{Ph} bond. A better comparison is provided by exchange reactions of (PMe₃)₄Ru(H)(CH₂Ph) with aniline or p-methylphenol (Scheme 1.6).⁴⁹ The BDE of the

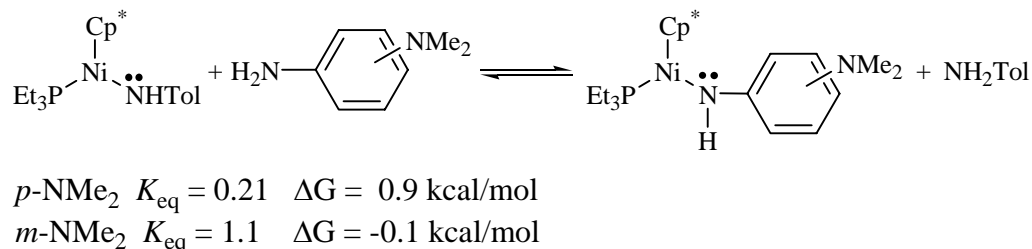


Scheme 1.6 Exchange reactions of (PMe₃)₄Ru(H)(CH₂Ph) with aniline and p-methylphenol favor π -donating oxide or amido ligands. This result suggests the importance of the ionic nature in M-X bonding.

benzylic C-H bonds of toluene is 88.0 ± 1 kcal/mol and the BDE of aniline N-H and p-methylphenol O-H is 86.5 ± 2 and 88.0 ± 2 respectively.^{43,49,50} The equilibria favor anilido

and *p*-methylphenoxide complexes and thus the Ru-X (X = N or O) bond strength is likely stronger than Ru-C of these complexes.

The extent to which π -conflict can impact thermodynamic preferences could be evaluated using exchange reactions with para/meta π -withdrawing/donating substituents on the anilido ligand. A meta substituent will have no π -effects, while the para substituent should impact K_{eq} relative the same substituent in the meta position. Based on π -conflict, π -donating substituents in the para position should be disfavored over the same substituents in the meta position. Bergman et al. have demonstrated that for the system $\text{Cp}^*\text{Ni}(\text{PEt}_3)\text{NHTol}$ the position (meta versus para) of the π -donating substituent does not significantly impact K_{eq} (Scheme 1.7).^{10,25}



Scheme 1.7 Meta versus para donating substituent does not significantly impact the respective K_{eq} of exchange reactions for the complex $\text{Cp}^*\text{Ni}(\text{PEt}_3)\text{NHTol}$. This result suggests π -conflict has a minimal effect on the bonding in such M-N linkages.

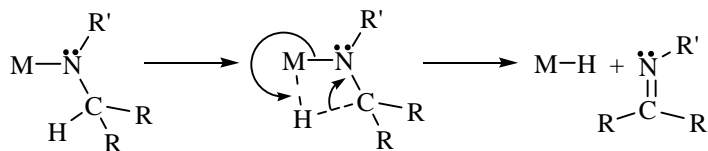
These observations are consistent with the *E-C* bonding model, yet they are incongruent with π -conflict (Scheme 1.7). Indeed, the extent to which π -interactions destructively interact with the metal d-orbital is challenging to quantify; however, rationalizing thermodynamic preferences for aryl substituents using an *E-C* approach is not intuitive because these substituents should decrease the overall ionic character of the bond and therefore should be disfavored. These π -only and σ -only theories are not exclusive of one another. Even

thought π -conflict may contribute to the reactivity, its overall effect on the bonding in these complexes is not definitive. Ultimately, more thermodynamic data regarding the bonding of these linkages are needed to discern the extent to which these models represent the bonding of these non-dative ligands.

1.4 General Reactivity of Late Transition Metal Complexes with Non-Dative π -Donating Ligands.

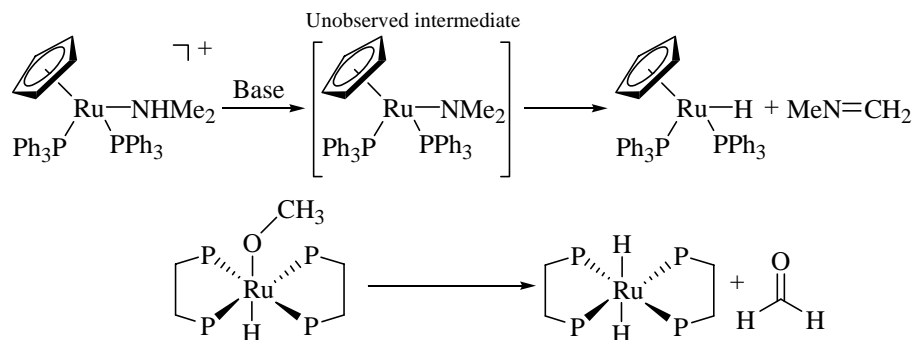
The understanding of the reactivity of late transition metal-oxide or metal-amido moieties is less developed than metal-carbon or metal-hydrogen ligands of late transition metals.^{10,11} Nevertheless, a diversity of reactivity patterns has been demonstrated for such complexes.¹¹ Generally, these ligands possess nucleophilic and basic character and thus can deprotonate weak acids and undergo reactions with electrophiles.^{2,11,13,51,52} In some cases, their reactivity in this regard is quite remarkable as they are reported to deprotonate very weak acids and attack weak electrophiles. In addition to their basic/nucleophilic reactivity, these complexes are known to undergo β -hydride eliminations, insertion reactions, reductive elimination, oxidative/reductive coupling, and σ -metathesis reactions.^{2,11}

Late transition metal oxide and amido complexes lacking hydrogen atom(s) on the β -carbon of the oxide/amido ligand are generally more stable than those with β -hydrogen atoms. The increased thermal stability results from the fact that β -hydrogens are susceptible to elimination.⁵³ In most cases, these reactions transfer a hydrogen atom from the ligand to the metal center via a four-member coplanar transition state (Scheme 1.8).³⁵



Scheme 1.8 Common mechanism of β -hydrogen elimination.

The reactive nature of amido and oxide ligands of late transition metal can result in β -elimination reactions that are not directly observed. Instead these transformations are inferred from reactions of alcohols and amines that form transition metal hydride products. For example, Roundhill et al. have reported that attempts to isolate the Ru(II) amido complex $\text{CpRu}(\text{PPh}_3)_2\text{NMe}_2$ were unsuccessful; specifically, deprotonation of corresponding amine complex $[\text{CpRu}(\text{PPh}_3)_2\text{NHMe}_2]^+$ results in formation of $\text{CpRu}(\text{PPh}_3)_2\text{H}$. Additionally, Bergman et al. have reported similar β -hydride elimination reactions with *trans*- $(\text{dmpe})_2\text{RuH}(\text{OMe})$ to form *trans*- $(\text{dmpe})_2\text{Ru}(\text{H})_2$ (*dmpe* = dimethylphosphinoethane) and formaldehyde (Scheme 1.9).

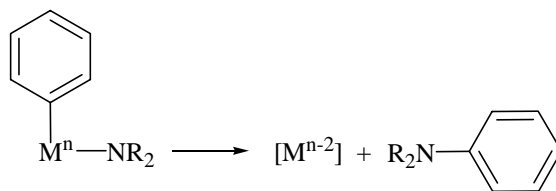


Scheme 1.9 β -hydride elimination reactions for late transition metal amido and oxide complexes.

Bennett and co-workers have observed β -hydride elimination directly from the complexes *trans*-Pt(PPh₃)₂(Ph)(OMe) and the analogue *cis*-(dppe)Pt(Ph)(OMe) (dppe = diphenylphosphinoethane).^{54,55} Thermolysis of these complexes results in β -hydride elimination to yield formaldehyde and Pt(PPh₃)₂(Ph)(H) or *cis*-(dppe)Pt(Ph)(H) respectively.

Oxidative addition reactions insert a metal center into a substrate bond. These reactions increase the metal's coordination number as well as formal oxidation state.^{1,35} Oxidative addition reactions generally are favored for complexes that are electron rich and can easily accommodate an increase in coordination number. The oxidative addition of N-H or O-H bonds, while infrequent, has been reported to yield late transition metal amido and oxide complexes.^{2,56} For example, bisphosphine platinum and palladium complexes are known to oxidatively add H-X bonds of phenol or pyrrole to form arylamido or aryloxy hydride complexes.^{57,58} Puddephatt et al. have reported similar oxidative addition of methanol and ethanol using (bipy)PtMe₂ to yield (bipy)Pt(H)(OR)Me₂ (R = Me or CH₂CH₃).^{59,60} The reversible oxidative addition of water by Pt(P(*i*-Pr)₃)₂ to form the corresponding hydroxo hydride has been reported.⁶¹ In addition, oxidative addition of aniline and ammonia to an unsaturated Ir(I) complex was reported by Hartwig, Goldman et al.⁴⁸ These reactions are potentially useful for olefin hydroamination where coordination and insertion of an olefin into the M-H or M-N bond followed by reductive elimination would catalytically produce alkylamines.

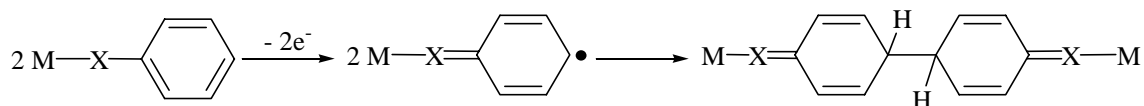
Reductive elimination is the microscopic reverse of oxidative addition and is a central step in many catalytic cycles including arylamination chemistry (Scheme 1.10). Compared to C-C or C-H reductive elimination, reports of C-N or C-O reductive elimination are few;



Scheme 1.10 Reductive elimination from a late transition metal amido complex to form an aryl amine.

however, the mechanism of this reaction has been studied in detail, and the nucleophilicity of amido moiety is proposed to be key to reductive elimination.^{16,17} Increasing the nucleophilicity of the amido nitrogen typically increases the rate of reductive elimination.

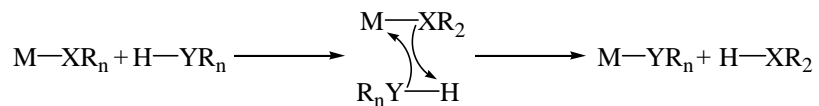
Aryl-aryl bond forming reactions are important in synthetic organic chemistry because these bonds are found in natural products, pharmaceutically active agents, agrochemicals, and dyes.⁶² Oxidative aryl couplings reactions of arylamido^{63,64,65} and aryloxo^{66,67,68} ligands have been reported (Scheme 1.11). For example, the oxidative



Scheme 1.11 Aryl-aryl coupling in late transition metal complexes with nondative and π -donating ligands that possess an aryl substituent.

coupling at ortho and para positions for $\text{Pt}(\text{PEt}_3)_2\text{Cl}(\text{NH}p\text{-tolyl})$ has been reported. In addition, the oxidative coupling of the related complex $\text{Pt}(\text{PEt}_3)_2\text{Cl}(4\text{-F-C}_6\text{H}_5)$ was reported. Interestingly, the regioselectivity for carbon-carbon (2,4 vs 2,2') bond formation is temperature dependent.⁶⁵ The mechanism of these coupling reactions are proposed to proceed through radical intermediates akin to the oxidative coupling of triaryl amines.⁶⁹

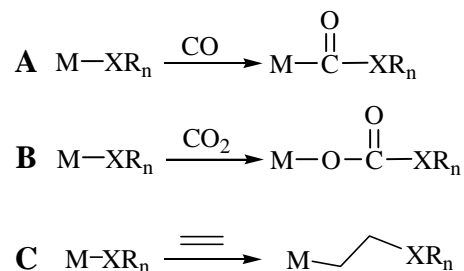
Late transition metal amido ligands are known to undergo σ -bond metathesis wherein the σ -bond of a ligand is replaced with the σ -bond of an incoming ligand (Scheme 1.12).



Scheme 1.12 σ -bond metathesis reaction scheme.

This reaction is common to d^0 early metal complexes where oxidative addition is prohibited; however net metathesis is also common for late transition metal amido and oxide complexes.⁷⁰ Typically the exchange occurs between an amido ($X = \text{N}$) and an amine or alcohol ($Y = \text{N}$ or O) or an alkyl ligand, such as methyl, exchanges with an amine ($X = \text{C}$ and $Y = \text{N}$) to form the corresponding amido complex. Examples of these reactions include the exchanges of $\text{Cp}^*\text{Ni}(\text{PEt}_3)\text{NR}_2$, $(\text{PMe}_3)_4\text{RuNR}_2$, $\text{Cp}^*\text{Ru}(\text{PMe}_3)_2\text{NR}_2$, and $(\text{dppe})\text{PtMeNR}_2$ with free amine/alcohol (above). It should be noted that these reactions are net metathesis and that a definitive reaction mechanism has not been proven for late transition metal amido or oxide systems.

Carbon monoxide, olefins, carbon dioxide, and heterocumenes are all known to undergo insertion chemistry with late transition metal amido and oxide ligands (Scheme 1.13). These reactions result in net placement of these moieties into the $\text{M}-\text{X}$ bond ($X =$ oxide or amido) bond, and several mechanisms of insertion have been proposed.^{2,11} The most common transformation of this type is observed for CO. For example, CO insertion reactions have been reported into the $\text{M}-\text{N}_{\text{amido}}$ bond of $\text{CpRu}(\text{PCy}_2\text{CH}_2\text{CH}_2\text{PCy}_2)\text{NH}_2$, $[\text{Cp}^*\text{Ni}(\mu\text{-NH}(p\text{-tol}))_2]$, and $(\text{dppe})\text{PtMe}\{\text{N}(\text{H})(\text{CH}_2\text{Ph})\}$ (Scheme 1.13 A).^{30,71,72} Olefin



Scheme 1.13 Insertion reactions of late transition metal amido and oxide complexes. **A** - CO insertion. **B** - Cumene and heterocumene insertion. **C** - Olefin insertion.

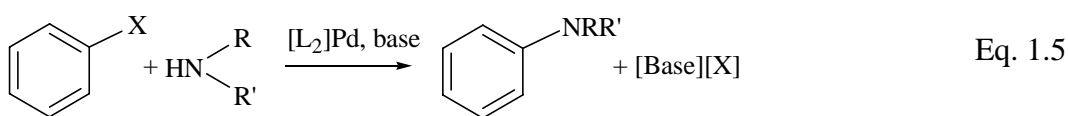
insertions of CF_2CF_2 into platinum oxide bonds have also been reported for $(\text{dppe})\text{PtMe}(\text{OR})$ ($\text{R} = \text{H}$ and Me) (Scheme 1.13C).^{73,74} For late transition metal amido and oxide complexes, generally these reactions are believed to proceed via a nucleophilic insertion mechanism. For example, Berman et al. have reported nucleophilic insertion of reactivity of $\text{Cp}^*\text{Ir}(\text{PPh}_3)(\text{H})(\text{NHPH})$ with the heterocumenes carbon disulfide and methyl isocyanate (Scheme 1.13B).

d^6 -Electron count amido and oxide complexes of iron(II) and ruthenium(II) have been demonstrated to undergo Bronsted acid/base transformations with C-H bonds. For example, the complexes *trans*- $(\text{dppe})_2\text{M}(\text{X})(\text{NH}_2)$ ($\text{M} = \text{Ru}$ or Fe) have been demonstrated to deprotonate C-H bonds of terminal acetylenes. Iron and ruthenium oxide complexes in oxidation states greater than two have also been demonstrated to initiate C-H bond cleavage reactions through net hydrogen atom abstraction reactions. Stack et al. have modeled the enzyme lipoxygenase using Fe(III) oxide complexes (see above). In addition, the Ru(IV) complex $[(\text{bpy})_2(\text{py})\text{RuO}]^{2+}$ has been demonstrated to cleave benzylic and allylic C-H bonds

through H-atom transfer reactions. These reactions result in single electron reductions of the metal center, and this reduction provides a driving force for the reaction.^{20,75}

The reactivity of late transition metal amido complexes has led to the utilization in a number of important chemical processes. One significant process is C-N bond formation reactions. The formation of carbon heteroatom bonds is fundamental in synthetic chemistry. Amines are a major class of compounds of interest to this area of chemistry. Their synthesis by transition metal mediated routes has been and intensely studied both in scope and mechanistic details.

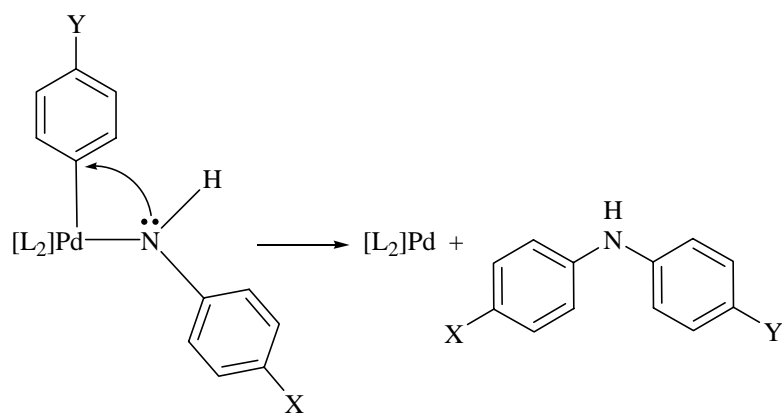
Arylamines can be challenging synthetic targets despite their simple nature. Many coupling methods are incompatible with functional groups, and reductive amination to form anilines is often sluggish. Approximately ten years ago, the Buchwald and Hartwig groups concurrently developed palladium catalyzed methods to couple aryl halides with aryl amines (Equation 1.5).¹⁵⁻¹⁸



This work was inspired by the earlier work of Kougi et al. where aryl bromides were coupled to tin amides using $[\text{PdCl}_2\{\text{P}(o\text{-C}_6\text{H}_4\text{Me})_3\}_2]$ as a catalyst.^{15,16} Buchwald and Hartwig's work eliminated the need for stoichiometric tin reagents, and since its introduction less than a decade ago, this methodology has enjoyed widespread use. Methods for cyclic-amination and heterocyclic amination are now known.^{15,16,18}

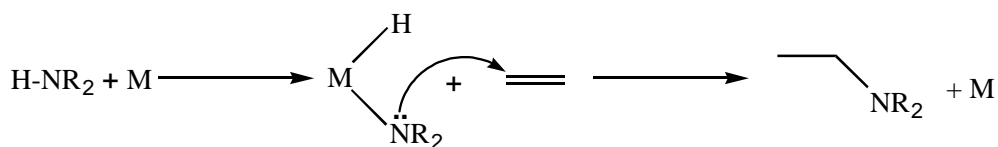
Hartwig and co-workers have studied the mechanism of aryl amination in detail. Kinetic studies have shown that C-N reductive eliminations are favored by increasing the

nucleophilicity of the amido as well as increasing the electrophilicity of the aryl group. Variation of the amido group's substituents reveal the rate of elimination favors alkylamido > arylamido > diarylamido. Hammett studies using para substituted anilines demonstrated the rate of elimination is increased for donating substituents, presumably due to a more nucleophilic intermediate, and a rate increase was also found for more electron withdrawing substituent arylhalides ($\rho_R = 3.9$, $\rho_I = 1.9$) (Scheme 1.14).



Scheme 1.14 Studies of palladium catalyzed aryl amination indicate the rate of reaction is increased by more donating amido substituents (X) and more electron-withdrawing aryl substituents (Y).

In addition to arylamination, hydroamination of olefins, where amines are added to alkenes or alkynes, is an important class of C-N bond forming reactions.^{15,16} One suggested pathway for this reaction involves the direct reaction of amines with unsaturated late metals to form amido hydride complexes. Subsequent binding of olefin or alkyne would then be followed by insertion into the amido bond (Scheme 1.15). Amine oxidative addition reactions are somewhat rare compared to C-H and H-H additions, and catalysts to prepare alkylamines as shown in Scheme 1.15 are not yet industrially relevant for large-scale



Scheme 1.15 Proposed scheme for amination of olefins. The nucleophilicity of the amido ligand is key to the reactivity.

synthesis; although, Pd and Rh catalysts for hydroamination have been developed by Hartwig et al.⁷⁶ As in the case of aryl amination, amido nucleophilicity is thought to be key to the C-N bond forming step.

Another focus of our research has been to examine aryl-aryl bond formation reactions that occur with late transition metal aryl amido complexes. Metal catalyzed methods for aryl-aryl couplings include the Ullmann reaction, Suzuki coupling, and Stille coupling and are important synthetic organic tools. All of these methods involve the use of aryl halides.^{70,77} Also, both Suzuki and Stille coupling require stoichiometric amounts of aryl organometallic reagents while the Ullmann reaction can require stoichiometric amounts of copper. The development of a catalytic system that couples aryl group of amines or alcohols to form bi-aryl species would simplify current multi-step synthesis as well as eliminate the need for aryl halide and stoichiometric quantities of aryl organometallic reagents.

1.5 Carbon-Hydrogen Bond Activation and Relevance to Late Transition Metal Amido Complexes.

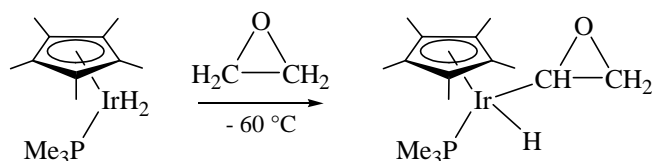
Alkanes and other hydrocarbons are an abundant and relatively inexpensive feedstock; unfortunately, their selective and controlled conversion to more useful chemicals remains a significant challenge.⁷⁸ The relatively non-coordinating nature of hydrocarbons

partly accounts for the challenge in activating them. Another difficulty with hydrocarbon functionalization is the tendency towards over oxidization. For example, the bond dissociation energy of methane is approximately 104 kcal/mol while the bond dissociation energy of methanol is approximately 93 kcal/mol. In addition, the polar nature of the alcohol renders it more coordinating. The result of these differences is a molecule with weaker C-H bonds and one that is much more coordinating, as such many methods that oxidize alkanes result in over oxidation to CO₂.

Free radicals are known to abstract hydrogen atoms from hydrocarbons, but these and other high-energy pathways are often selective towards undesirable functionalization (Equation 1.7).^{79,80}



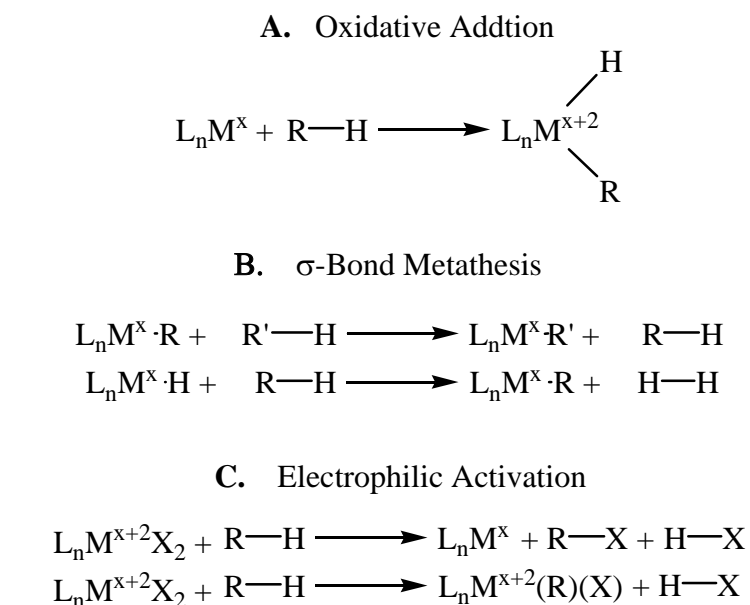
For example, these processes are selective for 3° > 2° > 1°, while industrially 1° functionality is often desired. Therefore, the development of methodologies for the controlled functionalization of hydrocarbons is of significant interest. The ability to directly convert hydrocarbons into functionalized products, for example methane to methanol or formaldehyde, would significantly reduce the processing and energy consumed by current methods to process hydrocarbons into useful end products.^{81,82} Homogeneous catalysis using transition metal-mediated methods to achieve C-H bond functionalization offer promise due to the possibility of controlling selectivity (1° > 2° > 3°).^{1,76} For example, Bergman et al. have reported activation of a C-H bond of ethyleneoxide (Scheme 1.16).⁸³



Scheme 1.16 C-H bond activation of ethylene oxide by Cp*Ir(PMe₃)₂. Ordinarily the epoxide functionality is considerably more reactive.

Under standard reaction conditions, the C-O epoxide linkage is substantially more reactive than a C-H bond.

In the arena of hydrocarbon functionalization, one noteworthy challenge is the activation methane.^{79,82,84} Methane is a significant portion of natural gas; unfortunately, much of its reserves are located in regions where transport difficulties render sequestration economically unfeasible.^{78,82} Developing methods for the direct conversion to methanol or other liquid fuels would increase the utilization of methane, and along these lines, many transition metal mediated routes for C-H activation have been developed (Scheme 1.17). For

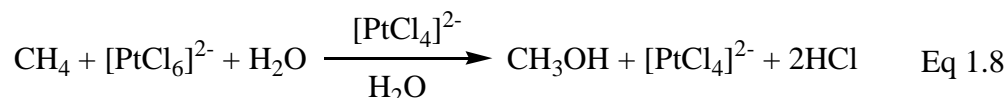


Scheme 1.17 General methods for metal-mediated C-H bond activation.

example, electron-rich, coordinatively unsaturated, late transition metal complexes, such as Pt, Pd, Ir, Rh, Ru, Fe, Re, or Os are known to oxidatively add C-H bonds across a metal (Oxidative Addition, Scheme 1.17a).^{1,70,77,78,79} Oxidative addition requires C-H coordination and thus a vacant coordination site on the metal; however such complexes are often unstable and involve *in situ* generation. A classic example is Cp*Ir(PMe₃)H₂ where photolysis results in loss of dihydrogen to form Cp*Ir(PMe₃).⁷⁹ This unsaturated intermediate has been demonstrated to undergo oxidative addition reactions with a host of C-H bonds.

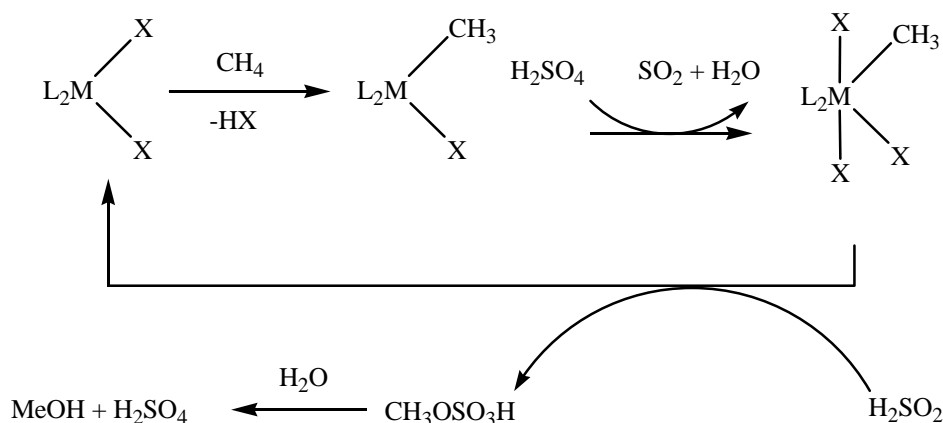
Complexes in higher oxidation states can initiate C-H activation through σ -bond metathesis (Scheme 1.17b). In this reaction, one alkyl or aryl ligand exchanges with an alkane or arene with concerted C-H bond-breaking and bond-forming. Definitive examples of C-H activation through σ -bond metathesis are only known for d⁰ complexes for which the metal cannot access higher oxidation states.^{1,70,78} Additional σ -bond metathesis reactions of transition metal hydride complexes have been reported to produce dihydrogen (Scheme 1.17b).⁷⁸

Despite several schemes to break C-H bonds, successful homogeneous catalytic routes for hydrocarbon functionalization remain scant. One of the first systems developed by Shilov et al. specifically for methane oxidation is the most successful. Shilov's chemistry incorporates chloroplatinum salts to achieve selective (1° > 2° > 3°) oxidation of alkanes (Equation 1.8).^{81,82,84}



This system is remarkable because of robust nature of the catalyst. It is water soluble and stable in the presence of oxidants such as dioxygen. The significant drawback of Shilov's system is the requirement of Pt(IV) as a stoichiometric oxidant, thus rendering it impractical for commercial use. Due to this drawback, considerable effort has been put forth to delineate the mechanism of this reaction which has proven difficult to study. C-H bond cleavage is the most important step because it controls both the rate and the selectivity. Goldberg, Templeton and others have studied Tp based Pt(II) systems to demonstrate that C-H activation most likely involves oxidative addition by an electrophilic Pt^{II} species.^{84,85,86}

Other methods of electrophilic activation using late transition metals (Pt, Pd, or Hg) in strong sulfuric acid media represent a significant advancement in this field (Scheme 1.18).



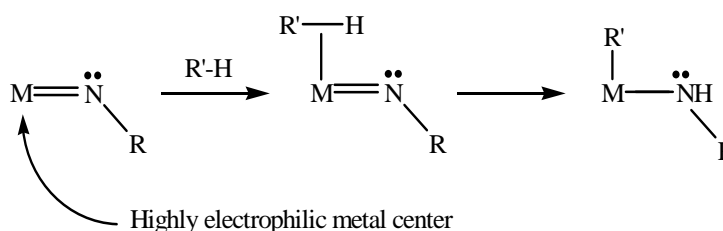
Scheme 1.18 Mechanism of electrophilic activation of methane using late transition metals in strong acidic media.

For example, Hg^{II} catalyzes the oxidation of methane to generate methylbisulfate. Methanol can be formed by hydrolysis of methylbisulfate with water; sulfuric acid is also a byproduct

of the latter reaction.⁸⁷ More recently the group of Prof. Roy Periana has published the efficient conversion of methane to using similar electrophilic methods and dichloro(η -2-{2,2'-bipyrimidyl})platinum(II) as a catalyst. At temperatures as low as 100 °C, yields of 72% have been achieved.⁸⁸

1.5.1 C-H Activation by Early Transition Metal Imido Complexes.

Electropositive early transition metal imido complexes with d^0 electron counts have been employed for the activation C-H bonds.^{89,90,91} For example, $\text{Cp}_2\text{Zr}=\text{N}^t\text{Bu}$ initiates the 1,2-addition of a benzene C-H bond across the $\text{Zr}=\text{N}$ bond resulting in formation of a zirconium amido/phenyl complex $\text{Cp}_2\text{Zr}(\text{Ph})(\text{NH}^t\text{Bu})$. Additionally, both $(t\text{-Bu}_3\text{SiNH})_2\text{Zr}=\text{NSi-}t\text{-Bu}_3$ and the d^0 tungsten analog $(^t\text{Bu}_3\text{SiN}=\text{)}_3\text{W}$ undergo similar 1,2-additions of benzene as well as alkanes (Scheme 1.19).⁹² Detailed examination and



Scheme 1.19 C-H activation by 1,2-addition across the $\text{M}=\text{N}$ bonds using early transition metals.

computational studies of related systems have revealed that the electrophilic nature of the metal centers facilitates cleavage of C-H bonds by increasing the affinity for hydrocarbon coordination and activation.^{90,91} In addition, increasing bond polarization of the metal-imido bond was also found to facilitate C-H activation.^{93,94} Theoretical studies also indicate that

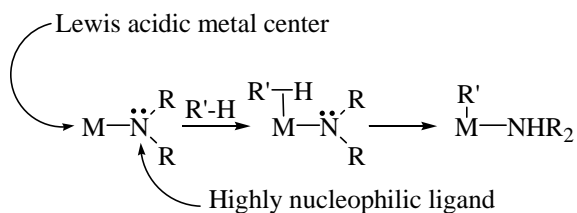
bulkier amido substituents increase reactivity by increasing metal-ligand polarization due to a decreased M-N bond order.

Although schemes utilizing 1,2-addition with early metals methods have been studied, the overall utility of such schemes for hydrocarbon functionalization is limited by the lack of metal redox flexibility. The addition of a C-H bond across the M=NR bond results in very stable amido complexes due to ligand to metal π -donation to an empty orbital of an electrophilic metal center.^{32,78} The formation of new organic molecules requires reductive elimination from the amido product, and this transformation is often disfavored for early transition metal complexes. The lack of redox flexibility and the robust nature of the metal-amido bond provide a thermodynamic sink rendering further reactivity improbable.⁹⁵

1.5.2 Activation of Non-Polar Bonds by Late Transition Metal Complexes that Possess Heteroatomic π -Donating Ligands.

We are interested in exploiting the reactivity of late transition metal amido, oxide, and imido complexes for the activation of non-polar bonds. One potential advantage of late transition metal systems over early transition metal imido complexes (above) is derived from their redox flexibility. For example, isolable complexes of ruthenium are known for all eight oxidation states, and ruthenium (II) and ruthenium (IV) complexes are common.⁹⁶ Thus, catalytic cycles in which the metal center mediates two electron processes are more likely to be accessible compared to related early transition metal systems. Furthermore, C-N and C-O reductive elimination reactions are well documented in catalytic arylamine and aryloxy ether systems that incorporate late transition metals.^{15,16,17} While the electrophilicity of late transition metal centers is anticipated to be reduced compared to early transition metal

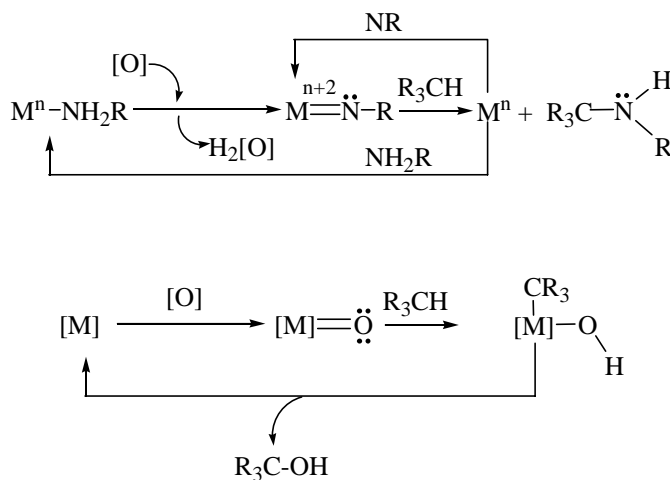
centers, the loss of electrophilicity may be compensated by the increased nucleophilicity of the non-dative ligands (Scheme 1.20). To our knowledge, C-H activation *across* M-N or M-



Scheme 1.20 C-H activation by 1,2-addition across the M-N bonds using late transition metals.

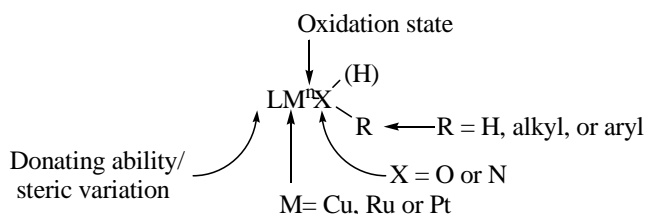
O has not been definitively demonstrated for the late transition metal system.

From an applied standpoint, we are interested in the 1,2-additions of C-H bonds across M-X (X = amido, oxide, imido, or oxo) bonds as a step to make functionalized organic molecules. Ultimately, catalytic cycles that involve amine oxidation or the generation of metal oxo bonds and C-H functionalization are envisioned (Scheme 1.21). From a



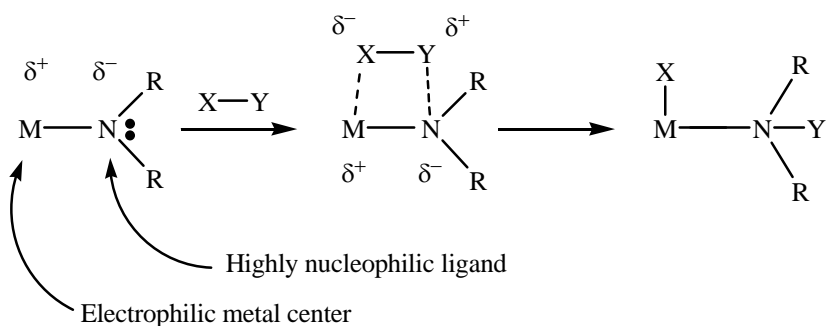
Scheme 1.21 Potential catalytic cycle for C-H functionalization using 1,2-addition with late transition metal imido or oxo complexes.

fundamental perspective, we have been studying the range of reactivity available with such complexes and the impact of various factors including metal identity, metal oxidation state, substituents on the non-dative ligand, as well as ancillary ligand identity (Scheme 1.22).



Scheme 1.22 Studies focused on the features that impact on amido reactivity, including metal identity, metal oxidation state, substituents on the non-dative ligand, as well as ancillary ligand identity.

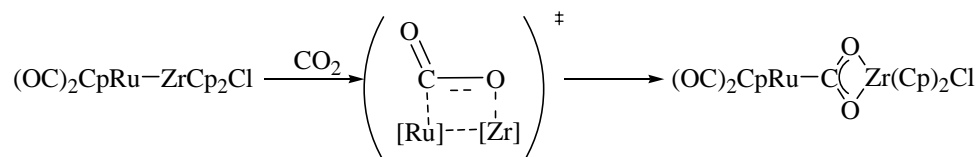
Specifically we are interested in investigating the potential chemistry that occurs with the “bifunctional activating” ability of complexes with non-dative ligands that result from an electrophilic metal center and an electron-rich nucleophilic ligand (Scheme 1.23).



Scheme 1.23 Bifunctional activation occurs between basic nucleophilic ligand and electrophilic metal center.

Such features of these complexes could facilitate unique and/or important chemistry.

Organometallic and inorganic examples of bifunctional activation have begun to emerge in the past decade.⁹⁷ For example, enolization of ketones using Rh(III) porphyrins with basic substituents has also been reported wherein the metal acts as a Lewis acid and the porphyrin substituent acts as a base.⁹⁸ Bimetallic examples of bifunctional activation has also been observed using combinations of early-late transition metal complexes. For example, CO₂ undergoes net insertion into the Ru-Zr bond of CpRu(CO)₂-Zr(Cl)Cp₂. The reactivity was attributed to the “push-pull” of electron density between ruthenium and zirconium (Scheme 1.24).⁹⁹ The proposed mechanism of this reaction is insertion of CO₂

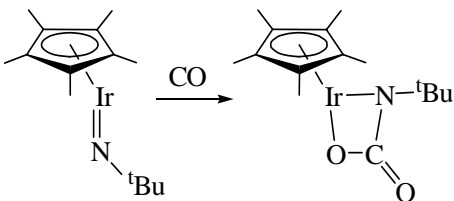


Scheme 1.24 The proposed mechanism of CO₂ into the Ru-Zr bond via a bifunctional activation resulting from the combination of an electron-rich and an electron-deficient metal center.

into the Ru-Zr bond via a bifunctional route where in stabilization occurs from coupling an electron-rich metal center with an oxophilic zirconium metal center. This reaction could also occur by heterolytic cleavage of the Ru-Zr bond, followed by net insertion; however, evidence for the mechanism in Scheme 1.24 is supported by ¹³C labeling studies whereby the product was reacted with ¹³CO₂. No labeled CO₂ was found to incorporate into the product, while the salt [CpRu(CO)₂(CO₂)]⁻ (presumably an intermediate product of the hetero-bimetallic scheme) undergoes ¹³CO₂ incorporation.

Most germane to the chemistry we propose is the cooperative reactivity which has been observed in late transition metal complexes with non-dative ligands. For example Bergman et al. have reported the terminal imido complex Cp^{*}IrN^tBu which undergoes

cycloazation with CO₂ (Scheme 1.25).²⁶ The activation of carbon dioxide was attributed to



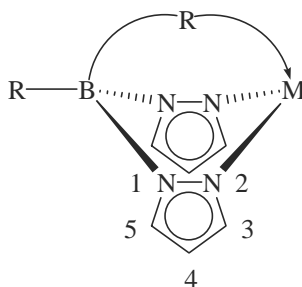
Scheme 1.25 Bifunctional activation of carbon dioxide by an iridium imido complex. The activation results from the metal center acting as a Lewis acid and the nitrogen of the imido ligand acting as a Lewis base.

the metal center acting as a Lewis acid and the nitrogen of the imido acting as a Lewis base.

This group has also published parallel chemistry with the related carbene complex Cp*Ir(PMe₃)(CH₂) and CO₂.¹⁰⁰

1.6 Rationale for the Choice of Ligands

Hydridotris(pyrazolyl)borate: The ligand Tp (Tp = hydridotris(pyrazolyl)borate) is a member of the scorpionate class of ligands, so named for the way the ligand binding resembles the attack of a scorpion (Scheme 1.26).^{101,102} Since their development in the late



Scheme 1.26 The Scorpionate ligand. Scorpionates are a versatile class of ligand often used for their ability to sterically protect the metal center, while serving as an unreactive spectator ligand. The name is derived from the way their coordination mode resembles the attack of a scorpion.

1960's, scorpionate ligands have found wide application in coordination chemistry, and scorpionate complexes have been reported with main group, transition metals as well as lanthanides and actinides. The attractiveness of these ligands results from their reliability as a stable spectator ligand that generally does not interfere with reactivity at the metal center. Also, these ligands provide an effective steric shield for the metal center that can impart stability, and the 3-position of the pyrazole ring can be altered to increase this steric shielding. Scorpionate ligands are often compared to the cyclopentadienyl coordination counterpart since both are mono-anionic, facially binding, 6-electron donor ligands.^{103,104,105} However, the Tp is more sterically bulky than Cp. The cone angle of Tp is 180° compared to 100° for Cp, and Tp tends to enforce an octahedral geometry, in contrast to Cp. Important differences in the donating ability of these ligands have been recently highlighted.¹⁰³ For example, Tp acts as σ -donor, while Cp is capable of π -donation. The difference in relative donating ability depends on the metal and oxidation state; however, for Ru(II) Tp would be expected to be less donating than Cp.

Our studies utilize the TpRu(L)(L') moiety which has attracted considerable attention because it offers the ability to systematically vary ligand sterics and donating ability.¹⁰⁶ Also, monomeric late transition metal amido and nitrene complexes can be challenging to synthesize due to their tendency to form binuclear complexes. The steric profile of Tp ligands may hinder the formation of binuclear systems.² NMR techniques play an integral role in our investigations. The Tp ligand, unlike cyclopentadienyl counterparts, provide valuable information on symmetry; C_3 , C_s , or C_1 (Figure 1.1 A-C). C_3 symmetric metal centers reveal a three 1:1:1 resonances for the Tp 3,4, and 5 positions, while C_1 symmetric

metal centers reveal 2:1 resonances for the Tp 3,4, and 5 positions, and nine 1:1:1 resonances are observed for asymmetric metal centers Tp 3,4, and 5 positions.

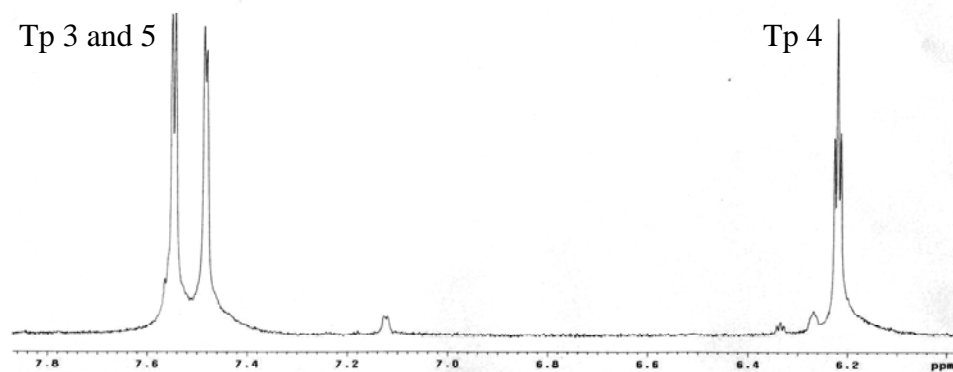


Figure 1.1A ^1H NMR spectrum of a Tp metal complex with C_3 symmetry.

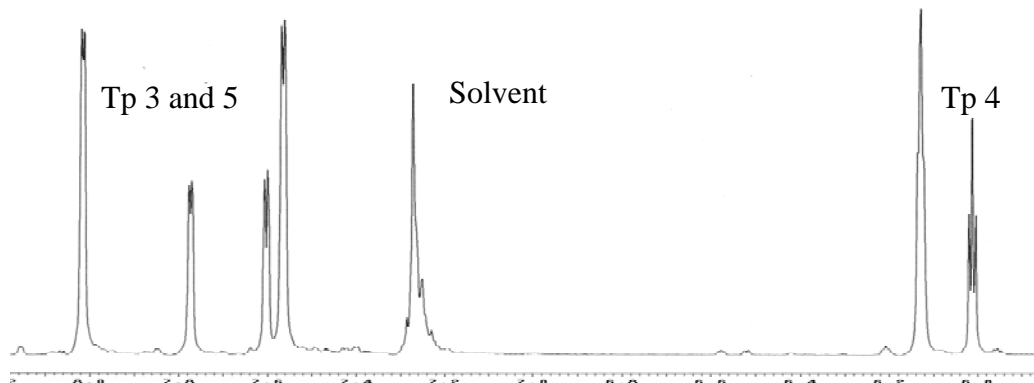


Figure 1.1B ^1H NMR spectrum of a Tp metal complex with σ -symmetry.

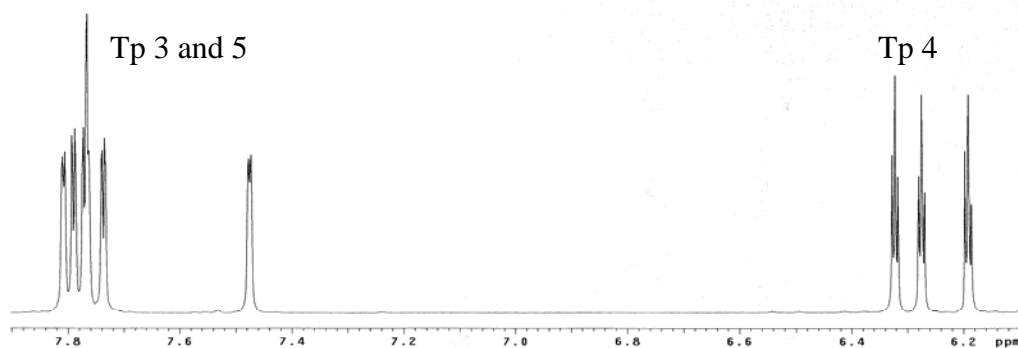


Figure 1.1C ^1H NMR spectrum of an asymmetric Tp metal complex.

The PCP pincer ligand: In addition to octahedral Tp based amido complexes, we have examined the reactivity of amido complexes based on the pincer ligand PCP (PCP = C₆H₃(CH₂P^tBu₂)-2,6) (Figure 1.2; X = H, R = ^tBu). Pincer ligands have received significant

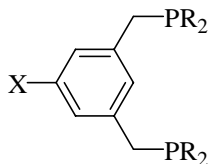


Figure 1.2 The PCP ligand. PCP ligands allow for tuning of steric and electronic effects through alteration of the phosphine substituent R, and variation of the X allows for further tuning of electronic effects.

attention due to their catalytic activity.¹⁰⁷ For example, these ligands have been demonstrated to possess relatively high activity towards dehydrogenation of hydrocarbons (alkanes, cycloalkanes, THF, and ethylbenzene).^{107,108} In addition dehydrogenation chemistry, pincer ligands have been demonstrated to effective for Heck-type catalysis. The balance of a robust nature as well as high reactivity has sparked the development of PCP and related ligands. These ligands also possess the ability allow modifications of the ligand's substituents which provide for steric and electronic tuning of the complex.

References.

- ¹ Atwood, J. D. *Inorganic and Organometallic Reaction Mechanisms Second Edition*; Wiley-VCH, Inc: New York, **1997**.
- ² Bryndza, H. E.; Tam, W. *Chem. Rev.* **1988**, *88*, 1163-1188.
- ³ Nugent, W. A.; Mayer, J. M. *Metal-Ligand Multiple Bonds: The Chemistry of Transition Metal Complexes Containing Oxo, Nitrido, Imido, Alkylidene, or Alkylidyne Ligands*; Wiley-Interscience: New York, **1988**.
- ⁴ Cundari, T. R. *Chem. Rev.* **2000**, *100*, 807-818.
- ⁵ Muller, T. E.; Beller, M. *Chem Rev.* **1998**, *98*, 675-703.
- ⁶ Wolfe, J. P.; Buchwald, S. L. *J. Am. Chem. Soc.* **1997**, *119*, 6054-6058.
- ⁷ Wagaw, S.; Rennels, R. A.; Buchwald, S. L. *J. Am. Chem. Soc.* **1997**, *119*, 8451-8458.
- ⁸ Goldsmith, C. R.; Jonas, R. T.; Stack, T. D. P, *J. Am. Chem. Soc.* **2002**, *124*, 83-96.
- ⁹ Mayer, J. M. *Comments Inorg. Chem.* **1988**, *8*, 125-135.
- ¹⁰ Holland, P. L.; Anderson, R. A.; Bergman, R. G. *Comments Inorg. Chem.* **1999**, *21*, 115-129.
- ¹¹ Fulton, R. J.; Holland, A. W.; Fow, D. J.; Bergman, R. G. *Acc. Chem. Res.* **2002**, *35*, 44-56.
- ¹² Conner, D.; Jayaprakash, K. N.; Cundari, T. R.; Gunnoe, T. B. *Organometallics* **2004**, *23*, 2724-2733.
- ¹³ Conner, D.; Jayaprakash, K. N.; Wells, M. B.; Manzer, S.; Gunnoe, T. B.; Boyle, P. D. *Inorg. Chem.* **2003**, *42*, 4759-4772.
- ¹⁴ Fulton, J. R.; Sklenak, S.; Bouwkamp, M. W.; Bergman, R. G. *J. Am. Chem. Soc.* **2002**, *124*, 4722-4737.
- ¹⁵ Wolfe, J. P.; Wagaw, S.; Marcoux, J.-F.; Buchwald, S. L. *Acc. Chem. Res.* **1998**, *31*, 805-818.
- ¹⁶ Hartwig, J. F. *Acc. Chem. Res.* **1998**, *31*, 852-860.
- ¹⁷ Hartwig, J. F. *Angew. Chem. Int. Ed.* **1998**, *37*, 2046-2067.
- ¹⁸ Hooper, M.W.; Utsunomiya M.; Hartwig J. F. *J. Org. Chem.* **2003**, *68*, 2861-2873.
- ¹⁹ Nicolaou, K. C.; Synder, S. A. *Classics in Total Synthesis: More Targets, Strategies, Methods*; John Wiley & Sons: New York, **2003**.
- ²⁰ Bryant, J. R.; Mayer, J. M. *J. Am. Chem. Soc.* **2003**, *125*, 10351-10361.
- ²¹ Mayer, J. M. *Acc. Chem. Res.* **1998**, *31*, 441-450.
- ²² Jonas, R. T.; Stack, T. D. P, *J. Am. Chem. Soc.* **1997**, *119*, 8566-8567.
- ²³ Fox, D. J.; Bergman, R. G. *Organometallics* **2004**, *23*, 1656-1670.
- ²⁴ Holland, A. W.; Bergman, R. G. *J. Am. Chem. Soc.* **2002**, *124*, 14684-14695.
- ²⁵ Holland, P. L.; Anderson, R. A.; Bergman, R. G.; Huang, J.; Nolan, S. P. *J. Am. Chem. Soc.* **1997**, *119*, 12800-12814.
- ²⁶ Glueck D. S.; Wu, J.; Hollander, F. J.; Bergman, R. G. *J. Am. Chem. Soc.* **1991**, *113*, 2041-2054.
- ²⁷ Michelman, R. I.; Bergman, R. G.; Andersen, R. A. *Organometallics* **1993**, *12*, 2741-2751.
- ²⁸ Dobbs, D. A.; Bergman, R. G. *Organometallics* **1994**, *13*, 4594-4605.
- ²⁹ Soper, J. D.; Bennett, B. K.; Lovell, S.; Mayer, J. M., *Inorg. Chem.* **2001**, *40*, 1888-1893.

-
- ³⁰ Joslin, F. L.; Johnson, M. P.; Mague, J. T.; Roundhill, M. D. *Organometallic* **1991**, *10*, 2781-2794.
- ³¹ Mindiola, D. J.; Hillhouse, G. L. *J. Am. Chem. Soc.* **2001**, *123*, 4623-4624.
- ³² Bryndza, H. E.; Fong, L. K.; Paciello, R. A.; Tam, W.; Bercaw, J. E. *J. Am. Chem. Soc.* **1987**, *109*, 1444-1456.
- ³³ Pearson, R. G. *J. Am. Chem. Soc.* **1963**, *85*, 3533-3539.
- ³⁴ Pearson, R. G. *J. Chem. Educ.* **1968**, *45*, 643.
- ³⁵ Miessler, G. L.; Tarr, D. A. *Inorganic Chemistry*; Prentice Hall Inc: Englewood Cliffs, NJ; 1991; pp 481-482.
- ³⁶ Wulfsberg, G. *Inorganic Chemistry*; University Science Books: Sausalito, CA; 2000.
- ³⁷ Hartwig, J. F.; Anderson, R. A.; Bergman, R. G. *J. Am. Chem. Soc.* **1991**, *119*, 1875-1887.
- ³⁸ Halpern, J. *Acc. Chem. Res.* **1982**, *15*, 238-244.
- ³⁹ Pearson R. G. *Chem. Rev.* **1985**, *85*, 41-49.
- ⁴⁰ Meyer T. Y.; Woerpel K. A.; Novak, B. M.; Bergman R. G. *J. Am. Chem. Soc.* **1994**, *116*, 10290-10291.
- ⁴¹ Torsten K.; Erikson, G.; Bryan, J. C.; Mayer, J. M. *Organometallics* **1988**, *7*, 1930-1938.
- ⁴² Caulton, K.G. *New J. Chem.* **1994**, *18*, 25-41.
- ⁴³ McMurry, J. *Organic Chemistry 4th ed.*; Brooks Cole Pub. Co.: Pacific Grove, CA, **1995**, pp 162-164.
- ⁴⁴ Conner, D.; Jayaprakash, K. N.; Gunnoe, T. B.; Boyle, P. D. *Inorg. Chem.* **2002**, *41*, 3042-3049.
- ⁴⁵ Antipin, I. S.; Gareyev, R. F.; Vedernikov, A. N.; Konovalov, A. I. *J. Phys. Org. Chem.* **1994**, *7*, 181-191.
- ⁴⁶ Kegley S. E.; Schaverien C. J.; Freudenberger J. H.; Bergman, R. G.; Nolan S. P.; Hoff, C. D. *J. Am. Chem. Soc.* **1987**, *109*, 6563-6565.
- ⁴⁷ Kim Y. J.; Osakada K.; Sugita K.; Yamamoto T.; Yamamoto A. *Organometallics* **1988**, *7*, 2182-2188.
- ⁴⁸ Kanzelberger, M.; Zhang, X.; Emge, T. J.; Goldman, A. S.; Zhao, J.; Incarvito, C.; Hartwig, J. F. *J. Am. Chem. Soc.* **2003**, *125*, 13644-13645.
- ⁴⁹ Hartwig, J. F.; Andersen, R. A.; Bergman, R. G. *Organometallics* **1991**, *10*, 1875-1887.
- ⁵⁰ McMillen, D. F.; Golden, D. M. *Annu. Rev. Phys. Chem.* **1982**, *33*, 493.
- ⁵¹ Jayaprakash, K. N.; Conner, D.; Gunnoe, T. B. *Organometallics* **2001**, *20*, 5254-5256.
- ⁵² Holland, A. W.; Bergman, R. G. *J. Am. Chem. Soc.* **2002**, *124*, 14684-14695.
- ⁵³ Fellmann J. D.; Schrock, R. R.; Traficante, D. D. *Organometallics* **1982**, *1*, 481-484.
- ⁵⁴ Bennett, M. A.; Yoshida, T. *J. Am. Chem. Soc.* **1978**, *100*, 1750-1759.
- ⁵⁵ Arnold, D. P.; Bennett, M. A.; Bilton, M. S.; Robertson, G. B. *J. Chem. Soc., Chem. Commun.* **1982**, 115.
- ⁵⁶ Muller, T. E.; Beller, M. *Chem Rev.* **1998**, *98*, 675-703.
- ⁵⁷ Fornies, J.; Green, M.; Spencer, J. L.; Stone, F. G. A. *J. Chem. Soc. Dalton Trans* **1977**, 1006-1009.
- ⁵⁸ Braga, D.; Sabatino, P.; Di Bugno, C.; Leoni, P.; Pasquali, M. *J. Organomet. Chem.* **1987**, *334*, 46-48.
- ⁵⁹ Monaghan, P. K.; Puddephatt, R. J. *Inorg. Chim. Acta.* **1982**, *65*, 59-61.

-
- ⁶⁰ Monaghan, P. K.; Puddephatt, R. J. *Organometallics* **1984**, *3*, 444-449.
- ⁶¹ Yoshida, T.; Matsuda, T.; Okano, T.; Kitani, T.; Otsuka, S. *J. Am. Chem. Soc.* **1979**, *101*, 2027-2038.
- ⁶² Hassan, J.; Sevignon, M.; Gozzi, C.; Schulz, E.; Lemaire, M. *Chem. Rev.* **2002**, *102*, 1359-1469.
- ⁶³ Ge, Y.; Ye, Y.; Sharp, P. R. *J. Am. Chem. Soc.* **1994**, *116*, 8384-8385.
- ⁶⁴ O'Sullivan, R. D.; Parkins, A. W.; Alcock, N. W. *J. Chem. Soc. Dalton Trans.* **1986**, 571-575.
- ⁶⁵ Albeniz, A. C.; Calle, V.; Espinet, P.; Gomez, S. *Chem. Comm.* **2002**, 610-611.
- ⁶⁶ Murahashi, S.; Naota, T.; Miyaguchi, N.; Noda, S. *J. Am. Chem. Soc.* **1996**, *118*, 2509-2510.
- ⁶⁷ Baesjou, P. J.; Driessen, W. L.; Challa, G.; Reedijk, J. *Macromolecules* **1999**, *32*, 270-276.
- ⁶⁸ Laszlo, S. I.; *Catalytic Activation of Dioxygen by Metal Complexes*; Kluwer Academic Publishers: Boston, **1992**.
- ⁶⁹ Li, X.; Huang, M.; Duan, W. *Chem. Rev.* **2002**, *102*, 2925-3030.
- ⁷⁰ Crabtree, R. H. *The Organometallic Chemistry of Transition Metals 3rd ed.*; John Wiley & Sons, INC.: New York, **2001**.
- ⁷¹ Holland, P. L.; Anderson, R. A.; Bergman, R. A. *J. Am. Chem. Soc.* **1996**, *118*, 1092-1104.
- ⁷² Bryndza, H. E.; Fultz, W. C.; Tam, W. *Organometallics* **1985**, *4*, 939-940.
- ⁷³ Bryndza, H. E. *Organometallics* **1985**, *4*, 406-408.
- ⁷⁴ Bryndza, H. E.; Calabrese, J. C.; Wreford S. S. *Organometallics* **1984**, *3*, 1603-1604.
- ⁷⁵ Mayer, J. M. *Acc. Chem. Res.* **1998**, *31*, 441-450.
- ⁷⁶ Hartwig, J.F. *Science* **2002**, *297*, 1653-1654.
- ⁷⁷ Miyaura, N.; Suzuki, A. *Chem. Rev.* **1995**, *95*, 2457-2483.
- ⁷⁸ Labinger, J. A.; Bercaw, J. E. *Nature* **2002**, *417*, 507-514.
- ⁷⁹ Bergman, R. G., *Science* **1984**, *223*, 902-908.
- ⁸⁰ Vollhardt, P. C. *Organic Chemistry 2nd ed.*; W.H. Freeman: New York, **1994**.
- ⁸¹ Crabtree, R. H. *Chem. Rev.* **1985**, *85*, 245-269.
- ⁸² Crabtree, R. H. *Chem. Rev.* **1995**, *95*, 987-1007.
- ⁸³ Wu, J.; Bergman, R. G. *J. Am. Chem. Soc.* **1983**, *111*, 7628-7630.
- ⁸⁴ Stahl, S. S.; Labinger, J. A.; Bercaw, J. E. *Angew. Chem. Int. Ed.* **1998**, *37*, 2180-2192.
- ⁸⁵ Jensen, M. P.; Wick, D. D.; Reinartz, S.; White, P. S.; Templeton, J. L.; Goldberg, K. I. *J. Am. Chem. Soc.* **2003**, *125*, 8614-8624.
- ⁸⁶ Wick, D. D.; Goldberg, K. I. *J. Am. Chem. Soc.* **1997**, *119*, 10235-10236.
- ⁸⁷ Periana, R. A.; Mironov, O.; Taube, D.; Bhalla, G.; Jones, C. J. *Science*, **1998**, *280*, 560-564.
- ⁸⁸ Periana, R. A.; Mironov, O.; Taube, D.; Bhalla, G.; Jones, C. *Science*, **2003**, *301*, 814-818.
- ⁸⁹ Walsh, P. J.; Hollander, F.J.; Bergman, R.G. *J. Am. Chem. Soc.* **1988**, *110*, 8729-8731.
- ⁹⁰ Cummins, C. C.; Baxter, S. M.; Wolczanski, P. T. *J. Am. Chem. Soc.* **1988**, *110*, 8731-8733.
- ⁹¹ Wolcaanzki, P. T.; Bennett, J. L. *J. Am. Chem. Soc.* **1994**, *116*, 2179-2180.
- ⁹² Schafer, D. F.; Wolczanski, P. T. *J. Am. Chem. Soc.* **1998**, *120*, 4881-4882.

-
- ⁹³ Cundari, T. R.; Klinckman, T. R.; Wolczanski, P. T. *J. Am. Chem. Soc.* **2002**, *124*, 1481-1487.
- ⁹⁴ Bennett, J. L.; Wolczanski, P. T. *J. Am. Chem. Soc.* **1997**, *119*, 10696-10719.
- ⁹⁵ Kempe, R. *Angew. Chem. Int. Ed.* **2000**, *39*, 468-493.
- ⁹⁶ Cotton, F. A.; Wilkinson, G.; Murillo, C. A.; Bochmann, M. *Advanced Inorganic Chemistry*, 6th ed.; Wiley-Interscience: New York, 1999, pp 1010-1012.
- ⁹⁷ Grotjahn, D. B.; Van, S.; Combs, D.; Lev, D. A.; Schneider, C.; Incarvito, C. D.; Lam, K.-C.; Rossi, G.; Rheingold, A. L.; Rideout, M.; Meyer, C.; Hernandez, G.; Mejorado, L. *Inorg. Chem.* **2003**, *42*, 3347-3355.
- ⁹⁸ Aoyama, Y.; Yamagishi, A.; Tanaka, Y.; Tio, H.; Ogoshi, H. *J. Am. Chem. Soc.* **1987**, *109*, 4735-4737.
- ⁹⁹ Pinkes, J. R.; Steffy, J. C.; Vites, J. C.; Cutler, A. R. *Organometallics* **1994**, *13*, 21-23.
- ¹⁰⁰ Klein, D. P.; Bergman, R. G. *J. Am. Chem. Soc.* **1989**, *111*, 3079.
- ¹⁰¹ Trofimenko, S. *Chem. Rev.* **1993**, *93*, 943-980.
- ¹⁰² Trofimenko, S. *Scorpionates: Polypyrazolylborate Ligands and Their Coordination Chemistry*; World Scientific Publishing Company: London, **1999**.
- ¹⁰³ Tellers, D. M.; Skoog, S. J.; Bergman, R. G.; Gunnoe, T. B.; Harman, W. D. *Organometallics* **2000**, *19*, 2428-2432.
- ¹⁰⁴ Bergman, R. G.; Cundari, T. R.; Gillespie, A. M.; Gunnoe, T. B.; Harman, W. D.; Klinckman, T. R.; Temple, M. D.; White, D. P. *Organometallics* **2003**, *22*, 2331-2337.
- ¹⁰⁵ Graziana, O.; Toupet, L.; Hamon, J.; Tilset, M. *J. Organomet. Chem.* **2003**, *669*, 200-206.
- ¹⁰⁶ Slugovc, C.; Schmid, R.; Kirchner, K. *Coord. Chem Rev.* **1999**, *185*, 109-126
- ¹⁰⁷ Van der Boom, M. E.; Milstein, D. *Chem. Rev.* **2003**, *103*, 1759-1792.
- ¹⁰⁸ Jensen, C. M. *Chem. Comm.* **1999**, 2443-2449.

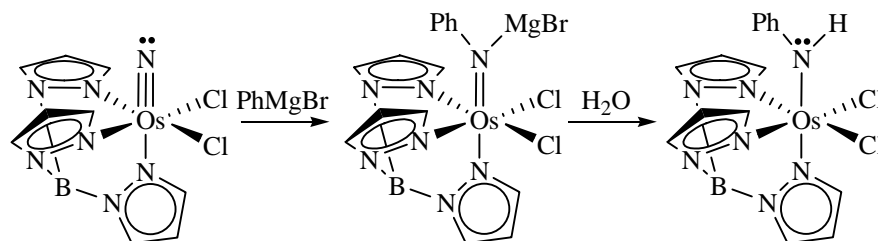
Chapter 2: Synthesis of Octahedral Ruthenium Amido Complexes and Initial Studies.

2.1 Introduction.

Late transition metal complexes with terminal amido or oxide ligands have received significant attention due their import role in C-N and C-O bond forming reactions; however, the synthesis and understanding of reactivity of such complexes has lagged relative to related early and middle transition metal complexes in high oxidation states.^{1,2,3,4,5,6} A misperception that the M-X (X = NR₂ or OR) bonds of these complexes are inherently "weak" has hindered their study, but recent interest has led to the preparation and detailed study of amido complexes of ruthenium, osmium, iridium, nickel, platinum, and copper.^{1,2,7,8,9,10}

The highly reactive nature of most late transition metal amido complexes renders the synthesis and study of these complexes challenging. As such, many synthetic strategies to prepare late transition metal complexes amido or oxide ligands have been employed, yet no single scheme works for all systems. For example, Bergman et al. have reported a series of Cp^{*}Ru(PMe₃)₂X (X = aryloxy, arylamido) complexes in which the synthesis of Cp^{*}Ru(PMe₃)₂(NPh₂) was achieved by a metathesis reaction with LiNPh₂ and Cp^{*}Ru(PMe₃)₂Cl.¹¹ However, Cp^{*}Ru(PMe₃)₂Cl was found to be inert in reactions with other alkali oxides and amides, thus more involved strategies were required to prepare the related complexes. Roundhill et al. have reported similar CpRu(PPh₃)₂NHR and CpRu(Cy₂PCH₂CH₂PCy₂)NHR amido complexes by deprotonation of the corresponding amine complexes [CpRu(PPh₃)₂NH₂R]⁺ and [CpRu(Cy₂PCH₂CH₂PCy₂)NH₂R]⁺ using strong bases.¹² In addition to basic preparation schemes, Mayer et al. have reported the synthesis of

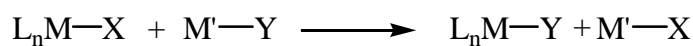
TpOs(Cl)₂NHPh by nucleophilic addition of phenyl anion to an electrophilic Os(VI) nitrido ligand using PhMgBr. The amido complex was subsequently formed via aqueous workup of the product of addition (Scheme 2.1).¹³ Given the difficulty in preparation of late transition



Scheme 2.1 Reduction of an Os(VI) nitrido using PhMgBr to form an Os(IV) amido complex.

metal amido complexes, methods for synthesizing these complexes remains an area of significant interest.

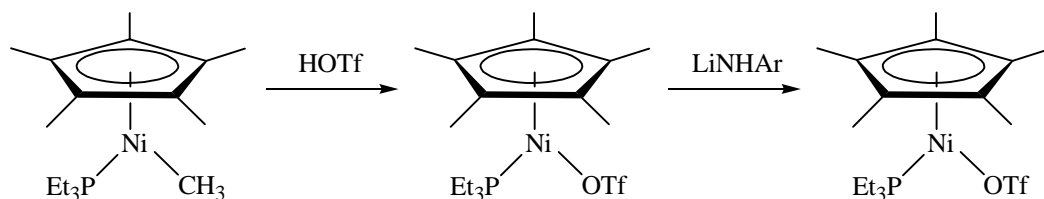
Metathesis reactions are the most commonly utilized strategy to prepare late transition metal amido or oxide complexes. In these reactions, the metal's leaving group is typically a halide, heteroatom, or alkyl group. Halide leaving groups undergo metathesis with amido and oxide salts, while amines and alcohols undergo exchange with alkyl, oxide or amido leaving groups.^{1,2} The most commonly employed of these exchange methods is direct preparation by salt metathesis of a transition metal halide with an alkali oxides or alkali amides (Scheme 2.2).^{1,14,15} These reactions work for early through late transition metal



Scheme 2.2 Salt metathesis strategy generate transition metal amido or oxide complexes
X = Halide, M' = Alkali, Y = NR₂ or OR.

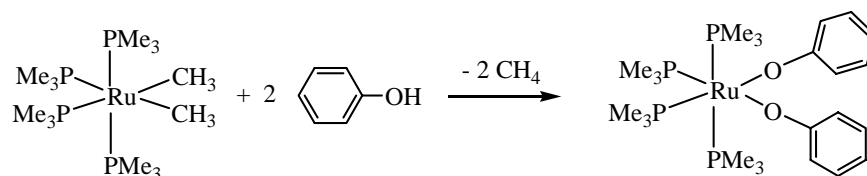
systems because the transmetalation reaction is generally favorable due to the strong ΔH_f of the alkali halide.¹⁶

Alternative synthetic schemes employed by Bercaw et al. and Bergman et al. exchange an alkyl leaving group with a free amine or alcohol to generate the respective amido or oxide ligand and free hydrocarbon.^{1,2,17,18} An analogous scheme treats the alkyl complex with triflic acid to release the hydrocarbon and form the corresponding triflate complex. Salt metathesis reactions similar to the transition metal halide metathesis reactions are then carried out (Scheme 2.3).^{2,19}



Scheme 2.3 Synthesis of a late transition metal amido complex from an alkyl complexes. Salt metathesis is performed with the triflate.

Elimination of hydrocarbons in the presence of an amine or alcohol is another method known to for synthesis of late transition metal oxide and amido complexes. For example, Berman et al. have reported the preparation of $\text{Ru}(\text{PMe}_3)_4(\text{OPh})_2$ by reacting $\text{Ru}(\text{PMe}_3)_4(\text{CH}_3)_2$ with phenol (Scheme 2.4). This reaction is driven by irreversible loss of



Scheme 2.4 Example of an alkyl exchange reaction to form late transition metal oxide or amido complex.

methane.

Building on the above chemistry, another synthetic method for the synthesis of late transition metal complexes with oxide or amido ligands is heteroatomic exchange reactions. This method utilizes a free amine or alcohol to exchange with an oxide or amido leaving group. These reactions yield the corresponding amido or oxide complex of the free amine or alcohol and the respective amine or alcohol of the original amido or oxide ligand (Scheme 2.5). Heteroatomic exchange reactions are known to be useful for synthesis if the exchange

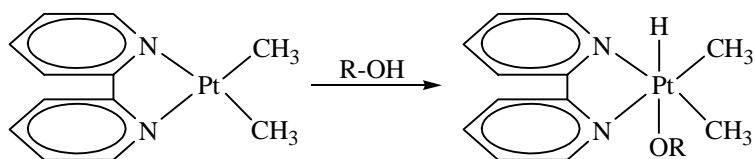


Scheme 2.5 Synthesis of a late transition metal amido or oxide by heteroatomic exchange of free amine or alcohol with an amido or oxide ligand (X/Y = NR₂ or OR).

equilibrium can be driven to products either by a strong thermodynamic preference for the amido or oxide complex being formed, or if the alcohol or amine being released is sequestered. For example, the preparation of the rhenium amido complexes Re(CO)₃(depe)X (depe = Et₂PCH₂CH₂PEt₂; X = NPh, NHC₆F₆, or NC₄H₄) is accomplished by exchange reactions of Re(CO)₃(depe)(OEt) with NH₂Ph, NH₂C₆F₆, or HNC₄H₄ respectively.²⁰ These exchange reactions are reversible, and the equilibrium strongly favors the Re-OEt and arylamine starting materials; however, 4Å sieves were used to sequester the ethanol released from exchange thus resulting in complete conversion to the respective rhenium amido complexes.

In addition to exchange reactions, oxidative addition of N-H or O-H bonds, while less frequent, are known to be a useful method for the synthesis of late transition metal complexes

with amido and oxide ligands.^{1,21} For example, bisphosphine platinum and palladium complexes are known to undergo oxidative addition reactions with the H-X (X = O or N) bonds of phenol or pyrrole to form the respective arylamido and aryloxy complexes.^{22,23} Puddephatt et al. have reported similar oxidative addition of methanol and ethanol using (bipy)PtMe₂ (Scheme 2.6).^{24,25} The reversible oxidative addition of water by Pt(P(*i*-Pr)₃)₂ to

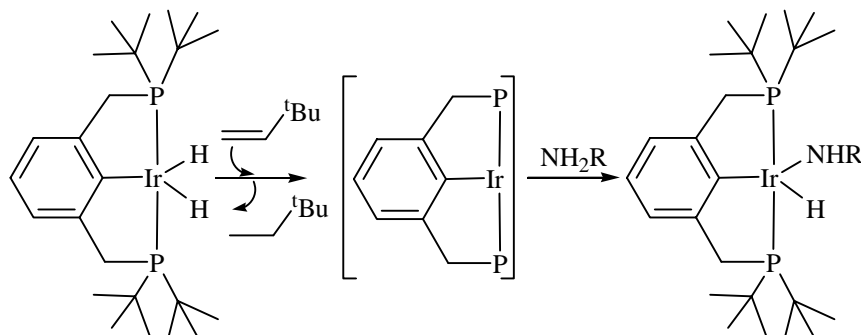


Scheme 2.6 Oxidative addition of alcohols to form a platinum (IV) oxide complex. (R = Me, or Et).

form the corresponding hydroxo hydride complex (P(*i*-Pr)₃)₂(H)(OH) has also been reported.²⁶ Also, the above oxidative addition reactions are potentially useful to olefins hydroamination chemistry, where coordination and insertion of an olefin into the M-H or M-N bond followed by reductive elimination can catalytically produce amines products.

Oxidative addition reactions to produce oxide or amido complexes of ruthenium and iridium have been reported by the Bergman et al. and Milstein et al. using the ethylene complexes Ru(PMe₃)₄(C₂H₄) and Ir(PEt₃)₂(C₂H₄)₂Cl respectively.^{2,27,28} At room temperature, the ruthenium system undergoes oxidative addition of water to form Ru(PMe₃)₄(OH)H and ethylene, and the iridium system oxidatively adds ammonia to form [Ir(PEt₃)₂(NH₂)H]₂ and ethylene. Both of the systems are proposed to proceed by loss of ethane to generate an unsaturated metal center to which the respective substrates can oxidatively add. In addition,

Hartwig, Goldman et al. have reported oxidative addition of aniline and ammonia to an unsaturated iridium metal center to generate the respective amido complexes (Scheme 2.7).²⁹



Scheme 2.7 Oxidative addition of amines to an unsaturated PCP Ir metal center to form amido complexes (R = H or Ph).

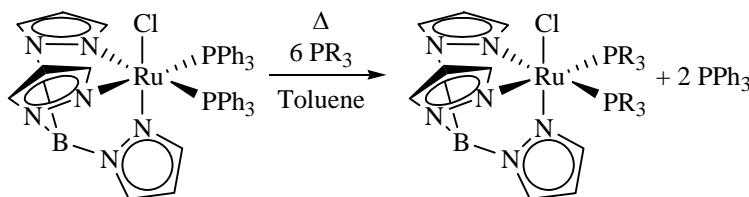
2.2 General Comments on Synthesis of TpRu(L)(L')NHR Complexes.

Our preliminary efforts focused on the synthesis of octahedral ruthenium (II) amido complexes. Ruthenium (II) was chosen because this d^6 metal center has a filled set of $d\pi$ orbitals that will disrupt ligand to metal π -donation resulting in π -conflict and providing enhanced reactivity. As discussed in Chapter 1, the {TpRu(L)(L')} moiety has received attention because the ancillary ligands L and L' can be varied to tune the steric and electronic nature of the metal center.³⁰ The {TpRu(L)(L')} backbone was also selected for our studies because the Tp ligand's steric bulk hinders the formation of bimetallic complexes as well as enforces the octahedral geometry.³¹ The Tp ligand also offers a higher degree of stabilization compared to the cyclopentadienyl ligand due to steric protection of the metal center.^{32,33,34} In addition, the cyclopentadienyl ligand can undergo ring slip that could potentially result in decomposition chemistry. The related transformation for the Tp ligand, a change from a K^3 to

a K^2 coordination mode often has a larger activation energy, thus decomposition pathways which involve initial opening of a coordination site are less likely for comparable Tp based complexes.

2.2.1 Synthesis of Tp Amido Precursor Complexes.

Our strategy to examine the chemistry of ruthenium amido complexes involved the preparation of a series of ligand sets followed by introduction of the amido fragment. The complex $\text{TpRu}(\text{PPh}_3)_2\text{Cl}$ has been used as a precursor due to the facile replacement of the triphenylphosphine ligand(s).³⁵ For example, we prepared $\text{TpRu}(\text{PMe}_3)_2\text{Cl}$ and $\text{TpRu}\{\text{P}(\text{OMe})_3\}_2\text{Cl}$ by refluxing $\text{TpRu}(\text{PPh}_3)_2\text{Cl}$ with an excess of PMe_3 or $\text{P}(\text{OMe})_3$. These reactions were performed by treating toluene solutions of $\text{TpRu}(\text{PPh}_3)_2\text{Cl}$ with 6 equivalents of corresponding phosphine (Scheme 2.8). Toluene was chosen because the relatively high



R = Me or OMe

Scheme 2.8 Preparation of $\text{TpRu}(\text{PMe}_3)_2\text{Cl}$ and $\text{TpRu}\{\text{P}(\text{OMe})_3\}_2\text{Cl}$ by refluxing by phosphine displacement of $\text{TpRu}(\text{PPh}_3)_2\text{Cl}$.

boiling point, 107 °C, facilitates dissociation of the triphenylphosphine ligands. Other non-coordinating or weakly coordinating solvents, such as THF or benzene, were found to be suitable for this reaction; however, extended reflux times were required due to the decreased

boiling points of these solvents. *In toluene*, the reactions were complete after approximately 48 H of reflux.

TpRu(PMe₃)₂Cl and TpRu{P(OMe)₃}₂Cl are yellow powders that are highly not air sensitive and can be stored under inert atmosphere for many months. The ¹H NMR spectra of these complexes reveal virtual triplets for the methyl groups of PMe₃ and P(OMe)₃ at 1.42 and 3.29 ppm, respectively. Consistent with C_s symmetry, the Tp pyrazolyl resonances are in a 2:1 pattern (Figures 2.1 and 2.2). In addition, the complex TpRu{P(OMe)₃}₂Cl has been characterized by X-ray crystallography (Figure 2.3). The X-ray structure of TpRu{P(OMe)₃}₂Cl shows a pseudooctahedral coordination sphere. The complete list of crystallographic data and bonds distances and angles are given in Appendix A. The Ru-P bond distances are 2.2362(5) and 2.2404(5) Å, and the P-Ru-P bond angle is 94.94(2) °. The Ru-N_{pyrazolyl} bond distance for the nitrogen trans to the chloride ligand is shorter (2.0767(17) Å) compared with the other two Ru-N_{pyrazolyl} bond distances (2.1534(18) and 2.1532(17) Å). The shorter bond distance for the trans nitrogen is due to the chloride trans effect.

Additionally, we have utilized [TpRu(CO)₂(THF)][PF₆] and TpRu(CO)(PPh₃)Cl as starting points in order to vary the electron density of the metal center more significantly. The syntheses of these complexes have been previously reported.^{36,37} The five ligand sets we have been utilizing in our investigations are shown in Figure 2.4.

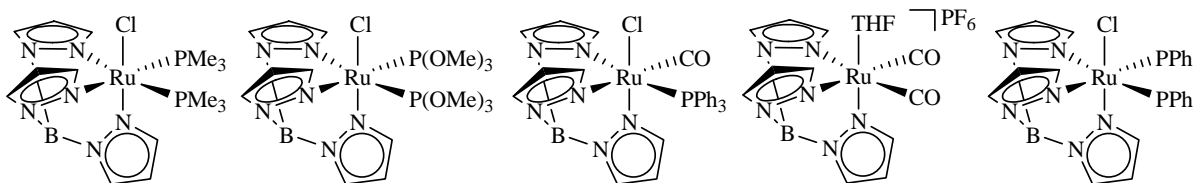


Figure 2.4 TpRu(L)(L')X systems used as precursors to octahedral Ru(II) amido complexes.

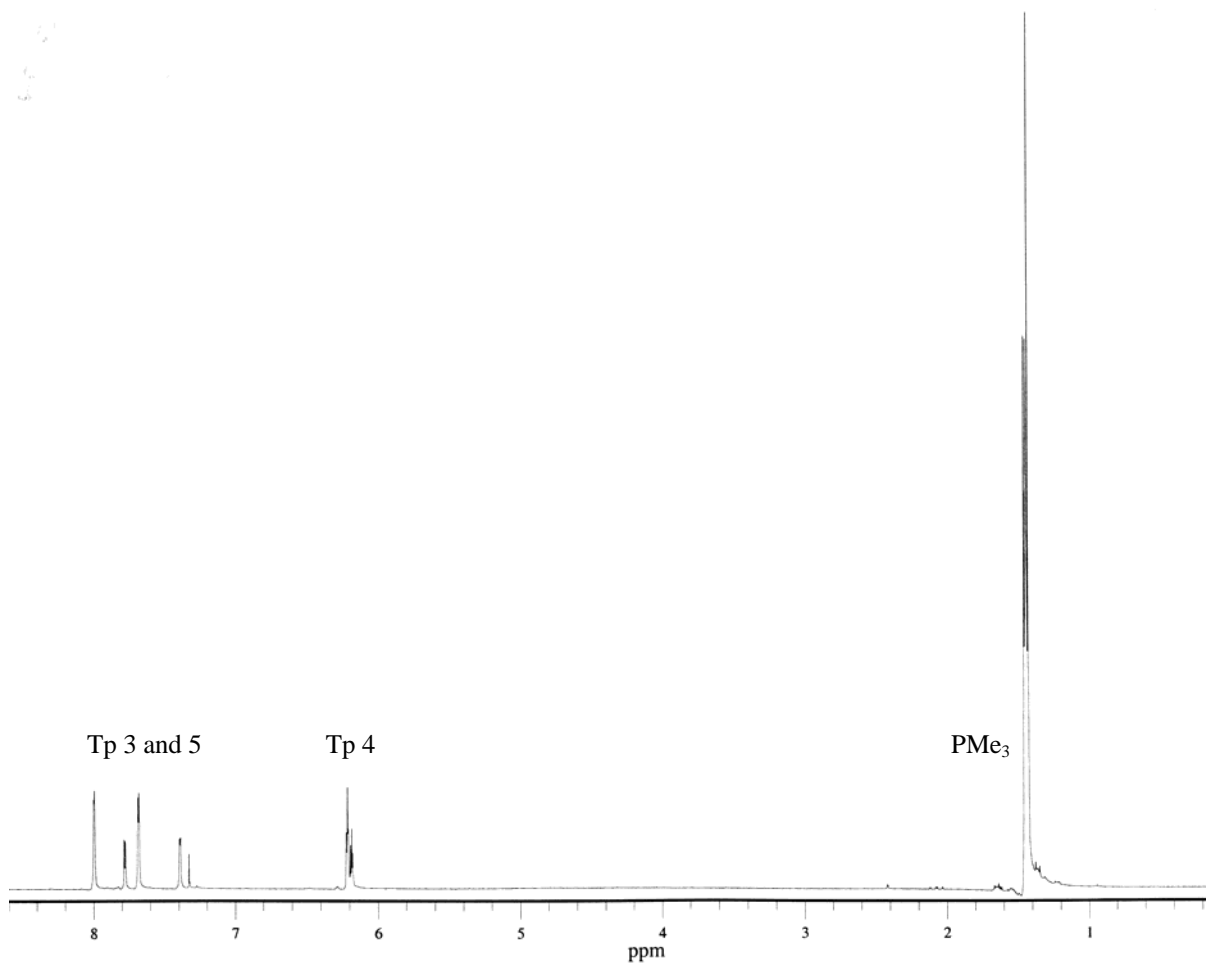


Figure 2.1 ^1H NMR spectrum of $\text{TpRu}(\text{PMe}_3)_2\text{Cl}$ in CDCl_3 .

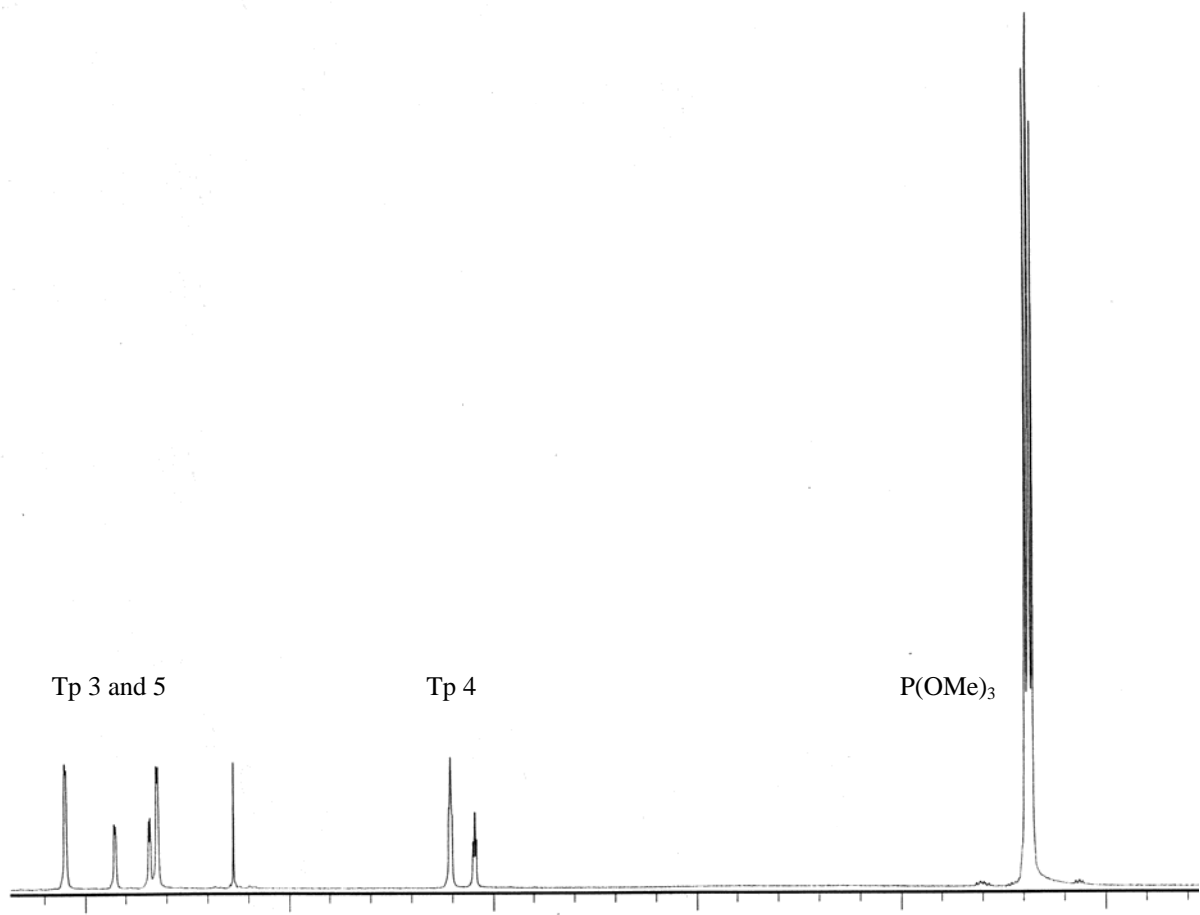


Figure 2.2 ^1H NMR spectrum of $\text{TpRu}\{\text{P}(\text{OMe})_3\}_2\text{Cl}$ in CDCl_3 .

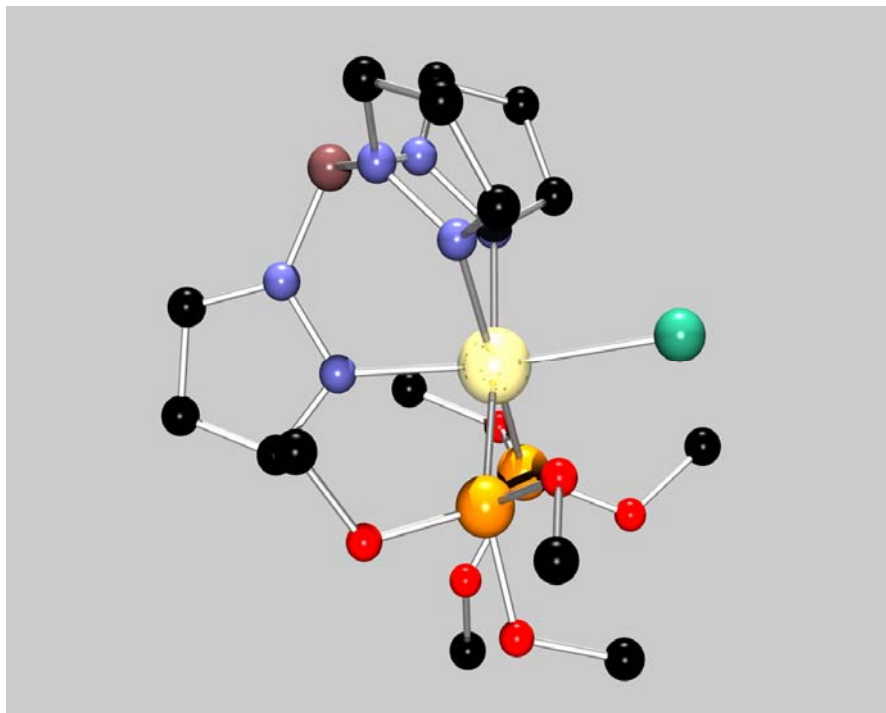


Figure 2.3 X-ray diagram of $\text{TpRu}\{\text{P}(\text{OMe})_3\}_2\text{Cl}$ (H omitted).

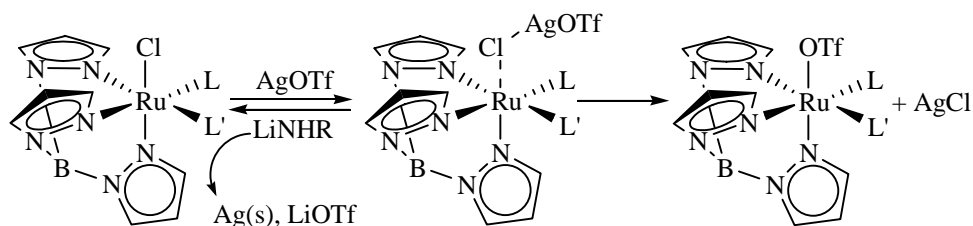
2.2.2 Synthesis of $\text{TpRu}(\text{PMe}_3)_2\text{OTf}$, $\text{TpRu}\{\text{P}(\text{OMe})_3\}_2\text{OTf}$, and $\text{TpRu}(\text{CO})(\text{PPh}_3)\text{OTf}$, and Their Reactivity with Alkali Amides.

The complexes $\text{TpRu}(\text{PMe}_3)_2\text{Cl}$, $\text{TpRu}\{\text{P}(\text{OMe})_3\}_2\text{Cl}$, and $\text{TpRu}(\text{CO})(\text{PPh}_3)\text{Cl}$ do not react with alkali amides. For example, reactions of THF solutions of $\text{TpRu}(\text{PMe}_3)_2\text{Cl}$ or $\text{TpRu}\{\text{P}(\text{OMe})_3\}_2\text{Cl}$ with LiNH_2 or LiNHPH refluxed for several days yielded ruthenium starting materials after workup. The anticipated metathesis reaction did not occur likely due to a kinetically inert Ru-Cl bond.

Trifluoromethanesulfonate (triflate, OTf) is commonly used as a ligand because its labile nature renders it susceptible to displacement. Also, metathesis reactions of this ligand

with alkali amides or oxides have been reported in the synthesis of late transition metal amido and oxide complexes.^{1,2,17,18} Thus, we sought to exchange the chloride ligand with OTf by using AgOTf to abstract the chloride ligand. AgOTf, in addition to its ability to abstract halides, can act as a relatively strong single-electron oxidant (the reduction potential of AgOTf in THF is 1.06 vs NHE).³⁸ For example, the complex (PCP^{Ph})Ru^{II}(Cl)(CO)(PPh₃) reacts with AgOTf to form the two products (PCP^{Ph})Ru^{II}(CO)(PPh₃)OTf and [(PCP^{Ph})Ru^{III}(CO)(PPh₃)Cl][OTf] in an approximately 1:1 ratio.³⁹

Reaction of TpRu(PMe₃)₂Cl, TpRu{P(OMe)₃}₂Cl, or TpRu(CO)(PPh₃)Cl with one equivalent of AgOTf in a non-coordinating solvent such as CH₂Cl₂ or THF resulted in the formation of the corresponding triflate complexes. Thus redox chemistry with AgOTf and the chloride complexes was not observed. *In THF*, the reactions were refluxed for 18 to 24 hours. The addition of AgOTf to THF solutions of TpRu(PMe₃)₂Cl, TpRu{P(OMe)₃}₂Cl, or TpRu(CO)(PPh₃)Cl resulted in the immediate formation of a precipitate. These precipitates are proposed to be TpRu(L)(L')Cl – AgOTf adducts wherein Ag⁺ is paired with the chloride ligand and triflate, and the chloride is still coordinated to ruthenium (Scheme 2.9). The



Scheme 2.9 Proposed intermediate in the synthesis of TpRu(L)(L')OTf.

proposed adduct complexes have not been fully characterized, but have been observed by ¹H NMR spectroscopy. Specifically, the addition of AgOTf to CDCl₃ solutions of

TpRu(PMe₃)₂Cl or TpRu{P(OMe)₃}₂Cl were found to yield a new products inconsistent with the ¹H NMR spectra of TpRu(PMe₃)₂OTf or TpRu{P(OMe)₃}₂OTf respectively. Also reactions of the adduct complexes with LiNHPPh yielded the TpRu(L)(L')Cl starting materials as well as solid silver. Heating the solutions of the intermediate complexes observed by ¹H NMR yielded the respective triflate complexes (Figure 2.5 A-C).

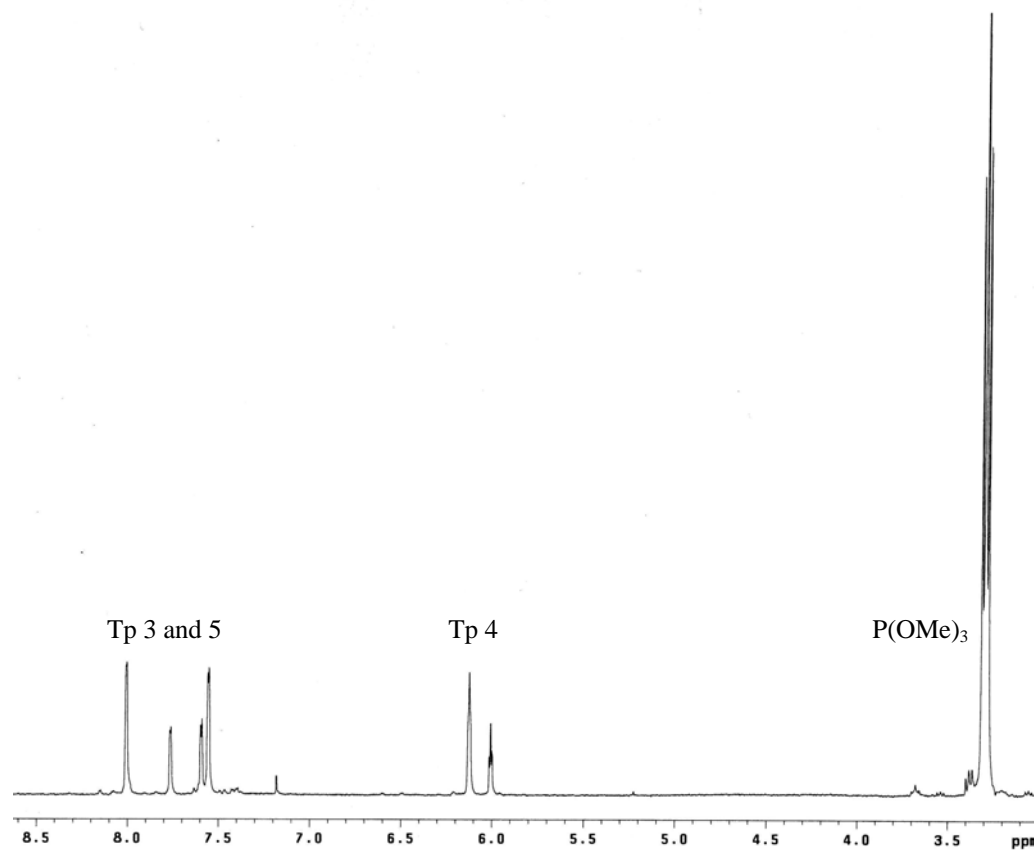


Figure 2.5 A ¹H NMR spectrum of TpRu{P(OMe)₃}₂Cl in CDCl₃.

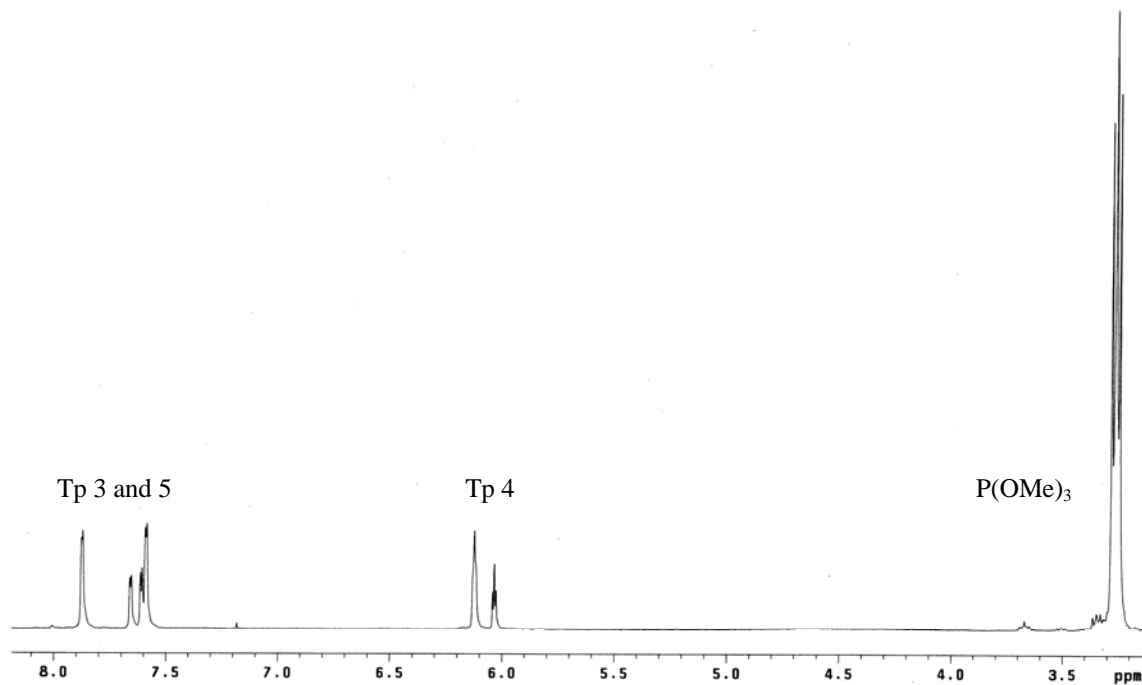


Figure 2.5 B ^1H NMR spectrum of the proposed adduct of formed by addition of AgOTf to $\text{TpRu}\{\text{P}(\text{OMe})_3\}_2\text{Cl}$.

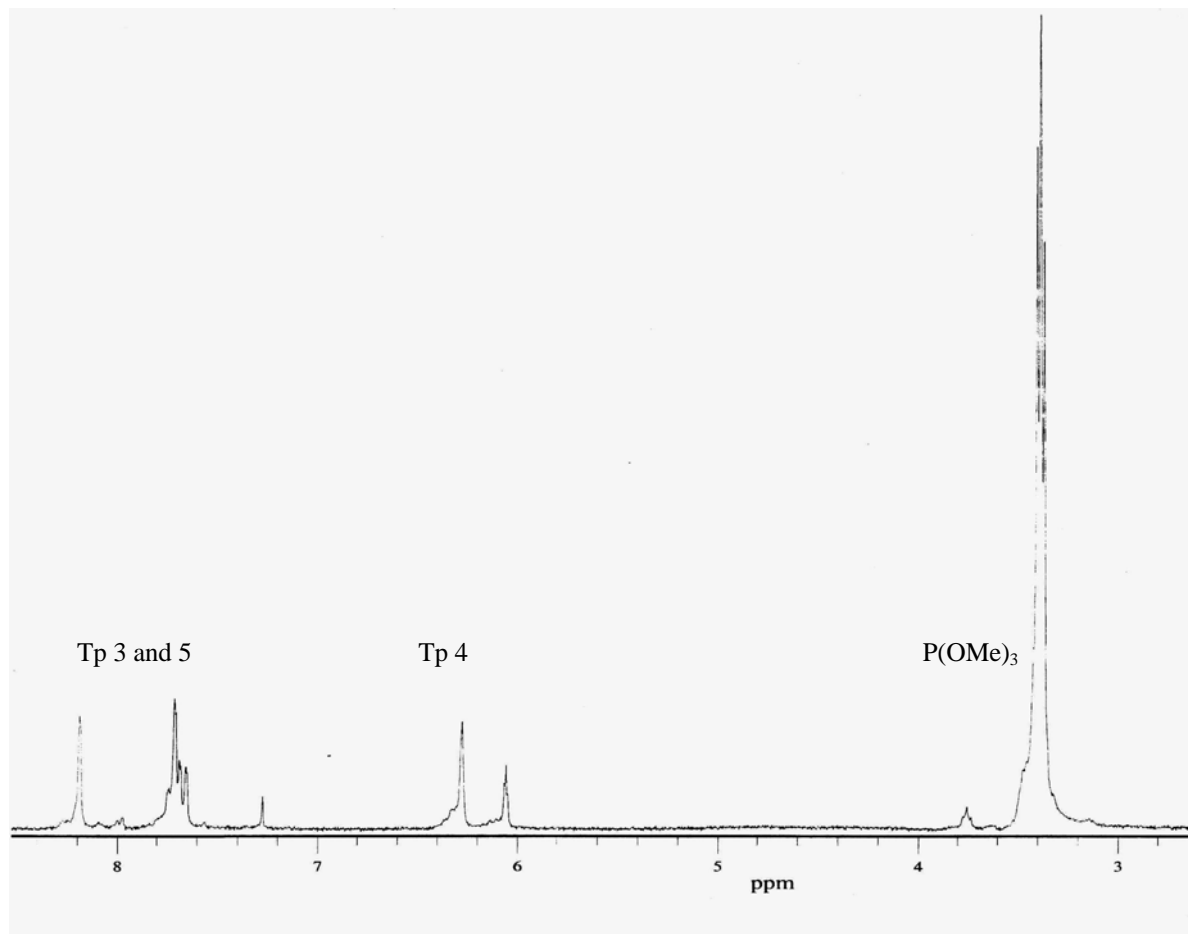


Figure 2.5 C ^1H NMR spectrum of $\text{TpRu}\{\text{P}(\text{OMe})_3\}_2\text{OTf}$ in CDCl_3 .

The triflate complexes are light yellow powders that are not air stable; however, they can be stored under inert atmosphere for several weeks. The ^1H NMR spectra of $\text{TpRu}(\text{PMe}_3)_2\text{OTf}$ and $\text{TpRu}\{\text{P}(\text{OMe})_3\}_2\text{OTf}$ show virtual triplets for the methyl groups of PMe_3 and $\text{P}(\text{OMe})_3$ at 1.41 and 3.18 ppm, respectively. Consistent with C_3 symmetry, the Tp pyrazolyl resonances are in a 2:1 pattern (Figure 2.6 and 2.7). The ^1H NMR of $\text{TpRu}(\text{CO})(\text{PPh}_3)\text{OTf}$ has Tp pyrazolyl resonances in 1:1:1 pattern consistent with C_1

symmetry. IR spectroscopy of $\text{TpRu}(\text{CO})(\text{PPh}_3)\text{OTf}$ reveals a single absorption due to the carbonyl ligand at $\nu_{\text{CO}} = 1986 \text{ cm}^{-1}$.

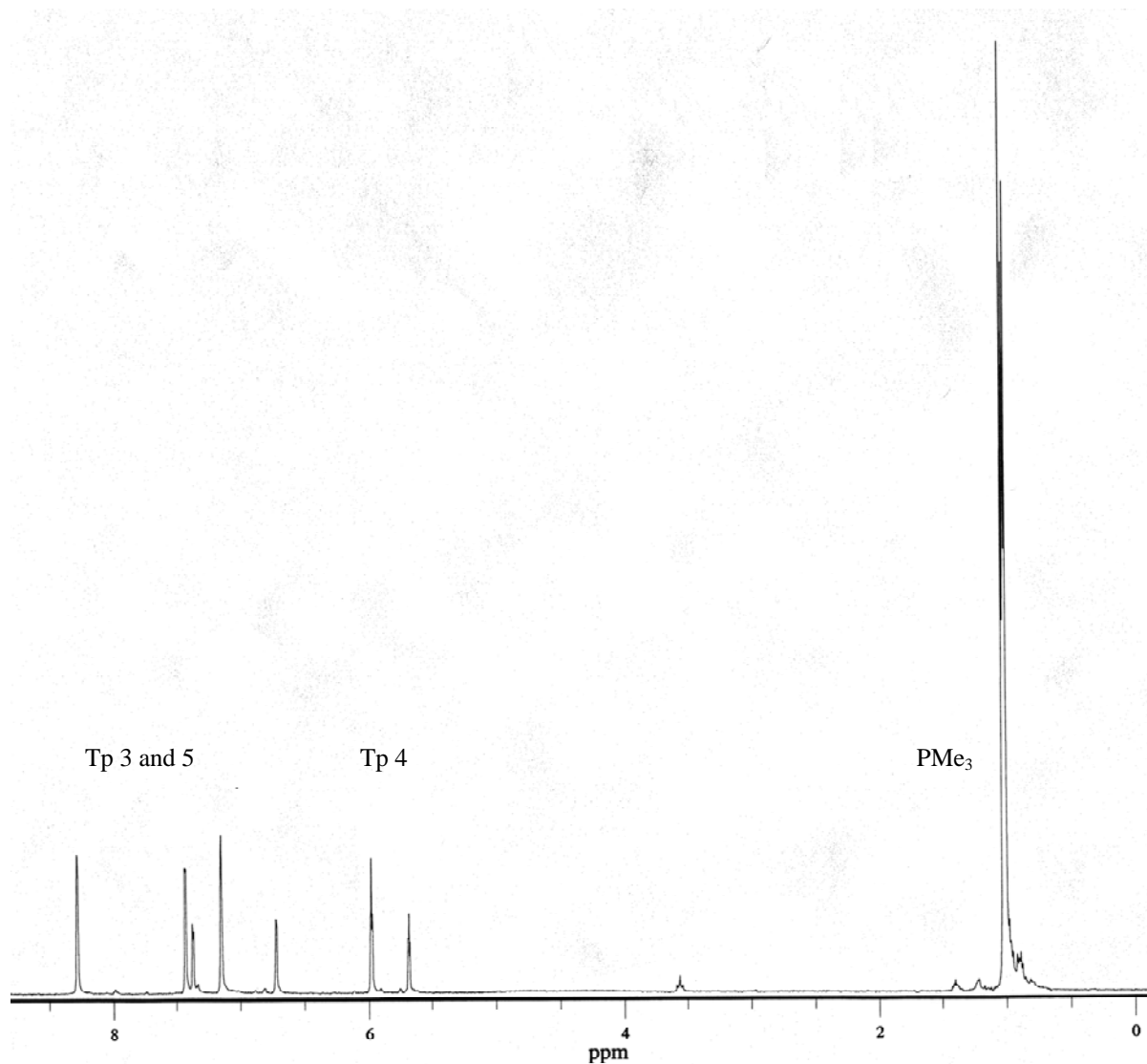


Figure 2.6 ^1H NMR spectrum of $\text{TpRu}(\text{PMe}_3)_2\text{OTf}$ in C_6D_6 .

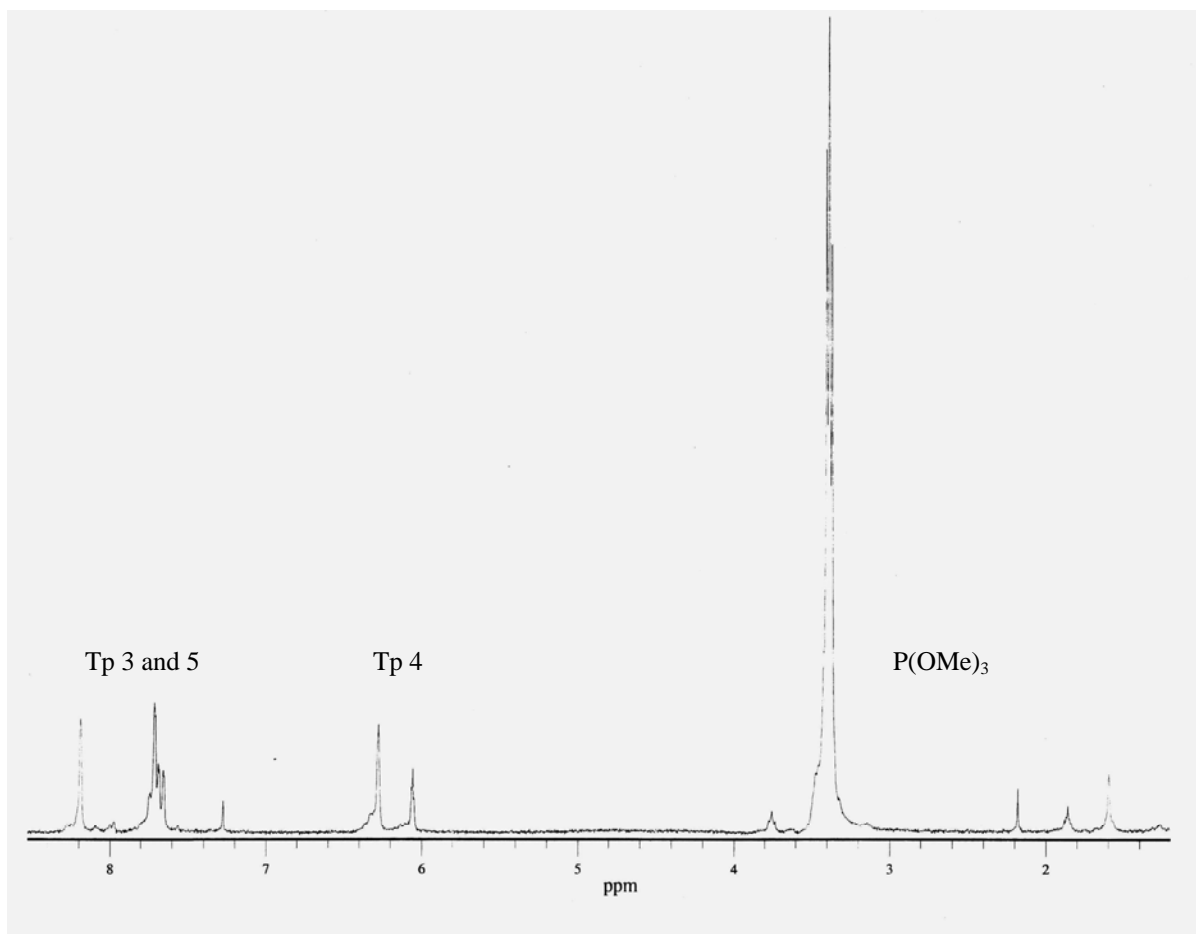


Figure 2.7 ^1H NMR spectrum of $\text{TpRu}\{(\text{P}(\text{OMe})_3)_2\text{OTf}\}$ in CDCl_3 .

2.2.3 Synthesis of Cationic Amine Complexes.

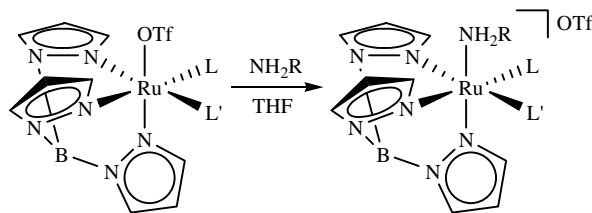
Although $\text{TpRu}(\text{CO})(\text{PPh}_3)\text{NHPh}$ was successfully prepared by reacting LiNHPh with $\text{TpRu}(\text{CO})(\text{PPh}_3)(\text{OTf})$ in THF, metathesis reactions of $\text{TpRu}(\text{PMe}_3)_2\text{OTf}$, $\text{TpRu}(\text{PMe}_3)_2\text{Cl}$, $\text{TpRu}\{(\text{P}(\text{OMe})_3)_2\text{OTf}\}$, or $\text{TpRu}\{(\text{P}(\text{OMe})_3)_2\text{Cl}\}$ with lithium or sodium amides were not an effective route for synthesis of these amido complexes of these starting materials. Specifically, the reaction of $\text{TpRu}(\text{L})(\text{L}')\text{Cl}$ with LiNH_2 , LiNHPh , or NaNH_2 in THF resulted in no reaction, and reactions of $\text{TpRu}(\text{PMe}_3)_2\text{OTf}$ or $\text{TpRu}\{(\text{P}(\text{OMe})_3)_2\text{OTf}\}$ with

LiNH₂ or NaNH₂ resulted in multiple Tp containing decomposition products. Bergman et al. have reported the preparation *trans*-(dmpe)₂(H)Ru(NH₂) (dmpe = bis(dimethylphosphino)ethane) by metathesis reaction of *trans*-(dmpe)₂(H)RuCl with NaNH₂ in THF and a carefully controlled concentration of 1 eq of NH₃.⁴⁰ Attempts to reproduce this chemistry with TpRu(PMe₃)₂Cl and TpRu{P(OMe)₃}₂Cl by reacting THF solutions of these complexes in with LiNH₂ in the presence of excess ammonia resulted in no reaction. Similar reactions with the triflate complexes TpRu(PMe₃)₂(OTf) or TpRu{P(OMe)₃}₂(OTf) with excess ammonia and LiNH₂ yielded the amine complexes [TpRu(PMe₃)₂(NH₃)] [OTf] and [TpRu{P(OMe)₃}₂(NH₃)] [OTf] respectively. The formation of the amine complexes in these latter reactions is like due to ammonia displacing the triflate ligand because treating these triflate complexes with excess ammonia results in the formation of the respective ammine complex [TpRu(L)(L')(NH₃)] [OTf] (see below); however, metathesis reactions to form the amido complex, followed by subsequent protonation have not been definitively ruled out.

Roundhill et al. have reported the preparation of a series of CpRu(PPh₃)₂NHR and CpRu(Cy₂PCH₂CH₂PCy₂)(NHR) amido complexes by using strong bases to deprotonate the respective amine complexes [CpRu(PPh₃)₂NH₂R] [OTf] and [CpRu(Cy₂PCH₂CH₂PCy₂)(NH₂R)] [OTf]. Given the difficulty in achieving clean chemistry with the above metathesis reaction methods, we chose to pursue a similar scheme for the preparation of the Tp base Ru(II) amido complexes.

A series of [TpRu(L)(L')(NH₂R)] [OTf] (L = L' = PMe₃ or P(OMe)₃; or L = CO and L' = PPh₃; R = H, Ph, or ^tBu) amine complexes were prepared by reaction of the triflate

complexes TpRu(L)(L')OTf with excess amine (NH_3 , NH_2Ar , or NH_2^tBu) in THF for 24 H (Scheme 2.10). Additionally, preparation of these complexes by in situ generation of the



Scheme 2.10 Preparation of cationic amine complexes by displacement of amine (NH_2R , $\text{R} = \text{H}$, Ph , or ^tBu).

triflate complex, rather than isolating the triflate, followed by addition of free amine was also successful. The amine complexes $[\text{TpRu(L)(L')NH}_2\text{R}][\text{OTf}]$ are white to pale yellow powders that are not air sensitive and can be stored under inert atmosphere for several months without significant decomposition. Note, successful storage of the ^tBu amine complexes $[\text{TpRu(L)(L')(NH}_2^t\text{Bu)}][\text{OTf}]$ required storage at $-20\text{ }^\circ\text{C}$, otherwise significant decomposition was found to occur within a 2-3 weeks. Additionally, the complexes $\text{TpRu(CO)(PPh}_3\text{)OTf}$, $[\text{TpRu(CO)(PPh}_3\text{)(NH}_3\text{)}][\text{OTf}]$, $[\text{TpRu(CO)(PPh}_3\text{)(NH}_2\text{Ph)}][\text{OTf}]$, or $[\text{TpRu(CO)(PPh}_3\text{)(NH}_2^t\text{Bu)}][\text{OTf}]$ were prepared by Dr. K. N. Jayaprakash.^{41,42,56}

The aniline complexes were prepared by in situ generation of TpRu(L)(L')OTf followed by addition of aniline. Highly colored (dark purple for $[\text{TpRu(PMe}_3\text{)}_2\text{NH}_2\text{Ph}][\text{OTf}]$ and blue/green for $[\text{TpRu}\{\text{P(OMe)}_3\}_2\text{NH}_2\text{Ph}][\text{OTf}]$) impurities were observed during preparation of these complexes if excess AgOTf was used. These impurities are likely (although not confirmed) the result of ruthenium based oxidation chemistry. The colored impurities were removed by washing the phenyl amine complexes with diethyl ether. $[\text{TpRu(PMe}_3\text{)}_2\text{NH}_2\text{Ph}][\text{OTf}]$ and $[\text{TpRu}\{\text{P(OMe)}_3\}_2\text{NH}_2\text{Ph}][\text{OTf}]$ have been characterized by

^1H NMR, ^{13}C NMR, ^{31}P NMR spectroscopy, as well as IR spectroscopy and elemental analysis. The ^1H NMR spectrum of these complexes reveals C_s symmetry (2:1 Tp pyrazolyl resonances), virtual triplets for the PMe_3 and $\text{P}(\text{OMe})_3$ groups at 1.30 and 3.44 ppm respectively, and broad resonances for the amine NH_2Ph protons at 4.77 and 4.74 ppm (Figure 2.8 and 2.9). IR spectroscopy reveals amine absorptions for $[\text{TpRu}(\text{PMe}_3)_2\text{NH}_2\text{Ph}][\text{OTf}]$ at 3285 and 3262 cm^{-1} . The complex $[\text{TpRu}\{\text{P}(\text{OMe})_3\}_2\text{NH}_2\text{Ph}]$ has IR absorptions for the amine ligand at 3318 and 3250 cm^{-1} . Cyclic voltammetry experiments reveal irreversible oxidation at 1.82 and 1.86 V (versus NHE) for $[\text{TpRu}(\text{PMe}_3)_2\text{NH}_2\text{Ph}][\text{OTf}]$ and $[\text{TpRu}\{\text{P}(\text{OMe})_3\}_2\text{NH}_2\text{Ph}][\text{OTf}]$ respectively, and the X-ray structure of $[\text{TpRu}(\text{PMe}_3)_2(\text{NH}_2\text{Ph})][\text{OTf}]$ reveal a pseudooctahedral coordination sphere (Figure 2.10). The data collection parameters and crystallographic data are listed in Appendix A. Additionally, selected bond distances and angles are displayed in Tables 2.1 and 2.2. The Ru-P bond distances are 2.3064(9) and 2.3116(10) Å. The Ru- $\text{N}_{\text{amine}}\text{-C}_{\text{ipso}}$ bond angle is 123.6(2), and the $\text{N}_{\text{amine}}\text{-C}_{\text{ipso}}$ bond distance is 1.444(5) Å. The Ru- N_{amine} bond distance (2.211(3) Å) is slightly longer than the Ru-N bond distances of the Tp ligand (average Ru-N bond distance for the three pyrazolyl rings is 2.142(5) Å). A shorter Ru-N bond distance is observed for the Tp nitrogen trans to the amine. Compared with the other two Ru-pyrazolyl bond distances (average 2.167(4) Å), the bond distance for the trans Ru-N (2.091(5) Å) is indicative of an amine trans effect. The ORTEP for the complex $[\text{TpRu}\{\text{P}(\text{OMe})_3\}_2\text{NH}_2\text{Ph}][\text{OTf}]$ indicates an amine orientation that is analogous to that of trimethylphosphine complex $[\text{TpRu}(\text{PMe}_3)_2\text{NH}_2\text{Ph}][\text{OTf}]$ (Figure 2.11). The Ru-P bond distances are 2.2336(6) and 2.2209(6) Å. The Ru- $\text{N}_{\text{amine}}\text{-C}_{\text{ipso}}$ bond angle (120.78(14)) is

slightly reduced compared with that of $[\text{TpRu}(\text{PMe}_3)_2\text{NH}_2\text{Ph}][\text{OTf}]$. The $\text{Ru-N}_{\text{amine}}$ bond distance ($2.1822(19) \text{ \AA}$) of $[\text{TpRu}\{\text{P}(\text{OMe})_3\}_2\text{NH}_2\text{Ph}][\text{OTf}]$ is shorter than that of the the complex $[\text{TpRu}(\text{PMe}_3)_2\text{NH}_2\text{Ph}][\text{OTf}]$ and is only slightly longer than the Ru-pyrazolyl bond distances (the average Ru-pyrazolyl bond distance is $2.139(31) \text{ \AA}$). As before, the Ru-N bond distance trans for the Tp nitrogen trans to the amine ligand ($2.0947(18) \text{ \AA}$) is shorter than the other two Ru-pyrazolyl bond distances (average bond distance of $2.1620(25) \text{ \AA}$).

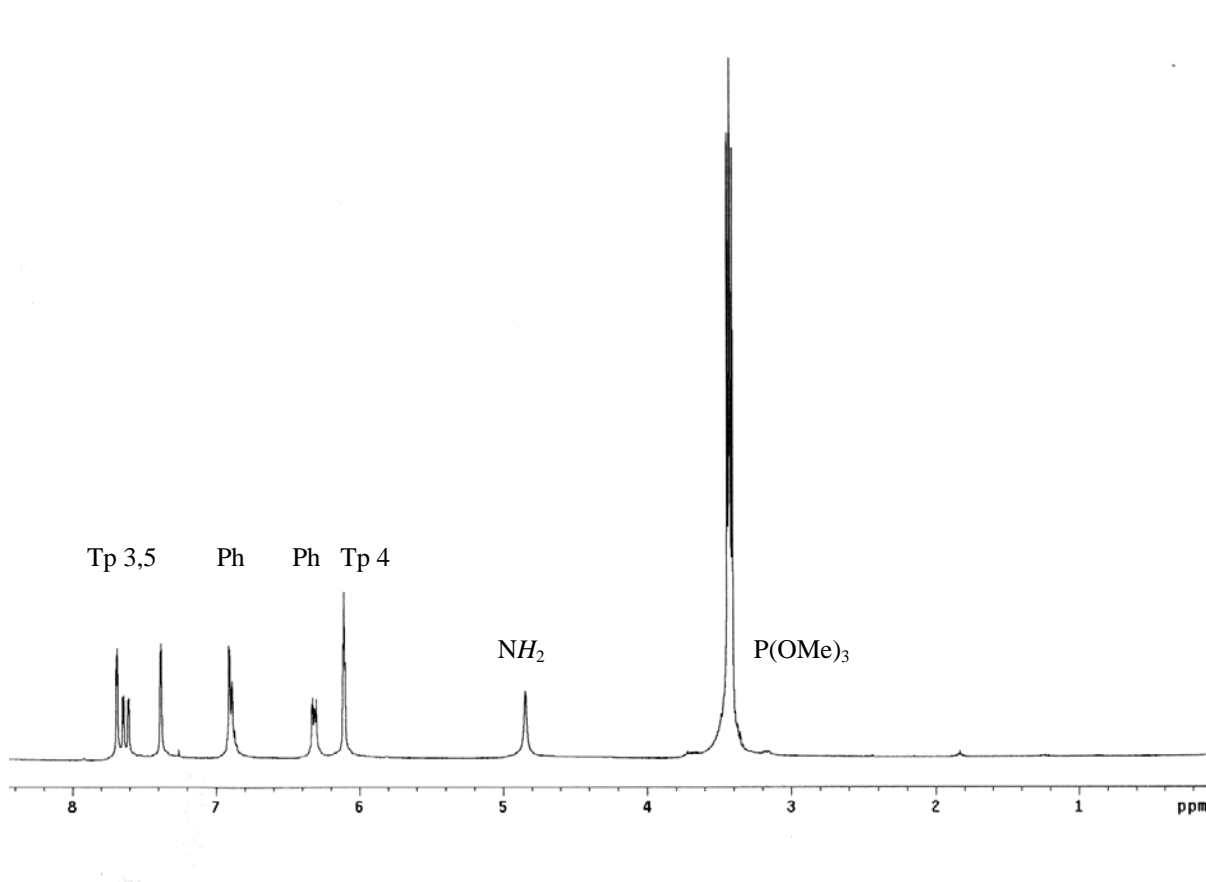


Figure 2.8 ^1H NMR spectrum of $[\text{TpRu}\{\text{P}(\text{OMe})_3\}_2\text{NH}_2\text{Ph}][\text{OTf}]$ in CDCl_3 .

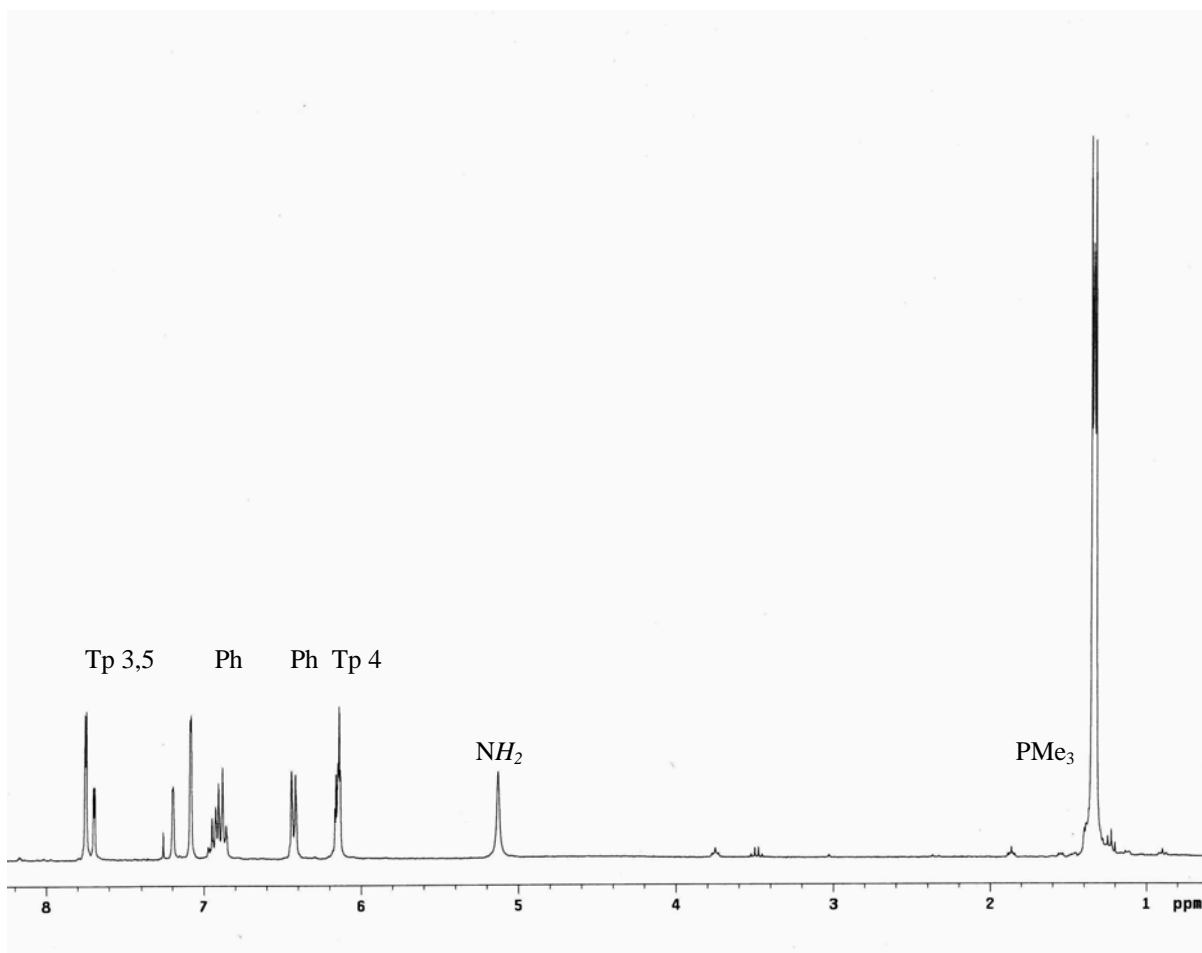


Figure 2.9 ^1H NMR spectrum of $[\text{TpRu}(\text{PMe}_3)_2\text{NH}_2\text{Ph}][\text{OTf}]$ in CDCl_3 .

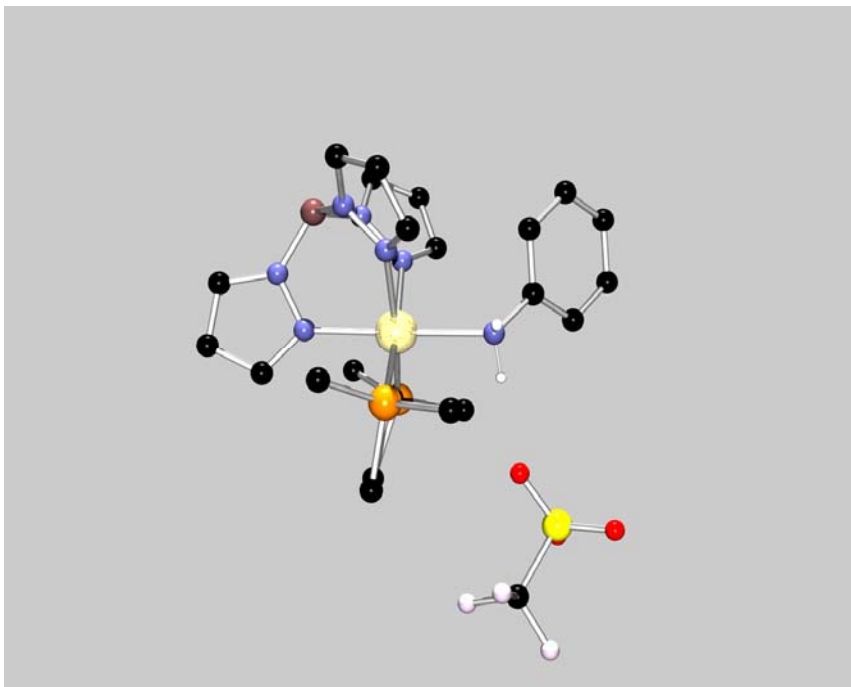


Figure 2.10 X-ray diagram of [TpRu(PMe₃)₂NH₂Ph][OTf].

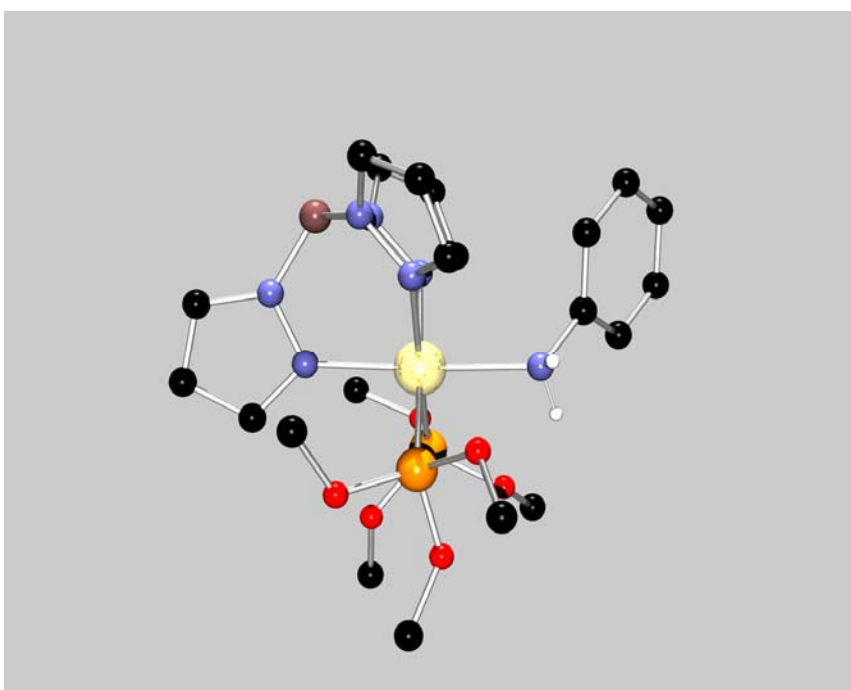


Figure 2.11 X-ray diagram of [TpRu{P(OMe)₃}₂NH₂Ph][OTf].

Table 2.1 Selected Bond Distances for [TpRuL₂NH₂Ph][OTf]

Atoms	L = PMe ₃	L = P(OMe) ₃
Ru-P1	2.3064(9)	2.2336(6)
Ru-P2	2.3116(10)	2.2209(6)
Ru-N1	2.091(3)	2.0947(18)
Ru-N3	2.176(3)	2.1620(18)
Ru-N5	2.158(3)	2.1620(18)
Ru-N7	2.211(3)	2.1822(19)
N7-C10	1.444(5)	1.451(3)

Table 2.2 Selected Bond Angles for [TpRuL₂NH₂Ph][OTf]

Atoms	L = PMe ₃	L = P(OMe) ₃
P1-Ru-P2	100.79(3)	9.29(2)
Ru1-N7-C10	123.6(2)	120.78(14)
N7-C10-C11	120.5(3)	119.4(2)
N7-C10-C15	119.6(3)	120.3(2)
N1-Ru-N3	86.77(11)	87.57(7)
N1-Ru-N5	88.65(11)	85.74(7)
N3-Ru-N5	83.02(11)	83.96(7)
N3-Ru-N7	90.51(11)	87.90(7)
P1-Ru-N7	88.71(8)	86.81(5)
P2-Ru-N7	95.79(9)	92.45(6)
N1-Ru-N7	176.74(11)	175.43(7)

Preparation of the dicarbonyl amine complex [TpRu(CO)₂(NH₂Ph)][PF₆] was accomplished by refluxing a mixture of the complex [TpRu(CO)₂(THF)][PF₆] with 10 equivalents of aniline in THF for 48 H. The phenyl amine complex [TpRu(CO)₂(NH₂Ph)][PF₆] is a pale gray solids. C_s symmetry (2:1 integration pattern for the Tp ligand) is observed in the ¹H NMR spectrum, and IR spectroscopy reveals ν_{CO} = 2084, 2022 cm⁻¹ and ν_{NH} = 3313, 3271 cm⁻¹.

The ammonia complexes [TpRu(PMe₃)₂NH₃][OTf] and [TpRu{P(OMe)₃}₂NH₃][OTf] were prepared by in situ generation of TpRu(L)(L)OTf in THF followed by addition of

excess ammonia. Workup by precipitation using hexanes or diethyl ether followed by filtration yielded clean products. The ^1H NMR spectra of the parent amine complexes $[\text{TpRu}(\text{PMe}_3)_2\text{NH}_3][\text{OTf}]$ and $[\text{TpRu}\{\text{P}(\text{OMe})_3\}_2\text{NH}_3][\text{OTf}]$ are consistent with C_s symmetry (2:1 Tp pyrazolyl resonances). Virtual triplets are observed for the PMe_3 and $\text{P}(\text{OMe})_3$ groups at 0.99 and 3.37 ppm respectively, and broad resonances for the ammine NH protons are observed at 2.34 and 2.09 ppm respectively. IR spectroscopy reveals ammine absorptions for the complex $[\text{TpRu}(\text{PMe}_3)_2\text{NH}_3][\text{OTf}]$ at 3123 and 3329 cm^{-1} . The NH absorption for the complex $[\text{TpRu}\{\text{P}(\text{OMe})_3\}_2\text{NH}_3][\text{OTf}]$ is observed at 3359 cm^{-1} . The complex $[\text{TpRu}(\text{PMe}_3)_2\text{NH}_3][\text{OTf}]$ has been characterized by X-ray spectroscopy. The structure reveals a pseudooctahedral coordination sphere (Figure 2.12). The data collection

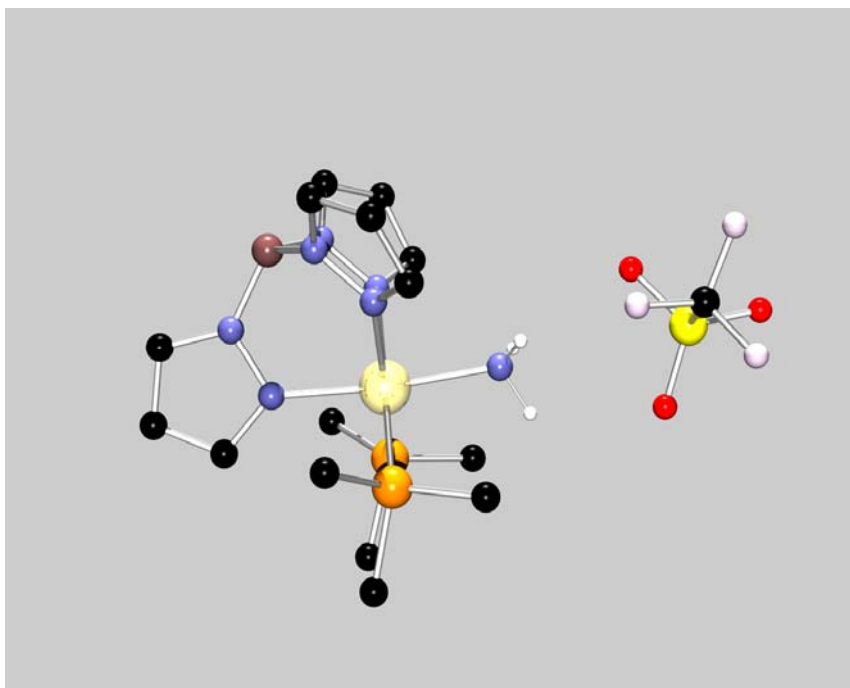


Figure 2.12 X-ray diagram of $[\text{TpRu}(\text{PMe}_3)_2\text{NH}_3][\text{OTf}]$.

parameters and crystallographic data are listed in Appendix A. The Ru-P bond distances are 2.2923(10) and 2.2916(10) Å, and the Ru-N_{amine} bond distance (2.136(3) Å) approximately equal than the Ru-N bond distances of the Tp ligand (average Ru-N bond distance for the three pyrazolyl rings is 2.129(5) Å). The shorter Ru-N (Tp) bond distance for the nitrogen trans to the amine (2.087(5) Å) compared with the other two Ru-pyrazolyl bond distances (average 2.151(4) Å) is indicative of an ammine trans effect.

Similar to the preparation of the ammonia complexes, the tert-butyl amine complexes [TpRu(PMe₃)₂NH₂^tBu][OTf] and [TpRu{P(OMe)₃}₂NH₂^tBu][OTf] were prepared by addition of excess tertbutyl amine to solutions TpRu(L)(L')OTf in THF that were generated in situ. Workup by precipitation using hexanes followed by isolation via filtration yielded clean products; however, the amine ligands of these complexes were found to be labile and readily dissociate in the presence of coordinating solvents such as CH₃CN. The ¹H NMR spectra of the tert-butyl amine complexes are consistent with C_s symmetry (2:1 Tp pyrazolyl resonances). Virtual triplets are observed for the PMe₃ and P(OMe)₃ at 1.28 and 3.41 ppm, respectively, broad resonances for the amine protons are observed at 2.55 and 2.59 ppm, and the ^tBu resonances are observed at 0.89 and 0.98 ppm, respectively.

Preparation of the dicarbonyl amine complex [TpRu(CO)₂(NH₂^tBu)][PF₆] was accomplished by refluxing a mixture of the complex [TpRu(CO)₂(THF)][PF₆] with an excess of tertbutyl amine in THF for 48 H. The tert-butyl amine complex [TpRu(CO)₂(NH₂^tBu)][PF₆] is a pale gray solid. C_s symmetry (2:1 integration) is observed in the ¹H NMR spectrum, and IR spectroscopy reveals ν_{CO} = 2084, 2022 cm⁻¹ and ν_{NH} = 3313, 3271 cm⁻¹.

2.3 Synthesis of Octahedral Ruthenium (II) Amido Complexes.

Deprotonation of the amine complexes was found to be the cleanest and most successful method to prepare the amido complexes. These reactions were carried out by low temperature (-78 °C) addition of the appropriate strong base to a THF solution of the amine complex. MeLi was used for all of the parent and ^tBu amine complexes, and NaN(SiMe₃)₂ was used to deprotonate the phenyl amine complexes. Work up for all of the amido complexes consisted of extraction into benzene or toluene followed filtration and removal of volatiles using vacuum. In addition, successful preparation of the amido complexes, particularly the parent and ^tBu amido complexes, required careful exclusion of all sources of water and air; otherwise incomplete conversion and/or decomposition was found to occur. Additionally, the parent and ^tBu amido complexes were found to react with solvents that possess acidic hydrogens, for example methanol, ethanol, methylene chloride, and chloroform.

The amido complexes are yellow solids that are air and moisture sensitive. Under inert atmosphere, the phenyl amido complexes TpRu(PMe₃)₂NHPh and TpRu{P(OMe)₃}₂NHPh are stable for up to one month; however, the complexes TpRu(PMe₃)₂NH₂ and TpRu(PMe₃)NH^tBu showed signs of decomposition after 1 day, and the complexes TpRu{P(OMe)₃}₂NH₂ and TpRu{P(OMe)₃}₂NH^tBu began to immediately decompose to multiple uncharacterized products. Where possible, the amido complexes have been characterized by ¹H NMR, ¹³C NMR, ³¹P NMR, and FT-IR spectroscopy. The most salient features of the ¹H NMR spectra are 2:1 integration for the complexes TpRuL₂NHR (L = PMe₃ or P(OMe)₃; R = H, Ph, or ^tBu) indicating C_s symmetry, and virtual triplets were

observed for the methyl protons of trimethylphosphine and trimethylphosphite. The amido resonances display upfield chemical shifts relative to amine complexes. Additionally, the phenyl amido complexes $\text{TpRu}(\text{PMe}_3)_2\text{NHPPh}$ and $\text{TpRu}\{\text{P}(\text{OMe})_3\}_2\text{NHPPh}$ display broad resonances for the aryl protons at room temperature. The nature of the broadening of the aryl resonances is discussed below.

The complex $\text{TpRu}\{\text{P}(\text{OMe})_3\}_2\text{NHPPh}$ has been characterized by X-ray crystallography. The structure shows a pseudooctahedral coordination sphere (Figure 2.13). The data collection parameters and crystallographic data are listed in Appendix A. The Ru-P bond distances are 2.2275(5) and 2.2186(5) Å. The Ru-N_{amido}-C_{ipso} bond angle {135.30(14)} is increased from the corresponding amine complex $[\text{TpRu}\{\text{P}(\text{OMe})_3\}_2\text{NH}_2\text{Ph}][\text{OTf}]$

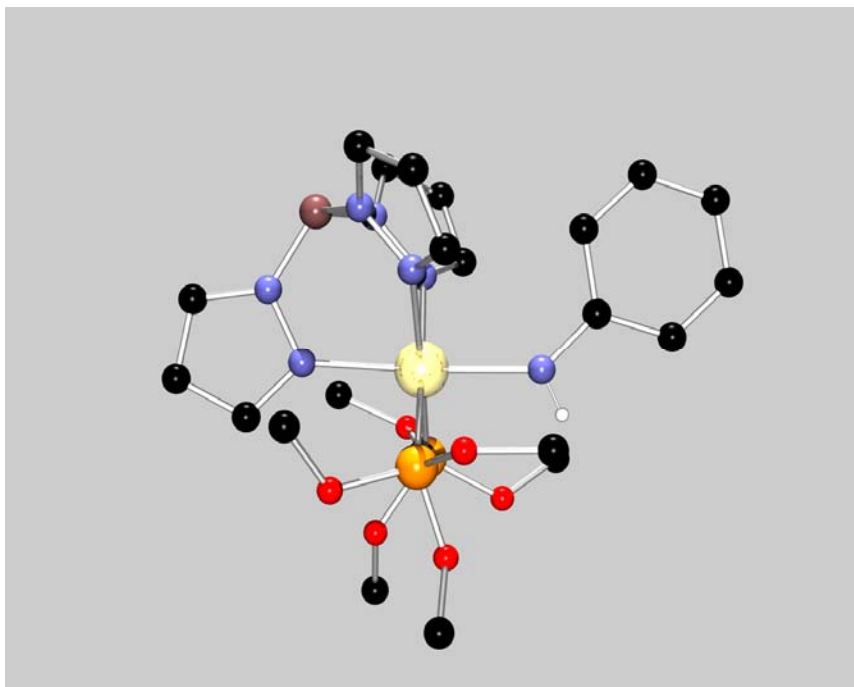
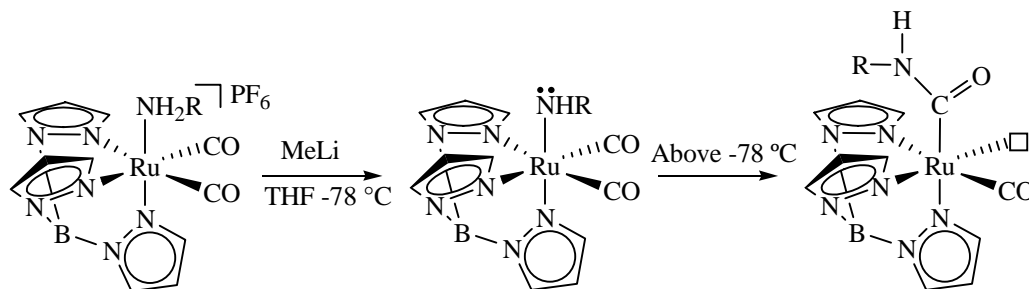


Figure 2.13 X-ray diagram of $\text{TpRu}\{\text{P}(\text{OMe})_3\}_2\text{NHPPh}$.

{120.78(14)}. The Ru-N_{amido} bond distance is {2.1012(15)} is shorter than the amine complex [TpRu{P(OMe)₃}₂NH₂Ph][OTf] {2.1822(19)Å}, and is shorter than the Ru-pyrazolyl bond distances (the average Ru-pyrazolyl bond distance is 2.1476(20) Å).

The amido complexes TpRu(CO)₂NHR (R = Ph, or ^tBu) have evaded isolation because the amido ligands of these complexes likely undergo CO insertion reactions (Scheme 2.11).⁴³ CO insertions involving late transition metal amido ligands are known.^{1,44,45}



Scheme 2.11 Proposed route of decomposition of TpRu(CO)₂NHR (R = Ph or ^tBu), CO insertion into the amido bond of TpRu(CO)₂NHR at elevated temperatures.

Although the amido complexes were not isolated, evidence for the formation of these complexes comes from in situ reactivity with the amido complex TpRu(CO)₂NHPh. For example, the addition of oxidants to low temperature solution of the anilido complex in solutions of THF results in aryl coupling to form [TpRu(CO)₂(NHC₆H₄-)]₂²⁺. Similar reactivity have been observed for the related anilido complexes TpRu(PMe₃)₂NHPh and TpRu{P(OMe)₃}₂NHPh (see Chapter 4). At temperatures above -78 °C, amido insertion into the carbonyl ligand likely occurs. The proposed CO insertion reaction is supported by IR spectroscopy. The starting aniline complex has CO absorptions of 2080 and 2020 cm⁻¹. Solutions of the putative amido complex that were allowed to warm to room temperature

exhibited a single broad CO absorption at 1960 cm^{-1} with an acyl absorption at 1650 cm^{-1} . These absorptions are consistent with amido insertion product in Scheme 2.11.

2.4 Electrochemical Studies of the Amido Complexes.

The preliminary studies of the amido complexes focused on determining the effect of the ancillary ligands and amido substituent on the electronic nature of the metal center. Cyclic voltammetry was performed on the complexes TpRu(L)(L')X , ($X = \text{Cl}, \text{NH}_2, \text{NHPh}$, or NH^tBu ; $L, L' = \text{P(OMe)}_3, \text{PMe}_3$ or $L = \text{CO}, L' = \text{PPh}_3$) and $[\text{TpRu(L)(L')X}][\text{OTf}]$, ($X = \text{NH}_3, \text{NH}_2\text{Ph}$, and NH_2^tBu ; $L, L' = \text{P(OMe)}_3, \text{PMe}_3$ or $L = \text{CO}, L' = \text{PPh}_3$). The experiments with complexes TpRu(L)(L')X ($X = \text{Cl}$ or OTf) and $[\text{TpRu(L)(L')X}][\text{OTf}]$, ($X = \text{NH}_3, \text{NH}_2\text{Ph}$, and NH_2^tBu) were conducted in CH_3CN using tetrabutylammonium hexafluorophosphate as an electrolyte and a scan rate of 100 mV/s . All potentials were referenced versus NHE using cobaltocenium hexafluorophosphate or ferrocene as an internal standard. Also, all experiments with the amido complexes were conducted as above except the experiments were performed in THF, and the electrolyte tetrabutylammonium hexafluorophosphate was dried under a dynamic vacuum at $140\text{ }^\circ\text{C}$ for 48 hours to remove all residual water.

The effect of the ligands on the Ru (III/II) potentials was as anticipated based on their respective donating/withdrawing ability. Specifically, more electron withdrawing ligand sets yielded less reduced metal centers. As such, the order of the RuIII/II reduction potential based on ancillary ligands was $\text{CO/PPh}_3 > \text{P(OMe)}_3 > \text{PMe}_3$. Interestingly, the amido substituent also has an effect on the III/II reduction potential. Amido ligands with aryl

substituents were found to yield less reduced metal centers (i.e. the III/II reduction potentials of the NH₂ amido complexes were more negative than the NHPPh amido complexes) (Table 2.3). Aryl substituents on the amido moiety are known to stabilize the amido ligands presumably due to the ability to delocalize electron density.^{6,46,47} This effect is observed as an increase in the reduction potential for the anilido complexes versus the parent amido complexes. Thus, the delocalization of the aryl substituents results in amido moieties which are less donating than their respective parent counterparts.

Table 2.3 III/II reduction potentials of the TpRu(L)(L') complexes

X =	Cl	OTf	NH ₃	NH ₂ Ph	NH ₂	NHPPh
L, L'						
CO/ PPh ₃	N/A	1.75	1.42	1.14	N/A	0.11*
P(OMe) ₃	0.97	1.28	1.4	1.86*	-0.34	-0.25
PMe ₃	0.64	1.00	1.08	1.82*	-0.47	-0.28

* = irreversible oxidation

2.5 ¹H NMR Chemical Shifts of the Amido Proton.

The parent amido complexes TpRu(PMe₃)₂NH₂, TpRu{P(OMe)₃}₂NH₂, and TpRu(CO)(PPh₃)NH₂ display upfield chemical shifts (¹H NMR) for the amido NH protons at -2.20, -1.91, and -1.79 ppm respectively. Dr. K. N. Jayaprakash has also prepared the amido complex [Li][TpRu(PPh₃)(NH₂)₂] and observed an upfield resonance at -2.60 ppm.⁴² Thus, a qualitative trend was observed in that the relative chemical shifts are consistent with the donating ability of L and L' ancillary ligands (Table 2.4). A similar trend was observed for the anilido complexes TpRu(PMe₃)₂NHPPh, TpRu{P(OMe)₃}₂NHPPh, and TpRu(CO)(PPh₃)NHPPh in that the relative NH chemical shifts were observed at 2.80, 1.98,

Table 2.4 ^1H NMR Chemical shifts of amido *NH* resonances

Complex	NHR resonance (ppm)
$\text{TpRu}(\text{PMe}_3)_2(\text{NH}_2)$	-2.20
$\text{TpRu}\{\text{P}(\text{OMe})_3\}_2(\text{NH}_2)$	-1.91
$\text{TpRu}(\text{CO})(\text{PPh}_3)(\text{NH}_2)$	-1.79
$[\text{Li}][\text{TpRu}(\text{PPh}_3)(\text{NH}_2)_2]$	-2.60
$\text{TpRu}(\text{PMe}_3)_2(\text{NHPh})$	2.80
$\text{TpRu}\{\text{P}(\text{OMe})_3\}_2(\text{NHPh})$	1.98
$\text{TpRu}(\text{CO})(\text{PPh}_3)(\text{NHPh})$	4.5

and 4.5 ppm. Additionally, downfield shifts were observed for these anilido complexes relative to parent amido systems. Thus, the more donating the amido moieties resulted in greater upfield chemical shifts for the *NH* resonances. This effect is likely due to increased electron density about the amido moiety. Thus, the chemical shift of the amido *NH* provides a qualitative predictor of the electron density on the amido. Using the shift of the *NH* resonance as a predictor could provide a rapid means of determining both the basicity and nucleophilicity of the amido moiety, and qualitatively we have observed that those complexes with greater upfield shifts are more basic/ nucleophilic. For example, our studies determined the parent amido complexes are much more reactive with regards to basic/ nucleophilic chemistry than the anilido complexes (see Chapter 3).

2.6 Variable Temperature ^1H NMR Spectra of the Amido Complexes.

For reversible processes that exchange NMR active nuclei, a quantitative description between the line shape and the kinetics of the dynamic process can be applied if the process

generates distinct Larmor frequencies for the nuclei.⁴⁸ Consider an equilibrium between A and B in which the resonance of nuclei exchanges.



The line shape of the resonance signal can be described by the equation

$$g(\nu) = [(1 + \tau\pi\Delta)P + QR] / (4\pi^2P^2 + R^2) \quad \text{Eq. 2.3}$$

where

$$P = (0.25\Delta^2) - \nu^2 + 0.25\delta\nu^2\tau + \Delta/4\pi$$

$$Q = [-\nu - 0.5(\rho_A - \rho_B) \delta\nu]\tau$$

$$R = 0.5(\rho_A - \rho_B) \delta\nu - \nu(1 + 2\pi\tau\Delta)$$

And

$$\tau = \tau_A\tau_B/(\tau_A + \tau_B)$$

τ_A, τ_B is the average time of nuclei in position A/B (s)

ρ_A, ρ_B is the molar fraction of components A and B

$\Delta\nu = \nu_A - \nu_B$ the difference in resonance frequencies (Hz)

Δ Width at half-height in the absence of exchange ($\tau \rightarrow \infty$)

ν Variable frequency (Hz)

Equation 2.3 is significant because it allows for the possibility of determining the rate constant of exchange for reactions in which the rate is too rapid for classical methods. Generally, this method is successful when the rate of exchange is between 10^{-1} Hz and 10^{-4} Hz or energy barrier to exchange is between approximately 5 kcal/mol and 25 kcal/mol.

Dynamic NMR methods are applicable to studies of internal dynamic or molecular structural changes such as inversions or rotations.

The complexity of equation 2.3 and difficulty in determining an accurate width at half height makes analysis using this equation difficult; however, workable approximate solutions are known. The most common approximation uses the coalescence temperature for exchange between equally populated sites ($\rho_A = \rho_B$). Under those conditions, the rate of exchange *at coalescence* can be calculated using equation 2.4.

$$k_{\text{coal.}} = \pi\Delta\nu/\sqrt{2} \quad \text{Eq. 2.4}$$

Using dynamic NMR techniques to determine the rate at coalescence, the Gibbs free energy of activation (ΔG^\ddagger) for the exchange process can be determined using the Eyring equation. This equation is derived from transition state theory, and it relates the rate of a process to temperature and free energy of activation (Equation 2.5).^{49,50}

$$k = k_b T/h * e^{(-\Delta G^\ddagger / RT)} \quad \text{Eq. 2.5}$$

where

T is the temperature (K)

R is the universal gas constant (8.31 J K⁻¹)

k_b is the Boltzmann constant (1.38 * 10⁻²³ J K⁻¹)

h is Planck's constant (6.63 * 10⁻³⁴ J s⁻¹)

Transition state theory assumes that for a reaction, for example $A + B \rightarrow C$, that the molecules collide to form an activated complex AB^\ddagger . This complex is unstable and will degenerate back to reagents or proceed to form bonds to make products. The energy required to generate the activated complex is the free energy of activation (ΔG^\ddagger) (Figure 2.14).

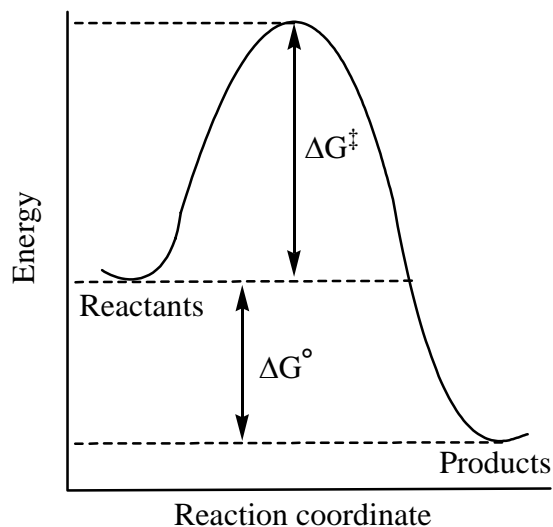


Figure 2.14 Transition state theory states the molecules collide to form an activated complex AB^\ddagger . The activation energy ΔG^\ddagger is the energy from reactants to AB^\ddagger .

Transition state theory also assumes the decomposition of the activated complex is extremely rapid, and using this statistical mechanics, the rate of decomposition is given by equation 2.6.

$$k^\ddagger = k_b T / h \nu \quad \text{Eq. 2.6}$$

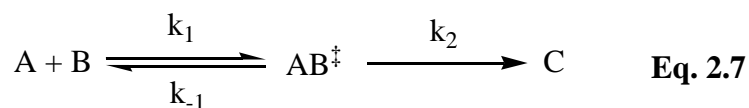
where

k_b is the Boltzmann constant ($1.38 \times 10^{-23} \text{ J K}^{-1}$)

T is the temperature (K)

h is Planck's constant ($6.63 \times 10^{-34} \text{ J s}^{-1}$)

In transition state theory, the activated complex is assumed to be in equilibrium with the starting materials (equation 2.7), and the rate of the reaction is given by equation 2.8.



$$\text{Rate} = \frac{k_b T}{h} \times K^\ddagger \quad \text{Eq. 2.8}$$

Additionally, the equilibrium constant of the reaction shown in equation 2.7 can be expressed by equation 2.9.

$$K^\ddagger = [AB^\ddagger]/[A][B] \quad \text{Eq. 2.9}$$

or

$$[AB^\ddagger] = K^\ddagger [A][B]$$

Substituting the above equation in to equation 2.8 these equations gives

$$k_r = \frac{k_b T}{h} \times K^\ddagger [A][B] \quad \text{Eq. 2.10}$$

Given $\Delta G^\ddagger = -RT \ln K^\ddagger$ or $K^\ddagger = e^{(-\Delta G^\ddagger / RT)}$ and the rate for a single step reaction can be expressed by rate = $k_r [A][B]$, substituting these equations into 2.10 yield the Eyring equation.

$$\text{Rate} = k_b T/h * e^{(-\Delta G^\ddagger / RT)} \quad \text{Eq. 2.11}$$

where

T is the temperature (K)

R is the ideal gas constant (8.31 J K⁻¹)

k_b is the Boltzmann constant (1.38 * 10⁻²³ J K⁻¹)

h is Planck's constant (6.63 * 10⁻³⁴ J s⁻¹)

$$\Delta G^\ddagger = RT[23.76 - \ln(k/T)] \quad \text{Eq. 2.12}$$

or

$$\Delta G^\ddagger = RT_{\text{coal}} [22.96 + \ln(T_{\text{coal}} / \delta v)] \quad \text{Eq. 2.13}$$

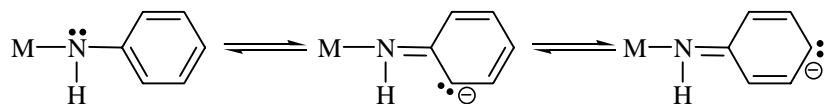
Equations 2.12 and 2.13 are simplified forms of that Eyring equation that are used to calculate the Gibbs free energy of activation of the chemical process, where T_{coal} is the coalescence temperature and $\delta\nu$ is the frequency difference in hertz. It should be noted the free energy of activation is temperature dependent since $\Delta G^\ddagger = \Delta H^\ddagger - T\Delta S^\ddagger$. Thus, comparisons of ΔG^\ddagger at different temperatures are only useful if the ΔS^\ddagger of the process is minimal.

In practice, the rate constant k is determined by monitoring a solution through a temperature range where, on the time scale of the experiment, the process transitions from the slow exchange to regime to rapid exchange. Careful observation near the coalescence temperature is needed to ensure this temperature is correct because it directly related to the energy of activation.

Since $\Delta\nu$ is dependent on the field strength, the coalescence temperature is also field dependent; stronger fields will increase the temperature of coalescence.

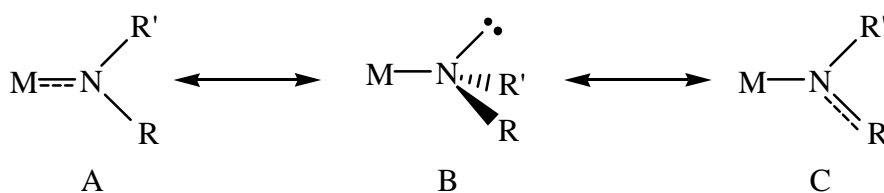
2.6.1 Dynamic ^1H NMR of the TpRu(L)(L')NPh Amido Complexes.

The phenyl ring of an anilido ligand can delocalize amido electron density into the aryl ring (Scheme 2.12).^{6,51,52} This rationalization has been employed to account for the



Scheme 2.12 Delocalization of the amido lone pair into an aryl substituent.

difference in pK_a between NHPH^- and NH_2^- .⁵³ The same rationalization has been used to account for a decreased reactivity/basicity of arylamido complexes as well as the thermodynamic preference for ligands that possess aryl substituents.^{6,46,47} The extent of multiple bond character can potentially be probed by dynamic NMR since the hindered N-C rotation will result from N=C double bonding character. In this examination, it is constructive to classify the ligand (Scheme 2.13).⁵⁴ In the first class (A), the amido ligand



Scheme 2.13 Amido bonding models. A. Donation to metal. B. Single bond with one lone pair. C. Ligand delocalization.

can effectively π -donate to the metal. This donation imparts multiple bonding character in the M-N bond. Class B is singly bonded with the amido lone pair localized on the nitrogen. With no electron delocalization, the reactivity of the amido ligand (basicity and nucleophilicity) is expected to be increased.⁵⁴ In class C, the lone pair is delocalized to the amido substituent(s). This delocalization should also impart multiple bonding character between the amido nitrogen and the substituent “R”.

The room temperature ^1H NMR spectrum of $\text{TpRu}(\text{PMe}_3)_2\text{NHPh}$ exhibits broadened resonances for the ortho protons of the amido phenyl group (Figure 2.15). Upon cooling, the

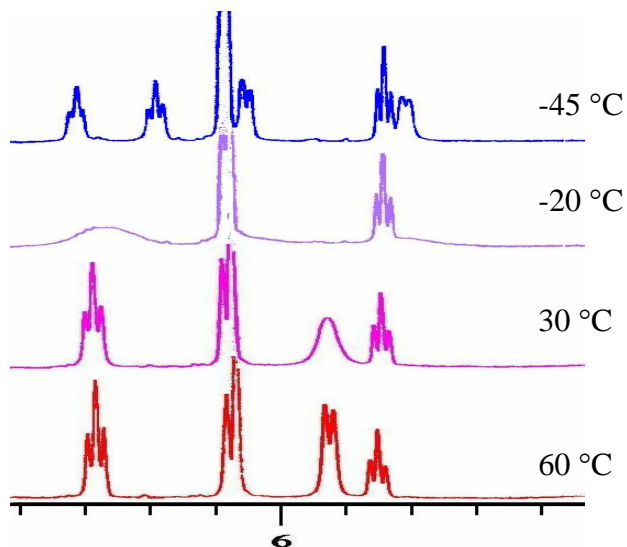
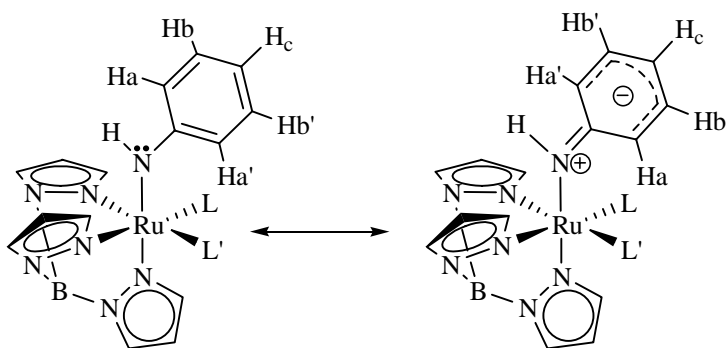


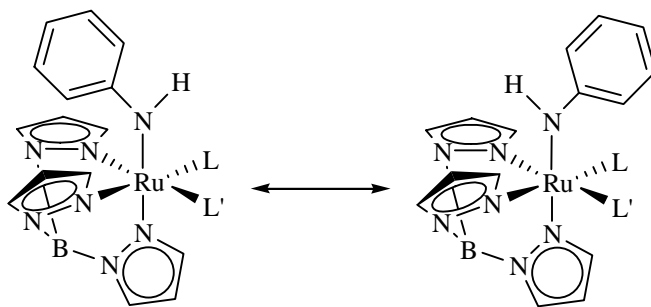
Figure 2.15 Variable temperature ^1H NMR spectroscopy of $\text{TpRu}(\text{PMe}_3)_2\text{NHPh}$.

resonances decoalesce into to doublets and the ^1H NMR spectrum at -45°C reveals five distinct resonances for the phenyl protons. Throughout the temperature range 60°C to -100°C , no changes are observed for the amido NH , anilido phenyl para hydrogen, Tp, or PMe_3 resonances (Figure 2.16). These observations are consistent with hindered rotation about the N-C_{ipso} bond ($\Delta G^\ddagger = 12.8$ kcal/mol) with rapid Ru-N bond rotation or a thermally preferred orientation (Scheme 2.14).⁵⁵



Scheme 2.14 Hindered rotation about the N-C_{ipso} bond and multiple bonding character results in broad aryl resonances in the ¹H NMR at room temperature.

The ¹H NMR spectra of TpRu{P(OMe)₃}₂NHPh exhibit similar results to approximately -50 °C. These observations are also attributed to hindered rotation about the N-C_{ipso} bond analogous to that of TpRu(PMe₃)₂NHPh ($\Delta G^\ddagger = 9.8$ kcal/mol). Continued cooling results in the broadening of the Tp, P(OMe)₃, and phenyl ortho, meta, and para resonances. This broadening is attributed to hindered Ru-N_{amido} bond rotation; however, the energy of activation of this process could not be determined because the slow exchange region could not be accessed (Scheme 2.15; Figure 2.16).⁵⁵



Scheme 2.15 Hindered rotation about the Ru-N_{amido} bond.

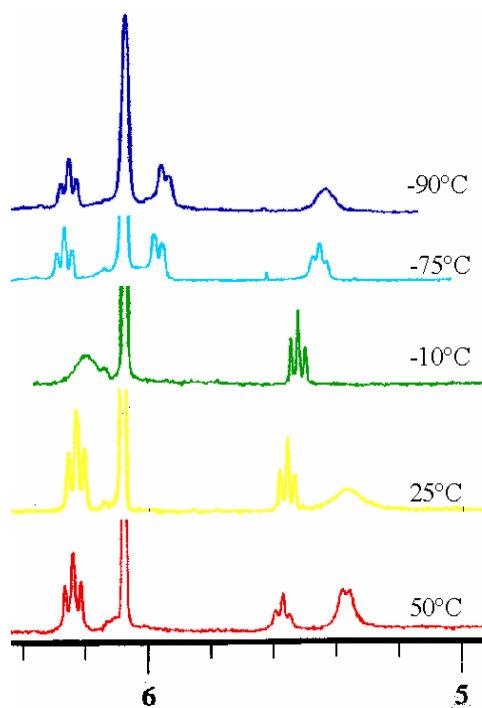


Figure 2.16 Variable temperature ^1H NMR spectra of $\text{TpRu}\{\text{P}(\text{OMe})_3\}_2\text{NHPH}$.

Additional work by Dr. K. N. Jayaprakash in the Gunnoe group has demonstrated that the complex $\text{TpRu}(\text{CO})(\text{PPh}_3)\text{NHPH}$ shows no evidence of hindered rotation about the $\text{N}-\text{C}_{\text{ipso}}$ bond down to $-100\text{ }^\circ\text{C}$. However, hindered rotational about the $\text{Ru}-\text{N}$ bond is observed.^{55,56} The rotational barriers for $\text{N}-\text{C}$ and $\text{Ru}-\text{N}$ for the series of $\text{TpRu}(\text{L})(\text{L}')$ anilido complexes are shown in Table 2.5.

Table 2.5 Rotational barriers about Ru-N and N-C bonds

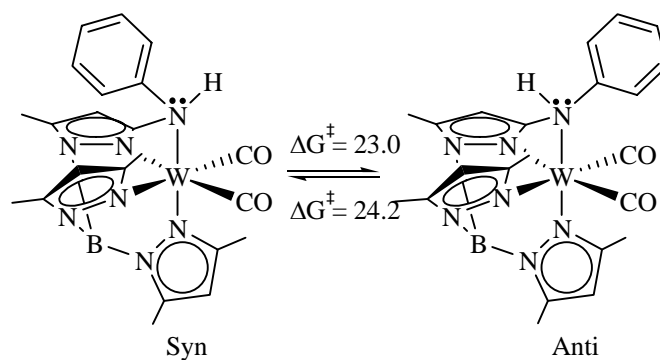
L/L'	Ru-N	N-C _{ipso}
CO/PPh ₃	12 kcal/mol	Not observed
P(OMe ₃)	≅ 9.5 kcal/mol	9.8 kcal/mol
P(Me ₃)	Not observed	12.8 kcal/mol

Hindered rotation about the N-C_{ipso} bond has been observed for other late transition metal anilido complexes.⁵⁴ For example, Flood et al. have report that the related d⁶ octahedral osmium phenyl amido system Os(PMe₃)₄(H)(NHPH) exhibits restricted rotation about the N-C_{ipso} bond, and this hindered rotation was attributed to steric interactions.⁵⁷ The rotational barrier for this process was not reported; however, the room temperature ¹H NMR spectrum has five distinct phenyl resonances, and the coalescence temperature for this rotational process was reported to be 100 °C. Thus, using this coalescence temperature to calculate activation barrier, ΔG[‡] is approximately 18 kcal/mol. Also, electron-withdrawing substituents at the para position of the anilido ligand of Os(PMe₃)₄(H)(*p*-NHC₆H₄R) were reported to decrease the temperature of coalescence. This observation suggests a strong electronic effect on this rotation; however, this cannot be demonstrated definitively because it does not rule out the possibility of Os-N rotation. Specifically, coalescence of four aryl resonances to two resonances would be anticipated for both processes.

Our observations are also inconsistent with the Ru-N rotation attributable solely to steric factors since the barrier for TpRu(PMe₃)₂NHPH is less than TpRu{P(OMe)₃}₂NHPH. Based on the cone angles, the PMe₃ (118 °) complex should be more sterically hindered than

the P(OMe)₃ (107 °) complex.⁵⁸ However, as classified above in Scheme 2.13, the Ru-N rotational barrier should be greater for metal centers that can more effectively π -accept. The observed trend for our Ru(II) amido complexes and the Flood's Os(II) amido systems are consistent with this trend in that less electron rich metal centers have a lower ΔG^\ddagger for M-N rotation.

One difficulty with the above rationalization is an uncertainty of the ability of a d^6 metal center to π -accept because these metal centers have filled orbitals of π -symmetry. Another possible rationalization for the observed trend in bond rotation (both M-N and N-C_{ipso}) involves a three-center, four-electron type of interaction between a metal orbital of π -symmetry, the amido lone pair, and the aryl substituent (Scheme 2.16). This interaction would result in a bonding orbital consisting of an ancillary ligand, a metal $d\pi$ -orbital, and the amido lone pair. This bonding interaction allows for restricted M-N bond rotation which is not attributable to steric influences occurs between the M-N bond. The three-center, four-electron would also result in a nonbonding amido lone and an antibonding orbital. More donating ancillary ligands would raise the energy the metal π -orbital, thus decreasing the mixing of this three-center interaction which would results in a decreased Ru-N bond order thus resulting in a decreased rotational barrier for this bond. As the ancillary ligand become more withdrawing, the energy of the metal π -orbital is decrease making it of more appropriate energy to undergo the three-center bonding.

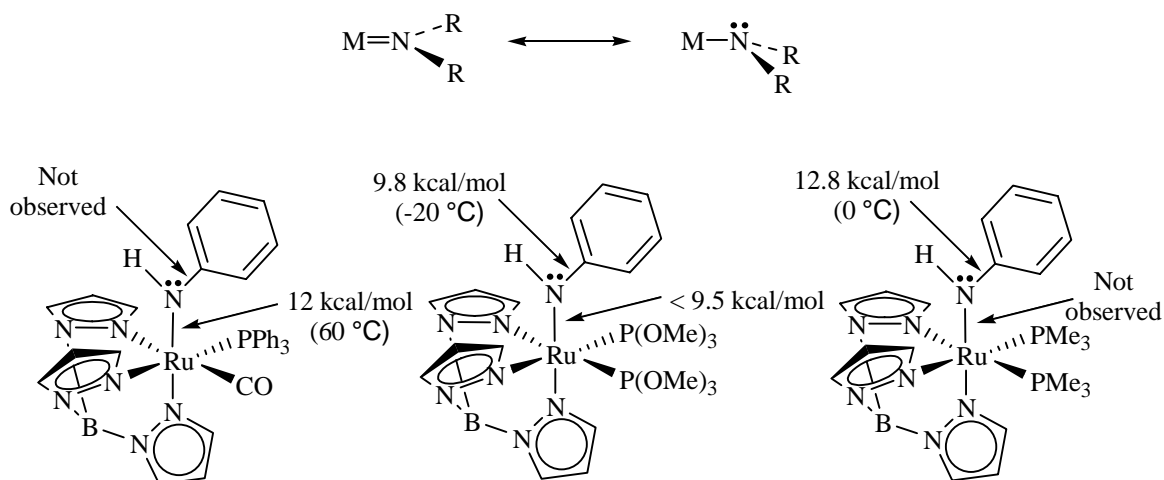


Scheme 2.17 Hindered rotation in $\text{Tp}^*\text{W}(\text{CO})_2\text{NHPH}$. The barrier to rotation is anticipated to be larger for the d^4 metal center compared to d^6 complexes because the amido ligand can more effectively π -donate.

electron count of the ruthenium complexes which disrupts amido to metal π -donation. However, the role of sterics is complicated by the presence of the more sterically imposing Tp^* ligand of the $\text{Tp}^*\text{W}(\text{CO})_2(\text{NHR})$ systems.

By comparison, the barrier to amido rotation for the isoelectronic $\text{CpRe}(\text{NO})(\text{PPh}_3)(\text{NMe}_2)$ complex has been determined to be 7.8 kcal/mol.⁶⁰ The difference in activation barriers between the TpRu anilido and $\text{CpRe}(\text{NO})(\text{PPh}_3)(\text{NMe}_2)$ is likely a result of the larger steric profile of the Tp ligand versus the Cp ligand.

While only a small data set is available, the rotational barriers for the series of $\text{TpRu}(\text{L})(\text{L}')\text{NHPH}$ systems demonstrate an inverse between Ru-N and N-C rotational barrier (Table 2.5). As the electron density increases at the metal center, so does the N-C rotational barrier, and this effect is concurrent with decrease in the rotational barrier about the Ru-N bond. We have rationalized these observations using a qualitative picture wherein the ligand to metal donation is increased for more accepting systems (Scheme 2.18).



Scheme 2.18 Summary of bond rotational barriers for the TpRu(L)(L)NHPPh amido complexes.

2.7 General Experimental Methods.

All reactions and procedures were performed under anaerobic conditions in a nitrogen-filled glovebox or by using standard Schlenk techniques. Glovebox purity was maintained by periodic nitrogen purges and monitored by an oxygen analyzer $\{\text{O}_2(\text{g}) < 15 \text{ ppm, for all reactions}\}$. Hexanes were purified by passage through a column of activated alumina. THF, toluene, benzene, and diethyl ether were dried by distillation over sodium/benzophenone. Benzene- d_6 and CD_3CN were purified by distillation from CaH_2 , degassed, and stored over 4 Å sieves. CDCl_3 and CD_2Cl_2 were degassed via three freeze-pump-thaw cycles and stored over 4 Å sieves. ^1H and ^{13}C NMR spectra were obtained on a Varian Mercury 300 MHz, Varian Mercury 400 MHz or General Electric 300 MHz spectrometer. Resonances due to the Tp ligand are reported by chemical shift and multiplicity only. All $^3J_{\text{HH}}$ values for the pyrazolyl rings are 2 Hz. All ^1H and ^{13}C NMR

spectra were referenced against tetramethylsilane using residual proton signals (^1H NMR) or the ^{13}C resonances of the deuterated solvent (^{13}C NMR). ^{31}P NMR spectra were obtained on a Varian 300 MHz spectrometer and referenced against external 85% H_3PO_4 . All variable-temperature NMR experiments were performed on a General Electric 300 MHz, Varian Mercury 300 MHz, or Varian Mercury 400 MHz spectrometer. UV-vis spectra were obtained on a Varian Cary 3E spectrophotometer. IR spectra were obtained on a Mattson Genesis II spectrometer either as thin films on a KBr plate or in a solution using a KBr solution plate. Electrochemical experiments were performed under a nitrogen atmosphere using a BAS Epsilon Potentiostat. Cyclic voltammograms were recorded in a standard three-electrode cell from -2.00 to +2.00 V with a glassy carbon working electrode and tetrabutylammonium hexafluorophosphate as an electrolyte. Tetrabutylammonium hexafluorophosphate was dried under a dynamic vacuum at 110 °C for 48 h prior to use. All potentials are reported versus NHE (normal hydrogen electrode) using cobaltocenium hexafluorophosphate of ferrocene as an internal standard. Elemental analyses were performed by Atlantic Microlabs, Inc. $\text{Li}\{(\text{NC})_2\text{CH}\}$ was generated by the reaction of malononitrile with 1 equiv of *n*-BuLi in benzene followed by vacuum filtration to collect the resulting white precipitate. All other reagents were used as purchased from commercial sources.

TpRu(PMe₃)₂Cl. A mixture of TpRu(PPh₃)₂Cl (9.59 g, 10.47 mmol) and trimethylphosphine (5.0 ml, 48 mmol) were refluxed in approximately 500 mL of toluene for 48 hours. The solution was subsequently cooled to room temperature, and the solution was concentrated under reduced pressure to approximately 150 mL. Approximately 200 ml dry, degassed hexanes were added slowly to precipitate the complex. The resulting mixture was

filtered and washed with hexanes 3 x 20 mL and ether 3 x 20 mL. A yellow solid was isolated and dried in vacuo (5.25g, 95% yield). ^1H NMR (CDCl_3 , δ): 7.97, 7.75, 7.67, 7.36 (6H, 2:1:1:2 integration, each a d, Tp CH 3 and 5 position), 6.18, 6.14 (3H 2:1 integration, each a t, Tp CH 4 position), 1.42 (18H, vt, $J_{\text{PH}} = 10\text{Hz}$, $\text{P}(\text{CH}_3)_3$). $^{13}\text{C}\{^1\text{H}\}$ NMR (CDCl_3 , δ): 145.0, 143.3, 136.1, 134.7 (Tp 3 or 5 position), 105.4, 105.0 (Tp 4 position), 18.0 (t, $J_{\text{PC}} = 12\text{Hz}$, $\text{P}(\text{CH}_3)_3$). $^{31}\text{P}\{^1\text{H}\}$ NMR (benzene- d_6 , δ): 14.8 (s, $\text{P}(\text{CH}_3)_3$). CV (CH_3CN , TBAH, 100 mV/s): $E_{1/2} = 0.64\text{ V}$ {Ru(III/II)}. Anal. Calculated for $\text{C}_{16}\text{H}_{28}\text{BClN}_6\text{P}_2\text{Ru}$: C, 35.91; H, 5.62; N, 16.75; Found: C, 36.36; H, 5.76; N, 16.56.

TpRu{P(OMe)₃}₂Cl. A mixture of TpRu(PPh₃)₂Cl (6.69 g, 7.68 mmol) and trimethylphosphite (10.0 ml, 84 mmol) were refluxed in approximately 500 mL of toluene for 48 hours. The solution was subsequently cooled to room temperature, and the solution was concentrated under reduced pressure to approximately 100 mL. Approximately 200 ml dry, degassed hexanes were added slowly to precipitate the complex. The resulting mixture was filtered and washed with hexanes 3 x 10 mL and ether 3 x 10 mL. A yellow solid was isolated and dried in vacuo (3.98g, 87% yield). ^1H NMR (benzene- d_6 , δ): 8.42, 8.06, 7.50, 7.49 (6H, 2:1:2:1 integration, each a d, Tp CH 3 and 5 position), 6.00, 5.88 (3H 2:1 integration, each a t, Tp CH 4 position), 3.29 (18H, vt, $J_{\text{PH}} = 10\text{Hz}$, $\text{P}(\text{OCH}_3)_3$). $^{13}\text{C}\{^1\text{H}\}$ NMR (CDCl_3 , δ): 147.8, 144.2, 136.3, 134.6 (each a s, Tp 3 or 5 position), 105.7, 105.5 (each a s, Tp 4 position), 51.6 (s, $\text{P}(\text{OCH}_3)_3$). $^{31}\text{P}\{^1\text{H}\}$ NMR (benzene- d_6 , δ): -15.0 (s, $\text{P}(\text{OCH}_3)_3$). CV (CH_3CN , TBAH, 100 mV/s): $E_{1/2} = 0.97\text{ V}$ {Ru(III/II)}. Anal. Calculated for $\text{C}_{15}\text{H}_{28}\text{BClN}_6\text{O}_6\text{P}_2\text{Ru}$: C, 30.14; H, 4.74; N, 14.06; Found: C, 30.23; H, 4.77; N, 14.06.

TpRu(PMe₃)₂OTf. To a yellow solution of TpRu(PMe₃)₂Cl (0.5450 g 1.087 mmol) in THF (30 mL) AgOTf (0.2800 g 1.087 mmol) was added and stirred. Immediately after addition a color change from pale yellow to red was observed. Additionally, the formation of a precipitate was noted after approximately 5 minutes. The solution is refluxed for 19 hours, then filtered through a fine porosity frit. The volatiles are removed under reduced pressure and product is extracted into benzene, filtered, washed with hexanes and ether, and dried in vacuo. The product is a pale yellow solid that is stable under inert atmosphere. (0.6200 g, 93% yield). ¹H NMR (benzene-*d*₆, δ): 8.04, 7.72, 7.69, 7.15 (6H, 2:1:2:1 integration, each a d, Tp CH 3 and 5 position), 6.24, 6.10 (3H 2:1 integration, each a t, Tp CH 4 position), 1.41 (18H, vt, J_{PH} = 11Hz, P(CH₃)₃). ¹³C{¹H} NMR (CDCl₃, δ): 147.8, 144.2, 136.3, 134.6 (each a s, Tp 3 or 5 position), 105.7, 105.5 (each a s, Tp 4 position), 51.6 (s, P(CH₃)₃). ³¹P{¹H} NMR (benzene-*d*₆ δ): 14.3 (s, P(CH₃)₃). CV (CH₃CN, TBAH, 100 mV/s): E_{1/2} = 1.0 V {Ru(III/II)}. Anal. Calculated for C₁₆H₂₈BF₃N₆O₃P₂RuS: C, 31.23; H, 4.59; N, 13.66; Found: C, 31.75; N, 4.66; N, 13.46.

TpRu{P(OMe)₃}₂OTf. To a yellow solution of TpRu{P(OMe)₃}₂Cl (0.1990 g 0.3335 mmol) in THF (20 mL) AgOTf (0.0860 g 0.3347 mmol) was added and stirred. . Immediately after addition a color change from pale yellow to dark yellow was observed. Additionally, the formation of a precipitate was noted after approximately 5 minutes. The solution is refluxed for 20 hours, then filtered through a fine porosity frit. The volatiles are removed under reduced pressure and product is extracted into benzene, filtered, washed with hexanes and ether, and dried in vacuo. The product is a pale yellow solid that is stable under inert atmosphere. (0.6200 g, 93% yield). ¹H NMR (benzene-*d*₆, δ): 8.57, 7.70, 7.49, 7.36 (6H,

2:1:2:1 integration, each a d, Tp CH 3 and 5 position), 6.07, 5.72 (3H 2:1 integration, each a t, Tp CH 4 position), 3.18 (18H, vt, $J_{\text{PH}} = 11\text{Hz}$, $\text{P}(\text{CH}_3)_3$). $^{13}\text{C}\{^1\text{H}\}$ NMR (CDCl_3 , δ): 147.8, 144.2, 136.3, 134.6 (each a s, Tp 3 or 5 position), 105.7, 105.5 (each a s, Tp 4 position), 51.6 (s, $\text{P}(\text{CH}_3)_3$). $^{31}\text{P}\{^1\text{H}\}$ NMR (benzene- d_6 δ): -19.6 (s, $\text{P}(\text{OCH}_3)_3$). CV (CH_3CN , TBAH, 100 mV/s): $E_{1/2} = 1.28\text{ V}$ {Ru(III/II)}.

TpRu(CO)(PPh₃)(OTf). To a yellow solution (1:1 v/v THF/ CH_2Cl_2 , 30 mL) of TpRu(CO)(PPh₃)(Cl) (0.6401 g, 1.016 mmol) was added a solution of AgOTf (0.261 g, 1.016 mmol dissolved in THF). The solution was stirred at room temperature for approximately 36 h, during which time the formation of a white precipitate (AgCl) was noted. The resulting pale yellow slurry was vacuum-filtered through a fine-porosity frit in order to remove the precipitate, and the volatiles were removed from the filtrate in vacuo. The resulting yellow solid was washed with diethyl ether and hexanes, dried in vacuo, and isolated (95% yield, 0.725 g). IR (thin film on KBr plate): $\nu_{\text{CO}} = 1986\text{ cm}^{-1}$. ^1H NMR (benzene- d_6 , δ): 8.99, 7.41, 7.37, 7.19, 7.06, 6.43 (each 1H, each a d, Tp CH 3 and 5 position), 5.78, 5.64, 5.25 (each 1H, each a t, Tp CH 4 position), 7.33, 6.95 (15H, each a m, $\text{P}(\text{C}_6\text{H}_5)_3$). $^{13}\text{C}\{^1\text{H}\}$ NMR (benzene- d_6 , δ): 203.6 (d, $^2J_{\text{PC}}$) 15 Hz, CO), 147.9, 146.8, 144.1 (each a s, Tp CH's), 137.5, 136.6, 135.7, 134.7, 134.5, 131.8, 131.2, 131.0, 129.1, 129.0 (resonances due to PPh₃, and Tp CH's, with J_{PC} to ispo, ortho, and meta PPh₃ carbons would expect a total of 10 lines due to 7 resonances), 107.5, 106.9 (2:1, coincidental overlap for first resonance, Tp 4 position CH's). $^{31}\text{P}\{^1\text{H}\}$ NMR (CD_2Cl_2 , δ): 39.0. CV (CH_3CN , TBAH, 100 mV/s): $E_{1/2} = 1.75\text{ V}$ {Ru(III/II)}. Anal. Calcd for $\text{C}_{29}\text{H}_{25}\text{BF}_3\text{N}_6\text{O}_4\text{PRuS}$: C, 46.23; H, 3.34; N, 11.15. Found: C, 46.27; H, 3.47; N, 11.12.

[TpRu(PMe₃)₂(NH₃)] [OTf]. In a 100 mL round bottom flask TpRu(PMe₃)₂OTf (1.030 g, 1.672 mmol) was dissolved in approximately 50 mL of THF. To the yellow solution, excess NH₃ dissolved in THF was added and the solution was stirred for 24 hours. The reaction was concentrated to 20 mL and approximately 60 mL of hexanes was added to precipitate the product. The precipitate was collected via filtration through a fine porosity frit and washed with hexanes (3 x 10 mL) to give a white solid. (1.00 g, 95%) IR (thin film on KBr plate): $\nu_{\text{BH}} = 2479 \text{ cm}^{-1}$, $\nu_{\text{NH}} = 3123, 3329 \text{ cm}^{-1}$. ¹H NMR (CD₃CN, δ): 7.89 (2H, d, Tp CH 3 and 5 position), 7.35-7.33 (3H, over-lapping d, Tp CH 3 and 5 position), 6.81 (1H, d, Tp CH 3 and 5 position), 5.99, (2H, t, Tp CH 4 position), 5.71(1H, t, Tp CH 4 position), 2.34 (3H, bs, NH₃), 0.99 (18H, vt, $J_{\text{PH}} = 10 \text{ Hz}$, P(CH₃)₃). ¹³C{¹H} NMR (CD₃CN, δ): 147.7, 143.8, 138.1, 137.5 (each a s, Tp 3 or 5 position), 105.5, 105.2 (each a s, Tp 4 position) 18.2 (t, $J_{\text{PC}} = 12 \text{ Hz}$, P(CH₃)₃). ³¹P{¹H} NMR (CD₃CN, δ): 14.5 (P(CH₃)₃). CV (CH₃CN, TBAH, 100 mV/s): $E_{1/2} = 1.08 \text{ V}$ {Ru(III/II)}. Anal. Calcd for C₁₆H₃₀BF₃N₇O₃PRuS: C, 29.92; H, 4.70; N, 15.26. Found: C, 30.57; H, 4.97; N, 15.42.

[TpRu{P(OMe)₃}₂(NH₃)] [OTf]. In a 100 mL round bottom flask, a solution of TpRu{P(OMe)₃}₂Cl (1.2549 g, 2.102 mmol) in approximately 50 mL of THF was reacted with a solution of AgOTf (0.5413 g 2.108 mmol) dissolved in 15 mL of THF. The reaction was refluxed for 20 hours. During the course of the reaction the formation of a white precipitate (AgCl) was noted. The reaction was cooled to room temperature, then filtered through a fine porosity frit. To the yellow filtrate, excess NH₃ dissolved in THF was added and the reaction was stirred for 24 hours during which time a color change to pale pink was observed. The reaction was concentrated to 40 mL and approximately 40 mL of hexanes was

added to precipitate the product. The precipitate was collected via filtration through a fine porosity frit and washed with hexanes (3 x 10 mL) to give a white solid. (1.134 g, 74%). IR (thin film on KBr plate): $\nu_{\text{NH}} = 3359 \text{ cm}^{-1}$. ^1H NMR (CD_2Cl_2 , δ): 7.79 (4H, overlapping m, Tp CH 3 and 5 position), 7.75-7.63 (each a 1H, d, Tp CH 3 and 5 position), 6.32 (2H, t, Tp CH 4 position), 5.99, (1H, t, Tp CH 4 position), 3.37 (18H, vt, $J_{\text{PH}} = 10 \text{ Hz}$, $\text{P}(\text{OCH}_3)_3$), 2.09 (3H, bs, NH_3). $^{13}\text{C}\{^1\text{H}\}$ NMR (CD_3CN , δ): 148.7, 144.6, 138.2, 137.3 (each a s, Tp 3 or 5 position), 107.6, 107.5 (each a s, Tp 4 position) 53.2 (s, $\text{P}(\text{OCH}_3)_3$). $^{31}\text{P}\{^1\text{H}\}$ NMR (CD_3CN , δ): -21.0 (s, $\text{P}(\text{OCH}_3)_3$). CV (CH_3CN , TBAH, 100 mV/s): $E_{1/2} = 1.40 \text{ V}$ {Ru(III/II)}. Anal. Calcd for $\text{C}_{16}\text{H}_{31}\text{BF}_3\text{N}_7\text{O}_6\text{PRuS}$: C, 26.39; H, 4.29; N, 13.46. Found: C, 26.22; H, 4.23; N, 13.23.

[TpRu(PMe₃)₂(NH₂^tBu)][OTf]. To a solution of TpRu(PMe₃)₂Cl (0.3364 g, 0.671 mmol) in approximately 30 mL of THF was added AgOTf (0.1732 g, 0.674 mmol). The resulting red solution was refluxed for 18 h. During the reaction, the formation of a white precipitate (AgCl) was noted. The solution was cooled to room temperature and filtered through a fine porosity frit. To the filtrate was added ^tBuNH₂ (0.37 g, 5.1 mmol), and the mixture was allowed to stir for an additional 24 h. The solution was concentrated to approximately 20 mL in vacuo, and diethyl ether (approximately 40 mL) was added to precipitate the product. The product was collected via vacuum filtration through a fine porosity frit and washed with diethyl ether (3 × 10 mL) to give a white solid. The solid was dried in vacuo and isolated (0.1368 g, 0.1987 mmol, 30%). ^1H NMR (CD_3CN , δ): 8.02, 7.91, 7.78, 7.35 (6H, 2:2:1:1 integration, each a d, Tp CH 3 and 5 position), 6.37, 6.17 (3H, 2:1 integration, each a t, Tp CH 4 position), 2.55 (2H, br s, NH), 1.28 (18H, vt, $N = 6 \text{ Hz}$,

$P(CH_3)_3$), 0.84 (9H, s, tBu). In THF- d_8 : 8.10, 7.89, 7.76, 7.40 (6H, 2:2:1:1 integration, each a d, Tp CH 3 and 5 position), 6.36, 6.14 (4H, 2:1 integration, each a t, Tp CH 4), 3.17 (2H, bs, NH_2^tBu), 1.33 (18H, vt, $N = 12$ Hz, $P(CH_3)_3$), 0.89 (9H, s, NH_2^tBu). $^{13}C\{^1H\}$ NMR (CD_3CN , δ): 148.2, 146.0, 138.7, 137.7 (Tp 3 or 5 position), 107.7, 107.1 (Tp 4 position), 53.8 ($C(CH_3)_3$), 31.7 ($C(CH_3)_3$), 18.7 ($P(CH_3)_3$). IR (thin film on KBr): $\nu_{NH} = 3262, 3114\text{ cm}^{-1}$, $\nu_{BH} = 2522\text{ cm}^{-1}$. $^{31}P\{^1H\}$ (CD_3CN , δ): 12.1. CV (CH_3CN , 100 mV/s): $E_{1/2} = 1.13$ V. Anal. Calcd for $C_{20}H_{38}BF_3N_7O_3P_2RuS$: C, 34.89; N, 14.24; H, 5.71. Found: C, 34.80; N, 14.02; H, 5.78

[TpRu{P(OMe) $_3$ } $_2$ (NH_2^tBu)][OTf]. A THF (50 mL) solution of TpRu{P(OMe) $_3$ } $_2$ Cl (0.6747 g, 1.129 mmol) and AgOTf (0.3050 g, 1.187 mmol) was refluxed for 24 h. The mixture was allowed to cool to room temperature and passed through a plug of Celite. To the yellow filtrate was added tBuNH_2 (1.19 mL, 11.3 mmol). The solution was stirred at room temperature for approximately 24 h. The solvent volume was reduced in vacuo to approximately 10 mL, and 20 mL of diethyl ether was added. The resulting white precipitate was collected and washed with four 20 mL portions of diethyl ether (0.4913 g, 56% yield). 1H NMR (CD_2Cl_2 , δ): 7.98, 7.85, 7.72, 7.66 (6H, 2:2:1:1 integration, each a d, Tp CH 3 and 5 position), 6.37, 6.15 (3H, 2:1 integration, each a t, Tp CH 4 position), 3.41 (18H, vt, $N = 10$ Hz, $P(OCH_3)_3$), 2.59 (2H, br s, NH), 0.98 (9H, s, tBu). $^{13}C\{^1H\}$ NMR ($CDCl_3$, δ): 147.7, 144.2, 137.1, 136.5 (Tp 3 or 5 position), 106.4, 106.3 (Tp 4 position), 53.0 (d, $^2J_{PC} = 5$ Hz, $P(OCH_3)_3$), 52.5 ($C(CH_3)_3$), 30.2 ($C(CH_3)_3$). IR (thin film on KBr): $\nu_{NH} = 3313, 3266\text{ cm}^{-1}$; $\nu_{BH} = 2498\text{ cm}^{-1}$. $^{31}P\{^1H\}$ ($CDCl_3$, δ): 138.0. CV (CH_3CN , 100 mV/s): $E_{1/2} = 1.45$ V. Anal.

Calcd for $C_{20}H_{39}BF_3N_7O_9P_2RuS$: C, 30.62; N, 12.50; H, 5.01. Found: C, 30.81; N, 12.37; H, 5.09.

[TpRu(CO)(PPh₃)(NH₂^tBu)][OTf]. To a solution of TpRu(CO)(PPh₃)Cl (0.9612 g, 1.50 mmol) in approximately 50 mL of THF was added AgOTf (0.3871 g, 1.51 mmol). The resulting solution was refluxed for 18 h. During the reaction, the formation of a white precipitate (AgCl) was noted. The solution was cooled to room temperature and filtered through a fine porosity frit, and ^tBuNH₂ was added to the filtrate. The mixture was allowed to stir for an additional 24 h and was then concentrated to approximately 30 mL under reduced pressure. Diethyl ether (approximately 50 mL) was added to precipitate the product. The product was collected via vacuum filtration through a fine porosity frit and washed with diethyl ether (3 × 10 mL) to give a white solid (0.8186 g, 0.9903 mmol, 79%). The product was recrystallized from THF/hexanes. ¹H NMR (CDCl₃, δ): 7.98 (2H, overlapping d's, Tp CH 3 or 5 position), 7.85, 7.77, 7.72, 6.12 (4H, 1:1:1:1 integration, each a d, Tp CH 3 and 5 position), 7.47, 7.01 (15H, 9:6 integration, m's, PPh₃), 6.28, 6.24, 5.90 (3H, 1:1:1 integration, each a t, Tp CH 4 position), 3.45 (1H, d, ²J_{HH} = 13 Hz, NH), 2.68 (1H, d, ²J_{HH} = 13 Hz, NH), 1.02 (9H, s, NH₂C(CH₃)₃). ¹³C{¹H} NMR (CDCl₃, δ): 204.7 (CO, d, ²J_{PC} = 14 Hz), 145.9, 145.5, 145.2, 137.8, 137.2, 137.1 (Tp 3 or 5 position), 133.6 and 129.6 (PPh₃ ortho and meta, each a d, ²J_{PC} = ³J_{PC} = 10 Hz), 131.5 (PPh₃ para), 129.7 (PPh₃ ipso, ¹J_{PC} = 44 Hz), 108.2, 107.2, 107.0 (Tp 4 position), 55.4 (C(CH₃)₃), 31.0 (C(CH₃)₃). IR (thin film on KBr): ν_{CO} = 1970 cm⁻¹, ν_{NH} = 3127, 3289 cm⁻¹, ν_{BH} = 2498 cm⁻¹. ³¹P{¹H} (CDCl₃, δ): 39.2. Anal. Calcd for C₃₃H₃₆BF₃N₇O₄PRuS·¹/₂(THF) (note that ¹/₂ equiv of THF was confirmed via ¹H NMR of the analysis sample): C, 48.73; N, 11.37; H, 4.67. Found: C, 48.21; N, 11.10; H, 4.69.

[TpRu(PMe₃)₂(NH₂Ph)][OTf]. TpRu(PMe₃)₂(OTf) (1.3674 g, 2.222 mmol) was dissolved in approximately 50 mL of THF. To this solution was added aniline (2.1295 g, 21.6 mmol), and the resulting mixture was allowed to stir for 24 h. The solution was concentrated to approximately 20 mL in vacuo, and diethyl ether (approximately 40 mL) was added to precipitate the product. The product was collected via vacuum filtration through a fine porosity frit and washed with diethyl ether (3 × 10 mL) to give a white solid (1.4089 g, 1.988 mmol, 90%). IR (thin film on KBr plate): $\nu_{\text{NH}} = 3285$ and 3262 cm^{-1} , $\nu_{\text{BH}} = 2481 \text{ cm}^{-1}$. UV-vis (THF): $\lambda_{\text{max}} = 267 \text{ nm}$ $\epsilon = 0.96 \times 10^4 \text{ M}^{-1} \text{ cm}^{-1}$. ¹H NMR (CD₃CN, δ): 7.85, 7.25 (each 2H, each a d, Tp CH 3 or 5 position), 7.80, 7.38 (each 1H, each a d, Tp CH 3 or 5 position), 6.95 (3H, m, overlap of NH₂C₆H₅ meta and para), 6.35 (2H, d, ³J_{HH} = 7 Hz, NH₂C₆H₅ ortho), 6.18 (2H, t, Tp CH 4 position), 6.14 (1H, t, Tp CH 4 position), 4.77 (2H, br s, NH₂Ph), 1.30 (18H, vt, $J_{\text{PH}} = 7 \text{ Hz}$, P(CH₃)₃). ¹³C{¹H}-NMR (CD₃CN, δ): 145.8, 142.7, 142.5, 136.9, 136.3 (each an s, Tp CH 3 or 5 position, and amine phenyl ipso carbon), 128.8, 125.1, 122.7 (each an s, amine phenyl ortho, meta, and para), 106.7, 106.0 (each an s, Tp CH 4 position), 18.1 (d, ¹J_{PC} = 12 Hz). ³¹P{¹H}-NMR (CDCl₃, δ): 10.9. CV (THF, TBAH, 100 mV/s): $E_{\text{p,a}} = 1.82 \text{ V}$ (Ru(III/II)). Anal. Calcd for C₂₂H₃₅BF₃N₇O₃P₂RuS: C, 37.29; H, 4.98; N, 13.84. Found: C, 37.16; H, 4.95; N, 13.61.

[TpRu{P(OMe)₃}₂(NH₂Ph)][OTf]. To a solution of TpRu{P(OMe)₃}₂Cl (1.2587 g, 2.106 mmol) in approximately 50 mL of THF was added AgOTf (0.5413 g, 2.107 mmol). The resulting solution was refluxed for 20 h. During the reaction, the formation of a white precipitate (AgCl) was noted. The solution was cooled to room temperature and filtered through a fine porosity frit. Aniline (2.0564 g, 20.9 mmol) was added to the resulting

solution. The mixture was allowed to stir for an additional 24 h. The solution was concentrated to approximately 20 mL in vacuo, and diethyl ether (approximately 40 mL) was added to precipitate the product. The product was collected via vacuum filtration through a fine porosity frit and washed with diethyl ether (3×10 mL) to give a white solid (1.5823 g, 1.967 mmol, 93%). IR (thin film on KBr plate): $\nu_{\text{NH}} = 3318$ and 3250 cm^{-1} , $\nu_{\text{BH}} = 2450 \text{ cm}^{-1}$. UV-vis (THF): $\lambda_{\text{max}} = 223 \text{ nm}$ ($\epsilon = 2.0 \times 10^4 \text{ M}^{-1} \text{ cm}^{-1}$). ^1H NMR (CD_2Cl_2 , δ): 7.77, 7.39 (each 2H, each a d, Tp CH 3 or 5 position), 7.71, 7.63 (each 1H, each a d, Tp CH 3 or 5 position), 6.99 (3H, m, overlapping $\text{NH}_2\text{C}_6\text{H}_5$ meta and para), 6.35 (2H, d, $^3J_{\text{HH}} = 7 \text{ Hz}$, $\text{NH}_2\text{C}_6\text{H}_5$ ortho), 6.16 (3H, m, overlapping Tp CH 4 position), 4.74 (2H, br s, $\text{NH}_2\text{C}_6\text{H}_5$), 3.44 (18H, vt, $J_{\text{PH}} = 10 \text{ Hz}$, $\text{P}(\text{OCH}_3)_3$). $^{13}\text{C}\{^1\text{H}\}$ NMR (CD_2Cl_2 , δ): 148.3, 144.7, 137.7, 137.0 (each an s, Tp CH 3 or 5 position), 142.7 (amine phenyl ipso carbon), 129.9, 127.1, 124.7 (each an s, amine phenyl ortho, meta, and para), 106.8, 106.7 (each an s, Tp CH 4 position), 53.2 (br s, $\text{P}(\text{OCH}_3)_3$). $^{31}\text{P}\{^1\text{H}\}$ NMR (CD_3CN , δ): 139.3 (s, $\text{P}(\text{OCH}_3)_3$). CV (THF, TBAH, 100 mV/s): $E_{\text{p,a}} = 1.86 \text{ V}$ (Ru(III/II)). Anal. Calcd for $\text{C}_{22}\text{H}_{35}\text{BF}_3\text{N}_7\text{O}_9\text{P}_2\text{RuS}$: C, 32.85; H, 4.39; N, 12.19. Found: C, 33.02; H, 4.28; N, 12.24.

[TpRu(CO)₂NH₂Ph][PF₆]. Aniline (0.2465 g, 2.65 mmol) was added to a THF solution of [TpRu(CO)₂(THF)][PF₆] (0.1027 g, 0.175 mmol). The resulting mixture was refluxed for 24 h, and the volatiles were removed under reduced pressure. The resulting beige solid was washed with approximately 4×30 mL of diethyl ether and was dried in vacuo (0.1015 g, 95%). ^1H NMR (acetone-*d*₆, δ): 8.18 (4H, overlap multiplet, Tp CH 3 and 5 position), 8.09, 8.03 (each 1H, each a d, Tp CH 3 or 5 position), 6.57, 6.42 (3H, 2:1 integration, each a t, Tp CH 4 position). 7.50 (4H, overlap multiplet, phenyl ortho, and meta),

7.34 (1H, t, phenyl para). $^{13}\text{C}\{^1\text{H}\}$ NMR (acetone- d_6 , δ): 194.5 (CO), 147.6, 145.0, 138.9, 138.6 (Tp 3 or 5 position), 146.5, 131.0, 127.4, 122.4 (amine phenyl), 108.7, 108.6 (Tp 4 position). IR (thin film on KBr): $\nu_{\text{CO}} = 2084, 2022 \text{ cm}^{-1}$, $\nu_{\text{NH}} = 3313, 3271 \text{ cm}^{-1}$, $\nu_{\text{BH}} = 2528 \text{ cm}^{-1}$. Anal. Calcd for $\text{C}_{17}\text{H}_{17}\text{BF}_6\text{N}_7\text{O}_2\text{Ru}$: C, 33.57; H, 2.82; N, 16.12. Found: C, 33.82; H, 2.93; N, 15.95.

TpRu(PMe₃)₂(NH^tBu). To a colorless THF (5 mL) solution of [TpRu(PMe₃)₂NH^tBu][OTf] (0.0710 g, 0.103 mmol) cooled to -78 °C was added dropwise a 1.0 M THF solution of [Na][N(SiMe₃)₂] (0.103 mmol). Upon addition of base, the mixture changed color to orange and was allowed to warm to room temperature. The solvent was removed in vacuo from the reaction mixture. The resulting orange residue was stirred with benzene, and the mixture was passed through a fine porosity frit. The benzene was removed in vacuo from the filtrate yielding a solid orange product. The product was recrystallized by dissolution in benzene and addition of hexanes (0.0308 g, 56% yield). ^1H NMR (C_6D_6 , δ): 8.36, 7.60, 7.54, 7.20 (6H, 2:2:1:1 integration, each a d, Tp CH 3 and 5 position), 6.04, 5.87 (3H, 2:1 integration, each a t, Tp CH 4 position), 1.19 (9H, s, ^tBu), 1.04 (18H, vt, $N = 6$ Hz, P(CH₃)₃), -2.45 (1H, br s, NH). $^{13}\text{C}\{^1\text{H}\}$ NMR (C_6D_6 , δ): 145.1, 144.7, 135.2, 134.7 (Tp 3 or 5 position), 104.6, 104.0 (Tp 4 position), 53.5 (C(CH₃)₃), 36.1 (C(CH₃)₃), 18.1 (vt, $N = 13$ Hz, P(CH₃)₃). IR (THF solution): $\nu_{\text{NH}} = 3294 \text{ cm}^{-1}$; $\nu_{\text{BH}} = 2460 \text{ cm}^{-1}$. $^{31}\text{P}\{^1\text{H}\}$ (C_6D_6 , δ): 14.8.

TpRu(PMe₃)₂(NHPh). A colorless solution of [TpRu(PMe₃)₂NH₂Ph][OTf] (0.1151 g, 0.162 mmol) in approximately 20 mL of THF was cooled to -78 °C. Sodium bis(trimethylsilyl)amide (0.178 mmol, 1.0 M in THF) was added dropwise via a microsyringe. After the addition of base, the color of the solution was noted to be pale

yellow. The solution was allowed to warm to room temperature, and a color change to dark brown/yellow was noted. The volatiles were removed under reduced pressure. The resulting solid was dissolved in benzene (approximately 60 mL) and filtered through a fine porosity frit. Benzene was removed from the filtrate under reduced pressure to yield a pale yellow solid (0.082 g, 0.147 mmol, 90%). IR (solution cell in THF): $\nu_{\text{NH}} = 3326 \text{ cm}^{-1}$, $\nu_{\text{BH}} = 2467 \text{ cm}^{-1}$. UV-vis (THF): $\lambda_{\text{max}} = 293 \text{ nm}$ ($\epsilon = 1.7 \times 10^4 \text{ M}^{-1} \text{ cm}^{-1}$). ^1H NMR (C_6D_6 , δ): 7.66, 7.47 (each 2H, each a d, Tp CH 3 or 5 position), 7.51, 6.89 (each 1H, each a d, Tp CH 3 or 5 position), 7.22 (2H, t, $^3J_{\text{HH}} = 7 \text{ Hz}$, phenyl meta), 6.45 (1H, t, $^3J_{\text{HH}} = 7 \text{ Hz}$, phenyl para), 5.88 (2H, t, Tp CH 4 position), 5.85 (1H, t, Tp CH 4 position), 2.80 (1H, br s, NHPH), 0.92 (18H, vt, $J_{\text{PH}} = 6 \text{ Hz}$, $\text{P}(\text{CH}_3)_3$). At room temperature in C_6D_6 , the resonances due to the ortho protons are broadened into the baseline. In CD_2Cl_2 at room temperature, the ortho protons are observed as a broad singlet at approximately 5.8 ppm. $^{13}\text{C}\{^1\text{H}\}$ NMR (C_6D_6 , δ): 163.3 (s, Ph ipso), 145.7, 142.8, 136.0, 135.8 (each an s, Tp CH 3 or 5 position), 129.4, 128.5, 115.9 (each an s, amido phenyl ortho, meta, and para), 106.0, 105.7 (each an s, Tp CH 4 position), 18.9 (d, $^1J_{\text{PC}} = 12 \text{ Hz}$, $\text{P}(\text{CH}_3)_3$). $^{31}\text{P}\{^1\text{H}\}$ NMR (C_6D_6 , δ): 17.5 (s, $\text{P}(\text{CH}_3)_3$). CV (THF, TBAH, 50 mV/s): $E_{1/2} = -0.28 \text{ V}$ (Ru(III/II)). Anal. Calcd for $\text{C}_{21}\text{H}_{31}\text{BN}_7\text{P}_2\text{Ru}$: C, 45.17; H, 6.14; N, 17.56. Found: C, 45.29; H, 6.17; N, 17.29.

TpRu(PMe₃)₂(NHPH). A colorless solution of [TpRu(PMe₃)₂NH₂Ph][OTf] (0.1151 g, 0.162 mmol) in approximately 20 mL of THF was cooled to -78 °C. Sodium bis(trimethylsilyl)amide (0.178 mmol, 1.0 M in THF) was added dropwise via a microsyringe. After the addition of base, the color of the solution was noted to be pale yellow. The solution was allowed to warm to room temperature, and a color change to dark

brown/yellow was noted. The volatiles were removed under reduced pressure. The resulting solid was dissolved in benzene (approximately 60 mL) and filtered through a fine porosity frit. Benzene was removed from the filtrate under reduced pressure to yield a pale yellow solid (0.082 g, 0.147 mmol, 90%). IR (solution cell in THF): $\nu_{\text{NH}} = 3326 \text{ cm}^{-1}$, $\nu_{\text{BH}} = 2467 \text{ cm}^{-1}$. UV-vis (THF): $\lambda_{\text{max}} = 293 \text{ nm}$ ($\epsilon = 1.7 \times 10^4 \text{ M}^{-1} \text{ cm}^{-1}$). ^1H NMR (C_6D_6 , δ): 7.66, 7.47 (each 2H, each a d, Tp CH 3 or 5 position), 7.51, 6.89 (each 1H, each a d, Tp CH 3 or 5 position), 7.22 (2H, t, $^3J_{\text{HH}} = 7 \text{ Hz}$, phenyl meta), 6.45 (1H, t, $^3J_{\text{HH}} = 7 \text{ Hz}$, phenyl para), 5.88 (2H, t, Tp CH 4 position), 5.85 (1H, t, Tp CH 4 position), 2.80 (1H, br s, NHPH), 0.92 (18H, vt, $J_{\text{PH}} = 6 \text{ Hz}$, $\text{P}(\text{CH}_3)_3$). At room temperature in C_6D_6 , the resonances due to the ortho protons are broadened into the baseline. In CD_2Cl_2 at room temperature, the ortho protons are observed as a broad singlet at approximately 5.8 ppm. $^{13}\text{C}\{^1\text{H}\}$ NMR (C_6D_6 , δ): 163.3 (s, Ph ipso), 145.7, 142.8, 136.0, 135.8 (each an s, Tp CH 3 or 5 position), 129.4, 128.5, 115.9 (each an s, amido phenyl ortho, meta, and para), 106.0, 105.7 (each an s, Tp CH 4 position), 18.9 (d, $^1J_{\text{PC}} = 12 \text{ Hz}$, $\text{P}(\text{CH}_3)_3$). $^{31}\text{P}\{^1\text{H}\}$ NMR (C_6D_6 , δ): 17.5 (s, $\text{P}(\text{CH}_3)_3$). CV (THF, TBAH, 50 mV/s): $E_{1/2} = -0.28 \text{ V}$ (Ru(III/II)). Anal. Calcd for $\text{C}_{21}\text{H}_{31}\text{BN}_7\text{P}_2\text{Ru}$: C, 45.17; H, 6.14; N, 17.56. Found: C, 45.29; H, 6.17; N, 17.29.

TpRu{P(OMe)₃}₂(NHPH). A colorless solution of [TpRu{P(OMe)₃}₂NH₂Ph][OTf] (0.1142 g, 0.142 mmol) in approximately 20 mL of THF was cooled to -78 °C. To this solution was added dropwise via a microsyringe sodium bis(trimethylsilyl)amide (0.156 mmol, 1.0 M in THF). After the addition of amide, the color of the solution was noted to be yellow. The solution was allowed to warm to room temperature, and a color change to dark yellow was noted. Removal of the volatiles under reduced pressure yielded a yellow solid.

The resulting solid was dissolved in benzene (approximately 60 mL) and filtered through a fine porosity frit. Benzene was removed from the filtrate under reduced pressure to yield a bright yellow solid (0.085 g, 0.130 mmol, 91%). IR (solution cell in THF): $\nu_{\text{NH}} = 3378 \text{ cm}^{-1}$, $\nu_{\text{BH}} = 2467 \text{ cm}^{-1}$. UV-vis (THF): $\lambda_{\text{max}} = 284 \text{ nm}$ ($\epsilon = 1.3 \times 10^4 \text{ M}^{-1} \text{ cm}^{-1}$). $^1\text{H NMR}$ (C_6D_6 , δ): 7.98, 7.56 (each 2H, each a d, Tp CH 3 or 5 position), 7.87, 7.46 (each 1H, each a d, Tp CH 3 or 5 position), 6.93 (2H, t, $^3J_{\text{HH}} = 7 \text{ Hz}$, phenyl meta), 6.36 (1H, t, $^3J_{\text{HH}} = 7 \text{ Hz}$, phenyl para), 6.00 (3H, m, overlap of Tp CH 4 position and phenyl ortho), 5.86 (1H, t, Tp CH 4 position), 3.14 (18H, vt, $J_{\text{PH}} = 10 \text{ Hz}$, $\text{P}(\text{OCH}_3)_3$), 1.98 (1H, br s, *NHPh*). $^{13}\text{C}\{^1\text{H}\}$ NMR (C_6D_6 , δ): 163.3 (s, phenyl ipso), 145.7, 142.8, 136.0, 135.8 (each an s, Tp CH 3 or 5 position), 129.4, 128.5, 115.9 (each an s, amido phenyl ortho, meta, and para), 106.0, 105.7 (each an s, Tp CH 4 position), 18.9 (d, $^1J_{\text{PC}} = 12 \text{ Hz}$, $\text{P}(\text{OCH}_3)_3$). $^{31}\text{P}\{^1\text{H}\}$ NMR (THF- d_8 , δ): 137.5 (s, $\text{P}(\text{CH}_3)_3$). CV (THF, TBAH, 50 mV/s): $E_{1/2} = -0.25 \text{ V}$ (Ru(III/II)). Anal. Calcd for $\text{C}_{21}\text{H}_{34}\text{BN}_7\text{P}_2\text{O}_6\text{Ru}-\text{C}_6\text{H}_6$: C, 44.27; H, 5.50; N, 13.38. Found: C, 42.50; H, 5.42; N, 13.22.

TpRu(PMe₃)₂(NH₂). A solution of [TpRu(PMe₃)₂(NH₃)] [OTf] (0.2423 g, 0.383 mmol) was dissolved in THF (50 mL) and cooled to -78 °C. MeLi (0.30 mL, 1.4 M solution in diethyl ether, 0.42 mmol) was added dropwise via a microsyringe. The solution turned immediately turned pale yellow, and stirring was continued for another 5 min at -78 °C. The slush bath was removed, and the reaction mixture was warmed to room temperature. The solvent was removed under reduced pressure to give a yellow-brown solid. The solid was dissolved in toluene (20 mL) and filtered through a fine-porosity frit. Removal of solvent from the filtrate in vacuo gave the desired product in 95% yield (0.175 g). IR (THF): $\nu_{\text{BH}} =$

2463 cm^{-1} , $\nu_{\text{NH}} = 3115, 3230 \text{ cm}^{-1}$. ^1H NMR (C_6D_6 , δ): 7.87, 7.55, 7.48, 7.15 (6H, 2:1:2:1 integration, each a d, Tp CH-3 or -5 position), 6.00, 5.88 (3H, 2:1 integration, each a t, Tp CH-4 position), 1.07 (18H, vt, $J_{\text{PH}} = 10 \text{ Hz}$, $\text{P}(\text{CH}_3)_3$), -2.20 (2H, bs, NH_2). $^{13}\text{C}\{^1\text{H}\}$ NMR (C_6D_6 , δ): 145.4, 142.8, 13.9, 135.3 (Tp 3- or 5-position), 105.8, 105.4 (Tp 4-position), 18.6 (t, $J_{\text{PC}} = 12 \text{ Hz}$, $\text{P}(\text{CH}_3)_3$). $^{31}\text{P}\{^1\text{H}\}$ NMR (C_6D_6 , δ): 17.5 (PMe_3). FAB MS (m/z): 483.1 $[\text{TpRu}(\text{PMe}_3)_2(\text{NH}_2)]^+$, 467.1 $[\text{TpRu}(\text{PMe}_3)_2]^+$.

$\text{TpRu}\{\text{P}(\text{OMe})_3\}_2(\text{NH}_2)$. A solution of $[\text{TpRu}\{\text{P}(\text{OMe})_3\}_2\text{NH}_3][\text{OTf}]$ (0.1072 g, 0.1473 mmol) in approximately 30 mL of THF was cooled to $-78 \text{ }^\circ\text{C}$. MeLi (0.22 mmol, 1.4 M in diethyl ether) was added dropwise via a microsyringe. After the addition of base, the color of the solution was noted to be pale yellow. The solution was stirred at $-78 \text{ }^\circ\text{C}$ then warmed to room temperature. The volatiles were removed under reduced pressure. The resulting solid was dissolved in benzene (approximately 30 mL) and filtered through a fine porosity frit. Benzene was removed from the filtrate under reduced pressure to yield a yellow solid (0.0804 g, 0.138 mmol, 94%). IR (THF): $\nu_{\text{NH}} = 3128, 2995 \text{ cm}^{-1}$. ^1H NMR (C_6D_6 , δ): 8.08, 7.66, 7.44, 7.41 (6H, 2:1:1:2 integration, each a d, Tp CH-3 or -5 position), 6.05, 5.84 (3H, 2:1 integration, each a t, Tp CH-4 position), 3.15 (18H, vt, $J_{\text{PH}} = 10 \text{ Hz}$, $\text{P}(\text{OCH}_3)_3$), -1.91 (2H, bs, NH_2). $^{13}\text{C}\{^1\text{H}\}$ NMR (C_6D_6 , δ): 146.4, 143.9, 135.9, 135.3 (each a s Tp 3 or 5-position), 106.3, 105.7 (each a s, Tp 4 position), 51.9 (s, $\text{P}(\text{OCH}_3)_3$). $^{31}\text{P}\{^1\text{H}\}$ NMR (C_6D_6 , δ): -11.3 $\text{P}(\text{OMe})_3$. FAB MS (m/z): 580.1 $[\text{TpRu}\{\text{P}(\text{OMe})_3\}_2(\text{NH}_2)]^+$, 563.1 $[\text{TpRu}\{\text{P}(\text{OMe})_3\}_2]^+$.

References.

- ¹ Bryndza, H. E.; Tam, W. *Chem. Rev.* **1988**, 88, 1163-1188.
- ² Fulton, R. J.; Holland, A. W.; Fox, D. J.; Bergman, R. G. *Acc. Chem. Res.* **2002**, 35, 44-56.
- ³ Mayer, J. M. *Comments Inorg. Chem.* **1988**, 8, 125-135.
- ⁴ Caulton, K. G. *New J. Chem.* **1994**, 18, 25-41.
- ⁵ Sharp, P. R. *Comments Inorg. Chem.* **1999**, 21, 85-114.
- ⁶ Holland, P. L.; Anderson, R. A.; Bergman, R. G. *Comments Inorg. Chem.* **1999**, 21, 115-129.
- ⁷ Kempe, R. *Angew. Chem. Int. Ed.* **2000**, 39, 468-493.
- ⁸ Conner, D.; Jayaprakash, K. N.; Wells, M. B.; Manzer, S.; Gunnoe, T. B.; Boyle, P. D. *Inorg. Chem.* **2003**, 42, 4759-4772.
- ⁹ Blue, E. D.; Davis, A.; Conner, D.; Gunnoe, T. B.; Boyle, P. D.; White, P. S. *J. Am. Chem. Soc.* **2003**, 125, 9435-9441.
- ¹⁰ Flood, T. C.; Lim, J. K.; Deming, M. A.; Keung, W. *Organometallics* **2000**, 19, 1166-1174.
- ¹¹ Hartwig, J. F.; Anderson, R. A.; Bergman, R. G. *Am. Chem. Soc.* **1991**, 119, 1875-1887.
- ¹² Joslin, F. L.; Johnson, M. P.; Mague, J. T.; Roundhill, D. M. *Organometallics* **1991**, 10, 2781-2794.
- ¹³ Soper, J. D.; Bennett, B. K.; Lovell, S.; Mayer, J. M. *Inorg. Chem.* **2001**, 40, 1888-1893.
- ¹⁴ Mindiola, D. J.; Hillhouse, G. L. *J. Am. Chem. Soc.* **2001**, 123, 4623-4624.
- ¹⁵ Holland, P. L.; Smith, M. E.; Anderson, R. A.; Bergman, R. G. *J. Am. Chem. Soc.* **1997**, 119, 12815-12823.
- ¹⁶ Salzer, Ch. E. *Organometallics – A Concise Introduction Second Edition*; Wiley VCH, Inc: New York, **1992**.
- ¹⁷ Bryndza, H. E.; Fong, L. K.; Paciello, R. A.; Tam, W.; Bercaw, J. E. *J. Am. Chem. Soc.* **1987**, 109, 1444-1456.
- ¹⁸ Glueck, D. S.; Bergman, R. G. *Organometallics* **1991**, 10, 1479-1486.
- ¹⁹ Holland, P. L.; Andersen, R. A.; Bergman, R. G.; Huang, J.; Nolan, S. P. *J. Am. Chem. Soc.* **1997**, 119, 12800-12814.
- ²⁰ Simpson, R. D.; Bergman, R. G. *Organometallics* **1992**, 11, 3980-3993.
- ²¹ Muller, T. E.; Beller, M. *Chem. Rev.* **1998**, 98, 675-703.
- ²² Fornies, J.; Green, M.; Spencer, J. L.; Stone, F. G. A. *J. Chem. Soc. Dalton Trans* **1977**, 1006-1009.
- ²³ Braga, D.; Sabatino, P.; Di Bugno, C.; Leoni, P.; Pasquali, M. *J. Organomet. Chem.* **1987**, 334, 46-48.
- ²⁴ Monaghan, P. K.; Puddephatt, R. J. *Inorg. Chim. Acta* **1982**, 65, 59-61.
- ²⁵ Monaghan, P. K.; Puddephatt, R. J. *Organometallics* **1984**, 3, 444-449.
- ²⁶ Yoshida, T.; Matsuda, T.; Okano, T.; Kitani, T.; Otsuka, S. *J. Am. Chem. Soc.* **1979**, 101, 2027-2038.
- ²⁷ Burn, M. J.; Fickes, M. G.; Hartwig, J. F.; Hollander, F. J.; Bergman R. G. *J. Am. Chem. Soc.* **1993**, 115, 5875-5876.
- ²⁸ Casalnuovo, A. L.; Calabrese, J. C.; Milstein, D. *Inorg. Chem.* **1987**, 26, 971-973

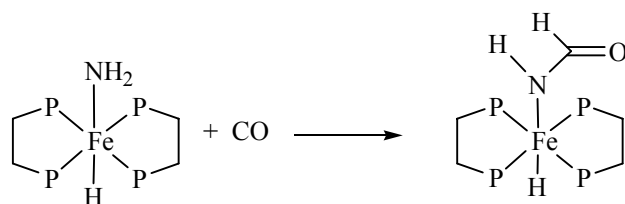
-
- ²⁹ Kanzelberger, M.; Zhang, X.; Emge, T. J.; Goldman, A. S.; Zhao, J.; Incarvito, C.; Hartwig, J. F. *J. Am. Chem. Soc.* **2003**, *125*, 13644-13645.
- ³⁰ Slugovc, C.; Schmid, R.; Kirchner, K. *Coord. Chem Rev.* **1999**, *185*, 109-126.
- ³¹ Trofimenko, S. *Chem. Rev.* **1993**, *93*, 943-980.
- ³² Tellers, D. M.; Skoog, S. J.; Bergman, R. G.; Gunnoe, T. B.; Harman, W. D. *Organometallics* **2000**, *19*, 2428-2432.
- ³³ Bergman, R. G.; Cundari, T. R.; Gillespie, A. M.; Gunnoe, T. B.; Harman, W. D.; Klinckman, T. R.; Temple, M. D.; White, D. P. *Organometallics* **2003**, *22*, 2331-2337.
- ³⁴ Graziana, O.; Toupet, L.; Hamon, J.; Tilset, M. J. *Organom. Chem.* **2003**, *669*, 200-206.
- ³⁵ Buriez, B.; Burns, D. I.; Hill, A. F.; White, A. J.; Williams, D. J.; Wilton-Ely, J. D. *Organometallics* **1999**, *18*, 1504-1516.
- ³⁶ Sun, N. Y.; Simpson, S. J. *J. Organomet. Chem.* **1992**, *434*, 341-349.
- ³⁷ Sorlie, M.; Tilset, M. *Inorg. Chem.* **1995**, *34*, 5199-5204.
- ³⁸ Connerly, N. G.; Gieger, W. E. *Chem. Rev.* **1996**, *96*, 877-901.
- ³⁹ Karlen, T.; Dani, P.; Grove, D. M.; Steenwinkel, P.; Van Koten, G. *Organometallic* **1996**, *15*, 5687-5694.
- ⁴⁰ Kaplan, A. W.; Ritter, J. C. M.; Bergman, R. G. *J. Am. Chem. Soc.* **1998**, *120*, 6828-6829.
- ⁴¹ Jayaprakash, K. N.; Gunnoe, T. B.; Boyle, P. D. *Inorg. Chem.* **2001**, *40*, 6481-6486.
- ⁴² Jayaprakash, K. N.; Conner, D.; Gunnoe, T. B. *Organometallics* **2001**, *20*, 5254-5256.
- ⁴³ Conner, D.; Jayaprakash, K. N.; Gunnoe, T. B.; Boyle, P. D. **2002**, *21*, 5265-5271.
- ⁴⁴ Wen, G. Y.; Sharp, P. R. *Inorg. Chem.* **1992**, *31*, 379-384.
- ⁴⁵ Holland, P. L.; Anderson, R. A.; Bergman, R. G. *J. Am. Chem. Soc.* **1996**, *118*, 1092-1104.
- ⁴⁶ Fulton, R. J.; Bouwkamp, M. W.; Bergman, R. G. *J. Am. Chem. Soc.* **2000**, *122*, 8799-8800.
- ⁴⁷ Holland, A. W.; Bergman, R. G. *J. Am. Chem. Soc.* **2002**, *124*, 14684-14695.
- ⁴⁸ Günther, H. *NMR Spectroscopy: Basic Principles, Concepts, and Applications in Chemistry, 2nd Edition*; John Wiley & Sons: New York, **1995**.
- ⁴⁹ Francis A. Carey, Richard J. Sundberg *Advanced Organic Chemistry: Structure and Mechanisms* 4th edition Plenum Publishing Corporation 2000
- ⁵⁰ Julio de Paula, Peter Atkins *Physical Chemistry* 7th ed. W. H. Freeman 2001.
- ⁵¹ Fulton, R. J.; Bouwkamp, M. W.; Bergman, R. G. *J. Am. Chem. Soc.* **2000**, *122*, 8799-8800.
- ⁵² Holland, A. W.; Bergman, R. G. *J. Am. Chem. Soc.* **2002**, *124*, 14684-14695.
- ⁵³ Vollhardt, P. C. *Organic Chemistry 2nd ed.*; W.H. Freeman: New York, **1994**.
- ⁵⁴ Albeniz, A. C.; Calle, V.; Espinet, P.; Gomez, S. *Inorg. Chem.* **2001**, *40*, 4211-4216.
- ⁵⁵ Conner, D.; Jayaprakash, K. N.; Gunnoe, T. B.; Boyle, P. D. *Inorg. Chem.* **2001**, *41*, 3042-3049.
- ⁵⁶ Jayaprakash, K. N.; Gunnoe, T. B.; Boyle, P. D. *Inorg. Chem.* **2001**, *40*, 6481-6486.
- ⁵⁷ Flood, T. C.; Lim, J. K.; Deming, M. A.; Keung, W. *Organometallics* **2000**, *19*, 1166-1174.
- ⁵⁸ C. A. Tolman *J. Am. Chem. Soc.* **1970**, *92*, 2956-2966.
- ⁵⁹ Powell, K. R.; Perez, P. J.; Luan, L.; Feng, S. G.; White, P. S.; Brookhart, M.; Templeton, J. L. *Organometallics* **1994**, *13*, 1851-1864.

⁶⁰ Kitajima, N.; Tolman, W. B. *Prog. Inorg. Chem.* **1995**, *43*, 419-531.

Chapter 3: Detailed Studies of the Amido Complexes.

3.1 Introduction.

Interest in late transition metal systems monomeric amido ligands is derived from their importance as intermediates in C-H bond activation reactions and catalytic C-N bond forming reactions such as hydroamination or arylation.^{1,2,3,4,5} Despite the importance of these complexes, a dearth of isolable late transition metal amido complexes has resulted in an insufficient understanding of their reactivity.^{5,6,7} Recent interest in the chemistry of such complexes has led to the preparation and detailed study of amido complexes of ruthenium, osmium, iridium, nickel, platinum, and copper.^{5,6,8,9,10,11} These studies revealed remarkable reactivity patterns. For example, Berman et al. have reported that octahedral Ru(II) complexes *trans*-(dmpe)₂Ru(NH₂)(H) and *cis*-(PMe₃)₄Ru(H)(NH₂) possess amido ligands with highly nucleophilic character, and these ligands are basic enough to deprotonate weak C-H bonds.^{5,7} The iron(II) analog *trans*-(dmpe)₂Fe(NH₂)(H) has been reported to undergo nucleophilic addition to free carbon monoxide (Scheme 3.1).^{12,13} While CO insertion into late transition metal



Scheme 3.1 Nucleophilic addition to free carbon monoxide by *trans*-(DMPE)₂Fe(NH₂)(H).

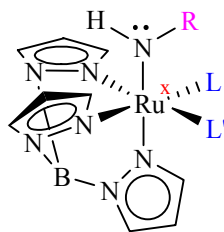
amido bonds is common, it has been suggested that the iron(II) amido/CO reaction proceeds by through initial nucleophilic attack on free carbon monoxide followed by

proton transfer.^{6,13} In contrast to these highly basic and nucleophilic complexes, Mayer et al. have reported that the Os(IV) amido complex $\text{TpOs}(\text{Cl})_2\text{NHPH}$ is inert strong to acids. Rather than exhibiting nucleophilic character, this complex has been demonstrated to activate the anilido ligand towards nucleophilic attack of the amido aryl ring.^{14,15}

Many biological systems and an increasing number of synthetic systems serve to activate C-H bonds remote to the metal center via ligand-based hydrogen abstraction. The electronic nature and coordination environment of the metal center dictate whether the C-H activation sequences occur via hydride, hydrogen atom, or proton removal.^{16,17,18,19} For example, Fe(III) hydroxide and methoxide complexes that mimic lipooxygenase enzymes undergo odd-electron hydrogen atom abstraction reactions have been reported.¹⁶ These reactions result in a change in formal metal oxidation state and are reliant upon the oxidizing ability of the transition metal center.^{20,21}

Such diversity of reactivity raises several questions, including: (1) What features control the amido reactivity? (2) What features of such complexes influence reactivity and to what extent do these features impact reactivity? We sought to begin to answer these questions by utilizing complexes where features such as the steric and the electronic nature of the metal center could be selectively tuned. As such, a system in which the ancillary ligands could be selectively varied was required. The $\{\text{TpRu}(\text{L})(\text{L}')\}$ moiety has received attention because of the ability to control steric and electronic features of the metal coordination sphere by variation of L and/or L'.²² In addition, we also sought to determine the effect of the amido substituent, metal identity, and metal oxidation state on reactivity. To our knowledge, this work is the first example of a series of octahedral d^6

amido complexes in which the ancillary ligands and amido substituents are varied (Scheme 3.2). A series of related Ru(II) amido complexes CpRuL_2NHR with phosphine



Scheme 3.2 Investigation of the reactivity of octahedral ruthenium amido complexes. We sought to determine the effect on reactivity of the amido substituent **R**, the oxidation state **x** and the ancillary ligand **L** and **L'**.

ligands have been reported by Roundhill et al.²³ These complexes were reported to undergo β -hydride elimination, reactions with electrophiles (such as NMe_4^+), and CO insertion into the Ru-N bond.²³ Also, Boncella et al. reported the Ru(II) amido complexes $\text{Cp}^*\text{Ru}(\text{PMe}_3)(\text{R})(\text{NR}'\text{R}'')$ ($\text{R} = \text{Ph}$ or Me , $\text{R}' = \text{H}$ or Me , $\text{R}'' = \text{Ph}$). These complexes were reported to undergo insertion reactions with CO_2 or dimethylacetylene dicarboxylate.²⁴

3.2 Linear Free Energy Relationship Studies of Ruthenium (II) Aryl Amido Complexes.

Linear free energy relationship (LFER) studies are often used to investigate the mechanism of a reaction or electronic features of a system by probing electronic effects.^{25,26} LFER studies can also be useful to correlate substituent effects on reaction rate and/or equilibrium. Most common are LFER studies that use substituted arenes because of the ability of the aryl ring to electronically communicate to a remote reaction site. Altering the electron-withdrawing/donating ability of the substituent results in thermodynamic changes from through-space electrostatic interactions called a field effect

(Figure 3.1).^{25,26} The thermodynamic changes due to aryl substituent's effect result in favorable or unfavorable interactions, and the electronic nature of the site that the substituent interacts with determine the favorability (Figure 3.1). Donating substituents

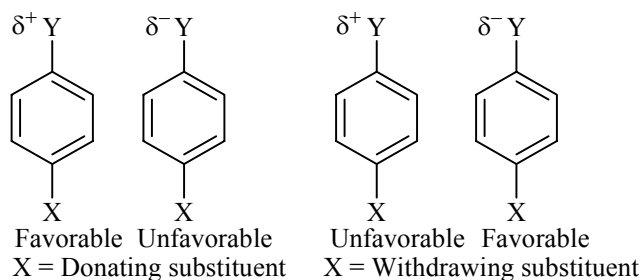
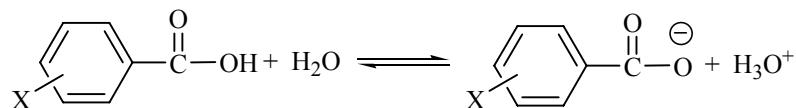


Figure 3.1 LFER studies use substituted arenes because of the ability of the aryl ring to electronically communicate to a remote reaction site.

interact favorably with electron-deficient reaction centers and unfavorably with electron-rich reaction centers. Electron-withdrawing substituents demonstrate the opposite preference. Only arenes which are substituted at the meta or para positions are suitable for these studies because these positions do not significantly perturb the reaction site through steric interactions. The quantitative parameters to describe the substituent effects were developed through examination of the change in pK_a of substituted benzoic acids (Scheme 3.3). Electron withdrawing substituents increase the ionization constant



Scheme 3.3 The σ parameter is determined from the pK_a of meta and para substituted benzoic acids.

(acidity) while donating substituents have the opposite effect.^{25,26} The values of σ are

defined by the ionization constants relative to the ionization constant of benzoic acid (Scheme 3.3; Equation 3.1)

$$\sigma_x = \log K_x - \log K_H \quad (\text{Eq. 3.1})$$

Where

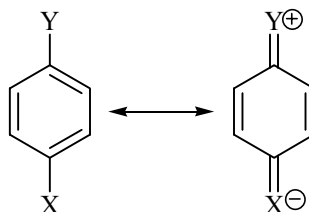
σ_x = σ -meta or σ -para

K_x = ionization constants of the substituted benzoic acids

K_H = ionization constant of benzoic acid in water at 25 °C

A result of defining benzoic acid as the standard is that electron withdrawing groups have $\sigma > 0$ for while $\sigma < 0$ is observed for electron donating groups.

In addition to through space interactions, substituent contributions from resonance effects can also impact the ionization constant. The parameters σ^+ and σ^- have been developed to account for the interactions that result from resonance contributions. The σ^+ parameter is used for reactions where resonance occurs with an electron-deficient reaction center, and σ^- is used for resonance with an electron-rich reaction site (Scheme 3.4).²⁶ Since σ^+ and σ^- are used for reaction sites where direct resonance occurs, these



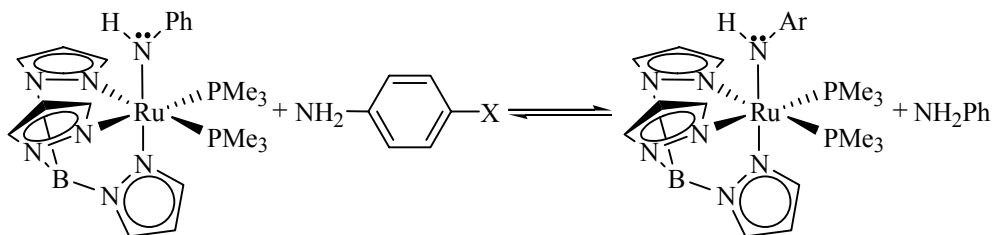
Scheme 3.4 The σ^+ and σ^- parameters. These parameters are used for LFER studies where the arene is in resonance with the reaction site.

values are appropriate when direct resonance with the reaction site is possible and thus only apply for para-substituted arenes.

The information from LFER studies is extracted by plotting the σ parameter versus $\log(k/k_0)$ when rate constants are used or by plotting the σ parameter versus $\log(K/K_0)$ when equilibria concentrations are measured. The value ρ is assigned as the slope of this plot, and this parameter provides information about the nature of the reaction site with which the arene interacts. A positive ρ indicates electron-withdrawing substituents increase the reaction rate or K_{eq} . Conversely, a negative ρ indicates electron deficiency in the transition state which can be stabilized by the donating arene groups.²⁶ The magnitude of ρ depends on the extent to which the arene can interact with the reaction center as well as the level of charge buildup; ρ increases with increased charge and arene interaction. Also, a plot with a sharply changing slope likely indicates an abrupt change of mechanism.^{25,26}

Analysis of bonding in late transition metal complexes with non-dative and π -donating ligands using Drago's EC theory as well as of the theory of π -conflict predicts that the M-N bond favors electron-withdrawing arene substituents on the aryl amido ligands.^{27,28,29} Studies of the thermodynamic trends for such complexes support the predictions of these two theories. For example, exchange reactions of $Cp^*Ir(silica)(Ph)(PMe_3)$ with para substituted phenols have been reported to favor electron-withdrawing substituents on the phenols.³⁰ In addition, LFER studies of the Ni(II) aryl amido complexes $Cp^*Ni(PEt_3)(NHPh)/NH_2(p-C_6H_4X)$ ($X = NMe_2, OMe, Me, F, CF_3$) have been reported with ρ determined to be 3.4 using σ_p^- parameters. The positive ρ indicates that electron-withdrawing groups are thermodynamically favored.³¹

In order to discern the extent of the amido lone pair delocalization into the phenyl ring of $\text{TpRu}(\text{PMe}_3)_2\text{NHPh}$, and to determine the thermodynamic preferences of the Ru(II) amido bond, a Hammett study was performed using the equilibria between $\text{TpRu}(\text{PMe}_3)_2\text{NHPh}$ and the para substituted anilines $p\text{-NH}_2\text{C}_6\text{H}_4\text{-X}$ ($\text{X} = \text{OMe}, \text{Me}, \text{F}, \text{CF}_3, \text{or NMe}_2$) (Scheme 3.5). The equilibrium constants were measured using NMR tube



Scheme 3.5 Hammett study of the $\text{TpRu}(\text{PMe}_3)_2\text{NHPh}$ amido complex. Exchange reactions with $p\text{-NH}_2\text{C}_6\text{H}_4\text{-X}$ ($\text{X} = \text{OMe}, \text{Me}, \text{F}, \text{CF}_3, \text{or NMe}_2$) were studied.

reactions in which an approximate 1:1 molar ratio of the amido complex $\text{TpRu}(\text{PMe}_3)_2\text{NHPh}$ and the respective arylamine was combined in C_6D_6 . The initial relative concentrations were determined by ^1H NMR spectroscopy by referencing against an internal standard (Cp_2Fe). The solutions were heated, and ligand exchange reactions were observed. The reactions were monitored periodically until equilibria were established. Equilibrium was assumed when no change in concentration was observed after 24 hours. The equilibrium constants were determined from the final ratios of amido complexes using ^1H and/or ^{31}P NMR spectroscopy. One to seven days heating was required depending on the arylamine and temperature. Temperatures ranging from 40 °C to 80 °C were required because decomposition was observed at higher temperatures for some of the systems. For example, the thermal instability of $\text{TpRu}(\text{PMe}_3)_2\{\text{NH}(p\text{-C}_6\text{H}_4\text{CF}_3)\}$ required gentle heating (40 °C) otherwise significant decomposition was

found to occur. In addition, the equilibrium for the reaction with $p\text{-NH}_2\text{C}_6\text{H}_4\text{CF}_3$ was confirmed by independently preparing the amido complex $\text{TpRu}(\text{PMe}_3)_2\{\text{NH}(p\text{-C}_6\text{H}_4\text{CF}_3)\}$ and reacting it with aniline. $\text{TpRu}(\text{PMe}_3)_2\{\text{NH}(p\text{-C}_6\text{H}_4\text{CF}_3)\}$ was prepared by deprotonation of the amine complex $[\text{TpRu}(\text{PMe}_3)_2\{\text{NH}_2(p\text{-C}_6\text{H}_4\text{CF}_3)\}][\text{OTf}]$ similar to the amido preparations discussed in Chapter 2. The reverse reaction was also conducted to confirm the K_{eq} because the strong thermodynamic preference ($K_{\text{eq}} \approx 1000$) for the $\text{NH}(p\text{-C}_6\text{H}_4\text{CF}_3)$ amido ligand over NHPH coupled with the low temperature (thus slow exchange) meant excessively long reaction time were required for the exchange of $\text{TpRu}(\text{PMe}_3)_2\text{NHPH}$ with $\text{NH}_2(p\text{-C}_6\text{H}_4\text{CF}_3)$, and during this reaction uncharacterized decomposition products were observed.

The LFER study of $\text{TpRu}(\text{PMe}_3)_2\text{NHAr}$ amido complexes indicate that amido ligands with electron-withdrawing groups favored binding to Ru, and the resulting equilibrium constants correlate well with σ_p^- parameters as shown in Figure 3.2 ($r^2 =$

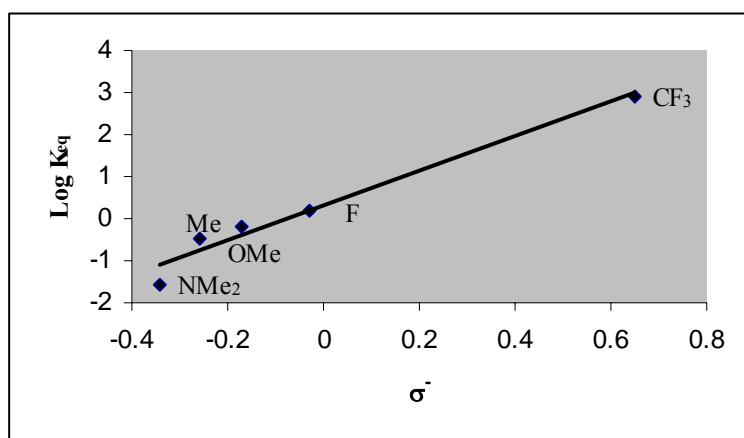
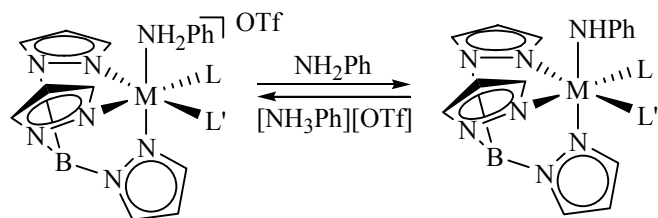


Figure 3.2 Hammett plot of $\log K_{\text{eq}}$ for aryl amido exchange reaction. $\rho = 4.1$; $r^2 = 0.97$.

0.97). The Hammett plot affords a ρ value of 4.1. Thus, negative charge is localized into the phenyl ring. Analogous exchange reactions with the complex $\text{TpRu}\{\text{P}(\text{OMe})_3\}_2\text{NHPh}$ and aryl amines were attempted; however, heating benzene solutions of this anilido complex with approximately one equivalent of para-substituted anilines resulted in decomposition.

3.3 Determination of the $\text{p}K_a$ of the Phenyl Amine Complexes and Ligand Effect on the $\text{p}K_a$.

The reactivity of π -donating ligands has been suggested to be increased for metal systems with filled $d\pi$ -orbitals due to disruption of ligand to metal π -donation.^{28,29,32} This heightened reactivity can be exemplified by contrasting the reactivity of analogous amido complexes of d^4 and d^6 metal centers. For example, the d^4 Os(IV) complex $\text{TpOs}(\text{Cl})_2\text{NHPh}$ is remarkably inert to strong acids, and the $\text{p}K_a$ of the conjugate acid of this complex $[\text{TpOs}(\text{Cl})_2\text{NH}_2\text{Ph}]^+$ was determined to approximately -3.¹⁴ Also, the d^4 W(II) complexes $[\text{Tp}^*\text{W}(\text{CO})_2(\text{NH}_2\text{Ph})]^+$ and $[\text{Tp}^*\text{W}(\text{CO})(\text{PhC}_2\text{H})(\text{NH}_2\text{Ph})]$ possess amine ligands acidic enough to be deprotonated by aniline.^{33,34} Excess aniline was used for the synthesis of $[\text{TpRu}(\text{L})(\text{L}')\text{NH}_2\text{Ph}][\text{OTf}]$ ($\text{L}, \text{L}' = \text{PMe}_3, \text{P}(\text{OMe})_3, \text{and CO}; \text{L} = \text{CO}, \text{L}' = \text{PPh}_3$), and unlike the d^4 tungsten complexes, aniline is insufficiently basic to deprotonate these d^6 amine complexes. The $\text{p}K_a$ of NH_3Ph^+ is approximately 3.2 in DMSO and is acidic enough to protonate $\text{TpRu}(\text{L})(\text{L}')\text{NHPh}$ (Scheme 3.5).³⁵ Based on the observation that aniline is not basic enough to deprotonate



Scheme 3.5 The Ru(II) d^6 anilido complexes are more basic than related W(II) d^4 systems. The amine complexes are not deprotonated in the presence of excess aniline.

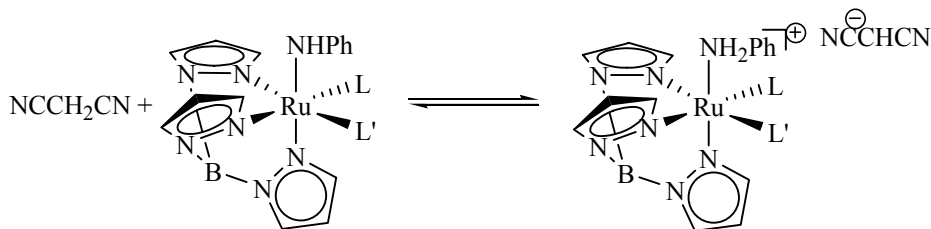
$[\text{TpRu}(\text{L})(\text{L}')\text{NH}_2\text{Ph}][\text{OTf}]$, qualitatively π -donation to serves to decrease the basicity of the amido ligand.

We sought to more accurately quantify the basicity of the amido complexes $\text{TpRu}(\text{CO})(\text{PPh}_3)(\text{NHPH})$, $\text{TpRu}(\text{PMe}_3)_2(\text{NHPH})$, and $\text{TpRu}\{\text{P}(\text{OMe})_3\}_2(\text{NHPH})$, as well as examine the influence of the donating ability of the ancillary ligands on $\text{p}K_a$. Mayer et al. have established the $\text{p}K_a$ of $[\text{TpOs}(\text{Cl})_2\text{NH}_2\text{Ph}]^{1+}$ is approximately -3 by observing an equilibrium with HOTf. Likewise, Bergman et al. have established the $\text{p}K_a$ of *trans*- $[(\text{dmpe})_2\text{Ru}(\text{NH}_3)(\text{H})]^{1+}$ is approximately 31 by observing an equilibrium with triphenylmethane.^{5,7} Thus, we sought to determine the approximate $\text{p}K_a$ values of amine complexes $[\text{TpRu}(\text{L})(\text{L}')\text{NHPH}]^+$ by observing the amido complexes in equilibrium with weak acids. To achieve this goal, we reacted the anilido complexes with increasingly stronger acids until equilibria were observed. Given the highly basic nature of *trans*- $(\text{dmpe})_2\text{Ru}(\text{NH}_2)(\text{H})$, phenylacetylene ($\text{p}K_a = 23$) was the first acid tested.³⁶ The complexes $\text{TpRu}(\text{L})(\text{L}')\text{NHPH}$ were reacted with HCCPh; however, no reaction was observed *at room temperature* after 24 H (reaction with phenylacetylene was observed with prolonged heating; details of these reactions are discussed below). Similarly, dissolution of $\text{TpRu}(\text{L})(\text{L}')\text{NHPH}$ in CD_2Cl_2 with 1 equivalent of methanol ($\text{p}K_a = 16$ in

water) resulted in no observable reaction after 24 hours. Ultimately, malononitrile (pK_a approximately 12 in CH_2Cl_2) was found to be of appropriate acidity to observe equilibria.³⁷

The addition of one equivalent of malononitrile to $\text{TpRu}(\text{PMe}_3)_2\text{NHPH}$ resulted in an immediate color change from yellow to pale purple. The ^1H NMR spectrum upon combination *with one equivalent* of malononitrile in CD_2Cl_2 revealed an immediate reaction at room temperature. For example, the resonance due to the amido NH proton of $\text{TpRu}(\text{PMe}_3)_2\text{NHPH}$ and the methylene CH protons of $\text{N}\equiv\text{CCH}_2\text{C}\equiv\text{N}$ were not observed and all other resonances were shifted toward $[\text{TpRu}(\text{PMe}_3)_2\text{NH}_2\text{Ph}]^+$ relative to starting materials (Figure 3.3). In addition, broad resonances were observed at 2.6 and 5.4 ppm. The addition of a second equivalent of malononitrile shifted the broad resonance at 2.6 ppm to 3.4 ppm (Figure 3.4).

These results are consistent with a rapid equilibrium in which the broad resonances at 2.6 and 5.4 ppm are due to a four-site rapid proton exchange between the amido proton of $\text{TpRu}(\text{PMe}_3)_2\text{NHPH}$, the amine protons of $[\text{TpRu}(\text{PMe}_3)_2\text{NH}_2\text{Ph}]^+$, the methylene protons of malononitrile, and the CH proton of the conjugate base of malononitrile (ion paired with the cationic amine complex) (Scheme 3.7).



Scheme 3.7 Equilibrium between the amido complexes/ malononitrile and amine ion pairs.

Variable temperature ^1H NMR spectroscopy was used to slow the exchange process. At $-90\text{ }^\circ\text{C}$ the resonance at 2.6 ppm decoalesces, and new broad resonances are observed at 3.8 and 1.6 ppm (Figure 3.5). The resonances at 3.8 and 1.6 ppm are assigned to the CH_2 and CH protons of malononitrile and its conjugate base. In CH_2Cl_2 , the methylene resonance of malononitrile is observed at 3.8 ppm. As an external confirmation for the assignment of the resonance at 1.6 ppm, the lithiated salt of malononitrile was prepared by deprotonation using butyl lithium.

Similar results were observed with the phenyl amido complexes $\text{TpRu}(\text{CO})(\text{PPh}_3)\text{NHPh}$ and $\text{TpRu}\{\text{P}(\text{OMe})_3\}_2(\text{NHPh})$. The reaction of $\text{TpRu}(\text{CO})(\text{PPh}_3)\text{NHPh}$ with one equivalent of malononitrile yields a ^1H NMR spectrum at $-90\text{ }^\circ\text{C}$ with broad resonances between 4.5 and 4.8 ppm (consistent with amido and amine proton chemical shifts), a broad resonance at approximately 3.8 ppm (malononitrile), and a broad resonance at 1.3 ppm (CH of malononitrile conjugate base). These four resonances coalesce at room temperature. The ^1H NMR spectrum of a 1/1 mixture of $\text{TpRu}\{\text{P}(\text{OMe})_3\}_2\text{NHPh}$ and malononitrile reveals resonances consistent with a single TpRu complex (presumably the amine and amido complex in rapid equilibrium) and a broad resonance at approximately 2.4 ppm. The resonance at 2.4 ppm is assigned as the time average between the CH_2 group of malononitrile and the CH group of the malononitrile conjugate base. The addition of a second equivalent of malononitrile shifts the resonance at 2.4 ppm to approximately 3.4 ppm. Thus based on ^1H NMR observation of the equilibria of these complexes with malononitrile, we established that the $\text{p}K_a$'s of the aniline complexes are approximately 12 in methylene chloride. Additionally, the

relative order of pK_a was assigned $PMe_3 \approx P(OMe)_3 > CO/PPh_3$, based on relative shift in the addition of one equivalent of malononitrile; i.e., $TpRu(PMe_3)_2NHPPh$ and $TpRu\{P(OMe)_3\}_2NHPPh$ were shifted to amine products, while $TpRu(CO)(PPh_3)NHPPh$ remained towards amido starting materials.

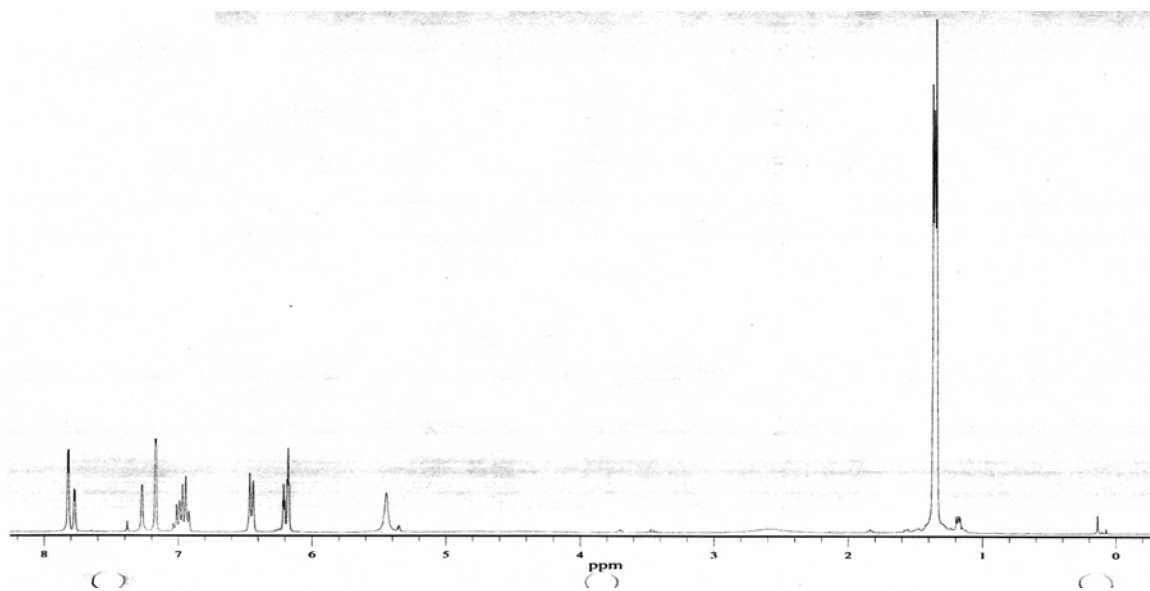


Figure 3.3 1H NMR spectrum of the reaction of $TpRu(PMe_3)_2NHPPh$ with one equivalent of malononitrile (room temperature).

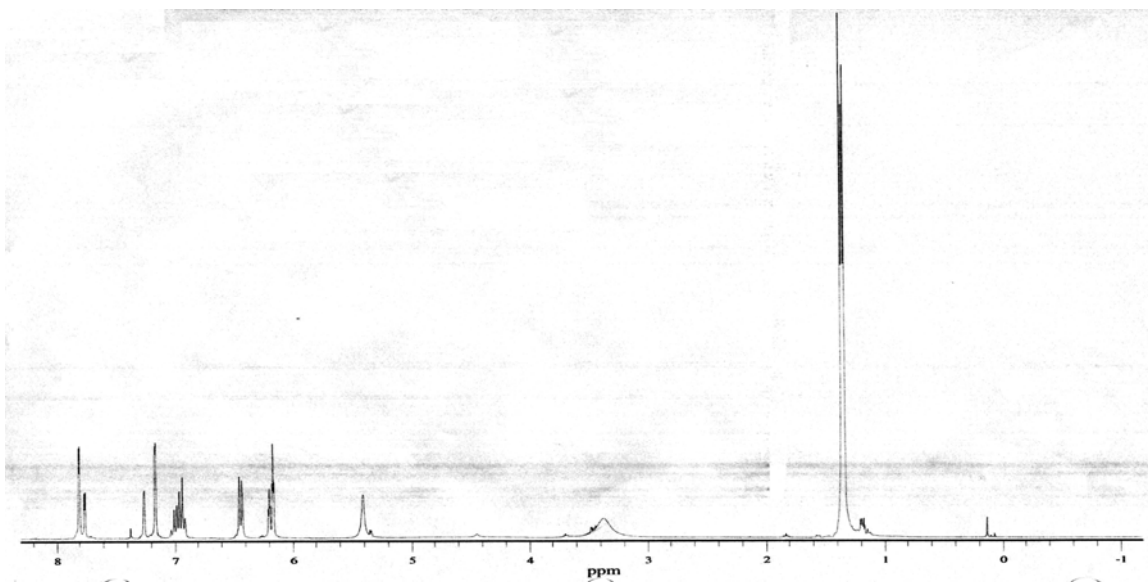


Figure 3.4 ¹H NMR spectrum of the reaction of $\text{TpRu}(\text{PMe}_3)_2\text{NHPPh}$ with two equivalent of malononitrile (room temperature).

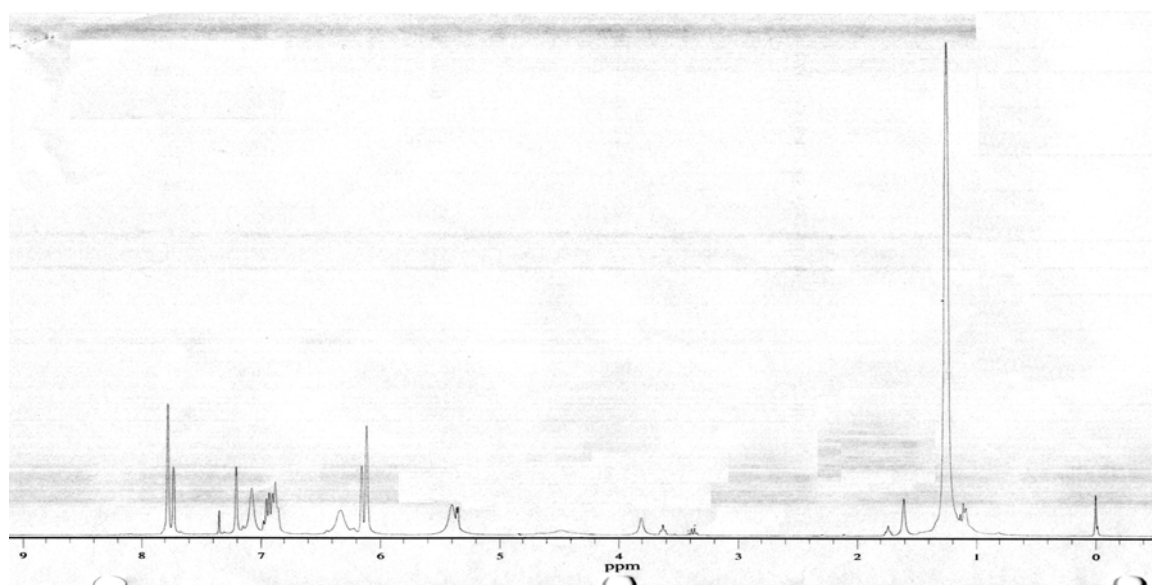


Figure 3.5 ¹H NMR spectrum of the reaction of $\text{TpRu}(\text{PMe}_3)_2\text{NHPPh}$ with one equivalent of malononitrile ($-90\text{ }^\circ\text{C}$).

3.4 UV-vis Studies of the Ru(II) Anilido-Malononitrile Reactions.

When one UV-vis absorbing species undergoes transformations to generate another absorbing species, a characteristic feature can be observed in the UV-vis spectrum provided the two species absorbencies overlap at some wavelength. A point in the spectra for which the absorbance remains constant throughout the transformation of the species is known as the isosbestic point, and the observation of such a point is good evidence only two principal species are present.³⁸

For our studies, stock solutions of each of the amido complexes were prepared. Also, stock solutions of malononitrile of equal concentrations to the amido solutions were prepared. Using a pipette, 1.00 mL of the amido solution was reacted with increasing amounts of the respective malononitrile solution (0.2 to 1.2 equivalents for each amido complex). Each of these reactions was then diluted to 5.00 mL, thus all total concentrations of Ru(II) remained constant (i.e., the concentration of $\text{TpRu(L)(L')NHPH} + [\text{TpRu(L)(L')NH}_2\text{Ph}]^+ = \text{constant}$ for each amido system).

To confirm that the amido complexes are in an acid/base equilibrium with malononitrile, UV-vis spectra of THF solutions of the amido complexes $\text{TpRu(PMe}_3)_2(\text{NHPH})$ or $\text{TpRu}\{\text{P(OMe)}_3\}_2(\text{NHPH})$ with malononitrile were acquired. λ_{max} of the amine and amido complexes are listed in Table 3.1. Neither malononitrile nor the lithium salt $[\text{Li}][\text{NCCHCN}]$ absorb in the range of interest ($\lambda_{\text{max}} < 220 \text{ nm}$).

Table 3.1 UV-Vis data for the Ru(II) amine and amido complexes in THF

Complex	λ_{\max} (nm)	ϵ ($M^{-1} \text{ cm}^{-1}$)
[TpRu(CO)(PPh ₃)(NH ₂ Ph)][OTf]	207	8.2×10^4
TpRu(CO)(PPh ₃)(NHPH)	216	1.2×10^4
[TpRu(PMe ₃) ₂ (NH ₂ Ph)][OTf]	267	0.96×10^4
TpRu(PMe ₃) ₂ (NHPH)	293	1.7×10^4
[TpRu{P(OMe) ₃ } ₂ (NH ₂ Ph)][OTf]	223	2.0×10^4
[TpRu{P(OMe) ₃ } ₂ (NHPH)]	284	1.3×10^4

The use of UV-vis spectroscopy to confirm an acid-base equilibrium with TpRu(CO)(PPh₃)NHPH and malononitrile was complicated by broad and overlapping absorptions for the anilido and amine complexes. For example, the addition of one 1 equivalent of malononitrile to a solution of TpRu(CO)(PPh₃)NHPH in THF reveals $\lambda_{\max} = 216$. Qualitatively this observation could suggest the equilibrium rests towards the amido; however, given the roughly 7 fold increase in the absorbance compared to the amine complex, and the extent overlap of the two absorbances, determination of the relative concentrations of the two complexes could not be achieved accurately.

The amido complex TpRu(PMe₃)₂(NHPH) exhibits $\lambda_{\max} = 293$ nm in its UV-vis spectrum, and the amine complex [TpRu(PMe₃)₂(NH₂Ph)][OTf] absorbs at $\lambda_{\max} = 267$ nm. The UV-vis spectrum of a combination of complex TpRu(PMe₃)₂(NHPH) with 1 equiv of malononitrile shows an absorption at $\lambda_{\max} = 227$ nm caused by the formation of

the cationic amine (via deprotonation of malononitrile) with a red-shifted shoulder due to the amido complex $\text{TpRu}(\text{PMe}_3)_2(\text{NHPh})$ ($\lambda_{\text{max}} = 293 \text{ nm}$). Similarly, the combination of amido complex $\text{TpRu}\{\text{P}(\text{OMe})_3\}_2(\text{NHPh})$ with malononitrile exhibits similar results, and variation of malononitrile concentrations results in the observation of isosbestic point (Figure 3.6 and 3.7).

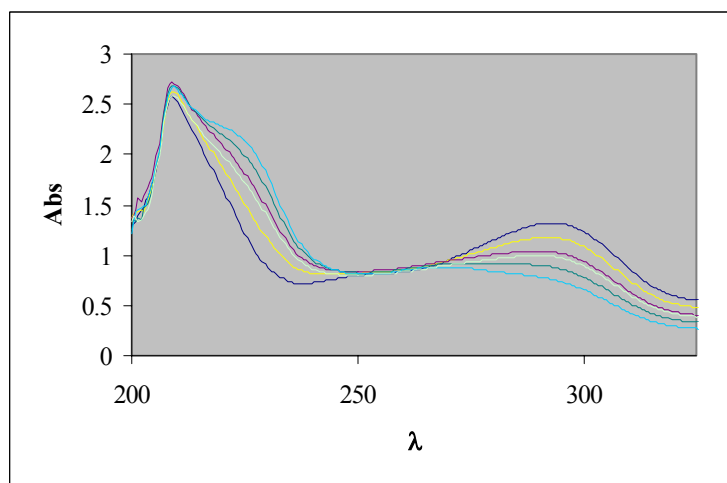


Figure 3.6 Isosbestic point of $\text{TpRu}(\text{PMe}_3)_2\text{NHPh}$ with addition of malononitrile

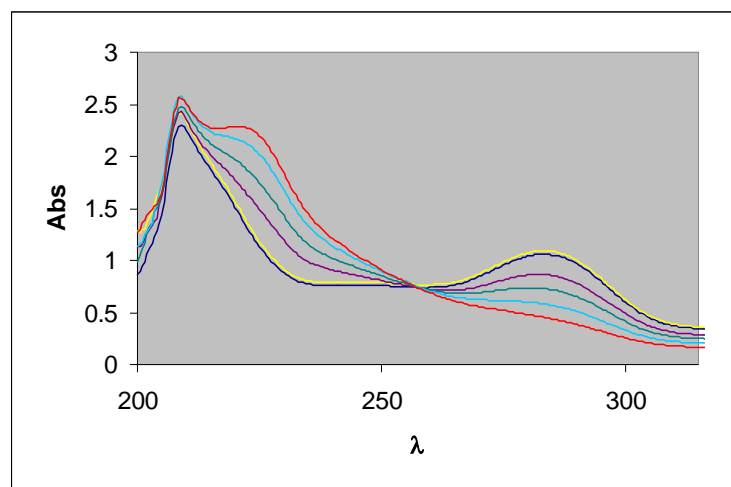


Figure 3.7 Isosbestic point of $\text{TpRu}\{\text{P}(\text{OMe})_3\}_2\text{NHPh}$ with addition of malononitrile.

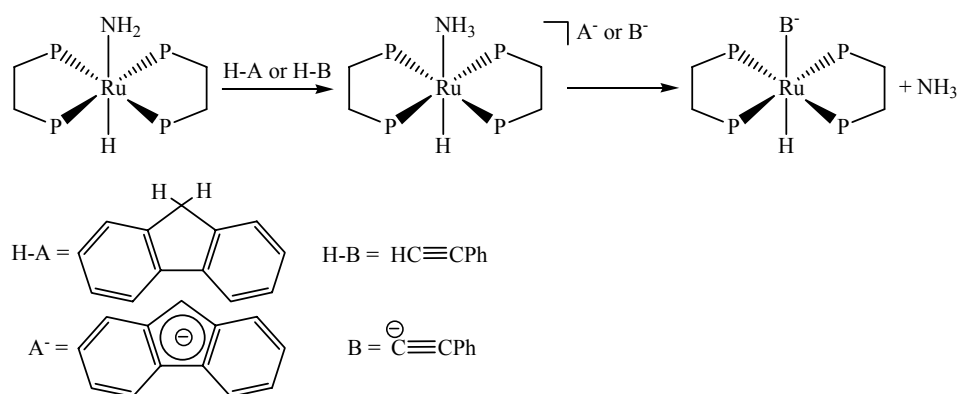
Based on the observation by ^1H NMR and UV-Vis spectroscopy of equilibria between the anilido complexes $\text{TpRu}(\text{PMe}_3)_2\text{NHPH}$, $\text{TpRu}\{\text{P}(\text{OMe})_3\}_2\text{NHPH}$, and $\text{TpRu}(\text{CO})(\text{PPh}_3)\text{NHPH}$ and malononitrile, the $\text{p}K_a$ of the phenyl amine complexes was established to be approximately 12 in CH_2Cl_2 . Compared to related the d^4 Os(IV) and W(II) systems discussed above, there is a shift of $\text{p}K_a$ approximately 15 orders of magnitude between the Os(IV) system, and at least 9 orders of magnitude between the W(II) system. The large difference in $\text{p}K_a$ is attributed to the ability of the d^4 systems to effectively π -accept the amido lone pair thereby stabilizing against basic reactivity. The qualitative trend of basicity was found to be $\text{PMe}_3 \approx \text{P}(\text{OMe})_3 > \text{CO}/\text{PPh}_3$. Interestingly, the effect of ancillary ligands donating/withdrawing ability did not significantly affect the $\text{p}K_a$, less than one $\text{p}K_a$ unit.

3.5 Reaction of the Amido Complexes with Weak Acids and Studies of the Reaction with Phenylacetylene.

Our initial reactivity studies focused on comparing the reactivity of our Tp based ruthenium amido systems to *trans*-(dmpe) $_2$ Ru(H)(NH $_2$) and *cis*-(PMe $_3$) $_4$ Ru(NH $_2$)(H) reported by Bergman et al.^{5,7³⁹} For example, *trans*-(dmpe) $_2$ Ru(H)(NH $_2$) was shown to be in equilibrium with triphenylmethane and H/D exchange was observed with the methyl protons of toluene- d_8 . Reactions of the amido complexes TpRuL_2NHR (L, = PMe $_3$ or P(OMe) $_3$; and R = H or ^tBu) with triphenylmethane show no deprotonation based on ^1H NMR spectroscopy. Thus, the TpRuL_2NHR amido complexes are qualitatively less basic than *trans*-(dmpe) $_2$ Ru(H)(NH $_2$) and *trans*-(dmpe) $_2$ Fe(H)(NH $_2$)

since both deprotonate triphenylmethane.^{5,7,39} Similarly, heating solutions of these complexes in toluene-*d*₈ do not result in H/D exchange of the methyl protons of toluene. Note, the amido complexes TpRu{P(OMe)₃}₂NHR (R = H or ^tBu) decompose rapidly at elevated temperatures thus decomposition complicates these reactions; however, the solutions of the TpRu(PMe₃)₃NHR (R = H or ^tBu) amido complexes were heated up to 80 °C for several hours and showed no H/D exchange.

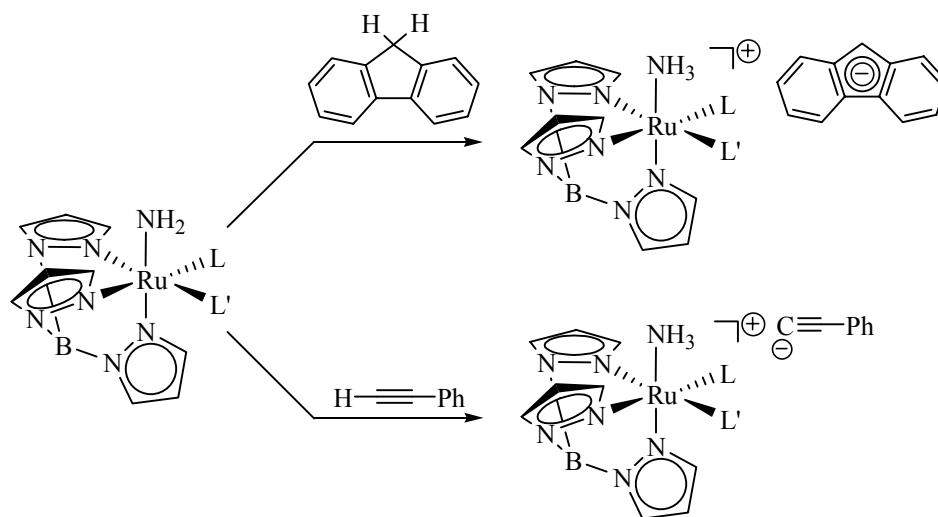
Bergman et al. have examined the reactivity of *trans*-(dmpe)₂Ru(H)(NH₂) with various other weak acids in an attempt to examine the coordination effects. For example both phenylacetylene and fluorene are deprotonated to form initial ion pairs. The acetylide anion coordinates to release ammonia, while the bulky fluorenyl anion was found not to coordinate (Scheme 3.8).



Scheme 3.8 Reactions of *trans*-(dmpe)₂Ru(H)(NH₂) with weak acids. The acetylide ion was found to displace ammonia while the bulky fluorenyl anion did not.

The TpRu(L)(L')NH₂ amido complexes exhibit similar reactivity to *trans*-(dmpe)₂Ru(H)(NH₂). For example, the TpRu(L)(L')NH₂ amido complexes also exhibit

the ability to deprotonate the C-H bonds of phenylacetylene or fluorene, and the reactions with these weak acids proceed to similar *initial* products (Scheme 3.9).



Scheme 3.9 Reactivity studies of the parent amido complexes TpRu(L)(L')NH_2 with phenylacetylene or fluorene.

Reactions with fluorene or phenylacetylene form Ru(II)-amine/organic anion ion pairs. For example, fluorene reacts immediately with the amido complexes $\text{TpRu(PMe}_3)_2\text{NH}_2$ or $\text{TpRu}\{\text{P(OMe)}_3\}_2\text{NH}_2$. Addition of one equivalent of fluorene to solutions of amido complexes in C_6D_6 or $\text{THF-}d_8$ revealed a color change from yellow to pale blue. The products of this reaction are highly air sensitive, and have only been characterized by ^1H NMR spectroscopy which revealed the disappearance of resonances due to fluorene CH_2 protons and Tp resonances were shifted towards the Ru(II) amine complexes $[\text{TpRu(PMe}_3)_2\text{NH}_3]^+$ or $[\text{TpRu}\{\text{P(OMe)}_3\}_2\text{NH}_3]^+$. Also, resonances consistent with a fluorenyl anion were observed.

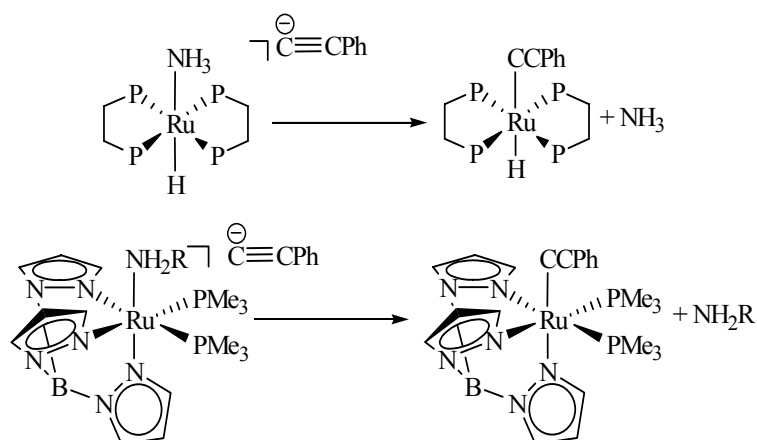
Likewise, the complexes $\text{TpRu}(\text{PMe}_3)_2\text{NH}_2$ and $\text{TpRu}\{\text{P}(\text{OMe})_3\}_2\text{NH}_2$ react immediately with phenylacetylene. The addition of 1 equivalent of $\text{HC}\equiv\text{CPh}$ to NMR tube solutions of the respective amido complexes in $\text{THF}-d_8$ resulted in an immediate color change from yellow to pale-yellow/colorless. The upfield resonances due to the amido proton were absent, as was the acetylene proton of phenylacetylene. A broad singlet that integrates for 3H relative to the Tp resonances was observed at approximately 2 ppm and aromatic resonances were observed between 7.3 and 7.4 ppm due to the acetylide anion. These observations are consistent with deprotonation of phenylacetylene to form the corresponding Ru(II) amine complexes with a phenylacetylide counterion. In contrast to the trimethylphosphine and trimethylphosphite parent amido complexes, the addition of phenylacetylene to $\text{TpRu}(\text{CO})(\text{PPh}_3)\text{NH}_2$ did not result in immediate deprotonation of phenylacetylene. More than 24 h were required for full deprotonation of phenylacetylene.

Similar reactivity to the parent amido complexes was observed with the amido complexes $\text{TpRuL}_2\text{NH}^t\text{Bu}$ ($\text{L} = \text{PMe}_3$ or $\text{P}(\text{OMe})_3$). Reactions with phenylacetylene conducted at room temperature in C_6D_6 or $\text{THF}-d_8$ undergo immediate deprotonation to form an amine ion pair complex $[\text{TpRuL}_2\text{NH}_2^t\text{Bu}][\text{CCPh}]$. ^1H NMR spectroscopy reveals similar results to the parent amido complexes (i.e., disappearance of the phenylacetylene terminal *CH* resonance and the amido *NH* resonance upon addition). Conversely, room temperature addition of phenylacetylene to $\text{TpRu}(\text{L})(\text{L}')\text{NHPh}$ ($\text{L}, \text{L}' = \text{PMe}_3$ or $\text{P}(\text{OMe})_3$; $\text{L} = \text{CO}$, $\text{L}' = \text{PPh}_3$) in THF or benzene does not yield reactions after

one week at room temperature. Thus the anilido complexes are at least 11 orders of magnitude less basic than the parent or ^tBu analogs.

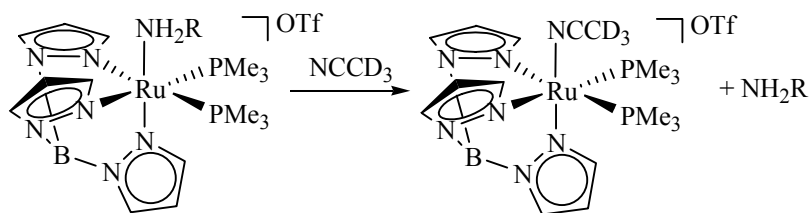
The ion pairs formed from the reaction with phenylacetylene have been characterized by ¹H, ¹³C, and ³¹P NMR spectroscopy, and can be isolated upon addition of phenylacetylene to solutions of the amido complexes in non-polar solvents such as benzene through precipitation of the amine/ ion pair complex which can be isolated by filtration through a fine porosity frit; however, these complexes are unstable and attempts at further analysis using techniques such as X-ray diffraction or elemental analysis were unsuccessful.

Bergman et al. have reported the ion pair complex [*trans*-(DMPE)₂Ru(H)(NH₃)] [CCPh] undergoes ligand exchange reactions to form *trans*-(DMPE)₂Ru(H)(CCPh) and ammonia. In contrast, solution of the complexes [TpRu(L)(L')(NH₃)] [CCPh] do not undergo phenylacetylide counter ion / ammonia ligand exchange reactions at room temperature, and heating solutions of these complexes at 80 °C for approximately 20 hours yield multiple intractable Tp containing complexes. Parallel reactions with the ^tBu amido complexes TpRu(PMe₃)₂NH^tBu readily undergo ligand exchange to form TpRu(PMe₃)₂CCPh and tert-butylamine (Scheme 3.10). Amine lability seemed likely attributable for the difference between these complexes.



Scheme 3.10 Reactivity of amine-acetylide ion pair complexes.

To examine the relative lability of the amine ligands, ligand exchange reactions were conducted in deuterated acetonitrile. Dissolution of the Ru(II) amine complexes $[\text{TpRu}(\text{PMe}_3)_2(\text{NH}_2\text{R})][\text{OTf}]$ ($\text{R} = \text{Ph}$ or ${}^t\text{Bu}$) in CD_3CN results in ligand exchange reactions to yield $[\text{TpRu}(\text{PMe}_3)_2(\text{N}\equiv\text{CCD}_3)][\text{OTf}]$ (Scheme 3.11). Each reaction was



Scheme 3.11 Examination of the amine ligand lability by reaction of the complexes $[\text{TpRu}(\text{PMe}_3)_2(\text{NH}_2\text{R})][\text{OTf}]$ ($\text{R} = \text{Ph}$ or ${}^t\text{Bu}$) with CD_3CN .

monitored starting with a 0.06 M solution of the $[\text{TpRu}(\text{PMe}_3)_2\text{NH}_2\text{R}][\text{OTf}]$ in CD_3CN at room temperature, and the resulting first-order kinetic plots are shown in Figure 3.8 ($R^2 = 0.99$ for both plots). The rate constant for the exchange reaction of the ${}^t\text{Bu}$ -amine

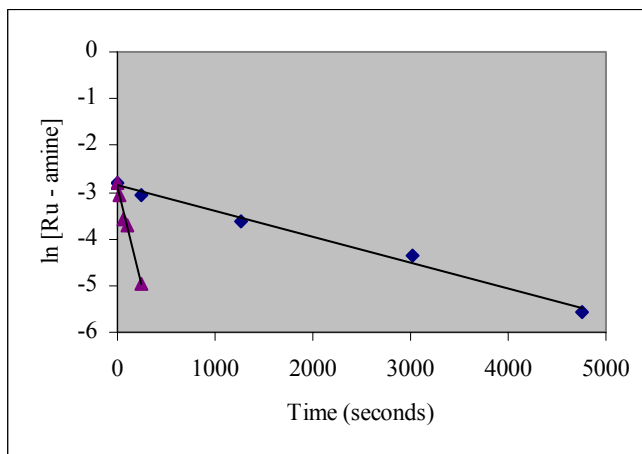


Figure 3.8 Kinetics of the reaction of $[\text{TpRu}(\text{PMe}_3)_2\text{NH}_2\text{R}][\text{OTf}]$ with CD_3CN . (\blacktriangle = $\text{R} = {}^t\text{Bu}$; \blacksquare = $\text{R} = \text{Ph}$).

complex $[\text{TpRu}(\text{PMe}_3)_2(\text{NH}_2{}^t\text{Bu})][\text{OTf}]$ is approximately an order of magnitude greater than that for $[\text{TpRu}(\text{PMe}_3)_2(\text{NH}_2\text{Ph})][\text{OTf}]$ ($k_{\text{obs}} = 1.4 \times 10^{-4} \text{ s}^{-1}$ for the ^tBu amine complex and $9.2 \times 10^{-6} \text{ s}^{-1}$ for the aniline complex at room temperature) (Figure 3.8). In contrast to aniline and ^tBu amine complexes, the parent ammine complex $[\text{TpRu}(\text{PMe}_3)_2(\text{NH}_3)][\text{OTf}]$ shows no evidence of ligand exchange after 5 days at room temperature and 48 h at 90 °C. In order to determine if the lack of reaction between $[\text{TpRu}(\text{PMe}_3)_2(\text{NH}_3)][\text{OTf}]$ and CD_3CN is due to kinetic or thermodynamic factors, $[\text{TpRu}(\text{PMe}_3)_2(\text{NCCH}_3)][\text{OTf}]$ was combined with a THF solution of ammonia in a sealed pressure tube. After 12 days at approximately 70 °C, a ¹H NMR spectrum of the nonvolatile products revealed only starting material (i.e., no ligand exchange occurred). In addition, dissolution of $[\text{TpRu}(\text{PMe}_3)_2(\text{NCCH}_3)][\text{OTf}]$ in CD_3CN at 80 °C for 48 h reveals no evidence of $\text{NCCH}_3/\text{NCCD}_3$ exchange. The failure of the acetonitrile ligand of $[\text{TpRu}(\text{PMe}_3)_2(\text{NCCH}_3)][\text{OTf}]$ to undergo exchange with deuterated acetonitrile

prevents conclusions about the inability to exchange the ammonia ligand of $[\text{TpRu}(\text{PMe}_3)_2(\text{NH}_3)][\text{OTf}]$ with CD_3CN .

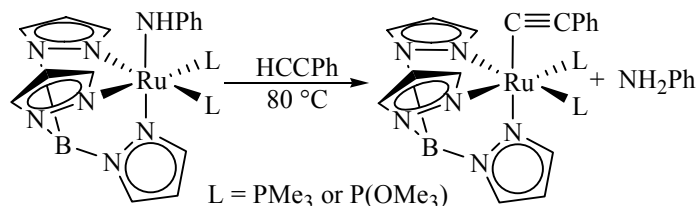
While the difference in basicity between the parent and ^tBu amido complexes $\text{TpRu}(\text{L})(\text{L}')\text{NHR}$ ($\text{L} = \text{L}' = \text{PMe}_3$ or $\text{P}(\text{OMe})_3$ and $\text{L} = \text{CO}$, $\text{L}' = \text{PPh}_3$; $\text{R} = \text{H}$ or ^tBu) cannot be discerned from the reactions with phenylacetylene, the $\text{p}K_a$ of the corresponding amine complexes of these amido complexes has been determined to be between 31.5 and 23. The parent and ^tBu amido complexes are significantly more basic than the phenyl amido complexes ($\Delta\text{p}K_a > 11$). The difference in basicity is attributed to the ability of the aryl ring of the anilido moiety to delocalize the nitrogen lone pair. In addition, amine lability can affect the final products of the deprotonation reactions. Specifically, more labile amines cleanly convert to products.

3.6 Reaction of the Phenyl Amido Complexes with Phenylacetylene.

While the parent and ^tBu amido complexes TpRuL_2NHR ($\text{L} = \text{PMe}_3$ or $\text{P}(\text{OMe})_3$; $\text{R} = \text{H}$ or ^tBu) undergo acid/base transformations with phenylacetylene, the complexes $\text{TpRuL}_2\text{NHPh}$ ($\text{L} = \text{PMe}_3$ or $\text{P}(\text{OMe})_3$) do not react with phenylacetylene at room temperature in solutions of THF or benzene. Thus, the phenyl substituent on the amido ligand serves to decrease the basicity of the ligand by approximately 11 orders of magnitude.

Heating THF- d_8 or benzene- d_6 solutions of the anilido complexes $\text{TpRuL}_2\text{NHPh}$ ($\text{L} = \text{PMe}_3$ or $\text{P}(\text{OMe})_3$) with 10 equivalents of phenylacetylene at approximately 80 °C results in the formation of the respective Ru(II) phenylacetylide complexes

TpRuL₂(C≡CPh) and aniline (Scheme 3.12). The reaction of TpRu(CO)(PPh₃)NHPPh



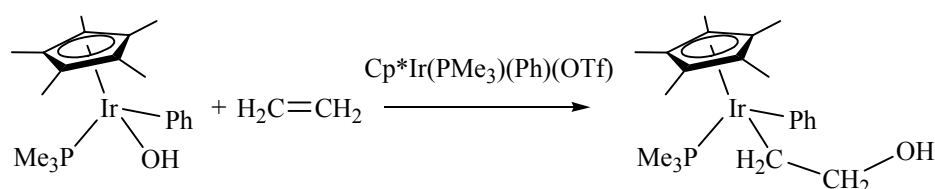
Scheme 3.12 Reaction of the amido complexes TpRuL₂NHPPh (L = PMe₃ or P(OMe)₃) with phenylacetylene at 80 °C yields the Ru respective acetylide complexes.

with 10 equiv of phenylacetylene results in decomposition to multiple intractable Tp containing species complexes.

Given, the anilido complexes TpRuL₂(NHPPh) (L = PMe₃ or P(OMe)₃) do not react with phenylacetylene at room temperature, but net deprotonation to form aniline and the respective Ru(II) acetylide complexes was observed with heating, we attempted to determine the mechanism of the reaction in Scheme 3.12 by examining the kinetics of this reaction. The reaction of TpRu(PMe₃)₂NHPPh in the presence of 10 and 20 equivalents of phenylacetylene show an increase in rate, and plots of these reactions were consistent with first order kinetics with respect to TpRu(PMe₃)₂NHPPh (i.e., plots of ln[TpRu(PMe₃)₂NHPPh] versus time were linear). Monitoring the reaction of TpRu{P(OMe)₃}₂NHPPh with 10 equivalents of phenylacetylene revealed inconsistent kinetic results. Specifically, a reproducible reaction rate could not be achieved, and the kinetics were consistent with zero order with respect to TpRu{P(OMe)₃}₂NHPPh (i.e., plots of [TpRu{P(OMe)₃}₂NHPPh] versus time were linear). The observation of complicated and varying kinetic results between TpRu(PMe₃)₂NHPPh and

TpRu{P(OMe)₃}₂NHPh suggested the possibility of an unobserved impurity catalyzing the reaction between these amido complexes and phenylacetylene.

Bergman et al. have reported the reaction of the iridium(II) hydroxide Cp*Ir(PMe₃)(Ph)(OH) with ethylene undergoes nucleophilic insertion to form the hydroxyethyl complex Cp*Ir(PMe₃)(Ph)(CH₂CH₂OH) by a mechanism catalyzed by the Ir(II) triflate complex Cp*Ir(PMe₃)(Ph)(OTf) (Scheme 3.13).⁴⁰ Based on this literature



Scheme 3.13 Reaction of Cp*Ir(PMe₃)(Ph)(OH) with ethylene. The triflate complex Cp*Ir(PMe₃)(OTf) was found to catalyze this reaction.

precedent, we anticipated an unobserved amount of TpRuL₂(OTf) or [TpRuL₂NH₂Ph][OTf] was catalyzing reaction of TpRuL₂NHPh and phenylacetylene. To test this hypothesis, reactions of amido complex TpRu(PMe₃)₂NHPh with 10 equivalents of phenylacetylene in the presence of catalytic amounts TpRu(PMe₃)₂OTf were conducted. These reactions revealed an increase in the rate of formation of TpRu(PMe₃)₂(C≡CPh) with increased concentration of TpRu(PMe₃)₂OTf. A plot of k_{obs} versus concentration of TpRu(PMe₃)₂(OTf) revealed a linear dependence of the concentration of the triflate complex TpRu(PMe₃)₂(OTf) (Figure 3.9). Also, addition of 0.4 equivalents of PMe₃ (based on the ruthenium amido) resulted in complete suppression of the formation of the acetylide complex TpRu(PMe₃)₂(C≡CPh); no reaction of was

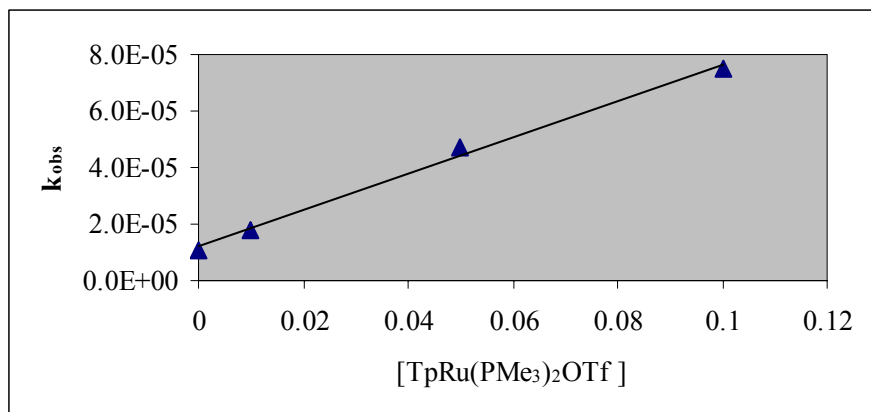
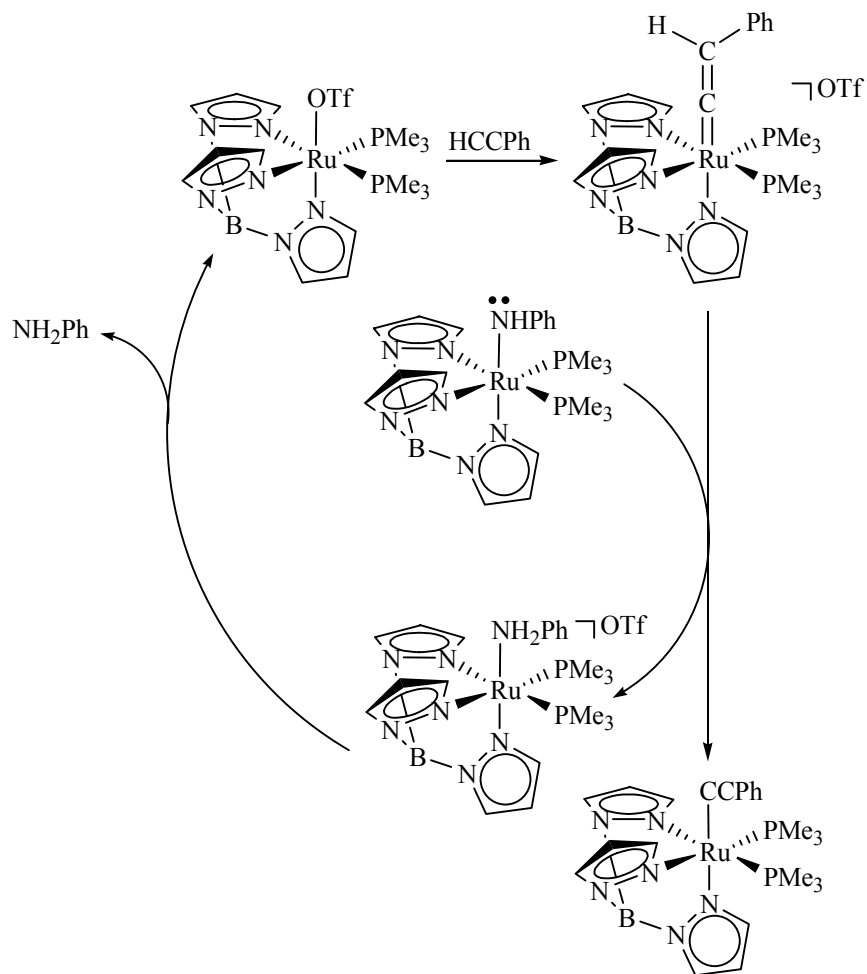


Figure 3.9 Plot of k_{obs} versus concentration of $\text{TpRu}(\text{PMe}_3)_2(\text{OTf})$.

observed after 24 hours of heating. Based on these observations, we suggest that the triflate complex catalyzes the reaction of $\text{TpRu}(\text{PMe}_3)_2\text{NHPH}$ and phenylacetylene to $\text{TpRu}(\text{PMe}_3)_2(\text{C}\equiv\text{CPh})$ and aniline. The proposed mechanism of this reaction involves initial reaction of $\text{TpRu}(\text{PMe}_3)_2\text{OTf}$ and phenylacetylene to form the vinylidene complex $[\text{TpRu}(\text{PMe}_3)_2(=\text{C}=\text{CHPh})][\text{OTf}]$. Subsequently, the vinylidene complex is deprotonated by $\text{TpRu}(\text{PMe}_3)_2\text{NHPH}$ to form the acetylide complex $\text{TpRu}(\text{PMe}_3)_2(\text{C}\equiv\text{CPh})$ and $[\text{TpRu}(\text{PMe}_3)_2\text{NH}_2\text{Ph}][\text{OTf}]$. The amine complex then releases aniline to regenerate the catalyst (Scheme 3.14). It is also possible that trace $[\text{TpRu}(\text{PMe}_3)_2\text{NH}_2\text{Ph}][\text{OTf}]$ in the reaction mixtures could serve as the catalyst if aniline was displaced by acetylene. Also, the suppression that is observed with addition of 0.4 equivalents of PMe_3 is likely attributable to phosphine coordination to the triflate complex $\text{TpRu}(\text{PMe}_3)_2\text{OTf}$ preventing the coordination of phenylacetylene. Phosphine binding to the triflate complex would result in formation of $[\text{TpRu}(\text{PMe}_3)_3][\text{OTf}]$. In a separate reaction, the



Scheme 3.14 Proposed mechanism of the reaction of $\text{TpRu}(\text{PMe}_3)_2\text{NHPH}$ with phenylacetylene.

addition of one equivalent of PMe_3 to solutions of $\text{TpRu}(\text{PMe}_3)_2\text{OTf}$ in CH_2Cl_2 resulted in rapid coordination of the phosphine to form the complex $[\text{TpRu}(\text{PMe}_3)_3][\text{OTf}]$. This complex has been characterized by ^1H NMR, ^{13}C and ^{31}P NMR spectroscopy and is consistent with a C_3 symmetric complex (Figure 3.10).

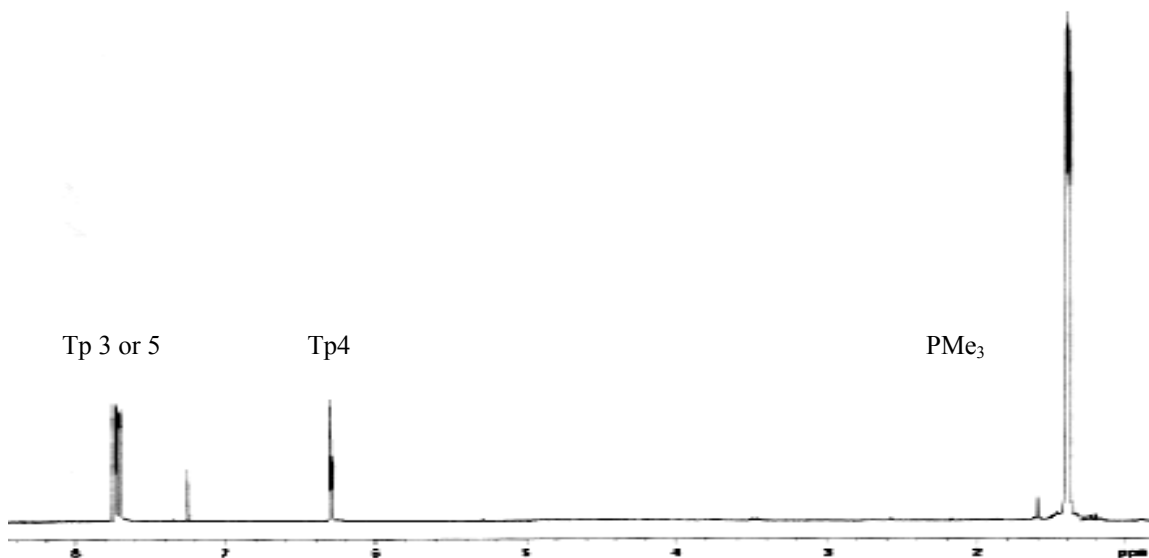
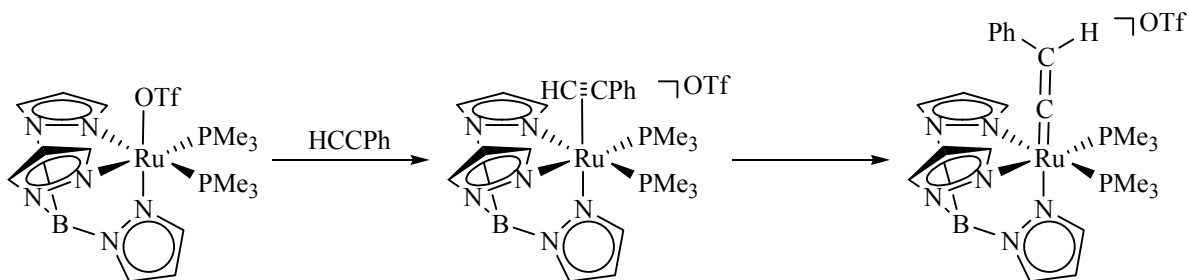


Figure 3.10 ^1H NMR spectrum of $[\text{TpRu}(\text{PMe}_3)_3][\text{OTf}]$ in CDCl_3 .

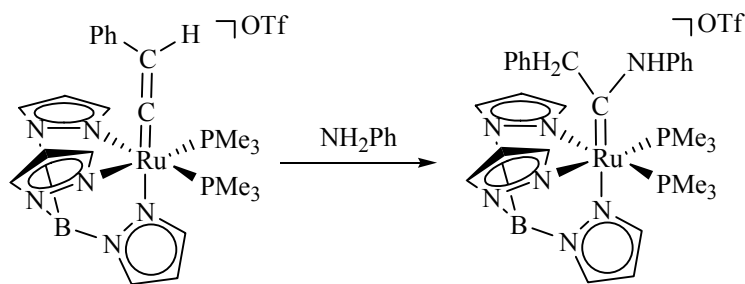
Monitoring the reaction of 10 mol % $\text{TpRu}(\text{PMe}_3)_2(\text{OTf})$ with $\text{TpRu}(\text{PMe}_3)_2\text{NHPh}$ and phenylacetylene by ^1H NMR spectroscopy revealed the presence of a mixture of species during the course of the reaction. For example, after approximately 50% conversion, aniline, $\text{TpRu}(\text{PMe}_3)_2(\text{C}\equiv\text{CPh})$, and the vinylidene complex $[\text{Tp}(\text{PMe}_3)_2\text{Ru}=\text{C}=\text{C}(\text{H})\text{Ph}][\text{OTf}]$ are observed. Also, the Tp resonances and the PMe_3 resonances were broadened. The vinylidene complex has been independently prepared by reacting $\text{TpRu}(\text{PMe}_3)_2\text{OTf}$ with phenylacetylene (Scheme 3.15). The ^1H NMR spectrum of the vinylidene complex is consistent with C_s -symmetry, and the vinylidene CH proton is observed as a triplet at 5.29 ppm ($^3J_{\text{PH}} = 3$ Hz). The broad Tp and PMe_3 resonances observed at 50% conversion are likely due to a mixture of amine and amido complexes undergoing self exchange. The combination of $[\text{TpRu}(\text{PMe}_3)_2(\text{NH}_2\text{Ph})][\text{OTf}]$



Scheme 3.15 Reaction of the triflate complex $\text{TpRu}(\text{PMe}_3)_2\text{OTf}$ with phenylacetylene yields the vinylidene complex $[\text{TpRu}(\text{PMe}_3)_2(\text{C}=\text{CHPh})][\text{OTf}]$.

and $\text{TpRu}(\text{PMe}_3)_2(\text{NHPh})$ in C_6D_6 confirms that the broadened resonances could be due to an amine/amido mixture (i.e., similarly broadened resonances are observed). In addition, after approximately 50% conversion to products, a new TpRu complex that exhibits a downfield singlet at 11.83 ppm is observed by ^1H NMR in small quantities (< 5%). This complex has been identified as the Fisher carbene complex $[\text{Tp}(\text{PMe}_3)_2\text{Ru}=\text{C}(\text{CH}_2\text{Ph})\{\text{N}(\text{H})\text{Ph}\}][\text{OTf}]$ and is formed upon reaction of $[\text{Tp}(\text{PMe}_3)_2\text{Ru}=\text{C}=\text{C}(\text{H})\text{Ph}][\text{OTf}]$ with aniline. This carbene complex has been independently prepared and by reaction of the vinylidene complex and aniline (Scheme 3.16). Consistent with the product observed towards the end of the reaction of $[\text{Tp}(\text{PMe}_3)_2\text{Ru}=\text{C}(\text{CH}_2\text{Ph})\{\text{N}(\text{H})\text{Ph}\}][\text{OTf}]$, the complex shows a NH resonance at 11.83 ppm and the carbene CH_2 resonance at 4.13 ppm.

The kinetic results for the reaction of $\text{TpRu}(\text{PMe}_3)_2\text{NHPh}$ with phenylacetylene demonstrate that the reaction is catalyzed by the presence of an impurity, likely a small amount of $[\text{TpRu}(\text{PMe}_3)_2\text{NH}_2\text{Ph}][\text{OTf}]$ or $\text{TpRu}(\text{PMe}_3)_2\text{OTf}$. The mechanism presented in Scheme 3.14 is supported by the isolation of the reaction intermediates, and the observation that excess trimethylphosphine results in suppression of reactivity. Thus it



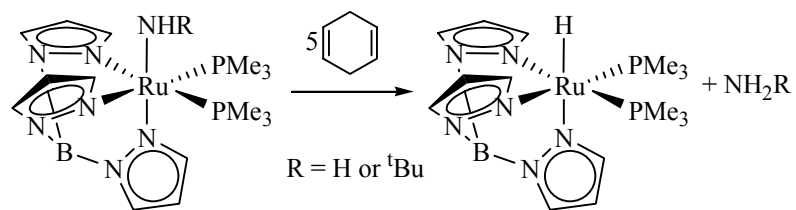
Scheme 3.16 Reaction of the vinylidene complex $[\text{TpRu}(\text{PMe}_3)_2(\text{C}=\text{CHPh})][\text{OTf}]$ with aniline yields the Fischer carbene $\text{TpRu}(\text{PMe}_3)_2\{\text{CC}(\text{H}_2\text{Ph})(\text{NHPh})\}$.

seems likely that coordination of phenylacetylene results in activation towards deprotonation.

3.7 Reaction of the Amido Complexes with 1,4-Cyclohexadiene.

In addition to the basic reactions with phenylacetylene, we examined the reactivity of the amido complexes $\text{TpRu}(\text{PMe}_3)_2\text{NHR}$ ($\text{R} = \text{H}$, ^tBu, or Ph) and $\text{TpRu}(\text{CO})(\text{PPh}_3)\text{NH}_2$ with 1,4-cyclohexadiene (1,4-CHD). This limited range of amido complexes was due to the instability resulting in rapid decomposition of the amido complexes $\text{TpRu}\{\text{P}(\text{OMe})_3\}_2\text{NHR}$ ($\text{R} = \text{H}$ or ^tBu) and $\text{TpRu}(\text{CO})(\text{PPh}_3)\text{NH}^t\text{Bu}$. Thus these amido complexes were not suitable for these studies.

The reaction of $\text{TpRu}(\text{PMe}_3)_2\text{NH}^t\text{Bu}$ with 5 equiv of 1,4-CHD at 80 °C results in the disappearance of resonances due to the amido complex and the formation of a ruthenium-hydride complex and benzene in approximately 24% yield (Scheme 3.17). These reactions were conducted in an NMR tube with THF-*d*₈ as the solvent, and the reactions were heated to 80 °C for 30 hours. The product yield was determined by integration of the benzene and $\text{TpRu}(\text{PMe}_3)_2\text{H}$ products versus a small amount of Cp_2Fe



Scheme 3.17 Reaction of $\text{TpRu}(\text{PMe}_3)_2\text{NH}^t\text{Bu}$ with 5 equiv of 1,4-CHD. This reaction forms the ruthenium-hydride complex $\text{TpRu}(\text{PMe}_3)_2\text{H}$ and benzene.

that was added as an internal standard. Reactions of the parent amido complex $\text{TpRu}(\text{PMe}_3)_2\text{NH}_2$ with 5 equivalents of 1,4-CHD at 80 °C conducted under identical conditions to the reactions above were found to yield $\text{TpRu}(\text{PMe}_3)_2(\text{H})$ and benzene. The ruthenium hydride complex was formed in approximately 48% yield after 3 days heating as determined by integration of the Ru-hydride triplet versus the internal standard. Also, approximately 1 equivalent of benzene was formed per equivalent of Ru-hydride formed. In contrast to the parent and ^tBu amido complexes above, solutions of the phenyl amido complexes $\text{TpRu}(\text{L})(\text{L}')\text{NPh}$ ($\text{L} = \text{L}' = \text{PMe}_3$ or $\text{P}(\text{OMe})_3$; $\text{L} = \text{CO}$, $\text{L}' = \text{PPh}_3$) with 1,4-CHD in C_6D_6 fail to react at elevated temperatures (up to 90 °C) up to 24 h; specifically, only starting materials are observed after heating.

The Ru-hydride complex $\text{TpRu}(\text{PMe}_3)_2\text{H}$ was assigned on the basis of a triplet at approximately -15.7 ppm with $^2J_{\text{PH}} = 31$ Hz. Independent preparation of $\text{TpRu}(\text{PMe}_3)_2\text{H}$ was achieved by reaction of $\text{TpRu}(\text{PMe}_3)_2\text{OTf}$ with LiAlH_4 in THF confirmed this assignment. $\text{TpRu}(\text{PMe}_3)_2(\text{H})$ has been characterized by ^1H , ^{13}C , and ^{31}P NMR spectroscopy (Figure 3.11).

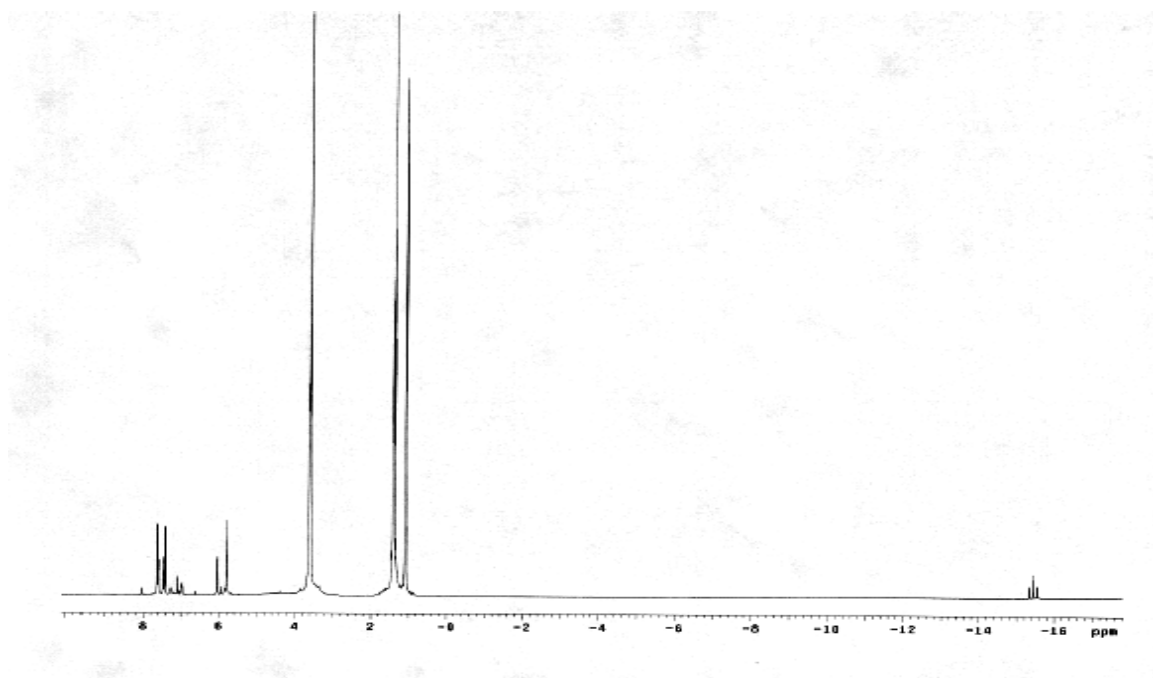
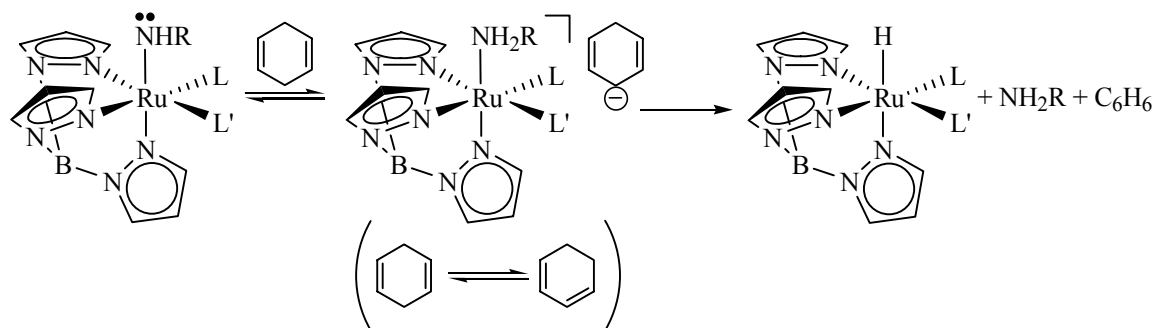


Figure 3.11 ^1H NMR spectrum of $\text{TpRu}(\text{PMe}_3)_2\text{H}$ in C_6D_6 .

During the course of the reactions of $\text{TpRu}(\text{PMe}_3)_2\text{NHR}$ ($\text{R} = \text{H}$ or ^tBu) or $\text{TpRu}(\text{CO})(\text{PPh}_3)\text{NH}_2$ with 1,4-CHD, 1,4-CHD was found to isomerize to 1,3-CHD (determined by ^1H NMR spectroscopy). Similar observations were reported for the reaction with *cis*- $(\text{PMe}_3)_4\text{Ru}(\text{H})(\text{NH}_2)$ with 1,4-CHD. We have attributed this isomerization to a basic mechanism where the amido ligand reversibly deprotonates 1,4-CHD to yield a cyclohexadienyl anion that is ion paired to the amine complex $[\text{TpRu}(\text{PMe}_3)_2\text{NH}_2\text{R}]^+$ (Scheme 3.18). Also, the reaction of phenyl amido complexes $\text{TpRu}(\text{PMe}_3)_2\text{NPh}$ or $\text{TpRu}\{\text{P}(\text{OMe})_3\}_2\text{NPh}$ with 5 equivalents of 1,4-CHD do not result in isomerization after 24 heating. These results were attributed to the decreased of



Scheme 3.18 Proposed pathway for the isomerization of 1,4-CHD to 1,3-CHD via deprotonation of 1,4-CHD to yield a cyclohexadienyl.

basicity of these amido complexes relative to those analogs with parent and ^tBu amido substituents.

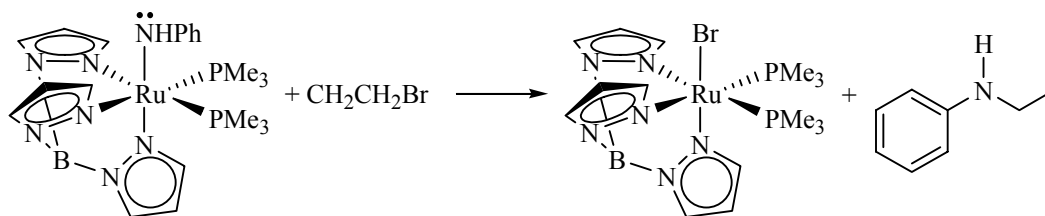
Monitoring the isomerization of 1,4-CHD to 1,3-CHD by $\text{TpRu}(\text{PMe}_3)_2\text{NH}_2$ revealed first order kinetics as determined by a plot of $\ln([\text{1,4-CHD}]_t - [\text{1,4-CHD}]_{\text{eq}})$ versus time ($k = 2.0 \times 10^{-5} \text{ s}^{-1}$). Also, the addition of 2 equivalents of trimethylphosphine to the reaction of $\text{TpRu}(\text{PMe}_3)_2\text{NH}_2$ with 1,4-CHD conducted similarly to those reactions above (i.e. in THF with 5 equivalents of 1,4-CHD and heating to 80 °C) resulted in isomerization of 1,4-CHD to 1,3-CHD and the rate of isomerization was identical to the reaction in the absence of trimethylphosphine. However, this reaction was found to form multiple decomposition products, but the hydride product $\text{TpRu}(\text{PMe}_3)_2(\text{H})$ and benzene products were not observed. Similar reactivity was observed for the amido complex *cis*- $(\text{PMe}_3)_4\text{Ru}(\text{H})(\text{NH}_2)$, the addition of trimethylphosphine does not impact the rate of isomerization. Thus, phosphine dissociation is not likely involved in the isomerization reaction. This supports the hypothesis that the isomerization is due to a basic mechanism.

Ultimately, these reactions produce benzene and $\text{TpRu}(\text{PMe}_3)_2(\text{H})$ in approximately 50% yield, and in analogy to reactions observed with other parent amido ruthenium-(II) complexes, we suggest an acid-base reaction mechanism to account for these results. Phosphine ligand dissociation appears to be important to the formation of $\text{TpRu}(\text{PMe}_3)_2(\text{H})$ since the addition of 2 equivalents of trimethylphosphine resulted in suppression of products. Thus the mechanism of formation of the products $\text{TpRu}(\text{PMe}_3)_2\text{H}$ and benzene likely involves coordination of the cyclohexadienyl counterion. Fe(III) oxide complexes have been reported to initiate H-atom abstraction reactions with 1,4-CHD to form benzene, but this reaction is due to a highly oxidized metal center.^{16,41,42} In contrast, the Ru(II) amido complexes reported herein are not reduced to -2.0 V (vs NHE). Thus H-atom abstraction reactions are unlikely. Also, the less basic Ru-(II) phenyl amido complex $\text{TpRu}(\text{PMe}_3)_2\text{NHPh}$ fail to react with 1,4-CHD; these metal centers are less reduced compared to the parent and ^tBu amido complexes $\text{TpRu}(\text{PMe}_3)_3\text{NHR}$ (R = H or ^tBu). These results in combination with the extensive studies of *trans*-(dmpe)₂Ru(NH₂)(H) and *cis*-(PMe₃)₄Ru(H)(NH₂) support an acid-base pathway for the deprotonation of 1,4-CHD.

3.8 Reaction of $\text{TpRu}(\text{PMe}_3)\text{NHPh}$ with Ethylbromide.

In addition to Bronsted base activity, the late transition metal amido complexes exhibit highly nucleophilic reactivity. For example, Bergman et al. have reported the reaction of *cis*-(PMe₃)₄Ru(H)(NH₂) with ethylbromide at room temperature results in the formation of the corresponding bromide complex *cis*-(PMe₃)₄(H)(Br) and ethylamine.^{5,39}

Reaction of the phenyl amido complex $\text{TpRu}(\text{PMe}_3)_2\text{NHPH}$ at room temperature show no reactivity after 24 hours. However, heating benzene solutions of $\text{TpRu}(\text{PMe}_3)_2\text{NHPH}$ with 10 equivalents of ethylbromide revealed slow conversion to $\text{TpRu}(\text{PMe}_3)_2\text{Br}$ and *N*-ethylaniline ($t_{1/2}$ approximately 22 hours) (Scheme 3.19). This reaction was found to be



Scheme 3.19 Reaction of the amido complex $\text{TpRu}(\text{PMe}_3)_2\text{NHPH}$ with ethylbromide.

first order with respect Ru(II)-amido ($k_{\text{obs}} = 8.6 \times 10^{-6} \text{ M}^{-1} \text{ s}^{-1}$ $R^2 = 0.99$; Figure 3.12).

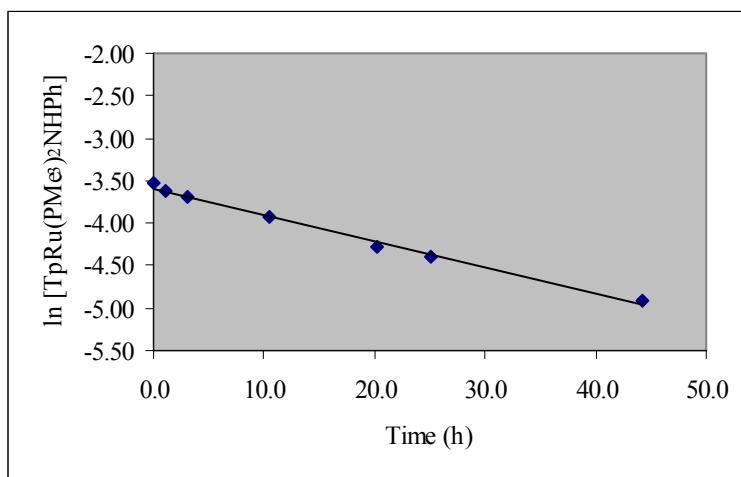


Figure 3.12 First order kinetic plot for the reaction of $\text{TpRu}(\text{PMe}_3)_2\text{NHPH}$ with ethyl bromide. ($k_{\text{obs}} = 8.6 \times 10^{-6} \text{ M}^{-1} \text{ s}^{-1}$)

Although suitable kinetic experiments could not be achieved, the parent amido complex $\text{TpRu}(\text{PMe}_3)_2\text{NH}_2$ was found to be significantly more nucleophilic than the anilido analog. Specifically, reactions of $\text{TpRu}(\text{PMe}_3)_2\text{NH}_2$ with 1.1 equivalents ethylbromide were found to yield $\text{TpRu}(\text{PMe}_3)_2\text{Br}$ and ethylamine after approximately 1 hour at room temperature. Thus the delocalizing ability of anilido ligand results in decreased nucleophilicity in addition to basicity.

3.9 Experimental Details.

General Methods. All reactions and procedures were performed under anaerobic conditions in a nitrogen filled glovebox or using standard Schlenk techniques. Glovebox purity was maintained by periodic nitrogen purges and monitored by an oxygen analyzer $\{\text{O}_2(\text{g}) < 15 \text{ ppm for all reactions}\}$. Acetonitrile was purified by passage through a column of activated alumina followed by distillation from CaH_2 .⁴³ Methylene chloride was purified by passage through a column of activated alumina followed by distillation from P_2O_5 . THF, hexanes, and diethyl ether were dried by distillation from sodium/benzophenone. Benzene was purified by distillation from CaH_2 . CD_3CN was purified by distillation from CaH_2 , degassed, and stored over 4 Å sieves. C_6D_6 , CDCl_3 , and CD_2Cl_2 were degassed via three freeze-pump-thaw cycles and stored over 4 Å sieves. $\text{THF-}d_8$ was distilled from Na metal, degassed via freeze-pump-thaw cycles, and stored over 4 Å sieves. ^1H and ^{13}C NMR spectra were obtained on Varian Mercury 300 MHz, Varian Mercury 400 MHz, and General Electric 300 MHz spectrometers. Resonances due to the Tp ligand are reported by chemical shift and multiplicity only. All $^3J_{\text{HH}}$ values for

pyrazolyl rings are 2 Hz. All ^1H and ^{13}C NMR spectra were referenced against tetramethylsilane using residual proton signals (^1H NMR) or the ^{13}C resonances of the deuterated solvent (^{13}C NMR). ^{31}P NMR spectra were obtained on a Varian 300 MHz spectrometer and referenced against external 85% H_3PO_4 . All NMR spectra were acquired at room temperature unless otherwise noted. IR spectra were obtained on a Mattson Genesis II spectrometer either as thin films on a KBr plate or in solution using a KBr solution plate. Electrochemical experiments were performed under a nitrogen atmosphere using a BAS Epsilon potentiostat. Cyclic voltammograms were recorded in a standard three-electrode cell from -2.00 to +2.00 V with a glassy carbon working electrode and tetrabutylammonium hexafluorophosphate as electrolyte. Tetrabutylammonium hexafluorophosphate was dried under dynamic vacuum at 110 °C for 48 h prior to use. All potentials are reported versus NHE (normal hydrogen electrode) using cobaltocenium hexafluorophosphate or ferrocene as an internal standard. Elemental analyses were performed by Atlantic Microlabs, Inc. $[\text{Li}][\text{CCPh}]$ was prepared by addition of BuLi to a benzene solution of phenylacetylene. The resulting white precipitate was collected via vacuum filtration and washed with hexanes. All other reagents were used as purchased from commercial sources.

NMR Tube Reactions of the Amido Complex with Malononitrile. All reactions followed the same general procedure. Inside a nitrogen-filled glovebox, an NMR tube was charged with a known amount of the appropriate amido complex. One equivalent of malononitrile was weighed out and dissolved in CD_2Cl_2 , and this solution was added to the NMR tube with the amido complex $\text{TpRu}(\text{L})(\text{L}')\text{NHPH}$ ($\text{L} = \text{L}' = \text{PMe}_3$

or P(OMe)₃; L = CO, L' = PPh₃). A ¹H NMR spectrum was immediately acquired at room temperature. Variable-temperature ¹H NMR experiments were performed by lowering the temperature of the NMR probe to -90 °C.

UV-Vis Reactions of TpRu(PMe₃)₂NHPh and TpRu{P(OMe)₃}₂NHPh with Malononitrile. The procedure that was utilized for the ¹H-NMR spectra of complexes TpRu(PMe₃)₂NHPh and TpRu{P(OMe)₃}₂NHPh with malononitrile was followed. The reaction solutions were transferred to a quartz cuvette (sealed under nitrogen), and UV-vis spectra were acquired.

[TpRu(PMe₃)₂{NH₂(p-C₆H₄CF₃)}][OTf]. A solution of TpRu(PMe₃)₂OTf (0.2603 g, 0.4233 mmol) and 4-(trifluoromethyl)aniline (0.2 mL, 1.6 mmol) in approximately 50 mL of THF was stirred for 24 hours at room temperature. The solvent was reduced in vacuo to approximately 15 mL, and 50 mL of diethylether were added. The product was collected by filtration through a fine porosity frit, washed with diethyl ether (3 x 10 mL), and dried in vacuo (0.2168g, 0.2792 mmol, 66%). ¹H NMR (CDCl₃, δ): 7.77, 7.67, 7.18, 7.10 (6H, 2:1:1:2 integration, each a d, Tp CH 3 and 5 position), 7.16, 6.54 (4H, 2:2 integration, each a d, NH₂C₆H₄CF₃, ³J_{HH} = 8 Hz), 6.16 (3H, m, overlapping Tp 4), 5.34 (2H, bs, NH₂C₆H₄CF₃), 1.35 (18H, vt, N = 16 Hz, P(CH₃)₃).

TpRu(PMe₃)₂{NH(p-C₆H₄CF₃)}. A solution of [TpRu(PMe₃)₂{NH₂(p-C₆H₄CF₃)}][OTf] (0.1104 g, 0.1422 mmol) was cooled to -78 °C. Sodium bis(trimethylsilyl)amide (1.0 M in THF, 156 μL, 0.156 mmol) was added drop wise using a microsyringe. A color change to dark yellow was observed during the addition. The solution was allowed to warm to room temperature, and the volatiles were removed in

vacuo. The product was extracted with dry benzene and filtered through a fine porosity frit. The volatiles were removed in vacuo to yield a dark yellow-brown powder (0.0859 g, 0.1371 mmol, 96%). ^1H NMR (CDCl_3 , δ): 7.47, 7.45, 7.41, 6.79 (6H, 2:1:2:1 integration, each a d, Tp CH 3 and 5 position), 5.85, 5.79 (3H, 2:1 integration, each a t, Tp CH 4 position), 2.71 (br s, Ru-NHAr), 0.76 (18H, vt, $N = 16$ Hz, PCH_3).

[TpRu(PMe₃)₂(NCMe)][OTf]. To a solution of TpRu(PMe₃)₂Cl (0.0976 g, 0.195 mmol) in approximately 30 mL of THF was added AgOTf (0.0512 g, 0.199 mmol). The resulting red solution was refluxed for 18 h. During the reaction, the formation of a white precipitate (AgCl) was noted. The solution was cooled to room temperature and filtered through a fine porosity frit. Approximately 5 mL of CH₃CN was added to the solution. The reaction was allowed to stir for an additional 4 h at room temperature. The solution was concentrated to approximately 15 mL in vacuo, and hexanes (approximately 60 mL) were added to precipitate the product. The resulting white solid was collected via vacuum filtration through a fine porosity frit and washed with hexanes (3 x 10 mL). The final product was collected in 72% yield after drying in vacuo (0.0919 g, 0.140 mmol). ^1H NMR (CDCl_3 , δ): 7.75, 7.72, 7.67, 7.33 (6H, 1:2:2:1 integration, each a d, Tp CH 3 and 5 position), 6.25, 6.22 (3H, 2:1 integration, each a t, Tp CH 4 position), 2.54 (3H, NCCCH_3), 1.35 (18H, vt, $N = 9$ Hz, $\text{P(CH}_3)_3$), 0.84 (9H, s, ^tBu). $^{13}\text{C}\{^1\text{H}\}$ NMR (CD_3CN , δ): 144.8, 142.5, 136.8, 135.6 (Tp 3 or 5 position), 124.9 (Ru-N \equiv CMe), 106.3, 106.0 (Tp 4 position), 17.5 (vt, $N = 29$ Hz, $\text{P(CH}_3)_3$), 4.3 (Ru-N \equiv CCH₃). IR (CDCl_3 solution): $\nu_{\text{CN}} = 2253$ cm^{-1} , $\nu_{\text{BH}} = 2485$ cm^{-1} . $^{31}\text{P}\{^1\text{H}\}$ (CDCl_3 , δ): 11.3. CV (CH_3CN , 100 mV/s): $E_{1/2} = 1.29$ V. Anal. Calcd for $\text{C}_{17}\text{H}_{31}\text{BF}_3\text{N}_7\text{O}_3\text{P}_2\text{RuS}, 1/2(\text{CH}_2\text{Cl}_2)$ (note that 1/2 equiv of

CH₂Cl₂ was confirmed via ¹H NMR of the analysis sample): C, 31.80; N, 14.03; H, 4.61. Found: C, 32.33; N, 14.03; H, 4.61.

TpRu(PMe₃)₂(C≡CPh). TpRu(PMe₃)₂(Cl) (0.5049 g, 1.01 mmol) was dissolved in approximately 40 mL of THF to give a pale yellow solution. To this solution was added AgOTf (0.2594 g, 1.01 mmol), and the resulting solution was refluxed for 21 h. After cooling to room temperature, the solution was filtered through a fine porosity frit, and 0.1364 g (1.26 mmol) of LiC₂Ph (dissolved in approximately 3 mL of THF) was added. After 5 h of reaction, the solvent was removed under reduced pressure. The products were extracted with approximately 15 mL of benzene and filtered through a fine porosity frit. The volume of the filtrate was reduced to 10 mL in vacuo, and 25 mL of hexanes was added. The resulting slurry was filtered through a fine porosity frit, and the collected solid was discarded. Volatiles were removed from the filtrate under reduced pressure to yield a beige solid. The solid was dried in vacuo to yield 0.2847 g of product (50% yield). ¹H NMR (CD₂Cl₂, δ): 7.95, 7.82 (3H, 2:1 integration, each a d, Tp CH 3 and 5 position), 7.65 (3H, overlapping d's, Tp CH 3 or 5 position), 7.26 (2H, d, ³J_{HH} = 7 Hz, phenyl ortho), 7.16 (2H, t, ³J_{HH} = 7 Hz, phenyl meta), 6.98 (1H, t, ³J_{HH} = 7 Hz, phenyl para), 6.28, 6.15 (3H, 1:2 integration, each a t, Tp CH 4 position), 1.42 (18H, vt, N = 9 Hz, P(CH₃)₃). ¹³C{¹H} NMR (CD₂Cl₂, δ): 144.4, 135.5, 135.0, 131.4, 130.8, 128.7, 128.0, 122.9 (Tp 3 or 5 and phenyl), 133.6 (t, ²J_{PC} = 19 Hz, R-C≡CPh), 107.3 (R-C≡CPh), 105.2, 105.0 (Tp 4 position), 19.1 (P(CH₃)₃). ³¹P{¹H} (CD₂Cl₂, δ): 14.8. CV (CH₃CN, 100 mV/s): E_{p,a} = 0.41 V. Anal. Calcd for C₂₃H₃₃BN₆P₂Ru: C, 48.69; N, 14.81; H, 5.86. Found: C, 48.55; N, 14.58; H, 5.77.

TpRu(CO)(PPh₃)(C≡CPh). A THF solution of TpRu(CO)(PPh₃)(Cl) (0.1532 g, 0.2394 mmol) and LiCCPh (0.0518 g, 0.4793 mmol) was refluxed for 20 h. After this time period, volatiles were removed in vacuo. The resulting brown oil was dissolved in approximately 15 mL of benzene and filtered through a fine porosity frit. Volatiles were removed from the filtrate to yield a light brown solid. The solid was dried in vacuo and collected (0.1285 g, 76% yield). Analytically pure product was obtained by layering a methylene chloride solution with hexanes. ¹H NMR (CDCl₃, δ): 8.09, 7.71, 7.66, 7.60, 6.98, 6.58 (6H, 1:1:1:1:1:1 integration, each a d, Tp CH 3 and 5 position), 7.44, 7.32 (17H, overlapping m's, phenyl ortho and PPh₃), 7.72 (2H, t, ³J_{HH} = 8 Hz, phenyl meta), 7.09 (1H, t, ³J_{HH} = 8 Hz, phenyl para), 6.20, 5.90, 5.87 (3H, 1:1:1 integration, each a t, Tp CH 4 position). ¹³C{¹H} NMR (CDCl₃, δ): 203.8 (d, ²J_{PC} = 16 Hz, CO), 144.3, 144.2, 143.9, 134.6, 134.4, 134.3, 128.2, 128.1, 127.7 (Tp 3 or 5 position and acetylide phenyl), 135.2 and 134.3 (each a d, ²J_{PC} = ³J_{PC} = 10 Hz, PPh₃ ortho and meta), 131.3 (PPh₃ para), 133.2 (¹J_{PC} = 44 Hz, PPh₃ ipso), 130.0 (d, ⁴J_{PC} = 4 Hz, acetylide phenyl ipso), 115.4 (d, ²J_{PC} = 17 Hz, R-C≡CPh), 109.0 (R-C≡CPh), 105.6 (d, ⁴J_{PC} = 2 Hz, Tp 4 position), 105.2, 105.0 (Tp 4 position). IR (THF solution): ν_{CO} = 1966 cm⁻¹, ν_{BH} = 2103 cm⁻¹. ³¹P{¹H} (CDCl₃, δ): 47.9. CV (CH₃CN, 100 mV/s): E_{1/2} = 1.16 V. Anal. Calcd for C₃₆H₃₀BN₆OPRu, CH₂Cl₂ (note that one molecule of CH₂Cl₂ was found in the analysis sample using ¹H NMR spectroscopy): C, 56.22; N, 10.63; H, 4.08. Found: C, 55.85; N, 10.67; H, 4.14.

TpRu{P(OMe)₃}₂(C≡CPh). A THF (50 mL) solution of TpRu{P(OMe)₃}₂Cl (0.1582 g, 0.2647 mmol) and AgOTf (0.0772 g, 0.3005 mmol) was refluxed for

approximately 24 h. The mixture was allowed to cool to room temperature and passed through a plug of Celite. LiCCPh (0.0572 g, 0.5294 mmol) was added to the pale yellow filtrate, and the resulting solution was refluxed for 5 h. The volatiles were removed in vacuo, and the remaining brown residue was dissolved in approximately 20 mL of diethyl ether and passed through a fine porosity frit. Approximately 20 mL of hexanes was added to the filtrate. The resulting light brown precipitate was collected (0.1528 g, 87% yield). ^1H NMR (C_6D_6 , δ): 8.34, 8.25, 7.55, 7.47 (6H, 2:1:1:2 integration, each a d, Tp CH 3 and 5 position), 7.50 (2H, d, $^3J_{\text{HH}} = 7$ Hz, phenyl ortho), 7.14 (2H, t, $^3J_{\text{HH}} = 7$ Hz, phenyl meta), 6.96 (1H, t, $^3J_{\text{HH}} = 7$ Hz, phenyl para), 6.02, 5.97 (3H, 1:2 integration, each a t, Tp CH 4 position), 3.35 (18H, vt, $N = 5$ Hz, $\text{P}(\text{OCH}_3)_3$). $^{13}\text{C}\{^1\text{H}\}$ NMR (C_6D_6 , δ): 146.4, 145.4, 135.5, 134.8, 131.8, 128.9, 128.5, 124.0 (Tp 3 or 5 position and acetylide phenyl), 132.3 (t, $^2J_{\text{PC}} = 13$ Hz, $\text{R}-\text{C}\equiv\text{CPh}$), 110.4 (s, $\text{R}-\text{C}\equiv\text{CPh}$), 105.7, 105.2 (Tp 4 position), 51.6 (br s, $\text{P}(\text{OCH}_3)_3$). $^{31}\text{P}\{^1\text{H}\}$ (C_6D_6 , δ): 152.4. CV (CH_3CN , 100 mV/s): $E_{\text{p,a}} = 0.65$ V. Anal. Calcd for $\text{C}_{23}\text{H}_{33}\text{BN}_6\text{O}_6\text{P}_2\text{Ru}$: C, 41.64; N, 12.67; H, 5.01. Found: C, 42.41; N, 12.35; H, 5.21.

TpRu(PMe₃)₂(H). To a THF solution (approximately 20 mL) of TpRu(PMe₃)₂OTf (0.0541 g, 0.0879 mmol) was added lithium aluminum hydride (0.0096 g, 0.2530 mmol). The reaction was stirred for 16 H at room temperature. The volatiles were removed in vacuo, and benzene was used to extract the residue. The solution was filtered through a fine porosity frit, and the volatiles were removed in vacuo. Additional purification of the product was achieved by column chromatography on silica gel with 80/20 benzene/THF as the eluent (0.034 g, 0.073 mmol, 81%). ^1H NMR (C_6D_6 , δ): 7.79,

7.69, 7.66, 7.48 (6H, 1:2:1:2 integration, each a d, Tp CH 3 and 5 position), 6.07, 5.84 (3H, 1:2 integration, each a t, Tp CH 4), 1.11 (18H, vt, $N = 8$ Hz, $P(CH_3)_3$), -15.69 (1H, t, $^2J_{PH} = 31$ Hz, RuH). $^{13}C\{^1H\}$ NMR (C_6D_6 , δ): 146.0, 143.2, 134.4, 133.8 (each a s, Tp 3 or 5 position), 104.7, 104.2 (each a s, Tp 4 position), 22.39 (vt, $N = 12$ Hz, $P(CH_3)_3$). $^{31}P\{^1H\}$ (C_6D_6 , δ): 19.5 (s, $P(CH_3)_3$).

TpRu(PMe₃)₃][OTf]. A CH_2Cl_2 (50 mL) solution of TpRu(PMe₃)₂Cl (0.1060 g, 0.2112 mmol) and AgOTf (0.0539 g, 0.2098 mmol) was refluxed for 18 h. During the reaction, the formation of a white precipitate (AgCl) was noted. To the resulting solution was added 0.3 mL of trimethylphosphine, and the reaction was allowed to stir for 6 h. The solution was concentrated to approximately 20 mL in vacuo, and diethyl ether (approximately 40 mL) was added to precipitate the product. The product was collected via vacuum filtration through a fine porosity frit and washed with diethyl ether (3 x 10 mL) to give a yellow solid (0.0845 g, 0.122 mmol, 58%). Additional purification was accomplished by dissolving the product in a minimal amount of $CHCl_3$ and cooling the solution to -20 °C, followed by vacuum filtration through a fine porosity frit. 1H NMR ($CDCl_3$, δ): 7.75, 7.71 (each 3H, each a d, Tp CH 3 or 5), 6.31 (3H, t, Tp CH 4) 1.40 (27H, m, $P(CH_3)_3$). $^{13}C\{^1H\}$ NMR ($CDCl_3$, δ): 145.2, 136.7 (each a s, Tp 3 or 5 position), 106.4 (s, Tp 4 position), 21.1 (m, $P(CH_3)_3$). $^{31}P\{^1H\}$ NMR ($CDCl_3$, δ): 4.1 (s, PMe_3).

[Tp(PMe₃)₂Ru=C=C(H)Ph][OTf]. TpRu(PMe₃)₂(Cl) (0.3965 g, 0.7903 mmol) was dissolved in approximately 10 mL of THF. To this solution was added AgOTf (0.2030 g, 0.7901 mmol, dissolved in ~2 mL of THF) and ~1.0 mL of phenylacetylene (9.1 mmol), and the resulting solution was refluxed for 19 h. After cooling to room

temperature, the solution was filtered through a fine porosity frit. The volatiles were removed in vacuo, and the crude reaction mixture was recrystallized from methylene chloride/ hexanes. A reddish-purple solid was collected (0.2436 g, 0.3395 mmol, 43% yield). ^1H NMR (CDCl_3 , δ): 7.94, 7.81, 7.70, 7.73 (6H, 1:1:2:2 integration, each a d, Tp CH 3 or 5 position), 7.12 (2H, t, $^3J_{\text{HH}} = 7$ Hz, phenyl meta), 7.03 (^1H , t, $^3J_{\text{HH}} = 7$ Hz, phenyl para), 6.72 (2H, d, $^3J_{\text{HH}} = 7$ Hz, phenyl ortho), 6.51, 6.23 (3H, 1:2 integration, Tp CH 4 position), 5.59 (1H, t, $^3J_{\text{PH}} = 3$ Hz, Ru=Cd C(H)Ph), 1.46 (18H, vt, $N = 10$ Hz, $\text{P}(\text{CH}_3)_3$). $^{13}\text{C}\{^1\text{H}\}$ NMR (CDCl_3 , δ): 373.0 (t, $2J_{\text{PC}} = 18$ Hz, Ru=C=C(H)Ph), 143.9, 137.5, 137.0, 129.1, 126.5, 126.4 (Tp 3 or 5 position and vinylidene phenyl, two resonances are missing due to overlap), 111.5 (s, Ru=C=C(H)Ph), 107.6, 106.5 (Tp 4 position), 18.0 (vt, $N = 28$ Hz, $\text{P}(\text{CH}_3)_3$). $^{31}\text{P}\{^1\text{H}\}$ (C_6D_6 , δ): 2.9. CV (CH_3CN , 100 mV/s): $E_{\text{p,a}} = 1.39$ V; $E_{\text{p,c}} = -1.30$ V. Anal. Calcd for $\text{C}_{24}\text{H}_{34}\text{BF}_3\text{N}_6\text{O}_3\text{P}_2\text{RuS}, (\text{CH}_2\text{Cl}_2)_{1/2}$ (note that 1/2 molecule of CH_2Cl_2 was found in the analysis sample using ^1H NMR spectroscopy): C, 38.72; N, 11.06; H, 4.64. Found: C, 39.53; N, 10.56; H, 4.70.

[Tp(PMe₃)₂Ru=C(CH₂Ph){N(H)Ph}][OTf]. A THF (50mL) solution of TpRu(PMe₃)₂Cl (0.4124 g, 0.8216 mmol) and AgOTf (0.2125 g, 0.8270 mmol) was gently refluxed for 24 h. During the reaction, the formation of a white precipitate (AgCl) was noted. The solution was cooled to room temperature and filtered through a fine porosity frit. Phenylacetylene (0.2 g, 1.9 mmol) was added to the solution, and the reaction was allowed to stir for 24 h. The solution was concentrated to approximately 20 mL in vacuo, and hexanes (approximately 40 mL) were added. Formation of a brown precipitate was noted. The precipitate was collected using a fine porosity frit and then

dissolved in THF (approximately 50 mL). Aniline (approximately 0.5 g) was added to the solution, and the reaction was allowed to stir for 24 h. The solution was concentrated to approximately 20 mL in vacuo, and diethyl ether (approximately 40 mL) was added to precipitate the product. The product was collected via vacuum filtration through a fine porosity frit and washed with diethyl ether (3 x 10 mL) to give a white solid (0.2576 g, 0.3178 mmol, 38%). ^1H NMR (CDCl_3 , δ): 11.83 (1H, bs, *NHPh*), 7.78, 7.71, 7.60, 7.41 (6H 1:2:1:2 integration, each a d, Tp *CH* 3 and 5 position), 7.19-7.10 (4H, m, Ph), 7.02 (1H, t, Ph para position, $^3J_{\text{HH}} = 7$ Hz), 6.90-6.63 (5H, m, Ph) 6.30, 6.14 (3H, 1:2 integration, each a t, Tp *CH* 4 position), 4.13 (2H, s, $\text{Ru}=\text{C}(\text{CH}_2\text{Ph})(\text{NHPh})$), 1.36 (18H, vt, $J_{\text{PH}} = 8$ Hz, $\text{P}(\text{CH}_3)_3$). $^{13}\text{C}\{^1\text{H}\}$ NMR (CDCl_3 , δ): 271.1 (t, $\text{Ru}=\text{C}(\text{CH}_2\text{Ph})(\text{NHPh})$, $^2J_{\text{PC}} = 24$ Hz), 144.3, (s, Tp 3 or 5 or Ph), 144.2-144.0 (m, Tp 3 or 5 or Ph), 141.0, 136.7, 136.4, 127.5, 125.8, 125.7 (each a s, Tp 3 or 5 position or Ph), 106.8, 106.4 (each a s, Tp 4 position), 52.7 (s, $\text{Ru}=\text{C}(\text{CH}_2\text{Ph})(\text{NHPh})$), 19.4 (m, $\text{P}(\text{CH}_3)_3$). Anal. Calcd for $\text{C}_{30}\text{H}_{41}\text{BF}_3\text{N}_7\text{O}_3\text{P}_2\text{SRu}$: C, 44.45; N, 12.10; H, 5.10. Found: C, 44.28; N, 11.87; H, 5.08.

[TpRu(PMe₃)₂(NH₂^tBu)][PhC₂]. In a screw cap NMR tube, TpRu(PMe₃)₂NH^tBu (0.0285 g, 0.0529 mmol) was dissolved in 0.8 mL of THF-*d*₈. Cp₂Fe was added as an internal standard, and a ^1H NMR spectrum was obtained. Phenylacetylene (6.0 μL , 0.0546 mmol) was added using a microsyringe. Quantitative conversion to [TpRu(PMe₃)₂(NH₂^tBu)][CCPh] was observed on the basis of integration. NMR spectra were obtained -50 °C. ^1H NMR (THF*d*₈, δ): 8.14, 7.85, 7.74, 7.42 (6H, 2:2:1:1 integration, each a d, Tp *CH* 3 and 5 position), 7.34 (2H, d, $J = 5$ Hz, phenyl ortho), 7.24 (2H, t, $J = 5$ Hz, phenyl meta), 7.18 (1H, t, $J = 5$ Hz, phenyl para), 6.31, 6.12 (3H, 2:1

integration, each a t, Tp CH 4), 1.34 (18H, vt, $J_{\text{PH}} = 6$ Hz, P(CH₃)₃), 0.88 (9H, s, NH₂^tBu). In THF-*d*₈, the resonance due to the amine protons is not observed; however, in C₆D₆, this resonance is observed as a broad singlet at 3.25 ppm. ¹³C{¹H} NMR (THF-*d*₈, δ): 146.6, 144.5, 136.6, 136.5 (each a s, Tp 3 or 5 position), 132.0, 130.9, 128.9, 128.6, 127.6, 123.9 (acetylide anion), 106.5, 105.7 (each a s, Tp 4 position), 52.4 (s, NH₂C(CH₃)₃), 30.3 (s, NH₂C(CH₃)₃), 17.4 (vt, $N = 10$ Hz, PMe₃). ¹³C{¹H} NMR of [PhC₂][Li] (THF-*d*₈, δ): 135.2, 131.1, 128.7, 127.6, 124.7, 114.9. ³¹P NMR (THF-*d*₈, δ): 15.8.

Ligand Exchange Reactions of [TpRu(PMe₃)₂(NH₂R)][OTf] (R = H, Ph, or ^tBu) with CD₃CN. The appropriate amine complex was weighed and dissolved in CD₃CN to bring the concentration to 0.06 M. A small amount of ferrocene was added as internal standard. The disappearance of resonances due to [TpRu(PMe₃)₂(NH₂R)][OTf] (R = H, Ph or ^tBu) was monitored with respect to time using ¹H NMR spectroscopy. The pulse delay of the spectrometer was set to 10 s in order to ensure accurate integration. The final ¹H NMR spectra for R = Ph and ^tBu displayed resonances consistent with the quantitative formation of [TpRu(PMe₃)₂(NCCD₃)][OTf] and NH₂R. Kinetic analysis revealed first-order transformations, and rate constants were abstracted from the slope ($R^2 > 0.99$). The ammonia complex [TpRu(PMe₃)₂(NH₃)][OTf] showed no evidence of ligand exchange even after heating at prolonged times.

Ligand Exchange Reactions of Ru(II) Phenyl Amido Complexes with Arylamines. In a representative reaction, 0.0230 g (0.0412 mmol) of TpRu(PMe₃)₂(NHPh) and 0.0059 g (0.0479 mmol) of *p*-anisidine were dissolved in

approximately 0.7 mL of C₆D₆ in a screw cap NMR tube. A ¹H NMR spectrum was acquired with the pulse delay set to 10 s. The resulting solution was heated to approximately 100 °C. ¹H NMR spectra were acquired periodically until equilibrium was established (approximately 5 days). The final distribution of TpRu(PMe₃)₂(NHPPh) and TpRu(PMe₃)₂{NH(*p*-C₆H₄OMe)} was determined using both ¹H and ³¹P NMR spectroscopy. Analogous procedures were used for all reactions with arylamines. The reaction with *p*-trifluoromethylaniline was slow; therefore, a catalytic (~1 mol %) amount of TpRu(PMe₃)₂(OTf) was added to the reaction solution. In addition, the equilibrium constant for this reaction was confirmed by preparing TpRu(PMe₃)₂{NH(*p*-C₆H₄CF₃)} and reacting it with aniline

Reaction of [TpRu(PMe₃)₂(NCMe)][OTf] with NH₃. TpRu(PMe₃)₂(NCMe) (0.0183 g, 0.0279 mmol) was dissolved in ~2 mL of THF in a pressure tube. To this solution was added a THF solution saturated with NH₃. The pressure tube was sealed. After 284 h at 70 °C, the solvent was removed under reduced pressure, and ¹H NMR spectroscopy of the resulting solid (CDCl₃) indicated [TpRu(PMe₃)₂(NCMe)][OTf] as the only TpRu complex.

Reactions of Ru(II) Amido Complexes with 1,4-Cyclohexadiene. In a glovebox, the appropriate amount of Ru(II) amido was weighed and dissolved in 0.7-1.0 mL of C₆D₆. This solution was transferred to a screw cap NMR tube, and 1,4-CHD was added along with ferrocene (as internal standard). ¹H NMR spectra were immediately acquired with a 10 s pulse delay in order to ensure accurate integration. Reaction

progress was monitored versus time by ^1H NMR spectroscopy. Percent yields of products were determined by integration versus ferrocene.

Reactions of $\text{TpRu}(\text{L})(\text{L}')(\text{NHR})$ with Phenylacetylene. In a representative reaction, 0.0224 g (0.040 mmol) of $\text{TpRu}(\text{PMe}_3)_2(\text{NHPH})$ was weighed into a glass vial and dissolved in 1.0 mL of C_6D_6 (0.04 M solution). To the resulting solution were added 0.044 mL of phenylacetylene (0.40 mmol) and a small amount of ferrocene. The solution was transferred to a screw cap NMR tube, and a ^1H NMR spectrum was acquired with a pulse delay of 10 s. The solution was heated to approximately 80 °C in an oil bath and periodically monitored by ^1H NMR spectroscopy.

Reactions of $\text{TpRu}(\text{PMe}_3)_2(\text{NHPH})$ with Phenylacetylene and Catalytic $\text{TpRu}(\text{PMe}_3)_2(\text{OTf})$. These reactions were analogous to reactions in the absence of $\text{TpRu}(\text{PMe}_3)_2(\text{OTf})$. Before heating, a known amount of $\text{TpRu}(\text{PMe}_3)_2(\text{OTf})$ was added to the reaction mixture. The reactions were monitored by ^1H NMR spectroscopy.

Kinetic Studies for the Conversion of $[\text{TpRu}(\text{PMe}_3)_2(\text{NH}_2^t\text{Bu})][\text{PhC}_2]$ to $\text{TpRu}(\text{PMe}_3)_2(\text{C}\equiv\text{CPh})$. In a screw cap NMR tube, a 1:1 molar mixture of $\text{TpRu}(\text{PMe}_3)_2(\text{NH}^t\text{Bu})$ and phenylacetylene was combined in $\text{THF-}d_8$. A ^1H NMR spectrum was acquired to confirm the clean formation of $[\text{TpRu}(\text{PMe}_3)_2(\text{NH}_2^t\text{Bu})][\text{PhC}_2]$. The NMR solution was taken into the glovebox, and the appropriate amount of PMe_3 or NH_2^tBu (1-5 equiv) was added. A second ^1H NMR spectrum was acquired at room temperature. Next, the probe was heated to 90 °C, and the conversion of the ion pair to $\text{TpRu}(\text{PMe}_3)_2(\text{C}\equiv\text{CPh})$ was monitored versus time. The half-lives for the all reactions

were approximately 15 min and did not vary substantially upon added phosphine or amine.

References.

- ¹ Muller, T. E.; Beller, M. *Chem Rev.* **1998**, *98*, 675-703.
- ² Wolfe, J. P.; Wagaw, S.; Marcoux, J.-F.; Buchwald, S. L. *Acc. Chem. Res.* **1998**, *31*, 805-818.
- ³ Hartwig, J. F. *Acc. Chem. Res.* **1998**, *31*, 852-860.
- ⁴ Hartwig, J. F. *Angew. Chem. Int. Ed.* **1998**, *37*, 2046-2067.
- ⁵ Fulton, R. J.; Holland, A. W.; Fow, D. J.; Bergman, R. G. *Acc. Chem. Res.* **2002**, *35*, 44-56.
- ⁶ Bryndza, H. E.; Tam, W. *Chem. Rev.* **1988**, *88*, 1163-1188.
- ⁷ Fulton, J. R.; Sklenak, S.; Bouwkamp, M. W.; Bergman, R. G. *J. Am. Chem. Soc.* **2002**, *124*, 4722-4737.
- ⁸ Kempe, R. *Angew. Chem. Int. Ed.* **2000**, *39*, 468-493.
- ⁹ Conner, D.; Jayaprakash, K. N.; Wells, M. B.; Manzer, S.; Gunnoe, T. B.; Boyle, P. D. *Inorg. Chem.* **2003**, *42*, 4759-4772.
- ¹⁰ Blue, E. D.; Davis, A.; Conner, D.; Gunnoe, T. B.; Boyle, P. D.; White, P. S. *J. Am. Chem. Soc.* **2003**, *125*, 9435-9441.
- ¹¹ Flood, T. C.; Lim, J. K.; Deming, M. A.; Keung, W. *Organometallics* **2000**, *19*, 1166-1174.
- ¹² Fox, D. J.; Bergman, R. G. *J. Am. Chem. Soc.* **2003**, *125*, 8984-8985.
- ¹³ Fox, D. J.; Bergman, R. G.; *Organometallics* **2004**, *23*, 1656-1670.
- ¹⁴ Soper, J. D.; Bennett, B. K.; Lovell, S.; Mayer, J. M. *Inorg. Chem.* **2001**, *40*, 1888-1893.
- ¹⁵ Soper, J. D.; Saganic, E.; Weinberg, D.; Hrovat, D. A.; Benedict, J. B.; Kaminsky, W.; Mayer, J. M. *Inorg. Chem.* **2004**, *43*, 5804-5815.
- ¹⁶ Goldsmith, C. R.; Jonas, R. T.; Stack, T. D. P. *J. Am. Chem. Soc.* **2002**, *124*, 83-96.
- ¹⁷ Bryant, J. R.; Mayer, J. M. *J. Am. Chem. Soc.* **2003**, *125*, 10351-10361.
- ¹⁸ Mayer, J. M. *Acc. Chem. Res.* **1998**, *31*, 441-450.
- ¹⁹ Bryant, J. R.; Mayer, J. M. *J. Am. Chem. Soc.* **2003**, *125*, 10351-10361.
- ²⁰ Binstead, R. A.; McGuire, M. E.; Dovletoglou, A.; Seok, W. K.; Roecker, L. E.; Meyer, T. J. *J. Am. Chem. Soc.* **1992**, *114*, 173-186.
- ²¹ Shultz, L. K.; Huynh, M. H. V.; Binstead, R. A.; Curry, M.; Meyer, T. J. *J. Am. Chem. Soc.* **2000**, *122*, 5984-5996.
- ²² Slugovc, C.; Schmid, R.; Kirchner, K. *Coord. Chem Rev.* **1999**, *185*, 109-126
- ²³ Joslin, F. L.; Johnson, M. P.; Mague, J. T.; Roundhill, D. M. *Organometallics* **1991**, *10*, 2781-2794.
- ²⁴ Boncella, J. M.; Eve, T. M.; Rickman, B.; Abboud, K. A. *Polyhedron* **1998**, *17*, 725-736.
- ²⁵ Hansch, C.; Taft, R. W. *Chem. Rev.* **1991**, *91*, 165-195.
- ²⁶ Sundberg, R.J.; Carey, F. A. *Advanced Organic Chemistry: Structure and Mechanism 4th ed.*; Plenum Publishing Company: New York, **2001**; pp 198-203.
- ²⁷ Holland, P. L.; Anderson, R. A.; Bergman, R. G. *Comments Inorg. Chem.* **1999**, *21*, 115-129.

-
- ²⁸ Mayer, J. M. *Comments Inorg. Chem.* **1988**, *8*, 125-135.
- ²⁹ Caulton, K.G. *New J. Chem.* **1994**, *18*, 25-41.
- ³⁰ Meyer T. Y.; Woerpel K. A.; Novak, B. M.; Bergman R. G. *J. Am. Chem. Soc.* **1994**, *116*, 10290-10291.
- ³¹ Holland, P. L.; Anderson, R. A.; Bergman, R. G.; Huang, J.; Nolan, S. P. *J. Am. Chem. Soc.* **1997**, *119*, 12800-12814.
- ³² Sharp, P. R. *Comments Inorg. Chem.* **1999**, *21*, 85-114.
- ³³ Powell, K. R.; Perez, P. J.; Luan, L.; Feng, S. G.; White, P. S.; Brookhart, M.; Templeton, J. L. *Organometallics* **1994**, *13*, 1851-1864.
- ³⁴ Gunnoe, T. B.; White, P. S.; Templeton, J. L. *J. Am. Chem. Soc.* **1996**, *118*, 6916-6923.
- ³⁵ Vollhardt, P. C. *Organic Chemistry 2nd ed.*; W.H. Freeman: New York, **1994**.
- ³⁶ Jayaprakash, K. N.; Conner, D.; Gunnoe, T. B.; *Organometallics* **2001**, *20*, 5254-5256.
- ³⁷ Antipin, I. S.; Gareyev, R. F.; Vedernikov, A. N. Kononov, A. I. *J. Phys. Org. Chem.* **1994**, *7*, 181-191.
- ³⁸ Harris D. C. *Quantitative Chemical Analysis 4th edition*; W.H. Freeman and Company: New York, **1995**.
- ³⁹ Holland, A. W.; Bergman, R. G. *J. Am. Chem. Soc.* **2002**, *124*, 14684-14695.
- ⁴⁰ Woerpel, K. A. Bergman, R. G. *J. Am. Chem. Soc.* **1993**, *115*, 7888-7889.
- ⁴¹ Jonas, R. T.; Stack, T. D. P. *J. Am. Chem. Soc.* **1997**, *119*, 8566-8567.
- ⁴² Binstead, R. A.; McGuire, M. E.; Dovletoglou, A.; Seok, W. K.; Roecker, L. E.; Meyer, T. J. *J. Am. Chem. Soc.* **1992**, *114*, 173-186.
- ⁴³ Pangborn, A. B.; Giardello, M. A.; Grubbs, R. H.; Rosen, R. K.; Timmers, F. J. *Organometallics* **1996**, *15*, 1518-1520.

Chapter 4: Aryl Coupling with Ruthenium Anilido Complexes.

4.1 Introduction and Importance of Biaryl Species.

Fundamental to the field of synthetic chemistry, biaryl species are present in a number of natural products, pharmaceuticals, electronic materials, and agrochemicals; their synthesis has been an area of significant study (Figure 4.1).^{1,2,3} For example, the synthesis of marine alkaloids has been an area of significant interest due to their high biological activity. Specifically, these compounds have been shown to inhibit topoisomerases, and their high cytotoxicity results in anti-tumor and anti-leukemia properties (Figure 4.1 A,B).⁴ Topoisomerases are enzymes that aid DNA replication by acting on the topology of DNA to decrease the degree of coiling and aid mobility. Without these enzymes, DNA is unable to replicate normally.⁵ Therefore, inhibitors of topoisomerases have been used as anti-cancer drugs to stop the proliferation of malignant cells.^{4,5} In addition, these compounds can act as DNA intercalating agents. Ascididemin and Neoamphimedine have specifically been shown to exhibit anti-leukemia properties through this ability (Figure 4.1 A,B).⁴

In the realm of drug discovery, the development and advancement of new/improved antibiotics is of special importance due to ever increasing bacteriological resistances to current pharmaceuticals. For example, the agent *Staphylococcus aureus* shows resistance to all current drugs save the very powerful group of antibiotics Vancomycins, sometimes referred to as the antibiotic of last resort (Figure 4.1C).^{6,7} Considerable efforts have been put forth over the past twenty years in the synthesis and modification of this drug to ensure its potency.^{6,7,8} Biaryl formation is an important step in the synthetic preparation of this antibiotic. The biaryl group is also a key feature in the group of drugs known as sartans which

are used to treat high blood pressure.⁹ The sartan Cozaar, a drug produced by Merck, is a shown below (Figure 4.1 D).

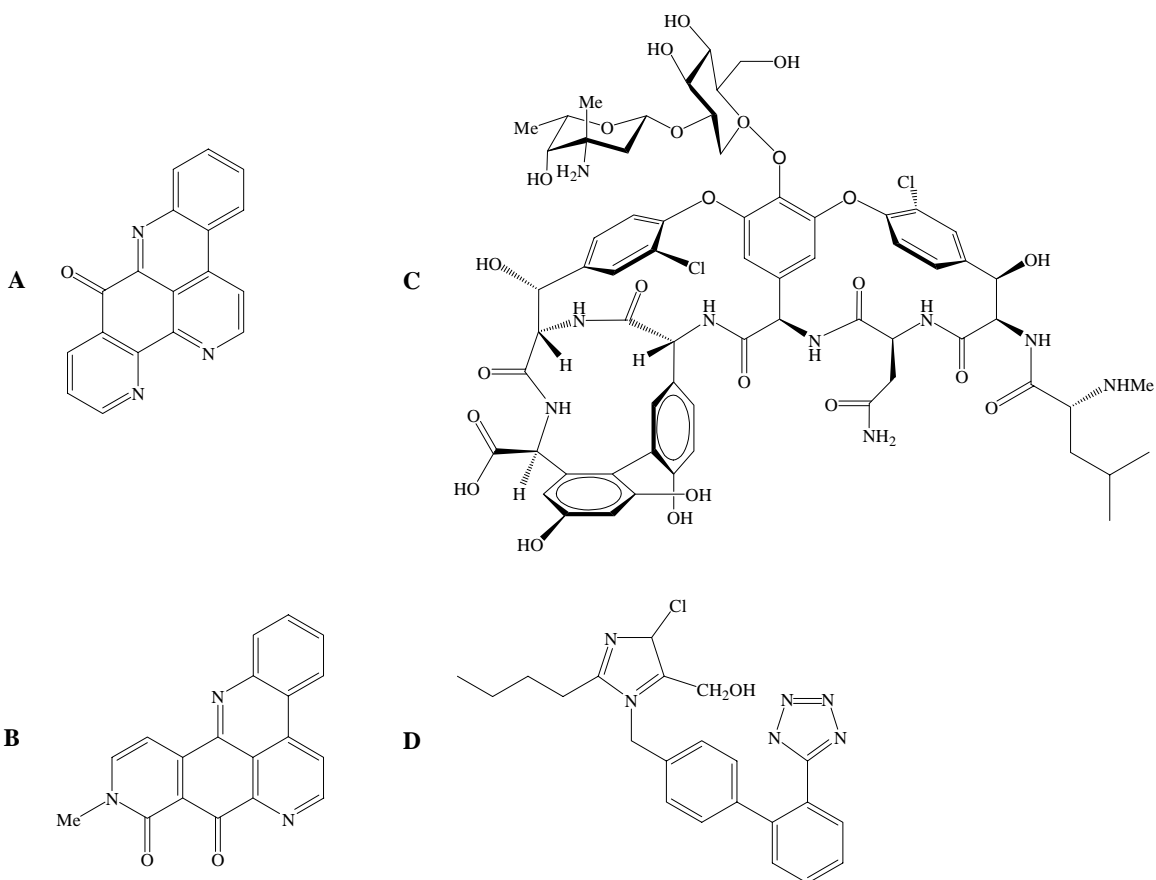
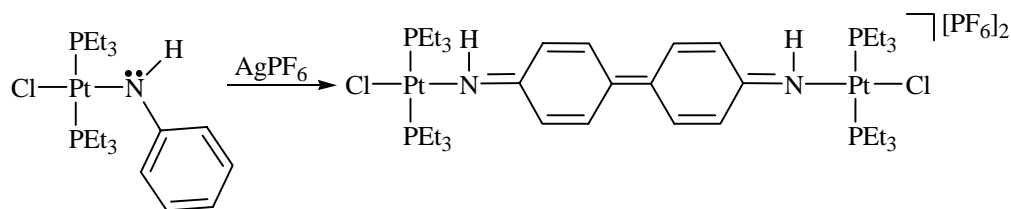


Figure 4.1 Examples of important biaryl species. **A.** Ascidiemin is a marine alkaloid shown to have biological activity. **B.** Neoamphimedine is a marine alkaloid shown to have biological activity. **C.** Vancomycin is a very powerful antibiotic. **D.** Sartans are a class of drugs used to treat high blood pressure.

4.1.1 Aryl-Aryl Bond Formation by Late Transition Metal Arylamido and Aryloxy Complexes.

Late transition metal complexes with arylamido and aryloxy ligands are known to undergo aryl-aryl bond forming reactions through coupling of those ligands upon oxidation.^{10,11,12,13,14,15,16} For example, Alcock et al. have reported the 4,4' coupling of the

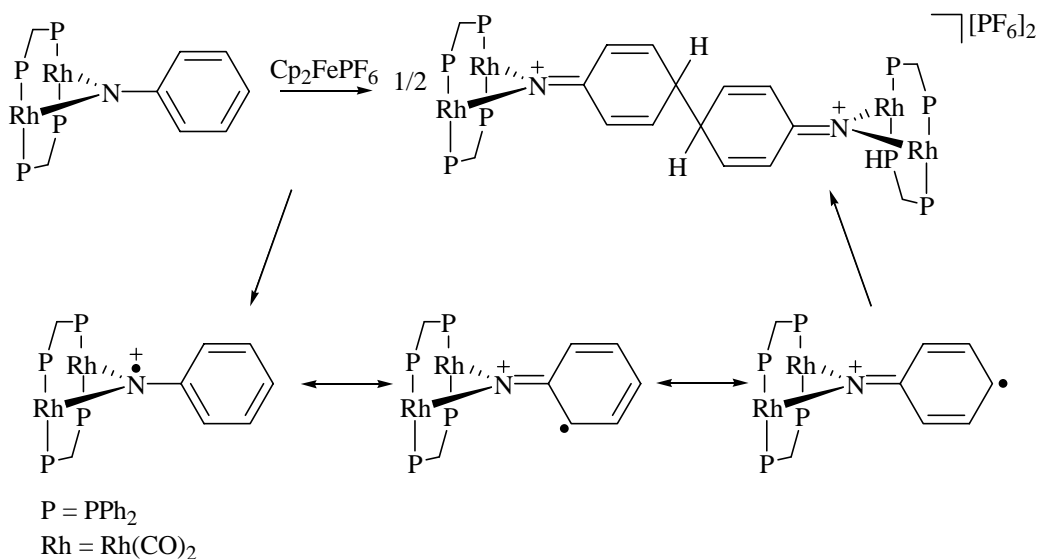
arylamido ligand of the Pt(II) complex $\text{PtCl}(\text{PEt}_3)_2\text{NHPH}$ by oxidation with AgPF_6 (Scheme 4.1).¹⁷ Similar oxidative coupling reactions have been reported with analogous para-methyl



Scheme 4.1 Oxidation of $\text{Pt}(\text{PEt}_3)_2\text{Cl}(\text{NHPH})$ results in aryl-aryl bond formation and C-H bond cleavage. This reaction yields two platinum metal centers bridged by a diimine ligand.

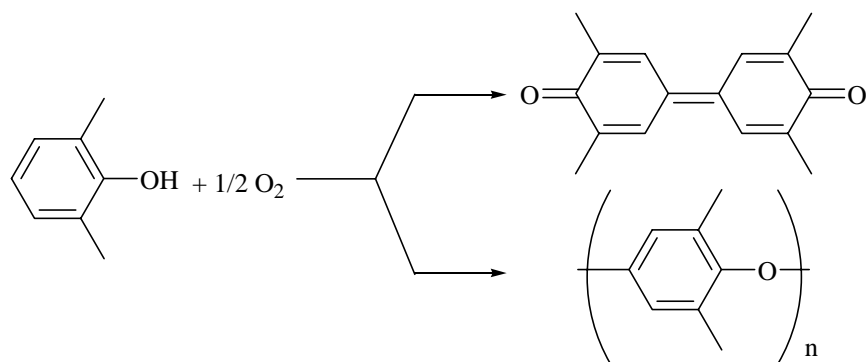
and para-fluoro substituted platinum aryl amido complexes.^{12,15} These oxidation reactions result in 2,4-coupling as well as 4,4' coupling. Approximately 20% ortho-para coupling was observed in the oxidation of $\text{Pt}(\text{PEt}_3)_2\text{Cl}(\text{NH}p\text{-tolyl})$.¹² Similarly, oxidation of the para-fluoro anilido analog of the platinum complex $\text{Pt}(\text{PEt}_3)_2\text{Cl}(\text{NH}p\text{-C}_6\text{H}_4\text{F})$ shows that the regioselectivity (4,4' versus 2,4-coupling) is temperature dependent. With increased temperature, the degree of 4,4'-coupling (C-F versus C-H bond activation) is increased.

The bridging rhodium imido complex $(\mu\text{-dppm})_2\text{Rh}_2(\text{NPh})(\text{CO})_2$ (dppm = bis(diphenylphosphino)methane) undergoes a similar coupling of the imido ligand to form an azavinylidene bridged dimer (Scheme 4.2).^{11,18} However, unlike the platinum chemistry above, C-H bond cleavage does not occur subsequent to the carbon-carbon coupling, but the para protons of the bridging ligand can be removed upon treatment with base to yield a benzidine bridged system. Also, the azavinylidene product in Scheme 4.2 can be formed by subsequent oxidation of this benzidine bridged system.



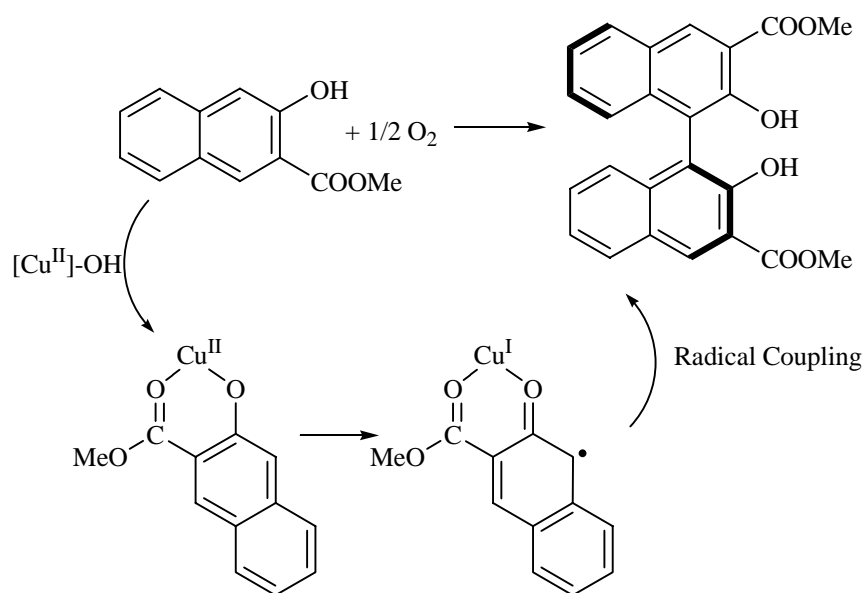
Scheme 4.2 Oxidation of the Rh μ -imido complex results in radical coupling at the 4 position of the imido ligand.

From a more synthetically practical standpoint, oxidation of phenolic compounds by metal-mediated routes has been of significant interest due to the increased selectivity of these methods compared to chemical/electrochemical oxidation because such methods with phenols results in the generation of radicals and non-selective coupling.¹⁹ Alternatively, the oxidation of phenols using late transition metal catalysts has been reported with increased selectivity compared to radical routes.^{19,20,21} For example, copper catalyzed oxidation of 2,6-dimethylphenol using $\text{Cu}(\text{NO}_3)_2$ as a catalyst and dioxygen as the oxidant results in the formation of diphenylquinone and polyphenylene ether (Scheme 4.3). The proposed mechanism of this reaction involves initial deprotonation of phenol followed by oxidation of the coordinated phenoxide to form a phenoxy radical. The biphenylquinone is formed through radical coupling, while the polymer is formed through nucleophilic attack by the phenoxide at the para position.



Scheme 4.3 Oxidation of 2,6-dimethylphenyl catalyzed by Cu(II). Radical coupling at the 4 position yields the biphenylquinones, and nucleophilic attack at the para position forms polymer.

The selective coupling of naphthols is important because optically active binaphthols can be used to induce chirality through axial dissymmetry, and thus the synthesis of 1,1'-binaphthols has been of significant interest.^{2,20,22,23} Copper-catalyzed oxidative coupling is one method to synthesize these compounds (Scheme 4.4).^{22,23} These reactions are proposed to proceed through metathesis of a Cu-OH with naphthol to form a copper naphthoxide complex that is oxidized by O₂. Reduction of Cu by a coordinated naphthoxide forms a

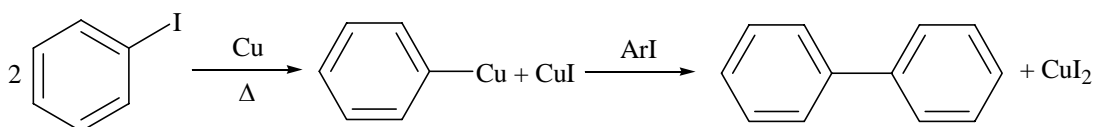


Scheme 4.4 Oxidative coupling of naphthols to form chiral binaphthols.

radical which can couple with another equivalent of the copper naphthoxide radical intermediate (Scheme 4.4). The chirality is induced through the steric direction by the copper catalyst's ancillary ligand(s) during the radical coupling. Specifically, the ancillary ligand(s) tend to enforce approach of the radicals. Depending on reaction conditions and particularly the Cu-ancillary ligand(s), enantiopurities in excess of 91 % have been reported.^{22,23}

4.1.2 Common Synthetic Methods to Form Aryl-Aryl Bonds.

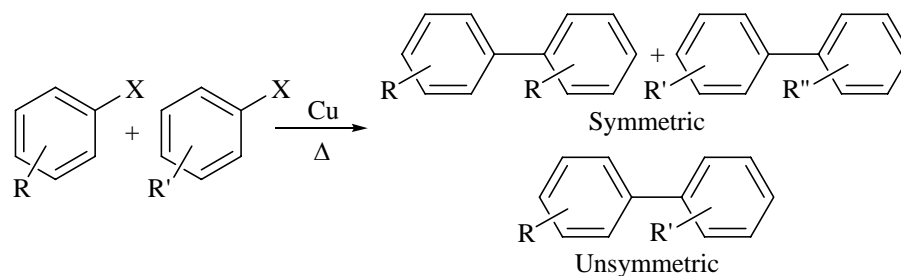
In the realm of organic synthesis, metal-mediated methods for aryl-aryl bond formation have long been developed. The earliest of these schemes is the Ullmann reaction. Developed in the early 1900's, this method reductively couples aryl-halides using metallic copper as a stoichiometric reductant.^{1,24} The reaction typically uses two equivalents of aryl-halide (usually aryl-iodide or bromide) to one equivalent of metallic copper powder, and the reaction is run at high temperatures (above 200 °C) (Scheme 4.5). The mechanism of this



Scheme 4.5 The Ullmann reaction couples aryl iodides in the presences of copper to form a biaryls and copper(II) iodide.

reaction is not definitively known; however, it has been proposed to proceed by a two step mechanism where halogen exchange occurs to form an organo-cuprate that reacts with aryl-iodide.^{1,24} Other mechanisms such as oxidative addition of aryl-halide followed by nucleophilic substitution have also been proposed.¹ The Ullmann reaction is most useful for

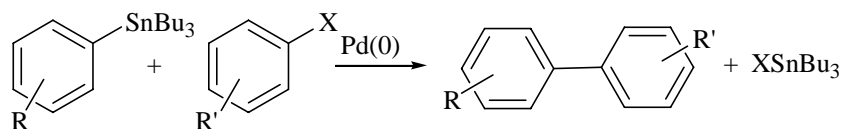
the synthesis of symmetric biaryls; however, unsymmetrical couplings have also been reported. A mixture of two different aryl-halides has three possible coupling products (two homocoupled and one heterocoupled) (Scheme 4.6).^{1,24}



Scheme 4.6 Symmetric vs. unsymmetric coupling for a mixture of two aryl-halides. Homocoupling yields two symmetric products and heterocoupling yields an unsymmetric product.

In addition to the Ullmann reaction, several common catalytic coupling methods have been developed that are applicable for the synthesis of biaryl species. In the 1970's, catalytic aryl coupling using aryl-Grignard reagents with aryl-halides in the presence of Ni or Pd catalysts was developed.^{1,24} This scheme is known as the Kharasch reaction. The significant shortcoming of this system is that the polar/reactive nature of Grignard reagents prohibits the use of many functional groups such as aldehydes, esters, and nitro groups.

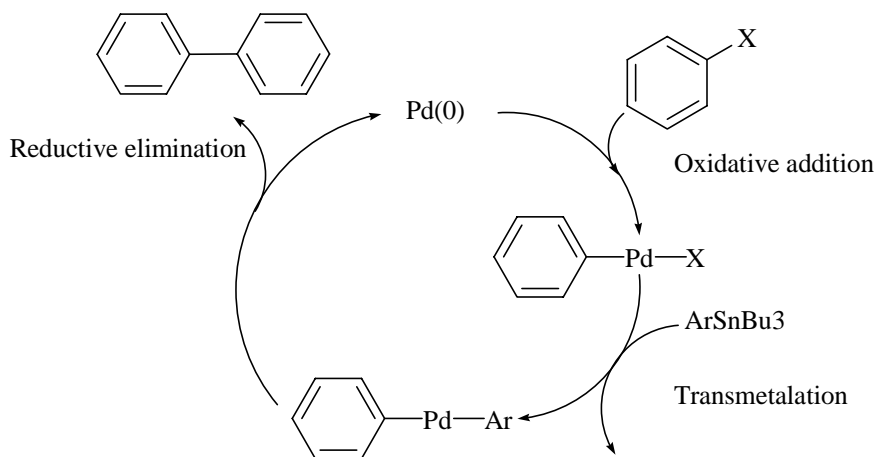
Stille coupling, also developed in the 1970's, is another prevalent method utilized to generate biaryl species. This reaction forms aryl-aryl bonds by coupling arylstannanes and arylhalides or triflates in the presence of a palladium catalyst (Scheme 4.7).^{1,25} The availability of aryl-tin reagents and their air and moisture stability is one advantage of Stille coupling over the Kharasch reaction. Stille coupling is also more versatile because the less reactive reagents will tolerate more functional groups on both organic halide as well as the



Scheme 4.7 The Stille reaction is used to form aryl-aryl bonds by reacting aryl-tin reagents with aryl-halides in the presence of a palladium catalyst.

aryl-tin reagents.^{24,25} The one significant drawback of Stille coupling is the organic stannyl reagents and byproducts associated with this reaction are toxic. Thus, there are negative implications for many end uses such as pharmaceutical chemistry.

The mechanism of this catalysis proceeds by oxidative addition of an aryl-halide or aryl-triflate to Pd(0) to form a Pd(II) aryl-halide/triflate. Transmetalation occurs between the Pd(II) intermediate and the arylstanne to form a Pd(II) bis-aryl complex and a stannylhalide byproduct. Reductive elimination from the Pd(II) bis-aryl species generates the biaryl product and regenerates the catalyst (Scheme 4.8).²⁵



Scheme 4.8 Mechanism of the Stille reaction. Initiation occurs by oxidative addition of aryl-halide or aryl-triflate to Pd(0), followed by transmetalation generate Pd(Ar)(Ar'), subsequently reductive elimination forms the biaryl bond and regenerates the catalyst.

Cross-coupling of arylboronic acids to aryl-halides or aryl-triflates using palladium catalysts in the presence of a base is known as the Suzuki coupling.^{1,24,25,26} Mechanistically similar to Stille coupling, this reaction proceeds by oxidative addition of an aryl-halide followed nucleophilic substitution of the halogen and reductive elimination to generate the biaryl product and regenerate the catalyst.²⁵ One significant advantage of Suzuki vs. Stille coupling is the removal of toxic reagents and by-products. In addition, aryl-boryl reagents are functional group tolerant.^{25,26}

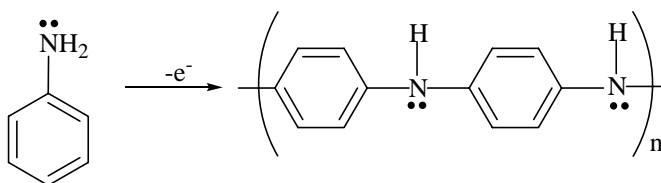
4.1.3 Potential Synthetic Utility of Aryl-Aryl Coupling by Oxidation of Late Transition Metal Amido Complexes.

We are interested in comparing the chemistry of non-dative ligands as a function of the metal oxidation state. The d^6 aryl amido complexes TpRu(L)(L')NHPH exhibit basic and nucleophilic character; however, the related d^4 osmium amine complex $[\text{TpOs}(\text{Cl})_2\text{NH}_2\text{Ph}]^+$ has a $\text{p}K_a$ of approximately -3 .^{10,27,28,29,30} In addition, Fe^{III} and Ru^{III} oxide complexes initiate hydrogen atom abstraction reactions.^{31,32} One possible reaction of the Ru^{III} anilido is a result of radical character in the amido phenyl substituent. Along these lines aryl-aryl coupling of late transition metal complexes with non-dative ligands has been reported.¹⁰⁻¹⁸ Based on this chemistry, schemes to form biaryl compounds through oxidization of arylamido and aryloxy complexes can be envisioned. In addition, the catalytic activity copper phenol oxidation catalysis suggests the possibility of catalytic formation of biaryl oxides and amines.^{1,2,20-23}

A catalytic system to promote aryl-aryl bond formation by indirect oxidation of anilines would potentially represent a significant advantage over commonly used methods.

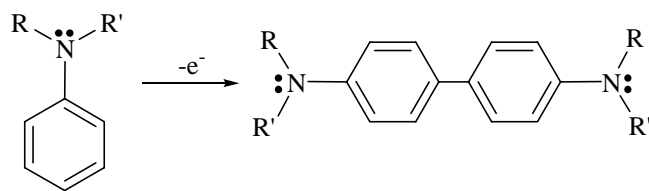
For instance, this method would eliminate the use of aryl-halides required in Kharasch, Ullman, Stille, and Suzuki couplings. Also, both Suzuki and Stille coupling require stoichiometric amounts of aryl organometallic reagents. Elimination of the toxic aryl-tin reagents used in Stille would be a particularly important advantage. Thus, direct catalytic coupling would eliminate the need for preparation and use of the organometallic aryl-tin and aryl-borate reagents; the latter of these can sometimes be difficult to prepare. Another potential advantage of direct catalytic oxidative coupling scheme is aryl-aryl bond formation using the Ullmann or Suzuki reactions are often inhibited by electron donating groups. In addition, although catalytic couplings have been communicated for the Ullmann reaction, it usually requires stoichiometric amounts of copper and oftentimes high temperature.¹

The direct formation of biaryl species through oxidation of aniline by chemical or electrochemical means has proven to be unsuccessful. This scheme results in the formation of polyaniline due to polymerization resulting from nitrogen based radical N-C bond formation (Scheme 4.9).³³ C-C bond formation occurs only if the nitrogen atom is sterically



Scheme 4.9 Oxidation of aniline. This reaction results in N-C bond formation through radical coupling.

protected from N-C bond formation. For example, the oxidation of triaryl amines on the surface of electrodes has been reported to result in C-C coupling (Scheme 4.10).^{44,45} Oxidative coupling catalysts using late transition amido or oxide complexes would be more

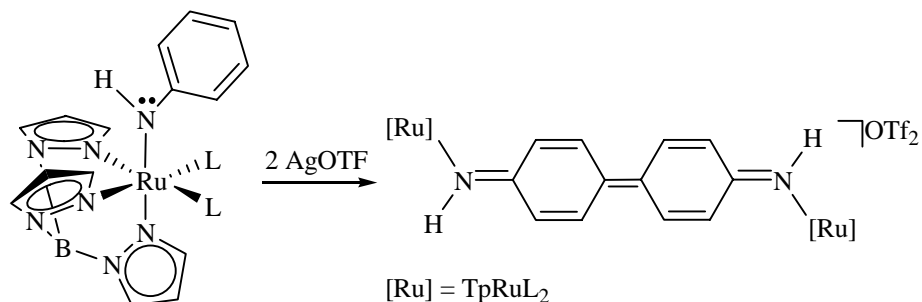


Scheme 4.10 Oxidation of sterically hindered arylamines results in carbon-carbon bond formation through radical coupling.

broadly applicable than aniline oxidations since the metal binds the nitrogen or oxygen atom of the ligand thereby acting as a protecting group preventing N-C or O-C bond formation.

4.2 Oxidation of $\text{TpRuL}_2\text{NHPH}$ $\text{L} = \text{CO}, \text{PMe}_3, \text{ or } \text{P(OMe)}_3$.

Reactions of THF or acetonitrile solutions of the phenyl amido complexes $\text{TpRu}(\text{CO})_2\text{NHPH}$, $\text{TpRu}\{\text{P(OMe)}_3\}_2\text{NHPH}$, or $\text{TpRu}(\text{PMe}_3)_2\text{NHPH}$ with 2 equivalents of AgOTf result in an immediate color change from yellow to red, blue, and green, respectively. The formation of a black precipitate (Ag), and the Ru(II) amine complexes $[\text{TpRuL}_2\text{NH}_2\text{Ph}][\text{OTf}]$ ($\text{L} = \text{CO}, \text{P(OMe)}_3, \text{ or } \text{PMe}_3$) were also observed. Attempts to perform these reactions in CH_2Cl_2 or CHCl_3 resulted in decomposition. The reactions were carried out at room temperature except for the amido complex $\text{TpRu}(\text{CO})_2\text{NHPH}$ which required in situ generation at -78°C due to the thermal instability of this amido complex (see Chapter 2). In addition to Ru(II) aniline complexes, the binuclear complexes $[\text{TpRuL}_2\text{NH}(\text{C}_6\text{H}_4^-)]_2[\text{OTf}]_2$ are formed in these oxidation reactions (Scheme 4.11). X-ray crystallography of $[\text{TpRu}\{\text{P(OMe)}_3\}_2\text{NH}(\text{C}_6\text{H}_4^-)]_2[\text{OTf}]_2$ indicates that a structure corresponding to Ru(II) metal centers linked by a diimine ligand contributes significantly to the bonding (see below). Thus, the oxidations of $\text{TpRuL}_2\text{NHPH}$ were found to proceed in a



Scheme 4.11 Oxidation of the phenyl amido complexes results in 4,4'-coupling of the phenyl group (L = CO, PMe₃, or P(OMe)₃).

similar fashion to that observed for the oxidation of Pt(PEt₃)₂(Cl)(NHPh).^{12,17} The binuclear complexes have been characterized by IR, ¹H NMR, ¹³C NMR, and ³¹P NMR spectroscopy, as well as FAB mass spectrometry.

[TpRu{P(OMe)₃}₂(NHC₆H₄-)]₂[OTf]₂ is a dark blue solid that is air stable. The most salient features of the ¹H NMR spectrum of [TpRu(CO)₂(NHC₆H₄-)]₂[OTf]₂ are downfield resonances due to the imine *NH* protons, and the ring protons of NHC₆H₄ are observed upfield of 5 ppm (Figure 4.2). The resonances for the ring protons are broadened due to fluxional processes involving ring rotation (see below). Virtual triplets were observed in the ¹H NMR spectrum for the trimethylphosphite ligands. Additionally, two isomers are possible based on orientation to the TpRu fragments (see below). Interestingly, a solvent dependence on the *K*_{eq} of these isomers was observed; specifically, *K*_{eq} approaches 1 in more polar solvents. The solvent dependence of *K*_{eq} is best observed with the imine *NH* and ring resonance. Figures 4.2 and 4.3 depict ¹H and ³¹P NMR spectra of [TpRu{P(OMe)₃}₂(NHC₆H₄-)]₂[OTf]₂ in CDCl₃ and CD₃CN; the insets provide the relative ratios; approximately 2:1 and 1:1 respectively. The two isomers are also distinguishable by ³¹P NMR. Two resonances are observed at approximately 135 ppm (depending on solvent),

and spectra confirm the relative ratio of the two isomers. (Figure 4.2 A and 4.3 A). The ^{31}P NMR in $\text{DMSO-}d_6$ reveals an approximate 1:1 ratio.

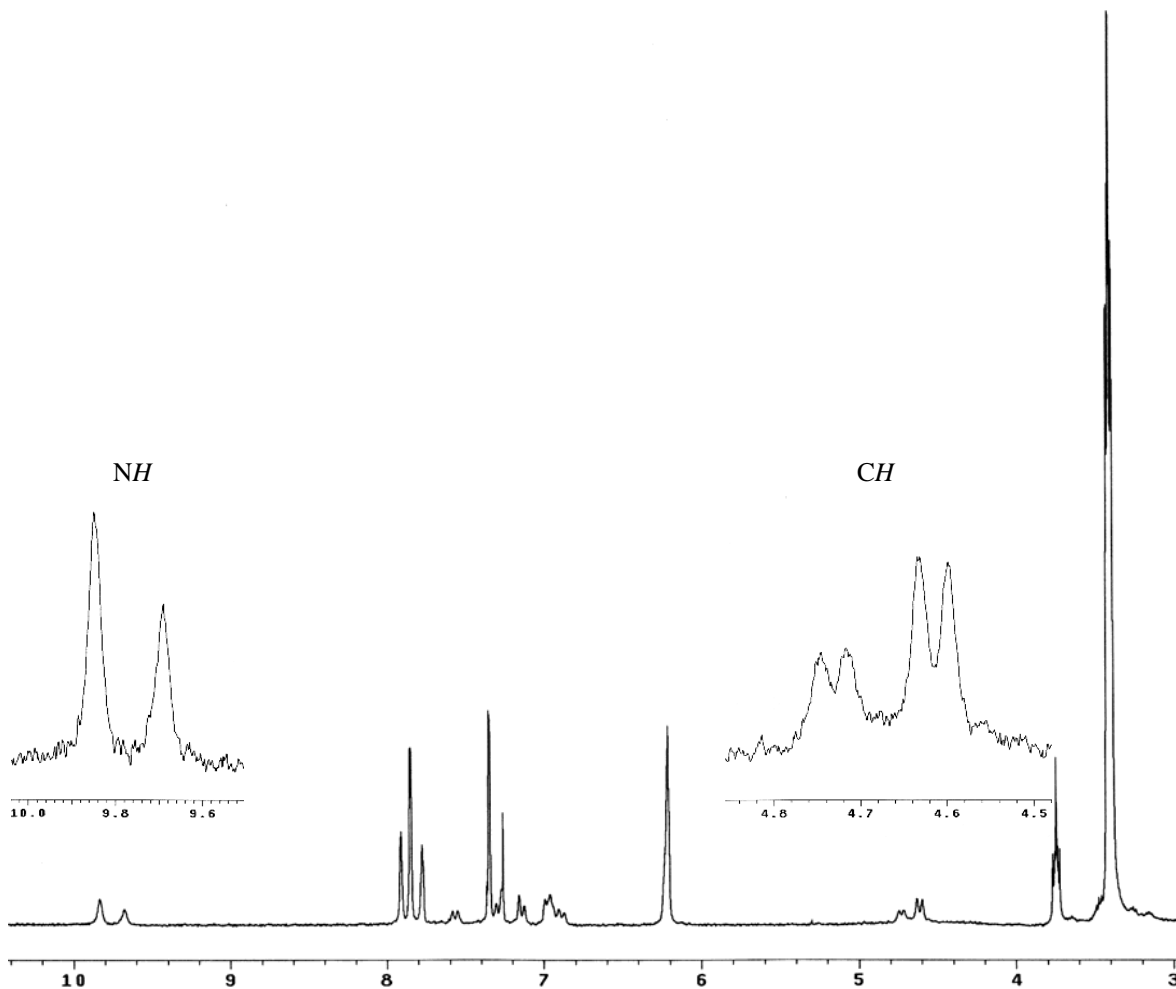


Figure 4.2 ^1H NMR spectrum of $[\text{TpRu}\{\text{P}(\text{OMe})_3\}_2(\text{NHC}_6\text{H}_4^-)_2][\text{OTf}]_2$ in CDCl_3 .

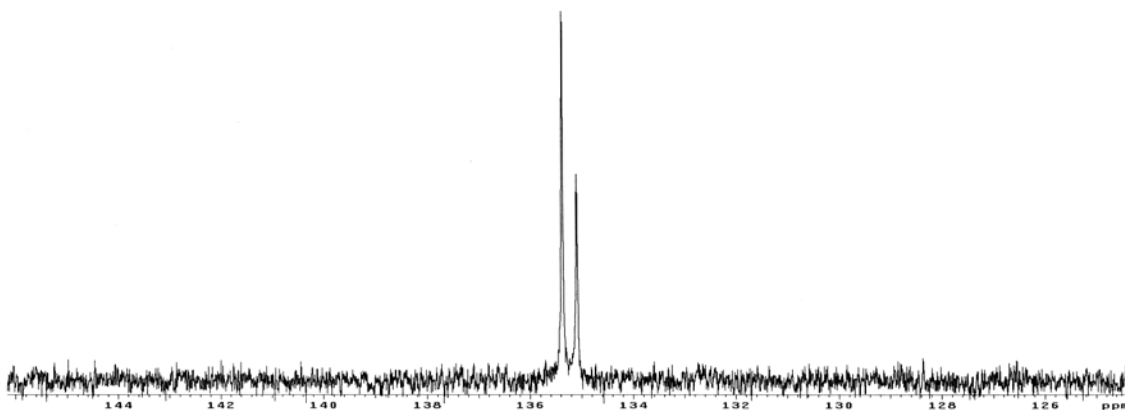


Figure 4.2A ^{31}P NMR spectrum of $[\text{TpRu}\{\text{P}(\text{OMe})_3\}_2(\text{NHC}_6\text{H}_4^-)_2][\text{OTf}]_2$ in CDCl_3 .

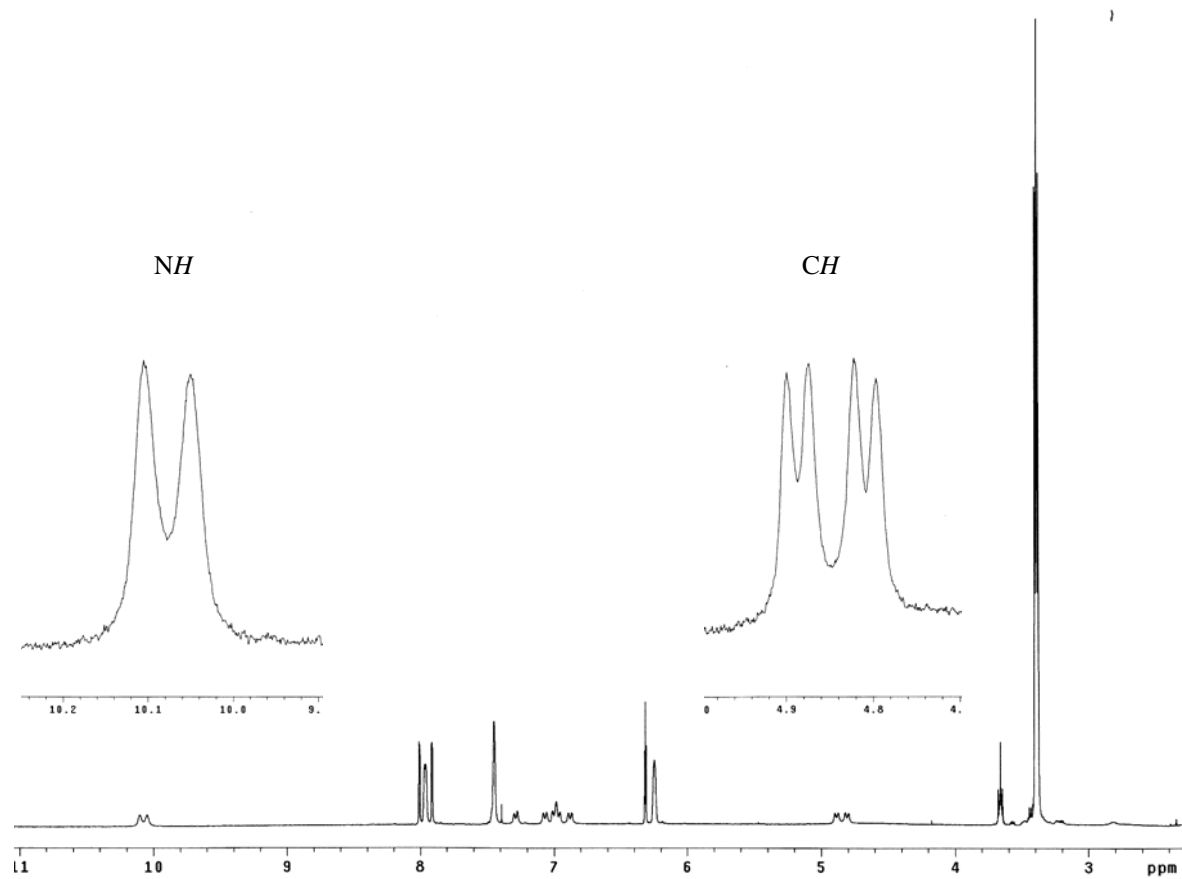


Figure 4.3 ^1H NMR spectrum of $[\text{TpRu}\{\text{P}(\text{OMe})_3\}_2(\text{NHC}_6\text{H}_4^-)]_2[\text{OTf}]_2$ in CD_3CN .

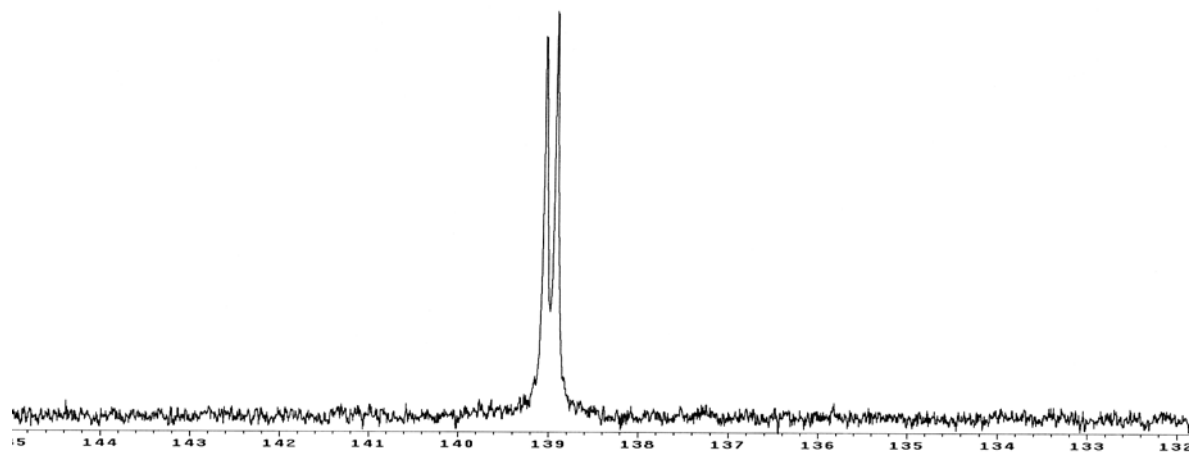


Figure 4.3 A ^1H NMR spectrum of $[\text{TpRu}\{\text{P}(\text{OMe})_3\}_2(\text{NHC}_6\text{H}_4^-)]_2[\text{OTf}]_2$ in $\text{DMSO-}d_6$.

$[\text{TpRu}(\text{CO})_2(\text{NHC}_6\text{H}_4^-)]_2[\text{OTf}]_2$ is a dark red solid that is air stable, and the ^1H NMR spectrum features are similar to $[\text{TpRu}\{\text{P}(\text{OMe})_3\}_2(\text{NHC}_6\text{H}_4^-)]_2[\text{OTf}]_2$. In $\text{DMSO-}d_6$, a single down field resonance due to the imine NH protons is observed at 11.33 ppm and the ring protons are observed at 5.9 ppm (Figure 4.4). Similar to $[\text{TpRu}\{\text{P}(\text{OMe})_3\}_2(\text{NHC}_6\text{H}_4^-)]_2[\text{OTf}]_2$, K_{eq} of the isomers display a dependence on solvent polarity. IR spectroscopy reveals $\nu_{\text{CO}} = 2080, 2024 \text{ cm}^{-1}$ and $\nu_{\text{NH}} = 3437 \text{ cm}^{-1}$. The carbonyl stretching frequency of $[\text{TpRu}(\text{CO})_2(\text{NHC}_6\text{H}_4^-)]_2[\text{OTf}]_2$ changes little from the CO stretch of the amine complex $[\text{TpRu}(\text{CO})_2(\text{NH}_2\text{Ph})][\text{PF}_6]$ ($\nu_{\text{CO}} = 2084, 2022 \text{ cm}^{-1}$). Thus, the relative donating abilities of

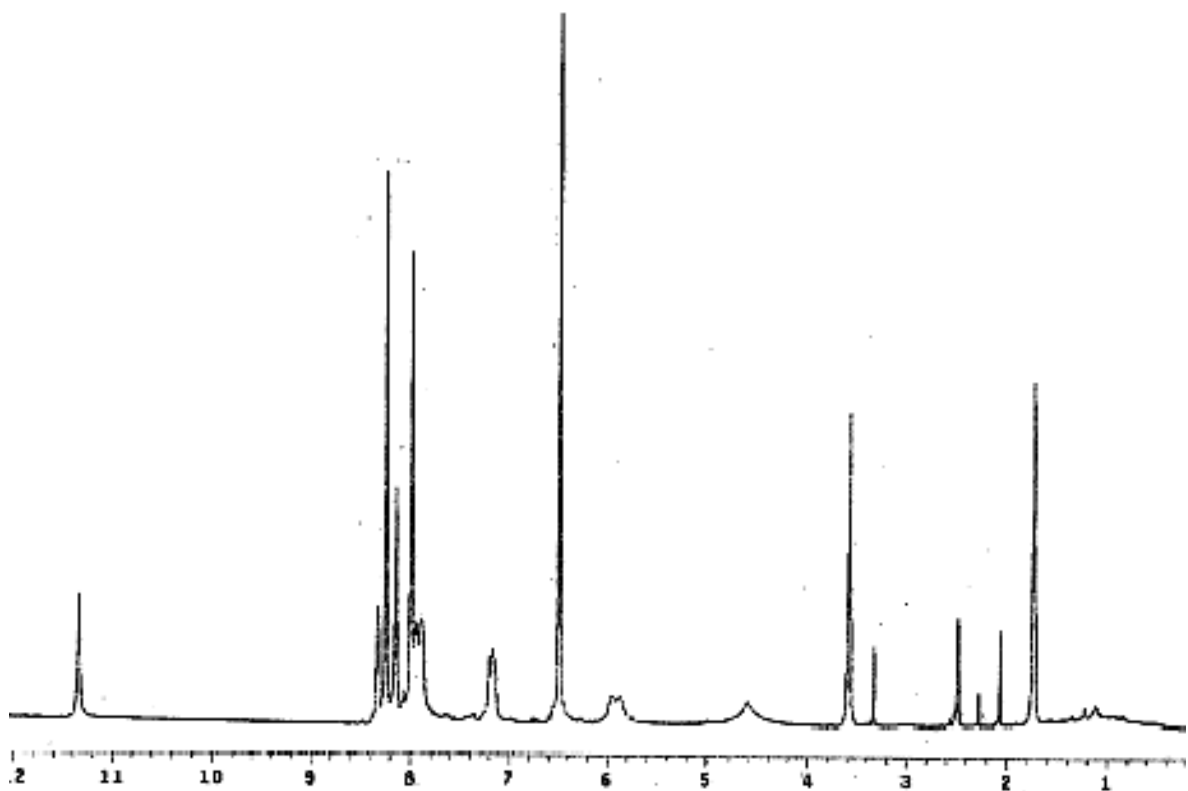


Figure 4.4 ^1H NMR spectrum of $[\text{TpRu}(\text{CO})_2(\text{NHC}_6\text{H}_4^-)]_2[\text{OTf}]_2$ in $\text{DMSO-}d_6$.

NH₂Ph and NHC₆H₄⁻ to the TpRu(CO)₂ fragment are similar.

[TpRu(PMe₃)₂(NHC₆H₄⁻)₂][OTf]₂ is a dark green solid that is not air sensitive. Like the complex [TpRu{P(OMe)₃}₂(NHC₆H₄⁻)₂][OTf]₂, the ¹H NMR spectrum in DMSO-*d*₆ reveals downfield a resonance due to the imine NH protons at 10.9 ppm and ring protons upfield of 4.9 ppm (Figure 4.5). IR spectroscopy reveals $\nu_{\text{NH}} = 3399 \text{ cm}^{-1}$. Only one

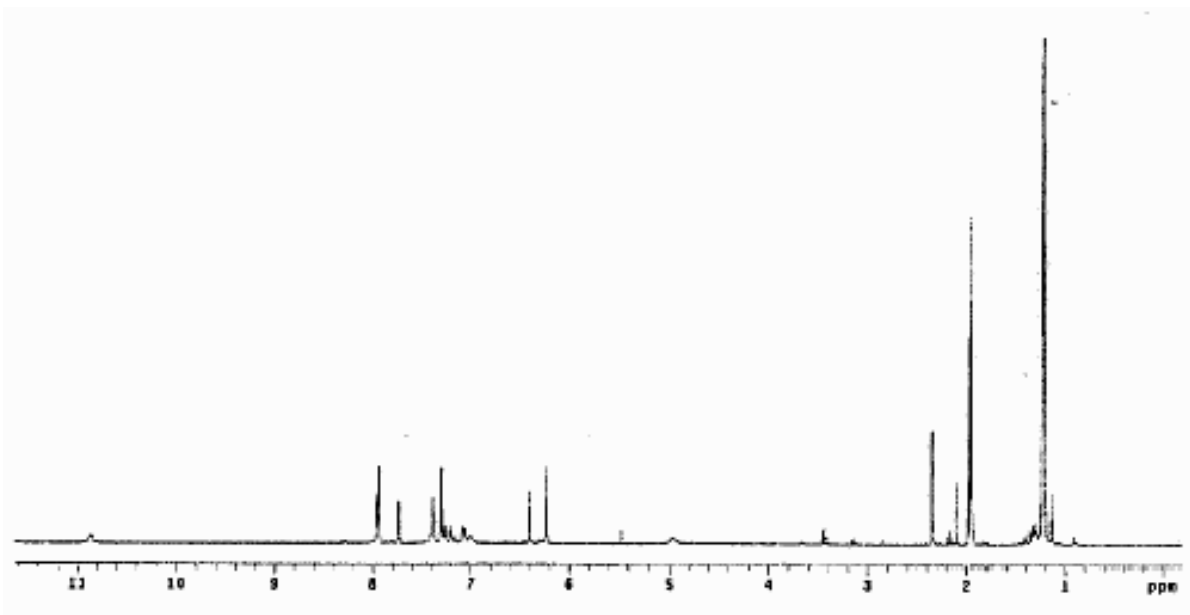


Figure 4.5 ¹H NMR spectrum of TpRu(PMe₃)₂(NHC₆H₄⁻)₂[OTf]₂ in DMSO-*d*₆

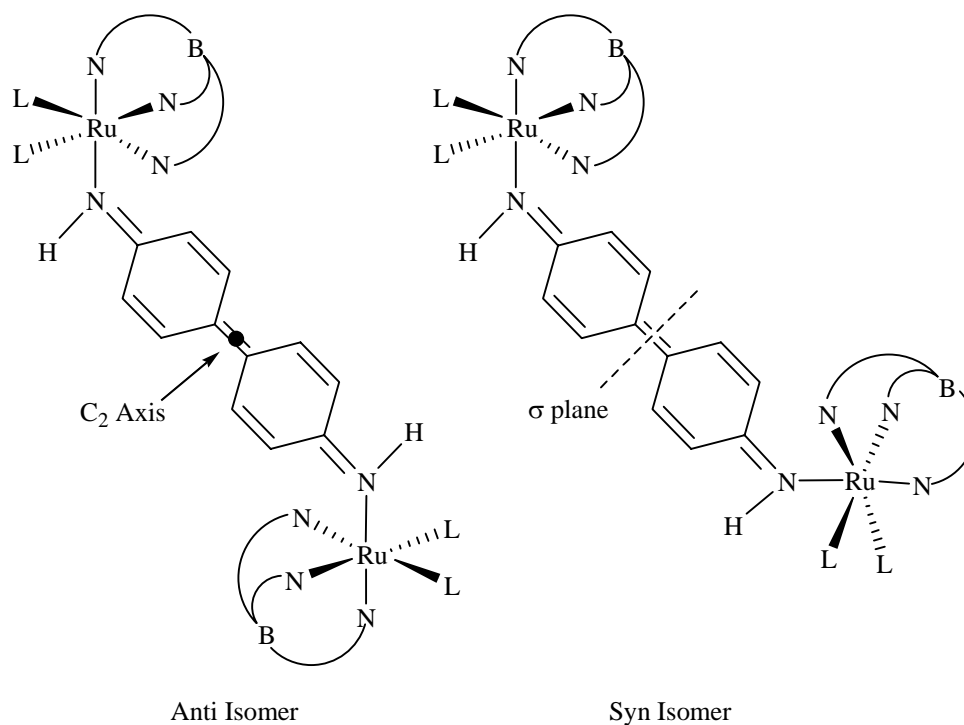
resonance is observed in the ³¹P NMR spectrum in CDCl₃, CD₃CN, or DMSO-*d*₆. This result is like attributable to coincidental overlap. In CDCl₃ or CD₃CN two isomers are observed in the ¹H NMR spectra based on the observation of two imine NH resonances as well as ring resonances.

4.3 Dynamic NMR Spectroscopy of the Complexes [TpRuL₂(NHC₆H₄-)][OTf]₂

Variable temperature ¹H and ³¹P NMR spectroscopy was used to analyze the fluxional behavior of the complexes [TpRuL₂(NHC₆H₄-)][OTf]₂ (L = PMe₃, P(OMe)₃, or CO). Appendix B provides selected spectra for [TpRu{P(OMe)₃}₂NH(C₆H₄-)]₂[OTf]₂, [TpRu(PMe₃)₂NH(C₆H₄-)]₂[OTf]₂, and [TpRu(CO)₂NH(C₆H₄-)]₂[OTf]₂.

The room temperature ¹H NMR spectrum of a CD₃CN solution of [TpRu{P(OMe)₃}₂NH(C₆H₄-)]₂[OTf]₂ reveals two downfield amido NH resonances at 10.12 and 10.06 ppm (*K*_{eq} ~ 1). The low temperature ¹H NMR spectrum (-40 °C) of this solution reveals eight unique resonances due to C₆H₄ rings. Heating the solution results in line broadening and coalescence of the resonances due to the imine ring and NH protons, and at 95 °C resonances consistent with a single isomer are observed. At room temperature, a single set of Tp resonances is observed. Upon cooling, the Tp resonances broaden and for some resonances decoalescence into two sets of peaks is observed.

The dynamic NMR behavior is consistent with two isomers based on relative positioning of {TpRuL₂} fragments about the bridging HN-C₆H₄-C₆H₄-NH ligands. Thus, the relative orientation of the two {TpRuL₂} fragments of a single binuclear complex can be "syn" or "anti" (Scheme 4.12). For each isomer, the two {TpRuL₂(NHC₆H₄-)} fragments are symmetry equivalent. For the anti isomer, a C₂ axis renders the two {TpRu} moieties equivalent, while a mirror plane of symmetry equilibrates the two {TpRu} fragments of the syn isomer. Thus, each isomer gives rise to four C₆H₄ resonances, a single NH resonance, and a single set of Tp resonances with a 2:1 integration pattern since both isomers possess



Scheme 4.12 “Syn” and “Anti” geometrical isomers due to relative orientations of {TpRuL₂} fragments about rigid π -system.

mirror symmetry in the plane of the ring linkages. Consistent with the solid-state structure of [TpRu{P(OMe)₃}₂NH(C₆H₄-)]₂[OTf]₂ (see below), Scheme 4.12 depicts an orientation with the C₆H₄ rings between two pyrazolyl rings. Heating the solution results in line broadening and coalescence of the resonances due to the NH protons. Using the coalescence temperature (40 °C) of the two NH resonances, the activation barrier for isomer interconversion has been calculated to be 15.9 kcal/mol.

Similar to [TpRu{P(OMe)₃}₂NH(C₆H₄-)]₂[OTf]₂, the ¹H NMR spectrum of [TpRu(PMe₃)₂NH(C₆H₄-)]₂[OTf]₂ at -50 °C reveals the presence of two NH resonances at 11.56 and 11.53 ppm (*K*_{eq} ~ 1), and the dynamic NMR features of the complex parallel those of the trimethylphosphite complex [TpRu{P(OMe)₃}₂NH(C₆H₄-)]₂[OTf]₂. At room

temperature, the ^{31}P NMR spectrum reveals a single resonance at 8.0 ppm; however, cooling the solution to $-45\text{ }^\circ\text{C}$ does not result in decoalescence. The inability to observe decoalescence is likely attributable to a small difference in chemical shift for the ^{31}P resonances of the two isomers. In the variable temperature ^1H NMR spectra, the coalescence of the two *NH* resonances ($-5\text{ }^\circ\text{C}$) results in a calculated barrier of 13.9 kcal/mol for isomer interconversion of $[\text{TpRu}(\text{PMe}_3)_2\text{NH}(\text{C}_6\text{H}_4^-)]_2[\text{OTf}]_2$.

In $\text{Me}_2\text{SO}-d_6$ or CD_3CN , the dicarbonyl complex $[\text{TpRu}(\text{CO})_2\text{NH}(\text{C}_6\text{H}_4^-)]_2[\text{OTf}]_2$ exhibits a single resonance for the *NH* protons. However, in CDCl_3 two *NH* resonances are observed in a 2.3 : 1 ratio at 10.64 and 10.31 ppm respectively. Heating this solution to $70\text{ }^\circ\text{C}$ does not result in significant line broadening; however, the addition of 3 drops of $\text{Me}_2\text{SO}-d_6$ results in an equilibrium shift to an approximate 1:1 ratio. This result indicates that K_{eq} is dependent on solvent identity, perhaps due to solvent polarity and differences in dipole of the geometrical isomers. Ion-pairing effects may also play a role in the solvent-dependent K_{eq} . Heating the $\text{CDCl}_3/\text{Me}_2\text{SO}-d_6$ solution of $[\text{TpRu}(\text{CO})_2\text{NH}(\text{C}_6\text{H}_4^-)]_2[\text{OTf}]_2$ to $40\text{ }^\circ\text{C}$ does not result in changes in chemical shift or line broadening. Thus, at room temperature the slow exchange regime has been accessed. Heating the solution to $70\text{ }^\circ\text{C}$ does result in line broadening; however, coalescence is not achieved at this temperature. Increasing the temperature further is limited by the boiling point of the solvent. Using these data, the ΔG^\ddagger for interconversion of the two isomers has been calculated to be >18.5 kcal/mol. The three complexes and the barriers to isomer interconversion are listed in Table 4.1. Although access to three data points is inadequate to reliably establish a trend, it is

notable that the ΔG^\ddagger values for isomer interconversion increase with decreasing donating ability of ligands "L" (i.e., for ΔG^\ddagger CO > P(OMe)₃ > PMe₃).

Table 4.1 Barriers to isomer interconversion for the binuclear complexes.

Complex	ΔG^\ddagger (kcal/mol)	T _{Coal} (°C)
[TpRu(CO) ₂ NH(C ₆ H ₄ -)] ₂ [OTf] ₂	>18.5	> 70
TpRu{P(OMe) ₃ } ₂ NH(C ₆ H ₄ -)] ₂ [OTf] ₂	15.9	40
[TpRu(PMe ₃) ₂ NH(C ₆ H ₄ -)] ₂ [OTf] ₂	13.9	-5

4.4 Solid-State Structure of [TpRu{P(OMe)₃}₂NH(C₆H₄-)]₂[OTf]₂.

The X-ray structure of [TpRu{P(OMe)₃}₂NH(C₆H₄-)]₂[OTf]₂ shows a binuclear complex with pseudooctahedral coordination spheres (Figure 4.6). Selected bond distances

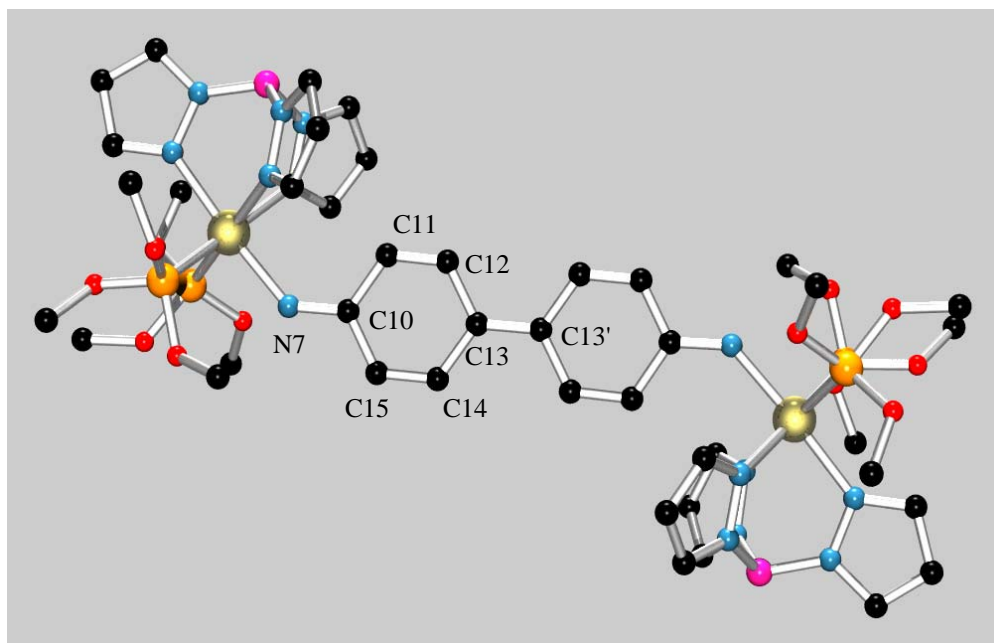


Figure 4.6 X-ray structural diagram of [TpRu{P(OMe)₃}₂NHC₆H₄-)]₂[OTf]₂

are given in Table 4.2, and the data collection parameters and complete list of bond distances and angles are provided in Appendix A. The molecule resides on a crystallographic center of symmetry, and the two $\{\text{TpRu}\{\text{P}(\text{OMe})_3\}_2(\text{NHC}_6\text{H}_4)\}$ fragments are equivalent. The C_6H_4 fragments are oriented syn to two pyrazolyl rings of the Tp ligands and are in a coplanar orientation. The Ru-N7 bond distance is 2.044(4) Å and is shorter than that observed for $\text{TpRu}^{\text{II}}(\text{L})(\text{L}')$ amido or amine complexes.^{16,34} The Ru-N7-C10 bond angle is 137.2(4)°. The N7-C10-C11 and N7-C10-C15 bond angles are 122.8(5)° and 120.7(5)°, respectively. The bond distance (1.425(10) Å) between the coupled carbon atoms (C13-C13') is shorter than a typical C-C single bond (1.54 Å).³⁵ In addition, the N7-C10 bond distance (1.315(7) Å) is shorter than expected for a N-C single bond (1.47 Å).³⁶ The bond distances of the C_6H_4 rings are consistent with quinoidal localization of the π -electrons. The C11-C12 and C14-C15 bond distances (1.363(7) and 1.352(8) Å) are shorter than the bond distances between C10-C11/C10-C15 (1.449(8)/1.441(8) Å) and C13-C12/C13-C14 (1.435(8)/1.440(8) Å).

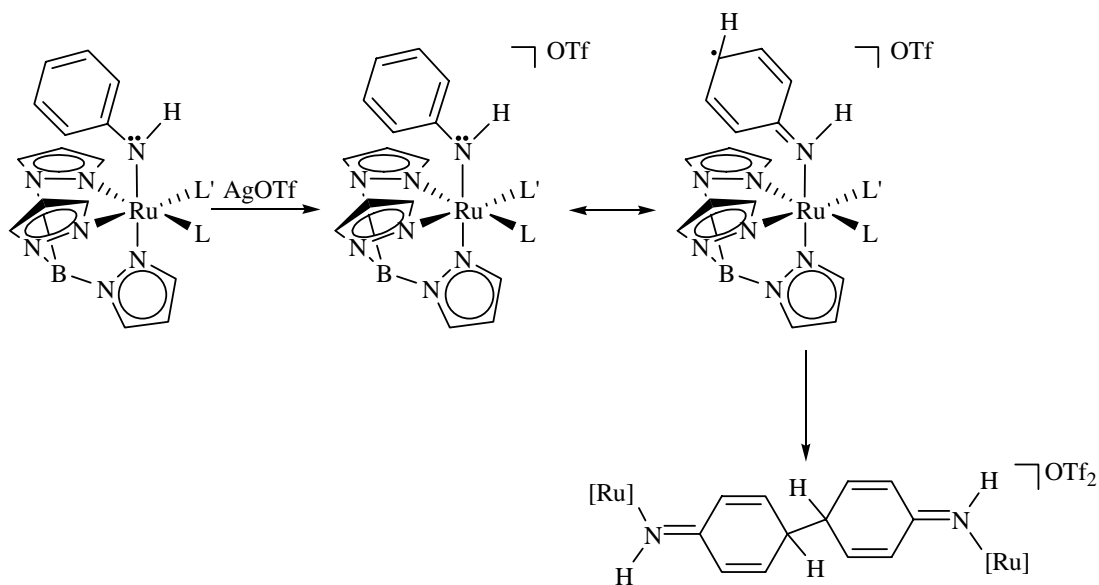
Table 4.2 Selected bond distances for $[\text{TpRu}\{\text{P}(\text{OMe})_3\}_2\text{NHC}_6\text{H}_4\text{-}]_2[\text{OTf}]_2$

Atoms	Distance (Å)	Atoms	Distance (Å)
Ru-N7	2.044(4)	C12-C13	1.435(8)
N7-C10	1.315(7)	C13-C13'	1.425(10)
C10-C11	1.449(8)	C13-C14	1.440(8)
C10-C15	1.441(8)	C14-C15	1.352(8)
C11-C12	1.363(7)		

4.5 Mechanism of Formation of the Binuclear Complexes $[\text{TpRuL}_2\text{NHC}_6\text{H}_4\text{-}]_2[\text{OTf}]_2$.

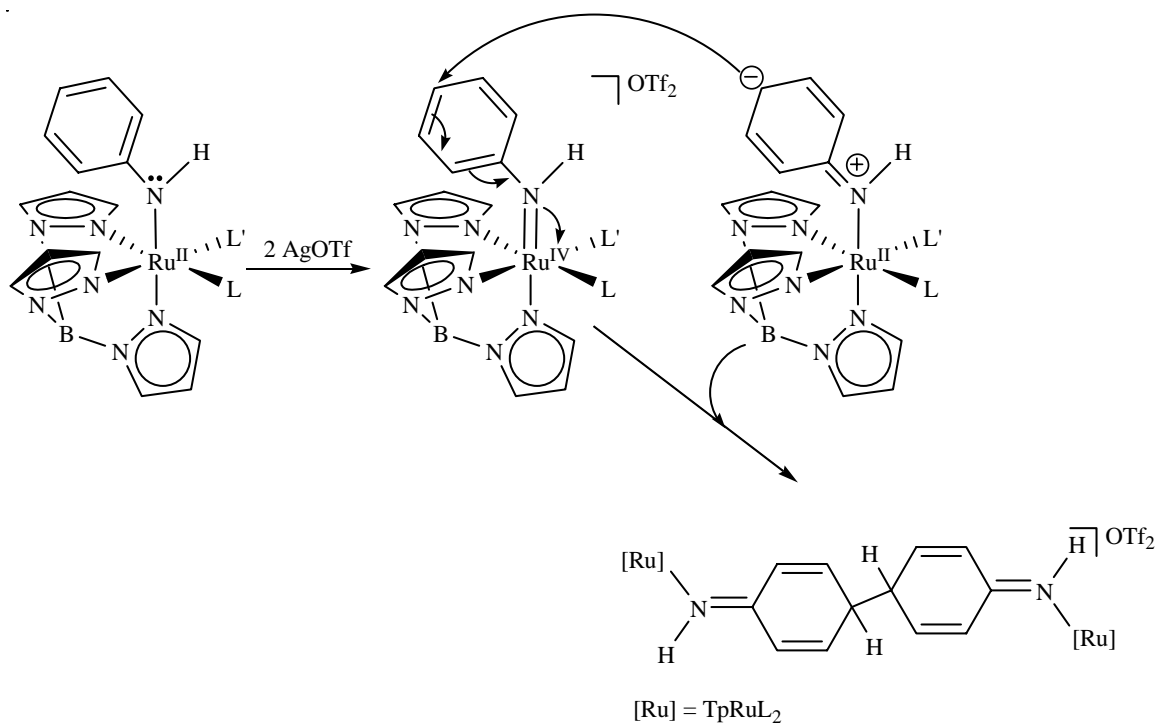
The mechanism of the oxidation reactions that form the binuclear complexes can be separated into two separate steps. The first step involves the formation of the carbon-carbon bond, and second step involves the formation of the imine through net deprotonation/oxidation.

The C-C bond forming step in these reactions likely proceeds through radical coupling akin to the oxidative coupling of aniline or the related coupling reactions of other late transition metal amido/oxide ligands (above). This reaction would occur via by initial oxidation of Ru(II) to Ru(III) to form the Ru(III) amido complex $[\text{TpRuL}_2\text{NHPH}][\text{OTf}]$. Subsequently, radical delocalization into the phenyl ring allows C-C coupling to occur (Scheme 4.13).



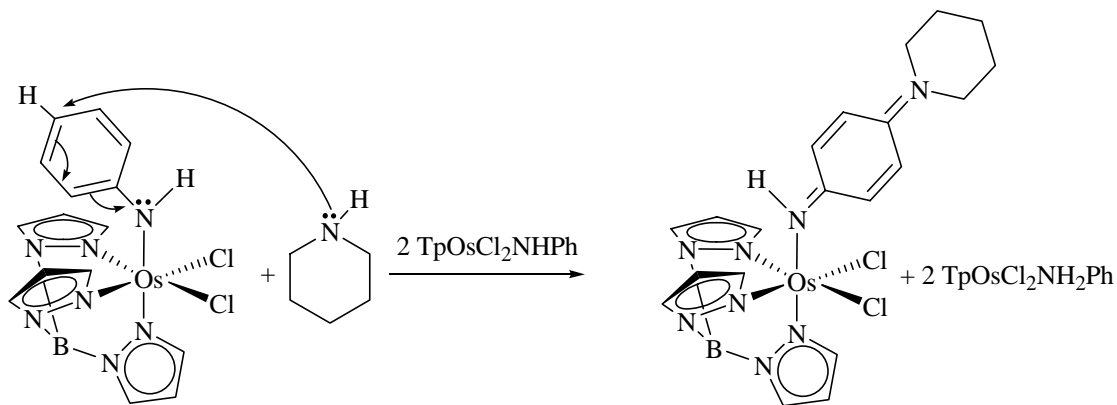
Scheme 4.13 Proposed mechanism for the formation of C-C bond in the oxidation of $\text{TpRuL}_2\text{NHPH}$ ($\text{L} = \text{CO}, \text{PMe}_3, \text{or P(OMe)}_3$; $[\text{Ru}] = \text{TpRuL}_2$).

To our knowledge, no direct evidence of radical intermediates for the coupling of late transition metal arylamido or aryloxo ligands has been reported (i.e., trapping of radical intermediates). An alternate mechanism based on nucleophilic aromatic substitution has also been considered. Indeed, both nucleophilic and radical mechanisms have been implicated in these couplings and questions about the specific mechanism(s) still exist.³⁷ This alternate mechanism would proceed via initial two electron oxidation of the Ru(II) amido complex to form a Ru(IV) amido complex. The Ru(IV) amido complex would likely exhibit similar reactivity patterns to the TpOs(IV) phenyl amido complex reported by Mayer et al. A second equivalent of the Ru(II) amido complex TpRuL₂NHPh would undergo nucleophilic attack of the Ru(IV) amido to form a bridging intermediate (Scheme 4.14).



Scheme 4.14 Proposed aryl-aryl bond formation based on a nucleophilic mechanism ([Ru] = TpRuL₂).

Support for this nucleophilic-based mechanism is drawn from the TpOs(IV) chemistry reported by Mayer et al. The addition of piperidine (or pyrrolidine) to the Os(IV) amido complex $\text{TpOs}(\text{Cl})_2\text{NHPH}$ results in nucleophilic attack at the para position of the anilido phenyl substituent (Scheme 4.15).³⁸ Under ordinary conditions, an arylamido ligand



Scheme 4.15 Formation of bridging binuclear amido complexes based on nucleophilic aromatic substitution.

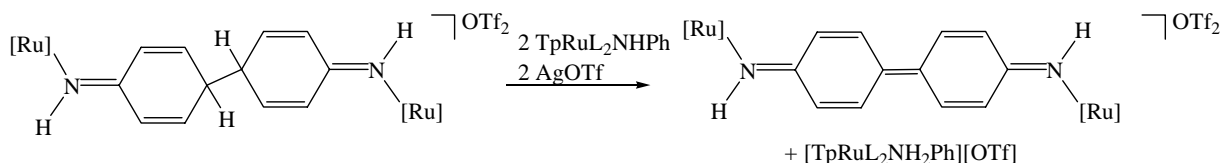
is electron rich and does not react with nucleophiles; however, the strongly oxidizing nature of the Os(IV) metal center is the key feature driving this reaction. One product of this reaction is an Os(II) imine, and a second major product of this reaction is the Os(III) amine complex $\text{TpOsCl}_2\text{NH}_2\text{Ph}$ (Scheme 4.15). The reaction yields a 2:1 ratio of Os(III) amine to Os(II) imine. The formation of $\text{TpOsCl}_2\text{NH}_2\text{Ph}$ is attributed to H-atom abstraction of an imine intermediate.³⁸

Hammett studies and variable temperature ^1H NMR spectroscopic studies of the phenyl amido complexes $\text{TpRu}(\text{L})(\text{L}')\text{NHPH}$ suggest negative charge build up in the aryl ring of the anilido ligand (see Chapter 3). While the nucleophilicity of the para position of the Ru(II) phenyl amido complex would be anticipated to be much less than piperidine or

pyrrolidine, the driving force for this reaction would also be increased since a Ru(IV) metal center would be anticipated to be more oxidizing than an Os(IV) metal center. This possible mechanism would also require the amido nitrogen of TpRuL₂NHPh to be too sterically hindered to undergo attack at para position of another Tp anilido center.

Two observations suggest the radical mechanism is more likely. First, the rate of reaction for the TpOsCl₂NHPh system is much slower than the oxidation of the TpRuL₂NHPh. Specifically, nucleophilic aromatic substitution was reported to occur over the course of several days while treatment of TpRuL₂NHPh with oxidant results in conversion to final products within minutes. Also, the observation that the oxidation reactions conducted in methylene chloride or chloroform result in decomposition products suggest the radical mechanism is more likely due to radical abstraction by the proposed Ru(II) anilido radical intermediate. The C-Cl bond strength of methylene chloride is 80 kcal/mol.³⁵ Thus, based on literature precedent with radical based coupling of anilines, the difference in reaction rates, and the incompatibility of this reaction with methylene chloride or chloroform, the mechanism of carbon-carbon bond formation most likely results from radical coupling.

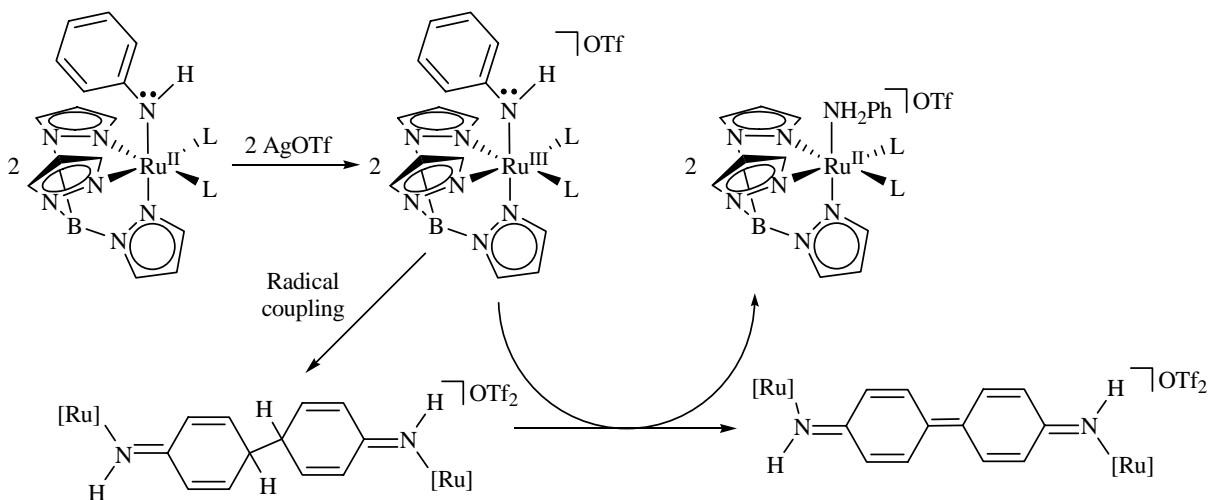
The second step in the mechanism to be considered is the net deprotonation/oxidation of the bridged intermediate (above). This step could occur by two possible pathways. The first is deprotonation of the intermediate by TpRuL₂NHPh followed by subsequent oxidation by residual oxidant (Scheme 4.16).



Scheme 4.16 The second step in the mechanism of formation of Ru(II) imine product base on deprotonation of the para protons followed by oxidation with residual oxidant ([Ru] = TpRuL₂).

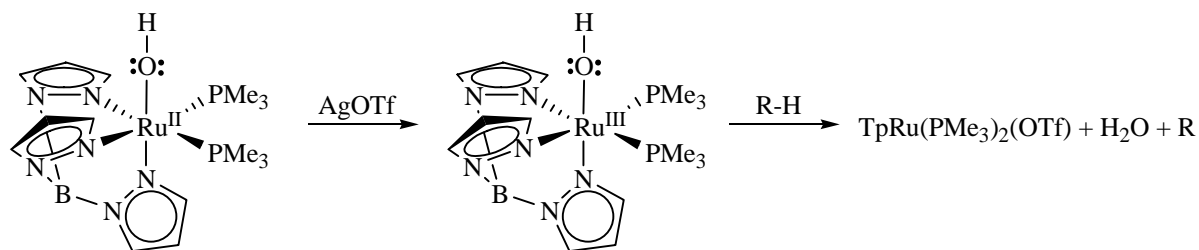
Sharp et al. have reported the oxidative coupling of the bridging imido ligand of $(\mu\text{-dppm})\text{Rh}_2(\text{NPh})(\text{CO})_2$ results in a bridged complex similar to the intermediated above.¹⁸ Sharp also reported treatment of the bridged complex with two equivalents of $[\text{Cp}_2\text{Fe}][\text{PF}_6]$ yields a bridged imine product (i.e. C-H bond cleavage occurs at the para position - see Scheme 4.2 above). Furthermore, the treatment of the bridged complex in Scheme 4.2 with the base $[\text{Li}][\text{N}(\text{SiMe}_3)_2]$ results in deprotonation of the para proton to form a benzidine bridged dimer. The observation of Ru(II) amine complexes in the oxidation of TpRuL₂NHPh could result from TpRuL₂NHPh acting as a base to deprotonate the para protons; the azavinylidene is formed by oxidation using residual oxidant. The TpRu(L)(L')NHPh complexes have been demonstrated to be basic enough to deprotonate malononitrile in CH_2Cl_2 ($\text{p}K_a \sim 12$). In addition, through the course of studying this reaction an increased ratio of binuclear complex to Ru(II) amine was discovered if the presence of added base such as triethylamine was added (see below). Based on this mechanism, this increased yield of binuclear complex would be rationalized by triethylamine competing as a base to deprotonate the intermediate (the possible effects of excess base on this reaction are discussed in further detail below).

Another possible pathway for the net deprotonation/oxidation step involves hydrogen atom abstraction of the coupled intermediate. This pathway would proceed via oxidation of the Ru(II) amido complex to form a Ru(III) amido complex. After coupling occurs, subsequent H-atom abstraction by a second equivalent of the Ru(III) amido would result in the formation of the dimer complexes and $[\text{TpRuL}_2\text{NH}_2\text{Ph}][\text{OTf}]$ (Scheme 4.17). Highly



Scheme 4.17 Mechanism of imine formation based on H-atom abstraction by Ru(III) amido on an unobserved bridged intermediate.

oxidized metal centers with amido or oxide ligand are known to undergo these transitions.^{39,40,41,42} For example, Mayer et al. have observed similar chemistry the reaction of $\text{TpOsCl}_2\text{NHPh}$ and nucleophiles (above). The strongest evidence for a H-atom abstraction mechanism comes from the work of Yuee Feng of the Gunnoe group.⁴³ The oxidation of $\text{TpRu}(\text{PMe}_3)_2\text{OH}$ in the presence of substrates that are susceptible to H-atom abstraction, such as 1,4 cyclohexadiene, results in the production of $\text{TpRu}(\text{PMe}_3)_2(\text{OTf})$, water, and organic products (Scheme 4.18). Consistent with a H-atom abstraction mechanism, the



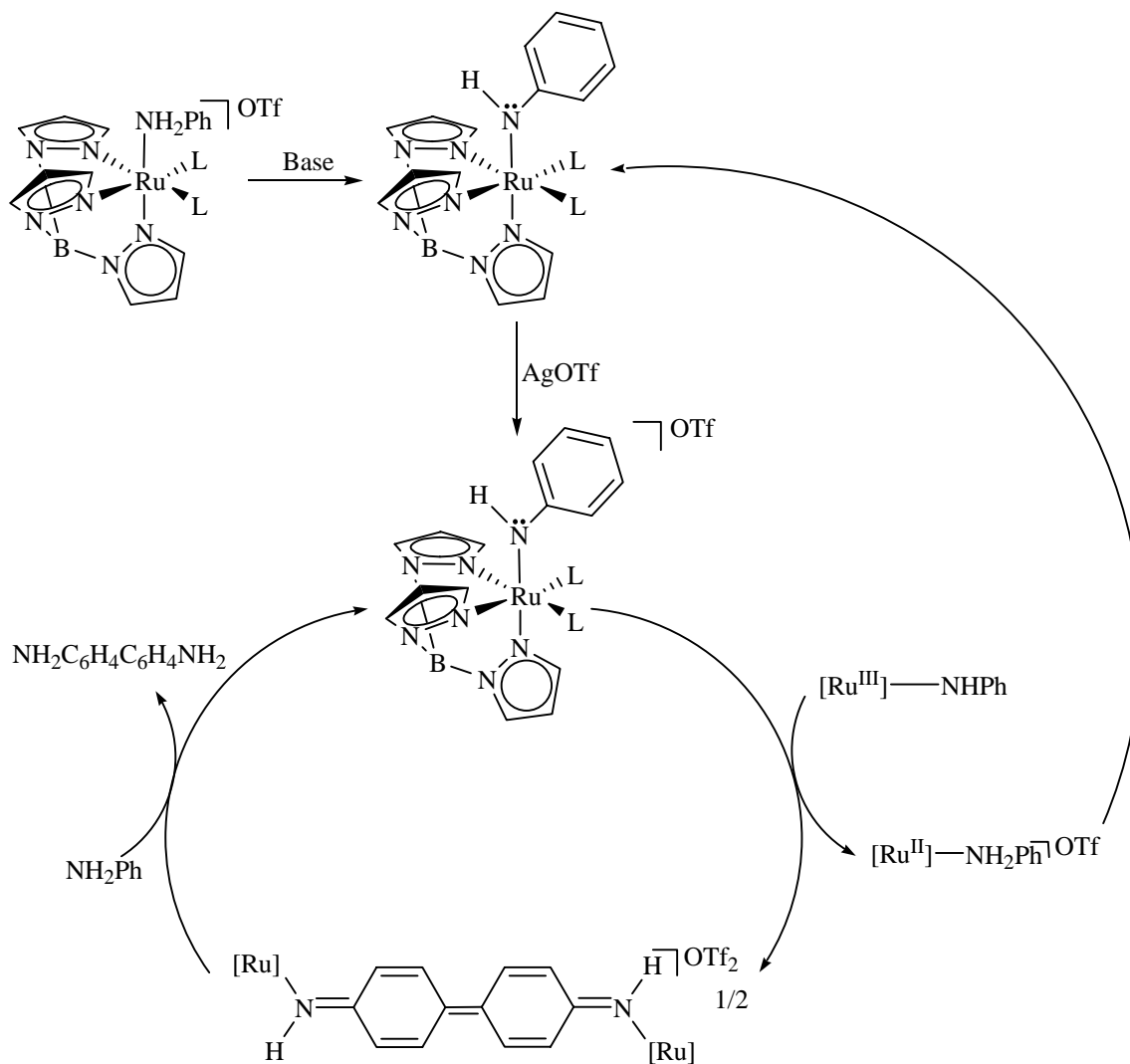
Scheme 4.18 Oxidation of $\text{TpRu}(\text{PMe}_3)_2(\text{OH})$ results in formation to $\text{TpRu}(\text{PMe}_3)_2(\text{OTf})$ and water by hydrogen atom abstraction.

yields of these oxidation reactions are directly related to the C-H strength. In light of this work, a mechanism of imine formation based on hydrogen atom abstraction seems most plausible; however, such a mechanism has not been definitively demonstrated.

For a H-atom abstraction mechanism, in the absence of excess base, the observed 50% yield of imine product would be anticipated. The observation that increased yields are observed in the presence of triethylamine or other bases would also be consistent with a H-atom abstraction mechanism (as opposed to the basic mechanism presented above) if the excess AgOTf (two equivalents were used) could serve to oxidize $[\text{TpRuL}_2\text{NH}_2\text{Ph}][\text{OTf}]$ in the presence of these bases. Thus, triethylamine would serve as a proton reservoir. Room temperature reactions of $[\text{TpRu}(\text{PMe}_3)_2\text{NH}_2\text{Ph}][\text{OTf}]$ or $[\text{TpRu}\{\text{P}(\text{OMe})_3\}_2\text{NH}_2\text{Ph}][\text{OTf}]$ in the presence of excess AgOTf and triethylamine were found to yield the respective binuclear complex; however, similar reactions of the dicarbonyl amine complex $[\text{TpRu}(\text{CO})_2\text{NH}_2\text{Ph}][\text{PF}_6]$ were unsuccessful, possibly due CO insertion reactions of an amido intermediate generated by deprotonation using triethylamine.

4.6 Effect of Base and Variation of Oxidant on the Oxidative Coupling of $\text{TpRuL}_2\text{NHPH}$.

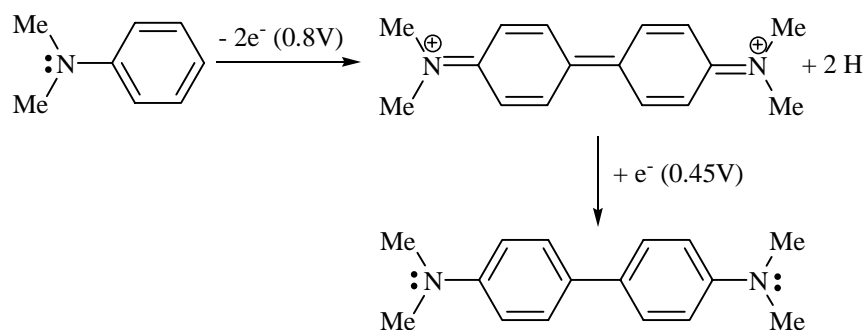
We have envisioned a catalytic cycle for the oxidative coupling reaction of our aryl amido complexes. This cycle would proceed by oxidation of the Ru(II) phenyl amido to from the dimer complex. Subsequently, the imine would exchange with free amine to form a Ru(III) amido which would then couple (Scheme 4.19).



Scheme 4.19 Potential cycle to catalytically convert aniline(s) to benzidine(s) by metal-mediated oxidation in the presence of base ($[\text{Ru}] = \text{TpRuL}_2$).

Along these lines, features of the proposed catalytic cycle have been explored. For example, the viability of cheaper and less harsh oxidants than AgOTf, and the effect of these oxidants, was investigated. The Ru(III/II) oxidation potentials for the amido complexes TpRu(L)(L')NPh ($\text{L, L}' = \text{PMe}_3$ or P(OMe)_3 and $\text{L} = \text{CO}$, $\text{L}' = \text{PPh}_3$) are -0.25 , -0.28 and 0.11 V (vs. NHE) respectively. These potentials suggest the possibility for a variety of suitable oxidants other than AgOTf.

If the mechanism of this reaction proceeds via deprotonation of a coupled intermediate (Scheme 4.16), oxidation of the intermediate formed after radical coupling would be required. This second oxidation in concert with deprotonation would form the imine product. While the potential of this second oxidation is difficult to predict, evidence in the oxidation of *N,N*-dimethylaniline (DMA) suggests the initial oxidation from Ru(II) to Ru(III) may be more difficult than oxidation of the intermediate.^{44,45} Surface electrode oxidation of DMA results in the formation of corresponding quinone. Dimethylbenzidine (DMB) is formed on the return sweep (Scheme 4.20). Thus the oxidation potential of DMB



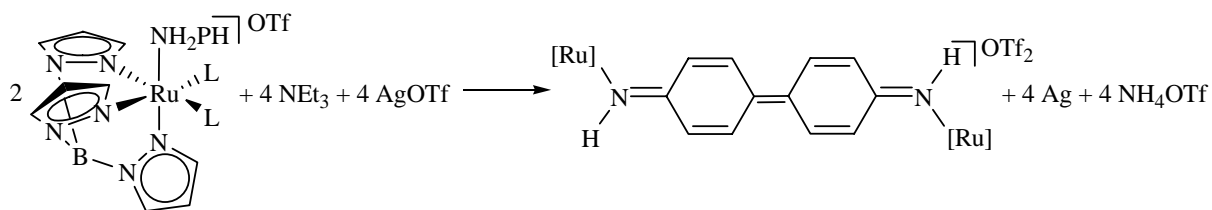
Scheme 4.20 Oxidation of DMA. DMB can not be directly formed because over-oxidation occurs due to the oxidation potential of DMB versus DMA. The oxidation potential DMB is about 0.4 V less than DMA.

is a few tenths of a volt less than DMA. This result suggests that oxidation of the dimer intermediate in the coupling of $\text{TpRuL}_2\text{NHPH}$ (assuming the mechanism in Scheme 4.16) may be more facile than the amido complexes themselves. Note, the alternate mechanism based on H-atom abstraction (Scheme 4.17) would only depend on the Ru amido (III/II) potential.

Solutions of the amido complex $\text{TpRu}(\text{PMe}_3)_2(\text{NHPH})$ in acetonitrile – d_3 were treated with two equivalents of the oxidant $[\text{Cp}_2\text{Fe}][\text{PF}_6]$ or I_2 in an analogous fashion to the reactions with AgOTf . The reduction potential of AgOTf (in THF) is 1.06 compared to the 0.65 and 0.54 (vs. NHE) for $[\text{Cp}_2\text{Fe}][\text{PF}_6]$ or I_2 respectively.^{46,47} These reactions revealed the formation of the complex $[\text{TpRu}(\text{PMe}_3)_2(\text{NHC}_6\text{H}_4^-)]_2[\text{X}]_2$ ($\text{X} = \text{PF}_6^-$ or I^-) in approximately 50% yield. Thus, the weaker oxidants were suitable to initiate the aryl coupling step. In addition, we attempted to use O_2 to oxidatively couple the amido complexes by purging THF solutions of the amido complex $\text{TpRu}(\text{PMe}_3)_2(\text{NHPH})$ with 1 atm of dioxygen. Unlike oxidations with AgOTf , $[\text{Cp}_2\text{Fe}][\text{PF}_6]$, or I_2 , no immediate reactivity was observed, and over the course of several hours the solution turned from yellow to dark brown. No coupled imine products were found after work up of the reaction. After approximately a 3 hour purge, workup of the reaction by removal of volatiles under vacuum revealed multiple decomposition products. Thus O_2 is not a suitable oxidant, likely attributable to decomposition pathway(s).

In the absence of added base, the oxidative coupling reaction yields an approximate 1:1 molar ratio of Ru(II) amine to Ru(II) imine based on ^1H NMR spectroscopy of the crude reaction mixture. In the course of studying these reactions, it was discovered excess base

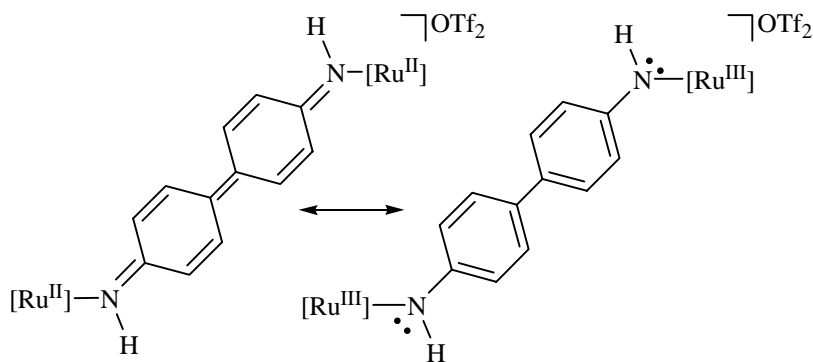
(approximately 15 equivalents) increased the yield of the bridging imine products complexes from 50% to approximately 75%. For example, the reaction of $\text{TpRu}(\text{PMe}_3)_2\text{NHPh}$ with 2 equivalents of AgOTf and 15 equiv of Et_3N resulted in the formation of the binuclear complex and amine complex in an approximate 3:1 molar ratio. These reactions involve C-H bond cleavage of two phenyl para protons via the net loss of 2 equivalents of hydride. The coupling reactions with added base, either Et_3N or 2,6-lutidine, resulted in an increase of the ratio of aryl coupled products $[\text{TpRu}(\text{PMe}_3)_2(\text{NHC}_6\text{H}_4^-)]_2[\text{OTf}]_2$ or $[\text{TpRu}\{\text{P}(\text{OMe})_3\}_2(\text{NHC}_6\text{H}_4^-)]_2[\text{OTf}]_2$ to the Ru(II) amine complexes $[\text{TpRu}(\text{PMe}_3)_2(\text{NH}_2\text{Ph})][\text{OTf}]$ or $[\text{TpRu}\{\text{P}(\text{OMe})_3\}_2(\text{NH}_2\text{Ph})][\text{OTf}]$, respectively. Reactions of the amido complexes $\text{TpRuL}_2\text{NHPh}$ ($\text{L} = \text{PMe}_3, \text{P}(\text{OMe})_3, \text{or CO}$) in acetonitrile- d_3 with 5 or 10 equivalents of triethylamine reveal an increase of in the yield of binuclear complex relative to Ru(II) amine products. Initially, the increases in yield were attributed to triethylamine acting as a base to deprotonate the bridged intermediate, and thus the increased yield would result from triethylamine competing with the basic amido complexes $\text{TpRuL}_2\text{NHPh}$. However, consistent results could not be achieved for the ratio of Ru(II) bridging imine to Ru(II) amine products relative to the amount of base that was added. Subsequent work revealed the treatment of the Ru(II) amine complexes $[\text{TpRu}(\text{PMe}_3)_2(\text{NH}_2\text{Ph})][\text{OTf}]$ or $[\text{TpRu}\{\text{P}(\text{OMe})_3\}_2(\text{NH}_2\text{Ph})][\text{OTf}]$ with excess triethylamine and AgOTf yielded the binuclear complexes (Scheme 4.21). Thus, the increased yield in the presence is of triethylamine results from this base serving as a proton reservoir, and the inconsistency observed with the oxidation reactions was likely due to the errors in the addition of oxidant.



Scheme 4.21 Reaction of [TpRuL₂(NH₂Ph)][OTf] with base and oxidation results in the formation of the binuclear complex (L = PMe₃ or P(OMe)₃; [Ru] = TpRuL₂).

4.7 Attempts at Catalytic Imine Formation.

The key catalytic step yet to be explored in detail is removal of the biaryl ligand from the metal center. X-ray crystallography and ¹H NMR spectroscopy indicate the dimer product of oxidation of the phenylamido complexes TpRu(L₂)NHPPh is best represented by TpRu fragments bridged by a coupled imine ligand rather than a Ru(III) amido complex; however, a resonance structure of the binuclear complexes can also be described as Ru(III) centers bridged by a coupled amido ligand (Scheme 4.22). A contribution of the Ru(III)

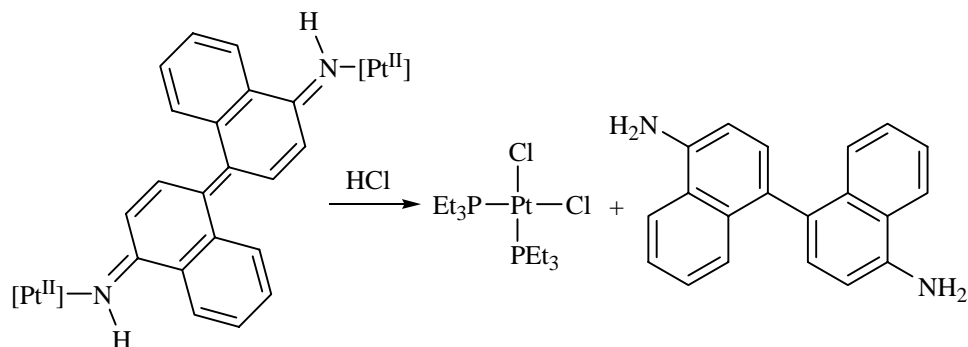


Scheme 4.22 A possible resonance structure for the Ru(II) binuclear imine complex is bridged Ru(III) amido complex. Metathesis reactions are well known for oxo and amido ligands bound to late transition metals ([Ru] = TpRuL₂).

amido resonance structure to the overall bonding would suggest the biaryl-ligand may exhibit similar reactivity patterns to other late transition metal amido complexes. Of particular importance are the exchange reactions late transition metal amido and oxide complexes undergo with free aryl amines (see Chapter 2 and Chapter 3). Furthermore, the Ru(II) phenyl amido complexes of this type have been demonstrated to undergo exchanges with aryl amines.

We attempted to exchange the imine ligand by the addition of 10 equivalents of aniline to NMR tube solutions of the complex $[\text{TpRu}(\text{PMe}_3)(\text{NHC}_6\text{H}_4^-)]_2[\text{OTf}]$ in $\text{DMSO-}d_3$ or CD_3CN ; however, no reaction was observed after prolonged heating at $80\text{ }^\circ\text{C}$. Further attempts at catalysis by reactions of the dimer complex $[\text{TpRu}(\text{PMe}_3)_2(\text{NHC}_6\text{H}_4^-)]_2[\text{OTf}]_2$ with aniline in the presence of the oxidant $[\text{Cp}_2\text{Fe}][\text{PF}_6]$ yielded no reactivity. The inert nature of the dimeric complexes is likely due to a tightly bound imine ligand.

Metal-nitrogen bond cleavage has been reported for a related bridged imine type system with a Pt metal center. Treatment of the complex $[\text{Pt}(\text{PEt}_3)_2\text{Cl}(\text{NH-1naphthyl-4-})]_2[\text{PF}_6]_2$ with 5 equivalents of HCl in methanol results in cleavage of the Pt-N bonds to form *cis*- $\text{Pt}(\text{PEt}_3)_2\text{Cl}_2$ and 4,4'-diamino-1,1'-binaphthyl (Scheme 4.23). This reaction suggests the



Scheme 4.23 Cleavage of a M-N imine bond by treatment with 5 equivalents of hydrochloric acid ([Pt] = $\text{Pt}(\text{PEt}_2)\text{Cl}$).

possibility of cleavage of the Ru-N imine bond; the only step that is unknown in the proposed catalytic cycle. However, this catalytic cycle is likely not compatible with strong acids since a base is required. Along lines continued, efforts are being directed towards Ru-N bond cleavage as well as oxidative coupling of ligands where the coupled products may be more dative (i.e. phenoxide systems). It is not yet known if these alternative ligands will be suitable for the proposed catalytic cycle, but realization of such systems would represent a significant advancement over current methods of aryl-aryl bond formation. Interestingly, the oxidative coupling of the Ru(II) acetylide complex $\text{TpRu}(\text{PPh}_3)_2(\text{CCPh})$ results in oxidative coupling at the para position of the phenyl group of the phenylacetylide ligand.⁴⁸ Thus reaction suggesting the generality of such oxidative coupling schemes for $\{\text{TpRuL}_2\}$ systems capable of delocalizing a radical.

4.8 Experimental Section.

General Methods. All reactions and procedures were performed under anaerobic conditions in a nitrogen-filled glovebox or using standard Schlenk techniques. Glovebox purity was maintained by periodic nitrogen purges and monitored by an oxygen analyzer $\{\text{O}_2(\text{g}) < 15 \text{ ppm for all reactions}\}$. Acetonitrile was purified by passage through a column of activated alumina followed by distillation from P_2O_5 . THF and diethyl ether were dried by distillation from sodium/benzophenone. CD_3CN was purified by distillation from CaH_2 , degassed, and stored over 4 Å sieves. $\text{Me}_2\text{SO}-d_6$ was used as received. Acetone- d_6 was degassed via 3 freeze-pump-thaw cycles and stored over 4 Å sieves. ^1H and ^{13}C NMR spectra were obtained on a Varian Mercury 300-MHz, Varian Mercury 400-MHz, or General Electric 300-MHz

spectrometer. Resonances due to the Tp ligand are reported by chemical shift and multiplicity only. All $^3J_{\text{HH}}$ for pyrazolyl rings are 2 Hz. All ^1H and ^{13}C NMR spectra were referenced against tetramethylsilane using residual proton signals (^1H NMR) or the ^{13}C resonances of the deuterated solvent (^{13}C NMR). ^{31}P NMR spectra were obtained on a Varian 300-MHz spectrometer and referenced against external 85% H_3PO_4 . All NMR spectra were acquired at room temperature unless otherwise noted. IR spectra were obtained on a Mattson Genesis II spectrometer either as thin films on a KBr plate or in solution using a KBr solution plate. Elemental analyses were performed by Atlantic Microlabs, Inc. All other reagents were used as purchased from commercial sources. The complexes $\text{TpRu}(\text{PMe})_3\text{NHPh}$, $\text{TpRu}\{\text{P}(\text{OMe})_3\}\text{NHPh}$, $[\text{TpRu}(\text{PMe})_3\text{NH}_2\text{Ph}][\text{OTf}]$, and $[\text{TpRu}\{\text{P}(\text{OMe})_3\}\text{NH}_2\text{Ph}][\text{OTf}]$ are discussed in Chapter 2.

$[\text{TpRu}(\text{CO})_2\text{NH}_2\text{Ph}][\text{PF}_6]$. Aniline (0.2465 g, 2.65 mmol) was added to a THF solution of $[\text{TpRu}(\text{CO})_2(\text{THF})][\text{PF}_6]$ (0.1027 g, 0.175 mmol). The resulting mixture was refluxed for 24 h, and the volatiles were removed under reduced pressure. The resulting beige solid was washed with approximately 4×30 mL of diethyl ether and was dried in vacuo (0.1015 g, 95%). ^1H NMR (acetone- d_6 , δ): 8.18 (4H, overlap multiplet, Tp CH 3 and 5 position), 8.09, 8.03 (each 1H, each a d, Tp CH 3 or 5 position), 6.57, 6.42 (3H, 2:1 integration, each a t, Tp CH 4 position), 7.50 (4H, overlap multiplet, phenyl ortho, and meta), 7.34 (1H, t, phenyl para). $^{13}\text{C}\{^1\text{H}\}$ NMR (acetone- d_6 , δ): 194.5 (CO), 147.6, 145.0, 138.9, 138.6 (Tp 3 or 5 position), 146.5, 131.0, 127.4, 122.4 (amine phenyl), 108.7, 108.6 (Tp 4 position). IR (thin film on KBr): $\nu_{\text{CO}} = 2084, 2022 \text{ cm}^{-1}$, $\nu_{\text{NH}} = 3313, 3271 \text{ cm}^{-1}$, $\nu_{\text{BH}} = 2528$

cm⁻¹. Anal. Calcd. for C₁₇H₁₇BF₆N₇O₂Ru: C, 33.57; H, 2.82; N, 16.12. Found: C, 33.82; H, 2.93; N, 15.95.

[TpRu(CO)₂NH(C₆H₄-)]₂[OTf]₂. [TpRu(CO)₂(NH₂Ph)][PF₆] (0.1402 g, 0.231 mmol) in approximately 50 mL of THF was cooled to -110 °C. To this solution was added sodium bis(trimethylsilyl)amide (0.253 mmol, 1.0 M in THF) dropwise via syringe. The resulting solution was pale yellow. This solution was transferred via cannula to a THF solution of AgOTf (0.1194 g, 0.465 mmol) and triethylamine (0.3511 g, 3.47 mmol) that was precooled to -110 °C. After the addition, the resulting solution was dark brown. The solution was warmed to room temperature, and a color change to dark red was noted. The volatiles were removed under reduced pressure to give a dark red solid. This solid was mixed with THF, filtered through a plug of Celite, and washed with THF until the filtrate was no longer red (approximately 50 mL of THF). The red filtrate was discarded. The remaining solids were eluted with acetonitrile until the filtrate was no longer red (approximately 100 mL of acetonitrile). The volatiles were removed under reduced pressure to give a dark purple solid (0.0763 g, 54%). Additional purification can be accomplished via recrystallization from methylene chloride and a nonpolar solvent such as hexanes or cyclohexane. ¹H NMR (Me₂SO-*d*₆, δ): 11.33 (2H, br s, NH), 8.33, 8.31, 8.24, 8.14, 7.98 (12H, 1:1:4:2:4 integration, each a d, Tp CH 3 and 5 position), 7.91, 7.16 (6H, 4:2 integration, overlapping d's, C₆H₄ rings), 6.49 (6H, overlapping t's, Tp CH 4 position), 5.90 (2H, overlapping d's, C₆H₄ rings). ¹³C{¹H} NMR (Me₂SO-*d*₆, δ): 193.4 (CO), 169.7 (amido C₆H₄ ipso), 146.7, 144.6, 138.0, 137.5 (Tp 3 or 5 position), 136.4, 133.4, 122.9, 118.6, 114.4 (C₆H₄ rings), 107.9, 107.7 (Tp 4 position). IR (thin film on KBr plate): ν_{CO} = 2080, 2024 cm⁻¹, ν_{NH} = 3437 cm⁻¹, ν_{BH} = 2513

cm⁻¹. FAB-MS: 923.1 [TpRu(CO)₂(NHC₆H₄)₂]⁺, 647.1 [TpRu(CO)₂NH(C₆H₄-)]₂²⁺, 553.1 [TpRu(CO)₂(NHC₆H₄-C₆H₄NH)]⁺, 371.0 [TpRu(CO)₂]⁺, 315.0 [TpRu]⁺. Note: Consistent elemental analysis of the complex could not be obtained. We attribute this to the difficulty in removing solvent from the precipitated products. Even after prolonged drying in vacuo and elevated temperatures, ¹H NMR spectroscopy revealed variable mixtures of acetonitrile, methylene chloride, THF, and/or hexanes.

[TpRu(PMe₃)₂NH(C₆H₄-)]₂[OTf]₂. A yellow solution of TpRu(PMe₃)₂(NHPh) (0.0529 g, 0.0947 mmol) in approximately 20 mL of THF was added dropwise to a solution of AgOTf (0.0452 g, 0.176 mmol) and triethylamine (0.1441 g, 1.42 mmol) in THF. Upon addition an immediate color change to dark blue-green was noted. The volatiles were removed under reduced pressure to give a dark green solid. This solid was mixed with THF, filtered through a plug of Celite, and washed with THF until the filtrate was no longer blue (approximately 50 mL of THF). The blue filtrate was discarded. The remaining solids were eluted with acetonitrile until the filtrate was no longer green (approximately 100 mL of acetonitrile). The volatiles were removed under reduced pressure to give a green solid (0.0401 g, 59%). Additional purification can be accomplished via recrystallization from methylene chloride and a nonpolar solvent such as hexanes or cyclohexane. ¹H NMR (CD₃CN, δ, 60 °C): 11.33 (2H, br s, NH), 7.96, 7.94, 7.78, 7.30 (12H, 2:4:2:4 integration, each a d, Tp CH 3 and 5 position), 7.43 (2H, d, ³J_{HH} = 9 Hz, C₆H₄ rings), 7.26, 7.18, 7.15, 7.06 (4H, 1:1:1:1, each a d, ³J_{HH} = 9 Hz, C₆H₄ rings), 6.39, 6.23 (6H, 2:4 integration, each a t, Tp CH 4 position), 4.99 (2H, d, ³J_{HH} = 9 Hz, C₆H₄ rings), 1.22 (36H, vt, N = 9 Hz, P(CH₃)₃). ¹³C{¹H} NMR (Me₂SO-*d*₆, δ): 169.5 (amido C₆H₄ ipso), 146.4, 143.1, 137.0, 136.6 (Tp 3 or

5 position), 133.5-118.5 (multiple overlapping resonances due to C₆H₄ rings), 107.1, 106.2 (Tp 4 position), 16.8 (P(CH₃)₃, vt, N = 29 Hz). ³¹P{¹H} NMR (CD₃CN, δ): 8.0 (s, PMe₃). IR (thin film on KBr plate): ν_{NH} = 3399 cm⁻¹, ν_{BH} = 2493 cm⁻¹. FAB-MS: 649.1 [TpRu(PMe₃)₂(NHC₆H₄-C₆H₄NH)]⁺, 573.0 [TpRu(PMe₃)(NHC₆H₄-C₆H₄NH)]⁺, 467.1 [TpRu(PMe₃)₂]⁺, 391.0 [TpRu(PMe₃)]⁺, 315.0 [TpRu]⁺. Note: Consistent elemental analysis of the complex could not be obtained. We attribute this to the difficulty in removing solvent from the precipitated products. Even after prolonged drying in vacuo and elevated temperatures, ¹H NMR spectroscopy revealed variable mixtures of acetonitrile, THF, methylene chloride, and/or hexanes.

TpRu{P(OMe)₃}₂NH(C₆H₄-)}₂[OTf]₂. A yellow solution of TpRu{P(OMe)₃}₂(NHPH) (0.1080 g, 0.165 mmol) in approximately 20 mL of THF was added dropwise to a solution of AgOTf (0.0856 g, 0.333 mmol) and triethylamine (0.2493 g, 2.46 mmol) in THF. Upon addition an immediate color change to dark blue was noted. The volatiles were removed under reduced pressure to give a dark-blue solid. The solid was mixed with THF, filtered through a plug of Celite, and washed with THF until the filtrate was no longer blue (approximately 50 mL of THF). The blue filtrate was discarded. The remaining solids were eluted with acetonitrile until the filtrate was no longer blue (approximately 100 mL of acetonitrile). The volatiles were removed under reduced pressure to give a dark-blue solid (0.0385 g, 29%). Additional purification can be accomplished via recrystallization from methylene chloride or THF and a nonpolar solvent such as hexanes or cyclohexane. ¹H NMR (CD₃CN, δ, 95 °C): 10.09 (2H, br s, amido NH) 8.04, 7.96, 7.91, 7.46 (12H, 2:4:2:4 integration, each a d, Tp CH 3 and 5 position), 7.39 (2H, d, ³J_{HH} = 9 Hz, amido

C₆H₄ ring), 6.97 (4H, overlapping resonances, amido C₆H₄ rings), 6.34, 6.27 (6H, 2:4 integration, each a t, Tp CH 4 position), 4.93 (2H, d, ³J_{HH} = 9 Hz, amido C₆H₄ rings), 3.46 (36H, vt, N = 10 Hz, P(OCH₃)₃). ¹³C{¹H} NMR (Me₂SO-*d*₆, δ): 169.8 (amido C₆H₄ ipso), 147.3, 144.0, 137.3, 136.5 (Tp 3 or 5 position), 136.4-122.8 (multiple overlapping resonances due to C₆H₄ rings), 106.5 (overlap, Tp 4 position), 52.2 (br s, P(OCH₃)₃). ³¹P{¹H} NMR (Me₂SO-*d*₆, δ): 139.0 and 138.9 (each a s, P(OMe)₃). IR (thin film on KBr plate): ν_{NH} = 3296 cm⁻¹, ν_{BH} = 2492 cm⁻¹. FAB-MS: 745.1 [TpRu{P(OMe)₃}₂(NHC₆H₄-C₆H₄NH)]⁺, 621.1 [TpRu{P(OMe)₃}(NHC₆H₄-C₆H₄NH)]⁺, 654.1 [TpRu{P(OMe)₃}₂NH(C₆H₄-)]₂²⁺, 563.0 [TpRu{P(OMe)₃}₂]⁺, 439.0 [TpRu{P(OMe)₃}]⁺, 315.0 [TpRu]⁺. Anal. Calcd. for C₄₄H₆₆B₂F₆N₁₄O₁₈P₄Ru₂S₂-THF: C, 34.38; H, 4.45; N, 11.69. Found: C, 34.40; H, 4.36; N, 11.12.

References.

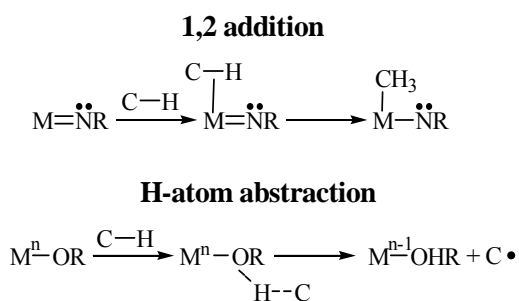
- ¹ Hassan, J.; Se´vignon, M.; Gozzi C.; Schulz, E.; Lemaire, M. *Chem. Rev.* **2002**, *102*, 1359-1469.
- ² Bringmann, G.; Walter, R.; Weirich, R. *Angew. Chem. Int. Ed.* **1990**, *29*, 997-991.
- ³ Stanforth, S. *Tetrahedron* **1998**, *54*, 263-303.
- ⁴ Molinski, T. F. *Chem. Rev.* **1993**, *93*, 1825-1838.
- ⁵ Riter, P. *Biochemistry, A Foundation*; Brooks/Cole Publishing Company: New York, **1996**; pp 653.
- ⁶ Nicolaou, K. C.; Synder, S. A. *Classics in Total Synthesis: More Targets, Strategies, Methods*; John Wiley & Sons: New York, **2003**.
- ⁷ Williams, P. L.; Giralt, E. *Chem. Soc. Rev.* **2001**, *30*, 145-157.
- ⁸ Nicolaou, K. C.; Boddy, C. N. C.; Brase, S; Winssinger, N. *Angew. Chem. Int. Ed.* **1999**, *38*, 2096-2152.
- ⁹ Littke A. F.; Dai, C.; Fu G. C. *J. Am. Chem. Soc.* **2000**, *122*, 4020-4028.
- ¹⁰ Bryndza, H. E.; Tam, W. *Chem. Rev.* **1988**, *88*, 1163-1188.
- ¹¹ Ge, Y.; Ye, Y.; Sharp, P. R. *J. Am. Chem. Soc.* **1994**, *116*, 8384-8385.
- ¹² O'Sullivan, R. D.; Parkins, A. W.; Alcock, N. W. *J. Chem. Soc. Dalton Trans.* **1986**, 571-575.
- ¹³ Murahashi, S.; Naota, T.; Miyaguchi, N.; Noda, S. *J. Am. Chem. Soc.* **1996**, *118*, 2509-2510.
- ¹⁴ Baesjou, P. J.; Driessen, W. L.; Challa, G.; Reedijk, J. *Macromolecules* **1999**, *32*, 270-276.
- ¹⁵ Albeniz, A. C; Calle, V.; Espinet, P; Gomez, S. *Chem. Comm.* **2002**, 610-611.
- ¹⁶ Conner, D.; Jayaprakash, K. N.; Gunnoe, T. B.; Boyle, P. D. **2002**, *21*, 5265-5271.
- ¹⁷ Alcock, N. W.; O'Sullivan, R. D.; Parkins, A. W. *J. Chem. Soc. Chem. Comm.* **1980**, 1216-1218.
- ¹⁸ Sharp, P. R. *J. Chem. Soc. Dalton Trans.* **2000**, 2647-2657.
- ¹⁹ Murahashi, S.-I.; Naota, T.; Miyaguchi, N.; Noda, S. *J. Am. Chem. Soc.* **1996**, *118*, 2509-2510.
- ²⁰ Nakajima, M.; Miyoshi, I.; Kanayama, K.; Hashimoto, S.; Noji, M.; Koga, K. *J. Org. Chem.* **1999**, *64*, 2264-2271.
- ²¹ Baesjou, P. J.; Driessen, W. L.; Challa, G.; Reedijk, J. *Macromolecules* **1999**, *32*, 270-276.
- ²² Li, X.; Yang, J.; Kozlowski, M. C. *Organic Letters* **2001**, *3*, 1137-1140.
- ²³ Hovorka, M.; Zavada, J. *Tetrahedron* **1992**, *48*, 9517-9530.
- ²⁴ Smith, M. B.; March, J. *March's Advanced Organic Chemistry: Reactions, Mechanism, and Structure 5th ed.*; John Wiley and Son, Inc: New York, **2001**; pp 870-871.
- ²⁵ Crabtree, R. H. *The Organometallic Chemistry of the Transition Elements 3rd ed.*; John Wiley and Son, Inc: New York, **2001**; pp 249-252.
- ²⁶ Miyaura, N.; Suzuki, A. *Chem. Rev.* **1995**, *95*, 2457-2483.
- ²⁷ Jayaprakash, K. N.; Conner, D.; Gunnoe, T. B. *Organometallics* **2001**, *20*, 5254-5256.
- ²⁸ Conner, D.; Jayaprakash, K. N.; Wells, M. B.; Manzer, S.; Gunnoe, T. B.; Boyle, P. D. *Inorg. Chem.* **2003**, *42*, 4759-4772.

-
- ²⁹ Fulton, R. J.; Holland, A. W.; Fow, D. J.; Bergman, R. G. *Acc. Chem. Res.* **2002**, *35*, 44-56.
- ³⁰ Soper, J. D.; Bennett, B. K.; Lovell, S.; Mayer, J. M. *Inorg. Chem.* **2001**, *40*, 1888-1893.
- ³¹ Goldsmith, C. R.; Jonas, R. T.; Stack, T. D. P. *J. Am. Chem. Soc.* **2002**, *124*, 83-96.
- ³² Mayer, J. M. *Acc. Chem. Res.* **1998**, *31*, 441-450.
- ³³ Li, X.; Huang, M.; Duan, W. *Chem. Rev.* **2002**, *102*, 2925-3030.
- ³⁴ Conner, D.; Jayaprakash, K. N.; Gunnoe, T. B.; Boyle, P. D. *Inorg. Chem.* **2001**, *41*, 3042-3049.
- ³⁵ McMurry, J. *Organic Chemistry 4th ed.*; Brooks Cole Pub. Co.: Pacific Grove, CA, **1995**.
- ³⁶ Dewar, M. J.; Thiel, W. *J. Am. Chem. Soc.* **1977**, *99*, 4709-4917.
- ³⁷ Baesjou, P. J.; Driessen, W. L.; Challa, G.; Reedijk, J. *Macromolecules* **1999**, *32*, 270-276.
- ³⁸ Soper, J. D.; Kaminsky, W.; Mayer, J. M. *J. Am. Chem. Soc.* **2001**, *123*, 5594-5595.
- ³⁹ Soper, J. D.; Mayer, J. M. *J. Am. Chem. Soc.* **2004**, *125*, 12217-12229.
- ⁴⁰ Mayer, J. M. *Acc. Chem. Res.* **1998**, *31*, 441-450.
- ⁴¹ Binstead, R. A.; McGuire, M. E.; Dovletoglou, A.; Seok, W. K.; Roecker, L. E.; Meyer, T. *J. Am. Chem. Soc.* **1992**, *114*, 173-186.
- ⁴² Shultz, L. K.; Huynh, M. H. V.; Binstead, R. A.; Curry, M.; Meyer, T. *J. Am. Chem. Soc.* **2000**, *122*, 5984-5996.
- ⁴³ Feng, Y.; Gunnoe, T. B. *Unpublished results*
- ⁴⁴ Mazoguchi, T.; Adams, R. N. *J. Am. Chem. Soc.* **1962**, *84*, 2058-2060.
- ⁴⁵ Galus, Z.; White, R. M.; Rowland, F. S.; Adams, R. N. *J. Am. Chem. Soc.* **1962**, *84*, 2065-2068.
- ⁴⁶ Connerly, N. G.; Gieger, W. E. *Chem. Rev.* **1996**, *96*, 877-910.
- ⁴⁷ Bard, A. J.; Faulkner, L. R. *Electrochemical Methods – Fundamentals and Applications Second Edition*; John Wiley & Sons, INC: New York, **2001**; pp 809.
- ⁴⁸ Rigaut, S.; Monnier, F.; Mousset, F.; Touchard, D.; Dixneuf, P. H. *Organometallic* **2002**, *21*, 2654-2661.

Chapter 5: Synthesis and Reactivity of Coordinatively Unsaturated Ruthenium(II) Amido Complexes.

5.1 Introduction and Importance of Unsaturation.

The study of metal mediated activation of methane and other hydrocarbons has received significant attention.^{1,2,3} Early transition metal imido complexes have been reported to undergo C-H activation reactions by 1,2-addition across the M-N bond.^{4,5,6} Such reactions are driven by the electrophilicity of the metal center and are kinetically favored for increased polarity of the M-N bond.^{7,8} Late transition metal oxide complexes in higher oxidation states also have been reported to initiate C-H bond activation reactions by hydrogen atom abstraction pathways (Scheme 5.1).^{9,10} These latter reactions

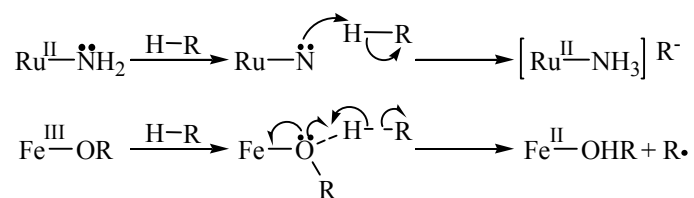


Scheme 5.1 C-H activation pathways. 1,2-Addition reactions are driven by electrophilic metal centers and polar M-N bonds. H-atom abstraction is driven by a favorable reduction of the metal center.

are driven by a favorable reduction of the metal center.^{11,12} One important distinction between these processes is that the metal center is directly involved in C-H bond activation for the 1,2-addition reaction, while it is not for ligand-centered H-atom abstraction. Thus, C-H bond activation based on H-atom abstraction pathways tend to be selective towards the weakest C-H bond; however, metal-mediated processes *potentially* offer the advantage of improved selectivity for activation and subsequent

functionalization. However, the overall utility of early transition metal imido complexes for C-H functionalization remains in doubt due to a lack of metal redox flexibility and the robust nature of the amido complexes that are formed (i.e. reductive elimination of an organic molecule is a disfavorable reaction).

Late transition metal amido and oxide complexes with high d-electron counts can cleave relatively acidic C-H bonds through intermolecular acid-base transformations as well as H-atom abstraction reactions (Scheme 5.2).^{9,10,13,14} For example, *trans*-

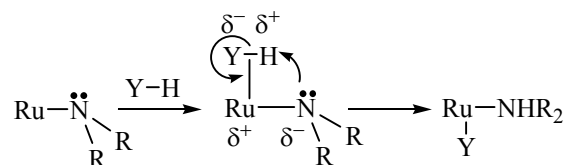


Scheme 5.2 C-H bond activation reactions for high d-electron count amido and oxide complexes.

(dmpe)₂M(NH₂)(H) (M = Ru or Fe) has been demonstrated to deprotonate triphenylmethane (pK_a ≈ 31 in THF) and terminal acetylenes.^{13,14,15} Studies of such complexes as well as our reactivity studies with the octahedral ruthenium(II) amido systems TpRu(L)(L')(NHR) (L = L' = PMe₃, P(OMe)₃ or L = CO and L' = PPh₃; R = H, Ph, and ^tBu) indicate that these deprotonation reactions result from highly basic amido or oxide moieties.^{13,14,16,17,18} Their reactive nature suggests the possibility of activating other inert bonds; however, results of our research with these complexes suggested that to achieve the increased reactivity needed to undergo transformation with less reactive substrates (i.e., those not susceptible to deprotonation or nucleophilic attack) required access to a metal coordination site. For example, the reaction of TpRu(PMe₃)₂NH₂ with

1,4-cyclohexadiene yields $\text{TpRu}(\text{PMe}_3)_2\text{H}$ and benzene. Also, 1,4-cyclohexadiene was observed to isomerize to 1,3-cyclohexadiene, likely by a deprotonation mechanism (see Chapter 3). The addition of excess PMe_3 (approximately 0.4 equivalents) was observed to suppress the formation of $\text{TpRu}(\text{PMe}_3)_2\text{H}$ and benzene, yet excess PMe_3 does not impact the rate of isomerization of 1,4-cyclohexadiene to 1,3-cyclohexadiene. Also, Bergman et al. have reported the rate of activation of dihydrogen- d_2 by *cis*- $(\text{PMe}_3)_4\text{Ru}(\text{H})(\text{NH}_2)$ was “slowed dramatically” by addition of two equivalents of PMe_3 .¹⁹ The effect of PMe_3 to decrease reactivity in these reactions is likely a result of competition for a coordination site. Hence, we sought to determine if coordinative unsaturation would yield systems that are able to activate otherwise inert substrates.

C-H bond cleavage by 1,2-additions for early metal imido complexes in high oxidation states are driven by the electrophilicity of the metal center (see Chapter 1). We anticipated that polar and basic/nucleophilic amido ligands coordinated to late transition metals with high d-electron counts would be able to achieve comparable reactivity via the reactive nature of the amido moiety. Thus, by accessing 16-electron Ru(II) amido complexes that possess an open coordination site, transient binding of non-polar H-H or C-H bonds might be feasible, thereby activating these substrates towards intramolecular deprotonation (Scheme 5.3).



Scheme 5.3 Activation of non-polar bonds using coordinatively unsaturated late transition metals with amido ligands. We anticipated polar and basic/nucleophilic amido moiety would promote functionalization.

Tridentate and monoanionic “pincer” ligands that coordinate in a meridional fashion have received significant attention in recent years due to the high catalytic activity and robustness of complexes possessing these ligands.²⁰ For example, pincer complexes of iridium(III) are active towards the dehydrogenation of alkanes, cycloalkanes, THF, and ethylbenzene.^{20,21} The complexes (PCP)Ir(H)₂ (PCP = [2,6-(CH₂PR₂)₂C₆H₃] {R = ^tBu or ⁱPr}) are thermally robust and do not decompose at temperatures up to 200 °C. Pincer ligands also allow tuning of steric and electronic properties of a metal center through the variation of phosphine substituents and the aryl para substituent (Figure 5.1).

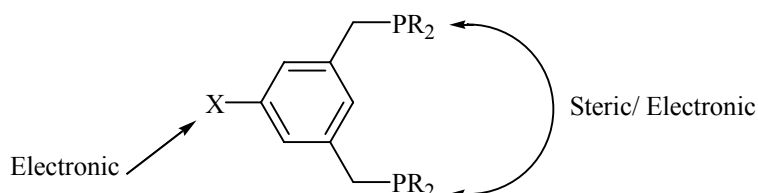


Figure 5.1 Pincer ligands allow tuning of steric and electronic effects through the phosphine substituent R, and, the variation of the X allows additional tuning of electronic effects.

The pincer ligand PCP (PCP = [2,6-(CH₂P^tBu₂)₂C₆H₃]) has provided a framework to prepare and study a coordinatively unsaturated Ru(II) amido system. (Figure 5.1, R = ^tBu and X = H).^{22,23}

5.2 Synthesis of Unsaturated Amido Complexes.

(PCP)Ru(CO)Cl provided the starting point for the preparation of unsaturated Ru(II) amido complexes. This ligand presents characteristic virtual triplets for the ^tBu resonances in the ¹H NMR spectrum as well as a diagnostic CO absorbance using IR

spectroscopy (Figure 5.2). Our initial attempts to prepare the amido complexes focused on methods similar to those used for preparation of TpRu(L)(L')NHR ($\text{L, L}' = \text{PMe}_3$ or P(OMe)_3 and $\text{L} = \text{CO}$, $\text{L}' = \text{PPh}_3$; $\text{R} = \text{H, Ph, } ^t\text{Bu}$); however, these methods did not allow the preparation of the amido complexes $(\text{PCP})\text{Ru}(\text{CO})\text{NHR}$ ($\text{R} = \text{H}$ or Ph). Specifically, attempted halide abstraction with AgOTf resulted in redox chemistry rather than halide/ OTf metathesis. The CO stretch of $(\text{PCP})\text{Ru}(\text{CO})\text{Cl}$ is observed at 1924 cm^{-1} while the CO stretch of $\text{TpRu}(\text{CO})(\text{PPh}_3)\text{Cl}$ appears at 1980 cm^{-1} .^{22,24} The difference in CO absorbance energy for these complexes suggests that the PCP system is more electron rich and is likely to be oxidized more readily. Our group has since discovered that reaction of $(\text{PCP})\text{Ru}(\text{CO})\text{Cl}$ with NaBAR'_4 ($\text{Ar}' = 3,5\text{-C}_6\text{H}_3(\text{CF}_3)_2$) affords the four coordinate complex $[(\text{PCP})\text{Ru}(\text{CO})][\text{BAR}'_4]$; however, the reaction is only successful under specific solvent and reaction conditions.²⁵

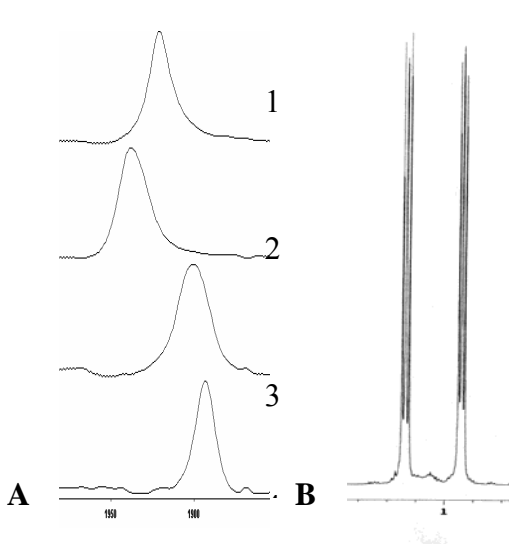
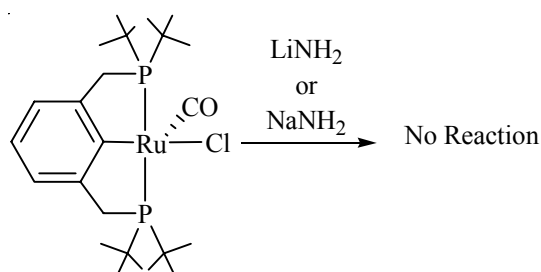


Figure 5.2 Spectroscopic handles for $(\text{PCP})\text{Ru}(\text{CO})\text{X}$ complexes. **A** CO absorptions (IR) **B** ^tBu resonances in the ^1H NMR spectrum.

Synthesis of the complex *trans*-(dmpe)₂Ru(H)(NH₂) was reported by reaction of *trans*-(dmpe)₂Ru(H)Cl with NaNH₂ in the presence of ammonia. A carefully controlled stoichiometry (1:1 liquid NH₃ to NaNH₂ in THF) was noted to be essential for synthesis.^{26,27} Attempts to translate this chemistry to (PCP)Ru(CO)Cl yielded ambiguous results. Room temperature reactions of (PCP)Ru(CO)Cl with one equivalent of LiNH₂ or NaNH₂ in THF yield no reaction after 24 hours based on IR spectroscopy (Scheme 5.4). Reaction of (PCP)Ru(CO)Cl with LiNH₂ in the presence of excess NH₃ in the THF

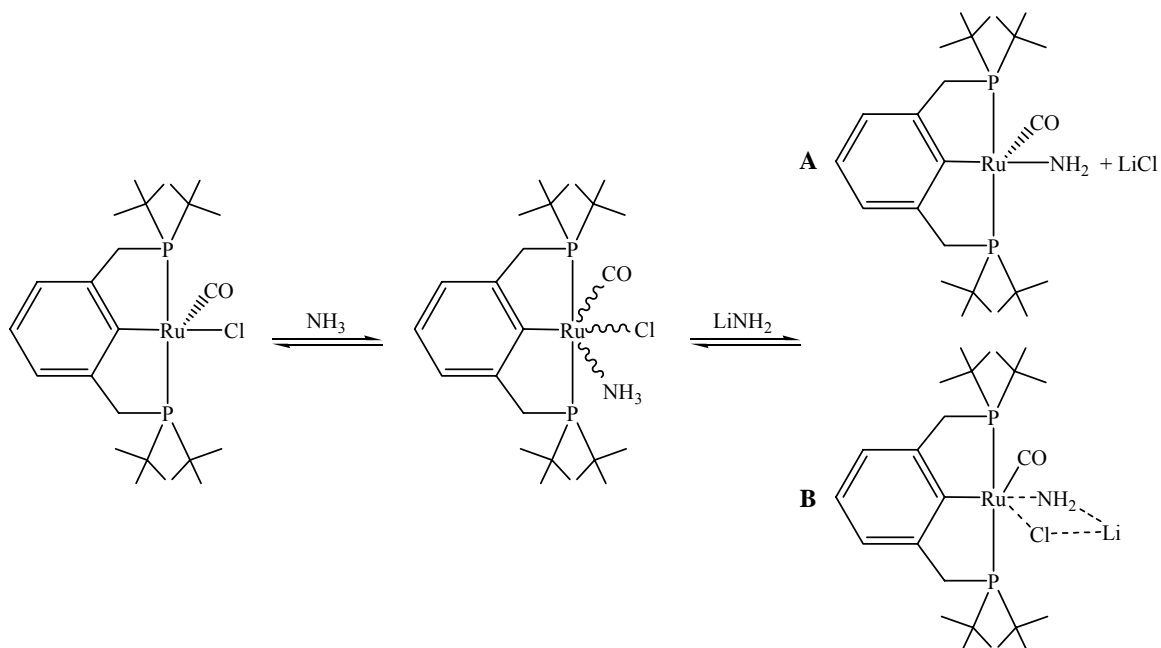


Scheme 5.4 Metathesis reactions of (PCP)Ru(CO)Cl with LiNH₂ or NaNH₂ were unsuccessful for preparation of the complex (PCP)Ru(CO)NH₂.

yielded new products based on IR spectroscopy; however, interpretation of these results was complicated by two factors. First, the addition of excess NH₃ to THF solutions of (PCP)Ru(CO)Cl results in coordination of ammonia. The CO absorption for the ammonia coordinated complex is observed at 1900 cm⁻¹, but multiple CO absorptions were observed depending on reaction conditions. The starting material has a CO absorbance of 1924 cm⁻¹. For example, for the reaction of (PCP)Ru(CO)Cl with 10 equivalents of LiNH₂ and excess NH₃, new CO absorptions were observed to form at 1880 and 1890 cm⁻¹ over the course of approximately 1 day. The absorption at 1900 cm⁻¹ likely corresponds to ammonia coordination to yield (PCP)Ru(CO)(NH₃)Cl. This

absorbance disappeared with growth of the new CO stretches. Although two CO absorptions were observed in the reaction mixture, work up of the reaction yielded only one product that was consistent with the formation of (PCP)Ru(CO)NH₂ ($\nu_{\text{CO}} = 1890 \text{ cm}^{-1}$; see below). The CO absorption at 1880 cm^{-1} likely attributable to ammonia coordination to (PCP)Ru(CO)NH₂, but this was not confirmed. Another factor complicating this reaction was the rate of disappearance of starting materials ($\nu_{\text{CO}} = 1924$ or 1900 cm^{-1}) and ratio of products ($\nu_{\text{CO}} = 1890$ or 1880 cm^{-1}) based on CO absorbance was dependant on equivalents of LiNH₂. For example, 10 equivalents were required to fully convert the starting material, while 1 or 5 equivalents did not yield clean conversion to the amido product; a new CO absorbance at 1897 cm^{-1} was observed before complete conversion. The CO absorbance at 1897 cm^{-1} is likely attributable to a decomposition pathway later discovered for (PCP)Ru(CO)(NH₂) (see below).

Based on the observation that addition of ammonia results in immediate coordination to (PCP)Ru(CO)Cl and no reactivity was observed in the absence of ammonia, ammine coordination likely precedes reactivity. The dependence of the rate of disappearance of (PCP)Ru(CO)Cl/(PCP)Ru(CO)(Cl)(NH₃) on the number of equivalents of LiNH₂ suggests an acid base equilibrium between an ammonia-coordinated intermediate and LiNH₂ (Scheme 5.5). Two likely products were postulated for this reaction. Product **A** is a neutral Ru(II) parent amido complex that results from deprotonation of the amine by LiNH₂, with loss of halide to form LiCl. Product **B** is formed via metathesis with LiNH₂ followed by loss of ammine. Scheme 5.5-A should result in irreversible precipitation of LiCl driving the equilibrium to products. Thus, the



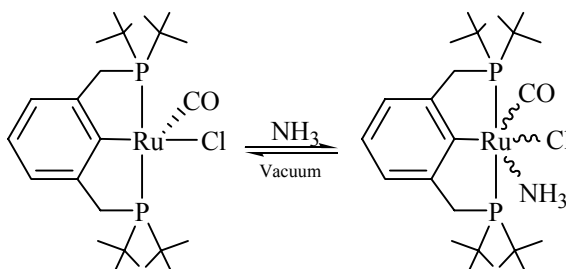
Scheme 5.5 Proposed pathways for reaction of (PCP)Ru(CO)Cl and LiNH₂ in the presence of ammonia.

observation 10 equivalents of LiNH₂ was required for complete conversion likely results from kinetic factors. Support for product **B** was found by work of Jubo Zhang in the Gunnoe group.²⁸ Specifically, reactions (PCP)Ru(CO)Cl and LiNHPh did not cleanly convert to (PCP)Ru(CO)(NHPh) and LiCl. Clean reactivity was only accomplished with coordination of PMe₃ prior to metathesis. It is suspected that in the absence of PMe₃ metathesis does not occur with the five coordinate system, and an analogous product to **B** in Scheme 5.5 is formed.²⁹ Concerns about such complications led us to pursue other synthetic routes.

5.2.1 Preparation of (PCP)Ru(CO)(NH₃)Cl, [(PCP)Ru(CO)(NH₃)₂][OTf], and (PCP)Ru(CO)NH₂.

Two general features of the PCP complexes discussed herein are the five coordinate systems are a dark orange color, and the six coordinate systems are pale yellow or white. Also, these complexes, both five and six coordinate, exhibit a high degree of solubility in organic solvents. For example, the complex (PCP)Ru(CO)Cl is soluble in THF, benzene, toluene, methylene chloride, chloroform, diethylether, and alkanes (e.g., hexanes, pentane, or cyclopentane).

Two routes were developed to prepare the PCP parent amido complex (PCP)Ru(CO)NH₂. The first route involved coordination of NH₃ to (PCP)Ru(CO)Cl, followed by deprotonation. The addition of excess NH₃ to a THF solution of (PCP)Ru(CO)Cl resulted in immediate coordination of ammonia as evidenced by an immediate color change from dark orange to colorless (Scheme 5.6). IR spectroscopy



Scheme 5.6 The addition of ammonia to (PCP)Ru(CO)Cl results in immediate coordination of NH₃.

also revealed a CO absorption of 1900 cm⁻¹ with the starting material exhibiting a CO stretch at 1924 cm⁻¹. Attempts to isolate (PCP)Ru(CO)Cl(NH₃) were unsuccessful due to lability of the ammonia ligand. Removal of excess ammonia via vacuum, isolation by

precipitation, or purging the solution with N₂ resulted in rapid ammine loss and formation of the starting material (Scheme 5.6).

Although isolation was not possible, the complex (PCP)Ru(CO)(NH₃)Cl has been characterized by ¹H, ¹³C, ³¹P NMR and IR spectroscopy. Characterization by ¹H NMR and ³¹P NMR was achieved by bubbling of NH₃ gas through solutions of (PCP)Ru(CO)Cl in CDCl₃. The ¹H NMR spectrum shows overlapping virtual triplets at 1.1 ppm for the ^tBu resonances of the PCP ligand, and a broad triplet for the ammine NH protons is observed at 2.85 ppm (Figure 5.3). A single resonance is observed in the ³¹P NMR spectrum at 78.3 ppm. IR spectroscopy of (PCP)Ru(CO)(NH₃)Cl reveals a CO absorbance of 1900 cm⁻¹ (in solutions THF or benzene). Excess NH₃ in solution

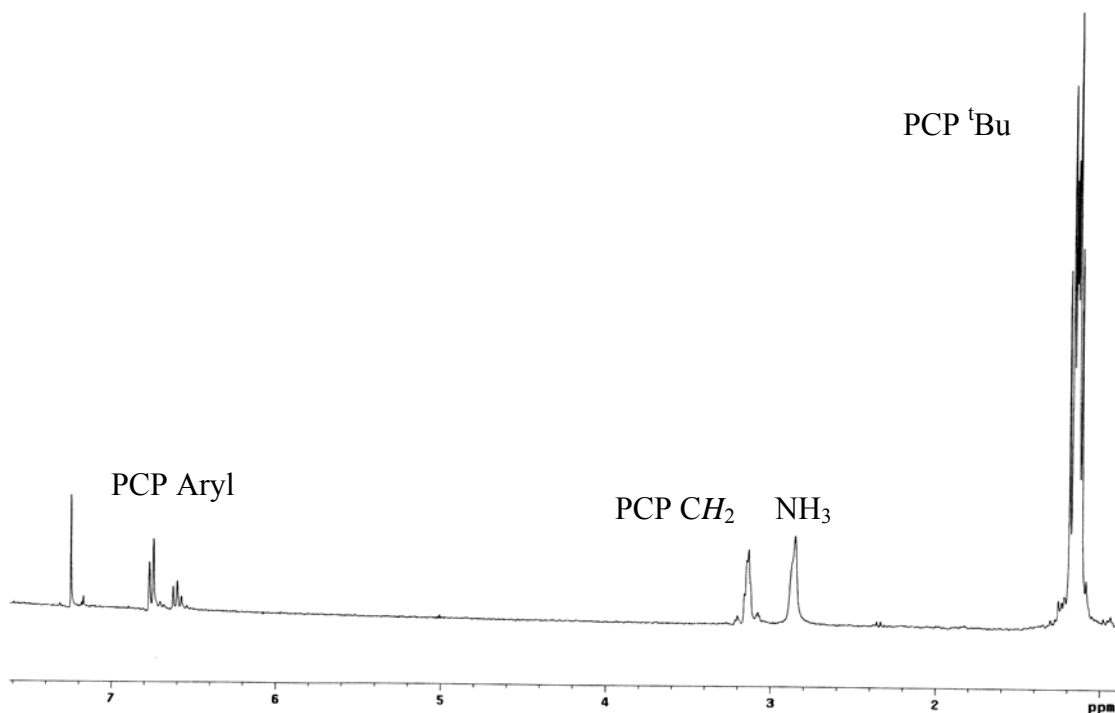
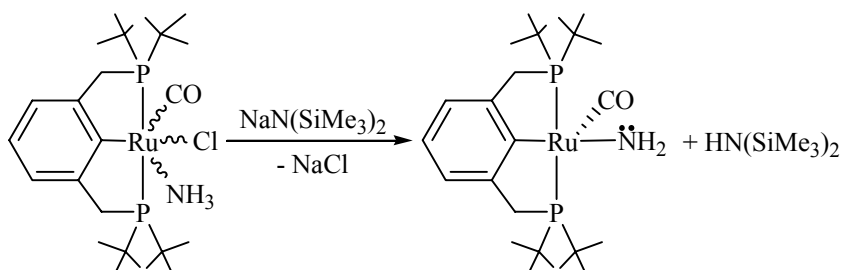


Figure 5.3 ¹H NMR spectrum of (PCP)Ru(CO)(Cl)(NH₃) in CDCl₃.

prevented determination of the N-H absorption.

Treatment of the complex (PCP)Ru(CO)(NH₃)Cl with the base NaN(SiMe₃)₂ resulted in an immediate color change from clear to dark orange. The product of this reaction is the amido complex (PCP)Ru(CO)NH₂ (Scheme 5.7). Workup by removal of



Scheme 5.7 Preparation of (PCP)Ru(CO)NH₂. (PCP)Ru(CO)Cl(NH₃) was prepared insitu and deprotonated using NaN(SiMe₃)₂.

volatiles followed by extraction with benzene allowed isolation of the product. The amido complex is an orange solid that is highly air and moisture sensitive. This complex has been characterized by ¹H, ¹³C, ³¹P NMR and IR spectroscopy as well as FAB mass spectrometry. The ¹H NMR spectrum shows virtual triplets for the ^tBu groups of the PCP ligand at 1.26 and 1.14 ppm, and a broad triplet for the amido NH protons at 3.09 ppm (Figure 5.4). The ³¹P NMR spectrum reveals a singlet at 72.9 ppm, and solution cell IR spectroscopy in THF reveals a CO absorption at 1890 cm⁻¹ with absorptions due to symmetric and asymmetric stretching at 3396 and 3306 cm⁻¹.

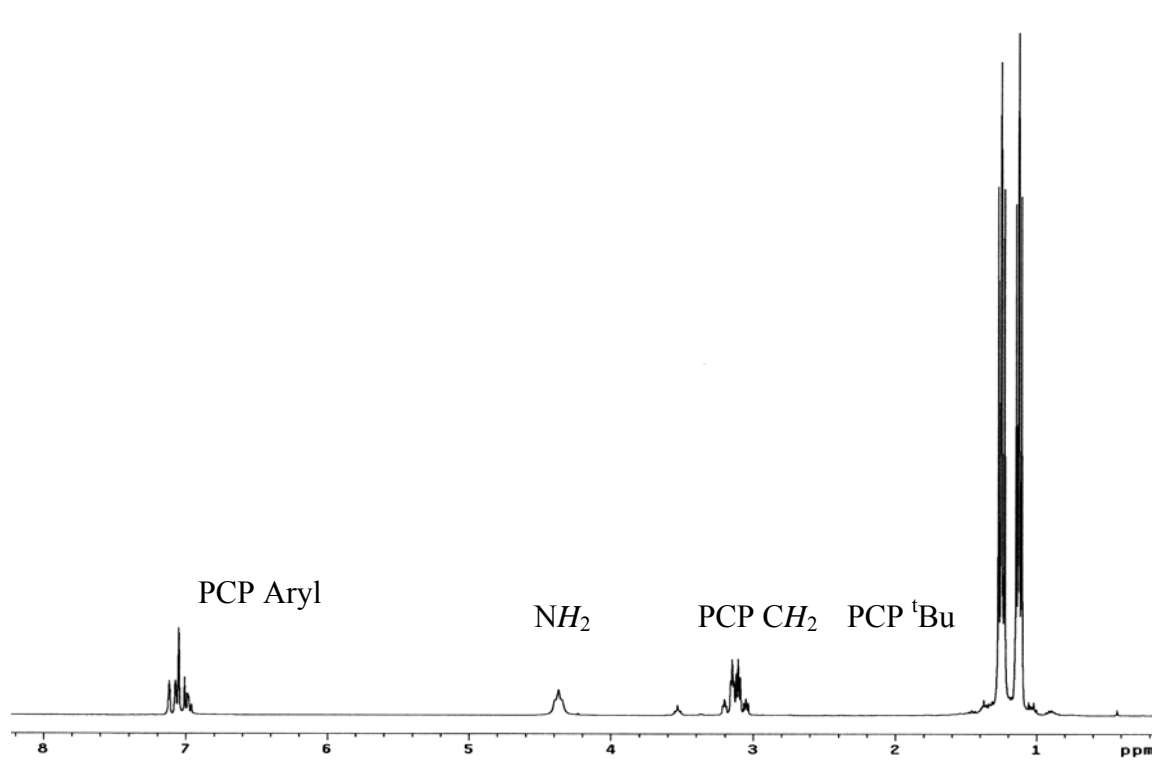
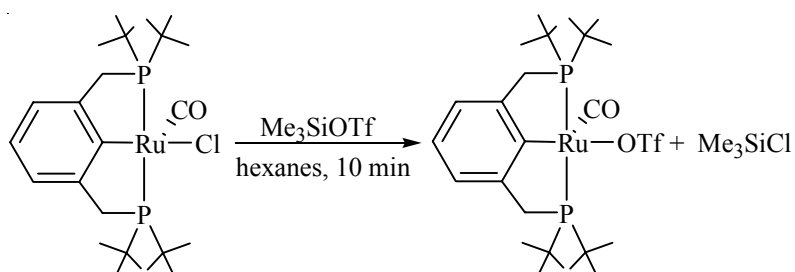


Figure 5.4 ^1H NMR spectrum of $(\text{PCP})\text{Ru}(\text{CO})\text{NH}_2$ in C_6D_6 .

A second method was also used to synthesize the parent amido complex $(\text{PCP})\text{Ru}(\text{CO})\text{NH}_2$. Me_3SiOTf is a strong Lewis acid. For example, this reagent is used in the preparation triphenylcarbenium triflate by heterolytic cleavage of the C-Cl bond of triphenylmethanechloride.³⁰ Similarly, reacting a hexanes or cyclopentane solution of $(\text{PCP})\text{Ru}(\text{CO})\text{Cl}$ with 10 equivalents of Me_3SiOTf resulted in formation of dark orange crystals after approximately ten minutes. Workup by filtration and washing with cold hexanes affords the corresponding triflate complex $(\text{PCP})\text{Ru}(\text{CO})\text{OTf}$ (Scheme 5.8). The triflate complex $(\text{PCP})\text{Ru}(\text{CO})\text{OTf}$ has been characterized by IR, ^1H , ^{13}C , and ^{31}P NMR spectroscopy as well as elemental analysis. The ^1H NMR spectrum shows virtual



Scheme 5.8 Preparation of (PCP)Ru(CO)OTf by halide abstraction from (PCP)Ru(CO)Cl using Me₃SiOTf.

triplets at 1.50 and 1.17 ppm (Figure 5.5), and a singlet is observed at 70.0 ppm in the ³¹P NMR spectrum. Solution cell IR spectroscopy in THF reveals a CO absorbance at 1936 cm⁻¹.

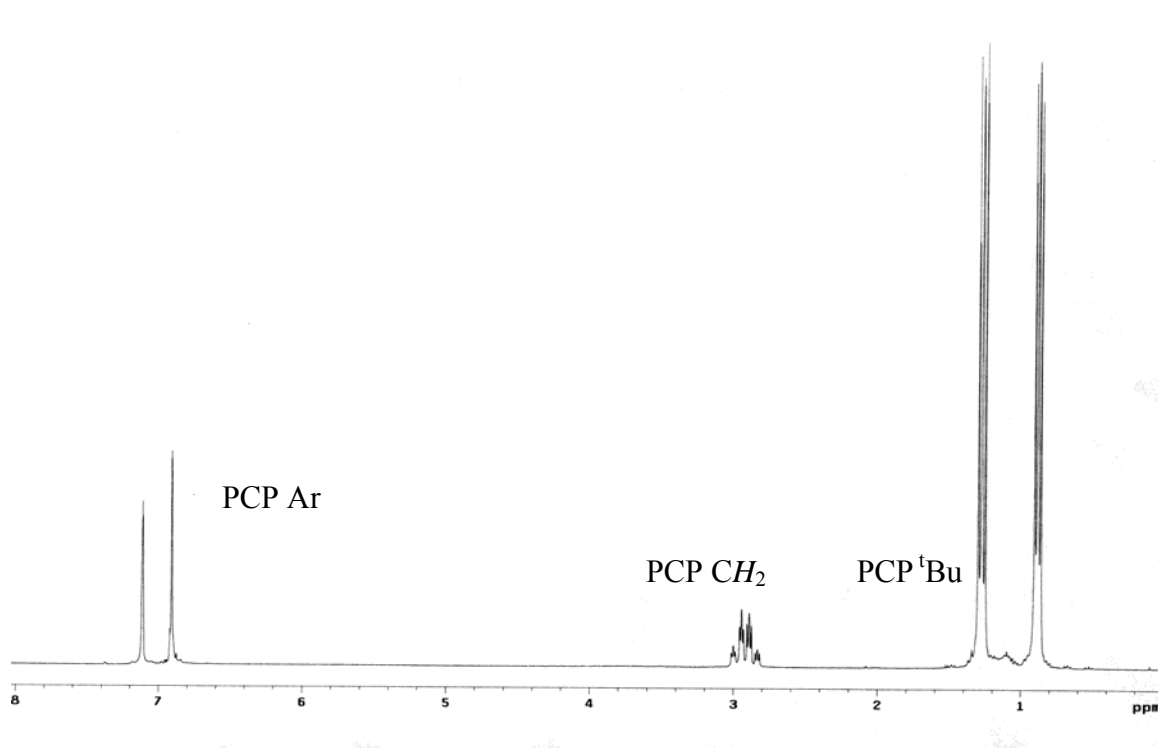


Figure 5.5 ¹H NMR spectrum of (PCP)Ru(CO)OTf in C₆D₆.

Reaction of (PCP)Ru(CO)OTf in THF with excess ammonia results in an immediate color change from dark orange to colorless. The reaction results in coordination of 2 equivalents of ammonia to form the cationic ammine complex [(PCP)Ru(CO)(NH₃)₂][OTf]. Interestingly, the amine ligands are not very labile even under reduced pressure. This observation is in contrast to other six coordinate ammine complexes of the (PCP)Ru(CO) system; however, over the course of several days [(PCP)Ru(CO)(NH₃)₂][OTf] slowly converts to an uncharacterized product which is likely the mono-ammonia complex (PCP)Ru(CO)(NH₃)OTf. IR spectroscopy of [(PCP)Ru(CO)(NH₃)₂][OTf] reveals a CO absorption at 1923 cm⁻¹, and N-H stretches at 3415, 3358, and 3292 cm⁻¹. The ¹H NMR spectrum shows distinct ammonia resonances at 2.50 and 2.45 ppm, indicating a cis geometry of these ligands (Figure 5.6). The reaction of this complex with the base NaN(SiMe₃)₂ results in formation of the parent amido complex (PCP)Ru(CO)NH₂.

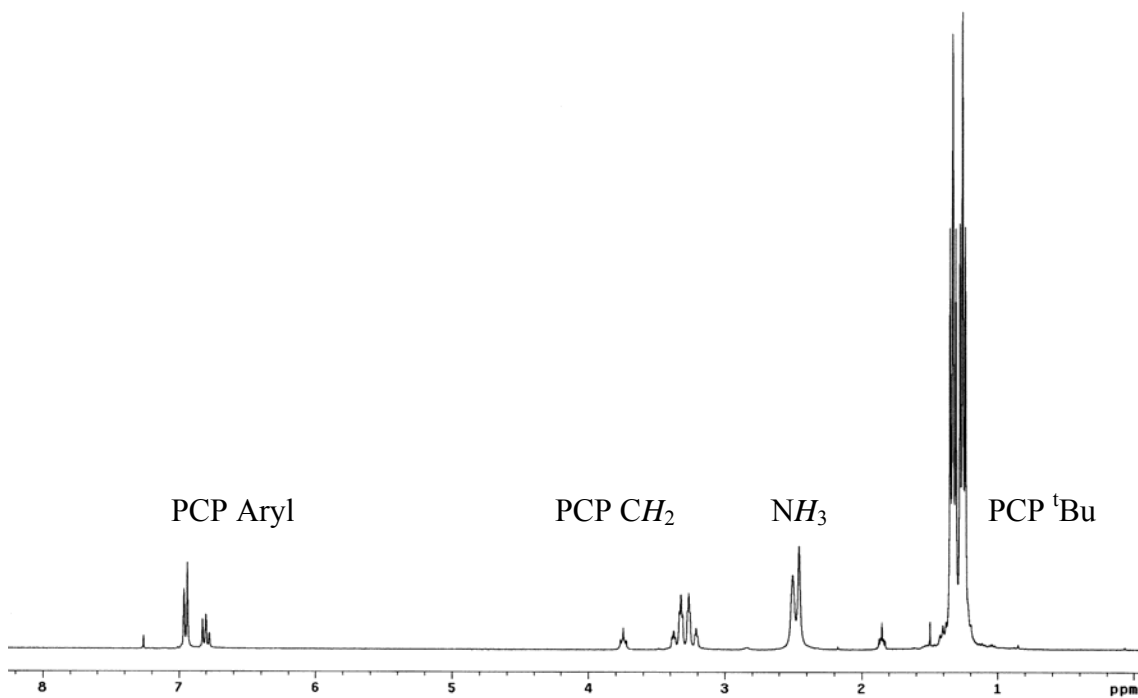
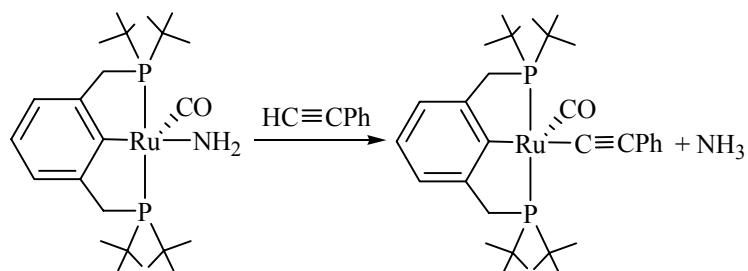


Figure 5.6 ^1H NMR spectrum of $[(\text{PCP})\text{Ru}(\text{CO})(\text{NH}_3)_2][\text{OTf}]$ in CDCl_3 .

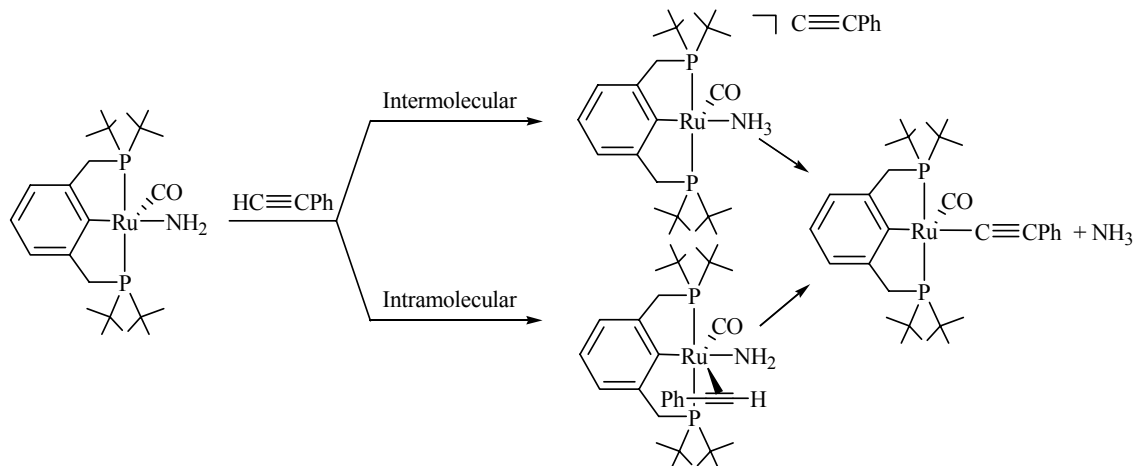
5.3 Reactivity of $(\text{PCP})\text{Ru}(\text{CO})\text{NH}_2$ with Phenylacetylene or Dihydrogen.

The reaction of the octahedral Ru(II) amido complexes $\text{TpRu}(\text{L})(\text{L}')\text{NHR}$ ($\text{R} = \text{H}$ or ^tBu) or *trans*-(dmpe)Ru(H)(NH₂) with phenylacetylene result in deprotonation of the terminal proton of phenylacetylene to form the ion pairs $[\text{TpRu}(\text{L})(\text{L}')\text{NH}_2\text{R}][\text{C}\equiv\text{CPh}]$ and *trans*-(dmpe)Ru(H)(NH₃)[C≡CPh], respectively.^{14,17} The unsaturated Ru(II) amido complex $(\text{PCP})\text{Ru}(\text{CO})\text{NH}_2$ also undergoes immediate reaction with phenylacetylene; however, rather than an ion pair, the product of this reaction is the acetylide complex $(\text{PCP})\text{Ru}(\text{CO})(\text{C}\equiv\text{CPh})$ and ammonia (Scheme 5.9).



Scheme 5.9 Reaction of (PCP)Ru(CO)(NH₂) with phenylacetylene results in immediate deprotonation to form (PCP)Ru(CO)(C≡CPh).

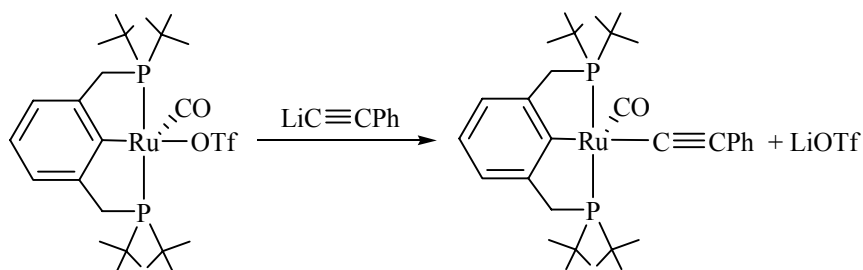
[TpRu(L)(L')NH₂R][C≡CPh] (R = H or ^tBu) and [*trans*-(dmpe)Ru(H)(NH₃)] [C≡CPh] are formed by intermolecular deprotonation of the acetylene C-H bond via a basic amido ligand.¹³⁻¹⁸ For the reaction of (PCP)Ru(CO)NH₂ with phenylacetylene, Ru-acetylide formation could result from a similar pathway. This reaction could also proceed by coordination of phenylacetylene to Ru, where by coordination provides a pathway to activate phenylacetylene towards intramolecular deprotonation (Scheme 5.10).



Scheme 5.10 Intra vs. inter molecular deprotonation of phenylacetylene. Intermolecular forms an ion pair, while intramolecular activates phenylacetylene towards deprotonation upon coordination to Ru.

We sought to determine if the deprotonation of phenylacetylene by (PCP)Ru(CO)NH₂ was occurring via an intramolecular or intermolecular pathway. To make this distinction, we attempted to observe reaction intermediates. Specifically, the observation of an ion pair complex would suggest an intermolecular pathway, while the complex (PCP)Ru(CO)(NH₃)(C≡CPh) is anticipated for an intramolecular pathway. The addition of phenylacetylene to a solution of (PCP)Ru(CO)NH₂ in toluene-*d*₈ that was cooled to -78 °C was performed. Low temperature ¹H NMR and ³¹P NMR spectroscopy were used to examine the reaction mixture for the ion pair intermediate [(PCP)Ru(CO)(NH₃)]⁺[C≡CPh]⁻ or the intramolecular intermediate the ammonia acetylide complex (PCP)Ru(CO)(NH₃)(C≡CPh). Unfortunately, the spectra from the low temperature reaction revealed complete conversion to the acetylide complex (PCP)Ru(CO)(C≡CPh) and ammonia. Thus, we were unable to determine the specific pathway of this reaction.

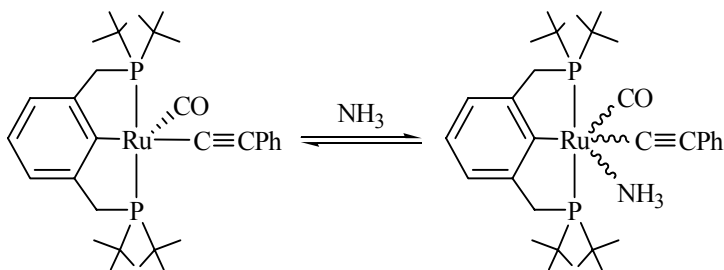
In order to confirm the identify the product from reaction of (PCP)Ru(CO) NH₂ with HC≡CPh, independent preparation of the acetylide complex was achieved by reaction of (PCP)Ru(CO)OTf with LiC≡CPh (Scheme 5.11). This product has been



Scheme 5.11 Preparation of the acetylide complex (PCP)Ru(CO)(C≡CPh) was achieved by reaction of (PCP)Ru(CO)OTf and LiC≡CPh.

characterized by ^1H , ^{13}C , and ^{31}P NMR spectroscopy as well as IR and elemental analysis. The IR spectrum shows a CO absorption at 1915 cm^{-1} , and the ^1H NMR spectrum shows virtual triplets for the ^tBu resonances at 1.53 and 1.18 ppm. The ^{31}P NMR spectrum shows a singlet at 80.0 ppm.

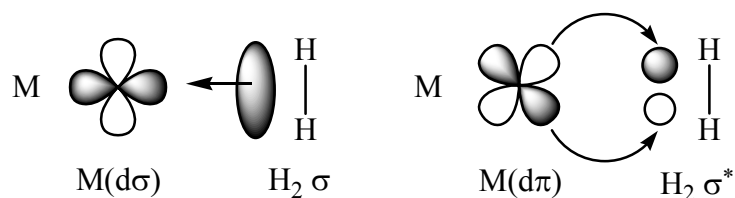
To aid in the identification of the reaction intermediates above, we also sought to prepare the intramolecular deprotonation intermediate $(\text{PCP})\text{Ru}(\text{CO})(\text{NH}_3)(\text{C}\equiv\text{CPh})$, but the addition of excess NH_3 to room temperature solutions of the acetylide complex $(\text{PCP})\text{Ru}(\text{CO})(\text{C}\equiv\text{CPh})$ did not result in coordination of ammonia based on ^1H NMR, ^{31}P NMR, and IR spectroscopy. Coordination was found only to occur at low temperature (approximately $-50\text{ }^\circ\text{C}$) and using a very highly concentrated mixture of toluene- d_8 and ammonia that was prepared by condensing NH_3 in the toluene (approximately 30% by volume). Under that condition, approximately 50% conversion to $(\text{PCP})\text{Ru}(\text{CO})(\text{C}\equiv\text{CPh})(\text{NH}_3)$ was observed based on ^{13}C and ^{31}P NMR spectroscopy (Scheme 5.12). The difficulty coordinating NH_3 to $(\text{PCP})\text{Ru}(\text{CO})(\text{C}\equiv\text{CPh})$ suggests *if* deprotonation of phenylacetylene occurs via an intramolecular pathway that the



Scheme 5.12 We attempted to prepare the intramolecular deprotonation intermediate $(\text{PCP})\text{Ru}(\text{CO})(\text{NH}_3)(\text{C}\equiv\text{CPh})$, by addition of NH_3 to $(\text{PCP})\text{Ru}(\text{CO})(\text{C}\equiv\text{CPh})$; however, only partial conversion was observed even under harsh condition.

intermediate would likely be unobservable due to rapid dissociation of the ammonia ligand. Ultimately, the reaction pathway, either intra/inter molecular or both could not be determined.

In a further effort to investigate the effects of coordinative unsaturation on the reactivity of late transition metal amido complexes, we reacted (PCP)Ru(CO)NH₂ with dihydrogen. Deprotonation of H₂ through an intermolecular pathway is not likely since the pK_a of dihydrogen in THF is approximately 49; however, coordination of dihydrogen to transition metal centers is known to increase its acidity.^{31,32} As a ligand, dihydrogen had long been postulated; however, the first complex was not isolated until mid 1980's.³³ Dihydrogen ligands can interact with metal centers through σ -donation of the H-H bond. In addition, dihydrogen can act as a π -acid by acceptance from metal a d π orbital into the H-H σ^* orbital (Scheme 5.13).^{34,35,36} Both interactions serve to weaken the H-H bond. σ -

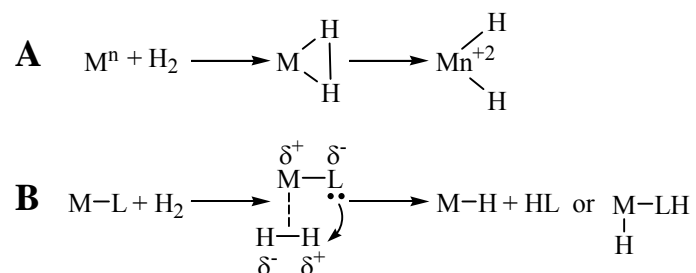


Scheme 5.13 Modes of η^2 -H₂ bonding. H₂ σ -donates from the H-H bonding electrons and π -accepts through the σ^* orbital.

Donation results in a three center two-electron interaction, and the metal-H₂ π -interaction involves an orbital that is antibonding character with respect to the H-H bond. The weakening of the H-H bond can result in increased acidity, thus dihydrogen ligands are more frequently acidic than free H₂. For example, Studies of a series of Cp and Cp* based ruthenium dihydrogen complexes with chelating phosphines, show a pK_a range

from 10 to -5 .³⁷ Generally, more π -basic metal centers increase acidity due to a greater degree of π -donation into the H-H σ^* orbital. Increased steric constraints by the ancillary ligands were found to favor dihydrogen binding, i.e. less acidic H₂ ligands, but the influence of steric interactions has been found to have a less pronounced effect on acidity.^{35,37}

η^2 -Dihydrogen bond cleavage can occur by either a homolytic or heterolytic bond scission mechanism (Scheme 5.14). Metal centers that are sufficiently π -donating



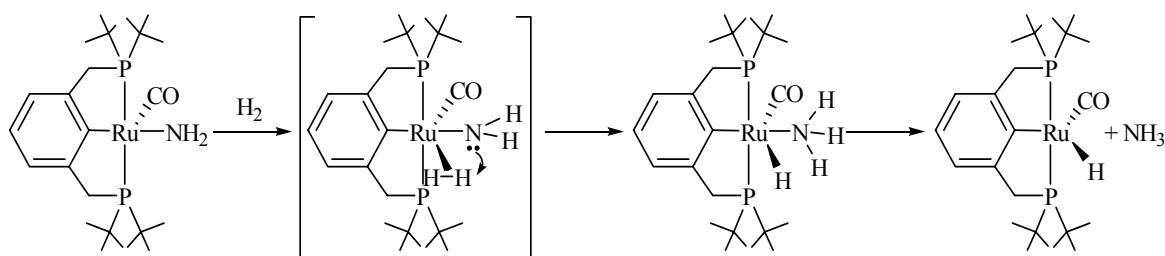
Scheme 5.14 Pathways for η^2 -H₂ bond scission. **A** – proceeds via oxidative addition and **B** – proceeds via base promoted heterolytic bond cleavage.

undergo homolytic cleavage occurs by oxidative addition of H₂, and heterolytic H-H bond cleavage proceeds via coordination in the presence of a basic ligand. The activation of dihydrogen by (PCP)Ru(CO)NH₂ would likely occur in a heterolytic fashion due to the basic nature of the amido ligand.

Placing a room temperature solution of (PCP)Ru(CO)NH₂ under 1 atm pressure of H₂ resulted in a color change from orange to pale yellow after four minutes. Workup of this reaction yielded the previously reported ruthenium (II) hydride complex

(PCP)Ru(CO)H.³⁸ Prior to workup, two CO absorptions at 1900 and 1925 cm^{-1} were observed in the IR spectrum of the reaction mixture. The low-energy absorption at 1900 cm^{-1} is consistent with the formation of the hydride complex (PCP)Ru(CO)H. Reaction of independently prepared (PCP)Ru(CO)H with H_2 results in a new CO absorption at 1925 cm^{-1} . Thus, the high energy stretch (1925 cm^{-1}) of the reaction mixture is likely due to the formation of (PCP)Ru(CO)(H)₃. The nature of the three hydrogen atoms is unknown.

Bond scission of H_2 by (PCP)Ru(CO)NH₂ likely occurs via coordination of H_2 followed by intramolecular deprotonation to form an ammonia/hydride complex that subsequently releases ammonia (Scheme 5.15). (PCP)Ru(CO)(NH₃)(H) is an anticipated



Scheme 5.15 Proposed scheme for the activation of dihydrogen by (PCP)Ru(CO)NH₂. Heterolytic bond cleavage occurs in the presence of the basic amido ligand.

intermediate in this proposed scheme. This complex was independently prepared by reaction of (PCP)Ru(CO)H with NH₃ in C₆D₆. Weak binding of the NH₃ ligand prevented isolation. For example, removal of excess NH₃ by placing solutions of this complex under vacuum or purging with N₂ results in formation of (PCP)Ru(CO)H. The complex (PCP)Ru(CO)(NH₃)(H) has been characterized by ¹H NMR, ³¹P NMR, and IR spectroscopy. The ¹H NMR spectrum shows a hydride triplet at -16.17 ppm with 21 Hz

coupling to phosphorous (Figure 5.7). Proton coupled ^{31}P NMR spectroscopy shows a doublet at 95.7 ppm with 21 Hz coupling to the hydride hydrogen. Solution cell IR spectroscopy in THF shows a CO absorption at 1905 cm^{-1} .

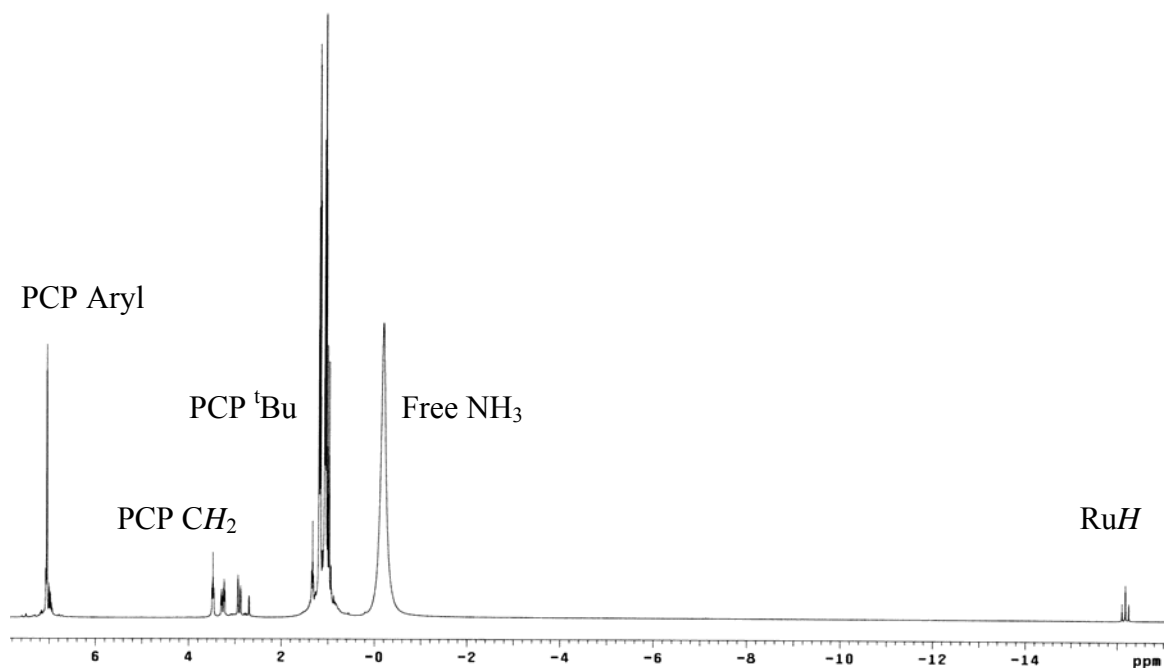
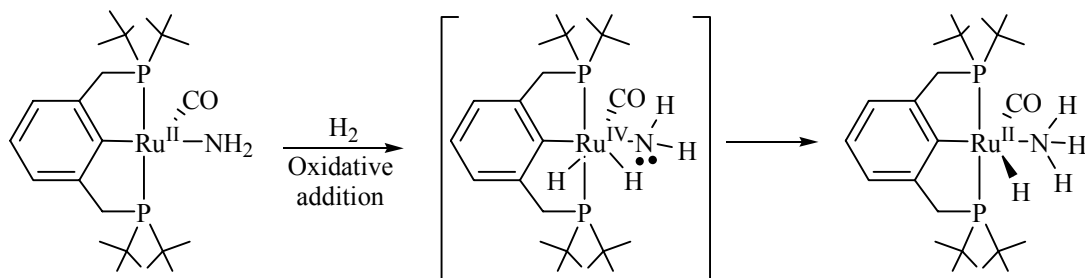


Figure 5.7 ^1H NMR spectrum of $(\text{PCP})\text{Ru}(\text{CO})(\text{NH}_3)(\text{H})$ C_6D_6 with NH_3 in solution.

The addition of dihydrogen to a toluene- d_8 solution of $(\text{PCP})\text{Ru}(\text{CO})\text{NH}_2$ at $-78\text{ }^\circ\text{C}$ in a gas tight NMR tube revealed the formation of $(\text{PCP})\text{Ru}(\text{CO})(\text{NH}_3)(\text{H})$ based on low temperature ^1H NMR and ^{31}P NMR spectroscopy ($-70\text{ }^\circ\text{C}$). Also, room temperature IR spectroscopy revealed three CO absorptions that are consistent a mixture of $(\text{PCP})\text{Ru}(\text{CO})(\text{NH}_3)\text{H}$, $(\text{PCP})\text{Ru}(\text{CO})(\text{H}_3)$, and $(\text{PCP})\text{Ru}(\text{CO})\text{H}$. The observation of $(\text{PCP})\text{Ru}(\text{CO})(\text{NH}_3)(\text{H})$ suggests coordination of H_2 activates it towards deprotonation

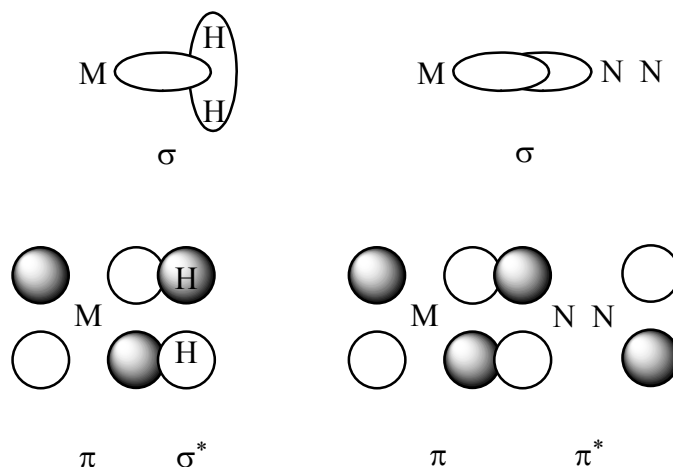
via intramolecular heterolytic H-H bond cleavage (i.e., 1,2-addition of H₂ across the Ru-N bond). It should be noted that (PCP)Ru(CO)(NH₃)(H) could also be formed by initial oxidative addition of H₂ to form the Ru(IV) dihydride complex (PCP)Ru(CO)(NH₂)(H)₂. Subsequent to oxidative addition, reductive N-H formation to form (PCP)Ru(CO)(NH₃)H (i.e. intramolecular proton transfer from ruthenium to the amido ligand) (Scheme 5.16).



Scheme 5.16 Formation of (PCP)Ru(CO)(NH₃)(H) by initial oxidative addition of H₂.

Reductive eliminations to form N-H bonds, although rare, have been reported for d⁶ metal centers. For example Bergman et al. have reported reductive elimination from Cp*Ir(PPh₃)(H)(NHPh) in the presence of coordinating ligands to form Cp*Ir(PPh₃)(L) (L = CO, C₂H₂, CNBu, PPh₃, and PPh₂Me) and aniline.³⁹ Also, Hartwig, Goldman et al. have reported reductive N-H bond formation from the Ir(III) complex (PCP)Ir(NH₂)H to form the Ir(I) complex (PCP)Ir and free ammonia.⁴⁰

H-H cleavage occurs with metal centers that are sufficiently π -basic since π -back donation is into the antibonding σ^* orbital of H₂.³⁶ A useful method for predicting a metal centers ability of cleave H-H bonds by oxidative addition upon coordination of H₂ has been developed.^{36,41} Morris et al. have suggested η^2 -H₂ and η^1 -N₂ interact similarly with the bonding site based comparable orbital diagrams (Scheme 5.17). A well followed



Scheme 5.17 Morris et al. suggest that η^2 -H₂ and η^1 -N₂ bond similarly to a metal center based on a comparable orbital diagrams.

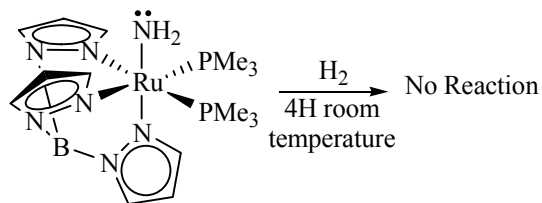
empirical trend has been established that octahedral d⁶ complexes with $\nu_{\text{NN}} > 2050 \text{ cm}^{-1}$ are insufficiently π -basic to cleave the H-H bond of the dihydrogen ligand when H₂ replaced N₂ in the coordination sphere.^{36,41} Thus, the energy of the N≡N stretching absorption is a reliable predictor of η^2 -H₂ versus dihydride coordination. The complex (PCP)Ru(CO)NH₂ was not found to coordinate N₂ in concentrations sufficient to be observed by IR spectroscopy. Given the predilection towards five coordinate complexes for the (PCP)Ru(CO) moiety, this observation is not surprising. A related complex (PCP)Ru(H)(N₂) has been reported to exhibit $\nu_{\text{NN}} = 2088 \text{ cm}^{-1}$. Thus, the complex (PCP)Ru(CO)(H)₃ (an observed product in the reaction of (PCP)Ru(CO)NH₂ and H₂) would be predicted to possess a single hydride ligand and an η^2 -H₂ ligand.

Initial cursory examination of differences between the complexes (PCP)Ru(CO)H and (PCP)Ru(CO)NH₂ suggest a suitable comparison of the prediction towards oxidative

addition versus η^2 -H₂ coordination based on Morris's scheme is not possible. Both of these complexes possess a strong π -acid and such ligands that are trans to η^2 -H₂ hinder oxidative addition due to decreased π -basicity of the metal center.^{35,41} However, the comparison is complicated by the fact that (PCP)Ru(CO)NH₂ also possesses a π -donating ligand that presumably increases the propensity toward oxidative addition by increasing metal π -basicity. Thus, the coordination site of η^2 -H₂ (cis or trans to CO and NH₂) may significantly impact the ability of the amido complex (PCP)Ru(CO)NH₂ to oxidatively add H₂. A number of octahedral Ru(II) complexes that possess N₂ ligands have been reported with $\nu_{\text{NN}} > 2050 \text{ cm}^{-1}$; however, to our knowledge none of these complexes possess related π -donating ligands.^{38,42,43,44,45} Thus, the overall impact of cis or trans π -donating ligands is unknown.

Ultimately, based on the basic nature of the amido ligand and the rare nature of reductive N-H bond formation, we believe the activation of dihydrogen likely occurs via heterolytic bond cleavage of a coordinated H₂ ligand (i.e., the 1,2-addition of H₂ across the Ru-N bond) rather than oxidative addition.

To probe the importance of a vacant coordination site for the dihydrogen activation, we reacted the parent amido complex TpRu(PMe₃)₂NH₂ with H₂ under identical conditions to the reaction with (PCP)Ru(CO)NH₂. Room temperature addition of 1 atm of H₂ with TpRu(PMe₃)₂NH₂ in benzene resulted in no reaction after several hours, and workup of the reaction yielded only starting material (Scheme 5.18). The activation of deuterated dihydrogen has been reported for octahedral Ru(II) amido complex *cis*-(PMe₃)₄Ru(H)(NH₂). This reaction yields the dihydride complex



Scheme 5.18 The combination of $\text{TpRu(PMe}_3)_2\text{NH}_2$ with dihydrogen results in no reaction after several hours.

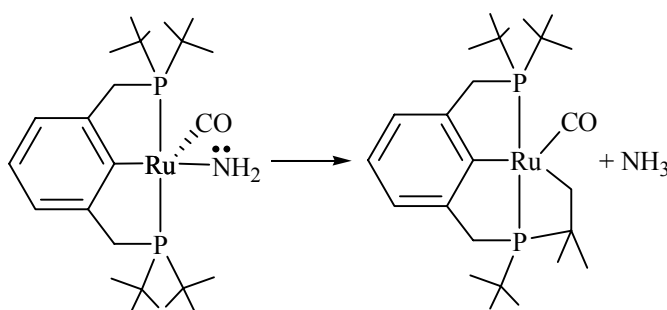
$(\text{PMe}_3)_4\text{Ru(H)(D)}$ and NDH_2 .^{19,46} For these reactions, the addition of two equivalents of PMe_3 to the reaction was reported dramatically suppress the rate of activation. The likely effect of the excess PMe_3 would hinder H_2 coordination. Thus, in the absence of a coordination site, these Ru(II) amido complexes are unable to activate the H-H bond. The inertness of the coordinatively saturated Ru(II) amido complexes suggest the activation of H_2 by the unsaturated amido complex $(\text{PCP})\text{Ru(CO)NH}_2$ occurs in an intramolecular fashion.

5.4 C-H Bond Activation of Methane by $(\text{PCP})\text{Ru(CO)NH}_2$.

The activation of dihydrogen by $(\text{PCP})\text{Ru(CO)NH}_2$ suggests the possibility of related transformations for other non-polar bonds such as C-H bonds. Generally, H_2 activation is more facile than C-H activation because H_2 activation has a greater thermodynamic driving force. Specifically, The bond dissociation energies of M-H bonds are approximately 60 kcal/mol, while M-C bonds are approximately 30-45 kcal/mol; the H-H bond dissociation energy is approximately 104 kcal/mol, and a typical C-H bond dissociation energy is of similar strength (95 kcal/mol for cyclohexane and 104

kcal/mol for methane).⁴⁷ Thus the products resulting from H-H activation are generally up to 20 kcal/mol more favorable than C-H activation. In addition, H-H bonds are less sterically demanding than C-H, and coordination of H-H is more facile.

Room temperature reactions of (PCP)Ru(CO)NH₂ with methane at 1 atm showed no reactivity after several hours (based on IR and ¹H NMR spectroscopy). Since coordination of a C-H bond of methane is more sterically demanding than H₂, similar reactions with methane in THF or benzene up to 50 psi and 50 °C were conducted. All attempted reactions with methane ultimately resulted in an intramolecular C-H activation of a ^tBu group of (PCP)Ru(CO)NH₂ to form a cyclometalated complex and ammonia (Scheme 5.19).



Scheme 5.19 (PCP)Ru(CO)NH₂ undergoes an intramolecular C-H activation with the ^tBu substituent to yield a cyclometalated complex and ammonia.

The cyclometalated complex is unstable and decomposes after a few days. The nature of the decomposition pathways is discussed below. This complex has been characterized by IR, ¹H, ¹³C, and ³¹P NMR spectroscopy. The IR spectrum reveals a CO absorption at 1897 cm⁻¹. The most salient features of the ¹H NMR spectrum are three doublets at 1.19, 1.00, and 0.71 ppm that each integrate for 9H due to the ^tBu groups. A 3H doublet is also observed at 0.90 ppm for the one of the methyl groups of the

cyclometalated ^tBu moiety; the other is not observed due to coincidental overlap. The methylene Ru-CH₂ protons are observed as a multiplet 0.44 ppm (Figure 5.8). The ³¹P NMR spectrum reveals doublets at 82.7 and 46.3 ppm with ²J_{PP} = 244 Hz (Figure 5.9).

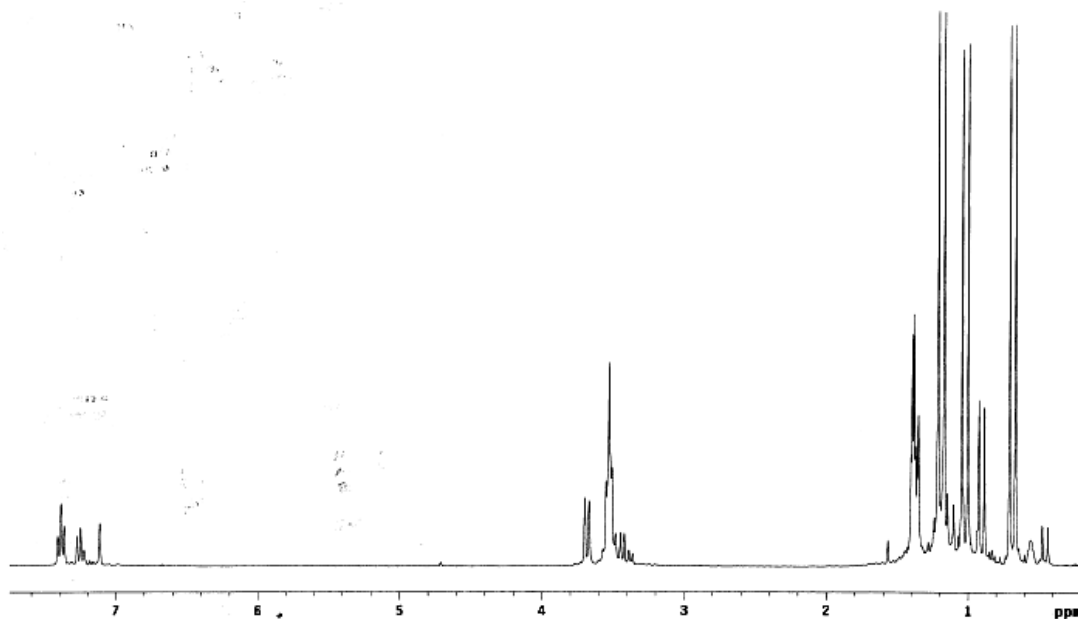


Figure 5.8 ¹H NMR spectrum of Ru(CO){C₆H₃-2-(CH₂P^tBu₂)-6-(CH₂P^tBu)-(CMe₂CH₂)} in C₆D₆.

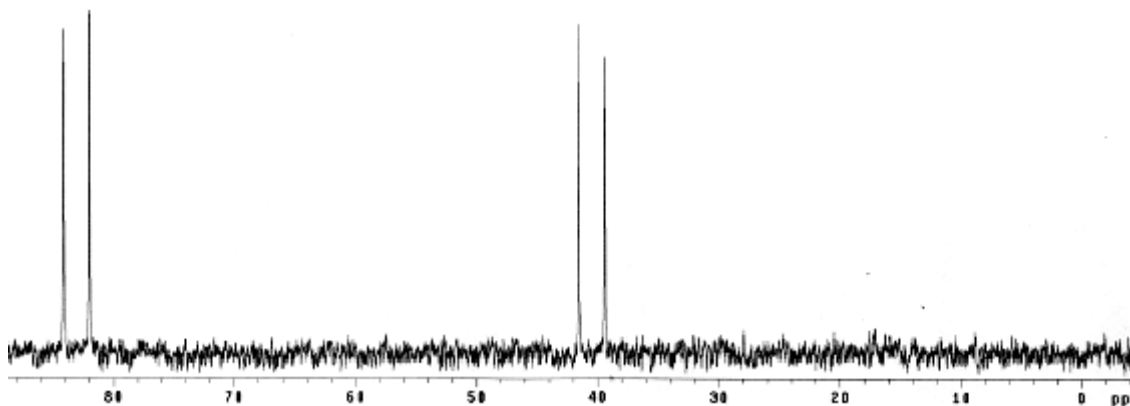
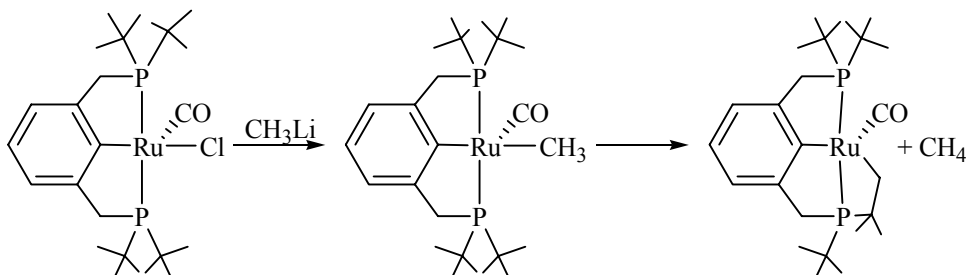


Figure 5.9 ³¹P NMR spectrum of Ru(CO){C₆H₃-2-(CH₂P^tBu₂)-6-(CH₂P^tBu)-(CMe₂CH₂)} in C₆D₆.

A related PCP iridium hydride complex (PCP)Ir(Cl)(H) has been observed in equilibrium with dihydrogen and a similar cyclometalated complex.⁴⁸ We attempted to determine if the ruthenium cyclometalated complex would establish a similar type equilibrium with ammonia or methane. These reactions would yield (PCP)Ru(CO)NH₂ or (PCP)Ru(CO)Me, respectively. Solutions of the cyclometalated complex in THF were placed under 50 psi pressure of ammonia or methane. Work up of reaction mixtures did not yield formation of (PCP)Ru(CO)NH₂ or (PCP)Ru(CO)Me. In addition, the ruthenium cyclometalated complex was not found to be in equilibrium based on ³¹P NMR spectroscopy. For the reaction with NH₃, two new sets of doublets were observed down field of the cyclometalated complex; however, the amido complex (PCP)Ru(CO)NH₂ was not observed in the ³¹P NMR spectrum. The second set of doublets observed in the reaction with NH₃ was attributed ammonia coordination to the cyclometalated complex. Additionally, ammonia coordination was confirmed by removing NH₃ by placing the solution under vacuum to reform the cyclometalated complex.

C-H bond activation of methane by (PCP)Ru(CO)NH₂ would result in formation of (PCP)Ru(CO)Me and ammonia. Since CH₄ activation was not observed, we wished to probe the stability of (PCP)Ru(CO)Me. The complex (PCP)Ru(CO)Me was independently prepared by reaction of (PCP)Ru(CO)Cl with methyl lithium. Like the amido complex, (PCP)Ru(CO)Me undergoes cyclometalation of a ^tBu group to release methane (Scheme 5.20). The formation of methane from the cyclometalation of (PCP)Ru(CO)Me has been confirmed using GC-MS.



Scheme 5.20 Methane C-H bond activation by $(\text{PCP})\text{Ru}(\text{CO})\text{NH}_2$ would form $(\text{PCP})\text{Ru}(\text{CO})\text{Me}$. This complex was synthesized by reacting $(\text{PCP})\text{Ru}(\text{CO})\text{Cl}$ with methyl lithium. The complex $(\text{PCP})\text{Ru}(\text{CO})\text{Me}$ undergoes cyclometalation.

$(\text{PCP})\text{Ru}(\text{CO})\text{Me}$ has been characterized by ^1H , ^{13}C , and ^{31}P NMR and IR spectroscopy. The IR spectrum of this complex shows a CO absorption at 1893 cm^{-1} , and salient features of the ^1H NMR spectrum include virtual triplets at 1.20 and 0.84 ppm for the ^tBu resonances of the PCP ligand and a triplet for the methyl ligand at 0.24 ppm ($^3J_{\text{PH}} = 4\text{ Hz}$) (Figure 5.10).

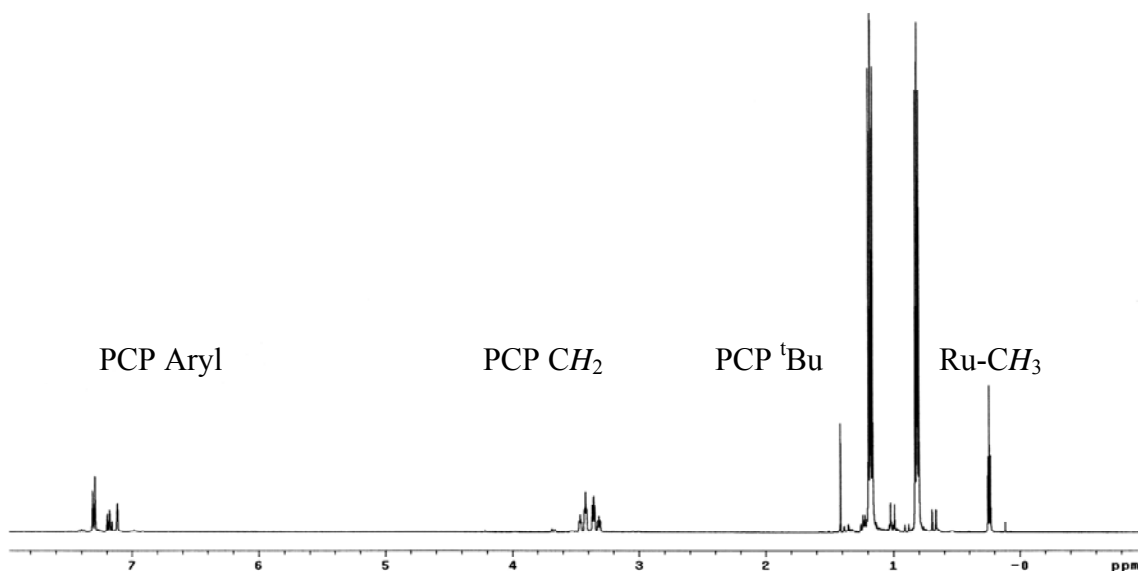


Figure 5.10 ^1H NMR spectrum of $(\text{PCP})\text{Ru}(\text{CO})\text{Me}$ in C_6D_6 .

The rate of conversion of the methyl complex to the cyclometalated complex is approximately 5 times faster ($k_{\text{obs}} = 3.2(1) \times 10^{-4} \text{ s}^{-1}$ at 50 °C) than the analogous conversion with the amido complex ($k_{\text{obs}} = 6.0(3) \times 10^{-5} \text{ s}^{-1}$ at 50 °C). Figure 5.11 shows first order kinetic plots at 40 °C.

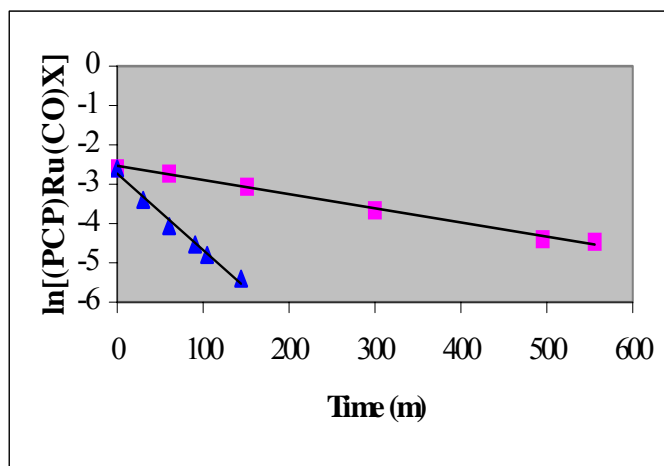


Figure 5.11 First order kinetic plot time for cyclometalation of (PCP)Ru(CO)Me and (PCP)Ru(CO)NH₂ at 40 °C (■ = (PCP)Ru(CO)NH₂ and ▲ = (PCP)Ru(CO)Me).

To determine the differences between the methyl ligand versus amido ligand impact on these reactions the activation parameters ΔH^\ddagger and ΔS^\ddagger were determined using an Eyring plot. The Eyring equation (equation 5.1; see Chapter 2) can be used to determine the entropy and enthalpy of activation by measuring the rate of reaction over a range of temperatures.⁴⁹

$$k = k_b T/h * e^{(-\Delta G^\ddagger/RT)} \quad \text{Eq. 5.1}$$

where

T is the temperature (K)

R is the universal gas constant (8.31 J K⁻¹ mol⁻¹)

k_b is the Boltzmann constant (1.38 * 10⁻²³ J K⁻¹)

h is Planck's constant ($6.63 \times 10^{-34} \text{ J s}^{-1}$)

Given $\Delta G = \Delta H - T\Delta S$, equation 5.1 can be rearranged to equation 5.2

$$k = k_b T/h * e^{(-\Delta H^\ddagger/RT)} * e^{(-\Delta S^\ddagger/T)} \quad \text{Eq. 5.2}$$

or

$$\ln(k/T) = -\Delta H^\ddagger/RT + \Delta S^\ddagger/R + \ln(k_b/h) \quad \text{Eq. 5.3}$$

Using equation 5.3, the activation parameters are determined by plotting the $\ln(k_{\text{obs}}/T)$ vs. $1/T$. The slope of this plot is equal to $-\Delta H^\ddagger/R$ and the intercept can be used to calculate ΔS^\ddagger .⁴⁹ Eyring plots provide accurate activation parameters if the reaction rate can be measured over a sufficient temperature range. The entropy of activation is more sensitive to the temperature range since small changes in the slope can translate into large shifts of the intercept.

Eyring plots were made over a 30 °C temperature range for the complexes (PCP)Ru(CO)NH₂ and (PCP)Ru(CO)Me to the cyclometalated complex and ammonia and methane respectively (Figure 5.12). The ΔH^\ddagger for both reactions is 18(1) kcal/mol. The ΔS^\ddagger for the conversion of complex (PCP)Ru(CO)NH₂ to the cyclometalated complex and ammonia is -23(4) eu, while the ΔS^\ddagger for the production of cyclometalated complex and methane from (PCP)Ru(CO)Me is -18(4) eu. Both reactions involve C-H bond breaking of a methyl group, thus the enthalpy gain for N-H or C-H bond forming in combination with Ru-N and Ru-C bond breaking must be nearly identical. Given that the C-H bond dissociation energy of methane is 104 kcal/mol and the N-H bond dissociation energy of ammonia is 86 kcal/mol, this result is somewhat surprising because the increased bond

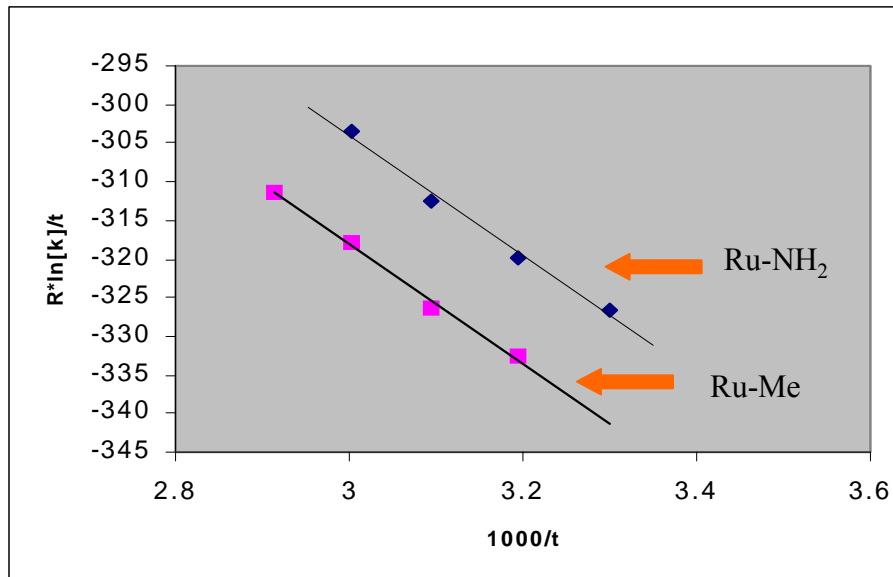


Figure 5.12 Eyring plots for the cyclometalation reactions of (PCP)Ru(CO)(X) (X = Me or NH₂). The ΔH^\ddagger for both reactions is 18(1) kcal/mol, and the ΔS^\ddagger is -23(4) and -18(4) for NH₂ and Me respectively.

strength of methane relative to ammonia should result in lower ΔH^\ddagger for (PCP)Ru(CO)Me relative to (PCP)Ru(CO)NH₂.^{47,50} The comparable ΔH^\ddagger for cyclometalation of (PCP)Ru(CO)Me and (PCP)Ru(CO)NH₂ suggest the difference could be due to the difference between the respective Ru-Me and Ru-NH₂ bond strengths as well as the extent of bond breaking. Specifically, the Ru-CH₃ bond forms a weakly bound C-H bond while Ru-NH₂ forms a stronger Ru-NH₃ bond. The results of the Eyring plots reveal that the difference in reaction rates result primarily from entropic factors; this has been attributed to methane leaving versus ammonia coordination in the transition state

Since both (PCP)Ru(CO)NH₂ and (PCP)Ru(CO)Me undergo cyclometalation, methane activation by (PCP)Ru(CO)NH₂ could occur but the product would remain unobserved. Isotopic labeling reaction using CD₄ should reveal if the amido ligand

initiates C-H activation of methane because this reaction would produce NDH_2 . However, a control experiment of a solution of the cyclometalated complex in the presence of a mixture of CH_4 and ND_3 revealed significant isotopic scrambling to produce CH_3D and ND_2H after approximately 1 hour (as determined by mass spectrometry; Figure 5.13). Therefore, production of NH_2D from the reaction of $(\text{PCP})\text{Ru}(\text{CO})\text{NH}_2$ with CD_4 would not allow differentiation between direct production of NH_2D and isotopic scrambling between NH_3 and CD_4 to produce NH_2D .

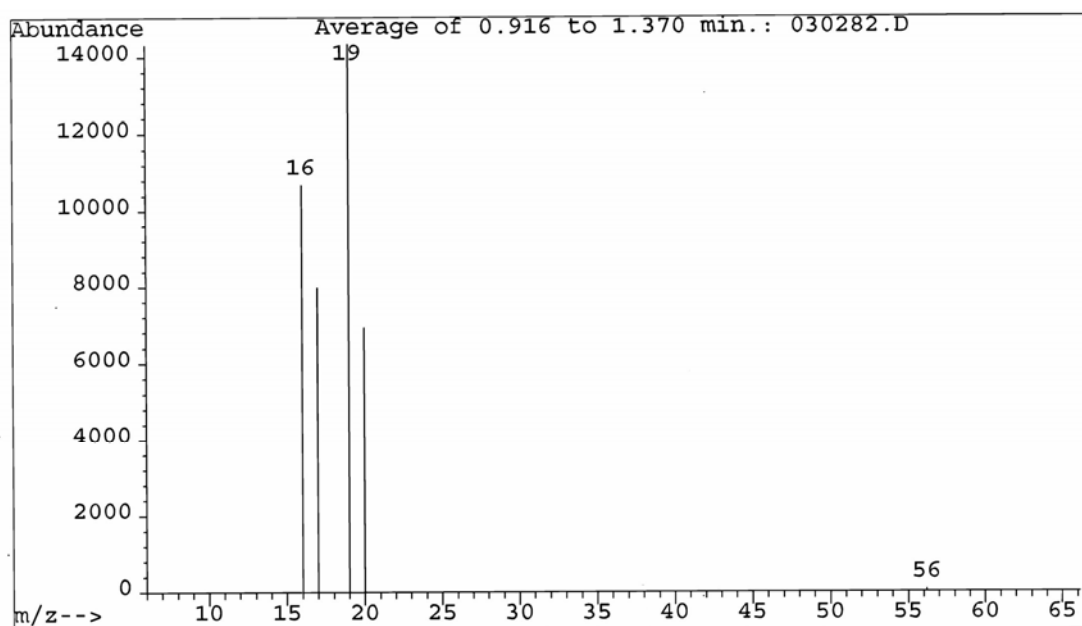
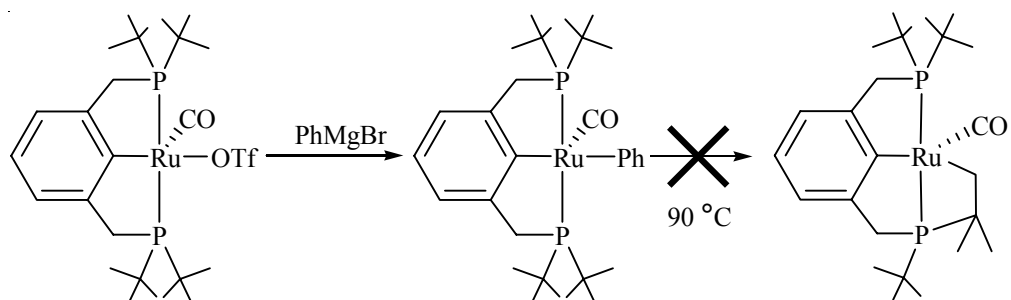


Figure 5.13 Mass spectrometry spectrum of the reaction of the cyclometalated complex and CH_4 and ND_3 . Isotopic scrambling prevented the determination of whether the amido complex $(\text{PCP})\text{Ru}(\text{CO})\text{NH}_2$ activates methane.

5.5 Attempted C-H Bond Activation of Benzene.

Initial difficulties with the activation of methane prompted us to attempt C-H activation reactions with hydrocarbons where bond activation would presumably be more facile. Since an ammonia N-H bond is formed and the Ru-N bond is going from an amido to amine regardless of hydrocarbon, the only difference in these activation reactions results from the R-H bond dissociation energy and M-R bond energy of the metal-hydrocarbyl bond being formed. Thus, we sought a reagent where such transformations would likely be more kinetically and thermodynamically favorable. Jones et al. have studied the oxidative addition of hydrocarbons in detail and found that oxidative addition favors the strongest C-H bond because this activation yields stronger M-C bond.^{51,52} The difference in the C-H bond strength of methane and benzene is 5 kcal/mol (104 versus 109 kcal/mol respectively).^{47,50} Thus, despite cleaving a stronger C-H bond, the thermodynamic loss is made up by energy gain in the energy of the M-C bond formation because metal aryl bonds are typically 10-20 kcal/mol stronger than metal-alkyl bonds. In addition, arenes are typically better ligands than alkanes.

As an independent check of the stability of the product of benzene activation by (PCP)Ru(CO)NH₂, the complex (PCP)Ru(CO)Ph was prepared by reaction of a THF solution of (PCP)Ru(CO)OTf with phenylmagnesiumbromide (Scheme 5.21). Unlike the amido and methyl complex, (PCP)Ru(CO)Ph was found to be quite robust. In the solid state, this complex is stable for several weeks, and in solutions of THF or benzene heated to 90 °C (PCP)Ru(CO)Ph shows no signs of decomposition after several days



Scheme 5.21 (PCP)Ru(CO)Ph is the anticipated product of benzene activation by (PCP)Ru(CO)NH₂. This complex was independently prepared by reaction of (PCP)Ru(CO)OTf and phenylmagnesiumbromide.

(based on IR and ¹H NMR spectroscopy). Thus (PCP)Ru(CO)Ph does not convert to the cyclometalated complex and benzene (Figure 5.21).

Monitoring reactions of benzene solutions of the amido complex (PCP)Ru(CO)NH₂ between room temperature and 50 °C by ¹H NMR and ³¹P NMR spectroscopy reveal conversion to the cyclometalated complex without formation of the product of benzene activation (PCP)Ru(CO)Ph. Considering the relative stability of (PCP)Ru(CO)Ph, C-H activation of benzene is likely not occurring. Whether this result was due to unfavorable thermodynamics for C-H cleavage, steric hindrance preventing benzene coordination or other kinetic issues has not been definitively determined.

5.6 Theoretical Studies of C-H versus H-H Bond Activation by (PCP)Ru(CO)NH₂.

The observations of H-H bond activation by (PCP)Ru(CO)NH₂ and intramolecular C-H activation with failure to achieve intermolecular C-H activation of methane or benzene prompted us to incorporate theoretical studies of these reactions. Professor Tom Cundari of the University of North Texas performed all theoretical calculations. DFT (density functional theory; B3LYP/SBK(d) level of theory) studies

were used to compare the energetics of X-H activation ($X = \text{H}$ or CH_3) by $(\text{PCP}')\text{Ru}(\text{CO})\text{NH}_2$ ($\text{PCP}' = 2,6\text{-(CH}_2\text{PH}_2)_2\text{C}_6\text{H}_3$).

PCP' was used to model the full PCP ligand and is generated by the replacement of the phosphine ^tBu substituents with hydrogen atoms. A variety of coordination isomers were investigated for the $(\text{PCP}')\text{Ru}(\text{CO})\text{NH}_2$ complex. In all cases, (both square pyramidal and trigonal bipyramidal geometries) the bound carbon and phosphorus atoms of the PCP' ligand were assumed to be meridonal (i.e., the P-C-P fragment is roughly coplanar with Ru). Two isomeric $(\text{PCP}')\text{Ru}(\text{CO})\text{NH}_2$ minima were found, both of which had psuedo square pyramidal geometry. Consistent with the structures of $(\text{PCP}')\text{Ru}(\text{CO})\text{NH}_2$ determined by these computational studies, the complexes $(\text{PCP})\text{M}(\text{CO})(\text{Cl})$ ($\text{M} = \text{Ru}$ or Os) exhibit square pyramidal structures in the solid state.^{23,53} The higher energy isomer of $(\text{PCP}')\text{Ru}(\text{CO})\text{NH}_2$ has CO trans to the aryl ring of the PCP' ligand and is 15.6 kcal/mol higher in energy (ΔG) than the lowest energy minimum found for $(\text{PCP}')\text{Ru}(\text{CO})\text{NH}_2$, in which the coordination site trans to the aryl ring of the PCP' ligand is vacant (Figure 5.14). The lower energy minimum was used in the calculation of all subsequent thermodynamic quantities.

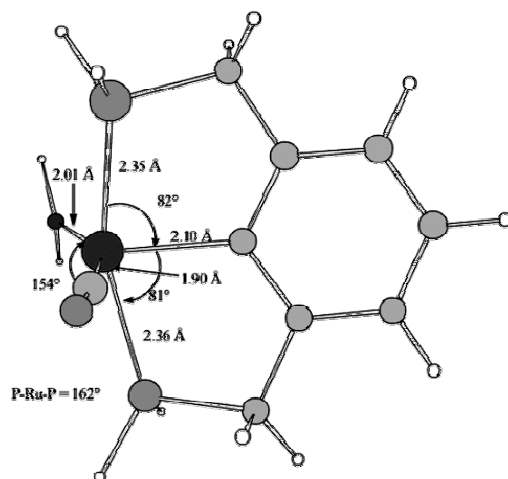


Figure 5.14 B3LYP/SBK(d) optimized geometry of (PCP')Ru(CO)(NH₂) model reactant showing pertinent bond lengths and bond angles as calculated by Prof. Tom Cundari of the University of North Texas.

Calculations of the energies of the dihydrogen and methane activation reactions by (PCP')Ru(CO)NH₂ were performed. As with the calculations for (PCP')Ru(CO)(NH₂), a variety of coordination isomers of the product (PCP')Ru(CO)(NH₃)(X) were investigated at the B3LYP/SBK (d) level of theory for both X = methyl and hydrogen. The most stable isomers found were used in the calculation of reaction enthalpies and reaction free energies. For dihydrogen activation, the reaction with (PCP)Ru(CO)NH₂ is exothermic by 16.9 kcal/mol and exoergic by 8.9 kcal/mol. The corresponding C-H activation of methane is strikingly different, being endothermic by 3.7 and endoergic by 13.6 kcal/mol. Hence, the calculations are in qualitative agreement with experimental observations. That is, (PCP)Ru(CO)NH₂ activates dihydrogen but not methane. In comparison to the attempted activation of methane, the entropy change for the

intramolecular C-H activation to yield the metallacycle complex should be more favorable and provide a driving force.

Perhaps the most interesting aspect of the computational comparison of dihydrogen versus methane activation is that the methane activation is endothermic rather than less exothermic than the dihydrogen activation. To understand the calculated endothermic nature of the methane activation, further calculations were carried out. First, the bond dissociation energies of dihydrogen and Me-H were calculated as an internal check. The enthalpies of the reactions are 105.3 kcal/mol (for H-H cleavage) and 101.9 kcal/mol (for C-H cleavage of methane). These numbers are in reasonable agreement with the experimental values. One can estimate the enthalpy of activation in terms of the appropriate bond enthalpies as shown in equation 5.4.

$$\Delta H \approx \text{BDE}_{\text{Ru-NH}_2} + \text{BDE}_{\text{X-H}} - \text{BDE}_{\text{Ru-NH}_3} - \text{BDE}_{\text{N-H}} - \text{BDE}_{\text{Ru-X}} \quad \text{Eq 5.4}$$

Calculation of the Ru-H bond enthalpy of (PCP')Ru(CO)(NH₃)(H) yields a value of 71.6 kcal/mol. Consistent with known differences in metal-alkyl versus metal-hydride bond dissociation energies, the corresponding Ru-CH₃ bond enthalpy (47.5 kcal/mol) is 24.1 kcal/mol weaker than the ruthenium-hydride bond enthalpy. This Ru-H/Ru-Me bond enthalpy difference is consistent with the difference in enthalpies for the activation of H₂ versus CH₄ ($\Delta\Delta H = 20.7$ kcal/mol).

More relevant in the context of the present research to identify novel hydrocarbon functionalization systems is the root cause of the surprising endothermicity of methane activation by (PCP')Ru(CO)NH₂. A significant enthalpic gain is expected by replacing a single C-H bond of methane with the N-H and Ru-C bonds of the

(PCP)Ru(CO)(Me)(NH₃) product. This gain is estimated to be 32 kcal/mol from the relevant B3LYP/SBK(d) bond enthalpies (Figure 5.15).

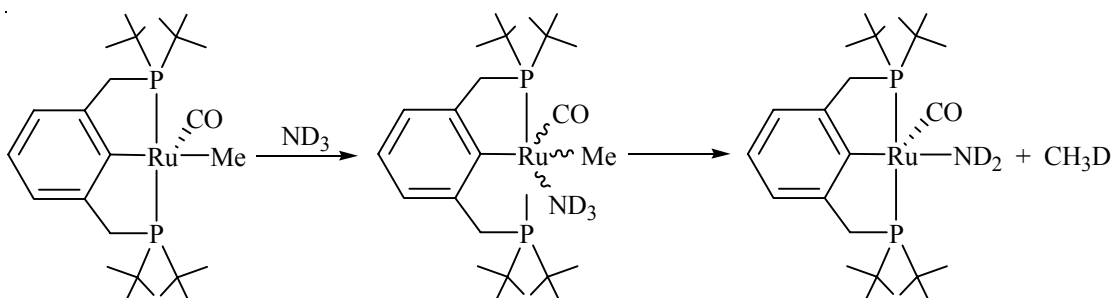
<i>Bonds Broken</i>	<i>Bonds Formed</i>
C-H = 102 kcal/mol	N-H = 86 kcal/mol
	Ru-C = 48 kcal/mol
102 kcal/mol -	134 kcal/mol = -32 kcal/mol

Figure 5.15 Based on theoretical calculations of methane activation, this reaction is anticipated to be thermodynamically favorable; however, a significant enthalpic loss for the Ru-N bond occurs in the transition from a non-dative amido ligand to a dative ammine ligand.

The only other potential source of a significant change in enthalpy is the conversion of the ruthenium-nitrogen linkage from a nondative amido to a dative ammine bond {although minor perturbations might be anticipated, the ΔH 's due to the Ru-phosphine, Ru-aryl, and Ru-CO bonds are unlikely to be substantial since both reactants and products are Ru(II)}. Clearly, if a change in enthalpy of the ruthenium-nitrogen bond is substantial and unfavorable, it is anticipated that methane activation would be prohibited. Indeed, calculation of the BDEs for Ru-NH₃ and Ru-NH₂ indicates that the difference is significant: BDE_{Ru-NH₂} = 52.5 kcal/mol; BDE_{Ru-NH₃} = 12.6 kcal/mol; Δ BDE = 39.9 kcal/mol. The calculations of a small BDE for the Ru-NH₃ linkage is consistent with the general experimental observation that ammonia is weakly coordinated to the (PCP)Ru(CO)(X)(NH₃) systems. The loss of approximately 40 kcal/mol upon converting from an amide to ammine linkage more than cancels the approximately 32 kcal/mol gain

due to breaking the methane C-H bond and forming Ru-CH₃ and N-H bonds and provides an explanation for the calculated endothermic nature of the methane activation.

The DFT calculations suggest that (PCP)Ru(CO)(NH₃)(Me) conversion to (PCP)Ru(CO)NH₂ and methane should be thermodynamically favorable. Experimentally, the addition of ammonia to (PCP)Ru(CO)Me forms an equilibrium between (PCP)Ru(CO)(Me)(NH₃) and (PCP)Ru(CO)(Me)/NH₃, and the mixture converts to methane and the cyclometalated complex (Scheme 5.22). However, whether the



Scheme 5.22 Addition of NH₃ to solutions of (PCP)Ru(CO)Me result in formation of the amine complex (PCP)Ru(CO)(Me)(NH₃). Subsequently, this amine complex converts to the cyclometalated complex.

formation of the cyclometalated complex and methane was derived from complex (PCP)Ru(CO)Me or (PCP)Ru(CO)(Me)(NH₃) cannot be definitively determined. In principle, isotopic labeling should allow for conformation of the reaction in scheme 5.22. The coordination of ND₃ and subsequent activation to yield the amido complex would form CH₃D, which is observable by ¹H NMR or mass spectrometry. However, isotopic labeling studies were not useful due to H/D scrambling in the presence of the cyclometalated complex. Specifically, solutions of the cyclometalated complex in C₆D₆ were treated with CH₄ and ND₃. GC/MS analysis of the head space of these reactions after approximately 1-2 hours revealed deuterium incorporation into methane to from

CH₃D. Since the reaction of (PCP)Ru(CO)Me with ND₃ yields the cyclometalated complex, it is not possible to determine if the deuterium incorporation into methane occurs due to initial formation of (PCP)Ru(CO)ND₂ or H/D scrambling after the this reaction.

For the reaction of (PCP)Ru(CO)Me and NH₃, the rate of cyclometalation for (PCP)Ru(CO)Me upon addition of NH₃ (1.5 equiv based ¹H NMR spectroscopy) was observed to be more rapid ($k_{\text{obs}} = 1.2 \times 10^{-4} \text{ s}^{-1}$ at 30 °C) than in the absence of ammonia ($k_{\text{obs}} = 5.5 \times 10^{-5} \text{ s}^{-1}$ at 30 °C; Figure 5.16). This result suggests the possibility of a direct conversion of (PCP)Ru(CO)(Me)(NH₃) to the cyclometalated complex and methane. Such a pathway would require the initial formation of (PCP)Ru(CO)NH₂ and methane with subsequent conversion of (PCP)Ru(CO)NH₂ to ammonia and the cyclometalated complex. However, the lack of observation of (PCP)Ru(CO)NH₂ as an intermediate in this reaction precludes a definitive conclusion on the feasibility of this pathway.

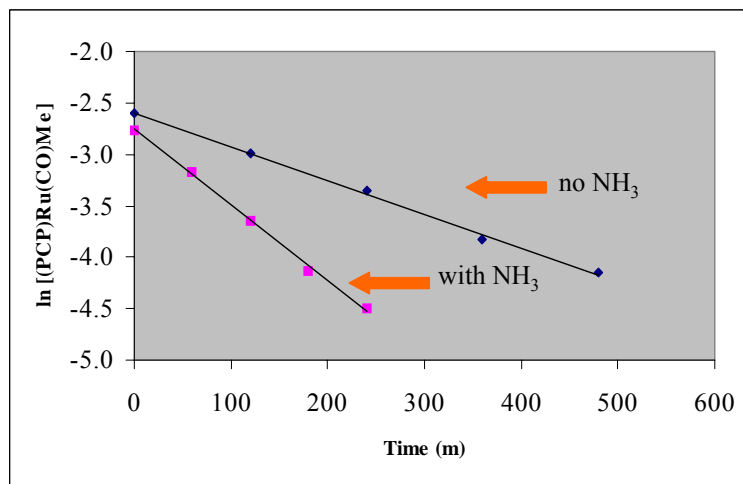
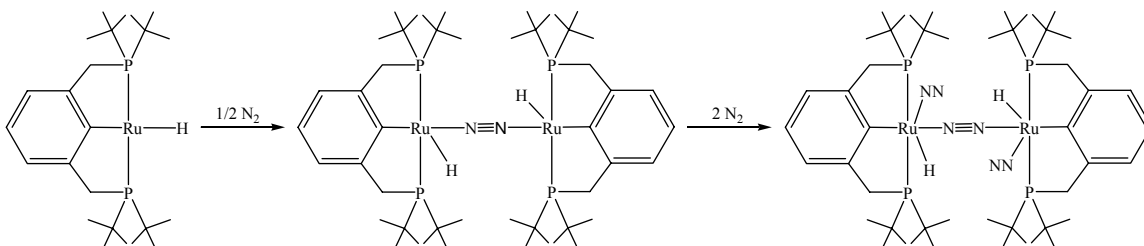


Figure 5.16 The addition of NH₃ increases the rate of disappearance of (PCP)Ru(CO)Me, possibly due to formation of (PCP)Ru(CO)NH₂ from methane elimination from (PCP)Ru(CO)(Me)(NH₃).

5.7 Reactivity of the Cyclometalated Complex.

The cyclometalated complex is air and moisture sensitive. In addition, isolation of this complex in the solid state, under N_2 atmosphere revealed complete conversion to an unidentified product after approximately 24 hours. While under vacuum or argon atmosphere, the cyclometalated complex stable for up to one week. Discussed below is a second decomposition pathway that was discovered to occur under nitrogen free conditions. Based on the dependence of dinitrogen on this decomposition pathway for the cyclometalated complex, N_2 is likely to be involved. Ruthenium(II) complexes with pincer ligands have been found to coordinate N_2 . For example, the complex $(PCP)Ru(CO)H$ was found to coordinate half an equivalent of N_2 to form a dimer that could subsequently pick up two equivalents of N_2 (Scheme 5.23).^{20,38} In addition, similar



Scheme 5.23 The Ru(II) pincer complex $(PCP)RuH$ has been reported to form nitrogen complexes by formation of a dimer that can subsequently add two equivalents of N_2 .

N_2 complexes have been reported with PCP complexes of Ir and Rh.^{54,55,56}

The product of the decomposition of the cyclometalated complex under N_2 atmosphere has been characterized by 1H NMR and ^{31}P NMR spectroscopy. The 1H NMR spectrum of this decomposition product shows overlapping virtual triplets for the tBu resonances, as well as a singlet at 67.3 ppm in the ^{31}P NMR (Figure 5.17). Thus, four symmetry equivalent tBu groups are present, and addition of a hydrogen atom must

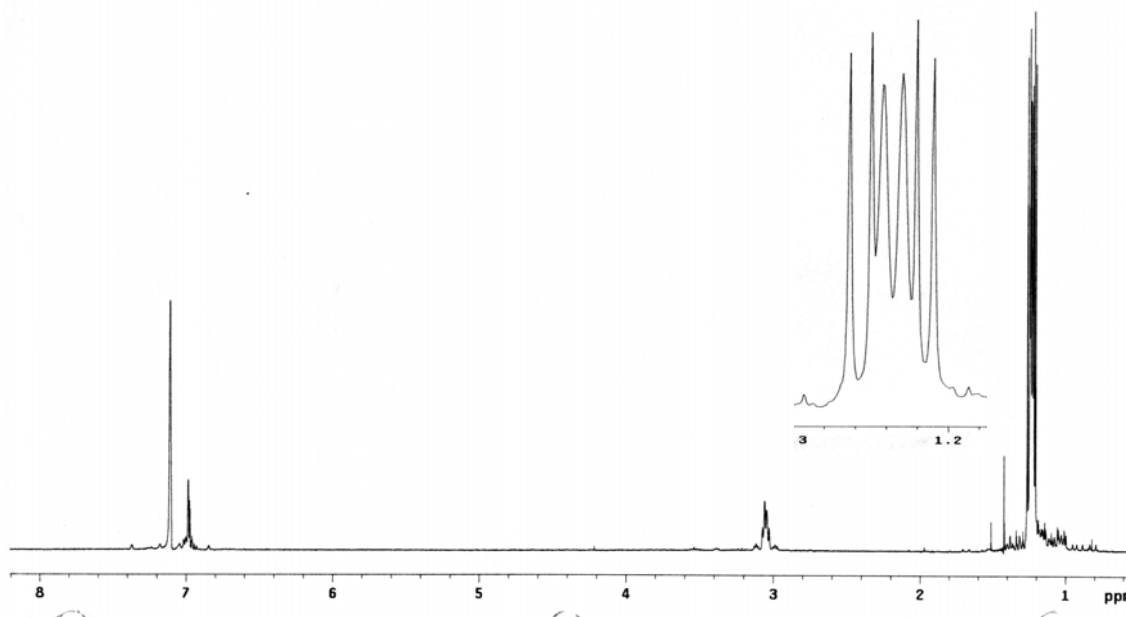


Figure 5.17 ^1H NMR spectrum of the decomposition product of the cyclometalated complex under N_2 atmosphere.

be involved in the formation of the product. All other ^1H NMR resonances can be assigned to the PCP ligand. Questions remain about the nature of this complex. First, what is the hydrogen source that allows for the formation of the C-H bond? Second what are the other ligand(s) in the coordination sphere? It seems likely that the hydrogen source could be residual solvent; however, this supposition remains untested. Also, it is believed that the ultimate product contains a bridging N_2 due to the observation that the cyclometalated complex reacts in the absence of N_2 to form a different product (see below), and no IR absorption(s) are observed in the anticipated range of a terminal dinitrogen ligand (from $2000\text{-}2200\text{ cm}^{-1}$).

Nitrogen free workup of the cyclometalated complex by isolation under vacuum or under an atmosphere of argon reveals transformation to a second product different than the one isolated under N_2 atmosphere. Monitoring a solution of the cyclometalated

complex in degassed C₆D₆ reveals the disappearance of the cyclometalated ^tBu moiety, and the formation of a multiplet at approximately 4.5 ppm. Also, the ³¹P NMR spectrum reveals two doublets at 99.3 and 76.5 ppm (²J_{PP} = 239 Hz). The multiplet has been assigned to isobutylene, and mass spectrometry of the headspace of this reaction revealed a product consistent with a C₄H₈ species (Figure 5.18). The isobutylene formed in this

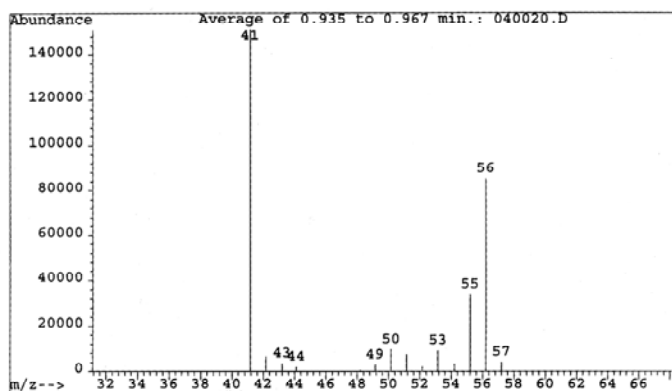
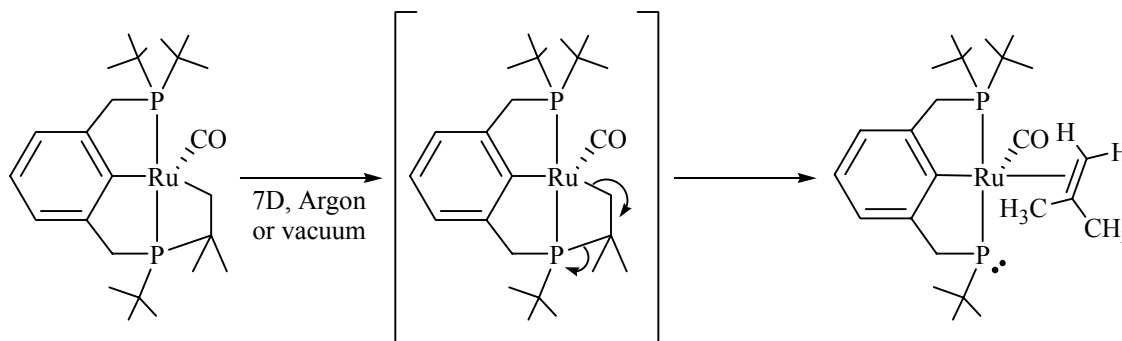


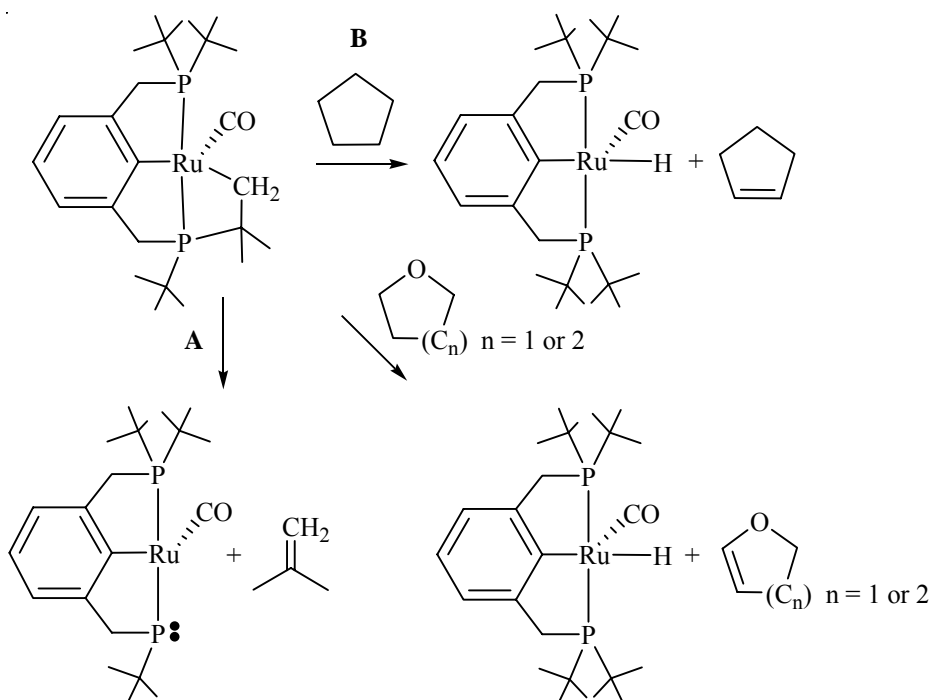
Figure 5.18 Mass spectrum of isobutylene.

reaction is likely due to cleavage of the cyclometalated ^tBu group. Thus, the product from decomposition of the cyclometalated complex in a N₂ free environment has been tentatively been assigned as a Ru(II) phosphido complex shown in Scheme 5.24.



Scheme 5.24 Conversion of the cyclometalated complex to a Ru(II) phosphido by elimination of isobutylene.

PCP metal centers are known to initiate dehydrogenation reactions with alkanes and THF.^{20,21} During the course of attempting to determine the nature of the cyclometalated decomposition pathway, degassed THF, tetrahydropyran, or cyclopentane solutions of the cyclometalated complex were observed to undergo reactions to form (PCP)Ru(CO)H. In these reactions the formation of the phosphido complex was also observed. Analysis of the reaction mixtures by GC/MS revealed the small amounts of the dehydrogenation products (i.e., cyclopentene, dihydrofuran, and dihydropyran) (Scheme 5.25). The ratio of the hydrocarbon dehydrogenation products based in integration of the



Scheme 5.25 Pathways for the decomposition of the cyclometalated complex. **A** -elimination of an isobutylene fragment. **B** - Initiation of dehydrogenation chemistry.

GC chromatograph was low relative to the yield of isobutylene; approximately 50%,

<5%, and <5% for cyclopentane, THF, and tetrahydropyran respectively. These results are consistent with two decomposition pathways for the cyclometalated complex (i.e., the cyclometalated complex can eliminate an isobutylene fragment or initiate dehydrogenation chemistry). Thus, the dehydrogenation pathway is kinetically competitive with the isobutylene elimination. Also, the qualitative yield of (PCP)Ru(CO)H was relative to the amount of hydrocarbon dehydrogenation product based on ^1H NMR spectroscopy. For example, work up the reaction of the cyclometalated complex with cyclopentane yielded approximately 33% (PCP)Ru(CO)H, while the reactions with THF and THP yields of (PCP)Ru(CO)H were much less < 5%. These observations are qualitative and this reaction has not been studied in detail. Nevertheless, the formation of (PCP)Ru(CO)H. is likely attributable to cyclometalated complex initiating dehydrogenation chemistry.

5.8 Experimental Section.

General Methods. All reactions and procedures were performed under anaerobic conditions in a nitrogen-filled glovebox or by using standard Schlenk techniques. Glovebox purity was maintained by periodic nitrogen purges and monitored by an oxygen analyzer $\{\text{O}_2(\text{g}) < 15 \text{ ppm, for all reactions}\}$. Toluene was dried by passage through a column of activated alumina. THF and benzene were dried by distillation over sodium/benzophenone. Pentane and cyclopentane were dried by distillation over P_2O_5 . Benzene- d_6 was purified by distillation from CaH_2 , degassed, and stored over 4 Å sieves.

CDCl_3 , toluene- d_8 , and CD_2Cl_2 were degassed via three freeze-pump-thaw cycles and stored over 4 Å sieves. Room-temperature ^1H and ^{13}C NMR spectra were obtained on a Varian Mercury 400 or 300 MHz spectrometer. All ^1H and ^{13}C NMR spectra were referenced against tetramethylsilane using residual proton signals (^1H NMR) or the ^{13}C resonances of the deuterated solvent (^{13}C NMR). ^{31}P NMR spectra were obtained on a Varian 300 MHz (observed frequency 161 MHz) spectrometer and referenced against external 85% H_3PO_4 . All variable-temperature NMR experiments were performed on a Varian 400 MHz spectrometer. IR spectra were obtained on a Mattson Genesis II spectrometer either as thin films on a KBr plate or in a solution using a NaCl solution plate. Elemental analyses were performed by Atlantic Microlabs, Inc. The syntheses of $\text{TpRu}(\text{PMe}_3)_2(\text{NH}_2)$, $(\text{PCP})\text{Ru}(\text{CO})\text{Cl}$, and $(\text{PCP})\text{Ru}(\text{CO})(\text{H})$ have been previously reported.^{16,38} $[\text{Li}][\text{C}\equiv\text{CPh}]$ was prepared by addition of butyllithium to a benzene solution of phenylacetylene. The resulting white precipitate was collected via vacuum filtration and washed with hexanes. All other reagents were used as purchased from commercial sources.

$(\text{PCP})\text{Ru}(\text{CO})(\text{NH}_3)(\text{Cl})$. A screw cap NMR tube was charged with approximately 0.025 g of $(\text{PCP})\text{Ru}(\text{CO})\text{Cl}$ in 1 mL of CDCl_3 . Ammonia was bubbled through the solution until it turned from orange to pale yellow. The solution was shaken, then vented to relieve excess pressure, and NMR and IR spectra were acquired. Quantitative conversion to $(\text{PCP})\text{Ru}(\text{CO})(\text{NH}_3)\text{Cl}$ was observed by ^1H , ^{13}C , and ^{31}P NMR and IR; however, removal of excess NH_3 by purging or placing the solution under reduced pressure results in rapid and quantitative formation of the starting material

(PCP)Ru(CO)(Cl). IR (solution cell CDCl₃): $\nu_{\text{CO}} = 1900 \text{ cm}^{-1}$. ¹H NMR (CDCl₃, δ): 6.76 (2H, d, $^3J_{\text{HH}} = 7 \text{ Hz}$, phenyl 3/5 position), 6.60 (1H, t, $^3J_{\text{HH}} = 7 \text{ Hz}$, phenyl 4 position), 3.14 (4H, m, CH₂), 2.85 (3H, bs, NH₃), 1.17, 1.14 (each 18 H, each a vt, $N = 12 \text{ Hz}$, CH₃). ¹³C{¹H} NMR (CDCl₃, δ): 207.4 (t, $^2J_{\text{PC}} = 13 \text{ Hz}$, CO), 147.7 (t, $^2J_{\text{PC}} = 12 \text{ Hz}$, PCP phenyl), 128.4, 123.9 (each a s, PCP phenyl), 122.5 (vt, $N = 13 \text{ Hz}$, PCP phenyl), 37.4, (vt, $N = 14 \text{ Hz}$, PC), 36.8 (vt, $N = 10 \text{ Hz}$, PC), 36.3 (vt, $N = 20 \text{ Hz}$, CH₂), 31.7, 31.2 (each a vt, $N = 4 \text{ Hz}$, CH₃). ³¹P{¹H} NMR (CDCl₃, δ): 78.3.

(PCP)Ru(CO)(NH₂). (PCP)Ru(CO)(Cl) (0.0969 g, 0.1736 mmol) was dissolved in approximately 30 mL of THF. Approximately 10 mL of a saturated solution of NH₃ in THF was added. Upon combination of the two solutions, a color change from dark orange to yellow was observed. Sodium bis(trimethylsilyl) amide (0.190 mmol, 1.0 M in THF) was added dropwise using a microsyringe. Upon addition of the amide, a color change to dark orange was observed. The solution was filtered through a fine porosity frit, and the volatiles were removed under reduced pressure (0.0771 g, 0.143 mmol, 82%). Orange microcrystalline product was obtained upon recrystallization from pentane at -20 °C (isolated yield of the recrystallization is approximately 50%). IR (solution cell THF): $\nu_{\text{CO}} = 1890 \text{ cm}^{-1}$, $\nu_{\text{NH}} = 3396, 3306 \text{ cm}^{-1}$. ¹H NMR (C₆D₆, δ): 7.06 (2H, d, $^3J_{\text{HH}} = 8 \text{ Hz}$, phenyl 3/5 position), 6.98 (1H, t, $^3J_{\text{HH}} = 8 \text{ Hz}$, phenyl 4 position), 4.36 (2H, br t, $^3J_{\text{PH}} = 9 \text{ Hz}$, NH₂), 3.19 (2H, dt, $^2J_{\text{HH}} = 17 \text{ Hz}$, $J_{\text{PH}} = 7 \text{ Hz}$, CH₂), 3.09 (2H, dt, $^2J_{\text{HH}} = 17 \text{ Hz}$, $J_{\text{PH}} = 9 \text{ Hz}$, CH₂), 1.26, 1.14 (each 18H, each vt, $N = 12 \text{ Hz}$, CH₃). ¹³C{¹H} NMR (C₆D₆, δ): 212.5 (t, $^2J_{\text{PC}} = 11 \text{ Hz}$, CO), 169.1 (PCP phenyl), 149.1 (t, $^2J_{\text{PC}} = 7 \text{ Hz}$, PCP phenyl), 121.8 (s, PCP phenyl), 121.5 (vt, $N = 14 \text{ Hz}$, PCP phenyl), 36.4 (vt, $N = 22 \text{ Hz}$, P-CH₂),

36.3 (vt, $N = 13$ Hz, PC), 36.2 (vt, $N = 13$ Hz, PC), 30.1-29.9 (m, CH_3). $^{31}\text{P}\{\text{H}\}$ NMR (C_6D_6 , δ): 72.9. High-resolution FAB-MS: 539.2 (PCP) $\text{Ru}(\text{CO})(\text{NH}_2)$, 523.2 (PCP) $\text{Ru}(\text{CO})$. Note: Elemental analysis could not be obtained due to instability of the product. This complex undergoes intramolecular elimination of ammonia to form the cyclometalated complex in approximately 24 h.

(PCP)Ru(CO)(OTf). In a 100 mL round-bottom flask, (PCP) $\text{Ru}(\text{CO})\text{Cl}$ (0.0675 g, 0.1209 mmol) was dissolved in approximately 40 mL of cyclopentane. Approximately 1 mL of trimethylsilyltriflate was added dropwise at room temperature. After 30 min the formation of an orange solid was observed. The reaction was stirred for 1 h. After removal of volatiles under reduced pressure, the resulting solids were dissolved in approximately 10 mL of THF, and the products were precipitated upon addition of 30 mL of cyclopentane. Orange crystals were isolated by filtration through a medium porosity frit (0.0690 g, 0.1027 mmol, 85%). IR (solution cell THF): $\nu_{\text{CO}} = 1936$ cm^{-1} . ^1H NMR (CDCl_3 , δ): 7.09 (2H, d, $^3J_{\text{HH}} = 7$ Hz, phenyl 3/5 position), 6.93 (1H, t, $^3J_{\text{HH}} = 7$ Hz, phenyl 4 position), 3.37 (4H, vt, $N = 8$ Hz, CH_2), 1.50 (18 H, vt, $N = 14$ Hz, CH_3), 1.17 (18 H, vt, $N = 13$ Hz, CH_3). $^{13}\text{C}\{\text{H}\}$ NMR (CDCl_3 , δ): 204.9 (t, $^2J_{\text{PC}} = 12$ Hz, CO), 157.2 (s, phenyl 4 position), 152.7 (t, $^2J_{\text{PC}} = 7$ Hz, phenyl ipso), 125.4 (s, phenyl 3/5 positions), 123.3 (vt, $N = 16$ Hz, phenyl 2/6 positions), 38.0 (vt, $N = 14$ Hz, PC), 36.7 (vt, $N = 16$ Hz, PC), 33.7 (vt, $N = 22$ Hz, CH_2), 30.1 (vt, $N = 4$ Hz, CH_3), 29.4 (vt, $N = 4$ Hz, CH_3). $^{31}\text{P}\{\text{H}\}$ NMR (CDCl_3 , δ): 70.0. Anal. Calcd for $\text{C}_{26}\text{H}_{43}\text{F}_3\text{O}_4\text{P}_2\text{RuS}$: C 46.42, H 6.45. Found: C 46.28, H 6.58.

[(PCP)Ru(CO)(NH₃)₂][OTf]. In a 50 mL round-bottom flask, 0.0816 g (0.121 mol) of (PCP)Ru(CO)(OTf) was dissolved in approximately 15 mL of THF. A THF solution of ammonia was added until the solution turned from orange to colorless. The volatiles were removed under reduced pressure. The solids were dissolved in approximately 5 mL of THF, and the product was precipitated with approximately 30 mL of cyclopentane. Pale yellow crystals were isolated by filtration through a fine porosity frit (0.0439 g, 0.0621 mmol, 51%). IR (solution cell THF): $\nu_{\text{CO}} = 1923 \text{ cm}^{-1}$, $\nu_{\text{NH}} = 3415, 3358, 3292, 3203 \text{ cm}^{-1}$. ¹H NMR (CDCl₃, δ): 6.95 (2H, d, ³J_{HH} = 8 Hz, phenyl 3/5 positions), 6.80 (1H, t, ³J_{HH} = 8 Hz, phenyl 4 position), 3.35 (2H, dt, ²J_{HH} = 16 Hz, J_{PH} = 7 Hz, CH₂), 3.23 (2H, dt, ²J_{HH} = 16 Hz, J_{PH} = 7 Hz, CH₂), 2.50 (3H, bs, NH₃), 2.45 (3H, bs, NH₃), 1.33 (18H, vt, N = 13 Hz, CH₃), 1.26 (18H, vt, N = 12 Hz, CH₃). ¹³C{¹H} NMR (CDCl₃, δ): 207.4 (t, ²J_{PC} = 13 Hz, CO), 164.2 (s, PCP 4 position), 147.7 (t, ²J_{PC} = 6 Hz, RuC), 124.3 (s, PCP 5 and 5 positions), 122.9 (vt, N = 13 Hz, PCP 2 and 6 positions), 37.3 (vt, N = 15 Hz, PC), 36.6 (vt, N = 11 Hz, PC), 36.0 (vt, N = 20 Hz, P-CH₂), 31.3 (vt, N = 5 Hz, CH₃), 31.0 (vt, N = 5 Hz, CH₃). ³¹P{¹H} NMR (CDCl₃, δ): 78.2. Note: Elemental analysis could not be obtained because drying under reduced pressure for a prolonged period of time results in the dissociation of ammonia.

PCP)Ru(CO)(C≡CPh) Method A. (PCP)Ru(CO)(Cl) (0.1096 g, 0.1964 mmol) was dissolved in approximately 30 mL of THF. Approximately 10 mL of a saturated solution of NH₃ in THF were added. Upon addition of the ammonia solution, a color change from dark orange to yellow was observed. Sodium bis(trimethylsilyl)amide (0.216 mmol, 1.0 M in THF) was added dropwise using a microsyringe, and a change in

color to dark orange was observed. The solution was filtered through a fine porosity frit, and the volatiles were removed under reduced pressure. Approximately 25 mL of THF was added to dissolve all solids. Phenylacetylene (24 μL , 0.219 mmol) was added using a microsyringe. Upon addition, a color change to dark red orange was observed. The volatiles were removed under reduced pressure to yield a dark red product (0.1112 g, 0.1781 mmol, 91%).

Method B. (PCP)Ru(CO)(Cl) (0.0977 g, 0.1750 mmol) was dissolved in approximately 30 mL of toluene. The solution was cooled to $-78\text{ }^{\circ}\text{C}$. The salt [Li][C \equiv CPh] (0.021 g, 0.194 mmol) was added to the solution of (PCP)Ru(CO)(Cl). A color change to dark red-orange was observed upon addition of the lithium acetylide salt. The volatiles were removed under reduced pressure, and the product was extracted with cyclopentane and filtered through a fine porosity frit. Removal of volatiles from the resulting filtrate allowed the isolation of a dark red solid (0.0850 g, 0.1362 mmol, 78%). This procedure yields product that is pure by NMR spectroscopy; however, additional purification can be achieved by column chromatography on silica gel with THF as eluent. IR (solution cell THF): $\nu_{\text{CO}} = 1915\text{ cm}^{-1}$. ^1H NMR (CD_2Cl_2 , δ): 7.29 (2H, t, $^3J_{\text{HH}} = 8\text{ Hz}$, acetylide phenyl meta position), 7.23-7.17 (4H, m, overlapping PCP and acetylide phenyl), 7.09 (1H, t, $^3J_{\text{HH}} = 8\text{ Hz}$, phenyl para/4 position), 6.95 (1H, t, $^3J_{\text{HH}} = 8\text{ Hz}$, phenyl para/4 position), 3.63 (4H, vt, $N = 8\text{ Hz}$, PCP CH_2), 1.53, 1.18 (each 18H, each a vt, $N = 14\text{ Hz}$, CH_3). $^{13}\text{C}\{^1\text{H}\}$ NMR (CD_2Cl_2 , δ): 209.0 (t, $^2J_{\text{PC}} = 13\text{ Hz}$, CO), 179.4 (t, $^2J_{\text{PC}} = 3\text{ Hz}$, ipso phenyl), 152.5 (vt, $N = 15\text{ Hz}$, PCP 3,5 or 2,6 position), 131.7 (t, $^2J_{\text{PC}} = 11\text{ Hz}$, C \equiv CPh), 130.3 (t, $N = 1.4\text{ Hz}$, PCP 4 or Ph o, m, p), 129.8 (t, $^4J_{\text{PC}} = 0.8\text{ Hz}$, Ph

ipso), 128.1 (s, PCP 4 or Ph o, m, p), 127.8 (t, $^3J_{PC} = 1.1$ Hz, $C\equiv CPh$), 124.5 (s, PCP 4 or Ph o, m, p), 124.4 (s, PCP 4 or Ph o, m, p), 121.8 (vt, $N = 15$ Hz, PCP 3,5- or 2,6-position), 37.9 (vt, $N = 23$ Hz, CH_2), 37.8 (vt, $N = 15$ Hz, PC), 37.0 (vt, $N = 17$ Hz, PC), 30.0, 29.8 (each a vt, $N = 5$ Hz, CH_3). $^{31}P\{^1H\}$ NMR (CD_2Cl_2 , δ): 80.0. Anal. Calcd for $C_{33}H_{48}OP_2Ru$: C 63.54, H 7.76. Found: C 63.52, H 7.74.

(PCP)Ru(CO)(NH₃)H. A screw cap NMR tube was charged with approximately 0.025 g of (PCP)Ru(CO)(H) and 1 mL of C_6D_6 . Ammonia was gently bubbled through the solution until it turned from orange to pale yellow. The solution was vigorously mixed and vented to relieve excess pressure, and NMR and IR spectra were acquired. Quantitative conversion to (PCP)Ru(CO)(NH₃)(H) was observed by 1H , ^{13}C , and ^{31}P NMR and IR spectroscopy; however, removal of excess ammonia by purging the solution with dinitrogen or placing the solution under reduced pressure results in the rapid formation of the starting material (PCP)Ru(CO)(H). IR (solution cell THF): $\nu_{CO} = 1905$ cm^{-1} . 1H NMR (C_6D_6 , δ): 7.07 (2H, d, $^3J_{HH} = 9$ Hz, phenyl 3/5 position), 6.98 (1H, t, $^3J_{HH} = 9$ Hz, phenyl 4 position), 3.26 (2H, dt, $^2J_{HH} = 16$ Hz, $J_{PH} = 8$ Hz, CH_2), 3.19 (2H, dt, $^2J_{HH} = 17$ Hz, $J_{PH} = 6$ Hz, CH_2), 1.18, 1.06 (each 18 H, each a vt, $N = 12$ Hz, CH_3), -16.17 (1H, t, $^2J_{PH} = 21$ Hz). The resonance due to bound NH_3 is not observed possibly due to overlap with a tBu resonance. $^{13}C\{^1H\}$ NMR (C_6D_6 , δ): 208.1 (t, $^2J_{PC} = 13$ Hz, CO), 149.9 (t, $^2J_{PC} = 11$ Hz, PCP phenyl), 123.4 (s, PCP phenyl), 122.5 (vt, $N = 16$ Hz, PCP phenyl), 39.4, (vt, $N = 14$ Hz, PC), 36.8 (vt, $N = 9$ Hz, PC), 36.5 (vt, $N = 21$ Hz, CH_2), 30.0-29.7 (m, overlapping CH_3); note: missing one PCP phenyl resonance possibly

due to coincidental overlap. ^{31}P NMR (hydrogen coupled; C_6D_6 , δ): 95.7 (d, $^2J_{\text{PH}} = 21$ Hz).

$\text{Ru}(\text{CO})\{\text{C}_6\text{H}_3\text{-2-(CH}_2\text{P}^t\text{Bu}_2\text{)-6-(CH}_2\text{P}^t\text{Bu})(\text{CMe}_2\text{CH}_2)\}$. In a 100 mL round-bottom flask, (PCP)Ru(CO)Cl (0.3837 g, 0.6876 mmol) was dissolved in approximately 50 mL of THF. Methyllithium (1.6 M in THF, 0.907 mmol) was added dropwise using a microsyringe. The volatiles were removed under reduced pressure, and the solids were dissolved in benzene. The solution was allowed to stir at room temperature for 48 h. Filtration of the solution through a fine porosity frit and removal of the volatiles under reduced pressure yielded a brown solid (0.3337 g, 0.6404 mmol, 93%). IR (solution cell benzene): ν_{CO}) 1897 cm^{-1} . ^1H NMR (C_6D_6 , δ): 7.37 (1H, d, $^3J_{\text{HH}} = 7$ Hz, phenyl 3/5 position), 7.34 (1H, d, $^3J_{\text{HH}} = 7$ Hz, phenyl 3/5 position), 7.22 (1H, t, $^3J_{\text{HH}} = 7$ Hz, phenyl 4 position), 3.67 (2H, d, $^2J_{\text{PH}} = 8$ Hz CH_2), 3.47 (1H, dd, $^2J_{\text{HH}} = 17$ Hz, $^2J_{\text{PH}} = 10$ Hz, P- CH_2), 3.37 (1H, dd, $^2J_{\text{HH}} = 17$ Hz, $^2J_{\text{PH}} = 6$ Hz CH_2), 1.37 (3H, d, $^3J_{\text{PH}} = 13$ Hz, $\text{PC}(\text{CH}_3)_2$), 1.19 (9H, d, $^3J_{\text{PH}} = 13$ Hz, $\text{PC}(\text{CH}_3)_3$), 1.00 (9H, d, $^3J_{\text{PH}} = 13$ Hz, $\text{PC}(\text{CH}_3)_3$), 0.90 (3H, d, $^3J_{\text{PH}} = 12$ Hz, $\text{PC}(\text{CH}_3)_2$), 0.71 (9H, d, $^3J_{\text{PH}} = 12$ Hz, $\text{PC}(\text{CH}_3)_3$), 0.49 (1H, d, $^2J_{\text{HH}} = 16$ Hz, Ru- CH_2), 0.44 (1H, d, $^2J_{\text{HH}} = 16$ Hz, Ru- CH_2). $^{13}\text{C}\{^1\text{H}\}$ NMR (C_6D_6 , δ): 207.4 (t, $^2J_{\text{PC}} = 13$ Hz, CO), 147.7 (t, $^2J_{\text{PC}} = 12$ Hz, phenyl ipso), 128.4 (s, phenyl 3/5 position), 123.9 (s, phenyl 4 position), 122.5 (vt, $N = 12$ Hz, phenyl 2/6 position), 37.4, (vt, $N = 14$ Hz, PC), 36.8 (vt, $N = 10$ Hz, PC), 36.3 (vt, $N = 20$ Hz, CH_2), 31.7, 31.2 (vt, $N = 4$ Hz, CH_3). $^{31}\text{P}\{^1\text{H}\}$ NMR (C_6D_6 , δ): 82.7 (d, $^2J_{\text{PP}} = 245$ Hz, P^tBu_2), 46.3 {d, $^2J_{\text{PP}} = 244$ Hz, $\text{P}^t\text{Bu}(\text{CMe}_2\text{-CH}_2)$ }. Note: satisfactory elemental analysis could not be obtained

due to instability of the product. This complex reacts to form an unidentified product in approximately 48 h at room temperature.

(PCP)Ru(CO)(CH₃). In a 100 mL round-bottom flask, (PCP)Ru(CO)Cl (0.0557 g, 0.0997 mmol) was dissolved in approximately 50 mL of THF. Methyllithium (1.6 M in the, 0.136 mmol) was added dropwise using a microsyringe. The volatiles were removed under reduced pressure, and the solids were dissolved in benzene. The solution was filtered through a fine porosity frit, and the volatiles were removed under reduced pressure to yield a brown solid (0.0471 g, 0.0877 mmol, 88%). Orange microcrystals were obtained upon recrystallization from pentane at -40 °C. IR (solution cell THF): $\nu_{\text{CO}} = 1893 \text{ cm}^{-1}$. ¹H NMR (C₆D₆, δ): 7.29 (2H, d, ³J_{HH} = 8 Hz, phenyl 3/5 position), 7.15 (1H, t, ³J_{HH} = 8 Hz, phenyl 4 position), 3.43 (2H, dt, ²J_{HH} = 17 Hz, J_{PH} = 7 Hz, P-CH₂), 3.32 (2H, dt, ²J_{HH} = 17 Hz, J_{PH} = 9 Hz, P-CH₂), 1.20, 0.84 (each 18 H, each a vt, N = 12 Hz, CH₃), 0.24 (3H, t, ³J_{PH} = 4 Hz). ¹³C{¹H} NMR (CDCl₃, δ): 208.7 (t, ²J_{PC} = 9 Hz, CO), 151.9 (t, ²J_{PC} = 11 Hz, RuC), 124.2 (s, PCP 4 position), 123.9 (s, PCP 3 and 5 position), 120.9 (vt, N = 17 Hz, PCP 2 and 6 position), 38.0 (vt, N = 15 Hz, PC), 37.6 (vt, N = 18 Hz, CH₂), 36.3 (vt, N = 13 Hz, PC), 31.2, 30.1 (each a vt, N = 5 Hz, CH₃). ³¹P{¹H} NMR (C₆D₆, δ): 84.9. Note: Elemental analysis could not be obtained due to instability of the product. This complex undergoes intramolecular elimination to form the cyclometalated complex after approximately 24 h.

Reaction of (PCP)Ru(CO)(NH₂) with H₂ at -78 °C. A screw cap NMR tube was charged with approximately 0.025 g of (PCP)Ru(CO)(NH₂) in 1 mL of toluene-*d*₈. The solution was cooled to -78 °C in a dry ice/acetone bath. Dihydrogen was bubbled through

the solution until the solution changed from orange to light yellow (approximately 5 min). The tube was kept at -78 °C until transferred to the NMR probe which was precooled to -50 °C. ^1H and ^{31}P NMR spectra were acquired at regular time intervals, allowing the observation of the formation of $(\text{PCP})\text{Ru}(\text{CO})(\text{H})(\text{NH}_3)$ as a reaction intermediate.

Reaction of $(\text{PCP})\text{Ru}(\text{CO})(\text{NH}_2)$ with $\text{PhC}\equiv\text{CH}$ at -78 °C. A screw cap NMR tube was charged with $(\text{PCP})\text{Ru}(\text{CO})(\text{NH}_2)$ (0.0311 g, 0.0577 mmol) in 1 mL of toluene- d_8 . The solution was cooled to -78 °C in a dry ice/acetone bath. Phenylacetylene (7 μL , 0.0637 mmol) was added via microsyringe. The tube was kept at -78 °C until transferred to the NMR probe which was precooled to -80 °C. Conversion to $(\text{PCP})\text{Ru}(\text{CO})(\text{C}\equiv\text{CPh})$ and NH_3 was observed in ^1H and ^{31}P NMR without observation of reaction intermediates.

Reaction of $\text{TpRu}(\text{PMe}_3)_2(\text{NH}_2)$ with H_2 . In a 50 mL round-bottom flask, $\text{TpRu}(\text{PMe}_3)_2(\text{NH}_2)$ was dissolved in approximately 20 mL of THF. Dihydrogen was bubbled through the solution for 2 h. The volatiles were removed under reduced pressure, and the resulting solids were dissolved in C_6D_6 to give a homogeneous solution. ^1H NMR spectroscopy revealed the presence of only $\text{TpRu}(\text{PMe}_3)_2(\text{NH}_2)$.

Kinetic Studies for the Cyclometalation of $(\text{PCP})\text{Ru}(\text{CO})(\text{NH}_2)$ or $(\text{PCP})\text{Ru}(\text{CO})(\text{Me})$. The general procedures for all kinetic analyses of cyclometalation reactions for $(\text{PCP})\text{Ru}(\text{CO})(\text{Me})$ and $(\text{PCP})\text{Ru}(\text{CO})(\text{NH}_2)$ were similar. A representative procedure is provided: In a reaction vial, $(\text{PCP})\text{Ru}(\text{CO})(\text{Me})$ (0.1251 g, 0.2320 mmol) was dissolved in 2.96 g of C_6D_6 . A small amount of Cp_2Fe was added as an internal standard. The solution was transferred into three screw cap NMR tubes, and ^1H NMR

spectra were acquired with the delay time set to 10 s. The solutions were then heated in an oil bath. The disappearance of complex (PCP)Ru(CO)(Me) was monitored at regular time intervals using ^1H NMR spectroscopy. The formation of the cyclometalated complex and methane was observed. In addition, the formation of methane and ammonia (for reactions with (PCP)Ru(CO)(NH₂)) was confirmed by GC/MS analysis.

Computational Methods. Quantum calculations were carried out using the Gaussian 98 package.⁵⁷ The B3LYP hybrid functional was employed for all calculations.⁵⁸ Heavy atoms were described with the Stevens relativistic effective core potentials (ECPs) and valence basis sets (VBSs).^{59,60} The valence basis sets of main group elements were augmented with a d polarization function. This ECP/VBS combination, termed SBK(d), has been validated for the calculation of a wide variety of transition metal properties in previous studies.^{61,62,63,64} All stationary points were fully optimized without symmetry constraint. All species investigated are closed-shell singlets. Several conformations of the different ligands were investigated by torsion about the appropriate metal-ligand bonds; the lowest energy conformers found were used in the analyses given below. The energy Hessian was calculated at all stationary points to characterize them as minima (no imaginary frequencies). The quoted energies include zero-point, enthalpy, and entropic corrections determined from unscaled vibrational frequencies calculated at the B3LYP/SBK(d) level of theory. All energetic determinations were done at 298.15 K and 1 atm.

References.

- ¹ Labinger, J. A.; Bercaw, J. E. *Nature* **2002**, *417*, 507-514.
- ² Crabtree, R. H. *Chem. Rev.* **1995**, *95*, 987-1007.
- ³ Stahl, S. S.; Labinger, J. A.; Bercaw, J. E. *Angew. Chem. Int. Ed.* **1998**, *37*, 2180-2192.
- ⁴ Walsh, P. J.; Hollander, F.J.; Bergman, R.G. *J. Am. Chem. Soc.* **1988**, *110*, 8729-8731.
- ⁵ Cummins, C. C.; Baxter, S. M.; Wolczanski, P. T. *J. Am. Chem. Soc.* **1988**, *110*, 8731-8733.
- ⁶ Wolcaanzki, P. T.; Bennett, J. L. *J. Am. Chem. Soc.* **1994**, *116*, 2179-2180.
- ⁷ Cundari, T. R.; Klinckman, T. R.; Wolczanski, P. T. *Am. Chem. Soc.* **2002**, *124*, 1481-1487.
- ⁸ Bennett, J. L.; Wolczanski, P. T. *J. Am. Chem. Soc.* **1997**, *119*, 10696-10719.
- ⁹ Jonas, R. T.; Stack, T. D. P. *J. Am. Chem. Soc.* **1997**, *119*, 8566-8567.
- ¹⁰ Goldsmith, C. R.; Jonas, R. T.; Stack, T. D. P. *J. Am. Chem. Soc.* **2002**, *124*, 83-96.
- ¹¹ Meyer h atom
- ¹² Mayer, J. M. *Acc. Chem. Res.* **1998**, *31*, 441-450.
- ¹³ Fulton, R. J.; Bouwkamp, M. W.; Bergman, R. G. *J. Am. Chem. Soc.* **2000**, *122*, 8799-8800.
- ¹⁴ Fulton, J. R.; Sklenak, S.; Bouwkamp, M. W.; Bergman, R. G. *J. Am. Chem. Soc.* **2002**, *124*, 4722-4737.
- ¹⁵ Fox, D. J.; Bergman, R. G. *Organometallics* **2004**, *23*, 1656-1670.
- ¹⁶ Jayaprakash, K. N.; Conner, D.; Gunnoe, T. B. *Organometallics* **2001**, *20*, 5254-5256.
- ¹⁷ Conner, D.; Jayaprakash, K. N.; Wells, M. B.; Manzer, S.; Gunnoe, T. B.; Boyle, P. D. *Inorg. Chem.* **2003**, *42*, 4759-4772.
- ¹⁸ Conner, D.; Jayaprakash, K. N.; Gunnoe, T. B.; Boyle, P. D. *Inorg. Chem.* **2002**, *41*, 3042-3049.
- ¹⁹ Holland, A. W.; Bergman, R. G. *J. Am. Chem. Soc.* **2002**, *124*, 14684-14695.
- ²⁰ Van der Boom, M. E. ; Milstein, D. *Chem. Rev.* **2003**, *103*, 1759-1792.
- ²¹ Jensen, C. M. *Chem. Comm.* **1999**, 2443-2449.
- ²² Moulton, C. J.; Shaw, B. L. *J. Chem. Soc. Dalton Trans.* **1976**, 1020-1024.
- ²³ Gusev, D. G.; Madott, M.; Dolgushin, F. M.; Lyssenko, K. A.; Antipin, M. Y. *Organometallics* **2000**, *19*, 1734-1739.
- ²⁴ Sun, N. Y.; Simpson, S. J. *J. Organomet. Chem.* **1992**, *434*, 341-349,
- ²⁵ Zhang, J.; Gunnoe, T. B. *Unpublished results.*
- ²⁶ Kaplan, A. W.; Ritter, J. C. M.; Bergman, R. G. *J. Am. Chem. Soc.* **1998**, *120*, 6828-6829.
- ²⁷ Fulton, R.J.; Holland, A. W.; Fow, D. J.; Bergman, R. G. *Acc. Chem. Res.* **2002**, *35*, 44-56.
- ²⁸ Zhang, J.; Gunnoe, T. B.; Boyle, P. D. *Organometallics* **2004**, *23*, 3094-3097.
- ²⁹ Zhang, J.; Gunnoe, T. B. *unpublished results.*
- ³⁰ Forbus, T. R.; Martin, J. C. *J. Org. Chem.* **1979**, *44*, 313-314.
- ³¹ Abdur-Rashid, K.; Fong, T. P.; Greaves, B.; Gusev, D. G.; Hinman, J. G.; Landau, S. E.; Lough, A. J.; Morris, R. J. *J. Am. Chem. Soc.* **2000**, *122*, 9155-9171.

-
- ³² Jia, G.; Lau, C.-P. *Coord. Chem. Rev.* **1999**, *190-192*, 83-108.
- ³³ Kubas, G. J.; Ryan, R. R.; Swanson, B. I.; Vergamini, P. J.; Wasserman, H. J. *J. Am. Chem. Soc.* **1984**, *106*, 451-452.
- ³⁴ Meisler, G. L.; Tarr, D. A. *Inorganic Chemistry 2nd ed.*; Prentice Hall: Upper Saddle River, NJ, **1998**; pp 445-446.
- ³⁵ Kubas, G. J. *Acc. Chem. Res.* **1988**, *21*, 120-128.
- ³⁶ Crabtree, R. H. *Acc. Chem. Res.* **1990**, *23*, 120-128.
- ³⁷ Ontko, A. C.; Houllis, J. F.; Schnabel, C.; Roddick, D. M.; Fong T.P.; Lough, A. J.; Morris, R. H. *Organometallics* **1998**, *17*, 5467-5476.
- ³⁸ Gusev, D. G.; Dolgushin, F. M.; Antipin, M. Y. *Organometallics* **2000**, *19*, 3429-3434.
- ³⁹ Glueck, D. S.; Newman Winslow, L. J.; Bergman, R. G. *Organometallics* **1991**, *10*, 1462-1479.
- ⁴⁰ Kanzelberger, M.; Zhang, X.; Emge, T. J.; Goldman, A. S.; Zhao, J.; Incarvito, C.; Hartwig, J. F. *J. Am. Chem. Soc.* **2003**, *125*, 13644-13645.
- ⁴¹ Morris, R. H.; Earl, K. A.; Luck, R. L.; Lazarowich, N. J.; Sella, A. *Inorg. Chem.* **1987**, *26*, 2647-2683.
- ⁴² Tenorio, M. J.; Tenorio, M. A.; Puerta, M. C.; Valerga, P. *Inorg. Chem. Acta.* **1997**, *259*, 77-84.
- ⁴³ Trimmel, G.; Glugovc, C.; Wiede, P.; Mereiter, K.; Sapunov, V. N.; Schmid, R.; Kirchner, K. *Inorg. Chem.* **1997**, *36*, 1076-1083.
- ⁴⁴ *Organometallics*, **1996**, *15*, 4565-4574.
- ⁴⁵ *Organometallics*, **2004**, *23*, 1424-1433.
- ⁴⁶ Holland, A. W.; Bergman, R. G. *J. Am. Chem. Soc.* **2002**, *124*, 14684-14696.
- ⁴⁷ Crabtree, R. H. *The Organometallic Chemistry of the Transition Metals 3rd ed.*; John Wiley & Sons: New York, **2001**.
- ⁴⁸ Mohammad, H. A. Y.; Grimm, J. C.; Eichele, K.; Mack, H.-G.; Speiser, B.; Novak, F.; Quintanilla, M. G.; Kaska, W. C.; Mayer, H. A. *Organometallics* **2002**, *21*, 5775-5784.
- ⁴⁹ Atwood, J. D. *Inorganic and Organometallic Reaction Mechanisms 2nd ed.*; Wiley-VCH: New York, **1997**.
- ⁵⁰ McMurry, J. *Organic Chemistry 4th ed.*; Brooks Cole Pub. Co.: Pacific Grove, CA, **1995**, pp 162-164.
- ⁵¹ Jones, W. D.; Hessel, E. T. *J. Am. Chem. Soc.* **1993**, *115*, 554-562.
- ⁵² Wick, D. D.; Jones, W. D. *Organometallic* **1999**, *18*, 495-500.
- ⁵³ Gusev, D. G.; Dolgushin, F. M.; Antipin, M. Y. *Organometallics* **2001**, *20*, 1001-1007.
- ⁵⁴ Vigalok, A.; Milstein, D. *Organometallics* **2000**, *19*, 2061-2064.
- ⁵⁵ Van der Boom, M. E.; Ben-David, Y.; Milstein, D. *J. Am. Chem. Soc.* **1999**, *121*, 6652-6656.
- ⁵⁶ Lee, D. W.; Jensen, C. M.; Morales, D. *Organometallics* **2003**, *22*, 4744-4749.
- ⁵⁷ Frisch, M. J.; Trucks, G. W.; Schlegel, H. B.; Scuseria, G. E.; Robb, M. A.; Cheeseman, J. R.; Zakrzewski, V. G.; Jr., J. A. M.; Stratmann, R. E.; Burant, J. C.; Dapprich, S.; Millam, J. M.; Daniels, A. D.; Kudin, K. N.; Strain, M. C.; Farkas, O.; Tomasi, J.; Barone, V.; Cossi, M.; Cammi, R.; Mennucci, B.; Pomelli, C.; Adamo, C.;

Clifford, S.; Ochterski, J.; Petersson, G. A.; Ayala, P. Y.; Cui, Q.; Morokuma, K.; Malick, D. K.; Rabuck, A. D.; Raghavachari, K.; Foresman, J. B.; Cioslowski, J.; Ortiz, J. V.; Baboul, A. G.; Stefanov, B. B.; Liu, G.; Liashenko, A.; Piskorz, P.; Komaromi, I.; Gomperts, R.; Martin, R. L.; Fox, D. J.; Keith, T.; Al-Laham, M. A.; Peng, C. Y.; Nanayakkara, A.; Challacombe, M.; Gill, P. M. W.; Johnson, B.; Chen, W.; Wong, M. W.; Andres, J. L.; Gonzalez, C.; Head-Gordon, M.; Replogle, E. S.; Pople, J. A. *Gaussian 98, Revision A.9*; Pittsburgh, PA, **1998**.

⁵⁸ Becke, A. D. *J. Chem. Phys.* **1993**, *98*, 5648-5652.

⁵⁹ Stevens, W. J.; Basch, H.; Krauss, M. *J. Chem. Phys.* **1984**, *81*, 6026-6033.

⁶⁰ Stevens, W. J.; Krauss, M.; Basch, H.; Jasien, P. G. *Can. J. Chem.* **1992**, *70*, 612-613.

⁶¹ Cundari, T. R.; Klinckman, T. R.; Wolczanski, P. T. *J. Am. Chem. Soc.* **2002**, *124*, 1481-1487.

⁶² Holland, P. L.; Cundari, T. R.; Perez, L. L.; Eckert, N. A.; Lachicotte, R. J. *J. Am. Chem. Soc.* **2002**, *124*, 14416-14424.

⁶³ Veige, A. S.; Slaughter, L. M.; Wolczanski, P. T.; Matsunaga, N.; Decker, S. A.; Cundari, T. R. *J. Am. Chem. Soc.* **2001**, *123*, 6419-6420.

⁶⁴ Bergman, R. G.; Cundari, T. R.; Gillespie, A. M.; Gunnoe, T. B.; Harman, W. D.; Klinckman, T. R.; Temple, M. D.; White, D. P. *Organometallics* **2003**, *22*, 2331-2337.

Appendix A: Crystallographic Data and Structural Refinements

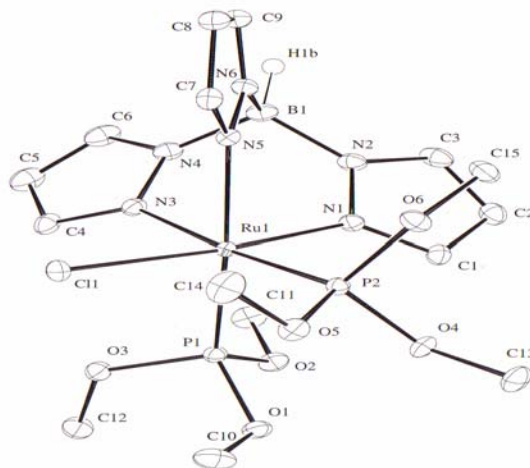


Figure A1 ORTEP diagram of $\text{TpRu}\{\text{P}(\text{OMe})_3\}_2\text{Cl}$

Table A.1 Crystal Data and Structure Refinement for $\text{TpRu}\{\text{P}(\text{OMe})_3\}_2\text{Cl}$

Identification code	x01026
Empirical formula	$\text{C}_{15}\text{H}_{28}\text{BClN}_6\text{O}_6\text{P}_2\text{Ru}$
Formula weight	597.70
Temperature	148 K
Wavelength	.71073
Crystal system	Monoclinic
Space group	P 21/n
Unit cell dimensions	
a	9.6277(3) Å
b	17.2937(5) Å
c	14.3109(4) Å

Table A.1 (continued)

α	90.00 °
β	90.00 °
χ	90.00 °
Volume	2359.96(12) Å ³
Z	4
Density (calculated)	1.682 Mg/m ³
Absorption Coefficient	.96
F(000)	1213.02
Crystal size	.40 x .36 x.24 mm
θ range for data collected	16.50 to 18.00
Limiting indices	-12 ≤ h ≤ 12, 0 ≤ k ≤ 22, 0 ≤ l ≤ 18
Reflections collected	5636
Independent reflections	5093
Absorption correction	psi-scan
Max and min transmission	0.9166 and 0.9977
Refinement method	Full matrix least squares of F ²
Data/restraints/parameters	0 / 0 / 294
Goodness of fit on F ²	2.57
Final R indices [I>2σ(I)]	R1 = 0.025, wR2 = 0.034
Final R indices (all data)	R1 = 0.025, wR2 = 0.034
Largest diff. peak and hole	-0.640 and 0.670 eÅ ⁻³

Table A.2 Atomic Coordinates and Thermal Parameters (x, y, z and u) for
TpRu{P(OMe)₃}₂Cl

	x	y	z	u
Ru1	.220074(16)	.239895(9)	.599555(11)	.00822(8)
Cl1	.25653(5)	.31888(3)	.74085(3)	.0137(2)
P1	.34041(6)	.32334(3)	.52229(4)	.0106(2)
P2	.00992(5)	.29125(3)	.54766(4)	.0097(2)
O1	.27712(16)	.39958(9)	.46790(11)	.0147(7)
O2	.40631(16)	.29172(9)	.43199(11)	.0152(7)
O3	.47462(16)	.35568(9)	.59115(11)	.0154(7)
O4	-.00201(15)	.32081(9)	.44150(10)	.0128(7)
O5	-.04959(16)	.36609(9)	.59602(10)	.0136(7)
O6	-.12634(16)	.23732(9)	.55110(11)	.0147(7)
N1	.19993(18)	.16276(10)	.48728(12)	.0115(8)
N2	.22839(19)	.08618(10)	.50348(13)	.0140(8)
N3	.41183(19)	.18045(10)	.65136(12)	.0123(8)
N4	.41668(19)	.10169(11)	.64215(13)	.0144(8)
N5	.12831(18)	.15085(10)	.67661(12)	.0113(7)
N6	.17143(19)	.07603(10)	.66885(12)	.0123(8)
B1	.2828(3)	.05648(14)	.60405(18)	.0148(11)
C1	.1574(2)	.17047(13)	.39462(15)	.0144(10)
C2	.1577(2)	.09891(14)	.34974(15)	.0174(10)
C3	.2031(3)	.04717(13)	.42095(16)	.0187(10)
C4	.5372(2)	.20255(14)	.69642(15)	.0162(10)
C5	.6239(2)	.13804(15)	.71699(18)	.0227(11)
C6	.5442(2)	.07570(14)	.68173(17)	.0206(10)
C7	.0376(2)	.15040(13)	.73935(15)	.0136(9)

C8	.0214(2)	.07531(13)	.77304(15)	.0163(9)
C9	.1090(2)	.03009(13)	.72648(15)	.0157(9)
C10	.2145(2)	.45737(14)	.52231(18)	.0209(12)
C11	.5045(2)	.22760(14)	.44465(17)	.0197(10)
C12	.5777(2)	.40239(14)	.55371(17)	.0200(11)
C13	-.1306(2)	.35128(14)	.38984(16)	.0173(10)
C14	-.0907(2)	.36247(15)	.68945(16)	.0203(11)
C15	-.1394(2)	.16235(13)	.50627(16)	.0172(10)
H1b	.306(3)	-.0096(16)	.6059(19)	.022(7)
H1	.131	.218	.363	.0243
H2	.132	.088	.284	.0276
H3	.215	-.007	.413	.0291
H4	.563	.255	.712	.0260
H5	.718	.137	.749	.0324
H6	.574	.023	.685	.0307
H7	-.010	.195	.759	.0234
H8	-.037	.059	.818	.0264
H9	.123	-.025	.734	.0255
H10a	.181	.500	.482	.0312
H10b	.137	.435	.549	.0312
H10c	.283	.476	.572	.0312
H11a	.535	.215	.385	.0302
H11b	.584	.242	.489	.0302
H11c	.460	.183	.468	.0302
H12a	.650	.417	.604	.0300
H12b	.618	.373	.507	.0300
H12c	.533	.448	.526	.0300

H13a	-.115	.366	.327	.0268
H13b	-.203	.313	.386	.0268
H13c	-.160	.396	.422	.0268
H14a	-.123	.412	.706	.0307
H14b	-.164	.325	.690	.0307
H14c	-.011	.348	.734	.0307
H15a	-.227	.139	.516	.0268
H15b	-.137	.168	.440	.0268
H15c	-.064	.130	.533	.0268

Table A.3 Anisotropic Displacement Parameters for $\text{TpRu}\{\text{P}(\text{OMe})_3\}_2\text{Cl}$

	u11	u22	u33	u12	u13	u23
Ru1	.00820(9)	.00843(9)	.00780(9)	-.00002(6)	.00025(6)	.00032(6)
Cl1	.0159(2)	.0140(2)	.0109(2)	-.00147(18)	.00041(18)	-.00244(18)
P1	.0100(2)	.0111(3)	.0107(2)	-.00051(19)	.00134(19)	.00113(19)
P2	.0090(2)	.0102(2)	.0098(2)	.00043(19)	.00038(18)	-.00016(19)
O1	.0143(7)	.0123(7)	.0169(8)	.0011(6)	.0003(6)	.0037(6)
O2	.0163(7)	.0169(8)	.0133(7)	.0015(6)	.0052(6)	.0020(6)
O3	.0122(7)	.0186(8)	.0146(7)	-.0047(6)	-.0004(6)	.0031(6)
O4	.0111(7)	.0166(8)	.0101(7)	.0032(6)	-.0003(6)	.0027(6)
O5	.0148(7)	.0136(7)	.0127(7)	.0036(6)	.0025(6)	-.0008(6)
O6	.0120(7)	.0137(8)	.0182(8)	-.0019(6)	.0020(6)	-.0008(6)
N1	.0116(8)	.0104(8)	.0126(9)	.0008(7)	.0015(6)	-.0004(7)
N2	.0173(9)	.0101(9)	.0150(9)	.0002(7)	.0039(7)	-.0008(7)
N3	.0121(8)	.0130(9)	.0116(8)	.0006(7)	.0008(7)	.0017(7)
N4	.0139(9)	.0129(9)	.0165(9)	.0039(7)	.0025(7)	.0027(7)
N5	.0121(8)	.0112(8)	.0101(8)	-.0005(7)	-.0001(6)	.0018(7)
N6	.0137(8)	.0096(8)	.0134(8)	-.0001(7)	.0014(7)	-.0001(7)
B1	.0167(12)	.0116(11)	.0167(12)	.0025(9)	.0047(9)	.0020(9)
C1	.0148(10)	.0164(11)	.0117(10)	-.0006(8)	.0009(8)	-.0011(8)
C2	.0197(11)	.0204(12)	.0127(10)	-.0041(9)	.0037(8)	-.0040(9)
C3	.0249(12)	.0132(11)	.0193(11)	-.0036(9)	.0078(9)	-.0054(9)
C4	.0111(10)	.0233(12)	.0136(10)	-.0014(9)	.0000(8)	.0032(9)
C5	.0128(11)	.0301(14)	.0244(12)	.0042(9)	-.0001(9)	.0089(10)
C6	.0158(11)	.0229(12)	.0233(12)	.0079(9)	.0036(9)	.0081(10)
C7	.0124(10)	.0158(11)	.0121(10)	-.0001(8)	.0002(8)	-.0010(8)
C8	.0170(10)	.0178(11)	.0143(10)	-.0042(8)	.0029(8)	.0034(9)

C9	.0180(10)	.0124(10)	.0159(10)	-.0022(8)	-.0008(8)	.0033(8)
C10	.0193(11)	.0136(11)	.0307(13)	.0016(9)	.0066(10)	.0025(9)
C11	.0201(11)	.0203(12)	.0203(11)	.0055(9)	.0081(9)	.0008(9)
C12	.0161(11)	.0235(12)	.0203(11)	-.0077(9)	.0026(9)	.0028(9)
C13	.0144(10)	.0200(11)	.0160(10)	.0065(9)	-.0031(8)	.0017(9)
C14	.0208(11)	.0269(13)	.0143(11)	.0061(10)	.0062(9)	-.0033(9)
C15	.0154(10)	.0131(10)	.0219(11)	-.0039(8)	-.0016(8)	-.0011(9)

Table A.4 Bond Distances for $\text{TpRu}\{\text{P}(\text{OMe})_3\}_2\text{Cl}$

Ru1 C11	2.4252(5)	N4 C6	1.356(3)
Ru1 P1	2.2362(5)	N5 N6	1.368(2)
Ru1 P2	2.2404(5)	N5 C7	1.336(3)
Ru1 N1	2.0767(17)	N6 B1	1.548(3)
Ru1 N3	2.1534(18)	N6 C9	1.345(3)
Ru1 N5	2.1532(17)	B1 H1b	1.16(3)
P1 O1	1.6078(16)	C1 C2	1.395(3)
P1 O2	1.6118(16)	C1 H1	.960(2)
P1 O3	1.6132(16)	C2 C3	1.381(3)
P2 O4	1.5919(15)	C2 H2	.960(2)
P2 O5	1.6100(16)	C3 H3	.960(2)
P2 O6	1.6159(16)	C4 C5	1.401(3)
O1 C10	1.449(3)	C4 H4	.960(2)
O2 C11	1.452(3)	C5 C6	1.378(4)
O3 C12	1.439(3)	C5 H5	.960(2)
O4 C13	1.451(3)	C6 H6	.960(2)
O5 C14	1.447(3)	C7 C8	1.401(3)
O6 C15	1.444(3)	C7 H7	.960(2)
N1 N2	1.366(3)	C8 C9	1.386(3)
N1 C1	1.339(3)	C8 H8	.960(2)
N2 B1	1.550(3)	C9 H9	.960(2)
N2 C3	1.353(3)	C10 H10a	.960(2)
N3 N4	1.370(3)	C10 H10b	.960(2)
N3 C4	1.343(3)	C10 H10c	.960(3)
N4 B1	1.542(3)	C11 H11a	.960(2)

C11 H11b .960(2)
C11 H11c .960(2)
C12 H12c .960(2)
C13 H13a .960(2)
C13 H13b .960(2)
C13 H13c .960(2)
C14 H14a .960(2)

C12 H12a .960(2)
C12 H12b .960(2)
C14 H14b .960(3)
C14 H14c .960(2)
C15 H15a .960(2)
C15 H15b .960(2)
C15 H15c .960(2)

Table A.5 Bond Angles for $\text{TpRu}\{\text{P}(\text{OMe})_3\}_2\text{Cl}$

C11 Ru1 P1	91.351(19)	O5 P2 O6	96.45(8)
C11 Ru1 P2	94.207(19)	P1 O1 C10	117.62(14)
C11 Ru1 N1	173.81(5)	P1 O2 C11	118.71(13)
C11 Ru1 N3	87.89(5)	P1 O3 C12	120.17(14)
C11 Ru1 N5	89.90(5)	P2 O4 C13	123.17(13)
P1 Ru1 P2	94.94(2)	P2 O5 C14	121.43(14)
P1 Ru1 N1	91.80(5)	P2 O6 C15	121.74(14)
P1 Ru1 N3	90.01(5)	Ru1 N1 N2	119.76(13)
P1 Ru1 N5	172.69(5)	Ru1 N1 C1	133.25(15)
P2 Ru1 N1	90.83(5)	N2 N1 C1	106.94(17)
P2 Ru1 N3	174.57(5)	N1 N2 B1	120.87(17)
P2 Ru1 N5	92.16(5)	N1 N2 C3	109.13(18)
N1 Ru1 N3	86.78(7)	B1 N2 C3	130.00(19)
N1 Ru1 N5	86.32(7)	Ru1 N3 N4	118.72(13)
N3 Ru1 N5	82.83(7)	Ru1 N3 C4	134.46(15)
Ru1 P1 O1	125.52(6)	N4 N3 C4	106.79(17)
Ru1 P1 O2	117.75(6)	N3 N4 B1	120.02(17)
Ru1 P1 O3	110.34(6)	N3 N4 C6	109.28(18)
O1 P1 O2	93.14(8)	B1 N4 C6	130.14(19)
O1 P1 O3	103.27(8)	Ru1 N5 N6	118.97(13)
O2 P1 O3	103.69(8)	Ru1 N5 C7	134.49(15)
Ru1 P2 O4	112.75(6)	N6 N5 C7	106.42(17)
Ru1 P2 O5	122.33(6)	N5 N6 B1	119.86(17)
Ru1 P2 O6	117.45(6)	N5 N6 C9	110.04(17)
O4 P2 O5	99.73(8)	B1 N6 C9	130.02(18)
O4 P2 O6	105.22(8)	N2 B1 N4	108.62(18)

N2 B1 N6	108.11(18)	C7 C8 H8	127.5(2)
N2 B1 H1b	112.7(13)	C9 C8 H8	127.8(2)
N4 B1 N6	106.97(18)	N6 C9 C8	108.32(19)
N4 B1 H1b	109.8(13)	N6 C9 H9	126.0(2)
N6 B1 H1b	110.5(13)	C8 C9 H9	125.7(2)
N1 C1 C2	110.34(19)	O1 C10 H10a	109.3(2)
N1 C1 H1	124.8(2)	O1 C10 H10b	109.5(2)
C2 C1 H1	124.8(2)	O1 C10 H10c	109.6(2)
C1 C2 C3	104.82(19)	H10a C10 H10b	109.5(2)
C1 C2 H2	127.7(2)	H10a C10 H10c	109.5(2)
C3 C2 H2	127.5(2)	H10b C10 H10c	109.5(2)
N2 C3 C2	108.77(20)	O2 C11 H11a	109.4(2)
N2 C3 H3	125.6(2)	O2 C11 H11b	109.3(2)
C2 C3 H3	125.6(2)	O2 C11 H11c	109.63(20)
N3 C4 C5	110.2(2)	H11a C11 H11b	109.5(2)
N3 C4 H4	124.9(2)	H11a C11 H11c	109.5(2)
C5 C4 H4	125.0(2)	H11b C11 H11c	109.5(2)
C4 C5 C6	105.09(20)	O3 C12 H12a	109.77(20)
C4 C5 H5	127.5(3)	O3 C12 H12b	109.4(2)
C6 C5 H5	127.4(3)	O3 C12 H12c	109.25(20)
N4 C6 C5	108.7(2)	H12a C12 H12b	109.5(2)
N4 C6 H6	125.6(2)	H12a C12 H12c	109.5(2)
C5 C6 H6	125.7(2)	H12b C12 H12c	109.5(2)
N5 C7 C8	110.53(19)	O4 C13 H13a	109.60(19)
N5 C7 H7	124.8(2)	O4 C13 H13b	109.45(19)
C8 C7 H7	124.7(2)	O4 C13 H13c	109.36(19)
C7 C8 C9	104.69(19)	H13a C13 H13b	109.5(2)

H13a C13 H13c 109.5(2)
O5 C14 H14a 109.5(2)
O5 C14 H14b 109.5(2)
O5 C14 H14c 109.39(19)
H14a C14 H14b 109.5(2)
H14a C14 H14c 109.5(2)
H14b C14 H14c 109.5(2)

H13b C13 H13c 109.5(2)
O6 C15 H15a 109.5(2)
O6 C15 H15b 109.37(20)
O6 C15 H15c 109.55(19)
H15a C15 H15b 109.5(2)
H15a C15 H15c 109.5(2)
H15b C15 H15c 109.5(2)

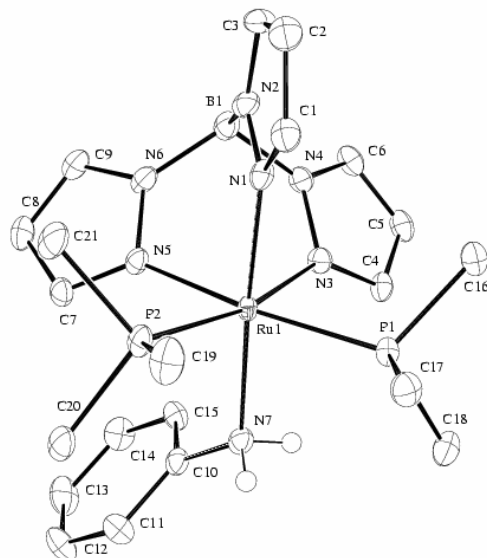


Figure A2 ORTEP diagram of [TpRuP(Me₃)₂NH₂Ph][OTf]

Table A.6 Crystal Data and Structure Refinement for [TpRu(PMe₃)₂NH₂Ph][OTf]

Identification code	x01040
Empirical formula	C ₂₂ H ₃₄ BF ₃ N ₇ O ₃ P ₂ RuR
Formula weight	707.43
Temperature	148 K
Wavelength	.71073
Crystal system	Triclinic
Space group	P -1
Unit cell dimensions	
a	9.4185(10) Å
b	11.9282(14) Å
c	14.0374(10) Å

Table A.6 (continued)

α	91.844(13) °
β	93.045(13) °
χ	106.552(8) °
Volume	1507.7(3) Å ³
Z	2
Density (calculated)	1.558 Mg/m ³
Absorption Coefficient	.75
F(000)	720.56
Crystal size	.32 x .28 x .18 mm
θ range for data collected	15.50 to 18.00
Limiting indices	-11 ≤ h ≤ 10, 0 ≤ k ≤ 14, -16 ≤ l ≤ 16
Reflections collected	5244
Independent reflections	4773
Absorption correction	psi-scan
Max and min transmission	0.9167 and 0.9979
Refinement method	Full matrix least squares of F ²
Data/restraints/parameters	0 / 0 / 498
Goodness of fit on F ²	3.49
Final R indices [I>2σ(I)]	R1 = 0.028, wR2 = 0.046
Final R indices (all data)	R1 = 0.028, wR2 = 0.045
Largest diff. peak and hole	-0.77 and 0.71 eÅ ⁻³

Table A.7 Atomic Coordinates and Thermal Parameters (x, y, z and u) for [TpRu(PMe₃)₂NH₂Ph][OTf]

	x	y	z	u
Ru1	.67400(3)	.77073(2)	.762835(18)	.01143(14)
P1	.46840(10)	.79084(8)	.67621(6)	.0141(5)
P2	.86273(10)	.89163(8)	.68320(6)	.0167(4)
N1	.6774(3)	.9181(2)	.8488(2)	.0164(14)
N2	.6964(3)	.9144(3)	.94538(20)	.0176(15)
N3	.5275(3)	.6681(2)	.86309(20)	.0158(14)
N4	.5604(3)	.7032(2)	.95735(20)	.0163(14)
N5	.8453(3)	.7420(2)	.85910(19)	.0153(14)
N6	.8361(3)	.7645(3)	.95467(20)	.0184(15)
N7	.6572(3)	.6104(3)	.6741(2)	.0167(16)
B1	.7033(5)	.7999(4)	.9907(3)	.020(2)
C1	.6655(4)	1.0248(3)	.8312(3)	.0196(20)
C2	.6748(4)	1.0900(3)	.9163(3)	.024(2)
C3	.6943(4)	1.0177(3)	.9864(3)	.0218(19)
C4	.4011(4)	.5803(3)	.8600(3)	.0171(18)
C5	.3504(4)	.5585(3)	.9514(3)	.0201(18)
C6	.4550(4)	.6384(3)	1.0106(3)	.0192(18)
C7	.9657(4)	.7056(3)	.8525(3)	.0185(18)
C8	1.0347(4)	.7027(3)	.9416(3)	.024(2)
C9	.9491(4)	.7405(3)	1.0044(3)	.0224(19)
C10	.7486(4)	.5335(3)	.6920(3)	.0171(17)
C11	.8450(4)	.5166(3)	.6249(3)	.0231(19)
C12	.9337(5)	.4430(4)	.6446(3)	.031(2)
C13	.9253(5)	.3870(4)	.7293(3)	.032(2)

C14	.8285(5)	.4029(3)	.7953(3)	.026(2)
C15	.7400(4)	.4765(3)	.7766(3)	.0189(19)
C16	.3380(4)	.8295(4)	.7536(3)	.021(2)
C17	.4800(4)	.8955(3)	.5832(3)	.0199(19)
C18	.3483(4)	.6614(3)	.6087(3)	.021(2)
C19	.8416(5)	1.0042(4)	.6021(3)	.026(2)
C20	.9715(4)	.8231(4)	.6096(3)	.023(2)
C21	1.0048(4)	.9835(4)	.7694(3)	.025(2)
S1	.68571(10)	.69821(8)	.37653(6)	.0177(5)
O1	.6131(3)	.5912(2)	.3228(2)	.0305(16)
O2	.6526(3)	.6998(3)	.47559(19)	.0320(17)
O3	.8384(3)	.7502(2)	.3585(2)	.0293(16)
C22	.5933(4)	.8006(3)	.3259(3)	.023(2)
F1	.6636(3)	.91019(19)	.35854(18)	.0361(14)
F2	.5931(3)	.7989(3)	.23113(16)	.0471(18)
F3	.4526(3)	.7778(2)	.34933(17)	.0312(13)
H1	.657(4)	1.046(3)	.771(3)	.018(10)
H1b	.726(4)	.807(3)	1.081(2)	.016(9)
H2	.667(5)	1.161(4)	.922(3)	.025(11)
H3	.700(4)	1.025(3)	1.046(3)	.020(10)
H4	.364(4)	.538(3)	.804(3)	.011(9)
H6	.470(4)	.643(3)	1.075(3)	.019(10)
H7	.992(5)	.688(3)	.796(3)	.022(11)
H7a	.566(6)	.574(5)	.678(3)	.048(15)
H7b	.658(5)	.642(4)	.612(3)	.035(12)
H8	1.116(5)	.682(3)	.955(3)	.020(10)
H9	.957(5)	.756(3)	1.073(3)	.025(11)

H11	.847(5)	.551(4)	.566(3)	.026(11)
H12	.995(5)	.433(4)	.600(3)	.028(11)
H13	.985(5)	.338(4)	.743(3)	.031(12)
H14	.825(4)	.371(3)	.852(3)	.016(10)
H15	.683(5)	.486(3)	.818(3)	.018(10)
H16a	.316(4)	.777(4)	.799(3)	.020(10)
H16b	.379(5)	.898(4)	.784(3)	.030(12)
H16c	.249(5)	.830(4)	.716(3)	.039(13)
H17a	.527(5)	.873(4)	.530(3)	.028(11)
H17b	.384(5)	.891(4)	.556(3)	.030(11)
H17c	.531(5)	.975(4)	.609(3)	.026(11)
H18a	.264(5)	.687(4)	.583(3)	.029(11)
H18b	.399(4)	.643(3)	.558(3)	.013(9)
H18c	.323(4)	.604(4)	.649(3)	.022(11)
H19a	.795(6)	1.057(5)	.631(4)	.054(16)
H19b	.930(6)	1.049(4)	.589(3)	.037(13)
H19c	.781(5)	.971(4)	.547(3)	.024(11)
H20a	.910(5)	.800(3)	.552(3)	.024(11)
H20b	1.053(5)	.884(4)	.596(3)	.028(11)
H20c	.998(4)	.761(4)	.641(3)	.019(10)
H21a	1.074(6)	1.039(5)	.737(4)	.064(17)
H21b	.969(5)	1.021(4)	.815(3)	.022(11)
H21c	1.043(4)	.935(3)	.806(3)	.018(10)

Table A.8 Anisotropic Displacement Parameters for [TpRu(PMe₃)₂NH₂Ph][OTf]

	u11	u22	u33	u12	u13	u23
Ru1	.00867(15)	.01051(15)	.01438(15)	.00132(10)	.00141(10)	.00196(10)
P1	.0113(4)	.0131(4)	.0179(4)	.0034(4)	.0005(3)	.0021(3)
P2	.0117(4)	.0176(5)	.0180(5)	-.0007(4)	.0023(4)	.0047(4)
N1	.0114(14)	.0148(15)	.0205(15)	.0001(12)	.0000(12)	.0016(12)
N2	.0151(15)	.0168(15)	.0171(15)	-.0014(12)	.0018(12)	-.0016(12)
N3	.0144(15)	.0151(15)	.0168(15)	.0020(12)	.0030(12)	.0019(12)
N4	.0149(15)	.0178(16)	.0156(14)	.0026(13)	.0050(12)	.0027(12)
N5	.0121(15)	.0172(15)	.0143(14)	.0003(12)	.0005(11)	.0025(12)
N6	.0159(16)	.0214(16)	.0136(14)	-.0010(13)	-.0009(12)	.0011(12)
N7	.0143(16)	.0175(16)	.0162(15)	.0013(13)	.0008(12)	.0011(12)
B1	.015(2)	.024(2)	.018(2)	.0005(17)	.0022(16)	.0008(16)
C1	.0171(19)	.0140(18)	.027(2)	.0029(15)	.0018(15)	.0019(15)
C2	.022(2)	.0119(18)	.037(2)	.0027(16)	.0016(17)	-.0023(16)
C3	.0213(20)	.0203(20)	.021(2)	.0031(16)	.0023(16)	-.0083(16)
C4	.0124(17)	.0110(17)	.0270(20)	.0021(14)	-.0002(15)	.0015(15)
C5	.0169(19)	.0170(18)	.0290(20)	.0076(15)	.0056(15)	.0064(15)
C6	.0192(19)	.0194(19)	.0210(19)	.0069(15)	.0086(15)	.0077(15)
C7	.0133(18)	.0194(19)	.0218(19)	.0025(15)	.0034(15)	.0015(15)
C8	.0147(19)	.026(2)	.030(2)	.0071(17)	-.0027(16)	.0026(16)
C9	.0188(19)	.025(2)	.0208(19)	.0037(16)	-.0051(15)	-.0002(15)
C10	.0131(17)	.0141(17)	.0229(18)	.0026(14)	-.0008(14)	-.0020(14)
C11	.025(2)	.024(2)	.0227(20)	.0098(17)	.0062(16)	.0023(16)
C12	.027(2)	.036(2)	.036(2)	.0182(20)	.0109(19)	-.0004(19)
C13	.025(2)	.029(2)	.047(3)	.0175(19)	.0013(19)	.0046(19)
C14	.028(2)	.022(2)	.028(2)	.0091(17)	.0005(17)	.0076(17)

C15	.0166(19)	.0176(19)	.0233(19)	.0052(15)	.0057(16)	.0037(15)
C16	.0154(19)	.024(2)	.0236(20)	.0065(16)	.0032(16)	.0034(17)
C17	.020(2)	.021(2)	.0203(19)	.0077(16)	.0008(16)	.0040(15)
C18	.0169(19)	.0174(20)	.029(2)	.0041(16)	-.0046(17)	.0002(17)
C19	.020(2)	.025(2)	.030(2)	.0015(18)	.0030(18)	.0144(18)
C20	.0141(19)	.031(2)	.0192(19)	-.0019(17)	.0034(15)	.0042(17)
C21	.0169(20)	.026(2)	.024(2)	-.0062(17)	.0026(17)	.0028(18)
S1	.0154(4)	.0140(4)	.0234(5)	.0033(4)	.0023(4)	.0017(3)
O1	.0278(16)	.0141(13)	.0491(18)	.0063(12)	.0000(13)	-.0069(12)
O2	.0319(16)	.0442(18)	.0220(14)	.0130(14)	.0038(12)	.0103(13)
O3	.0170(14)	.0216(14)	.0498(18)	.0054(12)	.0082(13)	.0009(13)
C22	.029(2)	.024(2)	.0194(19)	.0097(17)	.0056(16)	.0021(15)
F1	.0425(15)	.0146(11)	.0536(16)	.0096(11)	.0150(12)	.0039(10)
F2	.073(2)	.0630(19)	.0201(12)	.0421(17)	.0094(12)	.0097(12)
F3	.0223(12)	.0373(14)	.0372(13)	.0146(11)	-.0021(10)	-.0022(11)

Table A.9 Bond Distances for [TpRu(PMe₃)₂NH₂Ph][OTf]

Ru1 P1	2.3064(9)	N7 H7b	.96(5)
Ru1 P2	2.3116(10)	B1 H1b	1.27(4)
Ru1 N1	2.091(3)	C1 C2	1.388(5)
Ru1 N3	2.176(3)	C1 H1	.90(4)
Ru1 N5	2.158(3)	C2 C3	1.369(6)
Ru1 N7	2.211(3)	C2 H2	.88(4)
P1 C16	1.826(4)	C3 H3	.84(4)
P1 C17	1.821(4)	C4 C5	1.399(5)
P1 C18	1.833(4)	C4 H4	.92(4)
P2 C19	1.834(4)	C5 C6	1.377(5)
P2 C20	1.822(4)	C6 H6	.90(4)
P2 C21	1.834(4)	C7 C8	1.383(5)
N1 N2	1.362(4)	C7 H7	.88(4)
N1 C1	1.338(5)	C8 C9	1.375(6)
N2 B1	1.541(5)	C8 H8	.88(4)
N2 C3	1.349(5)	C9 H9	.98(4)
N3 N4	1.367(4)	C10 C11	1.391(5)
N3 C4	1.341(4)	C10 C15	1.382(5)
N4 B1	1.541(5)	C11 C12	1.399(6)
N4 C6	1.349(4)	C11 H11	.94(4)
N5 N6	1.372(4)	C12 C13	1.376(6)
N5 C7	1.332(5)	C12 H12	.90(4)
N6 B1	1.534(5)	C13 C14	1.379(6)
N6 C9	1.345(5)	C13 H13	.94(5)
N7 C10	1.444(5)	C14 C15	1.393(5)
N7 H7a	.85(6)	C14 H14	.89(4)

C15 H15	.83(4)	C16 H16a	.89(4)
C16 H16b	.89(5)	C20 H20b	.93(5)
C16 H16c	.96(5)	C20 H20c	.96(4)
C17 H17a	.96(4)	C21 H21a	.93(6)
C17 H17b	.95(5)	C21 H21b	.91(4)
C17 H17c	.98(4)	C21 H21c	.92(4)
C18 H18a	.98(5)	S1 O1	1.433(3)
C18 H18b	.93(4)	S1 O2	1.442(3)
C18 H18c	.90(4)	S1 O3	1.435(3)
C19 H19a	.97(6)	S1 C22	1.830(4)
C19 H19b	.89(5)	C22 F1	1.339(4)
C19 H19c	.95(4)	C22 F2	1.329(4)
C20 H20a	.95(4)	C22 F3	1.336(5)

Table A.10 Bond Angles for [TpRu(PMe₃)₂NH₂Ph][OTf]

P1 Ru1 P2	100.79(3)	C20 P2 C21	102.22(19)
P1 Ru1 N1	89.46(8)	Ru1 N1 N2	119.1(2)
P1 Ru1 N3	89.06(8)	Ru1 N1 C1	134.3(2)
P1 Ru1 N5	171.96(8)	N2 N1 C1	106.6(3)
P1 Ru1 N7	88.71(8)	N1 N2 B1	120.2(3)
P2 Ru1 N1	87.19(8)	N1 N2 C3	109.1(3)
P2 Ru1 N3	168.39(8)	B1 N2 C3	130.5(3)
P2 Ru1 N5	86.93(8)	Ru1 N3 N4	116.0(2)
P2 Ru1 N7	95.79(9)	Ru1 N3 C4	138.0(2)
N1 Ru1 N3	86.77(11)	N4 N3 C4	105.9(3)
N1 Ru1 N5	88.65(11)	N3 N4 B1	121.5(3)
N1 Ru1 N7	176.74(11)	N3 N4 C6	109.8(3)
N3 Ru1 N5	83.02(11)	B1 N4 C6	128.7(3)
N3 Ru1 N7	90.51(11)	Ru1 N5 N6	117.0(2)
N5 Ru1 N7	92.80(11)	Ru1 N5 C7	137.2(2)
Ru1 P1 C16	111.58(13)	N6 N5 C7	105.8(3)
Ru1 P1 C17	123.01(13)	N5 N6 B1	120.7(3)
Ru1 P1 C18	117.84(13)	N5 N6 C9	109.4(3)
C16 P1 C17	101.63(18)	B1 N6 C9	129.6(3)
C16 P1 C18	101.58(19)	Ru1 N7 C10	123.6(2)
C17 P1 C18	97.99(19)	Ru1 N7 H7a	100(3)
Ru1 P2 C19	125.34(14)	Ru1 N7 H7b	99(3)
Ru1 P2 C20	117.84(14)	C10 N7 H7a	110(3)
Ru1 P2 C21	109.98(14)	C10 N7 H7b	117(3)
C19 P2 C20	98.6(2)	H7a N7 H7b	102(4)
C19 P2 C21	99.3(2)	N2 B1 N4	108.1(3)

N2 B1 N6	109.2(3)	N6 C9 C8	108.8(3)
N2 B1 H1b	115.2(17)	N6 C9 H9	117(2)
N4 B1 N6	108.3(3)	C8 C9 H9	133(2)
N4 B1 H1b	111.8(17)	N7 C10 C11	120.5(3)
N6 B1 H1b	104.0(17)	N7 C10 C15	119.6(3)
N1 C1 C2	110.3(3)	C11 C10 C15	119.9(3)
N1 C1 H1	120(2)	C10 C11 C12	119.4(4)
C2 C1 H1	129(2)	C10 C11 H11	120(3)
C1 C2 C3	105.0(3)	C12 C11 H11	120(2)
C1 C2 H2	126(3)	C11 C12 C13	120.4(4)
C3 C2 H2	128(3)	C11 C12 H12	117(3)
N2 C3 C2	108.9(3)	C13 C12 H12	121(3)
N2 C3 H3	118(3)	C12 C13 C14	120.1(4)
C2 C3 H3	132(3)	C12 C13 H13	120(3)
N3 C4 C5	111.1(3)	C14 C13 H13	118(3)
N3 C4 H4	120(2)	C13 C14 C15	120.0(4)
C5 C4 H4	127(2)	C13 C14 H14	121(2)
C4 C5 C6	104.2(3)	C15 C14 H14	118(2)
N4 C6 C5	109.0(3)	C10 C15 C14	120.3(4)
N4 C6 H6	119(2)	C10 C15 H15	121(3)
C5 C6 H6	130(2)	C14 C15 H15	118(3)
N5 C7 C8	111.4(3)	P1 C16 H16a	108(2)
N5 C7 H7	119(3)	P1 C16 H16b	110(3)
C8 C7 H7	129(3)	P1 C16 H16c	109(3)
C7 C8 C9	104.6(3)	H16a C16 H16b	106(4)
C7 C8 H8	127(2)	H16a C16 H16c	110(4)
C9 C8 H8	127(2)	H16b C16 H16c	110(4)

P1 C17 H17a	109(2)	H20a C20 H20b	107(3)
P1 C17 H17b	110(3)	H20a C20 H20c	115(3)
P1 C17 H17c	110(2)	H20b C20 H20c	113(3)
H17a C17 H17b	102(3)	P2 C21 H21a	109(3)
H17a C17 H17c	112(3)	P2 C21 H21b	114(3)
H17b C17 H17c	110(3)	P2 C21 H21c	108(2)
P1 C18 H18a	104(2)	H21a C21 H21b	108(4)
P1 C18 H18b	108(2)	H21a C21 H21c	115(4)
P1 C18 H18c	107(3)	H21b C21 H21c	100(3)
H18a C18 H18b	109(3)	O1 S1 O2	115.00(18)
H18a C18 H18c	113(4)	O1 S1 O3	115.57(17)
H18b C18 H18c	113(3)	O1 S1 C22	102.48(17)
P2 C19 H19a	111(3)	O2 S1 O3	115.20(18)
P2 C19 H19b	109(3)	O2 S1 C22	102.76(17)
P2 C19 H19c	111(2)	O3 S1 C22	103.08(17)
H19a C19 H19b	104(4)	S1 C22 F1	110.2(3)
H19a C19 H19c	106(4)	S1 C22 F2	112.0(3)
H19b C19 H19c	113(4)	S1 C22 F3	112.3(3)
P2 C20 H20a	102(2)	F1 C22 F2	107.3(3)
P2 C20 H20b	105(3)	F1 C22 F3	107.1(3)
P2 C20 H20c	111(2)	F2 C22 F3	107.8(3)

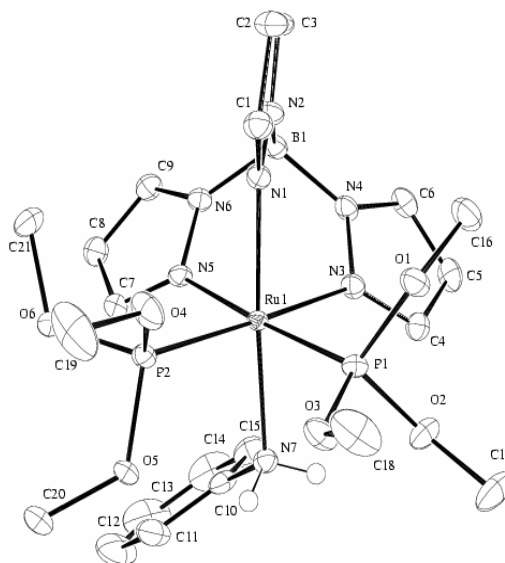


Figure A3 ORTEP diagram of [TpRu{P(OMe)₃}₂NH₂Ph][OTf]

Table A.11 Crystal Data and Structure Refinement for [TpRu{P(OMe)₃}₂NH₂Ph][OTf]

Identification code	x01041
Empirical formula	C ₂₂ H ₃₅ BF ₃ N ₇ O ₉ P ₂ RuS
Formula weight	804.43
Temperature	148 K
Wavelength	.71073
Crystal system	Monoclinic
Space group	P 21/c
Unit cell dimensions	
a	9.1753(6) Å
b	23.7851(18) Å
c	15.3015(10) Å

Table A.11 (continued)

α	90.00 °
β	92.307 °
χ	90.00 °
Volume	3336.6(4) Å ³
Z	4
Density (calculated)	1.682 Mg/m ³
Absorption Coefficient	.96
F(000)	1637.37
Crystal size	.32 x .22 x .14 mm
θ range for data collected	1.20 to 25.00
Limiting indices	-10 ≤ h ≤ 10, 0 ≤ k ≤ 28, 0 ≤ l ≤ 18
Reflections collected	5817
Independent reflections	5028
Absorption correction	psi-scan
Max and min transmission	0.8771 and 0.9960
Refinement method	Full matrix least squares of F ²
Data/restraints/parameters	0 / 0 / 555
Goodness of fit on F2	1.61
Final R indices [I > 2σ(I)]	R1 = 0.025, wR2 = 0.030
Final R indices (all data)	R1 = 0.025, wR2 = 0.030
Largest diff. peak and hole	-0.77 and 0.43 eÅ ⁻³

Table A.12 Atomic Coordinates and Thermal Parameters (x, y, z and u) for [TpRu{P(OMe)₃}₂NH₂Ph][OTf]

	x	y	z	u
Ru1	.093846(18)	.128309(7)	.727032(11)	.01117(10)
P1	.19031(6)	.11557(2)	.59679(4)	.0138(3)
P2	.21833(6)	.20759(2)	.74773(4)	.0145(3)
N1	-.08722(19)	.17134(7)	.67269(12)	.0142(9)
N2	-.22390(20)	.15525(8)	.69579(12)	.0169(9)
N3	-.03344(20)	.05212(8)	.71460(12)	.0156(9)
N4	-.17808(19)	.05427(8)	.73358(12)	.0161(9)
N5	-.01154(20)	.13667(7)	.85022(12)	.0152(9)
N6	-.1588(2)	.12760(8)	.85083(12)	.0161(9)
N7	.2732(2)	.07725(9)	.78131(12)	.0153(10)
O1	.09266(17)	.12589(6)	.50899(10)	.0183(8)
O2	.24434(18)	.05199(7)	.59041(10)	.0207(8)
O3	.32960(17)	.15186(7)	.57482(10)	.0200(8)
O4	.20768(18)	.24911(7)	.66554(11)	.0231(8)
O5	.38771(16)	.19776(6)	.77133(10)	.0175(7)
O6	.18193(16)	.24754(6)	.82890(10)	.0195(8)
B1	-.2441(3)	.10966(11)	.76612(17)	.0171(13)
C1	-.1056(3)	.21037(10)	.61027(15)	.0179(12)
C2	-.2542(3)	.21923(10)	.59192(16)	.0214(11)
C3	-.3248(3)	.18379(10)	.64681(16)	.0209(12)
C4	-.0064(3)	-.00140(9)	.69326(15)	.0184(12)
C5	-.1320(3)	-.03389(10)	.69884(16)	.0222(12)
C6	-.2381(3)	.00299(10)	.72400(15)	.0193(11)
C7	.0310(3)	.14981(10)	.93220(15)	.0185(11)

C8	-.0865(3)	.14932(11)	.98678(16)	.0222(12)
C9	-.2045(3)	.13504(10)	.93303(15)	.0203(11)
C10	.2823(2)	.06322(10)	.87366(15)	.0187(11)
C11	.3818(3)	.09139(12)	.92874(17)	.0284(14)
C12	.3916(3)	.07896(16)	1.01713(20)	.0443(18)
C13	.3006(4)	.03842(17)	1.0504(2)	.0511(20)
C14	.2010(4)	.01046(14)	.9955(2)	.0429(16)
C15	.1911(3)	.02270(11)	.90684(18)	.0278(13)
C16	-.0417(3)	.09439(12)	.49483(18)	.0243(13)
C17	.3319(4)	.03227(13)	.51976(19)	.0319(14)
C18	.3629(3)	.17490(15)	.49066(19)	.0346(15)
C19	.2874(4)	.30140(13)	.6610(2)	.0422(17)
C20	.4798(3)	.23373(11)	.82684(19)	.0265(13)
C21	.0413(3)	.27515(12)	.8291(2)	.0287(14)
S1	.40639(6)	.91179(2)	.69973(4)	.0202(3)
O7	.3402(2)	.90552(10)	.61368(14)	.0506(12)
O8	.54675(19)	.88584(7)	.71227(13)	.0310(10)
O9	.3948(2)	.96699(7)	.73665(15)	.0390(11)
C22	.2882(3)	.86929(10)	.76709(19)	.0274(14)
F1	.3380(2)	.86593(10)	.84916(13)	.0623(12)
F2	.27775(18)	.81654(6)	.73708(14)	.0494(11)
F3	.15235(17)	.88919(7)	.76680(14)	.0476(11)
H1	-.025(3)	.2268(11)	.5856(16)	.019(6)
H1b	-.360(2)	.1036(9)	.7801(14)	.006(5)
H2	-.295(3)	.2432(11)	.5504(17)	.021(7)
H3	-.422(3)	.1766(11)	.6571(17)	.026(7)
H4	.087(3)	-.0125(11)	.6753(17)	.028(7)

H5	-.143(3)	-.0713(12)	.6872(18)	.033(8)
H6	-.335(3)	-.0012(10)	.7321(16)	.019(6)
H7	.130(3)	.1579(11)	.9456(17)	.027(7)
H7a	.355(3)	.0952(11)	.7688(15)	.014(6)
H7b	.275(3)	.0463(12)	.7528(16)	.017(7)
H8	-.085(3)	.1556(11)	1.0472(18)	.026(7)
H9	-.307(3)	.1290(10)	.9453(16)	.019(7)
H11	.438(3)	.1188(12)	.9052(19)	.029(8)
H12	.456(3)	.0936(13)	1.055(2)	.038(8)
H13	.310(4)	.0283(15)	1.110(2)	.060(10)
H14	.138(4)	-.0183(14)	1.020(2)	.052(10)
H15	.126(3)	.0042(11)	.8681(18)	.026(7)
H16a	-.085(4)	.1095(14)	.445(2)	.046(9)
H16b	-.020(3)	.0549(13)	.4871(18)	.033(8)
H16c	-.103(3)	.0974(12)	.5423(19)	.033(8)
H17a	.351(4)	-.0069(16)	.531(2)	.059(11)
H17b	.294(4)	.0428(14)	.471(2)	.050(10)
H17c	.425(4)	.0512(14)	.521(2)	.049(10)
H18a	.464(4)	.1824(14)	.489(2)	.052(10)
H18b	.333(3)	.1535(14)	.443(2)	.041(9)
H18c	.305(4)	.2106(16)	.485(2)	.066(12)
H19a	.241(3)	.3213(13)	.612(2)	.043(9)
H19b	.286(3)	.3206(14)	.716(2)	.044(9)
H19c	.392(4)	.2931(15)	.645(2)	.062(11)
H20a	.577(3)	.2225(12)	.8142(19)	.038(8)
H20b	.462(3)	.2745(12)	.8151(17)	.024(7)
H20c	.456(3)	.2229(12)	.8898(20)	.036(8)

H21a	.033(4)	.2938(15)	.878(2)	.056(11)
H21b	.042(4)	.3026(16)	.783(3)	.070(12)
H21c	-.037(4)	.2512(15)	.825(2)	.051(10)

Table A.13 Anisotropic Displacement Parameters for [TpRu{P(OMe)₃}₂NH₂Ph][OTf]

	u11	u22	u33	u12	u13	u23
Ru1	.00742(10)	.01137(10)	.01476(10)	-.00052(7)	.00080(6)	-.00081(7)
P1	.0093(3)	.0161(3)	.0160(3)	.0007(2)	.0010(2)	.0003(2)
P2	.0100(3)	.0126(3)	.0208(3)	-.0013(2)	-.0007(2)	-.0009(2)
N1	.0092(9)	.0150(9)	.0185(9)	-.0020(7)	.0020(7)	-.0015(7)
N2	.0086(9)	.0218(10)	.0203(10)	-.0002(8)	.0012(7)	-.0016(8)
N3	.0118(9)	.0179(10)	.0171(9)	-.0025(8)	.0020(7)	-.0006(8)
N4	.0112(9)	.0202(10)	.0169(9)	-.0037(8)	.0009(7)	-.0019(8)
N5	.0089(9)	.0163(9)	.0205(10)	-.0002(7)	.0021(7)	-.0010(8)
N6	.0108(9)	.0184(10)	.0192(10)	-.0007(7)	.0017(8)	-.0010(8)
N7	.0128(10)	.0147(10)	.0187(10)	.0002(8)	.0021(8)	.0000(8)
O1	.0131(8)	.0241(9)	.0176(8)	-.0012(7)	-.0008(6)	-.0006(7)
O2	.0221(9)	.0209(8)	.0197(8)	.0063(7)	.0067(7)	-.0001(7)
O3	.0138(8)	.0303(9)	.0161(8)	-.0055(7)	.0015(6)	.0024(7)
O4	.0230(9)	.0170(8)	.0287(9)	-.0086(7)	-.0060(7)	.0048(7)
O5	.0091(8)	.0185(8)	.0246(8)	-.0026(6)	-.0011(6)	-.0052(7)
O6	.0121(8)	.0179(8)	.0282(9)	.0014(6)	-.0018(7)	-.0075(7)
B1	.0113(13)	.0215(13)	.0184(13)	-.0016(10)	-.0002(10)	-.0009(10)
C1	.0146(12)	.0174(12)	.0217(12)	.0001(9)	.0006(10)	.0003(9)
C2	.0156(12)	.0231(12)	.0251(13)	.0049(10)	-.0030(10)	.0028(10)
C3	.0098(11)	.0271(13)	.0257(13)	.0037(10)	-.0001(10)	-.0016(10)
C4	.0191(13)	.0153(11)	.0206(12)	-.0003(9)	.0004(10)	-.0013(9)
C5	.0272(14)	.0149(12)	.0243(13)	-.0070(10)	-.0015(10)	-.0009(10)
C6	.0168(13)	.0224(12)	.0188(12)	-.0091(10)	.0008(9)	.0017(9)
C7	.0146(12)	.0192(12)	.0216(12)	.0008(9)	-.0013(10)	-.0036(9)

C8	.0227(13)	.0262(13)	.0178(12)	.0021(10)	.0022(10)	-.0046(10)
C9	.0165(13)	.0243(13)	.0205(12)	.0021(10)	.0051(10)	-.0020(10)
C10	.0169(12)	.0207(12)	.0187(11)	.0083(9)	.0019(9)	.0015(9)
C11	.0173(13)	.0413(16)	.0264(14)	.0031(12)	-.0016(11)	.0001(12)
C12	.0314(16)	.075(2)	.0260(15)	.0105(16)	-.0107(13)	-.0023(16)
C13	.052(2)	.079(3)	.0233(15)	.0217(19)	.0037(15)	.0190(16)
C14	.0478(19)	.0437(18)	.0384(17)	.0117(15)	.0152(15)	.0220(14)
C15	.0286(14)	.0224(13)	.0326(15)	.0051(11)	.0050(12)	.0053(11)
C16	.0162(13)	.0328(15)	.0236(14)	-.0045(11)	-.0025(11)	-.0055(11)
C17	.0360(17)	.0345(16)	.0263(15)	.0157(14)	.0132(13)	-.0009(12)
C18	.0252(16)	.0548(20)	.0239(15)	-.0130(14)	.0021(12)	.0131(14)
C19	.051(2)	.0283(16)	.0459(19)	-.0230(15)	-.0169(16)	.0172(14)
C20	.0131(13)	.0269(15)	.0391(16)	-.0025(10)	-.0055(11)	-.0101(12)
C21	.0181(14)	.0234(14)	.0445(18)	.0063(11)	.0014(12)	-.0115(13)
S1	.0134(3)	.0163(3)	.0306(3)	.0002(2)	-.0034(2)	.0003(2)
O7	.0432(13)	.0705(16)	.0368(12)	-.0210(12)	-.0156(10)	.0085(11)
O8	.0142(9)	.0241(9)	.0547(12)	.0031(7)	.0019(8)	.0043(8)
O9	.0291(11)	.0156(9)	.0733(15)	-.0012(8)	.0136(10)	-.0068(9)
C22	.0175(13)	.0202(13)	.0444(16)	-.0009(10)	.0009(11)	.0015(11)
F1	.0505(12)	.0938(16)	.0423(11)	-.0291(11)	-.0006(9)	.0202(10)
F2	.0322(9)	.0182(8)	.0988(15)	-.0058(7)	.0162(9)	-.0014(8)
F3	.0166(8)	.0322(9)	.0950(15)	.0036(7)	.0161(9)	.0052(9)

Table A.14 Bond Distances for [TpRu{P(OMe)₃}₂NH₂Ph][OTf]

Ru1 P1	2.2336(6)	N7 C10	1.451(3)
Ru1 P2	2.2209(6)	N7 H7a	.89(3)
Ru1 N1	2.0947(18)	N7 H7b	.86(3)
Ru1 N3	2.1601(18)	O1 C16	1.451(3)
Ru1 N5	2.1620(18)	O2 C17	1.451(3)
Ru1 N7	2.1822(19)	O3 C18	1.443(3)
P1 O1	1.6034(16)	O4 C19	1.446(3)
P1 O2	1.5956(16)	O5 C20	1.452(3)
P1 O3	1.5893(16)	O6 C21	1.448(3)
P2 O4	1.5990(17)	B1 H1b	1.11(2)
P2 O5	1.5985(16)	C1 C2	1.397(3)
P2 O6	1.6094(16)	C1 H1	.93(3)
N1 N2	1.371(3)	C2 C3	1.370(4)
N1 C1	1.338(3)	C2 H2	.92(3)
N2 B1	1.544(3)	C3 H3	.93(3)
N2 C3	1.350(3)	C4 C5	1.393(3)
N3 N4	1.371(3)	C4 H4	.95(3)
N3 C4	1.340(3)	C5 C6	1.377(4)
N4 B1	1.541(3)	C5 H5	.91(3)
N4 C6	1.344(3)	C6 H6	.91(3)
N5 N6	1.368(3)	C7 C8	1.390(3)
N5 C7	1.336(3)	C7 H7	.94(3)
N6 B1	1.547(3)	C8 C9	1.375(3)
N6 C9	1.353(3)	C8 H8	.94(3)

C9 H9	.98(3)	C18 H18b	.92(4)
C10 C11	1.390(4)	C18 H18c	1.00(4)
C10 C15	1.386(4)	C19 H19a	.97(3)
C11 C12	1.384(4)	C19 H19b	.96(3)
C11 H11	.91(3)	C19 H19c	1.02(4)
C12 C13	1.386(5)	C20 H20a	.96(3)
C12 H12	.88(3)	C20 H20b	1.00(3)
C13 C14	1.386(5)	C20 H20c	1.03(3)
C13 H13	.95(4)	C21 H21a	.87(4)
C14 C15	1.387(4)	C21 H21b	.96(4)
C14 H14	.98(4)	C21 H21c	.92(4)
C15 H15	.94(3)	S1 O7	1.435(2)
C16 H16a	.92(4)	S1 O8	1.4341(18)
C16 H16b	.97(3)	S1 O9	1.4349(19)
C16 H16c	.94(3)	S1 C22	1.830(3)
C17 H17a	.96(4)	C22 F1	1.321(3)
C17 H17b	.85(4)	C22 F2	1.338(3)
C17 H17c	.96(4)	C22 F3	1.333(3)
C18 H18a	.95(4)		

Table A.15 Bond Angles for [TpRu{P(OMe)₃}₂NH₂Ph][OTf]

P1 Ru1 P2	91.29(2)	O5 P2 O6	98.17(8)
P1 Ru1 N1	92.78(5)	Ru1 N1 N2	118.71(13)
P1 Ru1 N3	92.29(5)	Ru1 N1 C1	134.25(15)
P1 Ru1 N5	176.01(5)	N2 N1 C1	106.69(18)
P1 Ru1 N7	86.81(5)	N1 N2 B1	120.83(18)
P2 Ru1 N1	92.11(5)	N1 N2 C3	109.28(18)
P2 Ru1 N3	176.43(5)	B1 N2 C3	129.86(19)
P2 Ru1 N5	92.47(5)	Ru1 N3 N4	118.33(13)
P2 Ru1 N7	92.45(6)	Ru1 N3 C4	135.53(15)
N1 Ru1 N3	87.57(7)	N4 N3 C4	106.12(18)
N1 Ru1 N5	85.74(7)	N3 N4 B1	119.80(17)
N1 Ru1 N7	175.43(7)	N3 N4 C6	109.80(18)
N3 Ru1 N5	83.96(7)	B1 N4 C6	130.28(19)
N3 Ru1 N7	87.90(7)	Ru1 N5 N6	117.89(14)
N5 Ru1 N7	94.37(7)	Ru1 N5 C7	135.76(16)
Ru1 P1 O1	119.92(6)	N6 N5 C7	106.35(18)
Ru1 P1 O2	108.56(6)	N5 N6 B1	120.28(18)
Ru1 P1 O3	117.77(6)	N5 N6 C9	109.18(18)
O1 P1 O2	104.97(9)	B1 N6 C9	130.50(19)
O1 P1 O3	99.59(8)	Ru1 N7 C10	120.78(14)
O2 P1 O3	104.32(9)	Ru1 N7 H7a	106.2(16)
Ru1 P2 O4	113.42(6)	Ru1 N7 H7b	108.4(17)
Ru1 P2 O5	113.44(6)	C10 N7 H7a	107.7(15)
Ru1 P2 O6	119.33(6)	C10 N7 H7b	107.2(16)
O4 P2 O5	107.22(9)	H7a N7 H7b	105(2)
O4 P2 O6	103.56(9)	P1 O1 C16	119.25(15)

P1 O2 C17	122.33(16)	N4 C6 H6	118.9(16)
P1 O3 C18	126.55(16)	C5 C6 H6	132.5(16)
P2 O4 C19	123.63(17)	N5 C7 C8	111.0(2)
P2 O5 C20	125.67(15)	N5 C7 H7	119.7(16)
P2 O6 C21	118.84(16)	C8 C7 H7	129.4(16)
N2 B1 N4	108.38(18)	C7 C8 C9	104.7(2)
N2 B1 N6	108.61(19)	C7 C8 H8	127.8(16)
N2 B1 H1b	111.7(11)	C9 C8 H8	127.5(16)
N4 B1 N6	108.31(18)	N6 C9 C8	108.8(2)
N4 B1 H1b	110.2(11)	N6 C9 H9	119.7(15)
N6 B1 H1b	109.5(11)	C8 C9 H9	131.4(15)
N1 C1 C2	110.0(2)	N7 C10 C11	119.4(2)
N1 C1 H1	120.3(15)	N7 C10 C15	120.3(2)
C2 C1 H1	129.7(15)	C11 C10 C15	120.3(2)
C1 C2 C3	105.4(2)	C10 C11 C12	120.3(3)
C1 C2 H2	126.9(16)	C10 C11 H11	118.2(18)
C3 C2 H2	127.7(16)	C12 C11 H11	121.5(18)
N2 C3 C2	108.6(2)	C11 C12 C13	119.5(3)
N2 C3 H3	117.1(16)	C11 C12 H12	124.5(20)
C2 C3 H3	134.2(16)	C13 C12 H12	115.9(20)
N3 C4 C5	110.5(2)	C12 C13 C14	120.2(3)
N3 C4 H4	120.9(16)	C12 C13 H13	119(2)
C5 C4 H4	128.5(16)	C14 C13 H13	119(2)
C4 C5 C6	105.1(2)	C13 C14 C15	120.5(3)
C4 C5 H5	127.9(18)	C13 C14 H14	118.8(19)
C6 C5 H5	127.1(18)	C15 C14 H14	120.7(19)
N4 C6 C5	108.5(2)	C10 C15 C14	119.2(3)

C10 C15 H15	118.4(16)	H19b C19 H19c	110(3)
C14 C15 H15	122.4(16)	O5 C20 H20a	104.0(18)
O1 C16 H16a	104.9(20)	O5 C20 H20b	112.2(15)
O1 C16 H16b	110.1(17)	O5 C20 H20c	105.0(16)
O1 C16 H16c	112.3(17)	H20a C20 H20b	112(2)
H16a C16 H16b	111(3)	H20a C20 H20c	110(2)
H16a C16 H16c	111(3)	H20b C20 H20c	111(2)
H16b C16 H16c	107(2)	O6 C21 H21a	109(2)
O2 C17 H17a	106(2)	O6 C21 H21b	105(2)
O2 C17 H17b	110(2)	O6 C21 H21c	114(2)
O2 C17 H17c	110.4(20)	H21a C21 H21b	106(3)
H17a C17 H17b	120(3)	H21a C21 H21c	106(3)
H17a C17 H17c	106(3)	H21b C21 H21c	113(3)
H17b C17 H17c	102(3)	O7 S1 O8	114.99(14)
O3 C18 H18a	109.9(19)	O7 S1 O9	114.89(14)
O3 C18 H18b	115.3(19)	O7 S1 C22	102.76(13)
O3 C18 H18c	105(2)	O8 S1 O9	114.95(12)
H18a C18 H18b	110(3)	O8 S1 C22	103.65(11)
H18a C18 H18c	110(3)	O9 S1 C22	103.21(12)
H18b C18 H18c	104(3)	S1 C22 F1	112.25(18)
O4 C19 H19a	104.4(18)	S1 C22 F2	111.14(19)
O4 C19 H19b	110.1(19)	S1 C22 F3	112.16(18)
O4 C19 H19c	109.1(20)	F1 C22 F2	106.7(2)
H19a C19 H19b	115(3)	F1 C22 F3	108.2(2)
H19a C19 H19c	106(3)	F2 C22 F3	106.1(2)

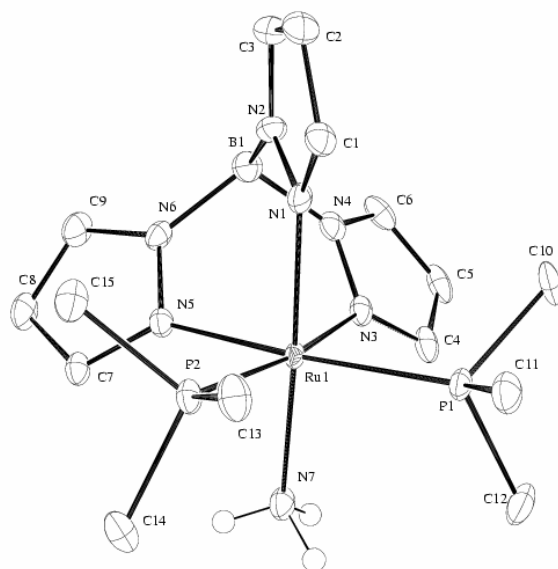


Figure A4 ORTEP diagram of $[\text{TpRu}(\text{PMe})_3]_2(\text{NH}_3)[\text{OTf}]$

Table A.16 Crystal Data and Structure Refinement for $[\text{TpRu}(\text{PMe})_3]_2(\text{NH}_3)[\text{OTf}]$

Identification code	x01046
Empirical formula	$\text{C}_{20}\text{H}_{39}\text{BF}_3\text{N}_7\text{O}_4\text{P}_2\text{RuS}$
Formula weight	704.45
Temperature	148 K
Wavelength	.71073
Crystal system	Triclinic
Space group	P -1
Unit cell dimensions	
a	9.4716(6) Å
b	11.6028(9) Å
c	14.3274(16) Å

Table A.16 (continued)

α	88.195(8) °
β	82.610(9) °
χ	74.679(6) °
Volume	1506.0(2) Å ³
Z	2
Density (calculated)	1.554 Mg/m ³
Absorption Coefficient	.75
F(000)	722.57
Crystal size	.40 x .26 x.10 mm
θ range for data collected	1.20 to 25.00
Limiting indices	-10 ≤ h ≤ 11, 0 ≤ k ≤ 13, -16 ≤ l ≤ 16
Reflections collected	5251
Independent reflections	4493
Absorption correction	psi-scan
Max and min transmission	0.7997 and 0.9926
Refinement method	Full matrix least squares of F ²
Data/restraints/parameters	0 / 0 / 508
Goodness of fit on F ²	1.64
Final R indices [I>2σ(I)]	R1 = 0.035, wR2 = 0.045
Final R indices (all data)	R1 = 0.035, wR2 = 0.045
Largest diff. peak and hole	-1.45 and 1.00 eÅ ⁻³

Table A.17 Atomic Coordinates and Thermal Parameters (x, y, z and u) for [TpRu(PMe)₃]₂(NH₃)]⁺[OTf]⁻

	x	y	z	u
Ru1	.61688(3)	.24754(2)	.721896(20)	.01062(15)
P1	.39840(10)	.23980(8)	.80829(7)	.0142(5)
P2	.77860(10)	.14228(8)	.81957(7)	.0146(5)
N1	.6276(3)	.0891(3)	.6530(2)	.0151(15)
N2	.6613(3)	.0836(3)	.5572(2)	.0153(15)
N3	.4945(3)	.3414(3)	.6138(2)	.0151(16)
N4	.5360(3)	.2976(3)	.5242(2)	.0170(16)
N5	.8010(3)	.2689(3)	.6242(2)	.0143(16)
N6	.8070(3)	.2355(3)	.5328(2)	.0158(15)
N7	.6138(4)	.4158(3)	.7797(3)	.0184(18)
B1	.6781(5)	.1947(4)	.5007(3)	.019(2)
C1	.6197(4)	-.0205(3)	.6808(3)	.0168(19)
C2	.6511(4)	-.0979(3)	.6039(3)	.023(2)
C3	.6758(4)	-.0289(3)	.5276(3)	.022(2)
C4	.3760(4)	.4344(3)	.6093(3)	.020(2)
C5	.3394(4)	.4501(3)	.5180(3)	.023(2)
C6	.4440(4)	.3628(3)	.4664(3)	.0209(20)
C7	.9206(4)	.3094(3)	.6278(3)	.0164(19)
C8	1.0048(4)	.3009(4)	.5403(3)	.022(2)
C9	.9295(4)	.2537(3)	.4815(3)	.022(2)
C10	.2683(4)	.2105(4)	.7346(3)	.023(2)
C11	.3778(5)	.1349(4)	.9028(3)	.021(2)
C12	.2941(5)	.3796(4)	.8680(3)	.026(2)
C13	.7365(5)	.0372(4)	.9095(3)	.0206(20)

C14	.8603(5)	.2311(4)	.8898(3)	.021(2)
C15	.9408(4)	.0446(4)	.7520(3)	.022(2)
S1	.47249(10)	.72792(8)	.84844(7)	.0177(5)
O1	.5176(3)	.8234(2)	.8873(2)	.0264(15)
O2	.4416(3)	.6390(3)	.9152(2)	.0324(16)
O3	.5565(3)	.6808(2)	.76002(20)	.0236(14)
C16	.2921(4)	.8026(4)	.8132(3)	.025(2)
F1	.2999(3)	.8948(2)	.75685(17)	.0317(13)
F2	.2403(3)	.7279(3)	.7666(2)	.0425(17)
F3	.1923(3)	.8444(3)	.88753(18)	.0401(15)
O1s	.9059(3)	.4974(2)	.79812(19)	.0232(14)
C1s	.8701(5)	.5488(4)	.8911(3)	.022(2)
C2s	.9264(5)	.6603(4)	.8848(3)	.028(2)
C3s	.9002(5)	.7036(4)	.7853(3)	.024(2)
C4s	.9314(5)	.5874(4)	.7314(3)	.026(2)
H1b	.701(5)	.173(4)	.424(3)	.030(12)
H1	.600(4)	-.035(3)	.743(3)	.015(10)
H2	.649(4)	-.184(3)	.609(3)	.012(9)
H3	.690(5)	-.040(4)	.469(3)	.029(13)
H4	.330(5)	.483(4)	.675(3)	.036(13)
H5	.263(5)	.506(4)	.493(3)	.019(10)
H6	.460(5)	.346(4)	.407(3)	.020(11)
H7	.945(5)	.332(4)	.683(3)	.026(12)
H7a	.698(5)	.427(4)	.778(3)	.021(11)
H7b	.562(6)	.478(5)	.760(4)	.053(18)
H7c	.572(6)	.427(5)	.846(4)	.049(15)
H8	1.091(5)	.322(4)	.527(3)	.032(12)

H9	.952(4)	.238(3)	.414(3)	.018(10)
H10a	.249(6)	.264(5)	.692(4)	.040(15)
H10b	.307(5)	.131(5)	.709(3)	.034(13)
H10c	.176(6)	.214(4)	.772(3)	.035(13)
H11a	.419(5)	.054(4)	.884(3)	.022(11)
H11b	.418(5)	.155(4)	.950(3)	.023(12)
H11c	.282(6)	.136(5)	.918(4)	.046(15)
H12a	.347(5)	.391(4)	.915(3)	.030(13)
H12b	.285(5)	.443(4)	.830(3)	.027(12)
H12c	.198(6)	.368(4)	.891(3)	.036(13)
H13a	.698(5)	-.021(4)	.884(3)	.021(11)
H13b	.825(5)	-.001(4)	.935(3)	.026(12)
H13c	.668(5)	.079(4)	.963(3)	.023(11)
H14a	.783(6)	.280(4)	.941(4)	.044(14)
H14b	.935(5)	.183(4)	.916(3)	.025(12)
H14c	.906(5)	.285(4)	.847(3)	.023(11)
H15a	.986(5)	.084(4)	.714(3)	.019(11)
H15b	1.006(6)	.010(4)	.799(4)	.042(14)
H15c	.910(5)	-.014(4)	.718(3)	.030(12)
H1sa	.768(6)	.568(4)	.910(3)	.037(13)
H1sb	.918(5)	.488(4)	.937(3)	.024(11)
H2sa	1.033(6)	.636(4)	.885(3)	.043(14)
H2sb	.876(6)	.713(4)	.929(3)	.037(14)
H3sa	.798(5)	.749(4)	.780(3)	.030(12)
H3sb	.966(4)	.752(3)	.756(3)	.015(10)
H4sa	1.029(6)	.568(4)	.705(3)	.038(14)
H4sb	.869(5)	.592(4)	.682(3)	.026(12)

Table A.18 Anisotropic Displacement Parameters for [TpRu(PMe)₃]₂(NH₃)[OTf]

	u11	u22	u33	u12	u13	u23
Ru1	.00738(15)	.00935(15)	.01501(17)	-.00338(10)	.00156(10)	-.00025(10)
P1	.0097(4)	.0151(5)	.0172(5)	-.0044(4)	.0027(4)	-.0003(4)
P2	.0104(4)	.0147(5)	.0192(5)	-.0049(4)	-.0004(4)	.0018(4)
N1	.0110(15)	.0146(15)	.0195(17)	-.0053(12)	.0032(12)	-.0021(12)
N2	.0170(16)	.0163(16)	.0125(15)	-.0046(12)	-.0005(12)	-.0027(12)
N3	.0110(15)	.0118(15)	.0229(17)	-.0044(12)	-.0004(13)	.0015(12)
N4	.0152(16)	.0143(15)	.0238(18)	-.0083(13)	-.0015(13)	.0009(13)
N5	.0114(15)	.0147(15)	.0170(16)	-.0042(12)	-.0010(12)	.0002(12)
N6	.0145(16)	.0159(16)	.0156(16)	-.0039(13)	.0039(12)	-.0006(12)
N7	.0129(17)	.0154(17)	.027(2)	-.0055(14)	.0022(14)	-.0020(14)
B1	.019(2)	.019(2)	.019(2)	-.0073(17)	-.0002(18)	.0003(17)
C1	.0161(19)	.0139(18)	.021(2)	-.0064(15)	-.0018(16)	.0015(15)
C2	.021(2)	.0120(19)	.036(2)	-.0063(16)	-.0032(18)	-.0033(16)
C3	.022(2)	.0176(20)	.026(2)	-.0073(16)	-.0001(17)	-.0070(17)
C4	.0130(19)	.0173(19)	.031(2)	-.0077(15)	-.0022(16)	.0050(16)
C5	.0153(19)	.0155(19)	.041(3)	-.0085(16)	-.0104(18)	.0095(17)
C6	.024(2)	.0204(20)	.025(2)	-.0160(17)	-.0085(17)	.0086(16)
C7	.0119(18)	.0153(18)	.022(2)	-.0052(14)	-.0001(15)	.0021(15)
C8	.0146(19)	.023(2)	.029(2)	-.0083(16)	.0049(16)	.0015(16)
C9	.0195(20)	.024(2)	.021(2)	-.0083(16)	.0057(16)	.0005(16)
C10	.0118(19)	.034(2)	.028(2)	-.0132(18)	-.0030(17)	.0046(20)
C11	.015(2)	.022(2)	.025(2)	-.0081(17)	.0016(17)	.0012(17)
C12	.016(2)	.020(2)	.036(3)	-.0025(17)	.0106(19)	-.0051(19)
C13	.0163(20)	.022(2)	.025(2)	-.0081(17)	-.0025(17)	.0071(17)
C14	.019(2)	.028(2)	.022(2)	-.0116(18)	-.0076(17)	.0048(17)

C15	.0163(20)	.021(2)	.028(2)	-.0030(17)	-.0009(18)	.0026(18)
S1	.0140(5)	.0158(5)	.0224(5)	-.0034(4)	-.0007(4)	.0001(4)
O1	.0229(15)	.0240(15)	.0328(17)	-.0060(12)	-.0041(13)	-.0065(12)
O2	.0310(17)	.0262(16)	.0373(18)	-.0062(13)	.0005(14)	.0113(13)
O3	.0197(14)	.0191(14)	.0295(16)	-.0024(11)	.0014(12)	-.0042(11)
C16	.0143(19)	.034(2)	.025(2)	-.0046(17)	-.0008(16)	.0003(18)
F1	.0243(13)	.0345(14)	.0312(14)	.0004(11)	-.0038(11)	.0097(11)
F2	.0270(14)	.0589(18)	.0511(18)	-.0253(13)	-.0093(13)	-.0042(14)
F3	.0162(12)	.0606(18)	.0320(15)	.0056(12)	.0056(11)	.0037(13)
O1s	.0286(15)	.0193(14)	.0234(15)	-.0109(12)	.0011(12)	-.0032(11)
C1s	.020(2)	.024(2)	.021(2)	-.0081(17)	.0025(17)	-.0014(17)
C2s	.028(2)	.027(2)	.029(2)	-.0104(19)	.0008(19)	-.0085(19)
C3s	.019(2)	.020(2)	.034(2)	-.0080(17)	-.0022(18)	.0027(17)
C4s	.028(2)	.031(2)	.021(2)	-.0105(19)	.0028(19)	.0016(18)

Table A.19 Bond Distances for [TpRu(PMe)₃]₂(NH₃)]⁺[OTf]⁻

Ru1 P1	2.2923(10)	N7 H7c	.98(6)
Ru1 P2	2.2916(10)	B1 H1b	1.12(4)
Ru1 N1	2.087(3)	C1 C2	1.395(5)
Ru1 N3	2.148(3)	C1 H1	.90(4)
Ru1 N5	2.154(3)	C2 C3	1.367(6)
Ru1 N7	2.136(3)	C2 H2	1.00(4)
P1 C10	1.825(4)	C3 H3	.85(5)
P1 C11	1.818(4)	C4 C5	1.391(6)
P1 C12	1.833(4)	C4 H4	1.09(5)
P2 C13	1.826(4)	C5 C6	1.372(6)
P2 C14	1.833(4)	C5 H5	.93(4)
P2 C15	1.830(4)	C6 H6	.86(5)
N1 N2	1.367(4)	C7 C8	1.387(6)
N1 C1	1.339(5)	C7 H7	.92(5)
N2 B1	1.534(5)	C8 C9	1.381(6)
N2 C3	1.352(5)	C8 H8	.91(5)
N3 N4	1.367(4)	C9 H9	.98(4)
N3 C4	1.342(5)	C10 H10a	.86(6)
N4 B1	1.553(5)	C10 H10b	.96(5)
N4 C6	1.346(5)	C10 H10c	.96(5)
N5 N6	1.367(4)	C11 H11a	.95(5)
N5 C7	1.343(5)	C11 H11b	.88(5)
N6 B1	1.547(5)	C11 H11c	.90(6)
N6 C9	1.354(5)	C12 H12a	.92(5)
N7 H7a	.84(5)	C12 H12b	.90(5)
N7 H7b	.82(6)	C12 H12c	.97(5)

C13 H13a	.95(5)	C13 H13b	.95(5)
C13 H13c	.99(5)	C2s H2sb	.89(5)
C14 H14a	1.03(5)	C3s C4s	1.515(6)
C14 H14b	.90(5)	C3s H3sa	.98(5)
C14 H14c	1.00(5)	C3s H3sb	.99(4)
C15 H15a	.85(5)	C4s H4sa	.93(5)
C15 H15b	.97(5)	C4s H4sb	.97(5)
C15 H15c	.97(5)	H7a H7b	1.32(8)
S1 O1	1.439(3)	H7a H7c	1.44(8)
S1 O2	1.446(3)	H7b H7c	1.36(8)
S1 O3	1.446(3)	H10a H10b	1.52(7)
S1 C16	1.826(4)	H10a H10c	1.45(7)
C16 F1	1.331(5)	H10b H10c	1.55(7)
C16 F2	1.336(5)	H11a H11b	1.53(6)
C16 F3	1.340(5)	H11a H11c	1.43(7)
F1 F2	2.151(4)	H11b H11c	1.49(7)
F1 F3	2.154(4)	H12a H12b	1.47(7)
F2 F3	2.158(4)	H12b H12c	1.53(7)
O1s C1s	1.440(5)	H13a H13b	1.55(7)
O1s C4s	1.440(5)	H13b H13c	1.54(6)
C1s C2s	1.520(6)	H14b H14c	1.51(6)
C1s H1sa	.93(5)	H15a H15b	1.47(7)
C1s H1sb	1.00(5)	H15a H15c	1.50(7)
C2s C3s	1.525(6)	H1sa H1sb	1.56(7)
C2s H2sa	.97(6)	H4sa H4sb	1.54(7)

Table A.20 Bond Angles for [TpRu(PMe)₃]₂(NH₃)[OTf]

P1 Ru1 P2	99.60(4)	C14 P2 C15	102.63(20)
P1 Ru1 N1	90.65(8)	Ru1 N1 N2	118.7(2)
P1 Ru1 N3	88.94(8)	Ru1 N1 C1	134.8(3)
P1 Ru1 N5	170.96(8)	N2 N1 C1	106.3(3)
P1 Ru1 N7	93.61(10)	N1 N2 B1	120.7(3)
P2 Ru1 N1	89.73(9)	N1 N2 C3	109.3(3)
P2 Ru1 N3	171.10(8)	B1 N2 C3	129.9(3)
P2 Ru1 N5	89.41(8)	Ru1 N3 N4	117.2(2)
P2 Ru1 N7	93.03(11)	Ru1 N3 C4	136.8(3)
N1 Ru1 N3	87.65(11)	N4 N3 C4	105.9(3)
N1 Ru1 N5	88.78(11)	N3 N4 B1	120.6(3)
N1 Ru1 N7	174.47(13)	N3 N4 C6	109.6(3)
N3 Ru1 N5	82.03(11)	B1 N4 C6	129.7(3)
N3 Ru1 N7	88.90(13)	Ru1 N5 N6	117.6(2)
N5 Ru1 N7	86.46(12)	Ru1 N5 C7	136.5(3)
Ru1 P1 C10	111.96(14)	N6 N5 C7	105.9(3)
Ru1 P1 C11	125.44(14)	N5 N6 B1	120.2(3)
Ru1 P1 C12	114.90(14)	N5 N6 C9	109.9(3)
C10 P1 C11	99.1(2)	B1 N6 C9	129.7(3)
C10 P1 C12	102.8(2)	Ru1 N7 H7a	113(3)
C11 P1 C12	99.5(2)	Ru1 N7 H7b	120(4)
Ru1 P2 C13	124.93(14)	Ru1 N7 H7c	114(3)
Ru1 P2 C14	116.05(14)	H7a N7 H7b	104(5)
Ru1 P2 C15	110.96(15)	H7a N7 H7c	104(4)
C13 P2 C14	99.43(19)	H7b N7 H7c	96(5)
C13 P2 C15	99.61(20)	N2 B1 N4	109.0(3)

N2 B1 N6	108.6(3)	C7 C8 H8	125(3)
N2 B1 H1b	109(2)	C9 C8 H8	129(3)
N4 B1 N6	107.2(3)	N6 C9 C8	108.1(3)
N4 B1 H1b	112(2)	N6 C9 H9	122(2)
N6 B1 H1b	110(2)	C8 C9 H9	129(2)
N1 C1 C2	110.6(4)	P1 C10 H10a	111(3)
N1 C1 H1	118(2)	P1 C10 H10b	108(3)
C2 C1 H1	130(2)	P1 C10 H10c	110(3)
C1 C2 C3	104.9(3)	H10a C10 H10b	113(4)
C1 C2 H2	123(2)	H10a C10 H10c	105(4)
C3 C2 H2	131(2)	H10b C10 H10c	107(4)
N2 C3 C2	108.9(4)	P1 C11 H11a	112(3)
N2 C3 H3	116(3)	P1 C11 H11b	106(3)
C2 C3 H3	134(3)	P1 C11 H11c	110(3)
N3 C4 C5	110.9(4)	H11a C11 H11b	113(4)
N3 C4 H4	116(2)	H11a C11 H11c	100(4)
C5 C4 H4	132(3)	H11b C11 H11c	113(4)
C4 C5 C6	104.6(3)	P1 C12 H12a	106(3)
C4 C5 H5	131(2)	P1 C12 H12b	112(3)
C6 C5 H5	124(2)	P1 C12 H12c	105(3)
N4 C6 C5	109.0(4)	H12a C12 H12b	107(4)
N4 C6 H6	118(3)	H12a C12 H12c	114(4)
C5 C6 H6	132(3)	H12b C12 H12c	110(4)
N5 C7 C8	111.0(4)	P2 C13 H13a	111(2)
N5 C7 H7	122(3)	P2 C13 H13b	107(3)
C8 C7 H7	126(3)	P2 C13 H13c	111(2)
C7 C8 C9	105.0(3)	H13a C13 H13b	110(4)

H13a C13 H13c	110(3)	C16 F1 F3	36.37(20)
H13b C13 H13c	105(4)	F2 F1 F3	60.16(13)
P2 C14 H14a	111(3)	C16 F2 F1	36.2(2)
P2 C14 H14b	109(3)	C16 F2 F3	36.31(20)
P2 C14 H14c	108(2)	F1 F2 F3	60.00(12)
H14a C14 H14b	110(4)	C16 F3 F1	36.1(2)
H14a C14 H14c	110(4)	C16 F3 F2	36.2(2)
H14b C14 H14c	105(4)	F1 F3 F2	59.85(12)
P2 C15 H15a	111(3)	C1s O1s C4s	109.1(3)
P2 C15 H15b	104(3)	O1s C1s C2s	105.5(3)
P2 C15 H15c	109(3)	O1s C1s H1sa	111(3)
H15a C15 H15b	107(4)	O1s C1s H1sb	108(2)
H15a C15 H15c	110(4)	C2s C1s H1sa	110(3)
H15b C15 H15c	113(4)	C2s C1s H1sb	113(2)
O1 S1 O2	115.40(19)	H1sa C1s H1sb	107(4)
O1 S1 O3	114.59(17)	C1s C2s C3s	101.9(3)
O1 S1 C16	103.32(18)	C1s C2s H2sa	108(3)
O2 S1 O3	115.03(17)	C1s C2s H2sb	110(3)
O2 S1 C16	103.72(19)	C3s C2s H2sa	106(3)
O3 S1 C16	102.30(18)	C3s C2s H2sb	112(3)
S1 C16 F1	111.1(3)	H2sa C2s H2sb	115(4)
S1 C16 F2	111.1(3)	C2s C3s C4s	102.4(3)
S1 C16 F3	111.9(3)	C2s C3s H3sa	113(3)
F1 C16 F2	107.5(3)	C2s C3s H3sb	114(2)
F1 C16 F3	107.5(3)	C4s C3s H3sa	108(3)
F2 C16 F3	107.5(3)	C4s C3s H3sb	109(2)
C16 F1 F2	36.3(2)	H3sa C3s H3sb	107(3)

O1s C4s C3s	107.3(3)	N7 H7a H7c	41(3)
O1s C4s H4sa	110(3)	H7b H7a H7c	58(4)
O1s C4s H4sb	109(3)	N7 H7b H7a	37(3)
C3s C4s H4sa	108(3)	N7 H7b H7c	46(4)
C3s C4s H4sb	113(3)	H7a H7b H7c	65(4)
H4sa C4s H4sb	108(4)	N7 H7c H7a	34(3)
N7 H7a H7b	37(3)	N7 H7c H7b	37(3)
H7a H7c H7b	55(4)	C12 H12b H12a	36(3)
C10 H10a H10b	35(3)	C12 H12b H12c	36(3)
C10 H10a H10c	39(3)	H12a H12b H12c	63(3)
H10b H10a H10c	62(3)	C12 H12c H12b	33(2)
C10 H10b H10a	31(3)	C13 H13a H13b	34(2)
C10 H10b H10c	36(3)	C13 H13b H13a	35(2)
H10a H10b H10c	56(3)	C13 H13b H13c	38(2)
C10 H10c H10a	34(3)	H13a H13b H13c	61(3)
C10 H10c H10b	36(3)	C13 H13c H13b	36(2)
H10a H10c H10b	60(3)	C14 H14b H14c	39(3)
C11 H11a H11b	32(2)	C14 H14c H14b	34(2)
C11 H11a H11c	38(3)	C15 H15a H15b	39(3)
H11b H11a H11c	60(3)	C15 H15a H15c	37(3)
C11 H11b H11a	34(2)	H15b H15a H15c	66(3)
C11 H11b H11c	33(3)	C15 H15b H15a	33(2)
H11a H11b H11c	56(3)	C15 H15c H15a	31(2)
C11 H11c H11a	40(3)	C1s H1sa H1sb	37(3)
C11 H11c H11b	33(3)	C1s H1sb H1sa	34(2)
H11a H11c H11b	63(3)	C4s H4sa H4sb	36(3)
C12 H12a H12b	35(3)	C4s H4sb H4sa	34(2)

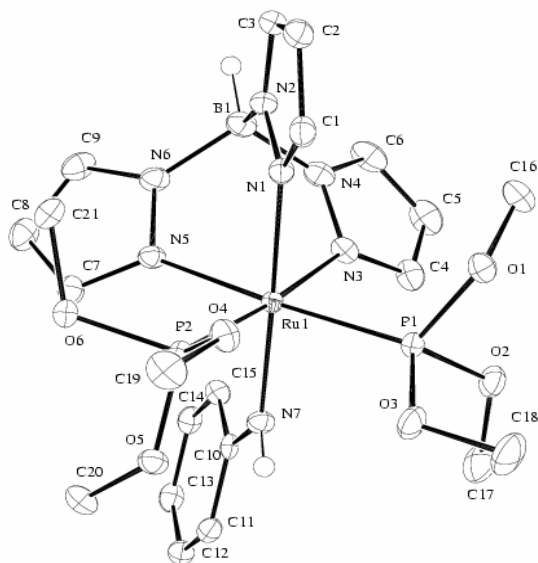


Figure A5 ORTEP diagram of $\text{TpRu}\{\text{P}(\text{OMe})_3\}_2\text{NHPh}$

Table A.21 Crystal Data and Structure Refinement for $\text{TpRu}\{\text{P}(\text{OMe})_3\}_2\text{NHPh}$

Identification code	x02014
Empirical formula	$\text{C}_{27}\text{H}_{40}\text{BN}_7\text{O}_6\text{P}_2\text{Ru}$
Formula weight	732.48
Temperature	148 K
Wavelength	.71073
Crystal system	Triclinic
Space group	P -1
Unit cell dimensions	
a	9.8449(4) Å
b	11.2687(4) Å
c	14.8435(5) Å

Table A.21 (continued)

α	86.667(3) °
β	87.380(4) °
χ	87.854(4) °
Volume	1641.22(10) Å ³
Z	2
Density (calculated)	1.482 Mg/m ³
Absorption Coefficient	.63
F(000)	754.30
Crystal size	.54 x .24 x.22 mm
θ range for data collected	1.20 to 25.00
Limiting indices	-11 ≤ h ≤ 11, 0 ≤ k ≤ 13, -17 ≤ l ≤ 17
Reflections collected	5751
Independent reflections	5397
Absorption correction	psi-scan
Max and min transmission	0.9320 and 0.9997
Refinement method	Full matrix least squares of F ²
Data/restraints/parameters	0 / 0 / 405
Goodness of fit on F2	1.50
Final R indices [I>2σ(I)]	R1 = 0.022, wR2 = 0.038
Final R indices (all data)	R1 = 0.022, wR2 = 0.038
Largest diff. peak and hole	-0.590 and 0.480 eÅ ⁻³

Table A.22 Atomic Coordinates and Thermal Parameters (x, y, z and u)
 TpRu{P(OMe)₃}₂NHPh

	x	y	z	u
Ru1	.192799(13)	.684007(11)	.728309(8)	.01120(9)
P1	.01293(4)	.57954(4)	.77565(3)	.0138(2)
P2	.32154(4)	.59974(4)	.83474(3)	.0124(2)
N1	.25915(15)	.55707(13)	.63528(10)	.0150(7)
N2	.29898(15)	.59488(14)	.54930(10)	.0166(8)
N3	.08149(16)	.76940(14)	.61737(10)	.0173(7)
N4	.14535(17)	.77619(14)	.53335(10)	.0197(8)
N5	.35785(16)	.78914(13)	.67253(10)	.0154(7)
N6	.38425(16)	.79466(14)	.58105(10)	.0180(7)
N7	.13066(16)	.81759(14)	.81586(11)	.0154(8)
O1	-.01923(13)	.46563(11)	.72109(9)	.0203(6)
O2	-.13641(13)	.64435(12)	.77020(9)	.0214(7)
O3	.01169(13)	.52120(13)	.87580(9)	.0233(7)
O4	.30224(13)	.46041(11)	.85537(8)	.0167(6)
O5	.30943(13)	.64454(11)	.93561(8)	.0160(6)
O6	.48528(12)	.60897(11)	.81988(8)	.0171(6)
B1	.2929(2)	.72816(19)	.51961(14)	.0194(11)
C1	.27449(18)	.43807(16)	.63973(13)	.0178(9)
C2	.32274(19)	.39846(17)	.55647(13)	.0212(9)
C3	.33737(19)	.50008(17)	.50179(12)	.0202(9)
C4	-.04350(19)	.81814(17)	.60733(13)	.0218(9)
C5	-.0615(2)	.85656(18)	.51771(15)	.0278(10)
C6	.0600(2)	.82914(18)	.47307(13)	.0260(10)
C7	.44917(19)	.85663(16)	.70703(13)	.0185(9)

C8	.5346(2)	.90609(17)	.63903(14)	.0239(9)
C9	.4902(2)	.86460(17)	.56012(13)	.0227(9)
C10	.13565(17)	.93866(16)	.81277(12)	.0141(8)
C11	.11777(18)	1.00104(16)	.89312(12)	.0164(8)
C12	.12129(19)	1.12375(17)	.89289(13)	.0198(9)
C13	.14253(19)	1.19256(16)	.81262(13)	.0200(9)
C14	.15948(18)	1.13316(16)	.73260(12)	.0187(8)
C15	.15630(19)	1.01012(16)	.73160(12)	.0171(8)
C16	-.0562(2)	.4814(2)	.62847(15)	.0307(10)
C17	-.1794(2)	.73673(20)	.82966(17)	.0340(11)
C18	-.0964(2)	.4433(2)	.90966(15)	.0310(10)
C19	.3782(2)	.39428(17)	.92360(13)	.0224(9)
C20	.36855(20)	.75330(17)	.95903(12)	.0196(8)
C21	.55139(19)	.56200(18)	.73978(13)	.0226(9)
H1b	.330(2)	.7349(19)	.4510(15)	.022(5)
H1	.255	.387	.693	.0279
H2	.341	.318	.541	.0317
H3	.370	.503	.440	.0304
H4	-.111	.826	.655	.0320
H5	-.142	.894	.493	.0381
H6	.081	.845	.410	.0360
H7	.455	.869	.770	.0288
H7n	.116(2)	.7946(19)	.8698(15)	.015(5)
H8	.608	.958	.645	.0342
H9	.528	.883	.501	.0322
H11	.103	.956	.950	.0263
H12	.109	1.162	.949	.0299

H13	.145	1.278	.812	.0301
H14	.174	1.179	.677	.0285
H15	.168	.973	.675	.0271
H16a	-.055(2)	.4054(3)	.6023(4)	.093(12)
H16b	.0078(12)	.5314(15)	.5955(3)	.062(9)
H16c	-.1458(9)	.5178(17)	.62577(19)	.068(10)
H17a	-.2724(6)	.7604(10)	.8194(8)	.067(10)
H17b	-.1229(11)	.8039(6)	.8179(8)	.032(6)
H17c	-.1717(16)	.7073(5)	.89127(12)	.046(8)
H18a	-.1004(12)	.4397(13)	.97450(14)	.064(9)
H18b	-.0780(10)	.3649(4)	.8889(10)	.061(9)
H18c	-.1818(3)	.4739(9)	.8879(10)	.044(7)
H19a	.3584(11)	.3115(2)	.9234(7)	.027(6)
H19b	.3531(11)	.4233(9)	.98181(14)	.032(6)
H19c	.47383(17)	.4040(10)	.9110(6)	.043(7)
H20a	.3492(11)	.7650(6)	1.0219(2)	.036(7)
H20b	.3305(10)	.81909(16)	.9234(6)	.014(5)
H20c	.4653(2)	.7481(5)	.9474(8)	.013(5)
H21a	.64822(17)	.5662(13)	.7432(5)	.030(6)
H21b	.5221(13)	.6080(9)	.68730(10)	.046(8)
H21c	.5278(13)	.4807(5)	.7357(6)	.069(10)
C1s	.5440(3)	.1803(2)	.78004(17)	.0397(12)
C2s	.5048(2)	.0908(2)	.84163(18)	.0389(12)
C3s	.6022(3)	.0200(2)	.88557(17)	.0381(12)
C4s	.7384(2)	.0392(2)	.86717(16)	.0339(11)
C5s	.7780(2)	.1280(3)	.80638(16)	.0398(13)
C6s	.6816(3)	.1998(2)	.76290(16)	.0424(13)

H1s	.477	.229	.749	.0503
H2s	.410	.077	.854	.0498
H3s	.575	-.042	.929	.0487
H4s	.806	-.010	.897	.0449
H5s	.873	.141	.794	.0501
H6s	.710	.263	.721	.0525

Table A.23 Anisotropic Displacement Parameters for $\text{TpRu}\{\text{P}(\text{OMe})_3\}_2\text{NHPH}$

	u11	u22	u33	u12	u13	u23
Ru1	.01050(10)	.01174(10)	.01146(10)	-.00178(6)	-.00034(6)	-.00074(6)
P1	.0110(2)	.0153(2)	.0154(2)	-.00242(18)	-.00003(18)	-.00141(18)
P2	.0115(2)	.0131(2)	.0128(2)	-.00178(17)	-.00038(17)	-.00071(17)
N1	.0134(8)	.0172(8)	.0147(8)	-.0020(6)	-.0008(6)	-.0009(6)
N2	.0161(8)	.0218(8)	.0121(7)	-.0022(6)	.0000(6)	-.0023(6)
N3	.0198(8)	.0158(8)	.0166(8)	-.0020(6)	-.0034(6)	-.0009(6)
N4	.0248(9)	.0193(8)	.0152(8)	-.0005(6)	-.0035(6)	-.0010(6)
N5	.0181(8)	.0155(8)	.0125(7)	-.0020(6)	.0010(6)	-.0007(6)
N6	.0215(8)	.0184(8)	.0138(7)	-.0033(6)	.0027(6)	.0006(6)
N7	.0178(8)	.0159(8)	.0122(8)	-.0016(6)	.0009(6)	.0005(6)
O1	.0194(7)	.0186(7)	.0239(7)	-.0061(5)	.0005(5)	-.0061(5)
O2	.0122(6)	.0226(7)	.0295(8)	.0004(5)	.0005(5)	-.0050(6)
O3	.0162(7)	.0349(8)	.0182(7)	-.0087(6)	.0018(5)	.0049(6)
O4	.0171(6)	.0136(6)	.0197(7)	-.0016(5)	-.0042(5)	.0005(5)
O5	.0190(6)	.0167(6)	.0124(6)	-.0030(5)	-.0002(5)	-.0009(5)
O6	.0116(6)	.0227(7)	.0174(6)	-.0021(5)	-.0012(5)	-.0031(5)
B1	.0225(11)	.0216(11)	.0143(10)	-.0009(8)	-.0014(8)	-.0011(8)
C1	.0137(9)	.0166(9)	.0235(10)	-.0021(7)	-.0016(7)	-.0027(7)
C2	.0176(9)	.0199(10)	.0272(10)	-.0016(7)	-.0003(8)	-.0099(8)
C3	.0158(9)	.0274(10)	.0184(9)	-.0019(8)	-.0003(7)	-.0104(8)
C4	.0201(10)	.0175(9)	.0282(11)	.0007(7)	-.0061(8)	-.0014(8)
C5	.0290(11)	.0231(10)	.0318(11)	.0036(8)	-.0134(9)	.0013(9)
C6	.0373(12)	.0228(10)	.0182(10)	.0002(9)	-.0110(9)	.0026(8)
C7	.0167(9)	.0167(9)	.0221(10)	-.0017(7)	-.0012(7)	-.0007(7)
C8	.0201(10)	.0187(9)	.0330(11)	-.0075(8)	.0031(8)	-.0012(8)

C9	.0250(10)	.0183(10)	.0238(10)	-.0049(8)	.0092(8)	.0023(8)
C10	.0077(8)	.0166(9)	.0180(9)	-.0009(6)	-.0020(7)	-.0007(7)
C11	.0137(9)	.0183(9)	.0171(9)	-.0004(7)	.0006(7)	.0002(7)
C12	.0177(9)	.0214(10)	.0210(9)	-.0010(7)	.0002(7)	-.0071(7)
C13	.0165(9)	.0138(9)	.0299(10)	-.0011(7)	-.0007(8)	-.0020(8)
C14	.0158(9)	.0194(9)	.0204(9)	-.0019(7)	-.0018(7)	.0042(7)
C15	.0174(9)	.0163(9)	.0178(9)	-.0012(7)	-.0024(7)	-.0019(7)
C16	.0247(11)	.0419(13)	.0279(11)	-.0065(9)	-.0058(9)	-.0159(9)
C17	.0194(10)	.0284(11)	.0545(15)	.0018(9)	.0067(10)	-.0133(10)
C18	.0218(11)	.0399(12)	.0299(11)	-.0108(9)	.0046(9)	.0101(9)
C19	.0264(10)	.0180(9)	.0226(10)	.0019(8)	-.0055(8)	.0033(8)
C20	.0242(10)	.0176(9)	.0180(9)	-.0024(7)	-.0055(8)	-.0039(7)
C21	.0133(9)	.0296(11)	.0249(10)	.0008(8)	.0026(7)	-.0060(8)
C1s	.0368(13)	.0456(14)	.0388(13)	.0111(11)	-.0164(11)	-.0161(11)
C2s	.0184(11)	.0392(13)	.0624(16)	-.0039(9)	.0004(11)	-.0310(12)
C3s	.0461(14)	.0259(11)	.0439(14)	-.0089(10)	.0016(11)	-.0148(10)
C4s	.0323(12)	.0351(12)	.0366(13)	.0088(10)	-.0116(10)	-.0203(10)
C5s	.0211(11)	.0657(17)	.0348(13)	-.0023(11)	.0028(10)	-.0240(12)
C6s	.0481(15)	.0554(16)	.0240(12)	-.0081(12)	.0029(11)	-.0056(11)

Table A.24 Bond Distances for $\text{TpRu}\{\text{P}(\text{OMe})_3\}_2\text{NHPH}$

Ru1 P1	2.2275(5)	N7 H7n	.83(2)
Ru1 P2	2.2186(5)	O1 C16	1.438(3)
Ru1 N1	2.1111(15)	O2 C17	1.443(2)
Ru1 N3	2.1772(15)	O3 C18	1.458(2)
Ru1 N5	2.1532(15)	O4 C19	1.442(2)
Ru1 N7	2.1012(15)	O5 C20	1.443(2)
P1 O1	1.6059(13)	O6 C21	1.447(2)
P1 O2	1.6201(13)	B1 H1b	1.07(2)
P1 O3	1.5898(14)	C1 C2	1.395(3)
P2 O4	1.5988(13)	C1 H1	.9601(19)
P2 O5	1.6055(12)	C2 C3	1.373(3)
P2 O6	1.6234(13)	C2 H2	.9551(18)
N1 N2	1.367(2)	C3 H3	.9597(18)
N1 C1	1.342(2)	C4 C5	1.392(3)
N2 B1	1.540(3)	C4 H4	.9586(20)
N2 C3	1.347(2)	C5 C6	1.374(3)
N3 N4	1.370(2)	C5 H5	.9597(20)
N3 C4	1.340(2)	C6 H6	.9599(20)
N4 B1	1.540(3)	C7 C8	1.389(3)
N4 C6	1.354(2)	C7 H7	.9596(19)
N5 N6	1.369(2)	C8 C9	1.381(3)
N5 C7	1.337(2)	C8 H8	.9577(19)
N6 B1	1.551(3)	C9 H9	.9585(19)
N6 C9	1.345(2)	C10 C11	1.420(3)
N7 C10	1.365(2)	C10 C15	1.421(3)

C11 C12	1.384(3)	C19 H19c	.960(3)
C11 H11	.9602(18)	C20 H20a	.960(4)
C12 C13	1.395(3)	C20 H20b	.960(7)
C12 H12	.9614(18)	C20 H20c	.960(3)
C13 C14	1.397(3)	C21 H21a	.960(3)
C13 H13	.9592(18)	C21 H21b	.960(7)
C14 C15	1.389(3)	C21 H21c	.960(7)
C14 H14	.9605(18)	C1s C2s	1.375(4)
C15 H15	.9602(18)	C1s C6s	1.390(4)
C16 H16a	.960(5)	C1s H1s	.960(2)
C16 H16b	.960(13)	C2s C3s	1.386(4)
C16 H16c	.960(11)	C2s H2s	.960(2)
C17 H17a	.960(7)	C3s C4s	1.379(4)
C17 H17b	.960(9)	C3s H3s	.961(3)
C17 H17c	.960(4)	C4s C5s	1.364(4)
C18 H18a	.960(3)	C4s H4s	.962(2)
C18 H18b	.960(7)	C5s C6s	1.383(4)
C18 H18c	.960(7)	C5s H5s	.960(2)
C19 H19a	.960(4)	C6s H6s	.964(3)
C19 H19b	.960(5)		

Table A.25 Bond Angles for $\text{TpRu}\{\text{P}(\text{OMe})_3\}_2\text{NHPPh}$

P1 Ru1 P2	92.822(17)
P1 Ru1 N1	92.54(4)
P1 Ru1 N3	91.36(4)
P1 Ru1 N5	175.25(4)
P1 Ru1 N7	90.01(4)
P2 Ru1 N1	92.13(4)
P2 Ru1 N3	175.38(4)
P2 Ru1 N5	91.81(4)
P2 Ru1 N7	89.52(4)
N1 Ru1 N3	85.71(6)
N1 Ru1 N5	86.24(6)
N1 Ru1 N7	176.89(6)
N3 Ru1 N5	83.98(6)
N3 Ru1 N7	92.45(6)
N5 Ru1 N7	91.08(6)
Ru1 P1 O1	117.65(5)
Ru1 P1 O2	118.07(5)
Ru1 P1 O3	117.50(5)
O1 P1 O2	97.00(7)
O1 P1 O3	100.13(7)
O2 P1 O3	103.02(7)
Ru1 P2 O4	115.18(5)
Ru1 P2 O5	120.44(5)
Ru1 P2 O6	117.60(5)
O4 P2 O5	100.11(7)

O4 P2 O6	103.05(7)
O5 P2 O6	97.18(7)
Ru1 N1 N2	119.20(11)
Ru1 N1 C1	134.32(13)
N2 N1 C1	106.48(14)
N1 N2 B1	120.66(14)
N1 N2 C3	109.37(15)
B1 N2 C3	129.96(16)
Ru1 N3 N4	117.90(11)
Ru1 N3 C4	135.90(13)
N4 N3 C4	106.17(15)
N3 N4 B1	120.38(15)
N3 N4 C6	109.51(16)
B1 N4 C6	130.10(16)
Ru1 N5 N6	118.98(11)
Ru1 N5 C7	134.75(13)
N6 N5 C7	106.27(15)
N5 N6 B1	119.62(15)
N5 N6 C9	109.69(15)
B1 N6 C9	130.67(16)
Ru1 N7 C10	135.30(13)
Ru1 N7 H7n	115.5(14)
C10 N7 H7n	107.3(15)
P1 O1 C16	119.72(13)
P1 O2 C17	121.39(12)
P1 O3 C18	121.08(12)
P2 O4 C19	121.22(11)

P2 O5 C20	122.07(11)
P2 O6 C21	118.82(11)
N2 B1 N4	108.67(16)
N2 B1 N6	108.52(15)
N2 B1 H1b	106.5(11)
N4 B1 N6	108.34(15)
N4 B1 H1b	113.5(11)
N6 B1 H1b	111.2(12)
N1 C1 C2	110.31(17)
N1 C1 H1	124.97(18)
C2 C1 H1	124.72(18)
C1 C2 C3	104.87(16)
C1 C2 H2	127.7(2)
C3 C2 H2	127.48(20)
N2 C3 C2	108.97(16)
N2 C3 H3	125.67(20)
C2 C3 H3	125.36(18)
N3 C4 C5	110.74(18)
N3 C4 H4	124.74(19)
C5 C4 H4	124.51(19)
C4 C5 C6	105.06(17)
C4 C5 H5	127.4(2)
C6 C5 H5	127.5(2)
N4 C6 C5	108.52(17)
N4 C6 H6	125.8(2)
C5 C6 H6	125.71(20)
N5 C7 C8	110.70(17)

N5 C7 H7	124.63(18)
C8 C7 H7	124.67(18)
C7 C8 C9	104.94(17)
C7 C8 H8	127.6(2)
C9 C8 H8	127.5(2)
N6 C9 C8	108.41(17)
N6 C9 H9	125.8(2)
C8 C9 H9	125.78(20)
N7 C10 C11	120.50(16)
N7 C10 C15	123.66(16)
C11 C10 C15	115.84(16)
C10 C11 C12	122.33(17)
C10 C11 H11	118.79(17)
C12 C11 H11	118.88(18)
C11 C12 C13	121.09(17)
C11 C12 H12	119.58(19)
C13 C12 H12	119.32(18)
C12 C13 C14	117.60(16)
C12 C13 H13	121.17(18)
C14 C13 H13	121.24(19)
C13 C14 C15	122.07(17)
C13 C14 H14	118.91(18)
C15 C14 H14	119.02(18)
C10 C15 C14	121.07(16)
C10 C15 H15	119.45(17)
C14 C15 H15	119.48(18)
O1 C16 H16a	109.5(5)

O1 C16 H16b 109.4(5)
O1 C16 H16c 109.5(3)
H16a C16 H16b 109.5(12)
H16a C16 H16c 109.5(15)
H16b C16 H16c 109.5(12)
O2 C17 H17a 109.5(7)
O2 C17 H17b 109.5(6)
O2 C17 H17c 109.5(5)
H17a C17 H17b 109.5(9)
H17a C17 H17c 109.5(11)
H17b C17 H17c 109.5(10)
O3 C18 H18a 109.5(8)
O3 C18 H18b 109.5(6)
O3 C18 H18c 109.5(6)
H18a C18 H18b 109.5(12)
H18a C18 H18c 109.5(11)
H18b C18 H18c 109.5(10)
O4 C19 H19a 109.4(6)
O4 C19 H19b 109.5(6)
O4 C19 H19c 109.5(6)
H19a C19 H19b 109.5(8)
H19a C19 H19c 109.5(10)
H19b C19 H19c 109.5(9)
O5 C20 H20a 109.4(5)
O5 C20 H20b 109.5(5)
O5 C20 H20c 109.5(4)
H20a C20 H20b 109.5(7)

H20a C20 H20c 109.5(10)
H20b C20 H20c 109.5(8)
O6 C21 H21a 109.5(6)
O6 C21 H21b 109.5(6)
O6 C21 H21c 109.5(6)
H21a C21 H21b 109.5(10)
H21a C21 H21c 109.5(12)
H21b C21 H21c 109.5(9)
C2s C1s C6s 119.6(2)
C2s C1s H1s 120.1(3)
C6s C1s H1s 120.3(3)
C1s C2s C3s 120.0(2)
C1s C2s H2s 119.9(3)
C3s C2s H2s 120.1(3)
C2s C3s C4s 119.9(2)
C2s C3s H3s 119.8(2)
C4s C3s H3s 120.3(3)
C3s C4s C5s 120.4(2)
C3s C4s H4s 119.8(3)
C5s C4s H4s 119.8(2)
C4s C5s C6s 120.1(2)
C4s C5s H5s 119.9(3)
C6s C5s H5s 120.0(3)
C1s C6s C5s 120.0(2)
C1s C6s H6s 120.0(3)
C5s C6s H6s 120.0(3)

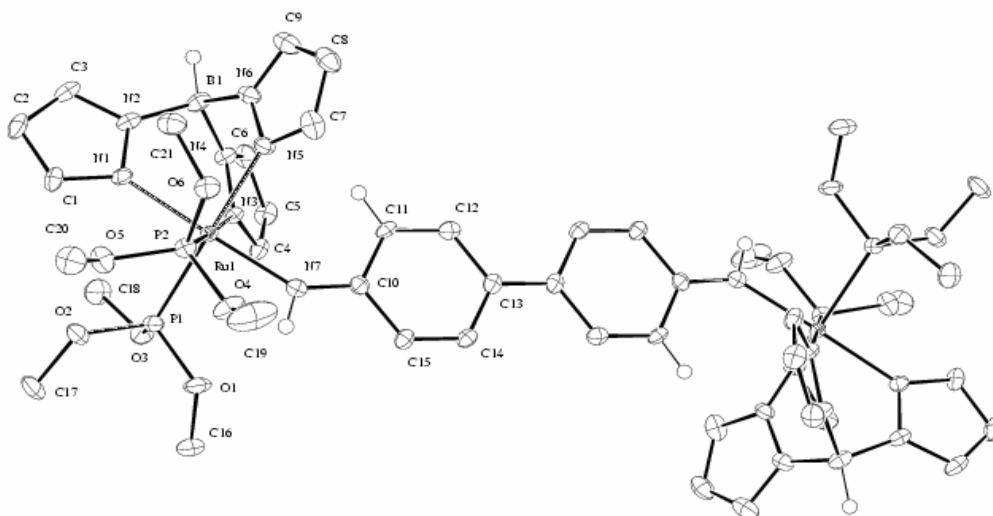


Figure A6 ORTEP diagram of $[\text{TpRu}\{\text{P}(\text{OMe})_3\}_2\text{NHC}_6\text{H}_4^-]_2[\text{OTf}]_2$

Table A.26 Crystal Data and Structure Refinement $[\text{TpRu}\{\text{P}(\text{OMe})_3\}_2\text{NHC}_6\text{H}_4^-]_2[\text{OTf}]_2$

Identification code	x02032
Empirical formula	$\text{C}_{23}\text{H}_{35}\text{BCl}_2\text{F}_3\text{N}_7\text{O}_9\text{P}_2\text{RuS}$
Formula weight	887.35
Temperature	148 K
Wave length	0.70930
Crystal system	Monoclinic
Space Group	P 21/c
Unit cell dimensions	$a = 9.6170(11) \text{ \AA}$ $b = 25.474(3) \text{ \AA}$ $c = 14.5857(18) \text{ \AA}$
Volume, z	$3568.4(7) \text{ \AA}^3$
Unit cell dimensions	

Table A.26 (continued)

a	9.6277(3) Å
b	17.2937(5) Å
c	14.3109(4) Å
α	90.00 °
β	92.974 °
χ	90.00 °
Volume	3568.4(7) Å ³
Z	4
Density (calculated)	1.652 Mg/m ³
Absorption Coefficient	0.86
F(000)	1798.58
Crystal size	0.32 x 0.14 x 0.10 mm
θ range for data collected	1.20 to 25.00
Limiting indices	-11 ≤ h ≤ 11, 0 ≤ k ≤ 30, 0 ≤ l ≤ 17
Reflections collected	6023
Independent reflections	4366
Absorption correction	psi-scan
Max and min transmission	0.8845 and 0.9937
Refinement method	Full matrix least squares of F ²
Data/restraints/parameters	4366 / 0 / 442

Table A.26 (continued)

Goodness of fit on F2	1.42
Final R indices [$I > 2\sigma(I)$]	R1 = 0.046, wR2 = 0.049
Final R indices (all data)	R1 = 0.046, wR2 = 0.050
Largest diff. peak and hole	-0.72 and 1.03 eÅ ⁻³

Table A.27 Atomic Coordinates and Thermal Parameters (x, y, z and u) for [TpRu{P(OMe)₃}₂NHC₆H₄-]₂[OTf]₂

	x	y	z	u
Ru1	.51232(4)	.103555(18)	.24192(3)	.0117(2)
P1	.58010(15)	.09033(6)	.38978(10)	.0163(7)
P2	.32670(14)	.05108(6)	.25174(10)	.0152(7)
O1	.6507(4)	.03458(15)	.4041(3)	.025(2)
O2	.4622(4)	.09563(16)	.4619(3)	.024(2)
O3	.7039(4)	.12690(15)	.4319(3)	.0209(19)
O4	.3671(4)	-.00934(15)	.2600(3)	.025(2)
O5	.2285(4)	.06363(16)	.3338(3)	.022(2)
O6	.2188(4)	.04887(15)	.1636(3)	.0190(20)
N1	.4007(5)	.17112(18)	.2724(3)	.017(2)
N2	.4158(5)	.21537(17)	.2203(3)	.017(2)
N3	.6854(4)	.15473(17)	.2225(3)	.014(2)
N4	.6620(5)	.20105(17)	.1769(3)	.016(2)
N5	.4618(5)	.12069(18)	.0996(3)	.017(2)
N6	.4639(5)	.17148(19)	.0717(3)	.018(2)
N7	.6318(5)	.04047(17)	.2098(3)	.015(2)
B1	.5127(7)	.2158(3)	.1398(5)	.018(3)
C1	.3066(5)	.1831(2)	.3344(4)	.018(3)
C2	.2624(6)	.2349(2)	.3227(4)	.023(3)
C3	.3324(6)	.2537(2)	.2501(4)	.023(3)
C4	.8220(6)	.1520(2)	.2433(4)	.018(3)
C5	.8888(6)	.1961(2)	.2125(4)	.021(3)
C6	.7852(6)	.2262(2)	.1703(4)	.023(3)
C7	.4198(6)	.0925(2)	.0258(4)	.024(3)

C8	.3959(6)	.1252(3)	-.0499(4)	.026(3)
C9	.4256(6)	.1747(3)	-.0184(4)	.025(3)
C10	.7274(6)	.0297(2)	.1513(4)	.016(3)
C11	.7595(5)	.0645(2)	.0768(4)	.015(3)
C12	.8612(6)	.0517(2)	.0191(4)	.017(3)
C13	.9441(5)	.0050(2)	.0290(4)	.016(3)
C14	.9096(5)	-.0295(2)	.1025(4)	.015(3)
C15	.8067(6)	-.0183(2)	.1592(4)	.016(3)
C16	.7463(7)	.0188(3)	.4800(4)	.032(3)
C17	.4903(7)	.0915(3)	.5604(4)	.035(4)
C18	.6779(7)	.1825(2)	.4428(4)	.029(3)
C19	.2854(8)	-.0534(3)	.2304(6)	.052(5)
C20	.0929(6)	.0398(3)	.3442(4)	.029(3)
C21	.1479(6)	.0968(2)	.1385(4)	.025(3)
S1	.03133(19)	.12596(6)	.64346(12)	.0316(9)
O7	.1215(6)	.1341(2)	.7216(4)	.053(3)
O8	.0463(6)	.0776(2)	.5957(4)	.062(4)
O9	-.1118(5)	.1418(2)	.6526(4)	.055(3)
C22	.0914(7)	.1742(3)	.5621(4)	.032(4)
F1	.2258(4)	.17044(18)	.5497(3)	.047(3)
F2	.0715(5)	.22302(16)	.5931(3)	.053(3)
F3	.0242(5)	.1704(2)	.4802(3)	.060(3)
C1s	.9028(7)	.1975(3)	.8676(5)	.037(4)
C11s	.73168(17)	.17992(7)	.89546(14)	.0431(11)
C12s	1.02681(19)	.17683(7)	.95281(12)	.0386(9)
H1b	.512	.256	.105	.0281
H1	.277	.160	.381	.0277

H2	.197	.254	.358	.0329
H3	.323	.288	.224	.0325
H4	.867	.123	.275	.0284
H5	.986	.204	.219	.0306
H6	.798	.259	.140	.0334
H7	.407	.055	.026	.0337
H7n	.633	.018	.254	.0247
H8	.367	.115	-.111	.0361
H9	.419	.207	-.053	.0351
H11	.707	.096	.068	.0247
H12	.879	.075	-.031	.0266
H14	.963	-.061	.112	.0251
H15	.785	-.043	.206	.0258
H16a	.775	-.017	.472	.0422
H16b	.827	.041	.482	.0422
H16c	.699	.022	.536	.0422
H17a	.405	.096	.591	.0446
H17b	.528	.057	.574	.0446
H17c	.556	.118	.580	.0446
H18a	.760	.199	.469	.0385
H18b	.653	.198	.384	.0385
H18c	.603	.187	.483	.0385
H19a	.336	-.085	.243	.0607
H19b	.202	-.053	.264	.0607
H19c	.261	-.051	.166	.0607
H20a	.053	.053	.399	.0387
H20b	.033	.048	.292	.0387

H20c	.103	.002	.349	.0387
H21a	.088	.091	.085	.0344
H21b	.094	.108	.188	.0344
H21c	.215	.123	.125	.0344
H1sa	.908	.235	.862	.0472
H1sb	.923	.182	.810	.0472

Table A.28 Anisotropic Displacement Parameters for [TpRu{P(OMe)₃}₂NHC₆H₄]₂[OTf]₂

	u11	u22	u33	u12	u13	u23
Ru1	.00970(20)	.0125(2)	.0189(3)	-.0009(2)	.00126(18)	-.0020(2)
P1	.0128(7)	.0163(8)	.0258(9)	-.0020(6)	.0015(6)	-.0027(7)
P2	.0143(7)	.0146(8)	.0230(8)	-.0016(7)	.0003(6)	-.0007(7)
O1	.021(2)	.028(2)	.024(2)	-.0088(18)	-.0041(18)	-.0023(18)
O2	.023(2)	.013(2)	.069(3)	-.0003(17)	.015(2)	-.001(2)
O3	.021(2)	.019(2)	.029(2)	-.0048(17)	.0026(17)	.0017(18)
O4	.0149(20)	.036(2)	.031(2)	-.0127(18)	-.0070(17)	.0017(19)
O5	.0191(20)	.043(3)	.027(2)	-.0042(20)	-.0037(17)	-.006(2)
O6	.019(2)	.023(2)	.069(3)	.0072(18)	-.021(2)	.000(2)
B1	.013(3)	.023(4)	.034(4)	.001(3)	.003(3)	-.003(3)
N1	.012(2)	.019(3)	.024(3)	.0013(20)	.0026(20)	-.008(2)
N2	.021(3)	.020(3)	.014(2)	-.002(2)	.0051(20)	-.002(2)
N3	.017(2)	.018(3)	.016(3)	.003(2)	.000(2)	-.001(2)
N4	.018(3)	.024(3)	.016(3)	.001(2)	.002(2)	-.005(2)
N5	.008(2)	.015(3)	.020(3)	.0008(19)	.003(2)	.002(2)
N6	.015(2)	.016(3)	.021(3)	-.002(2)	.002(2)	.000(2)
N7	.013(2)	.017(3)	.019(3)	.0043(20)	.0007(20)	-.004(2)
C1	.015(3)	.013(3)	.034(4)	-.001(2)	-.002(3)	-.005(3)
C2	.019(3)	.017(3)	.043(4)	.000(3)	.007(3)	-.013(3)
C3	.019(3)	.025(4)	.032(3)	-.002(3)	.009(3)	-.011(3)
C4	.016(3)	.026(4)	.031(3)	-.003(3)	-.003(3)	-.007(3)
C5	.016(3)	.026(4)	.036(4)	-.001(3)	-.008(3)	-.006(3)
C6	.030(3)	.019(3)	.022(3)	.005(3)	-.003(3)	.000(3)

C7	.014(3)	.021(3)	.024(3)	-.003(3)	.003(3)	-.006(3)
C8	.019(3)	.014(3)	.037(4)	-.001(3)	.002(3)	-.006(3)
C9	.020(3)	.011(3)	.045(4)	-.006(3)	.006(3)	.005(3)
C10	.015(3)	.012(3)	.017(3)	-.002(2)	-.002(2)	-.004(2)
C11	.013(3)	.011(3)	.023(3)	.000(2)	.000(2)	.004(2)
C12	.012(3)	.020(3)	.015(3)	-.002(2)	.006(2)	-.007(2)
C13	.011(3)	.016(3)	.021(3)	-.002(2)	-.003(2)	-.007(3)
C14	.015(3)	.015(3)	.011(3)	-.003(2)	-.001(2)	-.001(2)
C15	.013(3)	.020(3)	.014(3)	-.001(2)	.003(2)	.000(2)
C16	.048(4)	.030(4)	.028(4)	-.013(3)	-.002(3)	-.009(3)
C17	.036(4)	.014(3)	.081(6)	-.004(3)	.011(4)	.008(3)
C18	.031(3)	.033(4)	.037(4)	-.001(3)	.012(3)	.005(3)
C19	.020(3)	.042(4)	.033(4)	-.010(3)	.002(3)	-.002(3)
C20	.039(4)	.043(4)	.024(4)	-.006(3)	-.003(3)	-.012(3)
C21	.033(4)	.048(4)	.060(5)	.025(3)	-.021(3)	-.003(4)
Ru2	.0109(2)	.0122(3)	.0180(2)	-.0015(2)	.00122(19)	.0016(2)
P1'	.0152(7)	.0156(8)	.0240(9)	-.0005(6)	.0011(6)	-.0006(7)
P2'	.0145(7)	.0168(9)	.0213(8)	-.0034(7)	-.0011(6)	.0001(7)
O1'	.024(2)	.018(2)	.046(3)	.0018(18)	-.0058(20)	.0046(20)
O2'	.022 (2)	.011(2)	.046(3)	-.0066(17)	.0013(20)	-.0038(19)
O3'	.022 (2)	.025(2)	.042(3)	-.0010(18)	.0097(20)	-.0057(20)
O4'	.0158(19)	.028(2)	.036(2)	-.0025(19)	.0009(17)	-.006(2)
O5'	.027(2)	.027(2)	.026(2)	-.0082(19)	-.0085(19)	.0035(19)
O6'	.023(2)	.023(2)	.032(3)	-.0050(18)	.0011(19)	-.0056(19)
B2	.023(4)	.027(4)	.013(3)	.004(3)	.006(3)	-.001(3)
N1'	.014(2)	.015(3)	.022(3)	.0006(20)	.003(2)	.003(2)
N2'	.015(2)	.017(3)	.024(3)	.0025(20)	.0081(20)	.003(2)

N3'	.016(2)	.017(3)	.021(3)	-.003(2)	.000(2)	-.001(2)
N4'	.020(3)	.020(3)	.018(3)	-.003(2)	-.005(2)	.001(2)
N5'	.015(2)	.013(3)	.024(3)	-.001(2)	.003(2)	.003(2)
N6'	.017(2)	.018(3)	.019(3)	.002(2)	.004(2)	.000(2)
N7'	.012(2)	.011(3)	.026(3)	-.0031(19)	.001(2)	-.007(2)
C1'	.014(3)	.019(3)	.038(4)	-.004(3)	.003(3)	.008(3)
C2'	.021(3)	.020(3)	.040(4)	-.002(3)	.013(3)	.009(3)
C3'	.025(3)	.032(4)	.034(4)	.010(3)	.014(3)	.006(3)
C4'	.010(3)	.020(3)	.034(4)	-.001(3)	-.002(2)	.004(3)
C5'	.024(3)	.028(4)	.038(4)	-.004(3)	-.018(3)	.004(3)
C6'	.029(4)	.026(4)	.020(3)	-.003(3)	-.005(3)	.002(3)
C7'	.013(3)	.020(3)	.025(4)	.000(3)	.000(3)	.007(3)
C8'	.017(3)	.016(3)	.031(4)	.002(3)	.000(3)	.003(3)
C9'	.020(3)	.020(4)	.031(4)	.000(3)	.005(3)	-.007(3)
C10'	.014(3)	.017(3)	.011(3)	.002(2)	-.001(2)	.003(2)
C11'	.016(3)	.015(3)	.020(3)	.000(2)	.000(2)	-.003(3)
C12'	.016(3)	.027(4)	.010(3)	.001(3)	.001(2)	-.002(3)
C13'	.009(3)	.011(3)	.027(3)	.000(2)	.001(2)	.001(3)
C14'	.019(3)	.017(3)	.013(3)	-.002(3)	.003(2)	-.001(3)
C15'	.011(3)	.016(3)	.017(3)	-.002(2)	.003(2)	.000(3)
C16'	.049(4)	.025(4)	.038(4)	-.003(3)	-.016(3)	.009(3)
C17'	.037(4)	.015(3)	.058(5)	-.005(3)	.004(3)	-.006(3)
C18'	.027(4)	.040(4)	.087(6)	.009(3)	.017(4)	.001(4)
C19'	.016(3)	.032(4)	.038(4)	.009(3)	.002(3)	-.002(3)
C20'	.046(4)	.039(4)	.034(4)	-.002(3)	-.014(3)	.010(3)
C21'	.027(4)	.033(4)	.062(5)	-.010(3)	-.011(3)	-.005(4)
Ru3	.0101(2)	.0124(3)	.0217(3)	-.00142(19)	.00079(18)	.0018(2)

P1 "	.0126(7)	.0169(8)	.0280(9)	-.0014(6)	-.0013(6)	-.0008(7)
P2 "	.0151(7)	.0121(8)	.0295(9)	-.0007(6)	.0026(7)	.0010(7)
O1 "	.0160(19)	.030(3)	.031(2)	.0013(19)	-.0013(17)	-.002(2)
O2 "	.030(2)	.029(3)	.025(2)	-.0039(20)	-.0070(19)	.0087(20)
O3 "	.020(2)	.024(2)	.052(3)	-.0035(18)	-.006(2)	-.011(2)
O4 "	.028(2)	.022(2)	.023(2)	.0133(18)	.0019(19)	.0017(18)
O5 "	.024(2)	.020(2)	.026(2)	-.0055(18)	.0027(18)	.0009(18)
O6 "	.021(2)	.015(2)	.063(3)	-.0025(18)	.008(2)	.001(2)
B3	.024(4)	.019(4)	.017(4)	.002(3)	.005(3)	.004(3)
N1 "	.014(2)	.018(3)	.028(3)	-.002(2)	.003(2)	.002(2)
N2 "	.015(2)	.025(3)	.023(3)	.005(2)	.0034(20)	.006(2)
N3 "	.008(2)	.018(3)	.023(3)	.0004(20)	.0024(20)	.002(2)
N4 "	.013(2)	.017(3)	.028(3)	.002(2)	.002(2)	-.001(2)
N5 "	.016(2)	.018(3)	.019(3)	.000(2)	.0042(20)	.004(2)
N6 "	.018(3)	.022(3)	.028(3)	.001(2)	.003(2)	.009(2)
N7 "	.017(2)	.016(3)	.017(3)	.0025(20)	-.0031(20)	.001(2)
C1 "	.017(3)	.022(3)	.035(4)	.001(3)	.004(3)	.012(3)
C2 "	.013(3)	.018(3)	.052(5)	.000(3)	.004(3)	.012(3)
C3 "	.019(3)	.028(4)	.027(3)	.011(3)	.011(3)	.009(3)
C4 "	.018(3)	.013(3)	.028(4)	-.001(2)	-.003(3)	.003(3)
C5 "	.021(3)	.016(3)	.035(4)	.002(3)	.002(3)	-.001(3)
C6 "	.017(3)	.028(4)	.018(3)	-.002(3)	-.001(2)	-.006(3)
C7 "	.010(3)	.021(3)	.037(4)	.001(3)	.004(2)	.005(3)
C8 "	.017(3)	.031(4)	.032(4)	-.001(3)	-.006(3)	.003(3)
C9 "	.026(3)	.025(4)	.020(3)	-.006(3)	-.005(3)	-.001(3)
C10 "	.008(3)	.011(3)	.031(4)	.000(2)	-.001(2)	.000(3)
C11 "	.017(3)	.025(3)	.017(3)	.001(3)	.000(2)	.004(3)

C12"	.019(3)	.011(3)	.021(3)	-.003(2)	.005(3)	-.001(2)
C13"	.011(3)	.021(3)	.015(3)	.003(2)	.000(2)	.007(3)
C14"	.013(3)	.015(3)	.024(3)	-.004(2)	.001(2)	-.002(3)
C15"	.013(3)	.019(3)	.019(3)	.004(2)	.005(2)	.007(3)
C16"	.013(3)	.025(4)	.033(4)	.006(3)	.000(3)	-.001(3)
C17"	.039(4)	.047(5)	.025(4)	-.004(3)	-.017(3)	.008(3)
C18"	.030(4)	.032(4)	.093(6)	-.014(3)	-.009(4)	-.024(4)
C19"	.053(4)	.035(4)	.031(4)	.012(3)	.007(3)	.010(3)
C20"	.042(4)	.067(6)	.055(5)	.037(4)	.028(4)	.011(4)
C21"	.044(4)	.005(3)	.079(6)	-.006(3)	.012(4)	-.006(3)
S1	.0340(9)	.0266(9)	.0333(9)	-.0086(8)	-.0054(7)	-.0014(8)
O7	.037(3)	.050(3)	.034(3)	-.003(2)	-.017(2)	-.005(2)
O8	.071(4)	.038(3)	.056(3)	-.035(3)	-.018(3)	.011(3)
O9	.033(2)	.043(3)	.041(3)	-.005(2)	.004(2)	-.014(2)
C22	.027(4)	.068(6)	.010(3)	.004(4)	-.003(3)	-.002(3)
F1	.045(3)	.093(4)	.041(3)	.011(2)	-.013(2)	.007(2)
F2	.034(2)	.110(4)	.051(3)	.009(2)	.004(2)	.004(3)
F3	.050(3)	.046(3)	.089(4)	.010(2)	.000(3)	-.006(3)
S2	.0266(8)	.0273(9)	.0333(9)	-.0031(7)	.0008(7)	.0000(8)
O10	.038(3)	.051(3)	.028(3)	.006(2)	-.0109(20)	-.002(2)
O11	.028(2)	.053(3)	.034(3)	.004(2)	.0033(19)	-.011(2)
O12	.052(3)	.034(3)	.094(4)	-.023(3)	-.011(3)	.017(3)
C23	.021(3)	.055(5)	.017(3)	.008(3)	-.005(3)	-.003(3)
F4	.044(3)	.112(4)	.047(3)	.033(3)	.015(2)	-.004(3)
F5	.048(3)	.032(2)	.108(4)	.005(2)	-.014(3)	.008(2)
F6	.041(2)	.079(3)	.047(3)	.010(2)	-.024(2)	-.011(2)
S3	.0300(9)	.0382(10)	.0348(10)	-.0050(7)	.0014(7)	.0070(8)

O13	.054(3)	.027(3)	.083(4)	-.019(2)	-.004(3)	.026(3)
O14	.032(3)	.116(5)	.028(3)	-.027(3)	-.007(2)	.023(3)
O15	.066(3)	.056(3)	.055(3)	.018(3)	.028(3)	-.007(3)
F7	.046(2)	.030(2)	.069(3)	-.0122(18)	-.014(2)	.0106(20)
F8	.038(2)	.060(3)	.087(3)	.002(2)	.020(2)	.003(2)
F9	.053(3)	.058(3)	.082(3)	-.013(2)	-.035(2)	.019(3)
C1s	.034(4)	.045(4)	.033(4)	-.005(3)	-.006(3)	.003(3)
C11s	.0436(11)	.0565(13)	.0441(12)	.0143(9)	-.0050(9)	-.0020(10)
C12s	.0359(9)	.0636(13)	.0335(10)	.0059(9)	.0052(8)	.0041(9)
C13s	.0459(10)	.0417(11)	.0282(9)	-.0015(8)	-.0026(8)	.0016(8)
C2s	.030(4)	.033(4)	.041(4)	.002(3)	-.006(3)	-.001(3)
C14s	.0455(10)	.0458(11)	.0285(9)	.0064(9)	-.0028(8)	-.0038(8)
C15s	.0328(9)	.0552(12)	.0355(10)	-.0029(8)	.0032(8)	-.0016(9)
C16s	.0405(10)	.0558(12)	.0407(11)	-.0115(9)	.0011(8)	.0005(9)
C3s	.038(4)	.048(5)	.041(4)	.006(3)	.004(3)	-.004(3)
C17s	.0408(10)	.0498(11)	.0312(10)	.0111(8)	.0001(8)	.0005(8)
C18s	.0390(10)	.0814(14)	.0298(9)	.0035(10)	.0017(8)	-.0017(9)
C19s	.0370(10)	.0539(12)	.0611(13)	.0012(9)	-.0042(9)	-.0043(10)

Table A.29 Bond Distances for [TpRu{P(OMe)₃}₂NHC₆H₄-]₂[OTf]₂

Ru1 P1	2.2459(15)	N5 N6	1.357(7)
Ru1 P2	2.2406(15)	N5 C7	1.339(7)
Ru1 N1	2.088(4)	N6 B1	1.559(8)
Ru1 N3	2.144(4)	N6 C9	1.348(7)
Ru1 N5	2.152(4)	N7 C10	1.315(7)
Ru1 N7	2.044(4)	N7 H7n	.860(4)
P1 O1	1.583(4)	B1 H1b	1.140(6)
P1 O2	1.592(4)	C1 C2	1.393(8)
P1 O3	1.608(4)	C1 H1	.960(6)
P2 O4	1.591(4)	C2 C3	1.371(9)
P2 O5	1.595(4)	C2 H2	.960(5)
P2 O6	1.611(4)	C3 H3	.960(6)
O1 C16	1.458(7)	C4 C5	1.381(8)
O2 C17	1.452(7)	C4 H4	.960(6)
O3 C18	1.449(7)	C5 C6	1.377(9)
O4 C19	1.424(8)	C5 H5	.960(5)
O5 C20	1.454(7)	C6 H6	.960(6)
O6 C21	1.436(7)	C7 C8	1.393(9)
N1 N2	1.371(6)	C7 H7	.960(6)
N1 C1	1.347(7)	C8 C9	1.366(9)
N2 B1	1.537(8)	C8 H8	.960(6)
N2 C3	1.349(7)	C9 H9	.960(6)
N3 N4	1.368(6)	C10 C11	1.449(8)
N3 C4	1.335(7)	C10 C15	1.441(8)
N4 B1	1.554(8)	C11 C12	1.363(7)
N4 C6	1.354(7)	C11 H11	.960(5)

C12 C13	1.435(8)	C20 H20b	.960(6)
C12 H12	.960(5)	C20 H20c	.960(7)
C13 C13	1.425(10)	C21 H21a	.960(6)
C13 C14	1.440(8)	C21 H21b	.960(6)
C14 C15	1.352(8)	C21 H21c	.960(6)
C14 H14	.960(5)	S1 O7	1.411(6)
C15 H15	.960(6)	S1 O8	1.426(5)
C16 H16a	.960(6)	S1 O9	1.447(5)
C16 H16b	.960(7)	S1 C22	1.824(7)
C16 H16c	.960(6)	C22 F1	1.318(7)
C17 H17a	.960(6)	C22 F2	1.339(8)
C17 H17b	.960(7)	C22 F3	1.332(8)
C17 H17c	.960(7)	F1 F2	2.120(6)
C18 H18a	.960(6)	F1 F3	2.141(6)
C18 H18b	.960(7)	F2 F3	2.152(7)
C18 H18c	.960(6)	C1s C11s	1.773(7)
C19 H19a	.960(7)	C1s C12s	1.759(7)
C19 H19b	.960(9)	C1s H1sa	.960(7)
C19 H19c	.960(8)	C1s H1sb	.960(7)
C20 H20a	.960(6)		

Table A.30 Bond Angles for [TpRu{P(OMe)₃}₂NHC₆H₄-]₂[OTf]₂

P1 Ru1 P2	92.38(6)	O4 P2 O6	99.9(2)
P1 Ru1 N1	92.64(13)	O5 P2 O6	103.0(2)
P1 Ru1 N3	91.68(12)	P1 O1 C16	126.6(4)
P1 Ru1 N5	175.21(13)	P1 O2 C17	123.0(4)
P1 Ru1 N7	87.92(13)	P1 O3 C18	118.7(4)
P2 Ru1 N1	93.33(13)	P2 O4 C19	127.7(4)
P2 Ru1 N3	175.94(13)	P2 O5 C20	124.3(4)
P2 Ru1 N5	92.40(13)	P2 O6 C21	116.8(3)
P2 Ru1 N7	90.28(13)	Ru1 N1 N2	119.3(3)
N1 Ru1 N3	86.45(17)	Ru1 N1 C1	134.5(4)
N1 Ru1 N5	86.86(17)	N2 N1 C1	106.2(4)
N1 Ru1 N7	176.33(17)	N1 N2 B1	120.9(4)
N3 Ru1 N5	83.54(17)	N1 N2 C3	109.6(4)
N3 Ru1 N7	89.91(17)	B1 N2 C3	129.5(5)
N5 Ru1 N7	92.28(17)	Ru1 N3 N4	118.7(3)
Ru1 P1 O1	111.26(16)	Ru1 N3 C4	134.4(4)
Ru1 P1 O2	116.12(16)	N4 N3 C4	106.9(4)
Ru1 P1 O3	116.89(16)	N3 N4 B1	120.2(4)
O1 P1 O2	107.7(2)	N3 N4 C6	108.7(4)
O1 P1 O3	99.5(2)	B1 N4 C6	131.1(5)
O2 P1 O3	103.7(2)	Ru1 N5 N6	118.5(3)
Ru1 P2 O4	112.95(16)	Ru1 N5 C7	135.3(4)
Ru1 P2 O5	115.67(16)	N6 N5 C7	106.2(4)
Ru1 P2 O6	116.88(15)	N5 N6 B1	120.5(4)
O4 P2 O5	106.8(2)	N5 N6 C9	110.0(5)

B1 N6 C9	129.4(5)	C5 C6 H6	126.0(6)
Ru1 N7 C10	137.2(4)	N5 C7 C8	110.3(5)
Ru1 N7 H7n	109.2(3)	N5 C7 H7	124.1(6)
C10 N7 H7n	111.7(5)	C8 C7 H7	125.6(6)
N2 B1 N4	108.6(5)	C7 C8 C9	105.2(5)
N2 B1 N6	107.9(4)	C7 C8 H8	126.9(7)
N2 B1 H1b	110.5(5)	C9 C8 H8	127.8(6)
N4 B1 N6	106.8(4)	N6 C9 C8	108.3(5)
N4 B1 H1b	110.8(5)	N6 C9 H9	124.8(6)
N6 B1 H1b	112.0(5)	C8 C9 H9	126.9(6)
N1 C1 C2	110.2(5)	N7 C10 C11	122.8(5)
N1 C1 H1	124.6(5)	N7 C10 C15	120.7(5)
C2 C1 H1	125.2(5)	C11 C10 C15	116.5(5)
C1 C2 C3	105.4(5)	C10 C11 C12	120.3(5)
C1 C2 H2	127.9(6)	C10 C11 H11	119.4(5)
C3 C2 H2	126.7(6)	C12 C11 H11	120.3(5)
N2 C3 C2	108.7(5)	C11 C12 C13	123.3(5)
N2 C3 H3	125.2(6)	C11 C12 H12	119.0(5)
C2 C3 H3	126.1(6)	C13 C12 H12	117.7(5)
N3 C4 C5	110.6(5)	C12 C13 C13	121.4(5)
N3 C4 H4	124.6(5)	C12 C13 C14	115.7(5)
C5 C4 H4	124.8(5)	C13 C13 C14	122.9(5)
C4 C5 C6	105.1(5)	C13 C14 C15	122.0(5)
C4 C5 H5	127.5(6)	C13 C14 H14	118.5(5)
C6 C5 H5	127.4(6)	C15 C14 H14	119.5(5)
N4 C6 C5	108.7(5)	C10 C15 C14	122.1(5)
N4 C6 H6	125.4(6)	C10 C15 H15	118.9(5)

C14 C15 H15	118.9(5)	H16a C16 H16b	109.4(6)
O1 C16 H16a	110.0(6)	H16a C16 H16c	109.5(6)
O1 C16 H16b	109.8(5)	H16b C16 H16c	109.5(7)
O1 C16 H16c	108.5(5)		
O2 C17 H17a	109.7(6)	H20b C20 H20c	109.5(6)
O2 C17 H17b	109.0(5)	O6 C21 H21a	108.8(5)
O2 C17 H17c	109.7(6)	O6 C21 H21b	109.9(5)
H17a C17 H17b	109.5(7)	O6 C21 H21c	109.7(5)
H17a C17 H17c	109.5(6)	H21a C21 H21b	109.4(6)
H17b C17 H17c	109.5(7)	H21a C21 H21c	109.5(6)
O3 C18 H18a	109.5(6)	H21b C21 H21c	109.5(6)
O3 C18 H18b	109.5(5)	O7 S1 O8	116.6(4)
O3 C18 H18c	109.5(5)	O7 S1 O9	115.6(3)
H18a C18 H18b	109.5(6)	O7 S1 C22	103.0(3)
H18a C18 H18c	109.5(6)	O8 S1 O9	114.0(4)
H18b C18 H18c	109.5(6)	O8 S1 C22	102.8(3)
O4 C19 H19a	109.8(6)	O9 S1 C22	101.9(3)
O4 C19 H19b	107.5(7)	S1 C22 F1	112.7(5)
O4 C19 H19c	111.1(7)	S1 C22 F2	110.5(4)
H19a C19 H19b	109.5(8)	S1 C22 F3	112.2(5)
H19a C19 H19c	109.4(8)	F1 C22 F2	105.9(6)
H19b C19 H19c	109.5(7)	F1 C22 F3	107.8(5)
O5 C20 H20a	109.5(6)	F2 C22 F3	107.4(6)
O5 C20 H20b	109.5(5)	C11s C1s C12s	111.4(4)
O5 C20 H20c	109.4(5)	C11s C1s H1sa	108.9(5)
H20a C20 H20b	109.4(6)	C11s C1s H1sb	109.2(6)
H20a C20 H20c	109.5(6)	C12s C1s H1sa	108.7(6)

C12s C1s H1sb 109.2(5)

H1sa C1s H1sb 109.4(6)

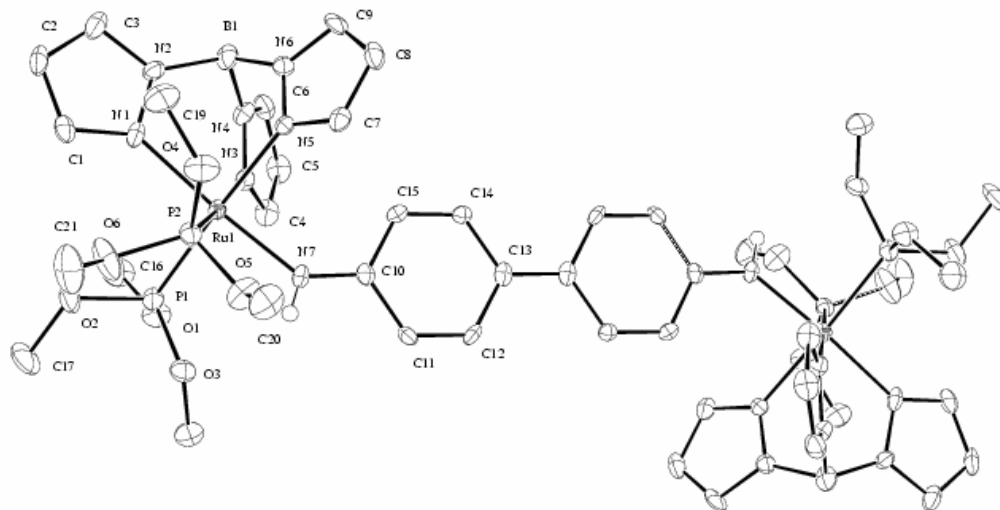


Figure A7 ORTEP diagram of $[\text{TpRu}\{\text{P}(\text{OMe})_3\}_2\text{NHC}_6\text{H}_4\text{-}]_2[\text{OTf}]_2$

Table A.31 Crystal Data and Structure Refinement $[\text{TpRu}\{\text{P}(\text{OMe})_3\}_2\text{NHC}_6\text{H}_4\text{-}]_2[\text{OTf}]_2$

Identification code	x02029
Empirical formula	$\text{C}_{46}\text{H}_{68}\text{B}_2\text{C}_{16}\text{F}_3\text{N}_{14}\text{O}_{18}\text{P}_4\text{Ru}_2\text{S}_2$
Formula weight	1843.59
Temperature	148 K
Wave length	.71073
Crystal system	Monoclinic
Space Group	P 21/n
Unit cell dimensions	$a = 9.6208(6) \text{ \AA}$
	$b = 28.276(2) \text{ \AA}$
	$c = 40.672(4) \text{ \AA}$

Table A.31 (continued)

α	90.00 °
β	90.443(10) °
χ	90.00 °
Volume, z	11064.0(15) Å ³
Density (calculated)	1.660 Mg/m ³
Absorption Coefficient	0.86
F(000)	5586.52
Crystal size	0.32 x 0.16 x 0.16 mm
θ range for data collected	1.20 to 25.00
Limiting indices	$-11 \leq h \leq 11, 0 \leq k \leq 33, 0 \leq l \leq 48$
Reflections collected	19340
Independent reflections	19340
Absorption correction	psi-scan
Max and min transmission	0.9992 and 0.9484
Refinement method	Full-matrix least-squares of F^2
Data/restraints/parameters	19340 / 0 / 1346
Goodness of fit on F^2	1.70
Final R indices [$I > 2\sigma(I)$]	$R1 = 0.077, wR2 = 0.085$
Final R indices (all data)	$R1 = 0.077, wR2 = 0.085$
Largest diff. peak and hole	2.06 and -1.34 eÅ^{-3}

Table A.32 Atomic Coordinates and Thermal Parameters (x, y, z and u) for [TpRu{P(OMe)₃}₂NHC₆H₄-]₂[OTf]₂

	x	y	z	u
Ru1	.99793(4)	.358764(16)	.953092(11)	.0137(2)
P1	.92917(15)	.28427(5)	.96237(4)	.0183(8)
P2	1.16786(14)	.35337(5)	.99118(4)	.0173(7)
O1	.7916(4)	.26550(13)	.94407(9)	.024(2)
O2	1.0414(4)	.24440(14)	.95595(11)	.035(3)
O3	.8817(4)	.27809(13)	.99927(9)	.023(2)
O4	1.2912(4)	.39138(14)	.98906(9)	.027(2)
O5	1.1158(4)	.36400(15)	1.02684(9)	.030(2)
O6	1.2461(4)	.30440(13)	.99208(11)	.037(2)
B1	1.0313(7)	.4133(2)	.88419(18)	.023(4)
N1	1.1322(4)	.34249(16)	.91458(11)	.018(2)
N2	1.1353(5)	.37257(16)	.88823(11)	.018(2)
N3	.8441(4)	.36990(16)	.91525(11)	.017(2)
N4	.8823(5)	.39315(17)	.88753(11)	.019(3)
N5	1.0536(4)	.43116(16)	.94499(11)	.014(2)
N6	1.0518(5)	.44802(16)	.91371(11)	.017(2)
N7	.8589(4)	.37825(15)	.98759(11)	.016(2)
C1	1.2359(6)	.31097(20)	.90997(15)	.021(3)
C2	1.3043(6)	.3215(2)	.88110(16)	.026(3)
C3	1.2414(5)	.3600(2)	.86799(14)	.025(3)
C4	.7067(5)	.3608(2)	.91251(15)	.024(3)
C5	.6573(6)	.3779(2)	.88286(16)	.026(3)
C6	.7706(6)	.3982(2)	.86743(14)	.024(3)
C7	1.0727(6)	.4683(2)	.96502(14)	.020(3)

C8	1.0826(6)	.5094(2)	.94679(16)	.023(3)
C9	1.0687(6)	.4952(2)	.91446(16)	.025(3)
C10	.7624(5)	.41124(19)	.99008(13)	.015(3)
C11	.6686(5)	.41090(19)	1.01770(14)	.016(3)
C12	.5694(5)	.44460(20)	1.02133(13)	.016(3)
C13	.5518(5)	.48272(19)	.99836(14)	.016(3)
C14	.6459(5)	.48249(19)	.97083(13)	.014(3)
C15	.7432(5)	.44858(20)	.96645(13)	.016(3)
C16	.8014(7)	.2530(2)	.90976(16)	.035(3)
C17	1.0171(7)	.1962(2)	.96646(19)	.044(4)
C18	.7659(6)	.2507(2)	1.01121(15)	.034(3)
C19	1.3712(6)	.3946(2)	.95912(16)	.032(4)
C20	1.1963(7)	.3838(2)	1.05346(16)	.035(4)
C21	1.3710(7)	.2950(2)	1.01111(17)	.047(4)
Ru2	.82720(4)	.855592(17)	.877589(11)	.0137(2)
P1'	.88933(15)	.78002(6)	.87015(4)	.0183(8)
P2'	.66571(14)	.85084(5)	.83752(4)	.0175(8)
O1'	.9834(4)	.75573(13)	.89810(11)	.029(2)
O2'	.7621(4)	.74455(13)	.86566(10)	.026(2)
O3'	.9823(4)	.76836(14)	.83859(10)	.029(2)
O4'	.5042(3)	.85462(14)	.84701(9)	.027(2)
O5'	.6926(4)	.89193(14)	.81128(10)	.027(2)
O6'	.6572(4)	.80588(13)	.81395(10)	.026(2)
B2	.7843(7)	.9088(2)	.94637(16)	.021(3)
N1'	.6854(4)	.83878(16)	.91501(11)	.017(2)
N2'	.6795(4)	.86825(16)	.94171(11)	.018(2)
N3'	.9749(4)	.86447(17)	.91693(11)	.018(2)

N4'	.9337(5)	.88802(17)	.94451(11)	.019(2)
N5'	.7733(5)	.92868(16)	.88640(12)	.017(3)
N6'	.7699(5)	.94429(16)	.91805(11)	.018(2)
N7'	.9682(4)	.87595(15)	.84326(11)	.016(2)
C1'	.5837(6)	.8065(2)	.91807(15)	.024(3)
C2'	.5118(6)	.8150(2)	.94699(16)	.027(3)
C3'	.5749(6)	.8537(2)	.96127(15)	.030(3)
C4'	1.1094(5)	.8543(2)	.92220(14)	.021(3)
C5'	1.1543(6)	.8703(2)	.95249(16)	.030(3)
C6'	1.0394(6)	.8919(2)	.96630(15)	.025(3)
C7'	.7627(6)	.9669(2)	.86683(14)	.020(3)
C8'	.7521(6)	1.0074(2)	.88606(16)	.021(3)
C9'	.7572(6)	.9917(2)	.91775(15)	.023(3)
C10'	1.0629(5)	.90979(19)	.84095(13)	.014(3)
C11'	1.1438(5)	.91511(19)	.81180(13)	.017(3)
C12'	1.2403(5)	.9495(2)	.80886(13)	.018(3)
C13'	1.2679(5)	.98307(19)	.83461(14)	.016(3)
C14'	1.1829(6)	.97808(20)	.86368(13)	.016(3)
C15'	1.0868(5)	.94398(19)	.86687(13)	.015(3)
C16'	.9278(7)	.7502(2)	.93045(16)	.038(4)
C17'	.7850(7)	.6953(2)	.85755(18)	.037(4)
C18'	1.1330(7)	.7720(3)	.8381(2)	.052(5)
C19'	.4540(6)	.8919(2)	.86815(16)	.029(3)
C20'	.6158(7)	.8943(2)	.78025(17)	.040(4)
C21'	.5437(6)	.7720(2)	.81349(18)	.041(4)
Ru3	1.81674(4)	1.146253(17)	.791212(11)	.0147(2)
P1"	1.97903(15)	1.14976(6)	.83114(4)	.0192(8)

P2 "	1.75014(15)	1.22082(5)	.80107(4)	.0189(8)
O1 "	2.1391(4)	1.14677(14)	.82130(9)	.026(2)
O2 "	1.9545(4)	1.10790(14)	.85663(10)	.028(2)
O3 "	1.9870(4)	1.19468(14)	.85482(11)	.032(2)
O4 "	1.6379(4)	1.24376(14)	.77662(9)	.024(2)
O5 "	1.6716(4)	1.22850(13)	.83525(9)	.023(2)
O6 "	1.8723(4)	1.25848(14)	.80247(11)	.033(3)
B3	1.8593(7)	1.0963(2)	.72055(16)	.020(3)
N1 "	1.9580(4)	1.16475(16)	.75501(12)	.020(3)
N2 "	1.9633(4)	1.13773(17)	.72738(11)	.021(2)
N3 "	1.8710(4)	1.07413(16)	.78086(11)	.017(3)
N4 "	1.8763(5)	1.05994(16)	.74881(12)	.019(3)
N5 "	1.6683(4)	1.13854(16)	.75175(11)	.018(2)
N6 "	1.7095(5)	1.11663(17)	.72379(12)	.023(3)
N7 "	1.6760(4)	1.12425(15)	.82548(11)	.016(2)
C1 "	2.0623(6)	1.1959(2)	.75227(15)	.025(3)
C2 "	2.1377(6)	1.1886(2)	.72394(16)	.028(3)
C3 "	2.0720(6)	1.1515(2)	.70808(14)	.025(3)
C4 "	1.8849(6)	1.0348(2)	.79909(15)	.020(3)
C5 "	1.8941(6)	.9950(2)	.77942(15)	.024(3)
C6 "	1.8880(6)	1.0126(2)	.74783(14)	.021(3)
C7 "	1.5328(5)	1.1485(2)	.74778(14)	.022(3)
C8 "	1.4859(6)	1.1327(2)	.71710(15)	.027(3)
C9 "	1.6001(6)	1.1129(2)	.70301(15)	.024(3)
C10 "	1.5804(5)	1.08982(19)	.82690(14)	.017(3)
C11 "	1.4971(6)	1.0850(2)	.85567(14)	.019(3)
C12 "	1.3994(5)	1.05120(19)	.85834(14)	.017(3)

C13 "	1.3728(5)	1.0180(2)	.83246(13)	.016(3)
C14 "	1.4588(6)	1.02254(19)	.80402(15)	.017(3)
C15 "	1.5567(5)	1.05678(19)	.80065(14)	.017(3)
C16 "	2.1886(6)	1.1092(2)	.80011(15)	.024(3)
C17 "	2.0290(7)	1.1048(2)	.88762(16)	.037(4)
C18 "	2.1021(7)	1.2270(2)	.8581(2)	.052(5)
C19 "	1.6742(7)	1.2551(2)	.74328(16)	.040(4)
C20 "	1.5211(7)	1.2298(3)	.83769(19)	.055(4)
C21 "	1.8450(7)	1.3073(2)	.81176(19)	.043(4)
S1	.58571(17)	.13745(6)	.94338(4)	.0313(8)
O7	.6529(4)	.15138(17)	.97342(11)	.040(3)
O8	.5125(5)	.09302(16)	.94433(12)	.055(3)
O9	.6654(4)	.14512(16)	.91428(10)	.039(3)
C22	.4423(7)	.1787(3)	.93930(15)	.035(4)
F1	.3683(4)	.17157(16)	.91217(10)	.059(3)
F2	.3583(4)	.17896(17)	.96424(10)	.065(3)
F3	.4907(4)	.22464(15)	.93742(11)	.062(3)
S2	1.07960(16)	.86452(6)	.72078(4)	.0291(9)
O10	1.0239(4)	.84720(16)	.69073(10)	.039(3)
O11	.9889(4)	.86177(16)	.74859(10)	.038(2)
O12	1.1609(5)	.90724(16)	.71823(14)	.060(3)
C23	1.2149(6)	.8219(3)	.73098(15)	.031(4)
F4	1.3082(4)	.81726(17)	.70793(10)	.068(3)
F5	1.1598(4)	.77750(14)	.73503(12)	.063(3)
F6	1.2793(4)	.83213(16)	.75906(10)	.056(3)
S3	.59287(17)	.33903(6)	.10716(4)	.0343(8)
O13	.5958(5)	.29185(15)	.11850(13)	.055(3)

O14	.5421(4)	.3442(2)	.07420(11)	.059(3)
O15	.5426(5)	.37335(17)	.13081(12)	.059(3)
C24	.7717(6)	.3566(2)	.10557(14)	.0233(13)
F7	.7919(4)	.40022(12)	.09686(9)	.049(2)
F8	.8383(4)	.33190(15)	.08075(11)	.061(3)
F9	.8426(4)	.34731(15)	.13234(11)	.065(3)
C1s	.3325(7)	1.0032(2)	.96416(16)	.037(4)
C11s	.15781(19)	1.01798(7)	.95423(5)	.0481(11)
C12s	.41147(18)	.97391(7)	.93075(4)	.0443(10)
C13s	.33909(18)	.96576(6)	.99860(4)	.0386(10)
C2s	.8216(6)	.4985(2)	.20229(17)	.035(4)
C14s	.82074(18)	.46104(6)	.16740(4)	.0400(10)
C15s	.73449(17)	.47028(7)	.23470(4)	.0411(10)
C16s	.99508(19)	.51259(7)	.21366(4)	.0457(11)
C3s	.4731(7)	.4838(2)	.13190(17)	.042(4)
C17s	.49363(18)	.52510(7)	.16452(4)	.0406(10)
C18s	.57737(18)	.50068(7)	.09899(4)	.0501(11)
C19s	.29896(19)	.47770(7)	.12031(5)	.0507(11)
H1	1.257	.285	.925	.0306
H1b	1.049	.432	.860	.0332
H2	1.382	.305	.872	.0360
H3	1.265	.376	.848	.0355
H4	.652	.345	.929	.0341
H5	.564	.376	.875	.0361
H6	.771	.413	.846	.0337
H7	1.079	.467	.989	.0296
H7n	.874	.362	1.005	.0262

H8	1.096	.541	.955	.0332
H9	1.069	.516	.896	.0353
H11	.676	.386	1.034	.0257
H12	.509	.443	1.040	.0256
H14	.640	.508	.955	.0235
H15	.800	.449	.947	.0256
H16a	.712	.242	.902	.0453
H16b	.830	.280	.897	.0453
H16c	.868	.228	.907	.0453
H17a	1.095	.177	.960	.0538
H17b	1.005	.195	.990	.0538
H17c	.935	.185	.956	.0538
H18a	.760	.253	1.035	.0436
H18b	.681	.262	1.001	.0436
H18c	.779	.218	1.005	.0436
H19a	1.440	.419	.961	.0416
H19b	1.416	.365	.955	.0416
H19c	1.311	.402	.941	.0416
H20a	1.139	.387	1.073	.0454
H20b	1.273	.363	1.058	.0454
H20c	1.230	.414	1.047	.0454
H21a	1.399	.263	1.008	.0569
H21b	1.443	.316	1.004	.0569
H21c	1.355	.300	1.034	.0569
H1'	.564	.782	.903	.0337
H2'	.435	.797	.955	.0372
H2b	.768	.926	.971	.0309

H3'	.549	.868	.982	.0402
H4'	1.166	.837	.907	.0314
H5'	1.245	.868	.962	.0398
H6'	1.035	.907	.987	.0351
H7'	.761	.966	.843	.0296
H7n'	.969	.859	.826	.0265
H8'	.744	1.039	.878	.0315
H9'	.753	1.011	.937	.0335
H11'	1.128	.894	.794	.0271
H12'	1.293	.952	.789	.0278
H14'	1.195	1.000	.881	.0263
H15'	1.034	.942	.887	.0248
H16a'	.995	.735	.944	.0477
H16b'	.905	.781	.939	.0477
H16c'	.845	.731	.929	.0477
H17a'	.697	.680	.856	.0466
H17b'	.833	.693	.837	.0466
H17c'	.839	.681	.875	.0466
H18a'	1.169	.763	.817	.0616
H18b'	1.159	.804	.843	.0616
H18c'	1.171	.751	.855	.0616
H19a'	.356	.888	.871	.0390
H19b'	.501	.890	.889	.0390
H19c'	.472	.922	.858	.0390
H20a'	.646	.921	.768	.0495
H20b'	.632	.866	.768	.0495
H20c'	.518	.897	.785	.0495

H21a'	.563	.748	.797	.0506
H21b'	.535	.758	.835	.0506
H21c'	.459	.788	.808	.0506
H1"	2.082	1.220	.768	.0347
H2"	2.218	1.206	.717	.0376
H3"	2.098	1.138	.687	.0346
H3b	1.885	1.079	.696	.0303
H4"	1.887	1.034	.823	.0300
H5"	1.904	.963	.786	.0340
H6"	1.890	.994	.728	.0308
H7"	1.477	1.164	.764	.0324
H7n"	1.683	1.140	.844	.0264
H8"	1.394	1.135	.708	.0366
H9"	1.602	1.098	.682	.0335
H11"	1.512	1.106	.874	.0293
H12"	1.345	1.049	.878	.0273
H14"	1.446	1.000	.786	.0275
H15"	1.610	1.059	.781	.0270
H16a"	2.287	1.113	.797	.0338
H16b"	2.170	1.079	.810	.0338
H16c"	2.141	1.111	.779	.0338
H17a"	2.000	1.077	.899	.0469
H17b"	2.127	1.103	.884	.0469
H17c"	2.010	1.132	.901	.0469
H18a"	2.080	1.251	.874	.0617
H18b"	2.184	1.210	.865	.0617
H18c"	2.118	1.242	.837	.0617

H19a"	1.595	1.269	.732	.0498
H19b"	1.749	1.278	.744	.0498
H19c"	1.703	1.227	.732	.0498
H20a"	1.494	1.235	.860	.0647
H20b"	1.485	1.255	.824	.0647
H20c"	1.485	1.200	.830	.0647
H21a"	1.930	1.325	.811	.0528
H21b"	1.779	1.321	.797	.0528
H21c"	1.807	1.308	.834	.0528
H1s	.384	1.032	.969	.0561
H2s	.774	.528	.197	.0524
H3s	.506	.454	.140	.0604

Table A.33 Anisotropic Displacement Parameters for [TpRu{P(OMe)₃}₂NHC₆H₄-
]2[OTf]₂

	u11	u22	u33	u12	u13	u23
Ru1	.00970(20)	.0125(2)	.0189(3)	-.0009(2)	.00126(18)	-.0020(2)
P1	.0128(7)	.0163(8)	.0258(9)	-.0020(6)	.0015(6)	-.0027(7)
P2	.0143(7)	.0146(8)	.0230(8)	-.0016(7)	.0003(6)	-.0007(7)
O1	.021(2)	.028(2)	.024(2)	-.0088(18)	-.0041(18)	-.0023(18)
O2	.023(2)	.013(2)	.069(3)	-.0003(17)	.015(2)	-.001(2)
O3	.021(2)	.019(2)	.029(2)	-.0048(17)	.0026(17)	.0017(18)
O4	.0149(20)	.036(2)	.031(2)	-.0127(18)	-.0070(17)	.0017(19)
O5	.0191(20)	.043(3)	.027(2)	-.0042(20)	-.0037(17)	-.006(2)
O6	.019(2)	.023(2)	.069(3)	.0072(18)	-.021(2)	.000(2)
B1	.013(3)	.023(4)	.034(4)	.001(3)	.003(3)	-.003(3)
N1	.012(2)	.019(3)	.024(3)	.0013(20)	.0026(20)	-.008(2)
N2	.021(3)	.020(3)	.014(2)	-.002(2)	.0051(20)	-.002(2)
N3	.017(2)	.018(3)	.016(3)	.003(2)	.000(2)	-.001(2)
N4	.018(3)	.024(3)	.016(3)	.001(2)	.002(2)	-.005(2)
N5	.008(2)	.015(3)	.020(3)	.0008(19)	.003(2)	.002(2)
N6	.015(2)	.016(3)	.021(3)	-.002(2)	.002(2)	.000(2)
N7	.013(2)	.017(3)	.019(3)	.0043(20)	.0007(20)	-.004(2)
C1	.015(3)	.013(3)	.034(4)	-.001(2)	-.002(3)	-.005(3)
C2	.019(3)	.017(3)	.043(4)	.000(3)	.007(3)	-.013(3)
C3	.019(3)	.025(4)	.032(3)	-.002(3)	.009(3)	-.011(3)
C4	.016(3)	.026(4)	.031(3)	-.003(3)	-.003(3)	-.007(3)
C5	.016(3)	.026(4)	.036(4)	-.001(3)	-.008(3)	-.006(3)
C6	.030(3)	.019(3)	.022(3)	.005(3)	-.003(3)	.000(3)
C7	.014(3)	.021(3)	.024(3)	-.003(3)	.003(3)	-.006(3)

C8	.019(3)	.014(3)	.037(4)	-.001(3)	.002(3)	-.006(3)
C9	.020(3)	.011(3)	.045(4)	-.006(3)	.006(3)	.005(3)
C10	.015(3)	.012(3)	.017(3)	-.002(2)	-.002(2)	-.004(2)
C11	.013(3)	.011(3)	.023(3)	.000(2)	.000(2)	.004(2)
C12	.012(3)	.020(3)	.015(3)	-.002(2)	.006(2)	-.007(2)
C13	.011(3)	.016(3)	.021(3)	-.002(2)	-.003(2)	-.007(3)
C14	.015(3)	.015(3)	.011(3)	-.003(2)	-.001(2)	-.001(2)
C15	.013(3)	.020(3)	.014(3)	-.001(2)	.003(2)	.000(2)
C16	.048(4)	.030(4)	.028(4)	-.013(3)	-.002(3)	-.009(3)
C17	.036(4)	.014(3)	.081(6)	-.004(3)	.011(4)	.008(3)
C18	.031(3)	.033(4)	.037(4)	-.001(3)	.012(3)	.005(3)
C19	.020(3)	.042(4)	.033(4)	-.010(3)	.002(3)	-.002(3)
C20	.039(4)	.043(4)	.024(4)	-.006(3)	-.003(3)	-.012(3)
C21	.033(4)	.048(4)	.060(5)	.025(3)	-.021(3)	-.003(4)
Ru2	.0109(2)	.0122(3)	.0180(2)	-.0015(2)	.00122(19)	.0016(2)
P1'	.0152(7)	.0156(8)	.0240(9)	-.0005(6)	.0011(6)	-.0006(7)
P2'	.0145(7)	.0168(9)	.0213(8)	-.0034(7)	-.0011(6)	.0001(7)
O1'	.024(2)	.018(2)	.046(3)	.0018(18)	-.0058(20)	.0046(20)
O2'	.022(2)	.011(2)	.046(3)	-.0066(17)	.0013(20)	-.0038(19)
O3'	.022(2)	.025(2)	.042(3)	-.0010(18)	.0097(20)	-.0057(20)
O4'	.0158(19)	.028(2)	.036(2)	-.0025(19)	.0009(17)	-.006(2)
O5'	.027(2)	.027(2)	.026(2)	-.0082(19)	-.0085(19)	.0035(19)
O6'	.023(2)	.023(2)	.032(3)	-.0050(18)	.0011(19)	-.0056(19)
B2	.023(4)	.027(4)	.013(3)	.004(3)	.006(3)	-.001(3)
N1'	.014(2)	.015(3)	.022(3)	.0006(20)	.003(2)	.003(2)
N2'	.015(2)	.017(3)	.024(3)	.0025(20)	.0081(20)	.003(2)
N3'	.016(2)	.017(3)	.021(3)	-.003(2)	.000(2)	-.001(2)

N4'	.020(3)	.020(3)	.018(3)	-.003(2)	-.005(2)	.001(2)
N5'	.015(2)	.013(3)	.024(3)	-.001(2)	.003(2)	.003(2)
N6'	.017(2)	.018(3)	.019(3)	.002(2)	.004(2)	.000(2)
N7'	.012(2)	.011(3)	.026(3)	-.0031(19)	.001(2)	-.007(2)
C1'	.014(3)	.019(3)	.038(4)	-.004(3)	.003(3)	.008(3)
C2'	.021(3)	.020(3)	.040(4)	-.002(3)	.013(3)	.009(3)
C3'	.025(3)	.032(4)	.034(4)	.010(3)	.014(3)	.006(3)
C4'	.010(3)	.020(3)	.034(4)	-.001(3)	-.002(2)	.004(3)
C5'	.024(3)	.028(4)	.038(4)	-.004(3)	-.018(3)	.004(3)
C6'	.029(4)	.026(4)	.020(3)	-.003(3)	-.005(3)	.002(3)
C7'	.013(3)	.020(3)	.025(4)	.000(3)	.000(3)	.007(3)
C8'	.017(3)	.016(3)	.031(4)	.002(3)	.000(3)	.003(3)
C9'	.020(3)	.020(4)	.031(4)	.000(3)	.005(3)	-.007(3)
C10'	.014(3)	.017(3)	.011(3)	.002(2)	-.001(2)	.003(2)
C11'	.016(3)	.015(3)	.020(3)	.000(2)	.000(2)	-.003(3)
C12'	.016(3)	.027(4)	.010(3)	.001(3)	.001(2)	-.002(3)
C13'	.009(3)	.011(3)	.027(3)	.000(2)	.001(2)	.001(3)
C14'	.019(3)	.017(3)	.013(3)	-.002(3)	.003(2)	-.001(3)
C15'	.011(3)	.016(3)	.017(3)	-.002(2)	.003(2)	.000(3)
C16'	.049(4)	.025(4)	.038(4)	-.003(3)	-.016(3)	.009(3)
C17'	.037(4)	.015(3)	.058(5)	-.005(3)	.004(3)	-.006(3)
C18'	.027(4)	.040(4)	.087(6)	.009(3)	.017(4)	.001(4)
C19'	.016(3)	.032(4)	.038(4)	.009(3)	.002(3)	-.002(3)
C20'	.046(4)	.039(4)	.034(4)	-.002(3)	-.014(3)	.010(3)
C21'	.027(4)	.033(4)	.062(5)	-.010(3)	-.011(3)	-.005(4)
Ru3	.0101(2)	.0124(3)	.0217(3)	-.00142(19)	.00079(18)	.0018(2)
P1"	.0126(7)	.0169(8)	.0280(9)	-.0014(6)	-.0013(6)	-.0008(7)

P2 "	.0151(7)	.0121(8)	.0295(9)	-.0007(6)	.0026(7)	.0010(7)
O1 "	.0160(19)	.030(3)	.031(2)	.0013(19)	-.0013(17)	-.002(2)
O2 "	.030(2)	.029(3)	.025(2)	-.0039(20)	-.0070(19)	.0087(20)
O3 "	.020(2)	.024(2)	.052(3)	-.0035(18)	-.006(2)	-.011(2)
O4 "	.028(2)	.022(2)	.023(2)	.0133(18)	.0019(19)	.0017(18)
O5 "	.024(2)	.020(2)	.026(2)	-.0055(18)	.0027(18)	.0009(18)
O6 "	.021(2)	.015(2)	.063(3)	-.0025(18)	.008(2)	.001(2)
B3	.024(4)	.019(4)	.017(4)	.002(3)	.005(3)	.004(3)
N1 "	.014(2)	.018(3)	.028(3)	-.002(2)	.003(2)	.002(2)
N2 "	.015(2)	.025(3)	.023(3)	.005(2)	.0034(20)	.006(2)
N3 "	.008(2)	.018(3)	.023(3)	.0004(20)	.0024(20)	.002(2)
N4 "	.013(2)	.017(3)	.028(3)	.002(2)	.002(2)	-.001(2)
N5 "	.016(2)	.018(3)	.019(3)	.000(2)	.0042(20)	.004(2)
N6 "	.018(3)	.022(3)	.028(3)	.001(2)	.003(2)	.009(2)
N7 "	.017(2)	.016(3)	.017(3)	.0025(20)	-.0031(20)	.001(2)
C1 "	.017(3)	.022(3)	.035(4)	.001(3)	.004(3)	.012(3)
C2 "	.013(3)	.018(3)	.052(5)	.000(3)	.004(3)	.012(3)
C3 "	.019(3)	.028(4)	.027(3)	.011(3)	.011(3)	.009(3)
C4 "	.018(3)	.013(3)	.028(4)	-.001(2)	-.003(3)	.003(3)
C5 "	.021(3)	.016(3)	.035(4)	.002(3)	.002(3)	-.001(3)
C6 "	.017(3)	.028(4)	.018(3)	-.002(3)	-.001(2)	-.006(3)
C7 "	.010(3)	.021(3)	.037(4)	.001(3)	.004(2)	.005(3)
C8 "	.017(3)	.031(4)	.032(4)	-.001(3)	-.006(3)	.003(3)
C9 "	.026(3)	.025(4)	.020(3)	-.006(3)	-.005(3)	-.001(3)
C10 "	.008(3)	.011(3)	.031(4)	.000(2)	-.001(2)	.000(3)
C11 "	.017(3)	.025(3)	.017(3)	.001(3)	.000(2)	.004(3)
C12 "	.019(3)	.011(3)	.021(3)	-.003(2)	.005(3)	-.001(2)

C13"	.011(3)	.021(3)	.015(3)	.003(2)	.000(2)	.007(3)
C14"	.013(3)	.015(3)	.024(3)	-.004(2)	.001(2)	-.002(3)
C15"	.013(3)	.019(3)	.019(3)	.004(2)	.005(2)	.007(3)
C16"	.013(3)	.025(4)	.033(4)	.006(3)	.000(3)	-.001(3)
C17"	.039(4)	.047(5)	.025(4)	-.004(3)	-.017(3)	.008(3)
C18"	.030(4)	.032(4)	.093(6)	-.014(3)	-.009(4)	-.024(4)
C19"	.053(4)	.035(4)	.031(4)	.012(3)	.007(3)	.010(3)
C20"	.042(4)	.067(6)	.055(5)	.037(4)	.028(4)	.011(4)
C21"	.044(4)	.005(3)	.079(6)	-.006(3)	.012(4)	-.006(3)
S1	.0340(9)	.0266(9)	.0333(9)	-.0086(8)	-.0054(7)	-.0014(8)
O7	.037(3)	.050(3)	.034(3)	-.003(2)	-.017(2)	-.005(2)
O8	.071(4)	.038(3)	.056(3)	-.035(3)	-.018(3)	.011(3)
O9	.033(2)	.043(3)	.041(3)	-.005(2)	.004(2)	-.014(2)
C22	.027(4)	.068(6)	.010(3)	.004(4)	-.003(3)	-.002(3)
F1	.045(3)	.093(4)	.041(3)	.011(2)	-.013(2)	.007(2)
F2	.034(2)	.110(4)	.051(3)	.009(2)	.004(2)	.004(3)
F3	.050(3)	.046(3)	.089(4)	.010(2)	.000(3)	-.006(3)
S2	.0266(8)	.0273(9)	.0333(9)	-.0031(7)	.0008(7)	.0000(8)
O10	.038(3)	.051(3)	.028(3)	.006(2)	-.0109(20)	-.002(2)
O11	.028(2)	.053(3)	.034(3)	.004(2)	.0033(19)	-.011(2)
O12	.052(3)	.034(3)	.094(4)	-.023(3)	-.011(3)	.017(3)
C23	.021(3)	.055(5)	.017(3)	.008(3)	-.005(3)	-.003(3)
F4	.044(3)	.112(4)	.047(3)	.033(3)	.015(2)	-.004(3)
F5	.048(3)	.032(2)	.108(4)	.005(2)	-.014(3)	.008(2)
F6	.041(2)	.079(3)	.047(3)	.010(2)	-.024(2)	-.011(2)
S3	.0300(9)	.0382(10)	.0348(10)	-.0050(7)	.0014(7)	.0070(8)
O13	.054(3)	.027(3)	.083(4)	-.019(2)	-.004(3)	.026(3)

O14	.032(3)	.116(5)	.028(3)	-.027(3)	-.007(2)	.023(3)
O15	.066(3)	.056(3)	.055(3)	.018(3)	.028(3)	-.007(3)
F7	.046(2)	.030(2)	.069(3)	-.0122(18)	-.014(2)	.0106(20)
F8	.038(2)	.060(3)	.087(3)	.002(2)	.020(2)	.003(2)
F9	.053(3)	.058(3)	.082(3)	-.013(2)	-.035(2)	.019(3)
C1s	.034(4)	.045(4)	.033(4)	-.005(3)	-.006(3)	.003(3)
C11s	.0436(11)	.0565(13)	.0441(12)	.0143(9)	-.0050(9)	-.0020(10)
C12s	.0359(9)	.0636(13)	.0335(10)	.0059(9)	.0052(8)	.0041(9)
C13s	.0459(10)	.0417(11)	.0282(9)	-.0015(8)	-.0026(8)	.0016(8)
C2s	.030(4)	.033(4)	.041(4)	.002(3)	-.006(3)	-.001(3)
C14s	.0455(10)	.0458(11)	.0285(9)	.0064(9)	-.0028(8)	-.0038(8)
C15s	.0328(9)	.0552(12)	.0355(10)	-.0029(8)	.0032(8)	-.0016(9)
C16s	.0405(10)	.0558(12)	.0407(11)	-.0115(9)	.0011(8)	.0005(9)
C3s	.038(4)	.048(5)	.041(4)	.006(3)	.004(3)	-.004(3)
C17s	.0408(10)	.0498(11)	.0312(10)	.0111(8)	.0001(8)	.0005(8)
C18s	.0390(10)	.0814(14)	.0298(9)	.0035(10)	.0017(8)	-.0017(9)
C19s	.0370(10)	.0539(12)	.0611(13)	.0012(9)	-.0042(9)	-.0043(10)

Table A.34 Bond Distances for [TpRu{P(OMe)₃}₂NHC₆H₄-]₂[OTf]₂

Ru1 P1	2.2408(16)	N3 C4	1.350(7)
Ru1 P2	2.2488(16)	N4 C6	1.353(8)
Ru1 N1	2.089(4)	N5 N6	1.359(7)
Ru1 N3	2.150(5)	N5 C7	1.342(7)
Ru1 N5	2.142(4)	N6 C9	1.345(7)
Ru1 N7	2.022(4)	N7 C10	1.321(7)
P1 O1	1.604(4)	C1 C2	1.383(8)
P1 O2	1.584(4)	C2 C3	1.353(9)
P1 O3	1.582(4)	C4 C5	1.381(9)
P2 O4	1.604(4)	C5 C6	1.387(8)
P2 O5	1.567(4)	C7 C8	1.382(8)
P2 O6	1.576(4)	C8 C9	1.381(9)
O1 C16	1.444(7)	C10 C11	1.446(7)
O2 C17	1.449(7)	C10 C15	1.439(8)
O3 C18	1.445(7)	C11 C12	1.358(7)
O4 C19	1.449(7)	C12 C13	1.435(8)
O5 C20	1.439(7)	C13 C13	1.403(10)
O6 C21	1.449(7)	C13 C14	1.445(7)
B1 N2	1.534(8)	C14 C15	1.353(8)
B1 N4	1.550(8)	Ru2 P1'	2.2400(16)
B1 N6	1.562(9)	Ru2 P2'	2.2470(16)
N1 N2	1.369(7)	Ru2 N1'	2.106(4)
N1 C1	1.352(7)	Ru2 N3'	2.146(5)
N2 C3	1.363(6)	Ru2 N5'	2.161(4)
N3 N4	1.358(6)	Ru2 N7'	2.037(4)

P1' O1'	1.602(4)	C4' C5'	1.379(9)
P1' O2'	1.592(4)	C5' C6'	1.385(9)
P1' O3'	1.604(4)	C7' C8'	1.392(8)
P2' O4'	1.608(4)	C8' C9'	1.364(9)
P2' O5'	1.600(4)	C10' C11'	1.432(7)
P2' O6'	1.594(4)	C10' C15'	1.447(8)
O1' C16'	1.433(8)	11' C12'	1.349(8)
O2' C17'	1.449(7)	C12' C13'	1.437(8)
O3' C18'	1.454(7)	C13' C14'	1.450(7)
O4' C19'	1.447(7)	C13' C13"	1.416(8)
O5' C20'	1.459(8)	C14' C15'	1.343(7)
O6' C21'	1.453(7)	Ru3 P1"	2.2464(16)
B2 N2'	1.537(8)	Ru3 P2"	2.2407(16)
B2 N4'	1.556(8)	Ru3 N1"	2.078(4)
B2 N6'	1.533(8)	Ru3 N3"	2.148(5)
N1' N2'	1.370(7)	Ru3 N5"	2.151(5)
N1' C1'	1.344(7)	Ru3 N7"	2.047(4)
N2' C3'	1.352(7)	P1" O1"	1.597(4)
N3' N4'	1.366(6)	P1" O2"	1.592(4)
N3' C4'	1.342(7)	P1" O3"	1.595(4)
N4' C6'	1.348(8)	P2" O4"	1.600(4)
N5' N6'	1.361(7)	P2" O5"	1.602(4)
N5' C7'	1.346(7)	P2" O6"	1.587(4)
N6' C9'	1.346(8)	O1" C16"	1.450(7)
N7' C10'	1.325(7)	O2" C17"	1.448(7)
C1' C2'	1.390(8)	O3" C18"	1.442(7)
C2' C3'	1.375(10)	O4" C19"	1.439(7)

O5 " C20 "	1.453(8)	S1 O7	1.433(5)
O6 " C21 "	1.457(7)	S1 O8	1.441(4)
B3 N2 "	1.564(8)	S1 O9	1.431(4)
B3 N4 "	1.549(8)	S1 C22	1.814(7)
B3 N6 "	1.558(8)	C22 F1	1.324(8)
N1 " N2 "	1.360(7)	C22 F2	1.302(7)
N1 " C1 "	1.340(7)	C22 F3	1.382(9)
N2 " C3 "	1.369(7)	F1 F2	2.131(6)
N3 " N4 "	1.365(7)	F1 F3	2.162(6)
N3 " C4 "	1.343(7)	F2 F3	2.122(6)
N4 " C6 "	1.345(8)	S2 O10	1.418(5)
N5 " N6 "	1.357(7)	S2 O11	1.436(4)
N5 " C7 "	1.342(7)	S2 O12	1.443(5)
N6 " C9 "	1.349(8)	S2 C23	1.820(7)
N7 " C10 "	1.341(7)	C23 F4	1.309(7)
C1 " C2 "	1.381(8)	C23 F5	1.373(8)
C2 " C3 "	1.382(9)	C23 F6	1.327(7)
C4 " C5 "	1.383(8)	F4 F5	2.131(6)
C5 " C6 "	1.378(9)	F4 F6	2.142(6)
C7 " C8 "	1.396(9)	F5 F6	2.156(6)
C8 " C9 "	1.364(8)	S3 O13	1.412(5)
C10 " C11 "	1.430(7)	S3 O14	1.431(5)
C10 " C15 "	1.435(8)	S3 O15	1.452(5)
C11 " C12 "	1.345(8)	S3 C24	1.792(6)
C12 " C13 "	1.431(8)	C24 F7	1.298(7)
C13 " C14 "	1.433(7)	C24 F8	1.389(7)
C14 " C15 "	1.359(7)	C24 F9	1.307(7)

F7 F8	2.089(6)	C2s C16s	1.773(7)
F7 F9	2.133(5)	C14s C15s	2.878(2)
F8 F9	2.143(6)	C14s C16s	2.903(3)
C1s C11s	1.775(7)	C15s C16s	2.912(2)
C1s C12s	1.768(7)	C3s C17s	1.778(7)
C1s C13s	1.757(7)	C3s C18s	1.746(7)
C11s C12s	2.908(2)	C3s C19s	1.745(7)
C11s C13s	2.903(3)	C17s C18s	2.874(2)
C12s C13s	2.860(2)	C17s C19s	2.913(3)
C2s C14s	1.772(7)	C18s C19s	2.896(2)
C2s C15s	1.760(7)		

Table A.35 Bond Angles for [TpRu{P(OMe)₃}₂NHC₆H₄-]₂[OTf]₂

P1 Ru1 P2	91.97(6)	O5 P2 O6	107.6(2)
P1 Ru1 N1	95.98(13)	P1 O1 C16	118.0(4)
P1 Ru1 N3	93.19(13)	P1 O2 C17	120.6(4)
P1 Ru1 N5	177.14(11)	P1 O3 C18	127.4(4)
P1 Ru1 N7	86.65(13)	P2 O4 C19	119.1(4)
P2 Ru1 N1	92.94(13)	P2 O5 C20	126.6(3)
P2 Ru1 N3	174.75(13)	P2 O6 C21	124.6(4)
P2 Ru1 N5	89.39(13)	N2 B1 N4	108.5(5)
P2 Ru1 N7	91.24(13)	N2 B1 N6	108.1(5)
N1 Ru1 N3	85.51(17)	N4 B1 N6	106.0(4)
N1 Ru1 N5	86.46(17)	Ru1 N1 N2	117.9(3)
N1 Ru1 N7	174.98(19)	Ru1 N1 C1	135.3(4)
N3 Ru1 N5	85.51(17)	N2 N1 C1	106.3(4)
N3 Ru1 N7	90.08(17)	B1 N2 N1	122.2(4)
N5 Ru1 N7	90.80(17)	B1 N2 C3	128.4(5)
Ru1 P1 O1	118.47(16)	N1 N2 C3	109.4(4)
Ru1 P1 O2	116.02(16)	Ru1 N3 N4	118.4(3)
Ru1 P1 O3	110.56(16)	Ru1 N3 C4	134.4(4)
O1 P1 O2	104.4(2)	N4 N3 C4	107.2(4)
O1 P1 O3	99.2(2)	B1 N4 N3	120.5(5)
O2 P1 O3	106.3(2)	B1 N4 C6	129.7(5)
Ru1 P2 O4	116.86(15)	N3 N4 C6	109.5(4)
Ru1 P2 O5	112.87(15)	Ru1 N5 N6	118.5(3)
Ru1 P2 O6	114.83(16)	Ru1 N5 C7	133.5(4)
O4 P2 O5	99.4(2)	N6 N5 C7	107.1(4)
O4 P2 O6	103.7(2)	B1 N6 N5	120.0(4)

B1 N6 C9	131.0(5)	P2' Ru2 N1'	93.59(13)
N5 N6 C9	109.0(5)	P2' Ru2 N3'	176.14(13)
Ru1 N7 C10	135.6(4)	P2' Ru2 N5'	90.68(14)
N1 C1 C2	109.4(5)	P2' Ru2 N7'	88.86(14)
C1 C2 C3	107.1(5)	N1' Ru2 N3'	85.21(17)
N2 C3 C2	107.8(5)	N1' Ru2 N5'	86.46(17)
N3 C4 C5	109.6(5)	N1' Ru2 N7'	175.97(18)
C4 C5 C6	105.9(5)	N3' Ru2 N5'	85.59(18)
N4 C6 C5	107.8(5)	N3' Ru2 N7'	92.14(17)
N5 C7 C8	110.1(5)	N5' Ru2 N7'	90.31(16)
C7 C8 C9	105.0(5)	Ru2 P1' O1'	117.57(16)
N6 C9 C8	108.7(5)	Ru2 P1' O2'	114.26(16)
N7 C10 C11	119.9(5)	Ru2 P1' O3'	117.07(16)
N7 C10 C15	123.6(5)	O1' P1' O2'	103.9(2)
C11 C10 C15	116.5(5)	O1' P1' O3'	99.5(2)
C10 C11 C12	121.5(5)	O2' P1' O3'	102.2(2)
C11 C12 C13	122.4(5)	Ru2 P2' O4'	119.07(16)
C12 C13 C13	122.8(5)	Ru2 P2' O5'	109.03(16)
C12 C13 C14	115.4(4)	Ru2 P2' O6'	121.06(16)
C13a C13 C14	121.8(5)	O4' P2' O5'	105.9(2)
C13 C14 C15	122.9(5)	O4' P2' O6'	98.8(2)
C10 C15 C14	121.1(5)	O5' P2' O6'	100.7(2)
P1' Ru2 P2'	91.64(6)	P1' O1' C16'	119.0(4)
P1' Ru2 N1'	93.29(13)	P1' O2' C17'	120.9(4)
P1' Ru2 N3'	92.09(13)	P1' O3' C18'	123.9(4)
P1' Ru2 N5'	177.68(14)	P2' O4' C19'	121.3(3)
P1' Ru2 N7'	89.84(13)	P2' O5' C20'	121.8(4)

P2' O6' C21'	124.7(4)	C4' C5' C6'	105.2(5)
N2' B2 N4'	108.5(5)	N4' C6' C5'	107.4(5)
N2' B2 N6'	109.9(5)	N5' C7' C8'	109.5(5)
N4' B2 N6'	106.8(4)	C7' C8' C9'	105.1(5)
Ru2 N1' N2'	117.8(3)	N6' C9' C8'	109.7(5)
Ru2 N1' C1'	134.1(4)	N7' C10' C11'	120.9(5)
N2' N1' C1'	107.7(4)	N7' C10' C15'	122.4(5)
B2 N2' N1'	121.3(4)	C11' C10' C15'	116.6(5)
B2 N2' C3'	130.2(5)	C10' C11' C12'	121.9(5)
N1' N2' C3'	108.4(5)	C11' C12' C13'	122.3(5)
Ru2 N3' N4'	118.3(3)	C12' C13' C14'	115.3(5)
Ru2 N3' C4'	136.6(4)	C12' C13' C13"	123.0(5)
N4' N3' C4'	105.0(4)	C14' C13' C13"	121.7(5)
B2 N4' N3'	119.9(4)	C13' C14' C15'	122.8(5)
B2 N4' C6'	129.1(5)	C10' C15' C14'	121.0(5)
N3' N4' C6'	110.9(5)	P1" Ru3 P2"	91.56(6)
Ru2 N5' N6'	118.3(3)	P1" Ru3 N1"	92.67(14)
Ru2 N5' C7'	133.4(4)	P1" Ru3 N3"	90.85(13)
N6' N5' C7'	107.2(4)	P1" Ru3 N5"	176.03(13)
B2 N6' N5'	119.7(4)	P1" Ru3 N7"	88.90(13)
B2 N6' C9'	131.8(5)	P2" Ru3 N1"	94.55(13)
N5' N6' C9'	108.5(5)	P2" Ru3 N3"	177.32(13)
Ru2 N7' C10'	135.6(4)	P2" Ru3 N5"	92.28(13)
N1' C1' C2'	109.1(5)	P2" Ru3 N7"	88.43(13)
C1' C2' C3'	105.9(5)	N1" Ru3 N3"	86.50(17)
N2' C3' C2'	108.8(5)	N1" Ru3 N5"	86.04(17)
N3' C4' C5'	111.5(5)	N1" Ru3 N7"	176.58(18)

N3 " Ru3 N5 "	85.33(18)	B3 N2 " N1 "	122.7(4)
N3 " Ru3 N7 "	90.45(16)	B3 N2 " C3 "	127.0(5)
N5 " Ru3 N7 "	92.20(17)	N1 " N2 " C3 "	110.3(5)
Ru3 P1 " O1 "	118.88(16)	Ru3 N3 " N4 "	118.5(3)
Ru3 P1 " O2 "	109.40(16)	Ru3 N3 " C4 "	134.6(4)
Ru3 P1 " O3 "	120.10(17)	N4 " N3 " C4 "	106.2(4)
O1 " P1 " O2 "	105.8(2)	B3 N4 " N3 "	120.6(4)
O1 " P1 " O3 "	98.7(2)	B3 N4 " C6 "	130.3(5)
O2 " P1 " O3 "	101.9(2)	N3 " N4 " C6 "	109.0(5)
Ru3 P2 " O4 "	117.57(16)	Ru3 N5 " N6 "	118.3(3)
Ru3 P2 " O5 "	114.86(16)	Ru3 N5 " C7 "	135.0(4)
Ru3 P2 " O6 "	115.15(16)	N6 " N5 " C7 "	106.6(5)
O4 " P2 " O5 "	99.4(2)	B3 N6 " N5 "	121.1(5)
O4 " P2 " O6 "	104.3(2)	B3 N6 " C9 "	129.5(5)
O5 " P2 " O6 "	103.4(2)	N5 " N6 " C9 "	109.2(4)
P1 " O1 " C16 "	120.6(3)	Ru3 N7 " C10 "	135.0(4)
P1 " O2 " C17 "	122.5(4)	N1 " C1 " C2 "	111.8(6)
P1 " O3 " C18 "	126.4(4)	C1 " C2 " C3 "	105.1(5)
P2 " O4 " C19 "	120.6(4)	N2 " C3 " C2 "	107.3(5)
P2 " O5 " C20 "	122.7(4)	N3 " C4 " C5 "	111.1(5)
P2 " O6 " C21 "	120.7(4)	C4 " C5 " C6 "	104.1(5)
N2 " B3 N4 "	107.6(5)	N4 " C6 " C5 "	109.5(5)
N2 " B3 N6 "	107.4(5)	N5 " C7 " C8 "	110.3(5)
N4 " B3 N6 "	105.9(4)	C7 " C8 " C9 "	104.5(5)
Ru3 N1 " N2 "	118.2(3)	N6 " C9 " C8 "	109.3(5)
Ru3 N1 " C1 "	135.9(4)	N7 " C10 " C11 "	119.6(5)
N2 " N1 " C1 "	105.5(4)	N7 " C10 " C15 "	123.0(5)

C11" C10" C15"	117.4(5)	C22 F3 F2	36.4(3)
C10" C11" C12"	122.0(5)	F1 F3 F2	59.7(2)
C11" C12" C13"	121.8(5)	O10 S2 O11	115.6(3)
C13' C13" C12"	122.4(5)	O10 S2 O12	115.4(3)
C13' C13" C14"	121.9(5)	O10 S2 C23	103.5(3)
C12" C13" C14"	115.8(5)	O11 S2 O12	115.8(3)
C13" C14" C15"	123.3(5)	O11 S2 C23	102.9(3)
C10" C15" C14"	119.7(5)	O12 S2 C23	100.6(3)
O7 S1 O8	115.7(3)	S2 C23 F4	113.3(5)
O7 S1 O9	115.0(3)	S2 C23 F5	110.9(4)
O7 S1 C22	103.8(3)	S2 C23 F6	112.3(5)
O8 S1 O9	114.8(3)	F4 C23 F5	105.2(5)
O8 S1 C22	101.1(3)	F4 C23 F6	108.6(5)
O9 S1 C22	103.8(3)	F5 C23 F6	105.9(5)
S1 C22 F1	112.5(5)	C23 F4 F5	38.4(4)
S1 C22 F2	114.1(5)	C23 F4 F6	36.0(3)
S1 C22 F3	110.7(4)	F5 F4 F6	60.6(2)
F1 C22 F2	108.5(5)	C23 F5 F4	36.4(3)
F1 C22 F3	106.0(5)	C23 F5 F6	36.3(3)
F2 C22 F3	104.4(6)	F4 F5 F6	59.95(20)
C22 F1 F2	35.4(3)	C23 F6 F4	35.4(3)
C22 F1 F3	37.9(4)	C23 F6 F5	37.8(3)
F2 F1 F3	59.2(2)	F4 F6 F5	59.5(2)
C22 F2 F1	36.1(3)	O13 S3 O14	114.0(3)
C22 F2 F3	39.1(4)	O13 S3 O15	114.9(3)
F1 F2 F3	61.1(2)	O13 S3 C24	104.9(3)
C22 F3 F1	36.0(3)	O14 S3 O15	116.1(3)

O14 S3 C24	105.0(3)	C1s C13s C12s	35.9(2)
O15 S3 C24	99.4(3)	C11s C13s C12s	60.60(6)
S3 C24 F7	114.8(4)	C14s C2s C15s	109.2(4)
S3 C24 F8	109.6(4)	C14s C2s C16s	110.0(3)
S3 C24 F9	114.2(4)	C15s C2s C16s	111.1(4)
F7 C24 F8	102.0(4)	C2s C14s C15s	35.3(2)
F7 C24 F9	109.9(5)	C2s C14s C16s	35.0(2)
F8 C24 F9	105.3(5)	C15s C14s C16s	60.49(6)
C24 F7 F8	40.6(3)	C2s C15s C14s	35.5(2)
C24 F7 F9	35.2(3)	2s C15s C16s	34.6(2)
F8 F7 F9	61.0(2)	C14s C15s C16s	60.18(6)
C24 F8 F7	37.4(3)	C2s C16s C14s	35.0(2)
C24 F8 F9	36.0(3)	C2s C16s C15s	34.3(2)
F7 F8 F9	60.49(19)	C14s C16s C15s	59.33(6)
C24 F9 F7	34.9(3)	C17s C3s C18s	109.3(4)
C24 F9 F8	38.7(3)	C17s C3s C19s	111.5(4)
F7 F9 F8	58.50(19)	C18s C3s C19s	112.1(4)
C11s C1s C12s	110.3(4)	C3s C17s C18s	35.0(2)
C11s C1s C13s	110.5(3)	C3s C17s C19s	33.9(2)
C12s C1s C13s	108.5(4)	C18s C17s C19s	60.04(6)
C1s C11s C12s	34.8(2)	C3s C18s C17s	35.7(2)
C1s C11s C13s	34.5(2)	C3s C18s C19s	34.0(2)
C12s C11s C13s	58.97(6)	C17s C18s C19s	60.64(6)
C1s C12s C11s	34.9(2)	C3s C19s C17s	34.6(2)
C1s C12s C13s	35.6(2)	C3s C19s C18s	34.0(2)
C11s C12s C13s	60.43(6)	C17s C19s C18s	59.32(6)
C1s C13s C11s	34.9(2)		

Appendix B: Variable Temperature Spectra

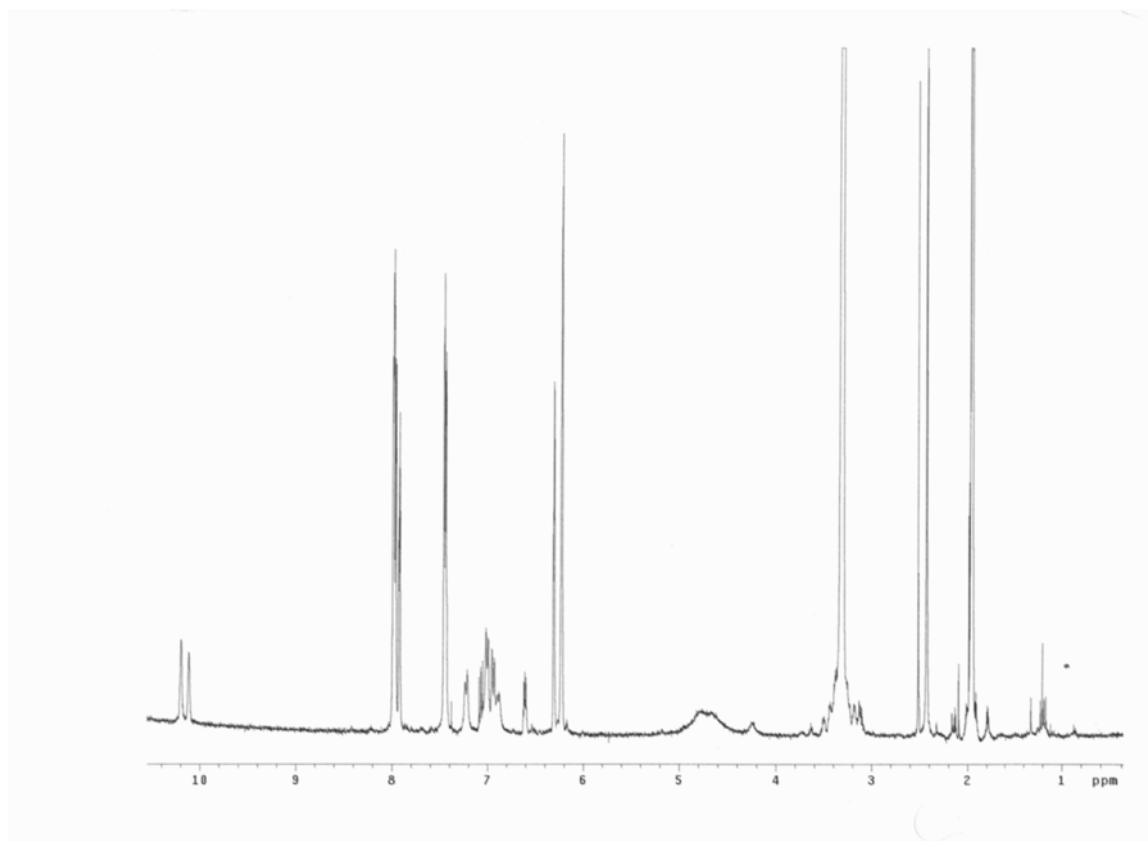


Figure B1 ^1H NMR spectrum of $[\text{TpRu}\{\text{P}(\text{OMe})_3\}_2\text{NC}_6\text{H}_4-]_2[\text{OTf}]_2$ in CD_3CN at $-45\text{ }^\circ\text{C}$.

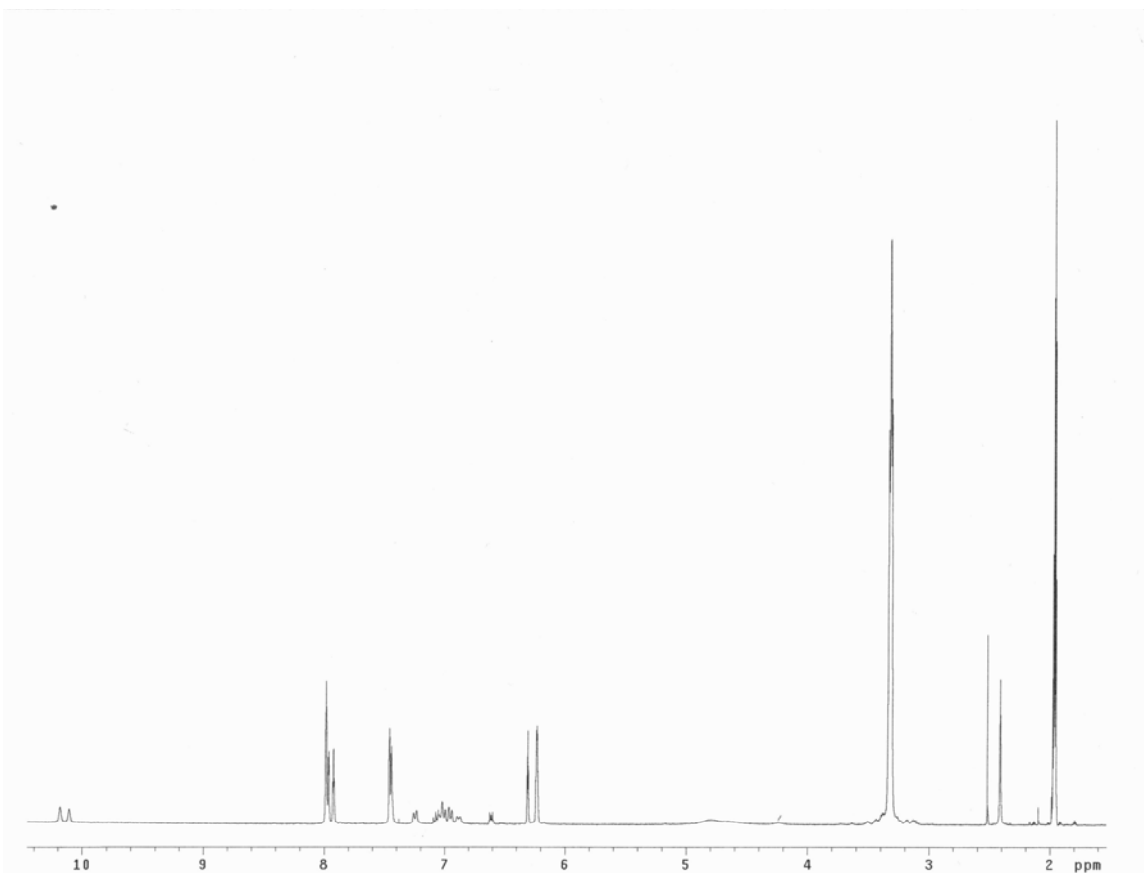


Figure B2 ^1H NMR spectrum of $[\text{TpRu}\{\text{P}(\text{OMe})_3\}_2\text{NC}_6\text{H}_4\text{-}]_2[\text{OTf}]_2$ in CD_3CN at $-40\text{ }^\circ\text{C}$.

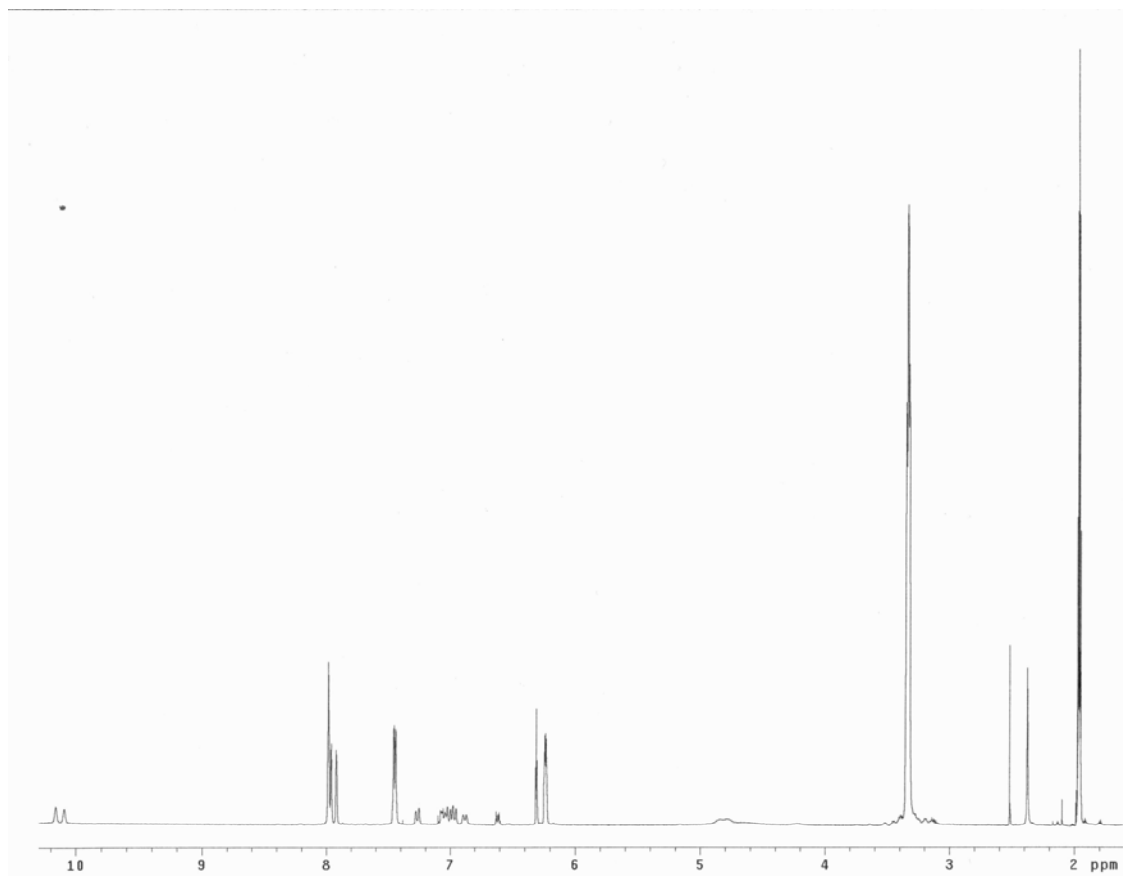


Figure B3 ¹H NMR spectrum of [TpRu{P(OMe)₃}₂NC₆H₄-]₂[OTf]₂ in CD₃CN at -30 °C.

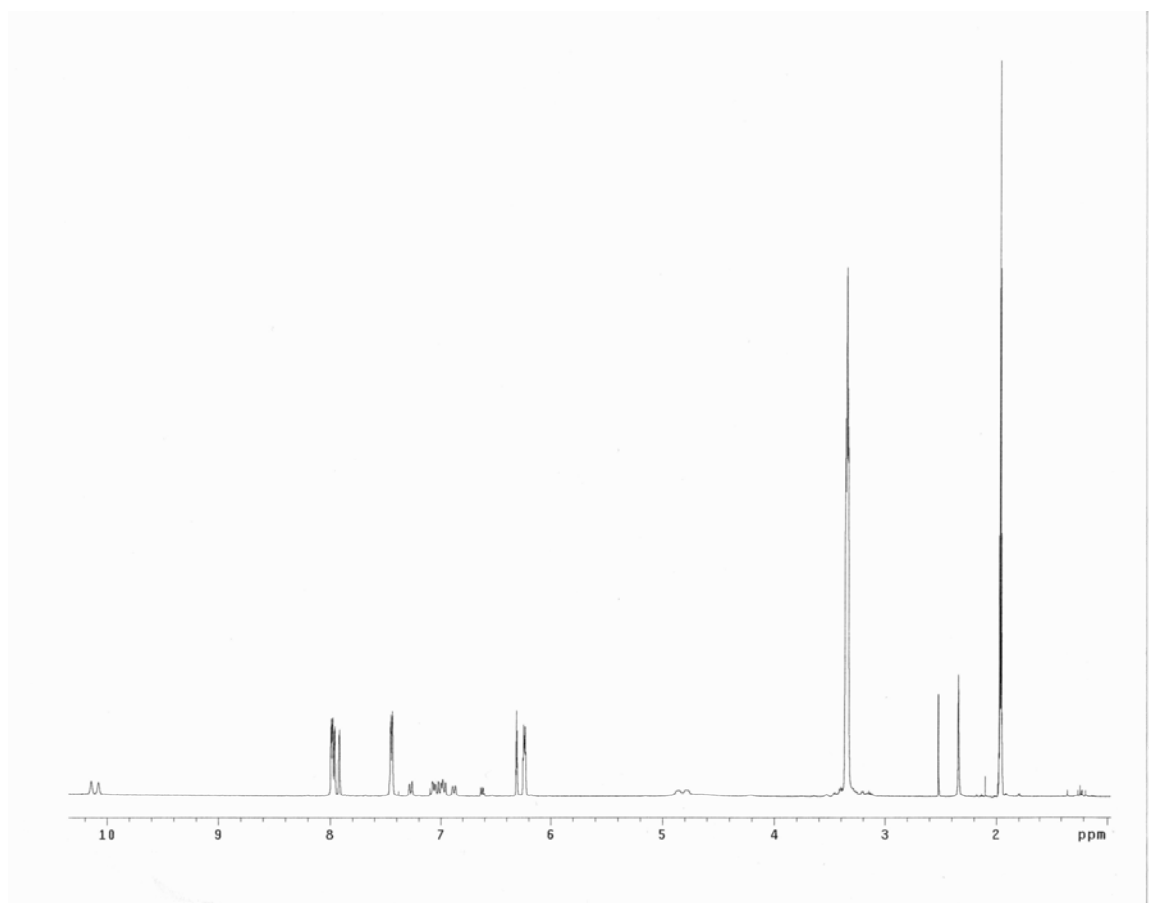


Figure B4 ¹H NMR spectrum of [TpRu{P(OMe)₃}₂NC₆H₄-]₂[OTf]₂ in CD₃CN at -20 °C.

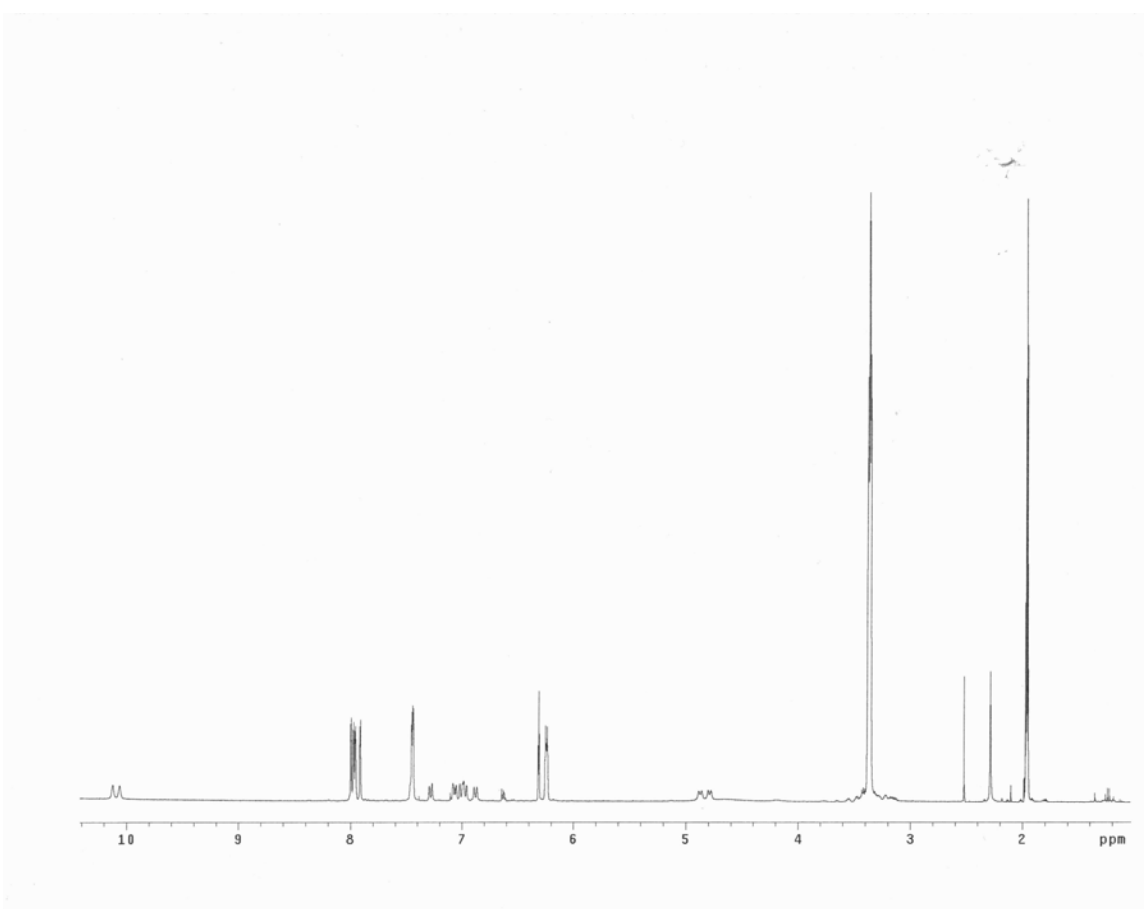


Figure B5 ¹H NMR spectrum of [TpRu{P(OMe)₃}₂NC₆H₄-]₂[OTf]₂ in CD₃CN at -5 °C.

" at 15°C.

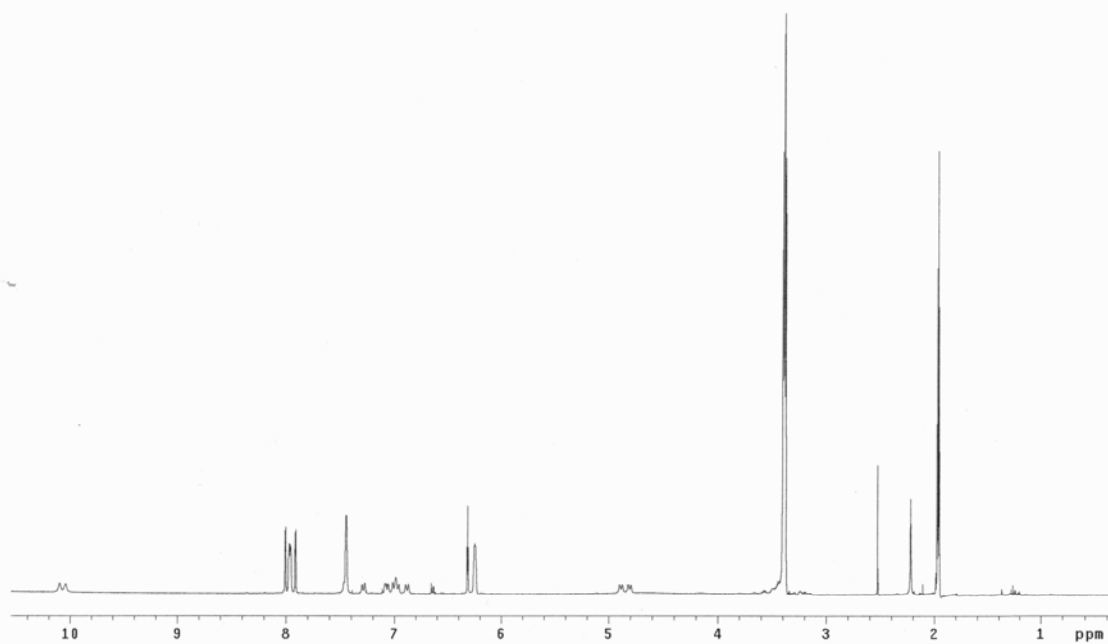


Figure B6 ¹H NMR spectrum of [TpRu{P(OMe)₃}₂NC₆H₄-]₂[OTf]₂ in CD₃CN at 15 °C.

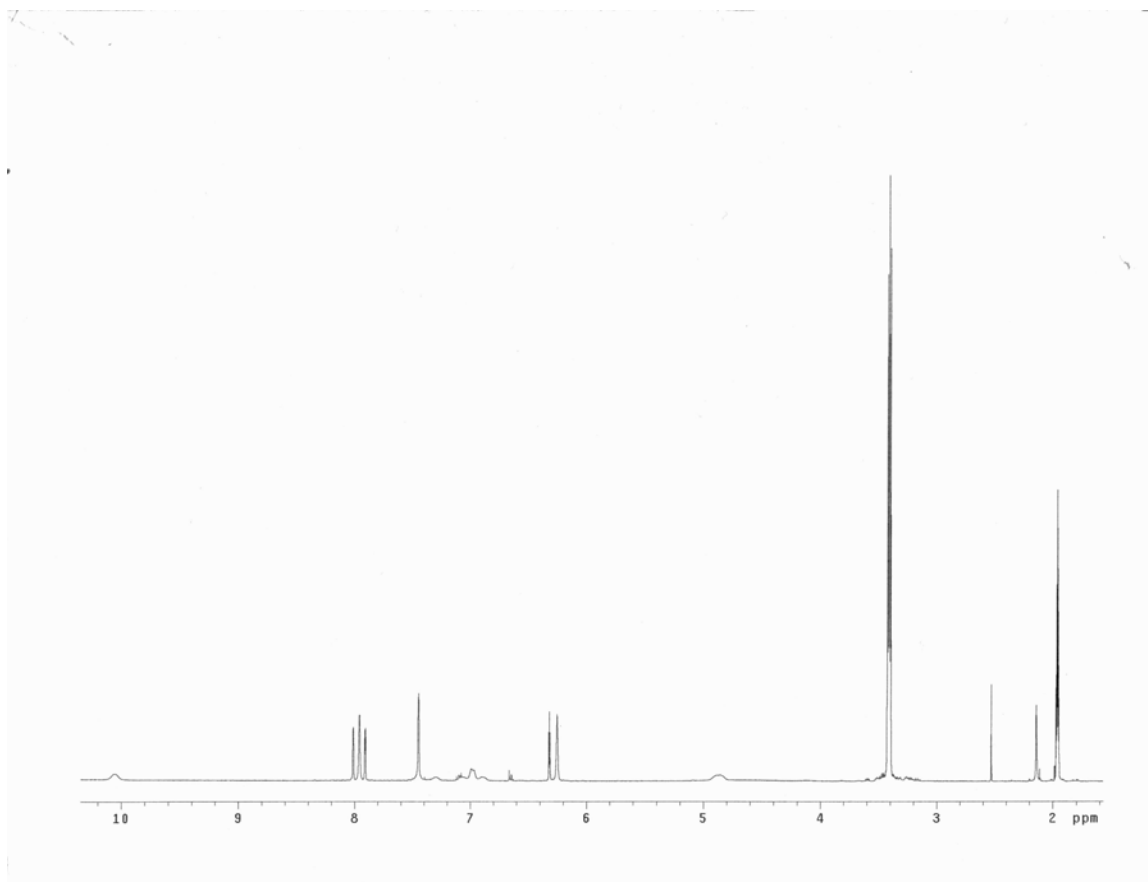


Figure B7 ^1H NMR spectrum of $[\text{TpRu}\{\text{P}(\text{OMe})_3\}_2\text{NC}_6\text{H}_4\text{-}]_2[\text{OTf}]_2$ in CD_3CN at $40\text{ }^\circ\text{C}$.

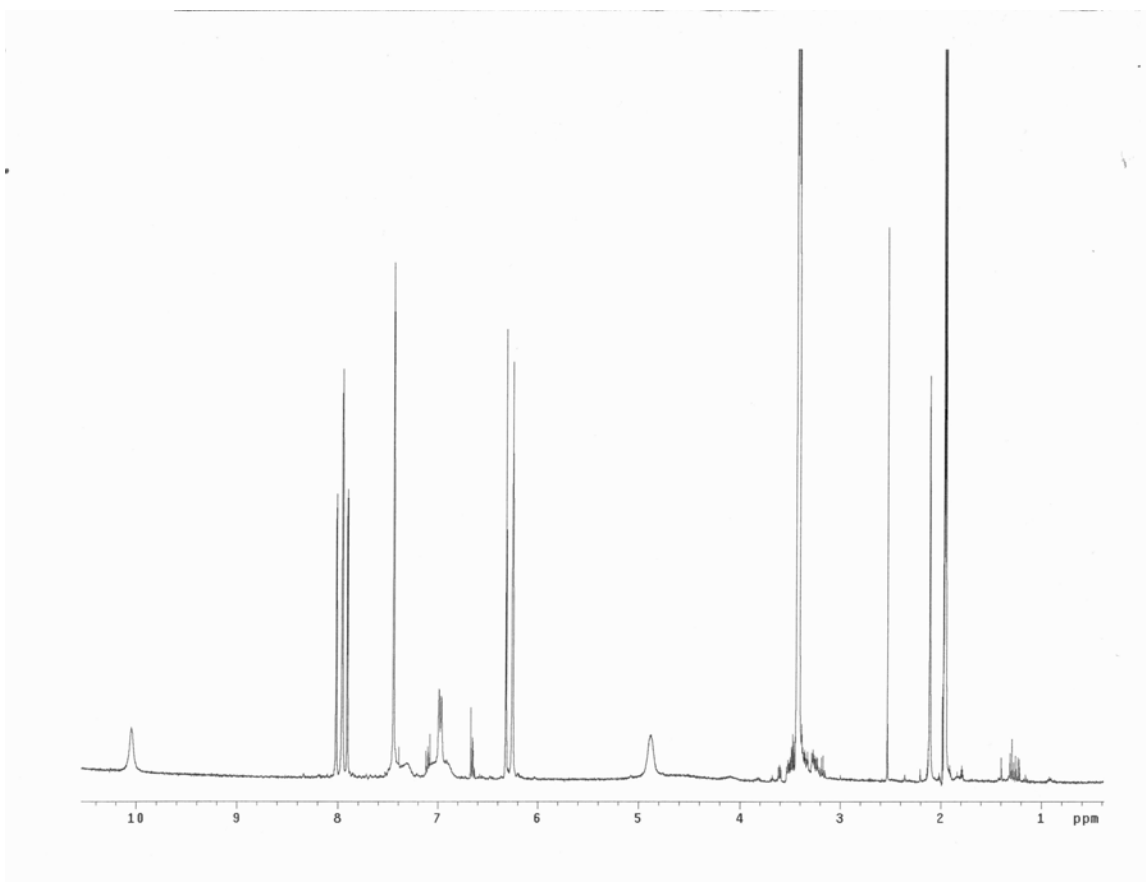


Figure B8 ^1H NMR spectrum of $[\text{TpRu}\{\text{P}(\text{OMe})_3\}_2\text{NC}_6\text{H}_4\text{-}]_2[\text{OTf}]_2$ in CD_3CN at $50\text{ }^\circ\text{C}$.

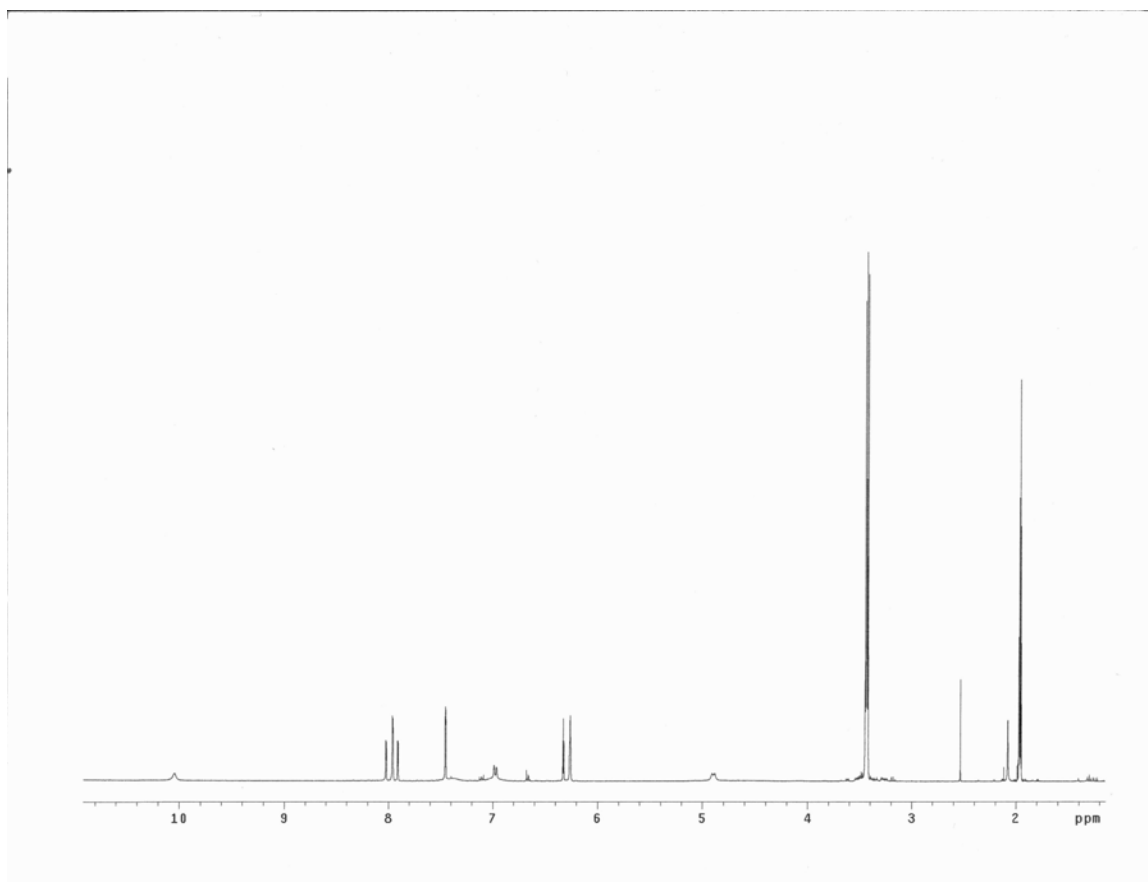


Figure B9 ^1H NMR spectrum of $[\text{TpRu}\{\text{P}(\text{OMe})_3\}_2\text{NC}_6\text{H}_4\text{-}]_2[\text{OTf}]_2$ in CD_3CN at $60\text{ }^\circ\text{C}$.

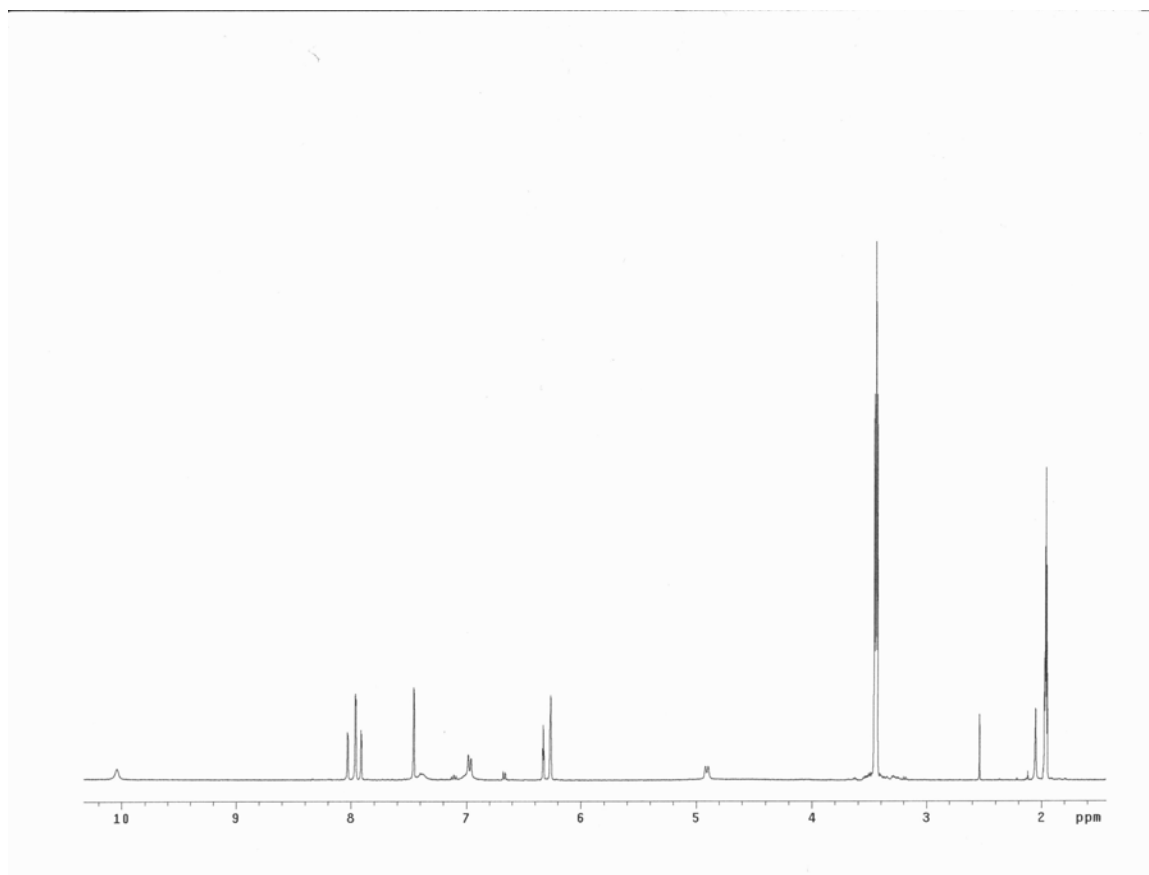


Figure B10 ¹H NMR spectrum of [TpRu{P(OMe)₃}₂NC₆H₄-]₂[OTf]₂ in CD₃CN at 70 °C.

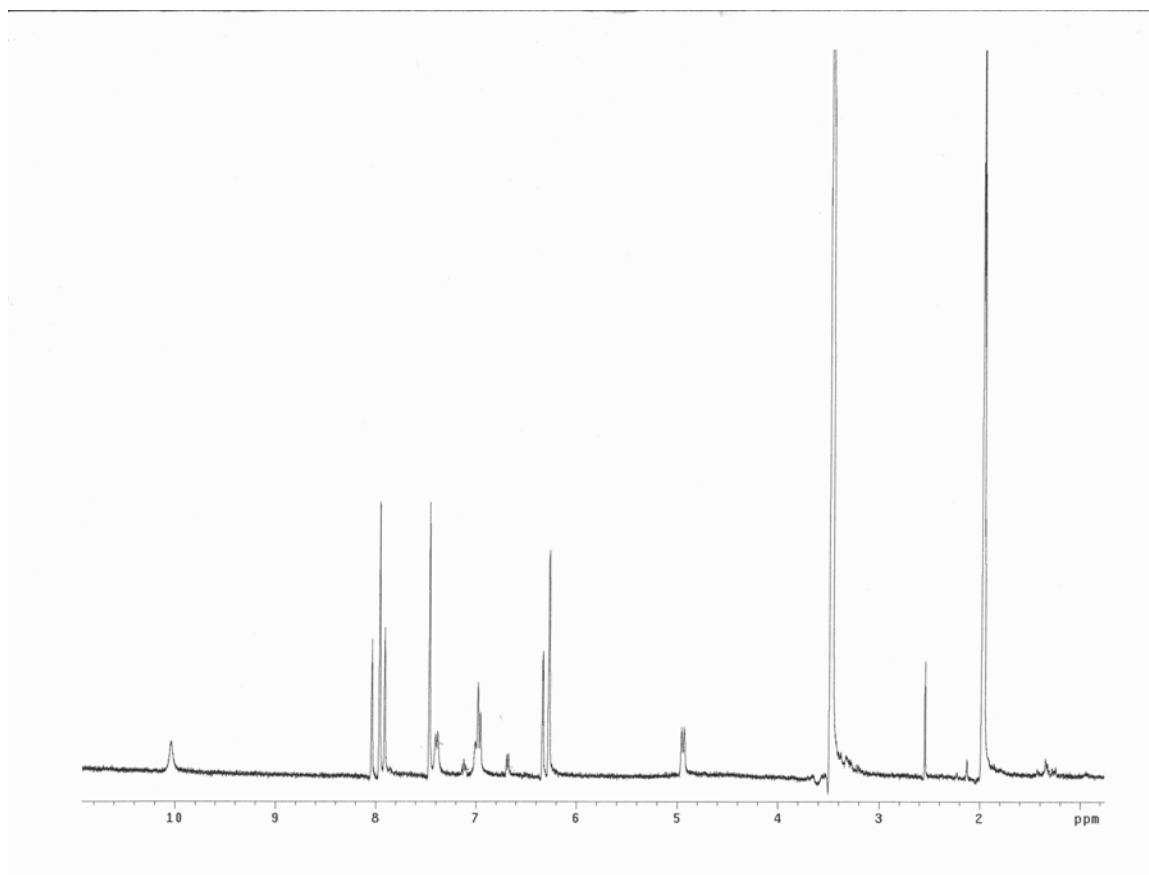


Figure B11 ¹H NMR spectrum of [TpRu{P(OMe)₃}₂NC₆H₄-]₂[OTf]₂ in CD₃CN at 95 °C.

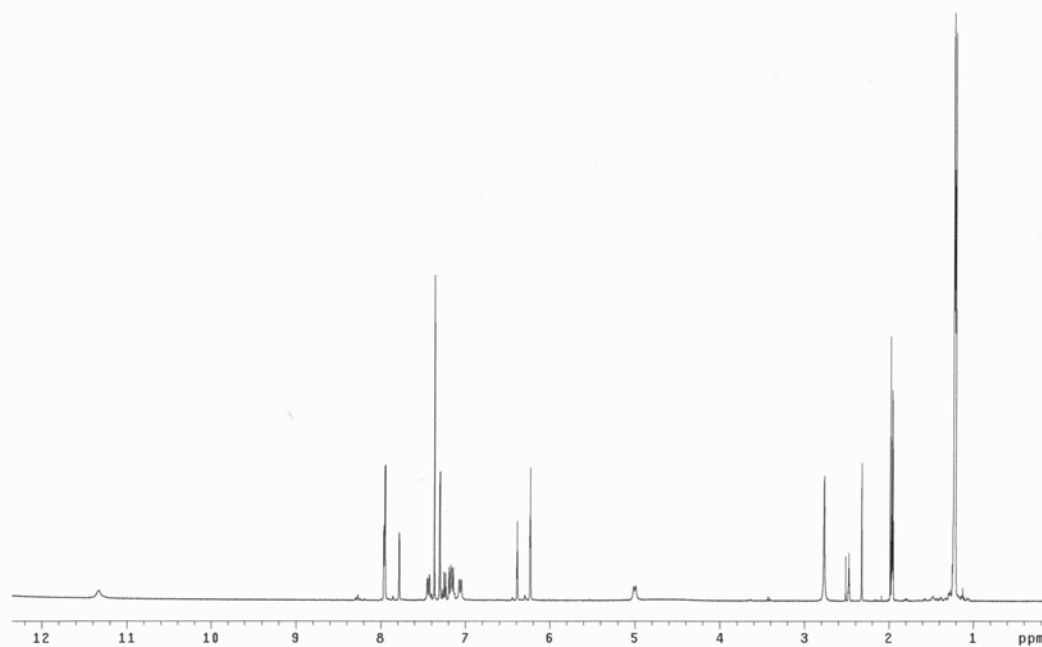


Figure B12 ¹H NMR spectrum of [TpRu(PMe₃)₂NC₆H₄-]₂[OTf]₂ in 80% CD₃CN 20 % DMSO-*d*₆ at 60 °C.

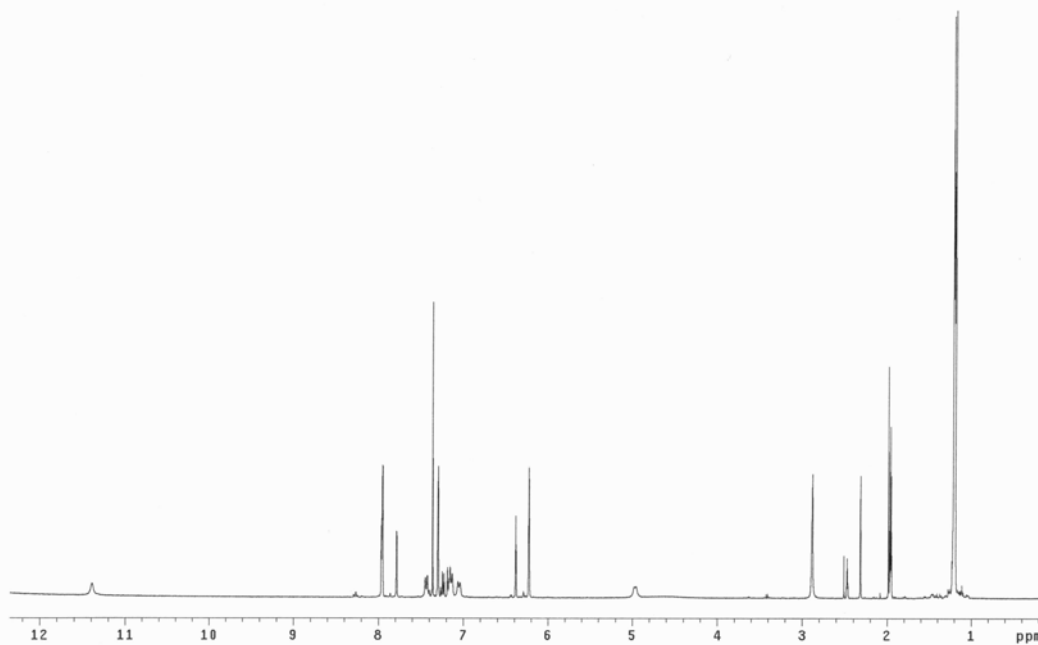


Figure B13 ¹H NMR spectrum of [TpRu(PMe₃)₂NC₆H₄-]₂[OTf]₂ in 80% CD₃CN 20 % DMSO-*d*₆ at 40 °C.

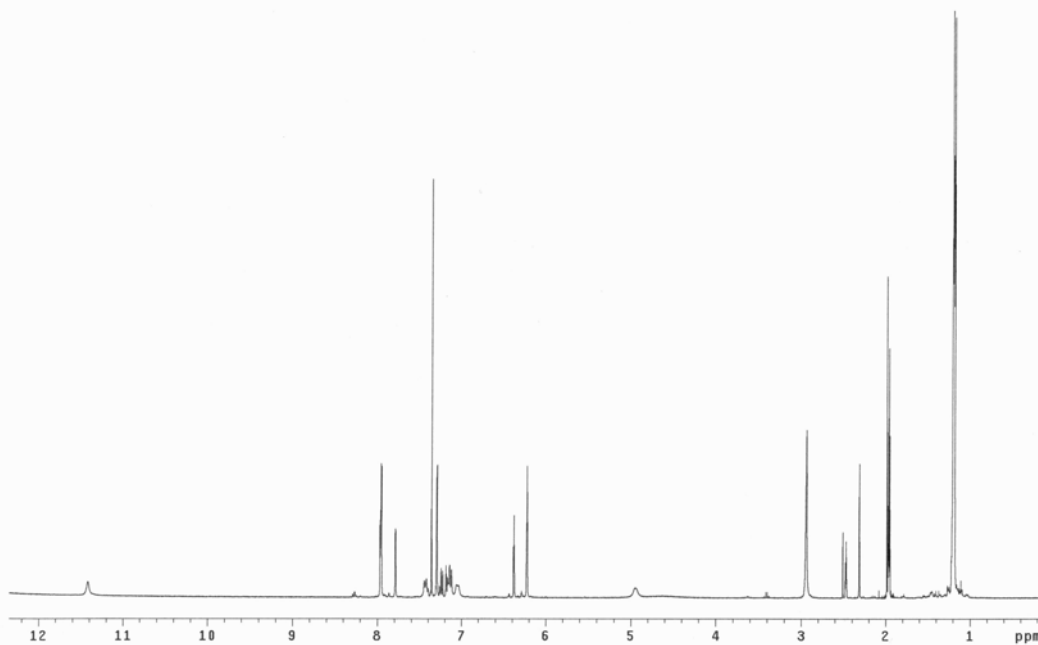


Figure B14 ¹H NMR spectrum of [TpRu(PMe₃)₂NC₆H₄-]₂[OTf]₂ in 80% CD₃CN 20 % DMSO-*d*₆ at 30 °C.

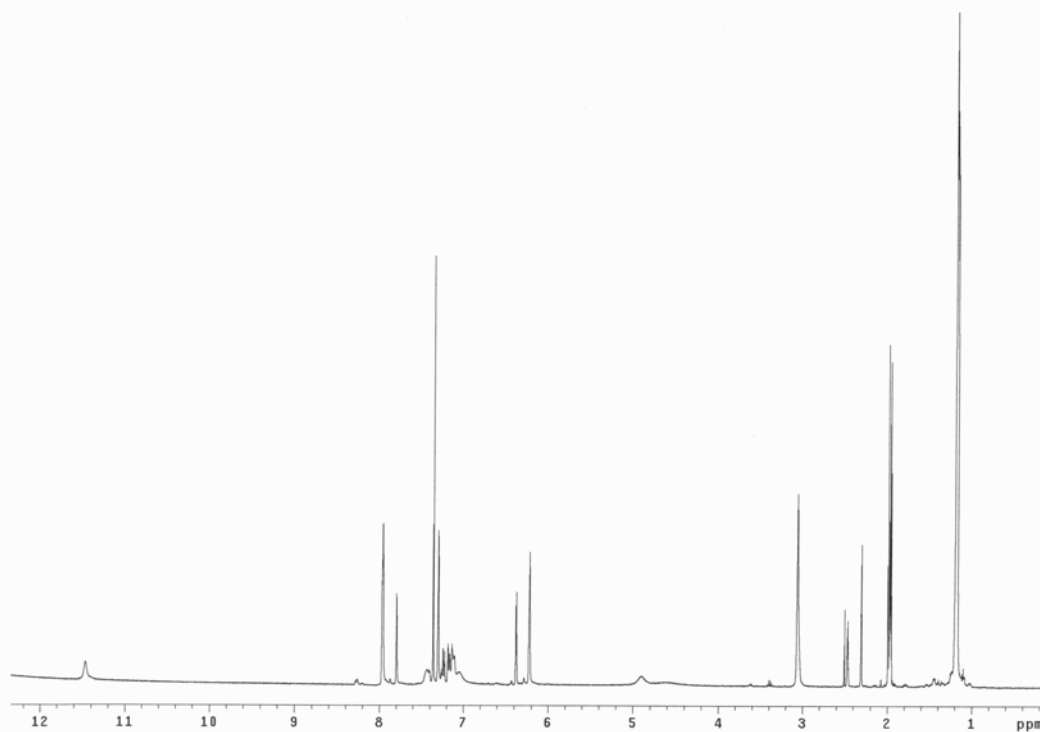


Figure B15 ¹H NMR spectrum of [TpRu(PMe₃)₂NC₆H₄-]₂[OTf]₂ in 80% CD₃CN 20 % DMSO-*d*₆ at 30 °C.

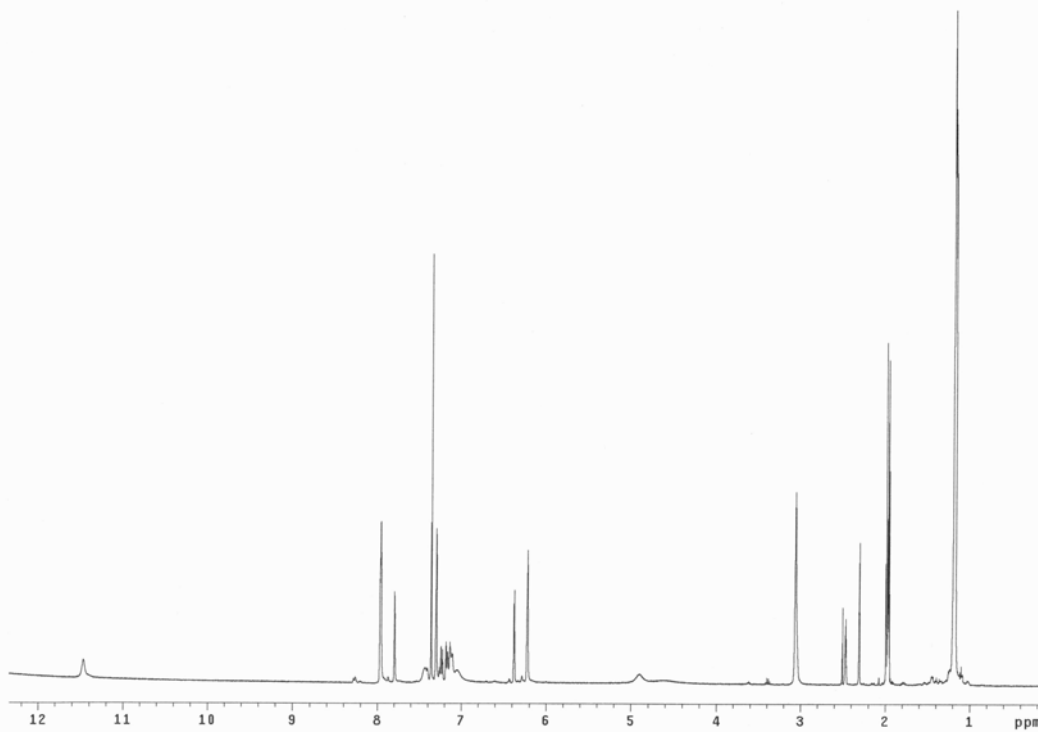


Figure B16 ¹H NMR spectrum of [TpRu(PMe₃)₂NC₆H₄-]₂[OTf]₂ in 80% CD₃CN 20 % DMSO-*d*₆ at 10 °C.

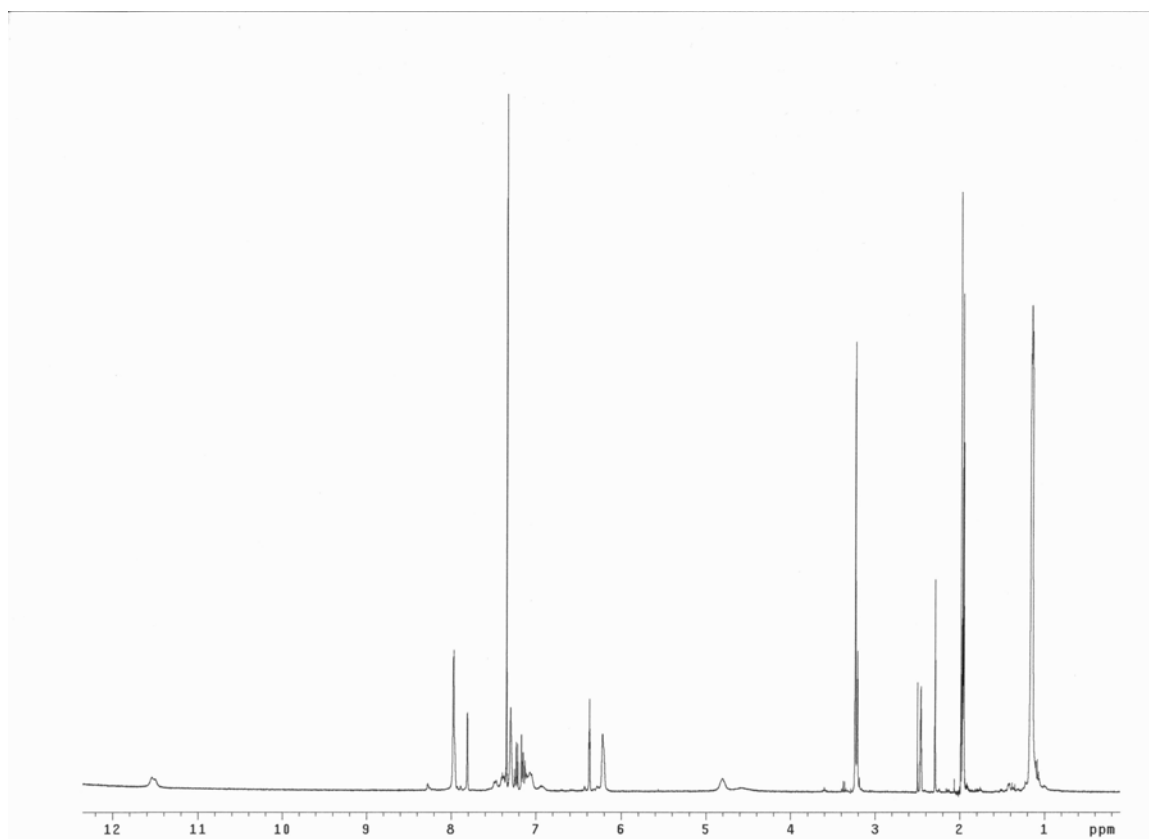


Figure B17 ¹H NMR spectrum of [TpRu(PMe₃)₂NC₆H₄-]₂[OTf]₂ in 80% CD₃CN 20 % DMSO-*d*₆ -20 °C.

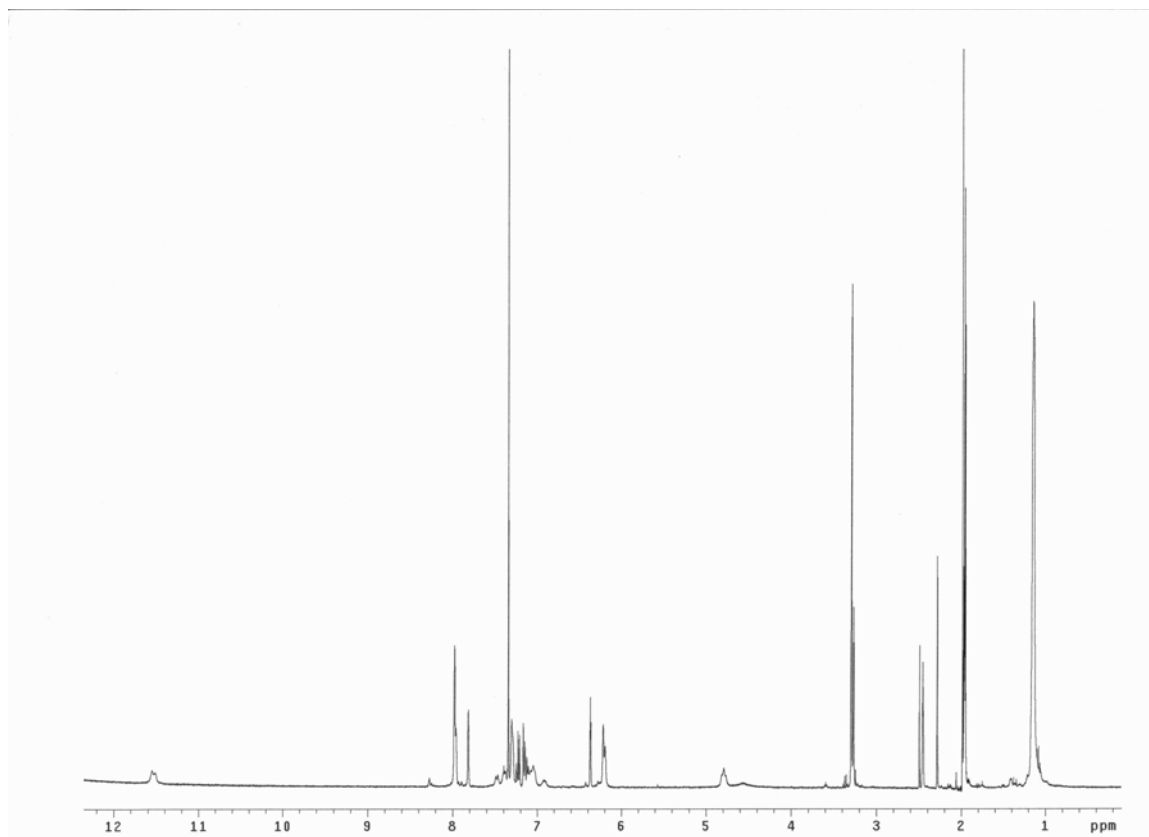


Figure B18 ¹H NMR spectrum of [TpRu(PMe₃)₂NC₆H₄-]₂[OTf]₂ in 80% CD₃CN 20 % DMSO-*d*₆ -30 °C.

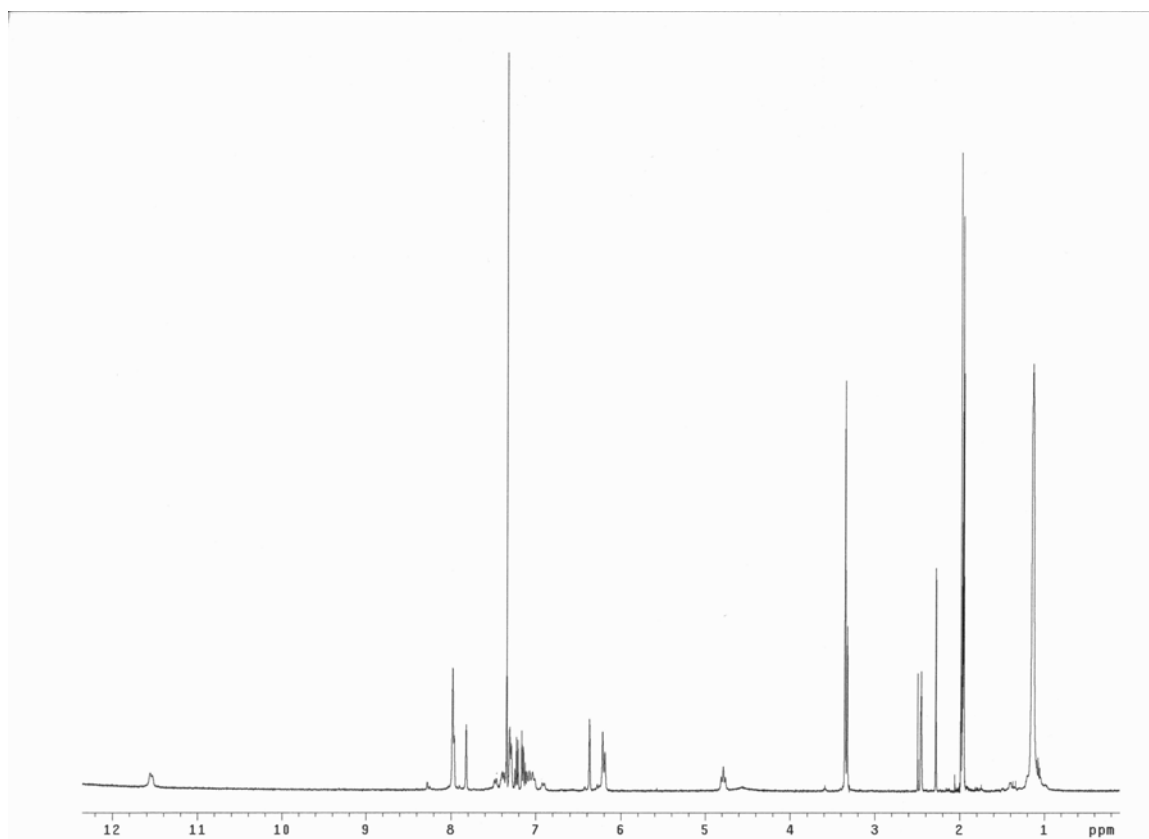


Figure B19 ¹H NMR spectrum of [TpRu(PMe₃)₂NC₆H₄-]₂[OTf]₂ in 80% CD₃CN 20 % DMSO-*d*₆ -40 °C.